Durability Properties of an Alkali Activated Cementitious Material

Olalekan Olayinka Ojedokun

A thesis submitted in partial fulfilment of the requirements of Sheffield Hallam University for the degree of Doctor of Philosophy

January 2018

Abstract

The utilization of Portland cement as a construction material is unsustainable due to the huge amount of CO_2 emissions coupled with the high energy demand during its production. New innovations in low impact construction materials require a reduction in the use of Portland cement with alternative binders, preferably utilising industrial waste materials and aggregates made from recycled waste. Alkali activated cementitious materials (AACMs) shows potential benefits when used in place of Portland cement in the construction industry. However, market forces mitigating against the acceptance of AACMs are fomidable. This is partly because of the limited knowledge of the in-service life of AACM concrete, which is linked to the inadequate durability investigations available in literature.

This research project investigates the durability properties of AACM concrete by exposing it to deleterious substances that cause deterioration and damage to reinforced concrete structures. The durability properties of AACM concrete were investigated under long term exposure to chloride and CO_2 environments which are the two main corrosion initiators in reinforced concrete structures. Four series of AACM concrete mixes were studied with a parallel OPC concrete mix used for the comparative analysis. Mix parameters investigated in the research included factors such as activator dilution and liquid/binder ratios which are given in relevant chapters.

Chapter 1 provides an Introduction to the thesis. Chapter 2 gives an overall Literaure Review and also provides information on the materials used in the research. A chapter specific literature review is given at the start of each chapter. The third chapter presents the investigation of the microsrtucture of AACM and OPC mortar mixes which shows that AACM mortar has less porosity than OPC mortar. However, a greater capillary pore volume was observed in AACM mortar than OPC mortar but the reverse was the case for gel pore volume. The fourth and fifth chapters investigate the physically bound, chemically bound and free chloride concentrations in both AACM and OPC concrete. The results show a lower degree of physically and chemically bound chlorides but a higher degree of free chloride in AACM concrete compared with OPC concrete. The free chloride/hydroxyl ion ratio which is an index for corrosion initiation in concrete is lower in AACM concrete than OPC concrete due to the higher pH of the former. The sixth chapter investigates the carbonation in AACM and control OPC concrete. The depth of carbonation is higher in AACM concrete than OPC concrete but the phenolpthlain test method has limitations for use in AACMs. Investigations on the pH of carbonation specimens gave a greater insight to carbonation in AACMs. The influence of mix design parameters of AACMs are reported in each chapter 3, 4, 5 and 6. The seventh chapter reports the monitoring of the corrosion activity of steel reinforcing bars embedded in AACM and OPC concrete until 860 days of cyclic exposure in a 5% NaCl solution and air. The corrosion potentials and current densities were higher in AACM concrete than OPC concrete under wet cycles, which is likely due to the insufficient oxygen concentration at the steel interface. The visual inspection of the reinforcing steel bars in AACM and OPC concrete to detect when corrosion begins will confirm the insufficient oxygen concentration at the steel interface.

Generally, AACM concrete shows better durability properties than OPC concrete except the carbonation aspect which requires further investigation. The likehood that the phenolpthalein indicator method which is a standard testing method for carbonation of OPC concrete might not be suitable for AACM concrete.

Declaration

I hereby declare that no portion of work presented in this thesis has been submitted in support of an application for another degree or qualification in this or any other university. All sources of information have been duly acknowledged.

Olalekan Olayinka Ojedokun

January 2018

Dedication

This research work is dedicated to God almighty, the giver of knowledge to do all kinds of work (Exodus 31:3).

I would like to appreciate my kind-hearted wife Olubunmi Ojedokun and our lovely kids Mark, Grace and Allison for their kind support, sacrifices and good wishes during the course of this project.

Also, I will like to thank my parents Hon. J.O. Ojedokun and late Mrs Grace Ojedokun for their early inspiration and encouragements.

Lastly, I would like to appreciate my siblings Dapo, Wale, Bayo and Damola for their love, kindness and understanding.

I love you all.

Acknowledgement

The author would like to express his profound gratitute to the director of studies Professor Pritpal S. Mangat for his insightful ideas, suggestions and professional relationship which has helped me develop careerwise, I will forever remain grateful. The author would also like to thank Professor Paul Lambert, Dr Finbarr J. O'Flaherty, Dr Vincenzo Starinieri and Shahriar Abubakri of the Centre for Infrastructure Management, the MERI administration team (Gail, Clare, Jane, Corrie and Rachael) and my PhD colleagues at Sheffield Hallam University for their guidance, support and patience throughout this research project. The author also wishes to express his appreciation to the assistance given by the technical staff of the Construction Materials Laboratory, Sheffield Hallam University.

The author acknowledges the part sponsorship of the Tertiary Education Trust Fund, Federal government of Nigeria and Sheffield Hallam University for the additional financial support in the completion of this research project.

Table of Contents

Abstract 2
Declaration 3
Dedication 4
Acknowledgement 5
Table of Contents 6
List of Tables 13
List of Figures 14

CHAPTER 1 22
INTRODUCTION 22
1.1 BACKGROUND 22
1.2 AIM OF THE RESEARCH 23
1.3 SCOPE OF THE CURRENT INVESTIGATION 23
1.4 THESIS LAYOUT 24

CHAPTER 2 28
GENERAL LITERATURE REVIEW 28
2.0 INTRODUCTION 28
2.1 ALKALI ACTIVATED CEMENTITIUOS MATERIALS (AACMs) 29
2.2 AACM BINDERS 31
2.2.1 High calcium AACM Binders 31
2.2.1.1 Ground granulated blast furnace slag (GGBS) 31
2.2.1.2 ASTM class C fly ash 33
2.2.2 Low calcium AACM Binders 34
2.2.2.1 ASTM class F fly ash 34
2.2.2.2 Silica Fume (SF) 34
2.2.2.3 Rice husk ash (RHA) 35
2.2.2.4 Metakaolin 36
2.3 ALKALINE ACTIVATORS 36
2.3.1 Sodium and Potassium Silicates *($Na_2O.rSiO_2$, $K_2O.rSiO_2$)* 36
2.3.2 Sodium, Calcium and Potassium Hydroxides *($NaOH$, $Ca(OH)_2$, KOH)* 37
2.3.3 Sodium and Pottasium Carbonate *(Na_2CO_3, K_2CO_3)* 38
2.4 METHODS OF MEASUREMENT 38
2.4.1 Activator Concentration 38
2.4.1.1 Percentage dilution 39
2.4.1.2 Molarity or Molar ratio 39
2.4.2 Liquid to Cementitious Ratios 40
2.4.2.1 Liquid/binder ratio 42
2.4.2.2 Activator/pozzolan ratio 43
2.4.3 Chloride Diffusion 43
2.4.3.1 Percent weight of binder 43

CHAPTER 3 45
POROSITY AND PORE STRUCTURE OF AN ALKALI ACTIVATED CEMENTITIOUS (AACM) MORTAR 45
3.1 INTRODUCTION 45
3.2 LITERATURE REVIEW 46
3.2.1 Concrete Pore Structure 46
3.2.1.1 Gel pores 46

3.2.1.2 Capillary pores 48
3.2.1.3 Unimodal and Bimodal 48
3.2.2 Pore System Parameters 49
3.2.2.1 Intrudable porosity Φ_{in} 50
3.2.2.2 Critical pore diameter d_c 51
3.2.2.3 Threshold pore diameter d_{th} 51
3.2.2.4 Effective Porosity 51
3.2.3 Factors Affecting Pore Structure 52
3.2.3.1 Pore System Characteristics 52
3.2.3.2 Experimental Factors 52
3.2.3.3 Hydration/Geopolymerisation of Binder 53
3.2.4 Materials 53
3.2.4.1 OPC 54
3.2.4.2 Water 54
3.2.4.3 Chemical Admixtures 55
3.2.4.4 Aggregates 55
3.3 TEST PROGRAMME 57
3.3.1 Materials and Mix Proportions 57
3.3.2 Specimen Preparation and Conditioning 60
3.3.2.1 Casting of Specimens 60
3.3.2.2 Specimen Preparation 60
3.3.2.3 Curing Regime 61
3.3.3 MIP Sample Preparation and Conditioning 62
3.3.3.1 Cube Crushing 62
3.3.3.2 Location of Test Samples 62
3.3.3.3 Oven Drying 63
3.3.3.4 Details of MIP Test Samples 63
3.3.4 Test Procedure 65
3.3.4.1 Mercury Intrusion Porosimetry 65
3.3.4.2 Mercury Intrusion Porosimetry Test Procedure 65
3.3.4.2.1 Pascal 140 66
3.3.4.2.2 Pascal 240 67
3.4 RESULTS AND DISCUSSION 67
3.4.1 Compressive Strength 67
3.4.1.1 Effect of Activator Dilution 67
3.4.1.2 Effect of Admixtures (R42 and SRA) 69
3.4.1.3 Effect of Liquid/Binder Ratio 69
3.4.1.4 Effect of Curing Regime (Wet/dry, Wet and Dry) 71
3.4.2 Classification of Pore Size Distribution 72
3.4.2.1 Unimodal and Bimodal Pore Distribution 72
3.4.2.1.1 Wet/dry Curing 75
3.4.2.1.2 Wet Curing 75
3.4.2.1.3 Dry curing 76
3.4.2.2 Gel and Capillary Pore Volumes 76
3.4.2.2.1 Wet/dry curing 77
3.4.2.2.2 Wet curing 77
3.4.2.2.3 Dry curing 78
3.4.2.2.4 Effect of admixtures 78
3.4.3 Pore System Parameters 81
3.4.3.1 Intrudable Porosity Φ_{in} 81
3.4.3.1.1 Effect of activator dilution 81
3.4.3.1.2 Effect of admixtures (R42 and SRA) 82

3.4.3.1.3 Effect of curing 83
3.4.3.2 Critical Pore Diameter d_c 84
3.4.3.2.1 Effect of activator dilution 85
3.4.3.2.2 Effect of admixtures 86
3.4.3.2.3 Effect of liquid/binder ratio 87
3.4.3.2.4 Effect of curing regimes (wet/dry, wet and dry) 88
3.4.3.3 Threshold Pore Diameter d_{th} 89
3.4.3.3.1 Effect of activator dilution 89
3.4.3.3.2 Effect of admixtures 90
3.4.3.3.3 Effect of liquid/binder ratio 91
3.4.3.3.4 Effect of curing regime (wet/dry, wet and dry) 92
3.4.3.4 Effective Porosity 93
3.4.3.4.1 Effect of activator dilution 93
3.4.3.4.2 Effect of admixtures (R42 & SRA) 94
3.4.3.4.3 Effect of liquid/binder ratio 95
3.4.3.4.4 Porosity of AACM and OPC mortar 96
3.4.4 Relationship between Effective Porosity and Strength 97
3.4.4.1 Effect of Curing 98
3.4.4.2 Effect of Liquid/Binder Ratio 99
3.4.4.2.1 Validation of the effect of liquid/binder ratio 100
3.5 CONCLUSIONS 101

CHAPTER 4 103
BOUND CHLORIDES IN ALKALI ACTIVATED CEMENTITIOUS (AACM) CONCRETE 103
4.1 INTRODUCTION 103
4.2 LITERATURE REVIEW 104
4.2.1 Alkali Activated Cementitious Materials (AACMs) 104
4.2.1.1 Gel Chemistry 104
4.2.2 Pore Structure of AACM and OPC Concrete 105
4.2.2.1 AACM Concrete 105
4.2.2.2 OPC Concrete 106
4.2.3 Durability Parameters of AACM Concrete 106
4.2.3.1 Introduction 106
4.2.3.2 Chloride Ingress and Transportation Mechanism 106
4.2.3.3 Rate of Chloride Ingress 108
4.2.3.4 Chloride Diffusion Parameters 108
4.2.3.5 Chloride Contents and Binding Capacity 111
4.2.3.6 Chloride Threshold 112
4.2.3.7 Chloride Diffusion Coefficient D_C 113
4.3 EXPERIMENTAL PROGRAMME 114
4.3.1 Mix Composition 114
4.3.2 Specimen Preparation 117
4.3.2.1 Chloride Samples 118
4.3.2.2 Compressive Strength 118
4.3.2.3 Shrinkage 118
4.3.3 Experimental Procedure 119
4.3.3.1 Chloride Ingress Test 119
4.3.3.2 Concrete Powder Sample Collection 120
4.3.4 Testing Procedure 121
4.3.4.1 Physically Bound Chloride Analysis 121
4.3.4.2 Chemically Bound Chloride Analysis 123

4.4 RESULTS AND DISCUSSION 123
4.4.1 Introduction 123
4.4.2 Compressive Strength 124
4.4.2.1 Strength Development of AACM and OPC concrete 125
4.4.2.2 Strength Development at Early Age 125
4.4.2.3 Influence of binder content 126
4.4.2.4 Influence of alkali activator dilution 127
4.4.3 Chloride ingress 128
4.4.3.1 Introduction 128
4.4.3.2 Chloride Diffusion Profiles 128
4.4.3.2.1 Water soluble chloride concentration 129
4.4.3.2.2 Acid soluble chloride concentration 131
4.4.3.3 Surface Chloride Concentration C_0 135
4.4.3.3.1 Influence of exposure period 135
4.4.3.3.2 AACM and OPC surface chloride concentrations C_0 138
4.4.3.3.3 Influence of activator dilution 139
4.4.3.4 Chloride Diffusion Coefficient D_c 141
4.4.3.4.1 Influence of exposure period 141
4.4.3.4.2 Influence of Activator Dilution 144
4.4.4 Relationship between Porosity and Chloride Diffusion Parameters 145
4.4.4.1 Chloride Diffusion Coefficient D_C 145
4.4.4.2 Surface Chloride Concentration C_0 146
4.5 CONCLUSIONS 147

CHAPTER 5 149
FREE CHLORIDE AND pH OF PORE SOLUTION IN ALKALI ACTIVATED CEMENTITIOUS (AACM) CONCRETE 149
5.1 INTRODUCTION 149
5.2 LITERATURE REVIEW 150
5.2.1 Concrete Pore Solution Composition 150
5.2.2 Concrete Chlorides 151
5.2.2.1 Free Chloride 151
5.2.2.2 Total Chloride 153
5.2.3 pH of Concrete Pore Solution 154
5.2.4 Hydroxyl Ion (OH^-) Concentration 155
5.2.5 Chloride Binding Isotherms 156
5.2.5.1 Introduction 156
5.2.5.2 Freundlich Isotherm 156
5.2.5.3 Langmuir Isotherm 157
5.2.5.4 Linear Isotherm 158
5.2.5.5 Chloride Binding Capacity 159
5.3 EXPERIMENTAL PROGRAMME 160
5.3.1 Mix Composition 160
5.3.2 Experimental Procedure 163
5.3.2.1 Concrete Coring 163
5.3.2.2 Pore Solution Expression 165
5.3.2.3 Concrete Pore Solution 167
5.3.3 Analytical Procedures 168
5.3.3.1 Determination of Free Chloride Concentration 168
5.3.3.2 Determination of pH 168
5.4 RESULTS AND DISCUSSION 169
5.4.1 Free Chloride Concentration 169

5.4.1.1 Free Chloride Diffusion Profiles....170
5.4.1.2 Activator Dilution....172
5.4.1.3 Free Chloride Content of AACM and OPC Concrete....173
5.4.2 Free Chloride Diffusion Parameters....175
5.4.2.1 Chloride Profiles....175
5.4.2.2 Surface Chloride Concentration $C_{0(f)}$....176
5.4.2.3 Diffusion Coefficient $D_{c(f)}$....178
5.4.3 Chloride Binding Isotherms....180
5.4.3.1 Free and Water-Soluble Chloride Relationship....180
5.4.3.1.1 Influence of Activator Dilution....183
5.4.3.2 Free and Acid-Soluble Chloride Relationship....184
5.4.3.2.1 Influence of Activator Dilution....184
5.4.3.2.2 Influence of Chloride Exposure Period....186
5.4.3.3 AACM and OPC Chloride Binding Capacity....187
5.4.4 pH and OH^- of AACM Concrete....189
5.4.4.1 Introduction....189
5.4.4.2 Effect of Activator Dilution and Penetration Depths....190
5.4.4.3 Effect of Chloride Exposure Period....193
5.4.5 Free Chloride/ Hydroxyl ion Ratio [Cl^-/OH^-]....194
5.4.5.1 Effect of Activator Dilution....194
5.4.5.2 Effect of Chloride Exposure Period....197
5.5 CONCLUSIONS....198

CHAPTER 6....200
CARBONATION OF ALKALI ACTIVATED CEMENTITIOUS (AACM) CONCRETE....200
6.1 INTRODUCTION....200
6.2 LITERATURE REVIEW....201
6.2.1 Carbonation in Concrete....201
6.2.2 Chemistry of Carbonation in Concrete....203
6.2.3 Factors Affecting Carbonation in Concrete....204
6.2.3.1 Humidity....204
6.2.3.2 Binder Content....204
6.2.3.3 CO_2 Exposure Concentration....205
6.2.4 Rate of Carbonation....206
6.2.5 Carbonation Shrinkage....208
6.3 EXPERIMENTAL PROGRAMME....209
6.3.1 Mix Composition....209
6.3.2 Specimen Preparation....212
6.3.2.1 Prism Specimens (300 x 75 x 75 mm)....212
6.3.2.1.1 Rate of carbonation specimens....212
6.3.2.1.2 Carbonation shrinkage specimens....213
6.3.2.2 Cylindrical Specimens (50mm diameter X 60mm Depth)....214
6.3.3 Experimental Procedure....215
6.3.3.1 Rate of Carbonation Test....215
6.3.3.1.1 Depth of carbonation d_k....216
6.3.3.2 Carbonation Shrinkage Test....217
6.3.3.3 Powder Collection....217
6.3.3.3.1 pH analysis....218
6.4 RESULTS AND DISCUSSION....219
6.4.1 Depth of Carbonation (Prism Tests)....219
6.4.1.1 AACM and OPC Concrete....220

6.4.1.2 Effect of liquid/binder ratio 222
6.4.1.3 Effect of Activator Dilution 222
6.4.1.4 Effect of Exposure Period 223
6.4.2 Rate of Carbonation 225
6.4.3 Shrinkage of AACM and OPC concrete 227
6.4.3.1 Carbonation Shrinkage 227
6.4.3.2 Drying Shrinkage 229
6.4.3.3 Carbonation and Drying Shrinkage 230
6.4.4 pH of Carbonated Zone 232
6.4.4.1 AACM and OPC Concrete and Mortar 232
6.4.4.2 Effect of Activator Dilution 233
6.4.5 Relationship between Carbonation Depth and Porosity 234
6.5 CONCLUSIONS 235

CHAPTER 7 237
CHLORIDE-INITIATED REINFORCEMENT CORROSION IN AACM CONCRETE 237
7.1 INTRODUCTION 237
7.2 LITERATURE REVIEW 238
7.2.1 Introduction 238
7.2.2 Corrosion process 240
7.2.2.1 The Anodic Reaction 240
7.2.2.2 The Cathodic Reaction 241
7.2.2.3 The Pourbaix Diagrams 241
7.2.3 Types of Corrosion 242
7.2.3.1 General or Uniform Corrosion 242
7.2.3.2 Localised Corrosion 242
7.2.3.2.1 Pitting corrosion 242
7.2.3.2.2 Crevice corrosion 243
7.2.3.2.3 Bimetallic corrosion 243
7.2.4 Corrosion Mechanisms in Concrete 243
7.2.4.1 Chloride induced corrosion 243
7.2.4.2 Carbonation induced corrosion 245
7.2.5 Service Life of Reinforced Concrete Structures 246
7.2.5.1 Service life models 246
7.2.5.2 Corrosion damage in steel reinforced concrete 249
7.3 EXPERIMENTAL PROGRAMME 250
7.3.1 Sample Preparation 250
7.3.1.1 Preparation of steel bars and electrical connection 250
7.3.1.2 Casting 252
7.3.1.3 Curing and exposure to corrosion environment 255
7.3.1.3.1 Chloride diffusion 255
7.3.1.3.2 Accelerated corrosion inducing environment 256
7.3.1.3.3 Climate chamber 257
7.3.2 Test Procedure 257
7.3.2.1 Corrosion potential E_{corr} 257
7.3.2.2 Corrosion current density I_{corr} 258
7.3.2.3 Sorptivity 259
7.3.2.4 Determination of [Cl/OH^-] ratio 260
7.3.2.4.1 Concrete coring 260
7.3.2.4.2 Concrete pore solution expression 262
7.3.2.4.3 Determination of free chloride and pH of pore solution 263

7.4 RESULTS AND DISCUSSION 264
7.4.1 Sorptivity 264
7.4.2 Corrosion Potential E_{corr} 265
7.4.2.1 Chloride diffusion period 266
7.4.2.2 Laboratory air exposure periods 267
7.4.2.3 Climate chamber exposure 268
7.4.3 Corrosion Current Density I_{corr} 269
7.4.4 Pore Solution 270
7.4.4.1 Free Cl concentration (mol/L) 270
7.4.4.2 Hydroxyl ion concentration (mol/L) 272
7.4.4.3 Chloride/Hydroxyl ion concentration $[Cl^-]/[OH^-]$ 273
7.5 CONCLUSIONS 275

CHAPTER 8 277
CONCLUSIONS AND RECOMMENDATIONS FOR FUTURE WORK 277
8.1 INTRODUCTION 277
8.2 GENERAL CONCLUSIONS 277
8.2.1 Porosity and pore structure of AACM and OPC mortars 277
8.2.2 Strength, shrinkage and bound chlorides of AACM and OPC concrete 278
8.2.3 Free chloride and pH of AACM and OPC concrete pore solution 279
8.2.4 Carbonation of AACM and OPC concrete 280
8.2.5 Chloride initiated corrosion in AACM and OPC concrete 281
8.2 RECOMMENDATIONS FOR FUTURE RESEARCH 282
APPENDIX I 284
APPENDIX II 285
REFERENCES 311

List of Tables

Table 2. 1: Performance level of combining different solid precursors with alkaline activators [3] 30

Table 3. 1: Classification of pore sizes in hydrated cementitious paste 46
Table 3. 2: Models of porosity and strength relationships for cement-based materials 52
Table 3. 3: Chemical composition of ordinary Portland cement 54
Table 3. 4: Chemical analysis of silica sand 57
Table 3. 5: Composition of AACM and OPC mortar mixes 59
Table 3. 6: Curing regimes for AACM & OPC mortar mixes 61
Table 3. 7: Mass and dimensions of samples under different curing regimes 64

Table 4. 1: Chloride transport mechanism for various marine exposure conditions 108
Table 4. 2: Published chloride diffusion coefficient Dc values for OPC concrete 111
Table 4. 3: Maximum allowable total chloride content in concrete [74] 113
Table 4. 4: Composition of AACM and OPC concrete mixes 116
Table 4. 5: Water and acid soluble surface chloride concentrations, C_0, (% weight of binder) 135

Table 5. 2: Published total and free Cl- content in OPC based concrete (laboratory conditions) [238] 152
Table 5. 3: Composition of AACM and OPC concrete mixes 162
Table 5. 4: Details of AACM and OPC concrete pore fluid extraction 167
Table 5. 5: Free chloride concentration (mg/L) for AACM and OPC concrete 170
Table 5. 6: Free Chloride diffusion parameters $C_{0(f)}$, $D_{c(f)}$ and the coefficient of correlation R^2 176
Table 5. 7: Binding coefficients for Langmuir, Freundlich and Linear isotherms 182
Table 5. 8: pH and OH^- concentration of AACM and OPC concrete pore solution 190

Table 6. 1: Depth of carbonation of concrete produced with CEM I Type Cement exposed to typical Nordic climate for 35 years. 207
Table 6. 2: Composition of AACM and OPC concrete mixes 211
Table 6. 3: Depth of Carbonation d_k (mm) for AACM and OPC concrete mixes S_2 to S_6 at different exposure periods to accelerated carbonation 220

Table 7. 1: Composition of AACM and control OPC concrete mixes 254
Table 7. 2: Exposure duration of corrosion specimens (batches "a" and "b") under different environments 254

List of Figures

Figure 2. 1: Example of relation between activator dilution and molarity for a 15 M activator 40
Figure 2. 2: The relationship between strength and water/cement ratio of OPC concrete [25] 42

Figure 3. 1: Conceptual Model for Geopolymerization [108] 47
Figure 3. 2: Unimodal pore size distribution in OPC concrete (Author's data) 49
Figure 3. 3: Bimodal pore size distribution in AACM concrete (Author's data) 49
Figure 3. 4: Definition of Pore System Parameters in OPC Mortar (Author's data) 50
Figure 3. 5: Definition of Pore System Parameters in AACM Mortar (Author's data) 50
Figure 3. 6: Model for Hydrated AACM Binder. (Myers et al. [129]) 53
Figure 3. 7: Model for Hydrated Portland Cement. (R. F. Feldman and P. J. Sereda, [130]) 53
Figure 3. 8: Grading curve for 10 mm uncrushed gravel 55
Figure 3. 9: Grading curve for silica sand 56
Figure 3. 10: Grading curve for sharp concrete sand 56
Figure 3. 11: AACM mortar specimens after demoulding 60
Figure 3. 12: Location of test sample used for MIP testing within a mortar cube core 62
Figure 3. 13: MIP specimens stored in self-sealing bags after oven drying 62
Figure 3. 14: Weighing of test sample 63
Figure 3. 15: Measuring the dimensions of samples 63
Figure 3. 16: Mercury intrusion porosimetry device used for analysis 65
Figure 3. 17: CD3 dilatometer showing the male cone and female bulb components 65
Figure 3. 18: Autoclave (1) upper valve (2) locking nut (3) lower valve [138] 66
Figure 3. 19: Filling with dielectric oil 66
Figure 3. 20: Placing the dilatometer into the autoclave 66
Figure 3. 21: Compressive strength of mortar batch "a" containing admixtures (R42 and SRA) 68
Figure 3. 22: Compressive strength of mortar batch "b" containing no admixtures (R42 and SRA) 68
Figure 3. 23*:* Effect of liquid/binder ratio on compressive strength of AACM mortars 70
Figure 3. 24: Compressive strength of AACM and OPC mortar batch "a" mixes with admixtures 71
Figure 3. 25: Compressive strength of AACM and OPC mortar batch "b" mixes without admixtures 71
Figure 3. 26: Pore size distribution for AACM and OPC mixes without admixtures under wet/dry curing 73
Figure 3. 27: Pore size distribution for AACM and OPC mixes without admixtures under wet curing 74
Figure 3. 28: Pore size distribution for AACM and OPC mixes without admixtures under dry curing 74
Figure 3. 29: Intrudable porosity for AACM and OPC mixes without admixtures under wet/dry, wet and dry curing 76

Figure 3. 30: Pore size distribution of AACM mortar mixes (with admixtures) under wet/dry curing 79
Figure 3. 31: Pore size distribution of AACM mortar mixes (without admixtures) under wet/dry curing 80
Figure 3. 32: Intrudable porosity of AACM mortar batch "a" mix with admixtures..... 82
Figure 3. 33: Intrudable porosity of AACM mortar batch "b" mix withot admixtures .. 82
Figure 3. 34: Relationship between liquid/binder ratio and intruded pore volume of AACM mortar mix M_3 (with admixtures)..... 84
Figure 3. 35: Effect of activator dilution on the critical pore diameters (with admixtures) 85
Figure 3. 36: Effect of admixtures (R42 and SRA) on the critical pore diameters of AACM mixes under wet/dry curing..... 86
Figure 3. 37: Relationship between liquid/binder ratio and critical pore diameter d_c of AACM mortar mix M_3 (with admixtures)..... 87
Figure 3. 38: Effect of curing regime (wet/dry, wet & dry) on the critical pore diameters of AACM and OPC mixes (without admixtures)..... 88
Figure 3. 39: Effect of activator dilution on the threshold pore diameters d_{th} of AACM mortar mixes M_2 to M_5 (without admixtures)..... 89
Figure 3. 40: Effect of admixtures (R42 & SRA) on threshold pore diameters d_{th} of AACM mortar mixes 90
Figure 3. 41: The relationship between threshold pore diameter d_{th} and liquid/binder ratio (with admixtures)..... 91
Figure 3. 42: Effect of curing on the threshold pore diameters d_{th} (without admixtures)92
Figure 3. 43: Effect of activator dilution on the porosity of AACM mortar with admixtures under different curing regimes. 93
Figure 3. 44: Effect of admixtures on the porosity of AACM mortar under different curing regimes. 94
Figure 3. 45: Relationship between porosity and liquid/binder ratio of AACM mortar M_3 under wet/dry, wet and dry curing (with admixture) 95
Figure 3. 46: Graph showing the porosity at the incremental diameter (µm) for AACM and OPC mortar mixes M_2 and M_6 under wet/dry curing. 96
Figure 3. 47*:* Graph showing the porosity at the incremental diameter (µm) for AACM and OPC mortar mixes M_2 and M_6 under wet curing. 96
Figure 3. 48: Graph showing the porosity at the incremental diameter (µm) for AACM and OPC mortar mixes M_2 and M_6 under dry curing. 96
Figure 3. 49: Porosity of AACM and OPC mortar mixes M_2 and M_6 under wet/dry, wet and dry curing. 97
Figure 3. 50: Strength-effective porosity relationship of AACM mortar under different curing..... 98
Figure 3. 51: Relationship between porosity and compressive strength. 99
Figure 3. 52: Strength-porosity relationship of AACM mortar mix M_3 (with admixtures) under different liquid/binder ratios 100

Figure 4. 1: Schematics of exothermic reaction of hydroxide (OH) alkali activators with binder..... 105

Figure 4. 2: Polystyrene moulds used for casting AACM Concrete 117
Figure 4. 3: AACM Concrete Specimens after demoulding 117
Figure 4. 4: Coated surfaces (top picture), exposed surface (bottom picture) 120
Figure 4. 5: Specimens immersed in 5% sodium chloride solution. 120
Figure 4. 6: AACM specimen sawn into half 120
Figure 4. 7: Some powder sample locations highlighted in red 120
Figure 4. 8: AACM powder passing a 150 µm sieve 121
Figure 4. 9: AACM powder passing (bottom picture) and retained (top picture) by a 150 µm sieve 121
Figure 4. 10: ISE reading of concrete powder solution 122
Figure 4. 11: pH reading of concrete powder solution 122
Figure 4. 12: Compressive strength with age of AACM concrete (wet cured, 20^0C) ... 124
Figure 4. 13: Compressive strength with age of AACM concrete (dry cured, 20^0C, 65% RH) 125
Figure 4. 14: Relationship between Compressive Strength and Activator Dilution 127
Figure 4. 15: Water-soluble chloride profiles (% weight of binder) at 55days exposure in 5% NaCl solution 129
Figure 4. 16: Water-soluble chloride profiles (% weight of binder) at 90days exposure in 5% NaCl solution 129
Figure 4. 17: Water-soluble chloride profiles (% weight of binder) at 120days exposure in 5% NaCl solution 130
Figure 4. 18: Water-soluble chloride profiles (% weight of binder) at 180days exposure in 5% NaCl solution 130
Figure 4. 19: Water-soluble chloride profiles for AACM mix S_3 and OPC mix S_6 at 20, 25 and 35 mm depths 131
Figure 4. 20: Acid-soluble chloride profiles (% weight of binder) at 55 days exposure in 5% NaCl solution 132
Figure 4. 21: Acid-soluble chloride profiles (% weight of binder) at 90 days exposure in 5% NaCl solution 132
Figure 4. 22: Acid-soluble chloride profiles (% weight of binder) at 120 days exposure in 5% NaCl solution 132
Figure 4. 23: Acid-soluble chloride profiles (% weight of binder) at 180 days exposure in 5% NaCl solution 133
Figure 4. 24: Acid-soluble chloride profiles (% weight of binder) at 270 days exposure in 5% NaCl solution 133
Figure 4. 25: Acid-soluble chloride profiles for AACM Mix S_3 and OPC Mix S_6 at 20, 25 and 35 mm depths 134
Figure 4. 26: Relationship between the water-soluble surface chloride concentration, $(C_0)_{ws}$ and exposure period 136
Figure 4. 27: Relationship between the acid-soluble surface chloride concentration, $(C_0)_{as}$ and chloride exposure period 137
Figure 4. 28: Water-soluble and acid-soluble surface chloride concentrations of mixes S_2, S_5 and S_6 at 55 days exposure 138
Figure 4. 29: Water-soluble and acid-soluble surface chloride concentrations of mixes S_2, S_5 and S_6 at 180 days exposure 138

Figure 4. 30: The relationship between water-soluble surface chloride concentration, $(C_0)_{ws}$ and activator dilution. 139
Figure 4. 31: The relationship between acid-soluble surface chloride concentration, $(C_0)_{as}$ and activator dilution. 141
Figure 4. 32: Relationship of acid-soluble chloride diffusion coefficient D_c with exposure period 142
Figure 4. 33: Relationship between acid soluble chloride diffusion coefficient, Dc and activator dilution 144
Figure 4. 34: Relationship between the chloride diffusion coefficient and intrudable porosity at different exposure periods. 145
Figure 4. 35: Relationship between the surface chloride concentration and intrudable porosity at different exposure periods to 5% NaCl solution. 146

Figure 5. 1: Free and bound chloride relationships using Freundlich, Langmuir and Linear binding isotherms 157
Figure 5. 2: Linear binding isotherm of published chloride concentrations from Table 5.1 159
Figure 5. 3: Coring of AACM and OPC specimens exposed to 5% NaCl solution. (a) Sawn halves, dimensions 250x125x75mm (180 and 270 days exposure) (b) Full specimen, dimensions 250x250x75 mm (540 days exposure). 163
Figure 5. 4: Cutting the concrete cores into discs of 50 mm diameter x 20 mm depth. 164
Figure 5. 5: Obtaining discs of 50mm diameter, 20mm depth from the concrete core. 164
Figure 5. 6: Concrete discs stored in self-sealing bags 165
Figure 5. 7: Pore fluid extraction device 166
Figure 5. 8: Cross section of pore fluid extraction device and concrete discs 166
Figure 5. 9: Pore fluid extractor placed under the compression testing machine platen 166
Figure 5. 10: Air tight plastic vials containing concrete pore solution. 166
Figure 5. 11: Double junction electrode and benchtop meter 3-in-1 used to measure pH 169
Figure 5. 12: Free chloride concentration profiles of AACM concrete exposed to 5% chloride solution. 171
Figure 5. 13: Effect of activator dilution on the free chloride concentrations of AACM concrete at 180 and 270 days of chloride exposure. 172
Figure 5. 14: Free chloride concentration profile of AACM and OPC concrete 174
Figure 5. 15: Experimental data and regression analysis profiles of free chloride concentration of AACM concrete at 180 days chloride exposure. 175
Figure 5. 16: Experimental data and regression analysis profiles of free chloride concentration of AACM and OPC concrete at 270 days chloride exposure. 175
Figure 5. 17: Experimental data and regression analysis profiles of free chloride concentration of AACM concrete at 540 days chloride exposure. 175
Figure 5. 18: Free surface chloride concentration, $C_{0(f)}$, of AACM and OPC concrete at 180, 270 and 540 days of chloride exposure. 177
Figure 5. 19: Diffusion coefficient, $D_{c(f)}$, of AACM and OPC concrete at 180, 270 and 540 days of chloride exposure. 178

Figure 5. 20: Langmuir, Freundlich and Linear binding isotherms for AACM concrete mix S_2 at 180 days chloride exposure.....181
Figure 5. 21: Langmuir, Freundlich and Linear binding isotherms for AACM concrete mix S_3 at 180 days chloride exposure.....181
Figure 5. 22: Langmuir, Freundlich and Linear binding isotherms for AACM concrete mix S_4 at 180 days chloride exposure.....181
Figure 5. 23: Langmuir, Freundlich and Linear binding isotherms for OPC concrete mix S_6 at 270 days chloride exposure.....182
Figure 5. 24: Effect of activator dilution on Langmuir binding isotherms of AACM concrete at 180 days chloride exposure. 183
Figure 5. 25: Effect of activator dilution on Langmuir binding isotherms of AACM concrete at 180 days chloride exposure 184
Figure 5. 26: Effect of activator dilution on Langmuir binding isotherms of AACM concrete at 270 days chloride exposure. 185
Figure 5. 27: Effect of chloride exposure period on Langmuir binding isotherms of AACM concrete. 186
Figure 5. 28: Acid-soluble chloride binding capacity of AACM and OPC concrete at 270 days chloride exposure period.....187
Figure 5. 29: Acid-soluble chloride binding capacity of AACM and OPC concrete at 180 days chloride exposure period.....187
Figure 5. 30: pH and OH^- profiles of AACM concrete at 180 days of chloride exposure 191
Figure 5. 31: pH and OH^- profiles of AACM and OPC concrete at 270 days of chloride exposure 191
Figure 5. 32: The relationship between $[OH^-]$ and mean depths (10, 30 and 50 mm) for AACM mixes S_2, S_3 and S_4 at 180 days of chloride exposure.....192
Figure 5. 33: The relationship between $[OH^-]$ and mean depths (10, 30 and 50 mm) for AACM and OPC mixes S_2, S_4 , S_5 and S_6 at 270 days of chloride exposure.....192
Figure 5. 34: pH and OH^- profiles of AACM concrete mix S_2 at 180, 270 and 540 days of chloride exposure.....193
Figure 5. 35: pH and OH^- profiles of AACM concrete mix S_4 at 180 and 270 days of chloride exposure 194
Figure 5. 36: Chloride/Hydroxyl ion $[Cl^-]/[OH^-]$ of AACM concrete at 180 days of chloride exposure 195
Figure 5. 37: Chloride/Hydroxyl ion $[Cl^-]/[OH^-]$ of AACM concrete at 270 days of chloride exposure 195
Figure 5. 38: The relationship between $[Cl^-]/[OH^-]$ and mean depths (10, 30 and 50 mm) for AACM mixes S_2, S_3 and S_4 at 180 days of chloride exposure. 196
Figure 5. 39: The relationship between $[Cl^-]/[OH^-]$ and mean depths (10, 30 and 50 mm) for AACM and OPC mixes S_2, S_4 , S_5 and S_6 at 270 days of chloride exposure. 196
Figure 5. 40: $[Cl^-]/[OH^-]$ of AACM concrete mix S_2 at 180, 270 and 540 days of chloride exposure 197
Figure 5. 41: $[Cl^-]/[OH^-]$ of AACM concrete mix S_4 at 180 and 270 days of chloride exposure 197

Figure 6. 1: Four sides coated with bitumen paint; the remaining two longitudinal (300 x 75mm) faces uncoated.....213
Figure 6. 2: Specimens exposed to 5% CO_2 concentration inside the accelerated carbonation chamber. 213
Figure 6. 3: Stainless steel demec points fixed along the two-parallel longitudinal (300 x 75 mm) faces 214
Figure 6. 4: Concrete specimens in 50mm diameter X 60mm depth cylindrical plastic moulds 215
Figure 6. 5: Self-adhesive tape fixed at the bottom of cylindrical moulds 215
Figure 6. 6: Phenolphthalein indicator applied to the two freshly cut faces. 216
Figure 6. 7: Bitumen paint applied to the freshly cut face of the prism. 216
Figure 6. 8: Depth of carbonation d_k measured from the two uncoated longitudinal faces of a prism 216
Figure 6. 9: Demoulded cylinders showing the section A-A of splitting.....218
Figure 6. 10: AACM and OPC concrete/mortar powder stored in air-proof plastic vials 218
Figure 6. 11: Filtering of AACM and OPC concrete/mortar powder 219
Figure 6. 12: Double junction electrode and benchtop meter 3-in-1 used to measure pH 219
Figure 6. 13: Relationship between depth of carbonation d_k and exposure period of AACM and OPC concrete (300 X 75 X 75 mm prism tests). 221
Figure 6. 14: Influence of activator dilution on the depth of carbonation d_k in AACM concrete 223
Figure 6. 15: Carbonation front at 28 days exposure to 5% CO_2 concentration. 224
Figure 6. 16: Carbonation front at 145 days exposure to 5% CO_2 concentration. 224
Figure 6. 17: Rate of carbonation graph for AACM and OPC concrete S_2 to S_6 225
Figure 6. 18: The carbonation coefficient k ($mm/yr^{0.5}$) for AACM and OPC concrete mixes 226
Figure 6. 19: Relationship between carbonation coefficient k ($mm/yr^{0.5}$) and activator dilution 227
Figure 6. 20: Carbonation shrinkage of AACM and OPC concrete 228
Figure 6. 21: Effect of capillary pores on carbonation and drying shrinkage 228
Figure 6. 22: Drying shrinkage of AACM and OPC concrete 229
Figure 6. 23: Relationship between carbonation and drying shrinkage of AACM and OPC concrete 231
Figure 6. 24: Decalcification of C-A-S-H in AACM concrete 232
Figure 6. 25: pH of pore solutions extracted from AACM and OPC concrete and mortar powder at the carbonated zones after 360 days exposure to 5% CO_2. 233
Figure 6. 26: Alkali activator dilution versus pH of pore solution extracted from carbonated AACM concrete and mortar powder. 234
Figure 6. 27: The relationship between depth of carbonation d_k and effective porosity of AACM concrete 235

Figure 7. 1: Schematic illustration of steel reinforcement corrosion showing the anodic and cathodic sites on the steel surface [323] 240

Figure 7. 2: Pourbaix diagram showing the potential pH of iron in aqueous solutions [327] 242
Figure 7. 3: Schematic model of corrosion process in steel reinforced concrete [90] .. 247
Figure 7. 4: Schematic model of pit formation during chloride induced corrosion [354] 248
Figure 7. 5: Grit blasted steel bars 251
Figure 7. 6: Cement slurry cast at the bar end..... 251
Figure 7. 7: Wire connection at one end 252
Figure 7. 8: Bars positioned in moulds 252
Figure 7. 9: Two coats of bituminous paint applied to five faces of the specimen..... 255
Figure 7. 10: Specimens immersed in 5% NaCl solution 255
Figure 7. 11: Specimens cured in laboratory air 256
Figure 7. 12: Specimens cured in alternative climate chamber 256
Figure 7. 13: Schematic diagram showing the Half-cell potential test [373]..... 258
Figure 7. 14: Galvanic current reading using the Zero Resistance Ammeter. 258
Figure 7. 15: PVC tape wrapped on five concrete faces 260
Figure 7. 16: Specimen supported on a strip of porous membrane..... 260
Figure 7. 17: Marked 50 mm diameter circle for coring..... 261
Figure 7. 18: Four cores (50 mm dia X 60 mm depth) drilled from corrosion specimens 261
Figure 7. 19: Concrete cores placed above water-filled enclosed container..... 261
Figure 7. 20: Concrete discs obtained from cores..... 261
Figure 7. 21: Repaired core holes 262
Figure 7. 22: Re-coating of bottom and the four side faces with bitumen paint..... 262
Figure 7. 23: Pore fluid extraction device..... 262
Figure 7. 24: Air tight plastic vials containing concrete pore solution. 262
Figure 7. 25: Free chloride measurement from concrete pore solution 263
Figure 7. 26: Double Junction Electrode and Benchtop Meter 3-in-1 used to measure pH 263
Figure 7. 27: Relationship between increase in mass of water per unit area and square root of time..... 264
Figure 7. 28: Graph of corrosion potential E_{corr} with exposure period for batch “a” corrosion specimens 265
Figure 7. 29: Graph of corrosion potential E_{corr} with exposure period for batch “b” corrosion specimens 266
Figure 7. 30: Graph of corrosion current density I_{corr} of AACM and control OPC concrete 269
Figure 7. 31: Schematic diagram illustrating (a) change of corrosion potential and current density as passive film grows (b) fall in corrosion potential and decrease in corrosion density as cathode is inhibited [378]..... 270
Figure 7. 32: Free chloride concentration (mol/L) of AACM and OPC concrete mixes S_2, S_3 and S_6 at 850 days exposure period..... 271
Figure 7. 33: Free chloride concentration (mol/L) of AACM S_2 and control OPC concrete S_6 specimens under (a) diffusion (b) water absorption and diffusion. 272

Figure 7. 34: Hydroxyl Ion concentration of AACM and OPC concrete mixes S_2, S_3 and S_6 at 850 days exposure period 272
Figure 7. 35: Hydroxyl Ion concentration (mol/L) of AACM S_2 and control OPC concrete S_6 specimens under (a) diffusion (b) water absorption and diffusion. 273
Figure 7. 36: $[Cl^-]/[OH^-]$ of AACM and OPC concrete mixes S_2, S_3 and S_6 at 850 days exposure period 273
Figure 7. 37: Chloride/Hydroxyl Ion $[Cl^-]/[OH^-]$ of OPC concrete mix S_6 at 270 and 850 days exposure period 274

CHAPTER 1
INTRODUCTION

1.1 BACKGROUND

The use of alkali activated cementitious materials (AACM) in place of ordinary Portland cement (OPC) has recently been recognised to have great potential in construction applications. There is the need for a viable alternative to OPC cement because of the high carbon footprint generated during its production with a huge energy demand, which is not sustainable in the future. The carbon footprint is significant because of the large volume of OPC cement consumed worldwide, which is ranked second after the volume of water [1]. A staggering yearly estimate of 1.5 Gt of CO_2 is emmitted into the atmosphere during the production of OPC cement worldwide [2]. To put this into perspective, for each tonne of cement produced an equivalent tonne of CO_2 is emitted into the atmosphere. This translates to the emission of 400 Kg of CO_2 when 1 m^3 of concrete is produced [3]. In addition, cement industry is the most energy intensive of all manufacturing industries, which consumes between 12 - 15% of the total industrial energy use [4]. The electric energy consumption for the burning process during cement production is estimated to be 65 kWh/tonne while the thermal energy consumption for cement grinding is 2.72 GJ/tonne [4]. Clearly, a dire need for replacing OPC cement with a less carbon foot print and a less energy demanding construction material is imperative.

Until recently, the research effort has been placed in fundamental investigations on AACMs and their engineering properties with less emphasis on the service life and durability properties. A number of papers have been published on the filler effect of AACM materials resulting in a denser microstructure than OPC concrete, thus leading to higher mechanical strengh [5][6]. Similarly, the fire resisting potential of AACM makes it an attractive construction material in thermal and nuclear stations and in other facilities including buildings prone to fire outbreak [3]. Other potential commercial applications include repair materials, overlays for bridge decks and pavements, mining and turnelling applications, industrial floors, marine structures.

However, with the preliminary research findings suggesting numerous attractive attributes associated with the use of AACM as a construction material over OPC cement, *RILEM TC 224-AAM* [3] pointed out that the market forces resisting the acceptance of AACM are formidable. Some of the reasons given are the 150 years track record of OPC cement while rapid advances in AACM began in the 70's with limited knowledge

of its durability and in-service life. The limited knowledge of the in-service life of AACM is linked to the inadequate laboratory durability investigations. Secondly, there are no existing standards which can serve as a user manual for consulting engineers and asset owners regarding liability and risk involved when using the product [3] although more recently PAS 8820: 2016 [7] has been published. AACM mix design and test methods are currently dependent on the standards used for OPC cement and its supplementary materials, which are not always appropriate for AACMs [3]. The research investigation carried out on the durability properties of AACM concrete in this study will address some of these concerns.

1.2 AIM OF THE RESEARCH

The research investigation focuses of the durability properties of an alkali activated cementitious concrete. It has been performed by subjecting AACM and parallel OPC concrete to long-term chloride and carbonation exposure, which are the two main corrosion initiators in reinforced concrete. The microstructure and corrosion behaviour of AACM concrete is also investigated and evaluated relative to OPC concrete. The durability and microscructure investigations have been carried out for optimum AACM concrete mixes which were developed during the first phase of the research. The investigation on the durability properties of AACMs will provide useful information for potential applications in deep water constructions.

1.3 SCOPE OF THE CURRENT INVESTIGATION

- Carry out a critical state of the art review on AACMs considering different types of AACM binders and alkaline activators.
- Investigate the microstructure of AACM and control OPC mortar through the classification of their pore sizes and distribution, pore system parameters and the relationship between strength and porosity.
- Investigate the physically and chemically bound chloride concentrations present in AACM and control OPC concrete when exposed in a 5% NaCl solution over long exposure periods up to 270 days.
- Investigate the free chloride concentrations and pH of AACM and control OPC concrete
- Establish the relationships between the free Cl^-/OH^- for corrosion activity and free Cl^-/ bound Cl^- for chloride binding capacity.
- Investigate the rate and depth of carbonation and also the carbonation and drying shrinkage of AACM and control OPC concrete.

- Investigate the pH of the carbonated and non carbornated zones in AACM concrete and determine the suitability of the phenolpthalien test for monitoring carbonation depth of AACMs.
- Investigate the corrosion behaviour of reinforcing steel embedded in AACM and control OPC concrete when exposed to long-term bulk chloride diffusion and an accelerated corrosion environment. Determine the capillary absorption effect of AACM and control OPC concrete by using the sorptivity technique and relate it to durability.

1.4 THESIS LAYOUT

The thesis reports the durability properties of AACM materials under the influence of two main corrosion initiators; chloride and carbon dioxide. The microstructure of AACM concrete and capillary absorption tendencies which directly relate to the transportation mechanism of the corrosion initiators within the matrix of the concrete has been investigated. The thesis is divided into eight chapters which includes this introductory chapter 1.

Chapter 2 presents a detailed critical literature review of AACM binders containing high and low calcium precursors, various alkaline activators normally used as a liquid content in the production of AACM concrete. The units of measurements and nomenclature of concrete materials reported by various researchers is also reviewed.

Chapter 3 presents the details of concrete and mortar mixes. Specimen preparation and test methods used during each investigation are presented seperately in each chapter. The microstructure of AACM mortar mixes M_2 to M_5 and the control OPC mortar mix M_6 are investigated. The AACM mortar mixes M_2 to M_5 incorporated varying levels of activator dilution of 2.15%, 4.25%, 8.12% and 12.0% respectively. The corresponding AACM and OPC concrete mixes S_2 to S_6 with the same levels of activator dilution were also used for other investigations reported in subsequent chapters. The microstructure of the AACM and OPC mortar was investigated by using the mercury intrusion porosimetry (MIP) technique. The experimental results were analysed to determine the pore size and distribution parameters such as the gel and capillary pore volume, unimodal and bimodal pore distribution, intrudable porosity, critical and threshold pore diameters. The strength-porosity relationship of AACM mortar is also presented. The results show higher capillary pore volume in AACM concrete than the control OPC concrete and the reverse for gel pore volume. The total porosity (i.e summation of capillary and gel pore volumes) is lesser in AACM concrete than OPC

concrete. A bimodal pore size distribution is observed in AACM concrete while OPC concrete has a unimodal pore size distribution.

Chapter 4 investigates the physically and chemically bound chlorides in AACM and OPC concrete mixes S_2 to S_6. A total of 50 slabs (250 mm X 250 mm X 75 mm) of AACM and OPC concrete specimens (10 slabs per each mix) were cast and cured for 28 days before immersing in 5% NaCl solution. The physically and chemically bound chloride tests were performed on 2 slabs per each concrete mix at 55, 90, 120, 180 and 270 days of exposure in the 5% NaCl solution. Chemical analysis were performed on the concrete powder collected at 8, 15, 20, 25, 35, 50 and 65 mm depths from the concrete surface. The powder samples were dissolved in water and acid solvents to extract the water and acid soluble chloride concentrations. Regression analysis were performed on the water and acid soluble chloride concentrations by applying Fick's second law of diffusion to determine the chloride diffusion profiles, rate of chloride diffusion and the surface chloride concentrations. The relationship between the porosity which was determined in chapter 3 and the chloride diffusion parameters is also determined.

Chapter 5 investigates the free chloride and pH of the pore solution that was obtained from the cores of AACM and OPC concrete mixes S_2 to S_6. The coring of the slabs of AACM and OPC concrete mixes S_2 to S_6 was performed at 180, 270 and 540 days exposure to 5% NaCl solution. An average of four cores (50 mm diameter X 60 mm depth) were drilled per mix at each test age making a total of 20 cores per each test age. Each concrete core was sliced into 20 mm thick discs (i.e. 0 - 20 mm is labelled 1, 20 - 40 mm is labelled 2 and 40 - 60 mm is labelled 3). The discs with the common number from the 4 cores for each mix (e.g. label 1 disc for mix S_2) were combined and placed inside a pore fluid extractor device. The pore fluid expression device with the concrete discs inside it was placed within the platens of a compression testing machine. The compression machine exerted pressure on the pore fluid extractor device which released the pore solution from the concrete matrix. The free chloride concentration and pH of the pore solution from AACM and control OPC concrete were determined. Regression analysis was performed on the free chloride concentration profiles by applying Fick's second law of diffusion to determine the chloride diffusion parameters. The chloride binding capacity between the free and bound chlorides (from chapter 4) was investigated. The free chloride/hydroxyl ion ratios for AACM and OPC concrete mixes S_2 to S_6 were also determined and related to the corrosion investigation reported in chapter 7.

Chapter 6 investigates the carbonation of AACM and control OPC concrete mixes S_2 to S_6 by the accelerated carbonation method. A total of 30 prisms (300 mm X 75 mm X 75 mm) per mix were produced to determine the rate of carbonation (10 prisms), carbonation shrinkage (10 prisms) and drying shrinkage (10 prisms) while 15 cylindrical specimens (50 mm diameter X 60 mm depth) were produced to determine the pH value at the carbonated and non carbonated zones in AACM and OPC concrete mixes S_2 to S_6. All the AACM and OPC concrete mixes S_2 to S_6 were cured in water (20 ± 2^0C) for 27 days after demoulding (1 day). The specimens were placed inside an accelerated carbonation chamber which was programmed to provide 5% CO_2 concentration at 20 ± 2^0C and 50% - 70% R.H for 360 days. The drying shrinkage control specimens were not placed in the carbonation chamber; instead they were cured in the laboratory air (20 ± 2^0C and 65% R.H) after the 27 days water curing. The carbonation depth was determined by the phenolpthalein test method. The rate of carbonation was, however, determined by applying regression analysis on the experimental data of the carbonation depth. The reading taken for both carbonation and drying shrinkage at regular intervals throughout the curing periods were analysed. The pH at the carbonated and uncarbonated zones was determined from the cylindrical specimens. The results show that the effect of carbonation is greater in AACM concrete than OPC concrete, however, the pH values suggest otherwise and, therefore, the phenolpthalein indicator method might not be appropriate for determing the depth of carbonation in AACM concrete.

Chapter 7 investigates the corrosion behaviour of AACM and OPC concrete mixes S_2 to S_6. A total of 10 reinforced concrete slabs (250 mm X 250 mm X 75 mm), each having 3 bars of 8 mm diameter steel reinforcement embedded in it, were produced for AACM and OPC concrete mixes S_2 to S_6 (i.e. 2 slabs per mix). Each concrete mix S_2 to S_6 was grouped into two seperate batches "a" or "b". Each batch was exposed to bulk chloride diffusion, alternative climate chamber, laboratory air and wet/dry cycles. The exposure period was 860 days. The steel potential difference and corrosion current densities were monitored at regular intervals. At 860 days age, cores were drilled on each specimen to investigate free chloride concentration and pH of the pore solution near the steel, similar to chapter 5. The results presented include the corrosion potential, corrosion current density and the free chloride/hydroxyl ratio. AACM and OPC concrete show no active corrosion activity even at the higher threshold value of 0.61 for free chloride/hydroxyl ratio.

Chapter 8 provides the overall conclusions from the study and gives recommendations for further research.

CHAPTER 2
GENERAL LITERATURE REVIEW

2.0 INTRODUCTION

This chapter presents the review of materials used in the prodution of AACM concrete and mortars. The unit of measurements and nomenclature used for the materials is also reviewed. However, the details of concrete and mortar mixes, specimen preparation and test methods are presented seperately in each chapter.

The production of Portland cement worldwide was estimated to be 2.9 billion tonnes in 2008, 3.6 billion tonnes in 2012, 4 billion tonne in 2013 and 4.3 billion tonnes in 2014 [8]; this makes Portland cement to be the second highest volume of commodity produced beside water [1]. Environmental challenges associated with such enormous production are quite significant. Its carbon footprint is topmost amongst these challenges with 5 to 8% of the total CO_2 emitted to the atmosphere being a result of CO_2 generated during the production of Portland cement [9].

The use of ordinary Portland cement as binder provides great challenges to the environment and makes its use unsustainable in the future. The *European commission* [10], proposed a technological roadmap for the possible reduction of CO_2 emissions in cement industry by 18% by 2050. To achieve this, the use of industrial alkalis with industrial pozzolanic materials offers a promising alternative to cement and is an important area of current research. New innovations in low impact construction materials require a reduction in the use of Portland cement with alternative binders, preferably utilising industrial waste materials and aggregates made from recycled waste.

Alkali activated concrete which is classified under geopolymer concrete is a relatively new technology with little understanding of its durability characteristics over a long period of time [3][11]. One reason for limited field application of geopolymer concrete is because of limited knowledge of its structural behaviour [12] when subjected to prolonged exposure to corrosion initiators such as chloride ion and carbonation. The importance of structural stability cannot be over emphasized since the primary aim of design is for a structure to perform optimally during its design lifespan [13]. Environmental factors contributing to structural defects or collapse could be attributed to the rate at which reinforcement steel corrodes under the prolonged influence of chloride; carbonation and the matrix deteriorates with sulphate attack. Millions of pounds (an estimate of £550m) [14] per year have been lost in repairs and structural

failures due to this corrosion mechanism in the UK [15]. The structural integrity of alkali activated concrete under these elements will be critically examined in this project.

2.1 ALKALI ACTIVATED CEMENTITIUOS MATERIALS (AACMs)

The production of an alkali activated cementitious material (AACM) comprises of an alumina-silica containing solid precursor such as fly ash, ground granulated blast furnace slag, silica fume and natural pozzolans and a suitable alkali activator (alkali cations of hydroxides, silicates, carbonates and sulphates) [3]. The first patent on AACM was by *Kuhl* [16] in 1908 which comprises of slag activated by alkalis of sulphate and carbonates. The AACM material was further developed by *Purdon* in 1940 and the results were published in scientific journals covering 30 different types of blast furnace slags activated by sodium hydroxide and calcium hydroxide [3]. The results showed that the compressive strength and heat evolution achieved were comparable to OPC concrete and a lower solubility of binder phase [17][18]. In the 1980s, cement shortage was experienced in former Soviet Union and China which led to the use of AACM as an alternative binder to OPC. Much work was carried out by *Glukhovsky* in the former Soviet Union [3]. Similarly, many patents on AACM are accredited to *Davidovits* in France, which were formed by the chemical reaction between alumino-silicate oxides and alkali polysilicates to yield polymeric Si-O-Al bonds [19] similar in composition to natural zeolites [20][21].

Unlike ordinary Portland cement, the setting mechanism of AACM is by geopolymerization which involves the dissolution of silica and alumina in a pozzolanic compound of geopolymer precursor species resulting in the formation of hydrated calcium silicates and aluminates (C-A-S-H) [22][23] as well as regeneration of caustic alkali solution [24]. The performance level of different solid precursors and alkaline activators reported in literature is presented in Table 2.1 [3]. The solid material formed from the AACM is comparable in mechanical and durability properties to hardened Portland cement [3].

Table 2. 1*:* Performance level of combining different solid precursors with alkaline activators [3]

Binder	Alkaline activators				
	MOH	$M_2O.rSiO_2$	M_2CO_3	M_2SO_4	Other
Blast furnace slag	Acceptable	Desirable	Good	Acceptable	-
Fly ash	Desirable	Desirable	Poor (acceptable with cement/clinker addition)	Acceptable (with cement/clinker addition)	Acceptable (with $NaAlO_2$)
Calcined clay	Acceptable	Desirable	Poor	Acceptable (with cement/clinker addition)	-
Natural pozzolans and volcanic ashes	Acceptable/Desirable	Desirable	-	-	-
Framework aluminosilicates	Acceptable	Acceptable	Acceptable (with cement/clinker addition)	Acceptable (with cement/clinker addition)	
Synthetic glassy precursors	Acceptable/Desirable (depending on glass composition)	Desirable	-	-	-
Steel slag	-	Desirable	-	-	-
Phosphorus slag	-	Desirable	-	-	-
Ferronickel slag	-	Desirable	-	-	-
Copper slag	-	Acceptable (grinding of slag is problematic)	-	-	-
Red mud	-	Acceptable (better with slag addition)	-	-	-

M is the cation of the alkali metal and ***r*** is the modulus.

Desirable: signifies that high compressive strength and durability of concrete can be achieved by using the activator. ***Good***: depicts slightly lower compressive strength than the optimal activator but good results can still be achievable. ***Acceptable***: depicts drawbacks in strength, durability and workability. ***Poor***: strength development is insufficient for most field application.

2.2 AACM BINDERS

Alkali activated binders are broadly classified as calcium rich precursors and low calcium precursors [3]. Fly ash class C and F are a good example representing high and low calcium precursors respectively. Other examples are ground granulated blast furnace slag (GGBS), silica fume, rice husk ash and metakaolin. These cementitious materials are normally incorporated into OPC concrete in varying percentages to achieve desirable properties such as high strength, improve workability, reduced bleeding and permeability amongst other properties. *Neville* [25] pointed out that the reason for these materials being used as supplementary or partial replacement to Portland cement was because cement was considered the best binder until fairly recently when AACM binders were used independently to produce concrete without the inclusion of OPC cement. Preliminary results from literature show that concrete produced from AACM binders possesses comparable mechanical strength and durability properties to OPC concrete [3][6][26]. The durability properties of concrete produced from AACM binder is investigated in this research project in parallel with control concrete produced from Portland cement.

2.2.1 High calcium AACM Binders

2.2.1.1 Ground granulated blast furnace slag (GGBS)

GGBS is a latent hydraulic binder which sets and hardens slowly when in contact with water or alkali activator unlike silica fume and class F fly ash which only sets and hardens when in contact with an alkali activator such as hydrating OPC. This is because of the high calcium content (about 45%) in ggbs [22]. The reaction process of AACMs based on ggbs involves dissolution of the glassy precursor resulting in the growth of initial solid phase, mechanical binding occurs in the phase formed, this is followed by the dynamic chemical equilibrium due to the ongoing reaction and lastly, the diffusion of reactive species from the curing medium [3]. The structure and composition of ggbs based system is strongly dependent on the type of activator used. Sodium hydroxide activator was suggested to produce a more structured geopolymerisation product with higher Ca/Si ratio than sodium silicate activator

[27][28]. The reason suggested was the availablity of silicate species in the pore solution of silicate activator based system [3] which produces lower Ca/Si ratio.

The main geopolymerisation products formed by ggbs based system are the aluminium substituted C-A-S-H type and the disordered tobermorit type C-S-H type structures [29][30]. This is followed by a secondary reaction which produces AFm type phase when sodium hydroxide activator is used [28][31], Si containing AFm phase when sodium silicate activator is used [32], hydrotalcite when ggbs containing high MgO content is used [33] and zeolite such as gismondine and garronite when ggbs containing high Al_2O_3 content is used [34]. The chemistry controlling the kinetics and equilibria of the secondary phase is not fully understood [3].

The performance of ggbs based systems is based on the type and concentration of activator used [3]. These activators include alkali hydroxides (NaOH, $Ca(OH)_2$, KOH), alkali silicate salts ($Na_2O.rSiO_2$, $K_2O.rSiO_2$), strong acid salts (Na_2SO_4, $CaSO_4.2H_2O$) and weak salts (Na_2CO_3, K_2CO_3, Na_2S, K_2S) [35]. In addition, all caustic alkalis whose anions react with Ca^{2+} component from ggbs to produce lower solubility than $Ca(OH)_2$ can act as activator [36]. The calcium rich content in the ggbs based system is produced during the initial reaction of anionic component of the activator with Ca^{2+} dissolved from ggbs binder [3]. The sodium hydroxide and sodium silicate are the commonly used activators for ggbs based systems because they produce high pore solution pH in its matrix. The pore solution pH of ggbs based system is slightly higher when activated with sodium hydroxide than sodium silicate but silicate activated system develops higher mechanical strength than hydroxide activated systems [37][38]. This is because of the additional supply of silicate species in silicate activator that reacts with Ca^{2+} dissolved from ggbs binder to form dense C-A-S-H products [27].

The dense microstructure of ggbs mortar made with OPC reduces water permeability up to a 100 times less than OPC mortar, particularly in resisting the penetration of chloride [39]. Other advantage observed in ggbs based OPC concrete systems is the high resistance to sulphate attack, for example *Hooton and Emery* [40] reported that supplementary cementitious materials containing 50% ggbs by mass with Portland cement (Type 1) produce high resistance to sulphate attack similar to sulphate resisting (Type 5) cement. The low permeability of ggbs based systems provides effective control over alkali-silica reaction because of the reduced mobility of alkali in the concrete matrix [25]. In the case of carbonation, no pore blocking formation of calcium carbonate was observed in ggbs based concrete because of the lower amount of

calcium hydroxide in its pore solution [25]. However, the tight pore structure reduces the depth of carbonation in ggbs based concrete [39].

2.2.1.2 ASTM class C fly ash

Class C fly ashes are artificial pozzolans produced from the combustion of younger lignite or subbituminous coal in large power plants [25]. The lime content in class C fly ash ranges from 15% to 30%. The high lime content in class C fly ash makes it a self-cementing binder similar to ggbs which sets and hardens when it reacts with water without necessarily using an alkali activator [41]. The lime will react with the silica and alumina content of the ash in the presence of water to produce geopolymerisation products. When incorporated as a supplementary cementitious material in OPC concrete, the additional lime content from the hydration products in OPC cement will dissolve the silica and alumina compound of class C fly ash rapidly [25]. This reaction of class C fly ash accounts for the rapid strength development of class C fly ash based systems.

The reaction mechanism in converting fly ash to a monolithic alkali activated gel is complex because of the variability of the material [3]. Variation in the properties of fly ash often occurs from one power station to the other. The non-uniformity in the coal used can also result in fly ash with varying properties from the same power station [25]. This is aided by the inhomogeneous mix of aluminosilicate and silica glasses and a small amount of crystalline materials such as quartz, hematite, magnetite and mullite present in fly ash [42]. *Ferna´ndez and Palomo* [43] suggested an optimum binding properties for fly ash content as less than 5% unburnt materials, less than 10% of Fe_2O_3, low CaO content, reactive silica should be between 40% -50%, particle size lesser than 45µm should be between 80% - 90% and the presence of high vitreous phase.

The beneficial influence of fly ash in OPC concrete is observed in the reduction of water content and increased workability [25]. A water reduction of 5% to 15% using fly ash based system compared to OPC based system is achieved for the same workability. These values increase as the water/cement ratio increases [44]. Other beneficial influence of fly ash on OPC concrete include cohesiveness which is an essential property for pumping, slipforming and finishing operation [25]. The fineness of the particle sizes of fly ash has been identified as the primary factor responsible for the desirable properties exhibited by fresh fly ash concrete [25][3].

2.2.2 Low calcium AACM Binders

2.2.2.1 ASTM class F fly ash

Class F fly ashes are artificial pozzolans produced from the combustion of older anthracite and bituminous coal in large power plants [25]. The lime content is less than 10% which is lower than the lime content in class C fly ash [26]. Thus, an alkali medium (e.g. an alkali activator, free lime from hydrating OPC cement) is required for class F fly ash to set and harden unlike class C fly ash which can set and harden when mixed with water only.

The rate of pozzolanic reaction of class F fly ash is slow when incorporated as supplementary cementitious material (in OPC) compared with when activated by an alkali solution. The pozzolanic reaction can be delayed when used as supplementary cementitious material for up to one week or more after mixing [25]. *Fraay et al.* [25] observed as much as 50% unreacted fly ash in OPC concrete after one year of mixing. The reason is the high alkalinity required to activate class F fly ash [45]. The pH of the pore solution should be at least 13.2 which requires a certain degree of cement hydration coupled with precipitation of the cement hydrate on the surface of class F fly ash, thus acting as a nuclei [25]. This distinctive behaviour is beneficial in the reduced evolution of heat [25].

Class F fly ash is deficient in calcium content (< 10%) [26] which accounts for the slow pozzolanic reaction but has sufficient aluminate content (< 35%) which is critical to the hardening process [26]. The aluminate content is believed to chemically trigger an irreversible hardening [46]. The author [46] suggested that dissolution of Al_2O_3 by an alkali activator controls the stoichiometry of the class F fly ash based system. Rapid strength development of about 80% is achieved within 24 hrs for high alumina cement after the initial setting [25]. Class F fly ash displays slow setting due to the high alkalinity demand but a rapid hardening process after the initial setting begins. This phase reaction is dependent on the temperature, pH of pore solution, Si/Al ratio and alkali concentration [46].

2.2.2.2 Silica Fume (SF)

Silica fume SF is also an artificial pozzolanic material which is produced from the oxidation of silicon dioxide gas when silicon metal or ferosilicon alloy from high purity quartz and coal is heated in a submerged-arc electric furnace [25][47]. The oxidized silicon dioxide gas condenses to form an extremely fine spherical particle in an amorphous phase [25]. The high reactivity of silica fume is as a result of its amorphous

form which contains high content of reactive silica (≥ 85%) [47]. The fast rate of pozzolanic reaction between the amorphous silica and $Ca(OH)_2$ from cement hydration product or alkali activator solution results in early strength development. Silica fume dissolves in $Ca(OH)_2$ or alkali activator within minutes [48]. In addition, nucleation sites are provided by the extreme fineness of SF particles for $Ca(OH)_2$ [25] or alkali activator.

The beneficial effects of using silica fume in OPC concrete include improved cohesion in the mix and reduced bleeding which enhance pumping, slipforming and finishing operation [25]. Other important property is the particle packing effect between cement grains and inter-transitional zones (ITZ) between the cement grains and aggregates. The particle packing is achieved due to the extreme fineness of the particle size which is 100 times smaller than the OPC grain [25]. The pore spaces between the inter-transitional zones (ITZ) provide the weakest link in concrete, thus the particle packing effect of silica fume close to the aggregate surface will improve the strength properties of concrete considerably [49]. The particle packing effect also improves the microstructure of silica fume concrete by possessing fewer pores for the ingress of deleterious substances like chloride, carbon dioxide and sulphate [50].

2.2.2.3 Rice husk ash (RHA)

Rice husk ash RHA is a natural pozzolan which is produced by slow incineration of rice husk at a temperature of 500^0C to 700^0C in an industrial furnace for few minutes until the carbon content is below 5% [51][25]. A high amorphous form of RHA is achieved by not exceeding 800^0C during the burning of the rice husk. Rice husk contains cellulose ($C_5H_{10}O_5$), lignin ($C_7H_{10}O_3$), hemicellulose, SiO_2 and holocellulose [52]. Similar to silica fume, RHA has high silica content between 87% to 97% depending on the source of rice husk and the efficiency of the combustion process [52][51]. It has a porous structure with specific surface as high as 50,000 m^2/Kg when measured by nitrogen absorption [25].

The beneficial influence of RHA in OPC concrete includes early strength development at 1 to 3 days [53]. There is reduction in the heat of hydration which helps in preventing drying shrinkage, thus facilitating the durability of the concrete [25]. The permeability of concrete containing RHA is reduced by particle packing effect similar to silica fume [53]. This concrete property will have positive impact on the resistance to deleterious substances.

2.2.2.4 Metakaolin

Metakaolin MK is a natural pozzolanic material produced from dehydroxylated product of calcinated kaolin clay by applying temperature of 500^0C to 800^0C [3][26]. Kaolin is a clay mineral containing layered tetrahedral silicon atom that is connected to octahedral aluminium atom via oxygen [26]. The calcination temperature is just high enough to remove the bound water from the clay structure but not so high as to lead to the formation of mullite [54][55]. The calcination temperature has been identified to be the dominant factor in determining the reactivity of MK with alkaline solution [56][57]. *Puertas et al* [58] suggested that the application of temperature above 550^0C will alter the hydroxyl ions that are strongly bonded to the aluminium framework leading to an ordered system with increased pozzolanic reactivity with alkali solution.

MK has been identified as a key component in cementitious blends particularly with fly ash and various slags because it provides supplementary alumina species to the reaction process [59][60][61]. The beneficial influence of incorporating MK in concrete is the increased thermal resistance and control over alkali-aggregate reaction.

2.3 ALKALINE ACTIVATORS

Alkaline activators are made up of alkali metals of hydroxides (NaOH, $Ca(OH)_2$, KOH), silicate salts ($Na_2O.rSiO_2$, $K_2O.rSiO_2$), strong acid salts (Na_2SO_4, $CaSO_4.2H_2O$) and weak salts (Na_2CO_3, K_2CO_3, Na_2S, K_2S) [35]. These activators when mixed with AACM binders prompt the precipitation and crystallization of the amorphous aluminosilicate species present in the mix [26] to form a hardened concrete. This process involves the dissolution of the solid AACM particles by releasing monomeric alumina and silica into the solution [62]. The dissolved monomers of alumina and silica in concentrated solutions lead to the formation of gel as the oligomers in the aqueous solution [62]. The gel formed grows into a well-crystallized structure [26]. The reaction process between the alkaline activator and AACM binders is termed geopolymerization.

A list of alkaline activators together with their use is shown in Table 2.1.

2.3.1 Sodium and Potassium Silicates *($Na_2O.rSiO_2$, $K_2O.rSiO_2$)*

Sodium and potassium silicates is a semi viscous liquid which is classified under caustic alkalis [63]. It is produced by blending sand (SiO_2) with sodium or potassium carbonate (Na_2CO_3, K_2CO_3) at a temperature of 1100 - 1200^0C [64]. The resulting product (glass) is dissolved with high pressured steam to form a clear, viscous liquid also known as waterglass. The waterglass can be spray dried to form quick dissolving, hydrous powder [64]. Sodium and potassium silicates are considered the best material to

activate pozzolans because of the effectiveness of both the cation and anion of the activator [29]. The cation (Na_2O, K_2O) activates the siliceous materials present in the pozzolans while the anion (SiO_2) facilitates the formation of calcium silicate hydrates.

The modulus ratio (SiO_2/Na_2O) is an important property that affects the geopolymerisation of AACM binder when sodium and potassium silicates are used as an activator. A range of 1.5 to 3.2 SiO_2/ Na_2O ratio is commercially available with 3.2 suggested to be best suited to enhance geopolymerization [65]. On the other hand, the degree of solubility of the silicate present in the anion is suggested to have positive influence on the compressive strength of AACM concrete and mortars [66]. This is because the activating solutions containing little or no soluble silicates will saturate in the concrete pore solution while the soluble silicate will promote inter-particle bonding within the AACM binder as well as the interfacial bonding between the aggregates and AACM paste [66].

2.3.2 Sodium, Calcium and Potassium Hydroxides *(NaOH, $Ca(OH)_2$, KOH)*

Sodium, calcium and potassium hydroxides are commonly used alkaline activator in the geopolymerization process of AACM concrete. It is used to buffer the pH of concrete pore solution due to its high pH. Unlike sodium and potassium silicates that can be used independently to produce desirable properties in AACM concrete, sodium, calcium and potassium hydroxides cannot be used independently. A mixture of hydroxides and silicates are often used as alkaline activator rather than using hydroxides independently [67][68]. This is because of the undesirable morphology and non-uniformity of the final product produced due to the excessive hydroxyl ion OH^- present in the concrete pore solution when hydroxide is used independently [24].

Sodium, calcium and potassium hydroxide activated AACM concrete displays lower compressive strength than the sodium and potassium silicate activated concrete of similar concentration particularly in high calcium content AACM binder. This is because calcium solubility decreases with high pH whereas the silica and alumina solubility increases [3]. Since the calcium content is high in GGBS and class C fly ash, the Ca^+ cation dissolved in hydroxide solution is lesser than silicate solution. Similar observations were reported for GGBS concrete showing higher compressive strength when activated by silicate solution than when activated by hydroxide solution [37][38][69].

2.3.3 Sodium and Pottasium Carbonate *(Na_2CO_3, K_2CO_3)*

Sodium and pottasium carbonate is classified among the weak salts. It has a low pH lesser than 12 which is lower than silicates and hydroxides activators. The advantage associated with sodium and pottasium carbonate activator is that it is cost effective, environmental and user friendly [70][71]. On the other hand, the prolonged setting and delayed compressive strength development are some of the practical challenges associated with using sodium and pottasium carbonate independently [72]. The delayed hardening process is because of the reduction in the alkalinity of the solution that is required to dissolve the reactive silica and alumina present in AACM binders [73]. The alkalinity of sodium and pottasium carbonate favours the dissolution of Ca^{+2} from the AACM binder which reacts with the CO_3^{2-} from the anionic component of the activator to form carbonate salts such as calcite and gaylussite whereas the Na^{2+} from the cation component of the activator reacts with the hydroxyl ions (OH^-) in the solution[71][72]. A later stage reaction of sodium carbonate activated AACM system is similar to sodium and pottasium hydroxide activated system once the CO_3^{2-} ions have been exhausted.

A mixture of carbonates and silicates is often used as alkaline activator similar to the combination of hydroxides and silicates activator. Partial substitution of carbonates by silicates reduces the carbonate ions in the pore solution which increases the alkalinity of the system compared with using carbonates independently to activate AACM binders [73].

2.4 METHODS OF MEASUREMENT

Literature often presents different measuring units for analysing the same result which could sometimes be confusing when used in the wrong context. A number of standard measuring units were adopted during the course of analysing the test results and in the discussions in this project report. This section addresses the variation in these measuring units for the same result.

2.4.1 Activator Concentration

Alkaline activator concentration plays a vital role in the geopolymerisation process of AACM concrete and consequently influences its durability and mechanical properties. Regardless of the activator type, an increased concentration facilitates faster reaction rate resulting in desirable AACM concrete properties [26]. However, optimum limits have been observed for certain activator types such as 10M for KOH solution

[24]. Exceeding these limits will reduce the effect on the desired concrete properties. A number of measuring units have been adopted in literature to quantify the activator concentrations which are discussed in the following subsections.

2.4.1.1 Percentage dilution

The activator concentration is expressed as a percentage dilution ratio when certain amount of distilled water is added to the concentrated alkaline activator. The alkaline activator when used without diluting with water may result in inferior properties of AACM concrete. For example, *Khale and Chaudhary* [24] observed a decrease in strength for AACM concrete when high concentration of potassium hydroxide KOH solution was used as activator. It was suggested that the excess K^+ ion in the framework may have contributed to the decrease in its strength. Similarly, *Smaoui et al.* [80] increased the alkali content of the mixing liquid used to produce AACM concrete by decreasing the amount of water added to sodium hydroxide NaOH activator. The alkali content was increased from 0.6% to 1.25% of Na_2O of cement mass. The resultant effect was a decrease in its strength, freeze-thaw resistance, increased shrinkage and a porous microstructure was observed [80].

On the other hand, when too much water is added to the concentrated alkaline activator provided by suppliers, it will have a negative effect on the mechanical and durability properties. For example, over-dilution of the activator will result in an increase in the net drying shrinkage, setting time and decrease in the reaction kinetics and strength [81]. Therefore, an optimum mix proportion between the alkali activator and water should be produced in order to obtain an activator concentration that can produce AACM concrete with desirable properties. The percentage dilution ratio between 2.15% to 12% will be adopted in this research project to produce AACM concrete mixes. This dilution can also be represented in terms of molarity which is discussed in the next section. The range of dilution (2.15% - 12%) was within the upper and lower limits of molarity beyond which AACM performance drops.

2.4.1.2 Molarity or Molar ratio

Molarity or molar ratio can be defined as the ratio of moles of solute by volume of the solution. In the case of quick dissolving hydrous powder of sodium silicate, the molarity of the activator is obtained by dissolving the powder in water to provide a solution of the required molarity. Similarly, sodium hydroxide activator, which is produced as a solid by electrolysis of NaCl solution, is dissolved in water to produce the required molarity or molar ratio [82].

The pH of AACM concrete pore solution is influenced by the degree of molarity present in the activator solution. *Williamson and Juenger* [83] suggested that an increase in the molarity of NaOH activating solution from 6 M to 8 M produced 11% increase in the pore solution alkalis while increasing it further to 10 M produced 27.3% increase in pore solution alkalis. The authors [83] suggested that the effect is greatest at the point of optimum concentration of activator needed to liberate silicate and aluminate species from the AACM binder. Presumably, additional alkalis beyond what are required for complete polymerization of AACM concrete end up in its pore solution [84] where they are charge-balanced by hydroxyl ions [83]. The molarity of any solution is given by equation 2.1.

$$Molarity = \frac{Mole\ of\ solute}{Litres\ of\ Solution} \qquad 2.1$$

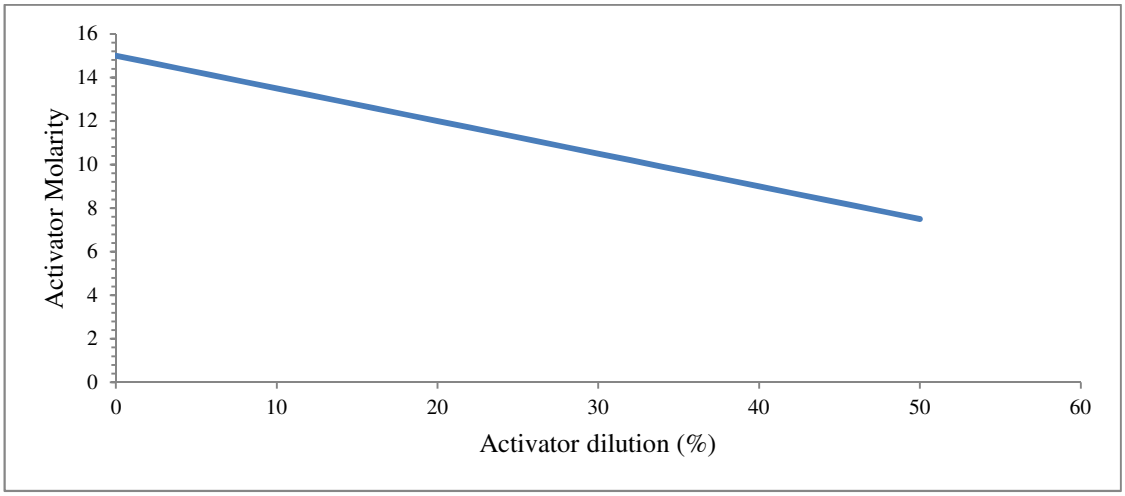

Figure 2. 1*:* Example of relation between activator dilution and molarity for a 15 M activator

2.4.2 Liquid to Cementitious Ratios

Various nomenclature in publications have been used to describe cementitious materials that play the role of binding together other aggregates present in a concrete mix [25]. Some of the generally accepted nomenclatures are as follows;

1. Portland cement contains 95% or more Portland cement clinker by mass of the total constituents.
2. Pozzolanic materials are substances of siliceous or silico-aluminous composition or a combination which reacts with water or alkali solution to produce concrete.

Variations in nomenclature have been used to describe the combination of Portland cement clinker lesser than 95% by mass and pozzolanic materials more than 5% by mass. ENV 197 – 1 [85] uses the term CEM cement to describe the component

containing Portland cement clinker lesser than 95% of the total mass. This nomenclature, however, is not sufficiently explicit for high alumina cements [25]. ASTM C 1157 - 94a uses the term hydraulic cement to describe a combination of inorganic constituents greater than 5% of total mass when present in cement which aid the strength development. Inorganic constituents in this case refer to the natural and industrially produced pozzolanic materials. *Neville* [25] suggested blended cement to describe the inter-grinding of Portland cement clinker and inorganic materials (pozzolanic materials). The author, therefore, proposed all these materials to be referred to as cementitious materials for simplicity and clarity [25]. The term cementitious materials are equally adopted in this thesis to describe the alkali activated cementitious materials (AACM) which were investigated.

Similarly, the term liquid is used to describe the mixtures of water and alkali metals of hydroxides (NaOH, $Ca(OH)_2$, KOH), silicate salts ($Na_2O.rSiO_2$, $K_2O.rSiO_2$), strong acid salts (Na_2SO_4, $CaSO_4.2H_2O$) and weak salts (Na_2CO_3, K_2CO_3, Na_2S, K_2S) to form an activator solution which is used to produce AACM concrete. However, for OPC concrete, the activation of cement was done with only water.

The strength of concrete at a given age, cured under a certain temperature and humidity is primarily dependent on its liquid/cementitious ratio and the degree of compaction [25]. The cementitious material in a mix remains inert until the liquid is added to the mix, which facilitates a chemical reaction of hydration in OPC concrete (with water) and geopolymerization in AACM concrete (with alkali activator). An inverse relationship was established between strength and water/cement ratio in a fully compacted OPC concrete by Duff Abrams [86] as shown in equation 2.2.

$$f_c = k_1 / k_2^{w/c} \qquad 2.2$$

Where w/c represents water/cement ratio, K_1 and K_1 are empirical constants and f_c is the strength.

Rene Feret proposed a similar general rule relating strength to volume of water and cement [25] as shown in equation 2.3.

$$f_c = k \left(\frac{c}{c+w+a}\right)^2 \qquad 2.3$$

Where f_c is the strength, c, w and a are the absolute volumetric proportions of cement, water and air and k is constant.

The inverse relationship between strength and water/cement ratio ceases to be valid at very low water/cement ratios when full compaction can not be achieved [25].

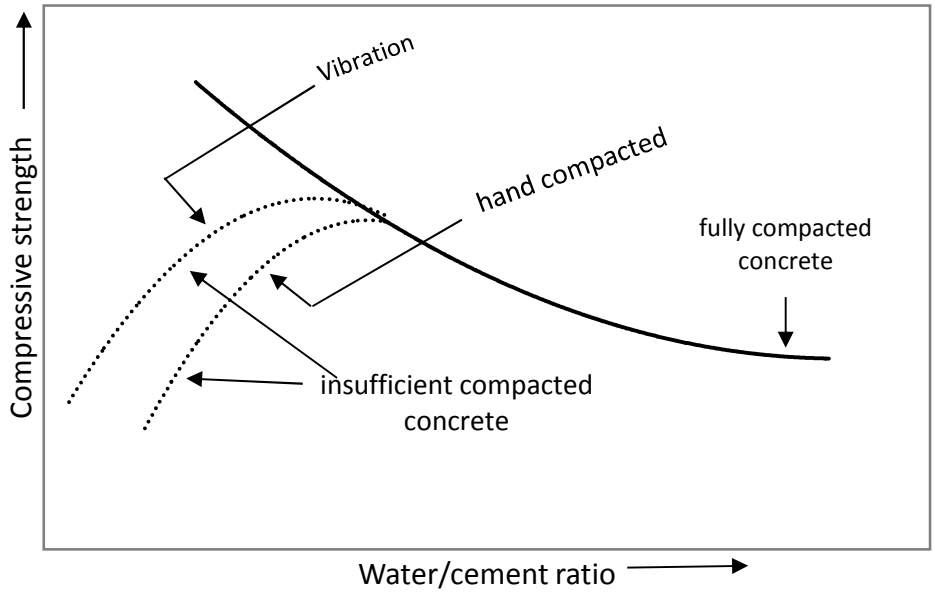

Figure 2. 2: The relationship between strength and water/cement ratio of OPC concrete [25]

2.4.2.1 Liquid/binder ratio

Liquid/binder ratio is the nomenclature used to describe the proportion by weight of liquid to cementitious material used to produce AACM concrete, mortar or paste. *Jaarsveld and Deventer* [87] acknowledge the importance of low liquid content in AACMs leading to the formation of amorphous zeolites with low porosity. Apart from temperature, the ratio of H_2O/Na_2O (liquid content) > Na_2O/SiO_2 (activator concentration) > SiO_2/Al_2O_3 (alkali metal) was proposed for zeolite formation in alkali-activated mixtures. Zeolite formation is the structural framework which has the controlling capacity for the polycondensation and crystal growth in AACMs.

In order to maintain a constant molar ratio of H_2O to Na_2O in a fly ash based geopolymer concrete, both the activator concentration (Na_2O content) and water content was increased but no significant effect was observed on the compressive strength [46]. In other words, the higher molar ratio of Na_2O/SiO_2 (activator concentration) had an insignificant impact on the compressive strength at higher liquid content. The durability properties of AACM material were enhanced by the presence of lower liquid content rather than a higher activator concentration. However, much attention has been given to Na_2O/SiO_2 in literature [26], [88] while limited data exist on the impact of liquid/binder ratio on porosity parameters of AACM materials. This aspect has been addressed in this project.

2.4.2.2 Activator/pozzolan ratio

Some literature uses the activator/pozzolan nomeclature to express the ratio between the effective liquid content to cementitious material in AACM concrete. The reason for this choice of nomenclature was to represent the effectiveness of the activator type and concentration in dissolving the silico-aluminous species present in the pozzolanic materials [89][88]. For example *Fernández-Jiménez et al*, [88] recommended 4% content of NaOH by weight in relation to slag for higher mechanical strength. Similarly, *Krizan and Zivanovic* [89] achieved the highest compressive strength by using 5 M of water glass activator and a liquid/fly ash ratio of 0.6.

2.4.3 Chloride Diffusion

Chlorides are present in concrete as free, acid soluble and water soluble [90]. Chloride concentrations that are physically absorbed by the walls of the binder gel are referred to as water-soluble chlorides. Acid-soluble chlorides are chemically bound to the concrete matrix which forms by the hydration/geopolymerisation process. The free chloride on the other hand is present in the pore solution of the concrete which is considered to facilitate chloride induced corrosion [91]. The wall of the binder gel which stores the water soluble chloride can either release or absorb chloride ions from the free chloride in the concrete pore solution. However, the acid soluble chloride forms part of the hydration/geopolymerisation product and cannot influence corrosion.

The results of acid and water soluble chlorides in concrete can be expressed as percentage by weight of binder or percentage by weight of concrete. The unit of measurement for free chloride concentrations is mol/L because it is obtained by expression of concrete pore fluid. Some authors have expressed it as a percentage by weight of binder because concrete powder was dissolved in water to measure the free chloride concentration [92][93]. However, these values do not strictly represent free chloride concentration and are more representative of water soluble chloride.

2.4.3.1 Percent weight of binder

The percentage by weight of binder nomenclature is often used in literature to express the acid and water soluble chloride concentrations relative to the weight of the binder in the concrete mix. The bound (acid and water soluble) chloride reacts directly with the binder gel to form Friedel's salt ($Ca_6Al_2O_6.CaCl_2.10H_2O$) and Kuzel's salt ($Ca_6Fe_2O_6.CaCl_2.10H_2O$) [94][95][90]. Regardless of the amount of aggregate in the concrete mix, the Friedel's salt ($Ca_6Al_2O_6.CaCl_2.10H_2O$) and Kuzel's salt ($Ca_6Fe_2O_6.CaCl_2.10H_2O$) is formed at the C-S-H gel of the binder paste. *BS EN 206*

[74] recommended the maximum permissible chloride concentrations in steel reinforced concrete to be 0.4% by weight of binder. However, a single value for chloride threshold level is not true for different types of concrete, steel and exposure environment [96]. This aspect is discused futher in chapter 4.

CHAPTER 3

POROSITY AND PORE STRUCTURE OF AN ALKALI ACTIVATED CEMENTITIOUS (AACM) MORTAR

3.1 INTRODUCTION

The durability properties of concrete have a strong relationship with its micropore structure. They are greatly influenced by the refinement of the micropore structure of the matrix. The important properties which are influenced by the concrete micropore structure include its strength, shrinkage, creep, permeability and diffusion. The resistance of concrete to the penetration of corrosion initiators such as chlorides is a function of its pore system characteristics [100]. Garboczi [101] applied three different types of pore structure and transport (PST) theories (Kozeny-Carman Theory, Archie's Law and Katz-Thompson Permeability Theory) to establish the direct relevance of pore system characteristics to the durability of concrete. The conclusion suggested that Katz-Thompson Permeability Theory was applicable to PST while Kozeny-Carman Theory and Archie's Law were found wanting.

Research shows that diffusivity of harmful ionic species (Cl^-, CO_2) in the concrete pore fluid causes corrosion of the embedded steel reinforcement and fibres in concrete [91][102][103]. The deterioration rate is controlled by the ease with which Cl, CO_2, O_2 and sulphate enter concrete and their movement within it. The attacks by these harmful species on concrete and steel reinforcement undermine the durability of concrete. AACM concrete is a porous cementitious material similar to OPC concrete and its porosity and pore structure will impact its properties. Hence, the need to investigate the pore structure characteristics of AACM concrete to better understand its durability properties with respect to these harmful ionic species (Cl^-, CO_2 and sulphate) is addressed in this chapter.

The permeability of fluid carrying harmful ionic species (Cl^-, CO_2 and Sulphate) into concrete is through its hardened cement paste and the interfacial transition zone (ITZ) between the cement paste and aggregate [25]. The ITZ which accounts for up to one-half of the total volume of hardened concrete could arguably be considered to be the predominant factor allowing the ingress of harmful elements. However, studies suggest that the diffusion of the ionic elements (Cl^- and Na^+) is mainly through the cement paste matrix [49]. The ITZ between the cement paste and aggregate was found to be discontinuous and the pores were isolated from each other thereby preventing the diffusion of harmful elements within the concrete matrix.

The common method of testing the microstructure of concrete by mercury intrusion porosimetry (MIP) is the application of mercury under high pressure through the mortar pores. The method is based on the "non-wetting" effects of mercury on the walls of the mortar pores. Mercury intrusion into the concrete matrix is suitable for pores within the range of 0.003 μm to 400 μm [104]. This method will be used for analysing the accessible pores within the AACM and the control OPC mortar samples.

Different mix compositions of the AACM mortar (four mixes) suitable for structural applications have been selected for pore structure analysis. These mixes represent different concentrations of the alkali activator, curing conditions and different binder content. Parallel investigations on control samples of normal OPC mortar of similar strength were also conducted. The research into the microstructure of AACM mortar will give quantitative measurements to determine the influence of pore parameters on the ingress of Cl^- and CO_2 within the AACM concrete matrix that cause its deterioration.

3.2 LITERATURE REVIEW

3.2.1 Concrete Pore Structure

Similar to the pore system in OPC paste, the hardened AACM paste comprises mainly of two types of pore sizes namely gel and capillary pores. Table 3.1 shows the classification of pore size in a conventional hydrated cementitious paste presented by Mindess et al. [105]. The pore system is further classified as unimodal or bimodal based on its distribution.

Table 3. 1: Classification of pore sizes in hydrated cementitious paste

Designation	Diameter	Description
Capillary Pores	10,000 - 50 nm	Large capillaries (macropores)
	50 - 10 nm	Medium capillaries (large mesopores)
Gel Pores	10 - 2.5 nm	Small isolated capillaries (small mesopores)
	2.5 - 0.5 nm	Micropores
	≤ 0.5 nm	Interlayer space

Source: *Mindess, Young, and Darwin, 2003* [105]

3.2.1.1 Gel pores

The gel pores are developed during the poor polymerization of aluminosilicate gel of the AACM binder. The polymerization and hardening of alkali activated

cementitious gel governs the desirable properties in AACM concrete, particularly in the context of durability, similar to the calcium silicate hydrate (C-S-H) gel in Portland cement hydrate [106]. The formation of aluminosilicate gel involves the dissolution of aluminosilicate precursor in the presence of alkali activator, thereby releasing silica and reactive alumina in monomeric form [107]. The silicate and aluminate species released become amorphous aluminosilicates in the presence of water. The amorphous aluminosilicate in concentrated solution results in gel formation [108]. The conceptual model for geopolymerization is presented in Fig. 3.1 [108].

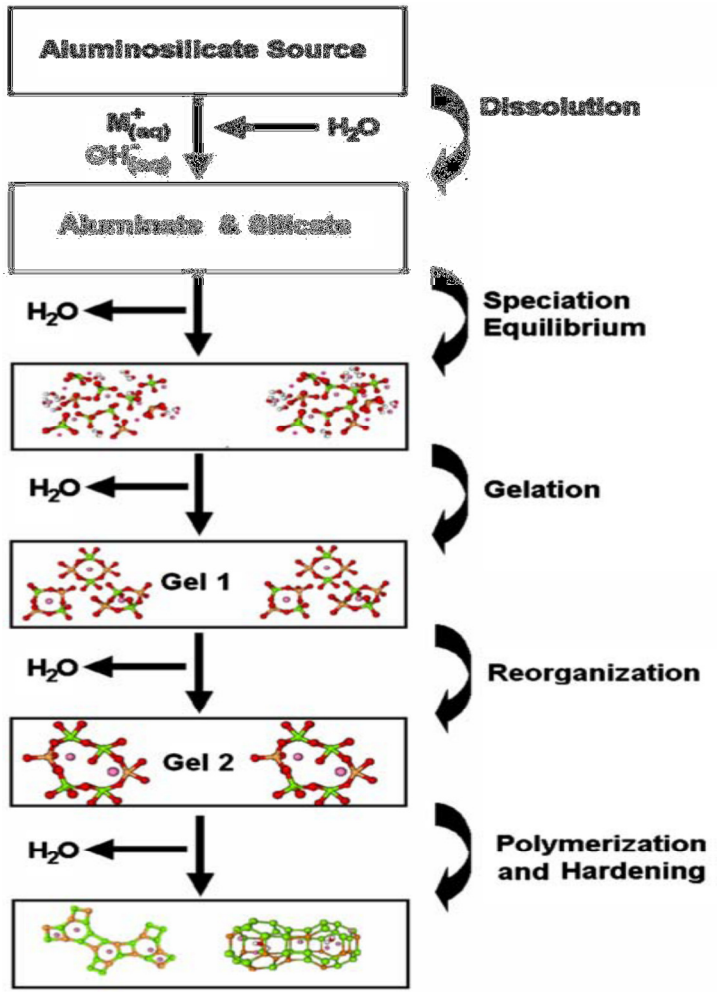

Figure 3. 1: Conceptual Model for Geopolymerization [108]

The gel pores of OPC are generally considered to occupy about 28 percent of the total volume of the gel after drying in a standard manner [109]. However, the gel pores of AACM are perceived to be less than 28 percent of the total volume of gel [106]. This is due to AACMs having a finer particle size than OPC, resulting in improved particle packing. The volume of gel pores in concrete is influenced by the type of cementitious binder, water/cement ratio and the hydration rate of hardened cementitious paste [25]. The total volume of gel pore increases in AACM with the progression of polymerization

and in OPC with hydration. On the other hand, the volume of capillary pores is simultaneously reduced as the gel pore volume increases [110].

The mix design factors affecting the pore formation in AACM mortar will be evaluated in this research work in order to develop optimal performing mixes in relation to engineering properties.

3.2.1.2 Capillary pores

The large capillary pores are orders of magnitude bigger than gel pores as shown in Table 3.1. An inverse relationship was suggested between the volume of gel pores and capillary pores as hydration progresses [110]. The volume of capillary pores decreases while the gel pores increases during the hydration process in the concrete matrix. This results in a lower cumulative pore volume within the concrete matrix because the comparatively large capillary pores are partially occupied by the binder gel. Ultimately, a denser microstructure evolves as the hydration progresses.

The capillary pores provide ease of ionic movement of harmful species (Cl^-, CO_2 and sulphate) within the concrete matrix, when in solution with water. Solutions of these ionic species (Cl^-, CO_2 and sulphate) are normally absorbed through the capillary pores within the concrete matrix because of their relatively large pore diameter. When water containing these harmful ionic species (Cl^-, CO_2 and sulphate) comes in contact with a dry concrete surface, it is driven into the concrete pore structure by a moisture gradient [111]. This process is known as capillary suction. It is a common transport mechanism prevalent in the tidal zone of marine structures and in coastal structures exposed to wetting and drying cycles. Therefore, capillary pores play a decisive role in the durability of concrete.

3.2.1.3 Unimodal and Bimodal

A unimodal pore distribution in OPC concrete is defined by the single range of pore volume within the differential pore distribution graph for OPC concrete as shown in Fig. 3.2. Other studies on the microstructure of OPC matrix also show a unimodal pore size distribution with most of the pore volume within the range of 0.01 to 0.1 μm of pore diameter [3][82].

A bimodal pore distribution, on the other hand, is defined by the double range of pore volume within the differential pore distribution graph as shown in Fig. 3.3. These pore sizes are normally observed between two separate zones. Current studies suggest that the pore size distribution of AACMs is bimodal with pores separated into two zones

(> 1 µm and < 0.02 µm ranges) unlike a similar grade of OPC matrix which is observed to be unimodal ranging between 0.01 to 0.1 µm [82].

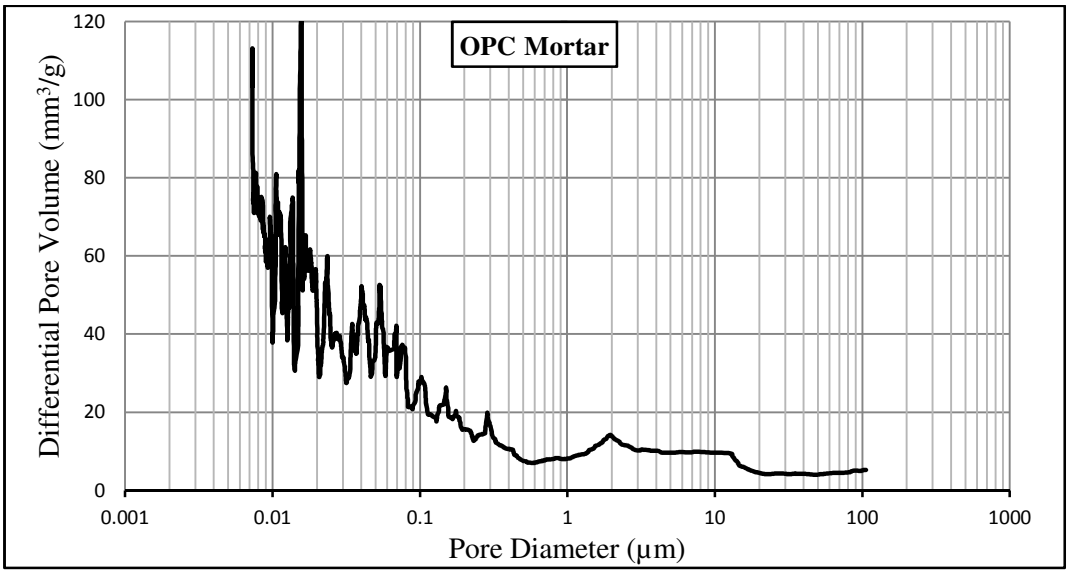

Figure 3. 2: Unimodal pore size distribution in OPC concrete (Author's data)

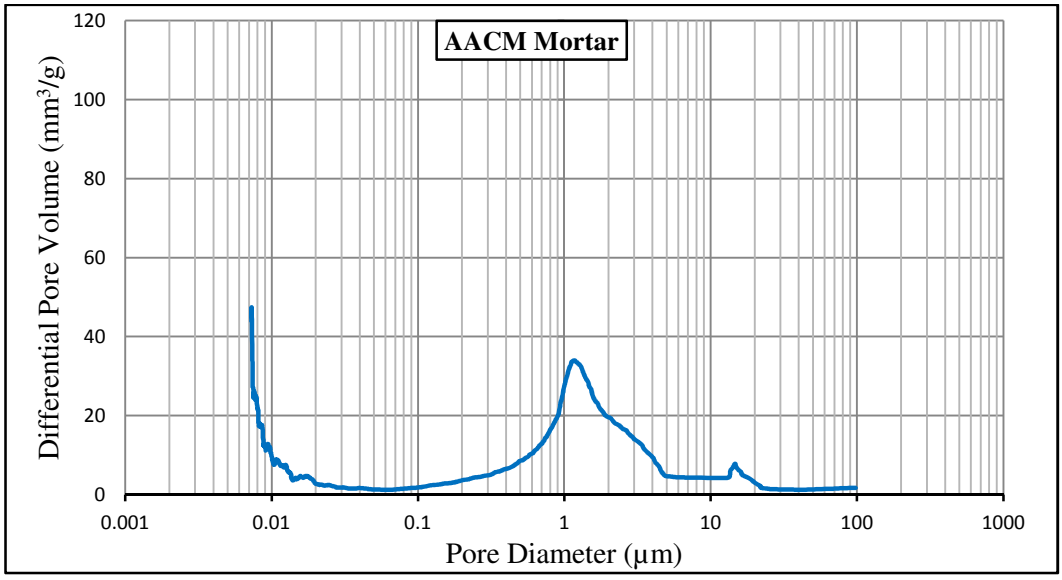

Figure 3. 3: Bimodal pore size distribution in AACM concrete (Author's data)

3.2.2 Pore System Parameters

There are three pore system parameters that are frequently used in analytical and empirical property-microstructure relationship models [112]. These are intrudable porosity $\boldsymbol{\Phi_{in}}$, critical pore diameter $\boldsymbol{d_c}$ and threshold pore diameter $\boldsymbol{d_{th}}$. These parameters are derived from the cumulative porosity curve and the logarithmic differential pore volume curve which are represented in Figures 3.4 and 3.5. The cumulative pore volume is the vertical scale on the left (blue graph) while the logarithmic differential pore volume is the vertical scale on the right (red graph) as shown in Figures 3.4 and 3.5. These pore system parameters are applicable to both OPC and AACM mortars (Figures 3.4 and 3.5 respectively).

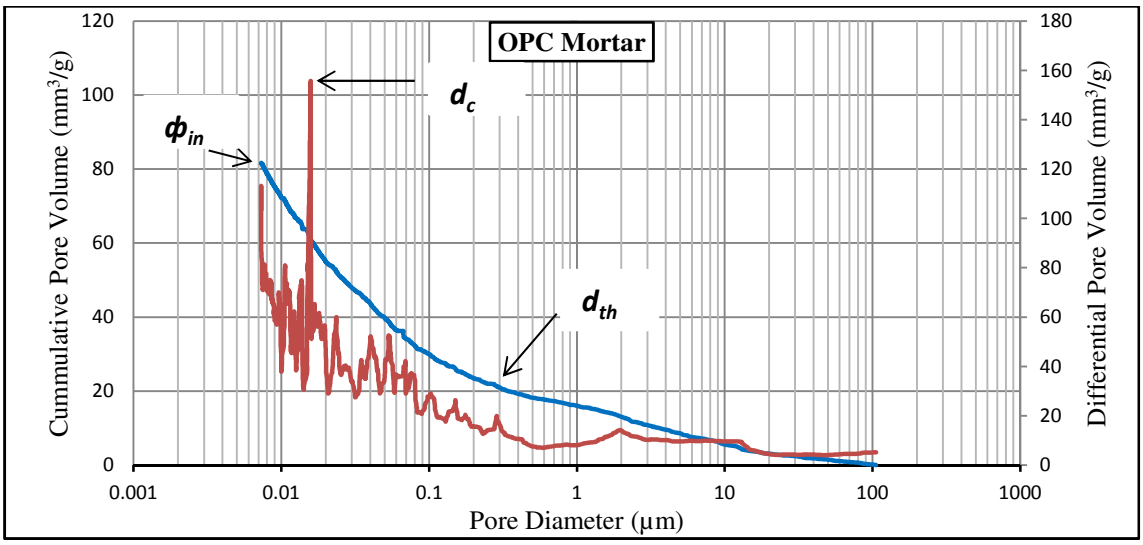

Figure 3. 4: Definition of Pore System Parameters in OPC Mortar (Author's data)

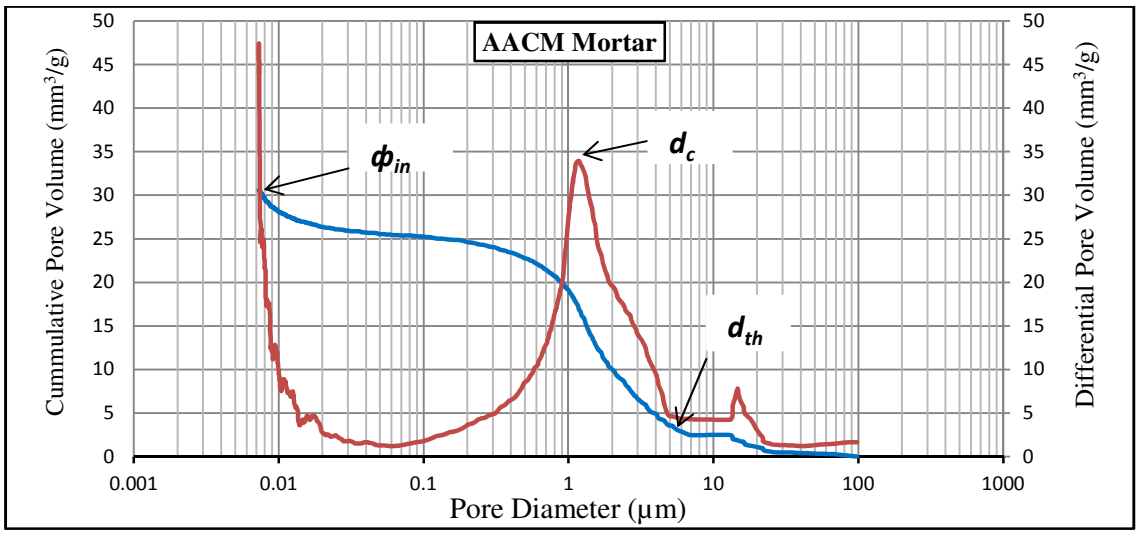

Figure 3. 5: Definition of Pore System Parameters in AACM Mortar (Author's data)

3.2.2.1 Intrudable porosity Φ_{in}

Intrudable porosity Φ_{in} which is obtained from the highest point on the cumulative porosity curve (Figures 3.4 and 3.5) depends on the connectivity of the capillary pores. A percolation intrudable porosity of 18% or less pores (equivalent to 82% or more solid fraction) was proposed for pore discontinuity in neat cement paste [113]. This threshold value is assumed to represent the degree of hydration where pore spaces are isolated from each other thereby limiting the intrusion of mercury within the pore spaces in a neat cement paste. How connected or disconnected these pores are, has a significant effect on the intrudable porosity Φ_{in}. The smaller the intrudable porosity Φ_{in}, the more refined the pore network thereby limiting the ingress of hazardous ions within the mortar matrix.

3.2.2.2 Critical pore diameter d_c

Critical pore diameter $\boldsymbol{d_c}$ is referred to as the pore diameter that exists between the interconnected net of voids within the concrete matrix [101]. This is used to characterise the extent by which harmful ionic species (Cl^-, CO_2 and sulphate) can penetrate into the concrete matrix through the network of these pores. Critical pore diameter $\boldsymbol{d_c}$ is shown in Figures 3.4 and 3.5 as the highest point on the logarithmic differential pore volume curve. At this pore diameter, a high volume of mercury intrusion within the concrete matrix is observed. Critical pore diameter $\boldsymbol{d_c}$ is applicable to AACM and OPC mortars as shown in Figures 3.4 and 3.5.

3.2.2.3 Threshold pore diameter d_{th}

Threshold pore diameter $\boldsymbol{d_{th}}$ was considered by some researchers as the diameter obtained from the inflexion point of the cumulative mercury intrusion curve [101] while others consider $\boldsymbol{d_{th}}$ as the diameter obtained from the point of abrupt variation in the same curve [114]. The inflexion point is often imperceptible and can be best observed by logarithm scale unlike the point of abrupt variation, which is visible by plotting on both normal and logarithm scales [115]. It was recommended that the values measured at the point of abrupt variation were useful indicators for assessing the quality of the concrete rather than at the point of inflexion [115][116]. Position of threshold pore diameter $\boldsymbol{d_{th}}$ is shown in Figures 3.4 and 3.5.

3.2.2.4 Effective Porosity

Porosity can be classified as total or effective porosity. Porosity is defined as the fractional volume of pores with respect to the bulk volume of the material [112]. Total porosity includes both open and closed pores unlike the effective porosity which takes account of only open pores that provide access for liquid to move within the concrete. Total porosity affects the bulk density, strength and thermal conductivity of concrete while the effective porosity relates to the permeability of concrete [112]. The porosity-strength relationships of concrete are often investigated in publications [117][118][119]. Four major empirical models relating porosity and strength of cement-based materials have been proposed [120][121][122][123]. A power function relationship was proposed by Balshin [120]. Ryshkevitch [121] proposed an exponential relationship. Hasselmann [122] and Schiller [123] proposed a linear and logarithmic relationship model respectively. These strength-porosity relationships are shown in Table 3.2., where σ =

Compressive strength, σ^0 = Compressive strength of fully dense material, p = Porosity and p_0 = Porosity of fully dense material.

Table 3. 2: Models of porosity and strength relationships for cement-based materials

Author and Year	Equation	Constant	Relationship	Application
Hasselmann [122]	$\sigma = \sigma_0 (1- bp)$	b	Linear	Originally for glass
Balshin [120]	$\sigma = \sigma_0 (1- p)^n$	n	Power	Originally for powder metals
Ryshkevitch [121]	$\sigma = \sigma_0 \exp(- cp)$	c	Exponential	Originally for ceramics and rocks
Schiller [123]	$\sigma = k \ln (p_0/p)$	k	Logarithmic	Originally for non-metallic brittle materials

3.2.3 Factors Affecting Pore Structure

3.2.3.1 Pore System Characteristics

The pore sizes and their distribution within the concrete matrix, obtained from mercury intrusion porosimetry, are used to characterise the concrete pore structure [116][124]. These pore system parameters are also crucial to the mechanical and durability properties of AACM concrete. Over the past few years, the AACM concrete pore system has been studied in relationship to its hardened properties such as compressive strength and durability. Preliminary experimental results reveal that the high degree of polycondensation of AACM concrete results in greater densification of the AACM paste within the concrete matrix when compared to the same degree of hydration of OPC concrete [26].

The complexity of concrete pore refinement is due to the complex nature of concrete pore system [116]. Many researchers [125][126][127] concluded that a true pore size distribution cannot be accurately determined in cement-based materials due to limitations of the mercury intrusion porosimeter test method (MIP). Mercury intrusion under pressure in MIP testing can access only the intrudable connecting pores within the concrete matrix, thereby leaving out the non-intrudable pores. It is also argued that mercury is accessible only to the connecting pores located at the outer surface of the specimen. Despite these limitations, MIP is the preferred alternative for assessing the pore structure of cement based materials.

3.2.3.2 Experimental Factors

Factors influencing the results of mercury intrusion porosimetry are the mercury contact angle with the pore walls, the surface tension of mercury, sample preparation and conditioning, rate and maximum pressure applied [124][128]. Appropriate input values of these factors are introduced in the MIP test for a given test material to obtain the output pore structure characteristics. Amongst the notable MIP input parameters are the contact angle and surface tension of mercury. Their values are 140^0 with the concrete pore wall and 0.48N/m surface tension respectively. These values were kept constant for all samples under investigation during the research work reported in this thesis.

3.2.3.3 Hydration/Geopolymerisation of Binder

The hydration/geopolymerisation in OPC and AACM concrete is dependent on time, temperature, type of binder and activator used. The AFm phase (Aluminate Ferritemono structure) is responsible for the adsorption and anion exchange with chloride ions. The formation of this AFm phase of AACM binder geopolymerisation lacks theoretical understanding [3][5] unlike the formation of hydrated calcium silicates and aluminates (C-A-S-H) in cement gel. There is little information on the formation of AFm phase in alkali-activated binders provided in the literature. Experimental studies show the formation of C-(N)-A-S-H gel during the geopolymerisation phase of AACM binder which has a mixture of cross-linked and non-cross-linked tobermorite based structures [129] as shown in Fig. 3.6. This is unlike the calcium silicate hydrate (C-S-H) of Portland cement, which is composed of only non-cross-linked tobermorite and jennite-like structures [130] as shown in Fig. 3.7. This difference could account for the high densification of AACM gel during hydration.

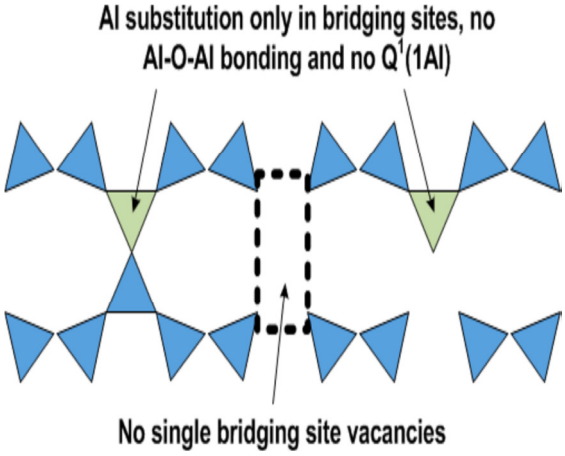

Figure 3. 6: Model for Hydrated AACM Binder. (Myers et al. [129])

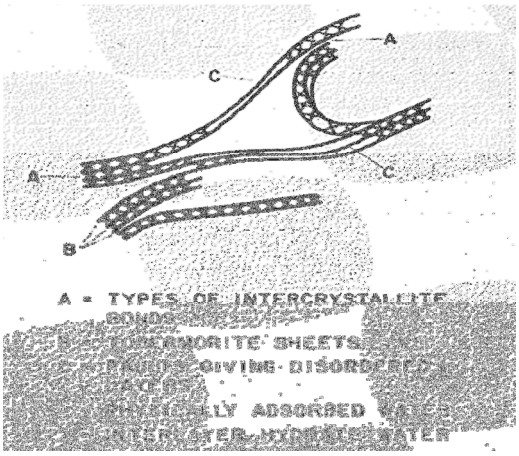

Figure 3. 7: Model for Hydrated Portland Cement. (R. F. Feldman and P. J. Sereda, [130])

3.2.4 Materials

3.2.4.1 OPC

The production of OPC has risen to 4.3 billion tonnes in 2014 which is the second highest commodity produced in the world [8]. The 1998 annual consumption is estimated to be 256 Kg of cement per head in UK, 261 Kg per head in US, 647 Kg per head in Spain, 664 Kg per head in Japan and 799 Kg of cement per head in Portugal [25].

The OPC used in this research project was supplied by Frank-key group, Sheffield. It was supplied in 25Kg bags conforming to CEM type 1 with above 95% clinker [74]. The ordinary Portland cement has a strength class of 42.5. The cement was used for the control concrete mixes used in the research. The chemical composition of the OPC used in this research is shown in Table 3.3

Table 3. 3: Chemical composition of ordinary Portland cement

CaO	SiO_2	Al_2O_3	Fe_2O_3	SO_3	MgO	K_2O	P_2O_5	TiO_2	MnO	SrO
64.2%	11.6%	8.35%	3.16%	3.14%	2.09%	1.19%	2.01%	1.88%	2.14%	0.23%

BSI 12 [75] suggests chemical composition requirements for the production of OPC as follows:

1. The sum of the reactive portion of CaO and SiO_2 should be greater than 50%
2. The CaO/SiO_2 ratio should be greater than 2 in order to ensure that the setting of cement paste is not inhibited as well as provide sufficient free lime within the concrete pore solution.
3. The quantity of MgO should not exceed 5%. The presence of high MgO in OPC will constitute unsightly cracks in concrete.
4. The SO_3 content should be less than 3.5 ± 0.1%. SO_3 content is known to accelerate the setting time of cement paste.
5. The maximum permissible Cl^- content should not be more than 0.4%. This is because of the possibility of chloride induced corrosion happening due to high amount above the specified limit when OPC is used in reinforced concrete structures.
6. Other chemical constituents such as Al_2O_3 and Fe_2O_3 aid the physical appearance of OPC as well as assist with faster setting time.

3.2.4.2 Water

The tap water used in each mix conforms to the requirement of *BS EN 1008* [76]. Additionally, distilled/ionized water was used for calibration of instruments, preparation

of NaCl solution, dissolving concrete powder into solution for analysis of chloride concentration and pH.

3.2.4.3 Chemical Admixtures

The retarder used was supplied by Oscrete Construction Products Ltd, Bradford, U.K. It was used in accordance with the manufacturer's specification of 0.75% binder weight. Its chloride ion content is less than 0.1% and the alkali content Na_2O (sodium oxide) is less than 3.5%. The introduction of the retarder in the AACM concrete mixes is aimed at prolonging the initial and final setting time of the geopolymerization reaction. This provides the time for the AACM concrete to be transported, placed and compacted easily. The shrinkage reducing agent SRA was supplied by Oscrete Construction Products Ltd, Bradford, U.K. SRA was added to the mix in accordance with the manufacturer's specification of 2% by binder weight. Its chloride ion content is less than 0.1% and the alkali content Na_2O (sodium oxide) is less than 3.5%.

3.2.4.4 Aggregates

The coarse aggregates used were 10 mm uncrushed gravel and 6 mm limestone. They were both supplied by Tarmac Ltd, Derbyshire. The proportion of 10mm uncrushed gravel to 6mm crushed limestone in each concrete mix was 2:1. The aggregates were in a saturated surface dry state when placed in the mixer. The main properties and oxide compositions of these aggregates conform to relevant standards [77]. The grading curve for the 10 mm uncrushed gravel is shown in Figure 3.8. Grading was performed in accordance with *BS EN 12620: 2002+ A1* [78] and *BS 812 - 103.2* [79].

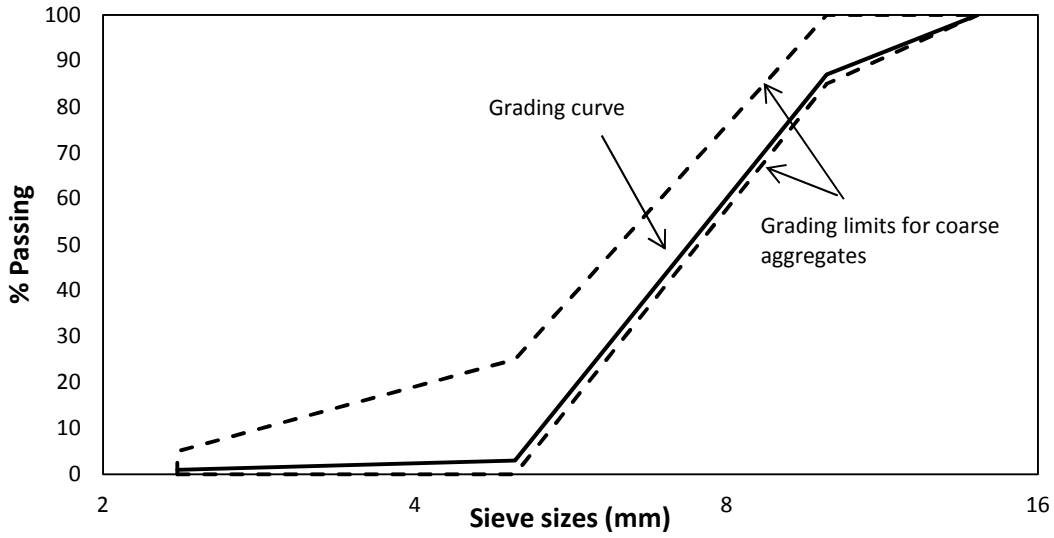

Figure 3. 8*:* Grading curve for 10 mm uncrushed gravel

Silica sand and sharp concrete sand were used as fine aggregates for the production of AACM and OPC concrete and mortar. The silica sand was used in the production of AACM concrete and mortar while sharp sand was used for OPC concrete and mortar. The silica sand and sharp concrete sand were both supplied by WBB Minerals Ltd, Congleton, Cheshire. The grading curves for silica and sharp sand are shown in Figures 3.9 and 3.10 respectively. The grading curves show a larger percentage of silica sand passing sieve size 1.008 mm compared with sharp concrete sand. This suggests that silica sand is finer than sharp concrete sand, but they fit the same grading zones.

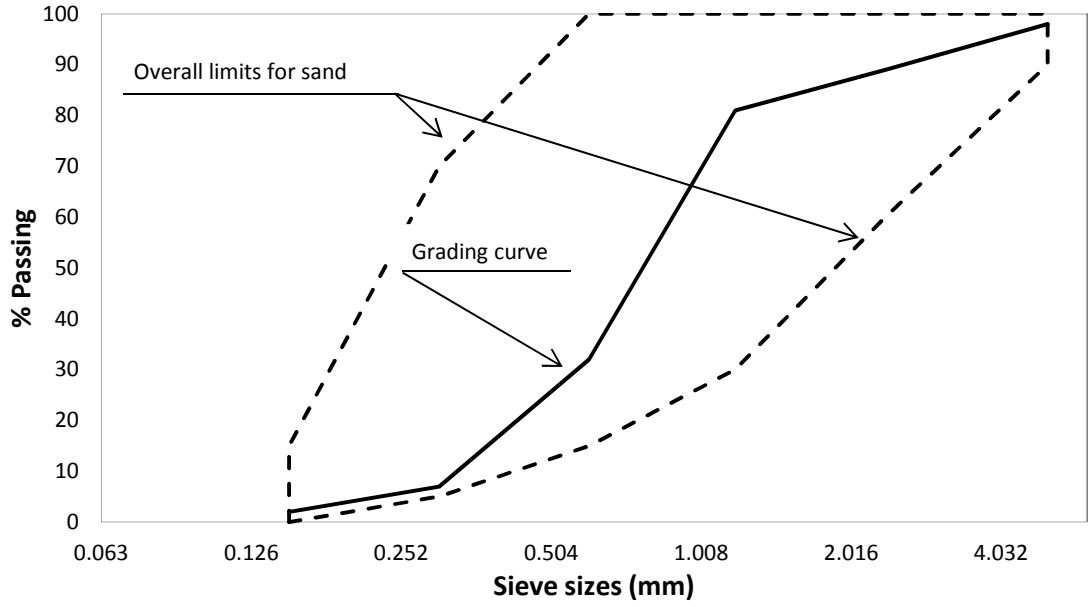

Figure 3. 9: Grading curve for silica sand

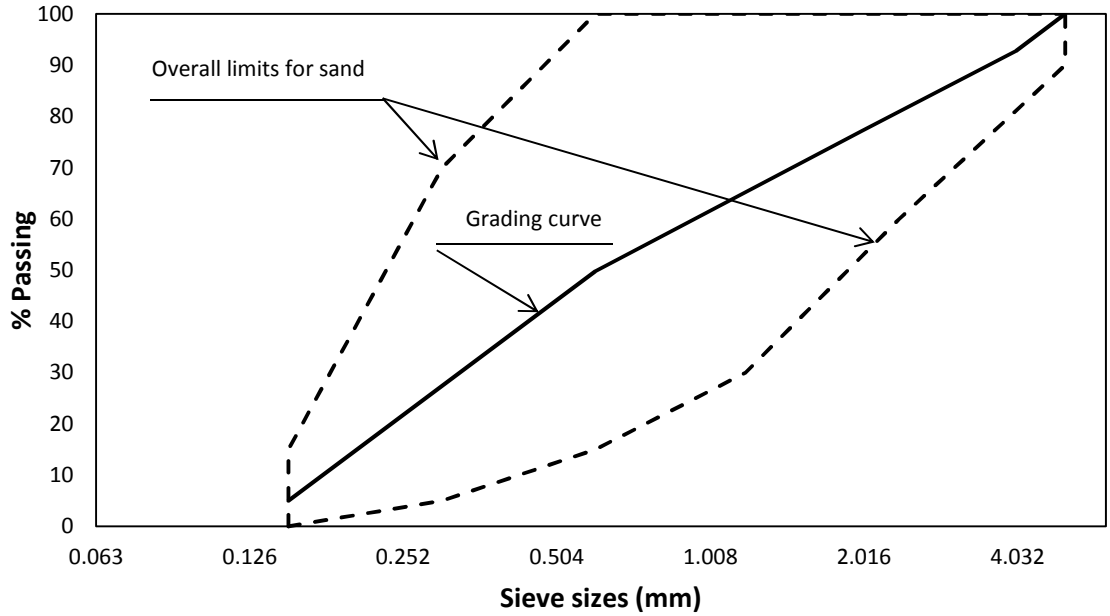

Figure 3. 10: Grading curve for sharp concrete sand

Silica sand was produced from consolidated sand deposits. It has high silica content (SiO_2) of 95.17% as shown in Table 3.4. It is free from impurities like clay and refractory minerals such as chromite.

Table 3. 4: Chemical analysis of silica sand

SiO_2	Fe_2O_3	Al_2O_3	K_2O	LOI
95.17	0.25	2.17	1.35	0.31

3.3 TEST PROGRAMME

3.3.1 Materials and Mix Proportions

Four different mix compositions of AACM mortar (M_2 to M_5) comprising a cementitious binder, fine aggregate, and alkali activator were produced and investigated. A pilot AACM mortar mix M_1 was initially produced to optimise the mix composition for AACM mortars (M_2 to M_5). A parallel control mix (M_6) of C40 grade mortar was also produced with 100% OPC binder. The AACM cementitious binder used was a proprietary hybrid alkali activated precursor comprising of low and high calcium constituents, which has been developed at Sheffield Hallam University [131]. A version of the AACM cementitious binder and activator is currently manufactured under licence. Medium grade silica sand (fine aggregate) was used for the AACM mortar mixes while sharp concrete sand was used for the OPC mortar mix. The experimental mortar mixes M_2 to M_6 used in this research were based on the practical mix compositions of AACM concrete which were investigated for chloride ingress reported in Chapter 4 and published by the author [132]. The samples for MIP study were prepared by replacement of coarse aggregate with fine aggregate and the binder to provide mortar mixes for MIP analysis. The replacement of the coarse aggregate content in AACM and OPC concrete were done by increasing the mix content of the fine aggregate and binder proportionately.

The liquid/binder and fine aggregate content were adjusted to achieve the workability and setting time required to produce practical AACM mortar mixes suitable for construction purposes. Two batches of AACM mixes were produced; the first batch of mixes had admixtures (retarder and shrinkage reducing admixtures) in it while the second batch was without admixtures. A retarder admixture (R42) containing less than 0.1% chloride ion and less than 3.5% alkali content Na_2O (Sodium oxide) was introduced in the first batch of AACM mortar mixes. The retarder in these mixes prolonged the initial and final setting time of the geopolymerization reaction, thereby

facilitating the required time for AACM mortar to be transported, placed and compacted easily. Similarly, a shrinkage reducing admixture (SRA) was added to AACM mortar mixes in accordance with the manufacturer's specification of 2% by binder weight. The composition of the five mixes M_2 to M_6 is given in Table 3.5. The alkali activator liquid [131] was diluted with tap water by 2.15%, 4.24%, 8.12% and 12% in mixes M_2 to M_5 respectively, similar to the AACM concrete specimens produced for chloride ingress investigation reported in Chapter 4. M_6 is an OPC mortar mix with water binder ratio of 0.486.

Table 3. 5: Composition of AACM and OPC mortar mixes

Mix	Batch	Total Binder (%)	Fine Agg. (%)	Total Liquid (%)	Liquid/Binder Ratio	Dilution (%)	R42 (% Binder)	SRA (% Binder)	Curing		
									Wet/Dry	Wet	Dry
M_1 Trial mix	a	45.0	33.0	22.0	0.488	9.93	0.75	2	-	-	√
	b	50.0	30.0	20.0	0.400	2.04	0.75	2	-	-	√
	c	50.0	33.0	17.0	0.340	1.60	0.75	2	-	-	√
	d	50.0	32.0	18.0	0.360	0.00	0.75	2	-	-	√
M_2	a	50.0	29.0	21.0	0.414	2.15	0.75	2	√	√	√
	b	50.0	29.0	21.0	0.414	2.15	0	0	√	√	√
M_3	a	48.2	28.9	23.0	0.477	4.24	0.75	2	√	√	√
	b	48.2	28.9	23.0	0.477	4.24	0	0	√	√	√
	c	48.5	29.1	22.3	0.460	4.24	0.75	2	√	√	√
	d	47.6	28.6	23.8	0.500	4.24	0.75	2	√	√	√
M_4	a	48.0	29.0	23.0	0.473	8.12	0.75	2	√	√	√
	b	48.0	29.0	23.0	0.473	8.12	0	0	√	√	√
M_5	a	48.0	29.0	23.0	0.470	12.00	0.75	2	√	√	√
	b	48.0	29.0	23.0	0.470	12.00	0	0	√	√	√
M_6	Ctrl	32(OPC)	53.0	15.0	0.486	-	-	-	√	√	√

3.3.2 Specimen Preparation and Conditioning

3.3.2.1 Casting of Specimens

The AACM mortar mixes were prepared to evaluate their pore structure using the mercury intrusion porosimetry technique. The dry binder and aggregate were placed in a 12 litre Hobart mixer with a 3-speed option. They were mixed in the Hobart mixer with the lowest speed (option-1) for 30 seconds to avoid dispersing the powder into the atmosphere. The Liquid component containing alkali activator, water, and retarder R42 were slowly added to the mix. The mixing continued for 2 minutes until a uniform paste was produced. The shrinkage reducing admixture was then slowly added while mixing continued. The mortar was further mixed for 1 minute before stopping the Hobart mixer.

The mortar was placed in 75 x 75 x 75 mm steel cube moulds which had been lightly oiled to prevent the hardened mortar from sticking to the surface. Each mould was filled in three layers. Each layer was properly compacted on the vibrating table for about 20 seconds to attain homogeneity and minimise the presence of voids. The mortar surface was gently trowelled to obtain a smooth and level surface. The cast specimens were placed on a flat surface and covered with polythene sheets to prevent rapid moisture loss. The specimens were left in the mould for 24 hours under a room temperature of 20 ± 2 ^{0}C and a relative humidity of about 65% before demoulding. The hardened AACM mortar specimens after 24hrs of casting are shown in Fig. 3.11. The OPC mortar mix M_6 was prepared similar to AACM mortar mixes except that the retarder R42 and shrinkage reducing admixture SRA were not added to the OPC mortar mix.

Figure 3. 11: AACM mortar specimens after demoulding

3.3.2.2 Specimen Preparation

Two batches (a) & (b) of AACM mortar mixes M_2, M_4 and M_5 were produced as shown in Table 3.5. Batch "a" as shown in Table 3.5 contains retarder R42 and

shrinkage reducing admixture (SRA) at 0.75% and 2% by weight of binder respectively. Batch "b" of the AACM mixes contained no retarder R42 and SRA admixture. However, for AACM mortar mix M_3, four batches were produced by varying the liquid binder ratios as shown in Table 3.5. Batches (a) and (b) of mix M_3 had the same liquid binder ratio of 0.477 while batches (c) and (d) had liquid/binder ratio of 0.460 and 0.500 respectively. In addition, batches (a), (c) and (d) contained retarder R42 and shrinkage reducing admixture (SRA) while batch "b" contained no retarder R42 and SRA, similar to batch "b" of AACM mixes M_2, M_4 and M_5. Mortar mix M_3 is based on the AACM concrete mix S_3 which gave optimum properties of strength, workability and shrinkage in the investigation reported in chapter 4 and authors' publication [132]. M_3 was, therefore, chosen for a more detailed investigation of liquid/binder ratio. The OPC control mix M_6 (one batch) contained no retarder R42 and shrinkage reducing admixture (SRA).

Six cubes (three per batch) were cast for each AACM mortar mix M_2, M_4 and M_5 and twelve cubes were cast for AACM mortar mix M_3 while three cubes were produced for OPC control mix M_6. A total of thirty-three cubes were cast.

3.3.2.3 Curing Regime

The curing regime is important for the development of the AACM mortar pore structure. Three practical curing regimes (wet/dry, wet and dry) applicable in the construction field were adopted in this research work as shown in Table 3.6.

Table 3. 6: Curing regimes for AACM & OPC mortar mixes

Age(days)	Wet/dry	Wet	Dry
0-3	Water (20^0C)	Water (20^0C)	Air (20^0C; 65%RH)
3-28	Air (20^0C; 65%RH)	Water (20^0C)	Air (20^0C; 65%RH)

Wet-dry curing involved placing the specimens in water at a temperature of 20 ± 2^0C for 3 days immediately after demoulding, followed by dry curing in the laboratory air at a temperature of 20 ± 2^0C and approximately 65% relative humidity for 25 days (total curing period of 28 days). For wet curing, the specimens were placed in water at a temperature of 20 ± 2 ^{0}C for 27 days immediately after demoulding. For dry curing, all the specimens were cured in the laboratory air at a temperature of 20 ± 2^0C and approximately 65% relative humidity for 27 days immediately after demoulding. The specimens cured in the laboratory air were securely covered with polyethene sheets during 28 days of dry curing to prevent rapid moisture loss. It simulates site practice of preventing moisture loss, for example, with the application of curing membranes.

Compressive strength tests on the 75mm cubes were conducted after the 28 days of curing under each regime (Wet/dry, Wet and Dry). Samples for MIP testing were obtained from the crushed cubes, which were then dried in an oven at a temperature of 50^0C for 3 days (28- 31 days age) and finally preserved in a desiccator for 3 days (31-34 days).

3.3.3 MIP Sample Preparation and Conditioning

3.3.3.1 Cube Crushing

Mortar test samples of small dimensions with an average length of 1cm were obtained for MIP testing from the 75mm mortar cubes which were crushed after 28 days of curing under regimes wet/dry, wet and dry (Table 3.6). This was achieved by performing compressive strength tests on the cubes in accordance with *BS EN 12390-3:2009* [133]. The results of the compressive strength tests are presented in section 3.4.1. Compression tests on the 75mm cubes produced large chunks of mortar samples. These chunks were further broken into smaller pieces by gentle crushing with the test machine to produce samples ideal for MIP testing. The aperture of the crushing machine was set to 1cm to obtain samples which would pass through the throat of the MIP dilatometer as discussed in section 3.3.5.1.

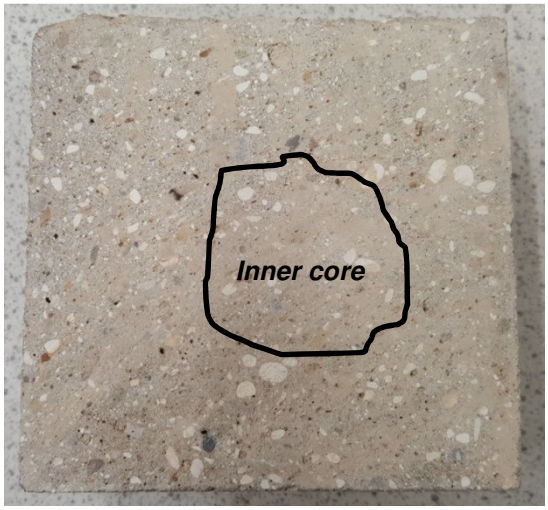

Figure 3. 12: Location of test sample used for MIP testing within a mortar cube core

Figure 3. 13: MIP specimens stored in self-sealing bags after oven drying

3.3.3.2 Location of Test Samples

The selection of samples from crushed cubes, that will be a true representation of the mortar matrix, was achieved by obtaining samples from the inner core of the crushed cube as shown in Fig. 3.12. The samples used for MIP testing after crushing the cube into suitable small pieces and oven drying were stored in self-sealing bags (Fig.

3.13). Using samples close to the concrete cube surface will not give an accurate result for the MIP test. An investigation was carried out to determine the influence of test sample location within the paste matrix relative to the casting position on porosity and pore size distribution [134]. The research revealed that the test sample from the top surface (trowelled) and the side surface of a paste has a larger pore volume and generally higher proportions of large pores compared to the middle (core). A conclusion was that test samples located near the surface are more sensitive to the curing regimes and settlement compared to the middle core.

3.3.3.3 Oven Drying

The crushed samples of 1cm average length were dried in an oven at a temperature of 50^0C for 3 days. This was carried out to remove adsorbed water from the pore fluid within the mortar pore system, which can obstruct its accessible porosity in MIP testing. Oven drying at a higher temperature than 50^0C was found to cause microcracking which may adversely affect the test results [135]. After oven drying at a temperature of 50^0C for 3 days, the samples were placed in a desiccator for another 3 days to cool down to 20^0C. The desiccator had silica gel at the bottom to further assist with removing adsorbed water and preventing moisture migration from the air. After cooling in the desiccator for 3 days, the test samples were stored in a self-sealing bag and labelled accordingly as shown in Fig. 3.13.

3.3.3.4 Details of MIP Test Samples

The mass and dimensions of each test sample subjected to MIP testing were obtained using an electronic weighing balance and digital callipers as shown Fig. 3.14 and 3.15.

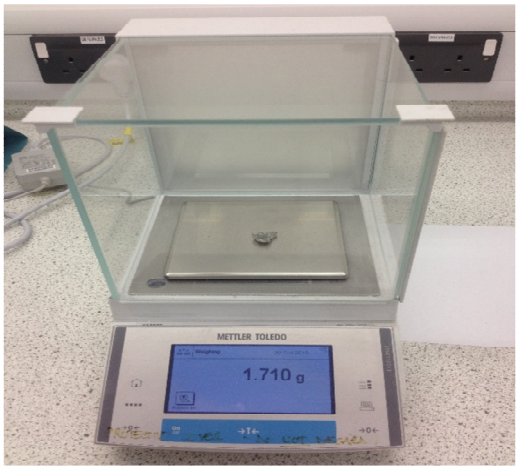

Figure 3. 14: Weighing of test sample

Figure 3. 15: Measuring the dimensions of samples

The mass and dimensions for each of these test samples are documented in Table 3.6. The dimensions of test specimens required for MIP test, as specified by *BS1902-316: 1990* [136] are a particle of maximum size 1cm^2. The dimensions of mortar test samples used for MIP analysis are within a range of 0.52 to 0.98 cm whose area falls within the specified 1cm^2 maximum particle size. However, the mass required for MIP analysis is not specified. It was observed that both the mass and dimensions affect the total intruded porosity even when many researchers fail to record these details in their investigation [137]. The higher mass and dimension give greater total intruded porosity when compared to samples of lower mass and dimension.

In this investigation, mass ranging between 1.022 to 1.647g was recorded for the test samples used for MIP analysis shown in Table 3.7. Both the mass (1.022 to 1.647 g) and dimensions (0.52 to 0.98 cm) of all test samples are within an acceptable range [136] to minimise the effect of specimen size on the results of MIP analysis of this study. The data given in Table 3.7 are an average result of three samples obtained from different cubes. The mass and dimension variation between each set of the three specimens are less than 5%.

Table 3. 7: Mass and dimensions of samples under different curing regimes

Mix	Batch	Wet/Dry		Wet		Dry	
		Mass (g)	Dimensions (cm)	Mass (g)	Dimensions (cm)	Mass (g)	Dimensions (cm)
M_2	a	1.148	0.92 x 0.61	1.198	0.93 x 0.62	1.460	0.94 x 0.92
	b	1.264	0.90 x 0.84	1.022	0.96 x 0.68	1.360	0.91 x 0.92
M_3	a	1.173	0.93 x 0.52	1.231	0.91 x 0.83	1.283	0.95 x 0.72
	b	1.147	0.90 x 0.67	1.177	0.94 x 0.97	1.211	0.97 x 0.62
	c	1.305	0.98 x 0.85	1.198	0.82 x 0.78	1.202	0.93 x 0.58
	d	1.148	0.89 x 0.91	1.320	0.98 x 0.76	1.103	0.81 x 0.65
M_4	a	1.330	0.90 x 0.89	1.330	0.91 x 0.76	1.647	0.98 x 0.99
	b	1.510	0.90 x 0.94	1.266	0.92 x 0.86	1.234	0.96 x 0.70
M_5	a	1.208	0.95 x 0.82	1.173	0.97 x 0.72	1.234	0.96 x 0.70
	b	1.192	0.85 x 0.89	1.255	0.98 x 0.74	1.370	0.97 x 0.72
M_6	Ctrl	1.156	0.93 x 0.58	1.162	0.89 x 0.60	1.165	0.98 x 0.63

3.3.4 Test Procedure

3.3.4.1 Mercury Intrusion Porosimetry

The mercury porosimetry analyses were performed using Pascal 140/240 Porosimeter [Fig 3.16]. This device is in two parts; Pascal 140 which applies pressure of up to 100 MPa and Pascal 240 which applies pressure of up to 200 MPa. The device measures pore sizes within the range of 0.007 to 100 µm. The computer microprocessor translates the data collected on applied pressures to pore radius using the Washburn equation (equation 3.1):

$$p = \frac{2y\cos\phi}{r} \qquad 3.1$$

Where $\boldsymbol{p}$ is the absolute applied pressure; $\boldsymbol{r}$ is the pore radius; $\boldsymbol{y}$ is the mercury surface tension (= 0.48N/m); $\boldsymbol{\phi}$ is the contact angle (= 140^0).

Washburn equation assumes that the pores in the concrete matrix are cylindrical in shape which has been criticised by many researchers. [137]

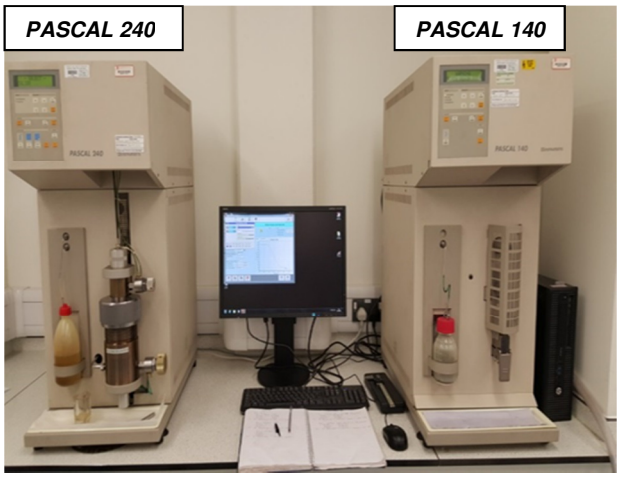

Figure 3. 16: Mercury intrusion porosimetry device used for analysis

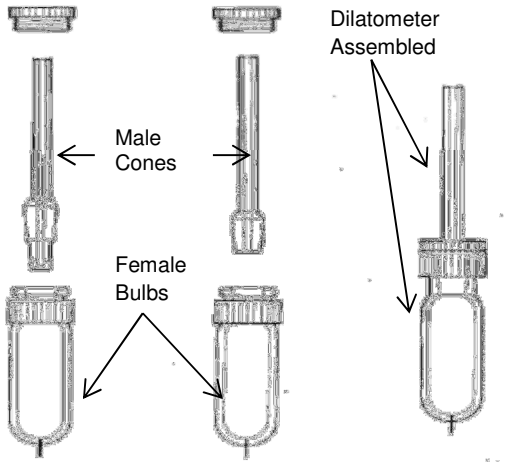

Figure 3. 17: CD3 dilatometer showing the male cone and female bulb components

3.3.4.2 Mercury Intrusion Porosimetry Test Procedure

Test samples of pre-determined mass and dimensions (Table 3.7) were placed inside a CD3 dilatometer. The dilatometer consists of a top male cone and a female bulb as shown in Fig. 3.17. The lower part of the male cone was lightly lubricated with silicon grease to prevent leaking. The male cone was then securely tightened to the female bulb (Fig. 3.17) and placed in the PASCAL 140 Porosimeter. The MIP test analysis was done in two parts, as follows:

3.3.4.2.1 Pascal 140

The test samples were analysed through seven stages in PASCAL 140 Porosimeter, which are: Outglass Countdown, Screw Dilatometer, Outglass Run, Outglass Ready, Filling Run, Air Pulse, Filling Wait and Analysis Run. The first four stages (Outglass Countdown, Screw Dilatometer, Outglass Run and Outglass Ready) involve degreasing the sample under vacuum. The essence of degreasing the test samples was to avoid the risk of powder elutriation. The mercury filling operation (Filling Run stage) commences once the minimum vacuum is reached after degreasing the sample. In between mercury filling operations, two air pulses were introduced to eliminate the possibility of bubble formation during the mercury filling operation. The maximum mercury fill was set to 450 mm^3. Once the mercury fill is completed, pressure increases from vacuum up to 100 MPa. The applied pressure up to 100MPa will allow mercury to intrude into large pore spaces of the mortar matrix. Depressurization (extrusion) begins when the pressure has reached 100 MPa. The 100 MPa is the set maximum pressure for PASCAL 140. The Depressurization (extrusion) decreases to atmospheric pressure before the data is collected and analysed by the computer microprocessor. After the seven stages of analysis in PASCAL 140 Porosimeter are completed, the sample, mercury fill and dilatometer were weighed and transferred to PASCAL 240 Porosimeter for further analysis.

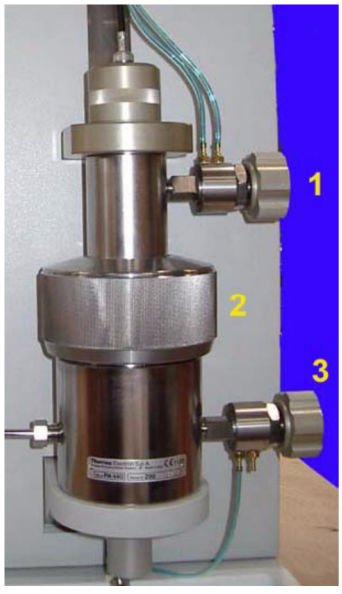

Figure 3. 18: Autoclave (1) upper valve (2) locking nut (3) lower valve [138]

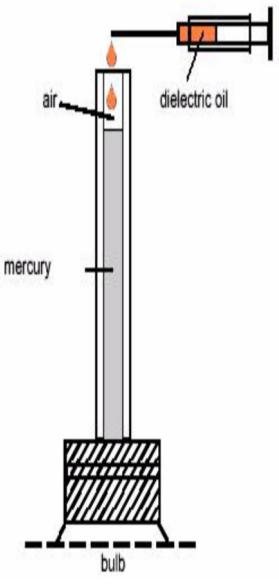

Figure 3. 19: Filling with dielectric oil

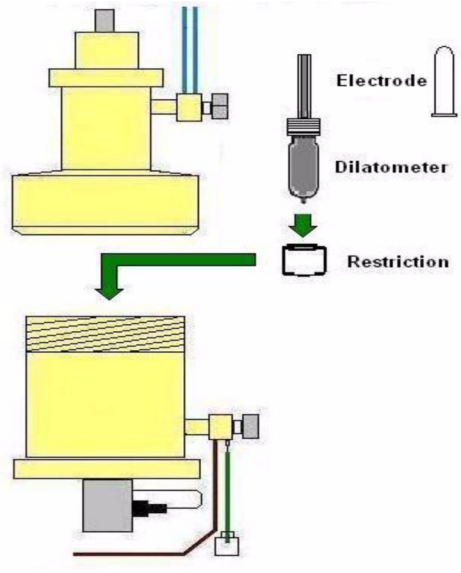

Figure 3. 20: Placing the dilatometer into the autoclave

3.3.4.2.2 Pascal 240

The CD3 dilatometer (Fig. 3.17) containing the mortar sample and filled with mercury is placed inside the autoclave of PASCAL 240 (Fig. 3.18). The autoclave contains dielectric oil to aid mercury intruding the mortar pore spaces under high pressure up to 200 MPa. Using a syringe, the empty space above the mercury fill in the male cone of the dilatometer was filled with dielectric oil to avoid any air remaining in the capillary, as shown in Fig. 3.19. The autoclave locking nut was tightened after properly placing the CD3 dilatometer (Fig. 3.20). The upper and lower valves were slightly loosened up to the red mark indicator before the filling operation of dielectric oil. The filling operation by dielectric oil was initiated to eliminate possible air bubbles in the hydraulic circuit. After all air bubbles were eliminated, the upper and lower valves were tightened. The first cycle of mercury intrusion was initiated after tightening the upper and lower valves. The first cycle involves the application of high pressure up to 200 MPa to aid intrusion of mercury through the pore spaces of the mortar sample to pore size down to 0.0073 μm. After the maximum pressure of 200 MPa is reached, the second cycle begins which involves the extrusion of mercury from the pore spaces of the mortar sample. The second cycle reduces the maximum pressure from 200 MPa until it reaches zero. The graphs of pore sizes and pore distribution were obtained at the end of the mercury intrusion porosimetry analysis.

3.4 RESULTS AND DISCUSSION

3.4.1 Compressive Strength

The compressive strengths of mortar mixes M_2 to M_6 were obtained as explained in section 3.3.3.4. The influence of activator dilution, admixtures (R42 and SRA), liquid/binder ratios and different curing regimes (wet/dry, wet and dry) has been investigated. Compressive strengths presented in this section represent an average of two specimens tested in accordance with *BS EN 12390-3:2009* [133].

3.4.1.1 Effect of Activator Dilution

The degree of alkali activator dilution for mortar mixes M_2 to M_5 is given in Table 3.5 (section 3.3.1). The dilution ratio is expressed as a percentage of water by mass which is mixed in the activator developed by *Sheffield Hallam University* [131]. Figures 3.21 and 3.22 show the relationship between compressive strength and activator dilution of 4.24% to 12% representing AACM mortar mixes M_3 to M_5 for batch "a" (with admixtures) and batch "b" (with no admixtures) respectively.

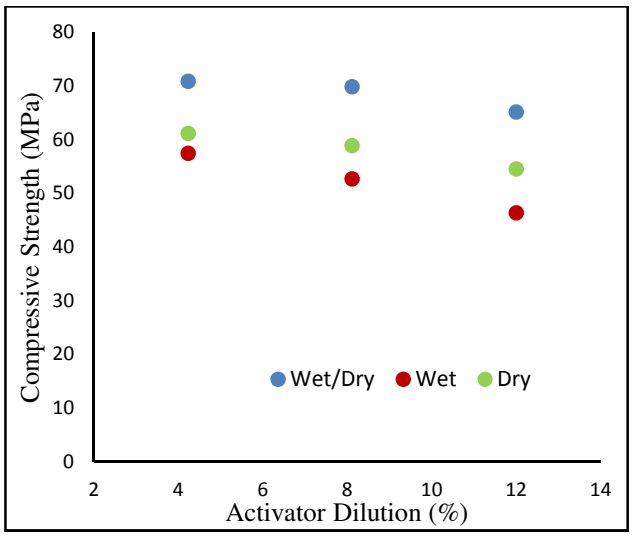

Figure 3. 21: Compressive strength of mortar batch "a" containing admixtures (R42 and SRA)

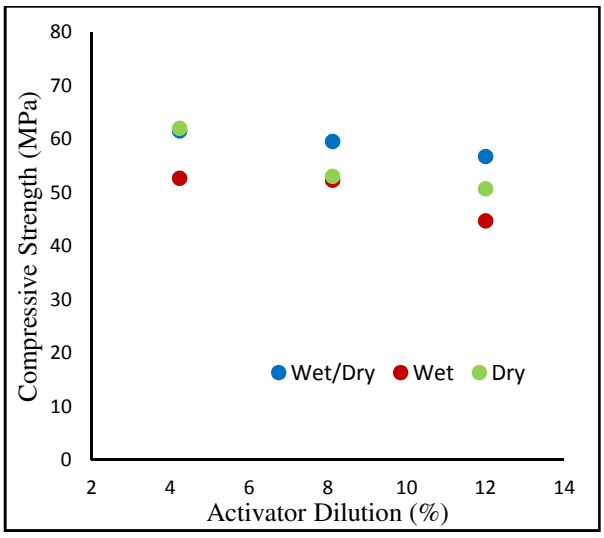

Figure 3. 22: Compressive strength of mortar batch "b" containing no admixtures (R42 and SRA)

The liquid/binder ratios of the AACM mortar mixes M_3 to M_5 are equal at approximately 0.47 and thus they have been used to investigate the influence of activator dilution on compressive strength of AACM concrete. Mix M_2 was excluded from this analysis since it has a different liquid/binder ratio (0.41).

A decrease in the compressive strength was achieved by increasing the degree of dilution of the activator. This was observed for AACM mortar mixes M_3 to M_5 under the three curing regimes for both batches (a) and (b) mixes (Figures 3.21 and 3.22). The lowest activator dilution of 4.24% (M_3) produced the highest compressive strength. For example, the compressive strengths of AACM mortar mixes with 4.24% (M_3), 8.12% (M_4) and 12.00% (M_5) dilution were 70.9 MPa, 69.9 MPa and 65.2 MPa respectively under wet/dry curing (Fig. 3.21).

A concentration between 8 to 16 molarity was recommended for sodium silicate activator [26] while a concentration of 10 molarity was recommended for potassium hydroxide [24]. These authors suggested that the geopolymer formations were delayed by a higher activator concentration due to excessive ions thereby limiting the mobility and potential to interact with reactive species. This reverse effect was, however, not observed in this study because the activator concentrations are within acceptable limits of the activator molarity.

The activator dilution affects the workability and strength of AACM concrete and mortar significantly [139]. A workability of 220 mm slump and compressive strength of 45 MPa was achieved by using a 35% activator concentration compared with 40% activator concentration which produced lower workability of 180 mm slump but higher strength of 54 MPa at 28 days age [139]. These results were based on an AACM

mix with a liquid/binder ratio of 0.37, binder content of 400 Kg/m^3 containing ground granulated blast-furnace slag (GGBS) and class F fly-ash cured under ambient conditions at a temperature of 20 ± 2^0C and 70 ± 10% relative humidity [139].

3.4.1.2 Effect of Admixtures (R42 and SRA)

Retarder R42 and shrinkage admixture SRA were introduced in the AACM mortar mixes M_3 to M_5 for batches (a)**.** The admixtures were not added to batches (b) mixes M_3 to M_5**.**

The presence of retarder and SRA admixtures in the AACM mortar mixes improved the compressive strength. For example, batch a (with admixtures, Fig. 3.21) produced higher strength of 80 MPa compared with 62 MPa for batch b (with no admixtures, Fig. 3.22) under wet/dry curing at activator dilution of 4.12%. The strength increase in batch "a" relative to batch "b" was observed under the three curing regimes although the wet/dry curing shows the greatest effect (Figures 3.21 and 3.22).

Similar results from literature show that a 2% (by mass of binder) dosage of SRA increases the compressive strength by approximately 8% at 28 days for a sodium silicate activated slag paste of liquid/binder ratio 0.5 cured at a temperature of 20 + 2^0C and 99% relative humidity [140]. The reasons proposed by the author [140] were a reduction in the surface tension leading to lesser internal stress when water evaporates and the redistribution of the pore structure by increasing the smaller pores while the larger pores are reduced simultaneously within the AACM concrete matrix.

3.4.1.3 Effect of Liquid/Binder Ratio

The liquid/binder ratios of the AACM mortar mix M_3 were varied between 0.46 and 0.50 to optimise strength and workability. The AACM mortar mix M_3 was selected for this fine-tuning of strength and workability instead of AACM mortar mixes M_2, M_4 and M_5 due to its superior resistance to chloride ingress [132] which is reported in chapter 4. Fig. 3.23 shows the compressive strength of the AACM mortar mix M_3 at liquid/binder ratios 0.46, 0.48 and 0.50 under wet/dry and dry curing alongside published compressive strength results for AACM mortars from other authors all cured under room temperature 20 ± 5^0C and 70 ± 10% R.H. [141][142][143].

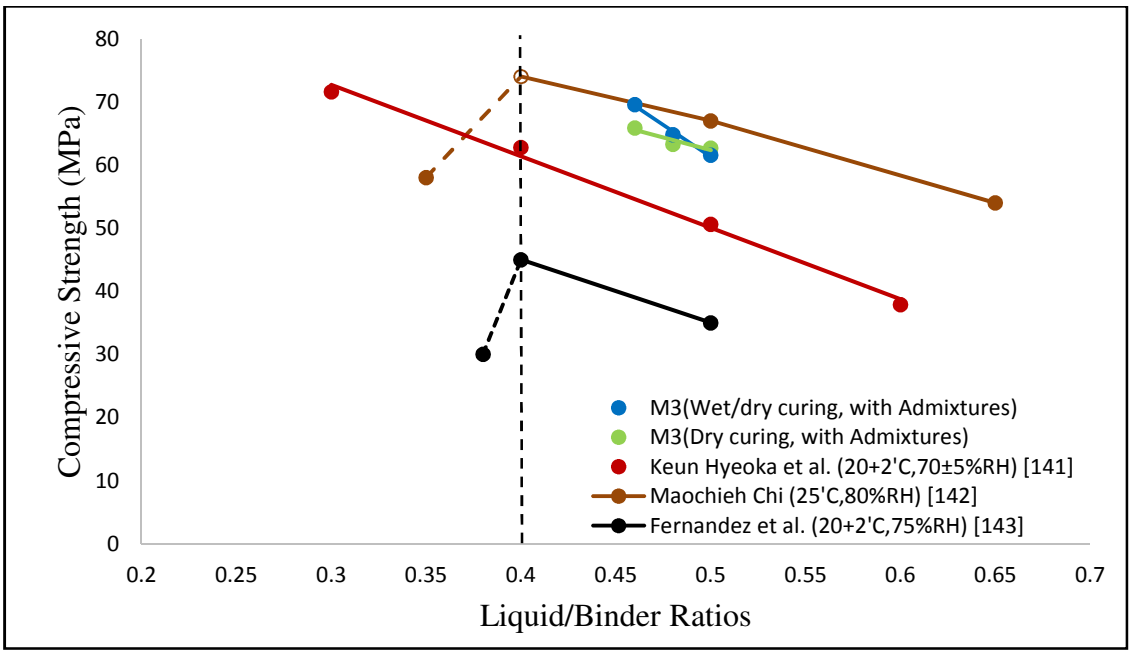

Figure 3. 23*:* Effect of liquid/binder ratio on compressive strength of AACM mortars

The strength of AACM mortar mix M_3 decreases with increasing liquid/binder ratios. The slope of the graph for mix M3 is similar to the graphs representing the data of the other authors [141][142][143]. The strength drops off at liquid/binder ratios under 0.4 in two cases [142][143] due to workability loss resulting in poor compaction. The close range of liquid binder ratios of 0.46 to 0.50 was used in this research work to optimise the strength and workability of mix M_3.

Keun-Hyeoka et al. [141] investigated a wider range of liquid/binder ratios 0.3, 0.4, 0.5 and 0.6 to give compressive strengths of 72 MPa, 63 MPa, 61 MPa and 38 MPa respectively for slag concrete activated by sodium silicate cured under room temperature (20 ± 2^0C) and relative humidity of 70 ± 5%. Another wide range of liquid binder ratios 0.65, 0.50 and 0.35 having compressive strengths of 54 MPa, 67 MPa and 58 MPa respectively were presented by *Maochieh Chi* [142]. The concrete was cured at a room temperature of 25^0C and relative humidity of 80%. The graph of *Maochieh Chi* [142] in Fig. 3.23 gives the highest compressive strength values due to the high temperature of curing (25^0C) compared with the ambient curing temperature of (20 ± 2^0C) adopted by the other researchers.

The results of *Fernandez-Jimenez and Palomo* [143] show the lowest compressive strength values of specimens cured at room temperature (20 ± 2^0C and 75 R.H). The mix composition used by *Maochieh Chi* [142] was 574 Kg/m^3 of class F fly ash, 1581 Kg/m^3 of fine aggregate and 270 Kg/m^3 of sodium silicate and sodium hydroxide activator while the mix details by *Keun-Hyeoka et al.* [141] and *Fernandez-Jimenez and Palomo* [143] were not stated.

The graphs in Fig. 3.23 show a sudden loss of strength at low liquid/binder ratios due to poor workability of mortar or concrete. The explanation for the poor performance at the lowest liquid binder ratio 0.35 (58 MPa) presented by *Maochieh Chi* [142] was an insufficient alkali solution for the formation of crystallized structure. *Fernandez-Jimenez and Palomo* [143] presented results similar to *Maochieh Chi* [142] showing the lowest compressive strength of 30 MPa at lowest liquid binder ratio 0.38. The data from *Maochieh Chi* [142] and *Fernandez-Jimenez and Palomo* [143] show a sharp decline in strength at liquid/binder ratios below 0.4 as seen in Fig. 3.23. The optimum limits for liquid/binder ratios for compressive strength, recommended by *Fernandez-Jimenez and Palomo* [143], are between 0.40 and 0.50. A liquid/binder ratio below 0.40 limits the plasticity of the fresh mortar which results in inadequate consolidation and strength loss.

3.4.1.4 Effect of Curing Regime (Wet/dry, Wet and Dry)

Three curing regimes (wet/dry, wet and dry) were employed for mortar mixes M_2 to M_6. The strengths of batch "a" mixes (with admixtures) are shown in Figures 3.21 and 3.24, while the batch "b" mixes (with no admixtures) are represented in Figures 3.22 and 3.25. The significance of applying practical curing methods (wet/dry, wet and dry) is to investigate strength performance under these curing conditions. These curing methods are often applied in the field application. The shrinkage reducing admixture SRA and retarder R42 will equally influence the concrete mechanical properties.

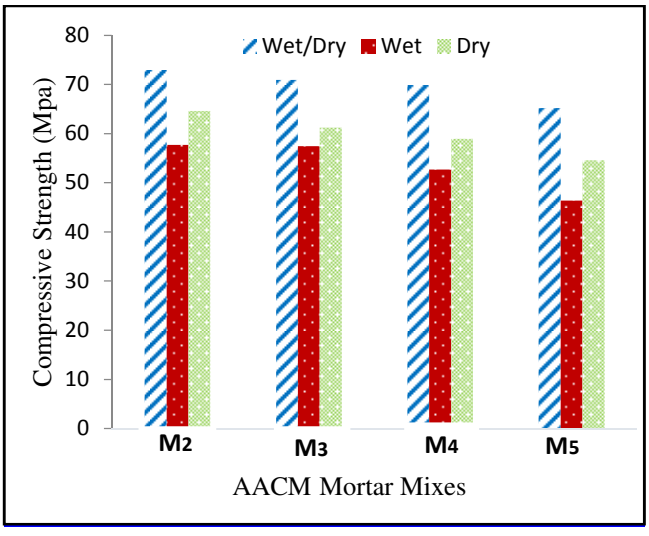

Figure 3. 24: Compressive strength of AACM and OPC mortar batch "a" mixes with admixtures

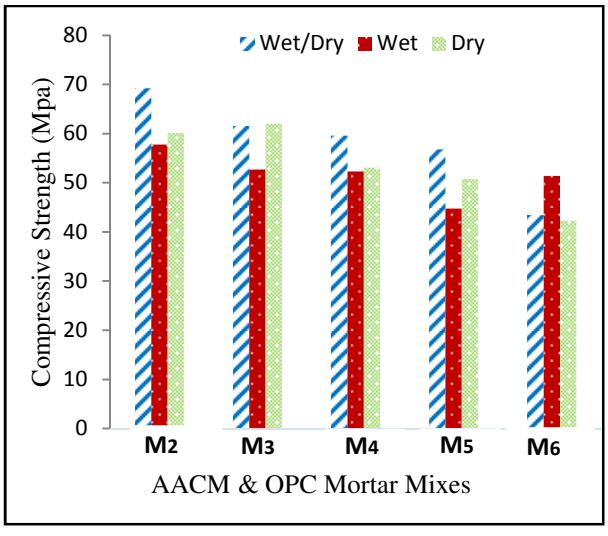

Figure 3. 25: Compressive strength of AACM and OPC mortar batch "b" mixes without admixtures

For AACM mortar mixes M_2 to M_5, the wet/dry curing which is 3 days in water at 20 ± 2^0C followed by 25 days in the laboratory air (20 ± 2^0C, 65% R.H.) had the

highest compressive strength for both batches (a) and (b) mixes as shown in Figures 3.24 and 3.25. This was followed by dry curing (28 days curing in laboratory air at 20 ± 2^0C, 65% R.H.). The least compressive strength was recorded for wet curing (28 days curing in water at 20 ± 2^0C).

Arie at al., [144] achieved a compressive strength of 63 MPa under moist curing at a temperature of 20 ± 2^0C for a slag/fly ash AACM mortar blend, other researchers presented compressive strength as high as 100 MPa for fly ash-based AACM mortar at elevated temperature curing (50-80^{0}C) [26][145][146]. Heat treatment is required for fly ash-based AACM mortar to synthesize. The beneficial effect of heat curing is the increased pozzolanic reactions in geopolymer concrete when compared with ambient temperature curing. Whilst it may be practicable to expose specimens of geopolymer to heat curing in the laboratory, it is impractical on construction sites.

The effect of curing conditions on OPC mortar contrasts the AACM mortars by providing the maximum compressive strength under wet curing. The availability of moisture in OPC concrete supports cement hydration which produces strength. The geopolymer reactions in AACMs do not rely on moisture as OPC. The OPC mortar mix M_6 recorded the highest compressive strength of 51 MPa (Fig. 3.25) under wet curing followed by 43 MPa for wet-dry curing, which is slightly higher than 42 MPa for dry curing as shown in Fig. 3.25. The results of OPC mortar mix M_6 are consistent with the work of other researchers which also show a similar effect of curing conditions on strength of OPC concrete [147][148]. The relative humidity of moisture in the OPC capillary pores is maintained above 80% when cured in water, which favours hydration reactions [25]. There will be little loss of moisture when OPC concrete is cured in any medium above 80% R.H., hence curing in water may not be needed for continuing hydration.

3.4.2 Classification of Pore Size Distribution

3.4.2.1 Unimodal and Bimodal Pore Distribution

The distribution of pore sizes in AACM and OPC mortar mixes was determined from the differential pore volume graphs under wet/dry, wet and dry curing as shown in Figures 3.26, 3.27 and 3.28 respectively**.** The results of two AACM mortar mixes M_2 (2.15% activator dilution) and M_5 (12% activator dilution) alongside the OPC mortar mix M_6 are presented. All mixes were without the admixtures R42 and SRA. AACM mixes M_3 and M_4 provide similar results as mixes M_2 and M_5, which are recorded in Appendix 3.2(a - d).

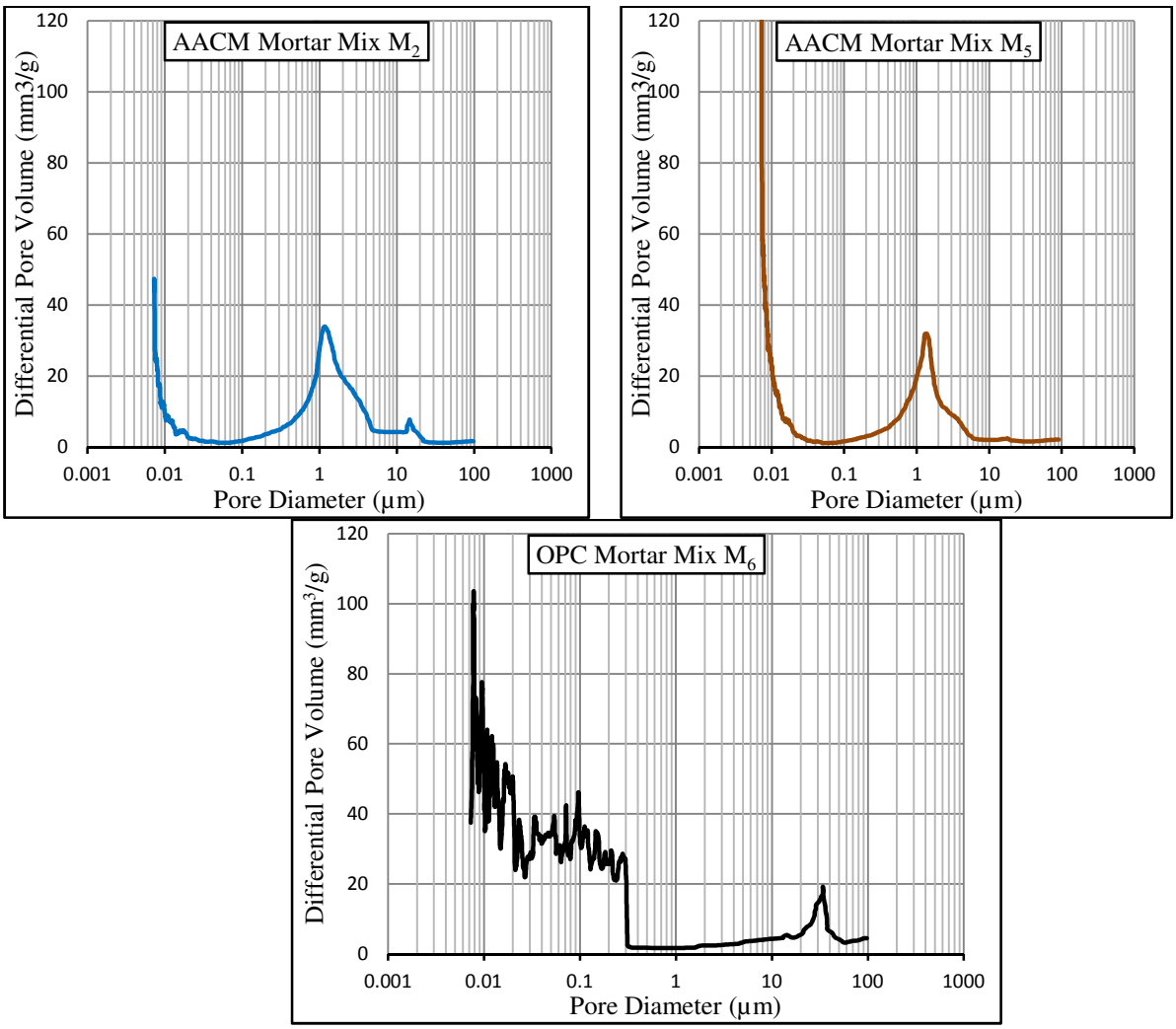

Figure 3. 26: Pore size distribution for AACM and OPC mixes without admixtures under wet/dry curing

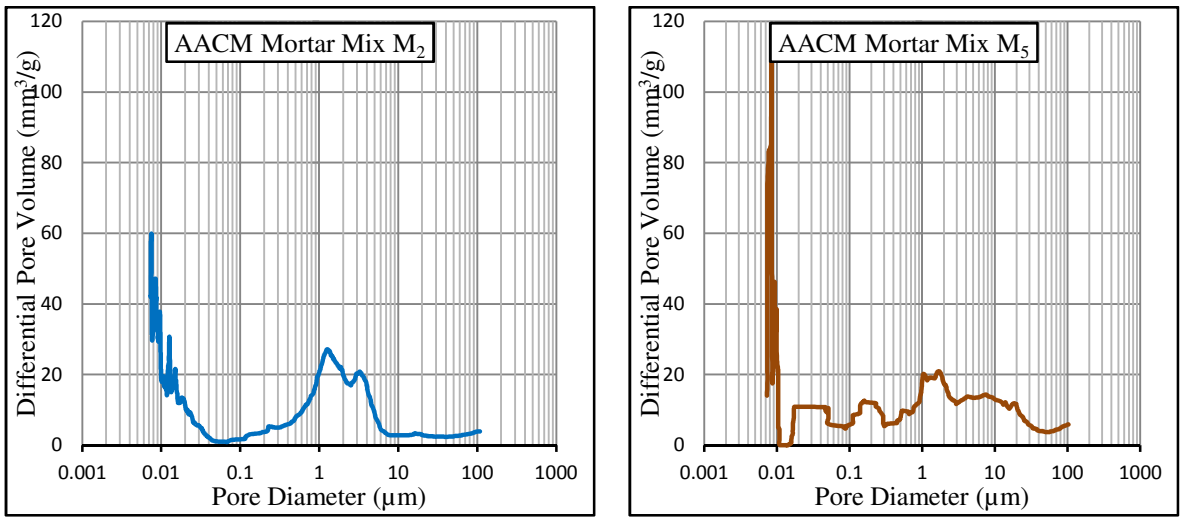

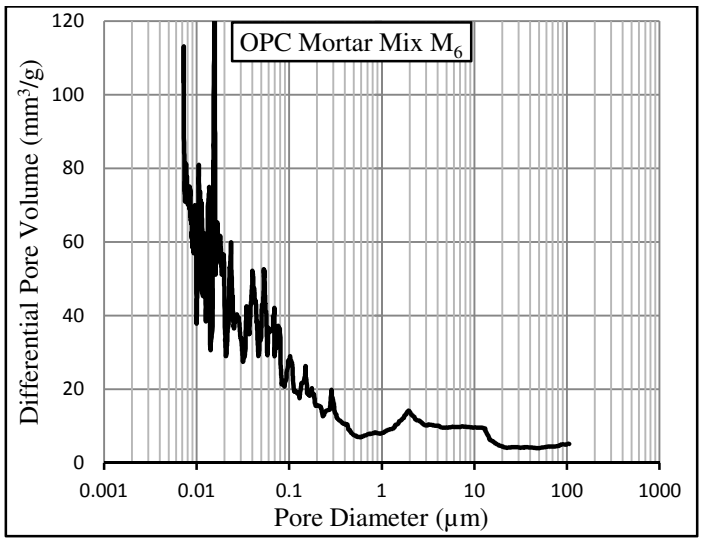

Figure 3. 27: Pore size distribution for AACM and OPC mixes without admixtures under wet curing

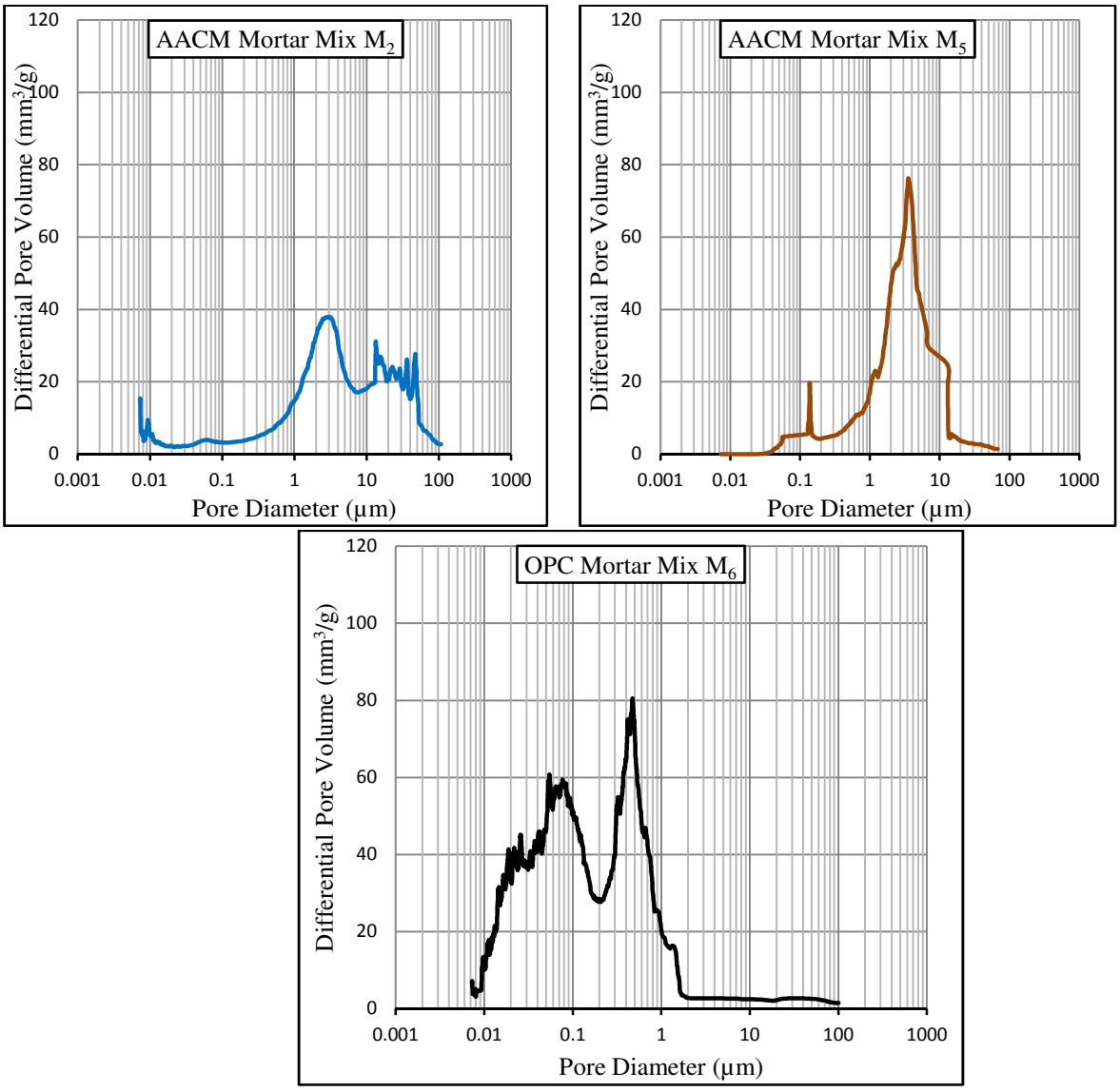

Figure 3. 28: Pore size distribution for AACM and OPC mixes without admixtures under dry curing

A unimodal pore distribution in OPC mortar is defined by the single range of pore volumes observed within the differential pore distribution graphs for OPC mortar shown in Figures 3.26, 3.27 and 3.28. Other studies on the microstructure of OPC matrix also show a unimodal pore size distribution with most of the pore volume within the range of 0.01 to 0.1 µm pore diameter [3][82]. However, under dry curing, OPC mortar also shows the presence of pore diameters up to 1 µm.

A bimodal pore distribution in AACM mortar, on the other hand, is defined by the double range of pore volume observed within the differential pore distribution graphs in Figures 3.26, 3.27 and 3.28 for the AACM mixes. These pore sizes are normally observed between two separate zones of > 1 µm and <0.02 µm [3]. The results of this investigation in Figures 3.26, 3.27 and 3.28 show AACM mortar falls under this category with significant porosity observed at > 1 µm and <0.02 µm while there is little porosity between these pore size ranges. AACM mixes with admixtures show similar bimodal pore distribution which will be discussed in section 3.4.2.2.4.

3.4.2.1.1 Wet/dry Curing

The pore sizes in AACM mortar mixes under wet/dry curing presented in Fig. 3.26 show a bimodal pore size distribution. The first range of pore sizes in the AACM mortar mix M_2 is <0.02 µm pore diameter while the second range is predominantly > 0.2 µm. AACM mortar mix M_5 shows similar trend of bimodal pore distribution, the pore sizes range from under 0.03 µm and greater than 0.2 µm. The OPC mortar mix M_6 shows a unimodal pore size distribution (Fig. 3.26) within the approximate range of 0.01 to 0.3 µm. The bimodal distribution of pores in AACM mortar mixes M_2 and M_5 has a larger maximum pore diameter than the OPC mortar M_6.

3.4.2.1.2 Wet Curing

The bimodal pore size distribution in AACM mortar mix M_5 is less pronounced under wet curing (Fig. 3.27) than under wet/dry (Fig. 3.26) or dry curing (Fig. 3.28) due to its highest activator dilution. There is significant continuity of differential pore volume above pore diameters 0.01 µm which do not appear under both wet/dry and dry curing. There is the possibility of interconnection of pores in wet cured AACM mortar mix M_5 (12% activator dilution) between the gel pores (0.005 to 0.01 µm) and capillary pores (0.01 to 100 µm) which provides continuity to the pores. The interconnection is represented by the distribution of peaks throughout the range of pore sizes 0.01 to 100 µm. The less geopolymerisation product formed in AACM mortar mix M_5 due to its higher activator dilution are likely to cause interconnected capillary pores. This leads to

vulnerability of the wet cured AACM mortar mix M_5 to greater permeability of harmful ionic elements like Cl^-, CO_2 and sulphate [132].

AACM mortar mix M_2 which has a lower degree of activator dilution (2.15%), on the other hand, shows the typical bimodal distribution similar to that observed under wet/dry curing in Fig. 3.26.

3.4.2.1.3 Dry curing

AACM mortar mixes M_2 and M_5 under dry curing (Fig. 3.28) show a bimodal pore size distribution similar to wet/dry curing. The first range of pores in AACM mortar mix M_2 are less than 0.01 µm while the second range of the bimodal pore size distribution is greater than 1 µm. AACM mortar mix M_5 has a coarser pore range of less than 0.2 µm and greater than 1 µm. OPC mortar mix M_6 revealed a unimodal pore distribution between 0.01 µm to approximately 2 µm, the pore size range is slightly higher compared to wet/dry and wet curing.

3.4.2.2 Gel and Capillary Pore Volumes

The total pore volumes within the AACM and OPC mortars were determined from the cumulative pore volume curves under wet/dry, wet and dry curing, which are shown in Appendix 3.1 (a -c) respectively. Fig. 3.29 shows the total pore volume of AACM and OPC mortar mixes under the three types of curing. Only AACM mortar mixes M_2 and M_5 are considered in this section.

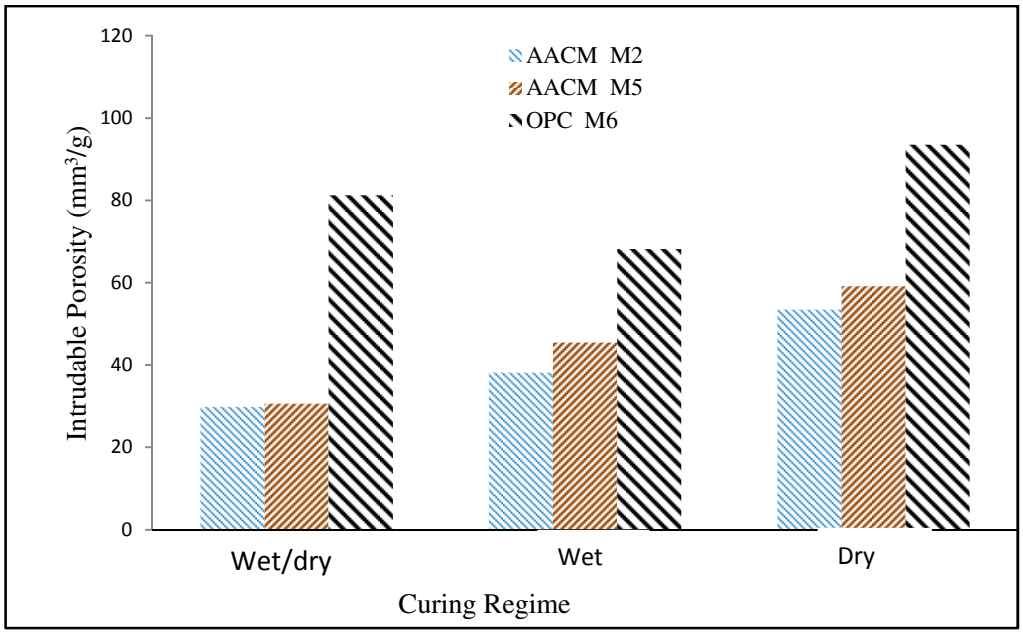

Figure 3. 29: Intrudable porosity for AACM and OPC mixes without admixtures under wet/dry, wet and dry curing

3.4.2.2.1 Wet/dry curing

AACM mortar mix M_2 had a lower pore volume of 29.82 mm^3/g compared with 81.21 mm^3/g for the OPC mortar mix M_6 as shown in Fig. 3.29. The application of wet/dry curing to AACM concrete was observed to enhance its resistance to chloride ingress under prolonged exposure to salt laden environment which is reported in chapter 4, section 4.4.3. The resistance of heat cured AACM mortar to chloride penetration is best achieved when it is initially subjected to adequate wet curing before the application of external heat source [149]. The 3 days initial wet curing under the wet/dry curing method (Table 3.5) used in this research project provided the much-needed moisture to improve particle packing [149] around the aggregates in the AACMs. This together with the geopolymer reactions resulted in lower pore volume when compared to the OPC mortar at later ages.

The pore volume for AACM mortar mix M_2 (2.15% activator dilution) is slightly less than AACM mortar mix M_5 (12% activator dilution). The pore volume in AACM mortar mix M_2 is 29.82 mm^3/g while it is 30.60 mm^3/g for AACM mortar mix M_5 under wet/dry curing as shown in Fig. 3.29. The higher activator dilution of 12% in AACM mortar mix M_5 under wet/dry curing reveals almost the same pore refinement as AACM mortar mix M_2 with 2.15% activator dilution.

3.4.2.2.2 Wet curing

The wet curing of OPC mortar resulted in a pore volume of 68.16mm^3/g compared with 81.21 mm^3/g and 93.51 mm^3/g for wet/dry and dry curing respectively (Fig. 3.29). The wet curing method normally provides the best mechanical and durability properties to OPC concrete. The saturation of OPC mortar pore spaces with water supports cement hydration. The hydration is greatly reduced when the relative humidity within the capillary pores drops below 80% [60][61]. Since both the wet/dry and dry curing methods exposed the specimens to laboratory air curing at relative humidity of 65% before cement paste hydration was completed, the result was a slow hydration rate with more pores than under wet curing. This is more prominent under dry curing (Fig. 3.29) than wet/dry curing because of the lack of wet curing at a very early stage.

The pore volume of AACM mortar mix M_2 under wet curing is greater than under wet/dry curing (Fig. 3.29). The intrudable pore volume under wet curing of 38.14 mm^3/g is higher than 29.82 mm^3/g under wet/dry curing. AACM mortar mix M_5 shows a similarly higher pore volume under wet curing (Fig. 3.29). The OPC mortar mix M_6

on the contrary, has a lower pore volume under wet curing (68.16 mm^3/g) compared to wet/dry curing (81.21 mm^3/g). The wet curing favoured the hydration process of OPC mortar resulting in lower pore volume.

3.4.2.2.3 Dry curing

AACM mortar mix M_5, under dry curing, has pore volume of 59.13 mm^3/g compared with 93.51 mm^3/g for the OPC mortar mix M_6 under the same dry curing (Fig. 3.29). The results presented in Fig. 3.29 show that AACM mortars possess significantly less pore volume than OPC mortars under the three curing methods. This suggests AACM mortar contains less pore spaces accessible by mercury than OPC mortar. Since the dimensions and mass of all test samples are within the same range (Table 3.6), the effect of hysteresis and entrapment will be minimal [137]. The pore volume of the OPC mortar mix M_6 is higher than the AACM mortar mixes for all curing conditions.

RILEM TC 224-AAM [3] reported that the total pore volume (i.e. summation of both gel and capillary pores) of AACM is somewhat similar or sometimes higher than comparative OPC. On the contrary, the results of this study show that the total intruded pore volume was higher in OPC mortar than in AACM mortar. Nevertheless, a higher capillary pore volume (0.01 to 100 µm) was observed in AACM mortar than OPC mortar, while the gel pore volume (0.0073 to 0.01 µm) was much lower in AACM mortar. For example, AACM mortar mixes M_2 and M_5 under wet/dry curing (Fig. 3.23) have a higher capillary pore volume compared to OPC mortar mix under the same wet/dry curing as shown later in section 3.4.3.4.4.

3.4.2.2.4 Effect of admixtures

The distribution of pore sizes of batch "a" mixes (with admixtures) are presented in Fig. 3.30. The corresponding data for batch "b" mixes (without admixtures) are plotted in Fig. 3.31. The specimens under wet/dry curing were only considered amongst the three curing methods employed due to the optimal performance of AACM mixes under this curing condition as discussed later in section 3.4.3.2. The graphs for other curing conditions are shown in Appendix 3.2 (a-d), which is similar to Figures 3.30 and 3.31.

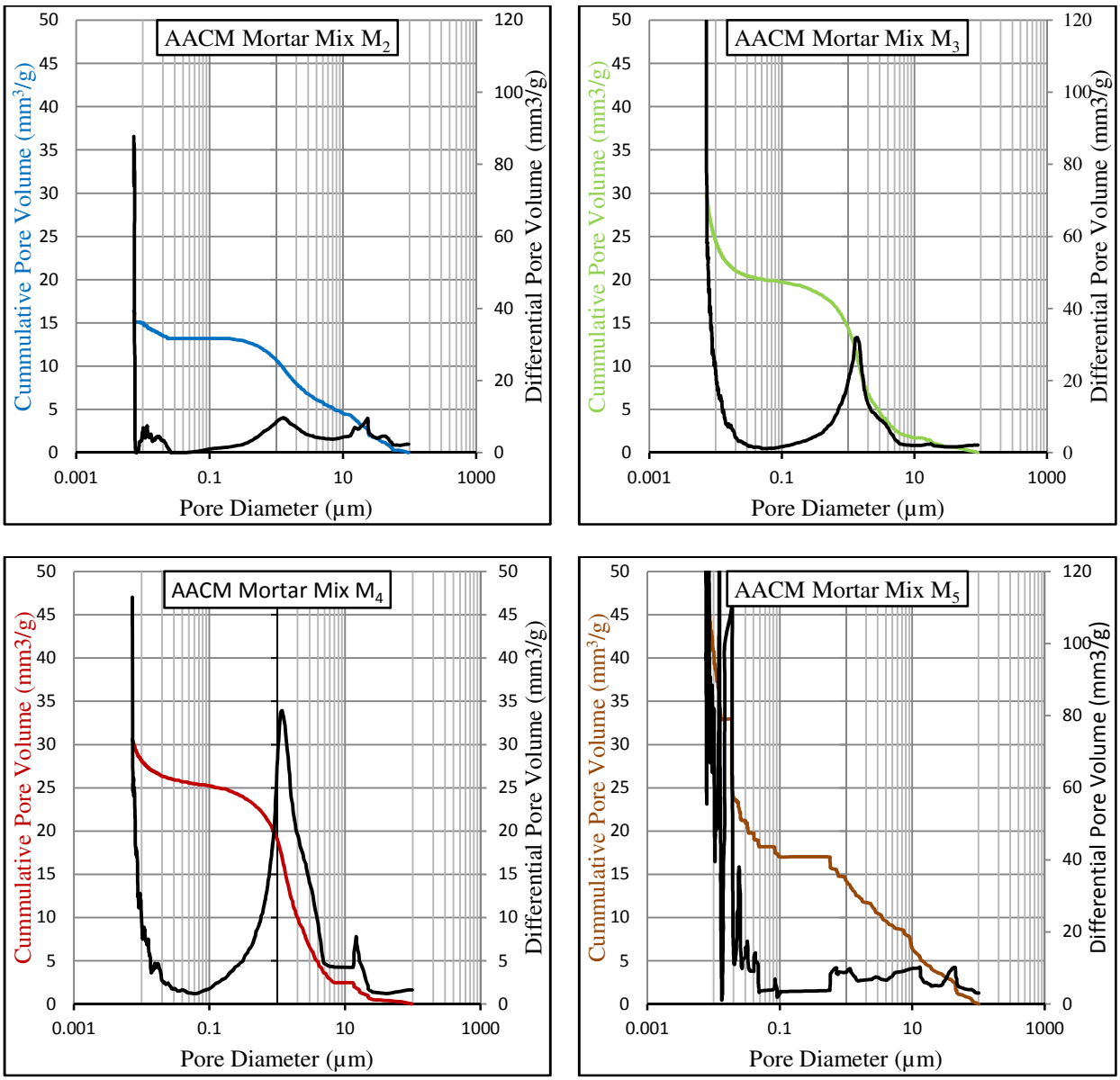

Figure 3. 30: Pore size distribution of AACM mortar mixes (with admixtures) under wet/dry curing

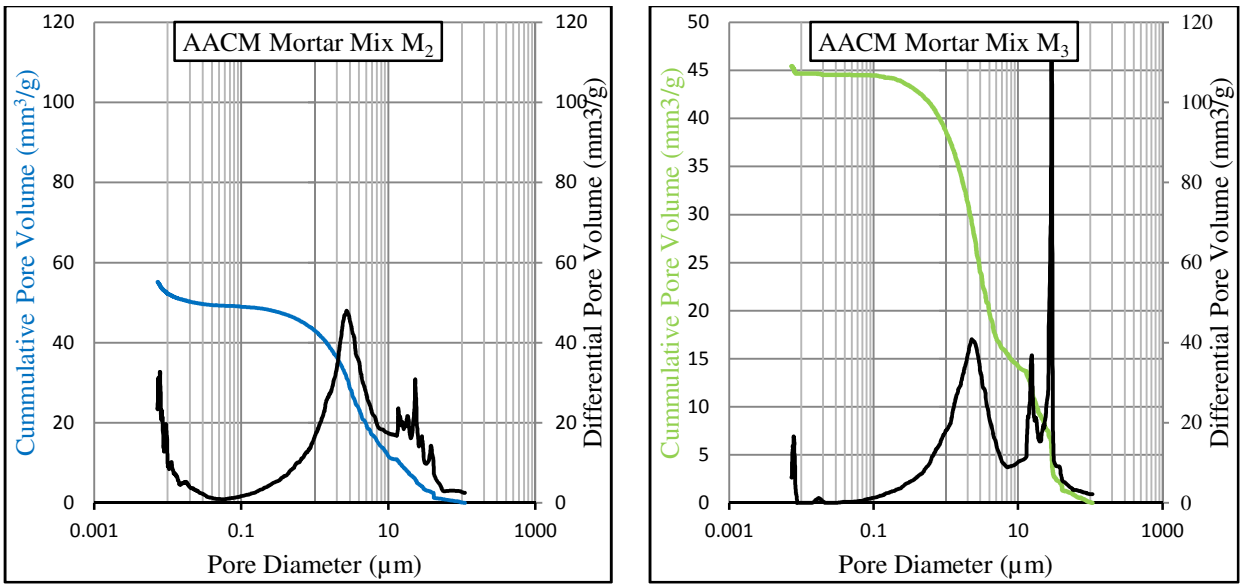

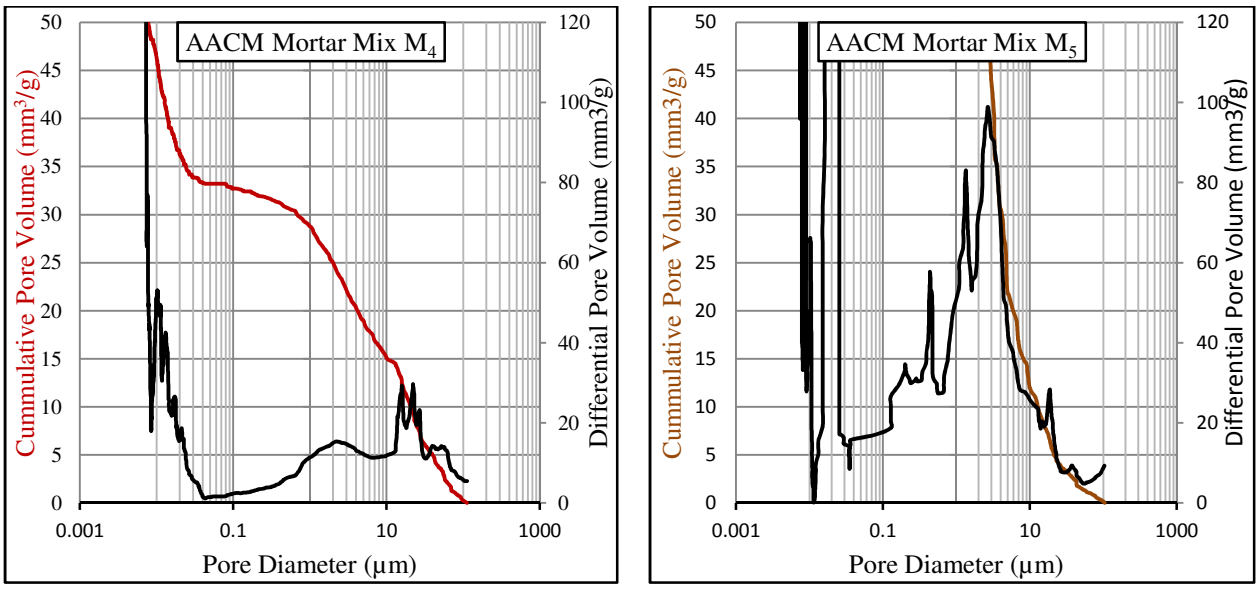

Figure 3. 31: Pore size distribution of AACM mortar mixes (without admixtures) under wet/dry curing

The introduction of chemical admixtures in AACM mortar reduces the pore sizes as shown in Figures 3.30 and 3.31. The reduction indicates significant pore refinement when admixtures were added in the AACM mortar mixes M_2 to M_5. Chemical admixtures (R42 and SRA) induce a better distribution of cementitious particles consequently leading to better hydration [152]. Similarly, the inclusion of polycarboxylate admixture in OPC cement paste has shown significant reduction in total porosity after 2 days of hydration and the pore structure becomes more refined by the rise in the percentage of gel pores and a decrease in the capillary pore sizes [152].

However, *RILEM TC 224-AAM* [3] report reveals inconsistencies in the rheological properties as well as the hydration process of AACMs by the addition of most available admixtures designed for Portland cement-based materials. The differences in the chemistry of AACM materials compared with OPC based materials, in particular the high pH obtained during the synthesis of most alkali-activated binders, is likely to account for such differences in their rheological properties and activation process.

The volume of pores is reduced under the combined influence of admixture and a lower activator dilution. For instance, batch "a" (with admixture) displayed a lower pore volume which is 15 mm^3/g for mix M_2 (Fig. 3.30) compared with batch "b" (without admixture) which is 57 mm^3/g for mix M_2 (Fig. 3.31). Similarly, AACM mortar with lower activator dilution (2.15%) has the lowest pore volume of 15 mm^3/g compared with 46 mm^3/g for AACM mortar with highest activator dilution (12%) as seen in Fig. 3.30. The porosity results indicated that the permeability of AACM mortars

is reduced by the inclusion of chemical admixtures (R42 and SRA) and by lower activator dilution.

3.4.3 Pore System Parameters

The pore system parameters were derived from the cumulative porosity curve and logarithmic differential pore volume curves as discussed in section 3.2.3. These parameters are classified as intrudable porosity $\boldsymbol{\Phi_{in}}$, critical pore diameter $\boldsymbol{d_c}$ and threshold pore diameter $\boldsymbol{d_{th}}$ and their location on the curves is shown in Figures 3.4 and 3.5 for OPC and AACM mortar respectively. The location of $\boldsymbol{\Phi_{in}}$ on the cumulative pore volume curve is similar for both OPC and AACM mortars (Figures 3.4 and 3.5). The location of $\boldsymbol{d_c}$ and $\boldsymbol{d_{th}}$ is different with both values representing larger pore volumes for AACM mortars. Mercury intrusion porosimetry tests were performed on two samples per mix and their average results were calculated.

3.4.3.1 Intrudable Porosity Φ_{in}

The Intrudable porosity $\boldsymbol{\Phi_{in}}$ is obtained by reading the highest point on the cumulative porosity curve. This corresponds to the lowest equivalent diameter on the cumulative porosity curve. The influence of activator dilution, admixtures, liquid/binder ratio and different curing regime (wet/dry, wet and dry) on the the intrudable porosity $\boldsymbol{\Phi_{in}}$ was determined. The intrudable porosity $\boldsymbol{\Phi_{in}}$ values which were derived from the highest point of the cumulative porosity curves are presented in Appendix 4.3 (a-f) for all mixes. The liquid/binder of the mixes was 0.48 except mix M_2 (2.15% dilution) for which it was 0.41.

3.4.3.1.1 Effect of activator dilution

The influence of activator dilution on the intruded pore volume is presented in Figures 3.32 and 3.33.

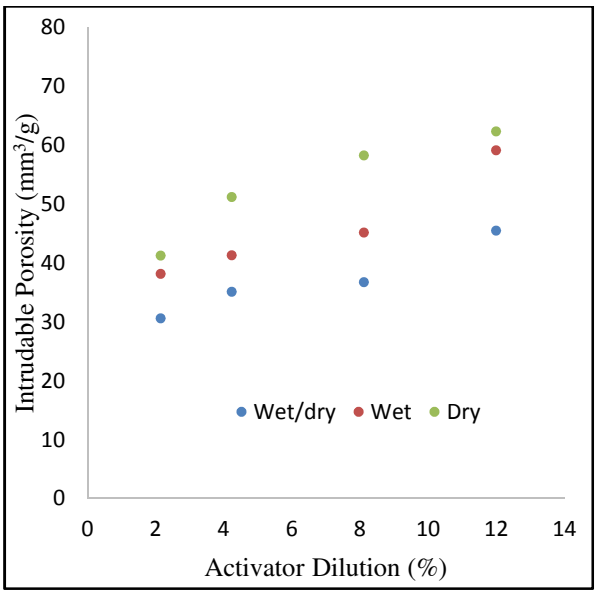

Figure 3. 32: Intrudable porosity of AACM mortar batch "a" mix with admixtures

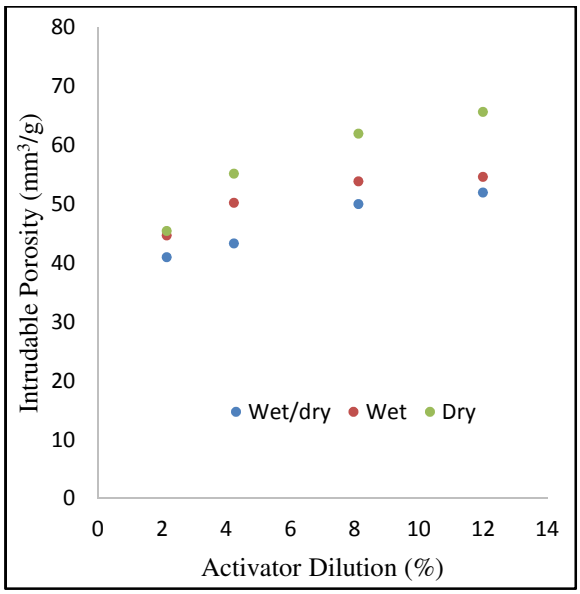

Figure 3. 33: Intrudable porosity of AACM mortar batch "b" mix withot admixtures

Figures 3.32 and 3.33 show that the intrudable porosity increases as the activator dilution increases. The increase in activator dilution reduces the pore refinement of the mortar matrix.

A gas sorption analysis was performed on a fly-ash based AACM system to study the influence of activator concentration [153][154]. The authors observed pore refinement of the fly-ash based alkali activated material with an increase in the activator concentration which is similar to results obtained from this study. A high dosage of activator improves the pore refinement of AACM mortar [89].

3.4.3.1.2 Effect of admixtures (R42 and SRA)

The intruded pore volume of mixes with and without admixtures (R42 and SRA) is shown in Figures 3.32 and 3.33 respectively**.** A lower intruded pore volume was observed in batch "a" mixes (with admixtures) compared with batch "b" mixes (without admixtures). This could be due to the modified crystal growth or morphology produced by the admixtures [3]. A similar modification was observed in the microstructure of OPC pastes when 1% polycarboxylate retarding admixture was used, which resulted in a slight reduction in the porosity [152]. A similar reduction in the total intrudable pore volume of cement paste by inclusion of admixtures was observed [155].

The beneficial influence of the shrinkage reducing agent SRA is explained by two factors, firstly, the reduction of surface tension of water present in the pore system leading to smaller internal stress when water evaporates and secondly, the redistribution of cement particle due to the decreased capillary stress of water induced during the

mixing process [156]. On the other hand, the retarder reduces the reaction rate of tricalcium silicate with water, thereby, impeding the early growth of calcium hydroxide in OPC concrete. During the delayed growth of calcium hydroxide, which is the hydration product, realignment of cement particles occurs in the concrete matrix to form a denser pore structure [157]. The admixture R42 has a similar retarding effect on the early age reactions of the AACMs, which slow down its setting and hardening process. However, the chemical processes involved are not clear at present.

3.4.3.1.3 Effect of curing

The lowest intruded pore volumes in batches "a" and "b" occur under wet/dry curing, followed by wet curing and then dry curing (Figures 3.32 and 3.33). The combined influences of admixtures and wet/dry curing have a more beneficial effect on the pore structure than either wet or dry curing. This is due to the high volume of pore blocking effect induced by wet/dry curing regime. Figures 3.32 and 3.33 show that the intrudable porosity under dry curing is highest at all activator dilution values. This is contrary to the results on compressive strength (section 3.4.1.1) which show higher strengths achieved by AACMs under dry curing compared to wet curing. For example, AACM mortar M_2 batch "a" (with admixtures) had intruded porosity of 30.60 mm^3/g, 38.14 mm^3/g and 53.44mm^3/g for wet/dry, wet and dry curing respectively (Fig 3.32) while their corresponding strengths are 73 MPa, 58 MPa and 65 MPa respectively (Fig 3.24).

The availability of water during early age allows for more hydration to take place in concrete containing mineral admixtures. This results in the formation of more calcium silicate gel [134]. In the case of supplementary cementitious materials, reduction of pore spaces occurs with wet/dry curing. Research results from *Khatib and Mangat* [134] agree with the reduction of pore spaces when wet/dry curing is employed for cement pastes with 22% and 9% replacement with fly ash and silica fume. The authors [134] adopted 14 days moist curing after casting followed by air curing at 45^0C and 25% relative humidity for further 14 days. This phenomenon may be applicable to AACM concrete where fewer pores are produced under wet curing at early age due to initial hydration reactions which proceed along with geopolymerisation reactions.

3.4.3.1.3 Effect of liquid/binder ratio

The intruded pore volumes for AACM mortar mix M_3 with three liquid/binder ratios of 0.46, 0.48 and 0.50 are presented in Fig 3.34. The intrudable porosity was obtained from the graphs of cumulative pore volume presented in Appendix 3.4 (a-c).

The AACM mortar mixes were subjected to curing regimes wet/dry, wet and dry. Despite the small range of liquid/binder ratios (0.46 - 0.50), a clear linear relationship is observed with the intrudable porosity as shown by the best-fit regression lines plotted in Fig 3.34.

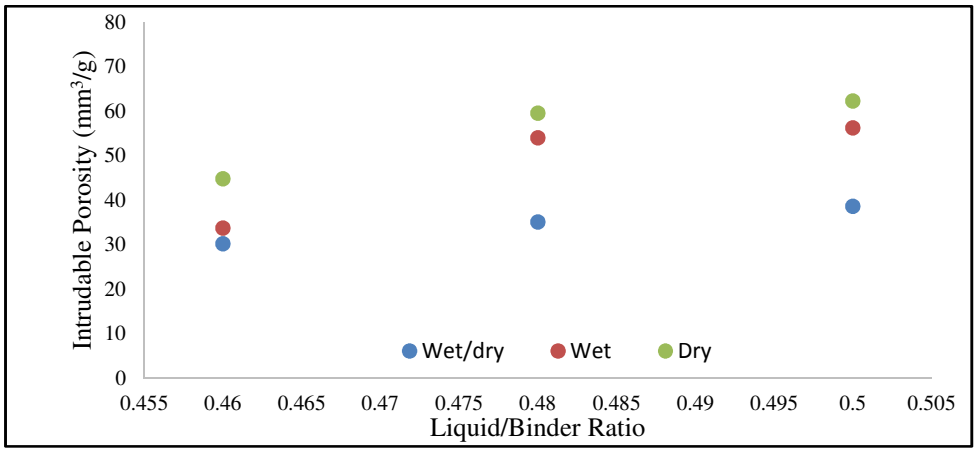

Figure 3. 34: Relationship between liquid/binder ratio and intruded pore volume of AACM mortar mix M_3 (with admixtures)

Liquid/binder ratio 0.46 had the lowest intruded pore volume of 30.23 mm^3/g compared with 38.63 mm^3/g at liquid binder ratio 0.5 under wet/dry curing.

The lowest intruded pore volumes were recorded for wet/dry curing, followed by wet curing and lastly dry curing for the AACM mortar M_3 as shown in Fig 3.34, each curing condition showing a linear relationship between liquid/binder ratio and porosity. This relationship is similar to the strength-liquid/binder ratio relationships discussed in section 3.4.1.3 except the contradictory effect of wet and dry curing on the relationships. It has been suggested that the reason for lesser intruded pore volume in hardened cement paste with low water/cement ratio is the smaller distances between unhydrated cement grains [126].

3.4.3.2 Critical Pore Diameter d_c

The tortuosity and randomness of interconnected pores of AACM and OPC mortars M_2 to M_6 are determined by the critical pore diameter $\boldsymbol{d_c}$. This represents the extent to which these pores are connected to each other. The influence of parameters such as activator dilution, admixtures, liquid/binder ratio and curing regime on the critical pore diameter $\boldsymbol{d_c}$ was analysed, similar to intrudable porosity $\boldsymbol{\Phi_{in}}$. The first highest point on the logarithmic differential pore volume curve (pore diameter versus dv/dlogD curve) is considered as the critical pore diameter $\boldsymbol{d_c}$ as shown in Figures 3.4 and 3.5, discussed in section 3.2.3.

3.4.3.2.1 Effect of activator dilution

Four levels of activator dilution of 2.15%, 4.24%, 8.12% and 12.00% were adopted for the AACM mortar mixes M_2, M_3, M_4 and M_5 respectively. Their critical pore diameters $\boldsymbol{d_c}$ were obtained from the differential pore volume graphs under wet/dry (Fig. 4.31), wet (Appendix 3.2a) and dry curing (Appendix 3.2c) respectively. The critical pore diameter $\boldsymbol{d_c}$ is plotted against activator dilution in Fig. 3.35.

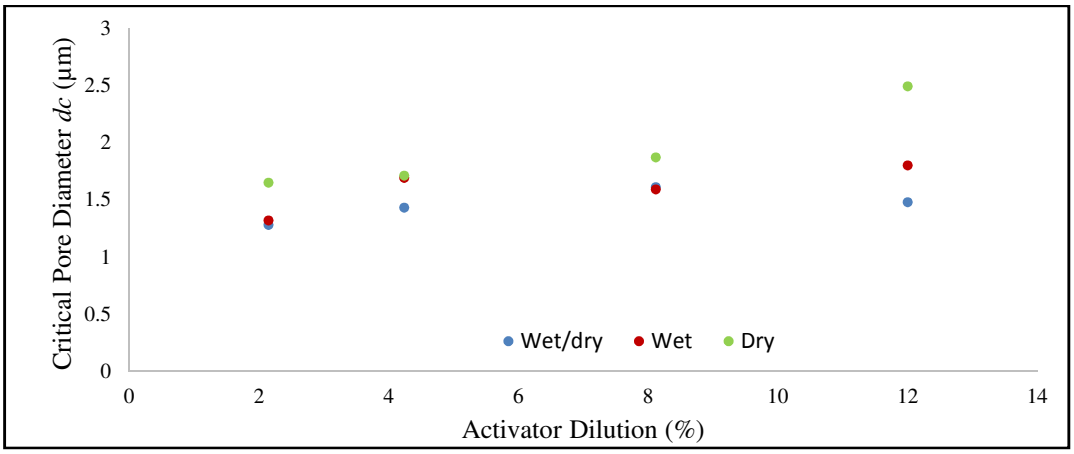

Figure 3. 35: Effect of activator dilution on the critical pore diameters (with admixtures)

The dilution of alkali activator increases the critical pore volume $\boldsymbol{d_c}$ as shown in Fig. 3.35**.** This pattern is similar for the three curing regimes wet/dry, wet and dry although the slope of the dry cured graph is significantly steeper. The increase in the critical pore diameter $\boldsymbol{d_c}$ within the AACM mortar matrix leads to greater diffusion of deleterious substances such as chlorides and sulphates. The durability properties of AACM mortars are, thereby, impaired by higher critical pore diameter $\boldsymbol{d_c}$ produced by the dilution of alkali activator.

The highest critical pore diameters $\boldsymbol{d_c}$ were observed under dry curing as shown in Fig. 3.35. The combined effect of 3 days wet curing followed by the 25 days dry curing (wet/dry curing) improved the crystallinity and pore structure of AACM mortar leading to superior mechanical and durability properties compared to dry curing, as shown in chapter 4.

The pore size distribution of capillary pores in AACM mortar determines its permeability to deleterious elements such as chlorides and sulphates [82] while the gel/space ratio determines the strength properties of the cementitious materials [25]. Consequently, the influence of activator dilution on $\boldsymbol{d_c}$ is likely to have greater impact on the durability properties of AACM mortar rather than its mechanical strength. In conclusion, the wet/dry curing displayed the best result for the critical pore diameter $\boldsymbol{d_c}$ followed by wet curing and lastly dry curing for AACM mortar.

3.4.3.2.2 Effect of admixtures

The critical pore diameter d_c under wet/dry curing plotted against activator dilution is shown in Figures 3.36 for batch "a" (with admixtures) and batch "b" (without admixtures). The critical pore diameters d_c is derived from the differential pore volume curves presented in Figures 3.30 and 3.31 respectively.

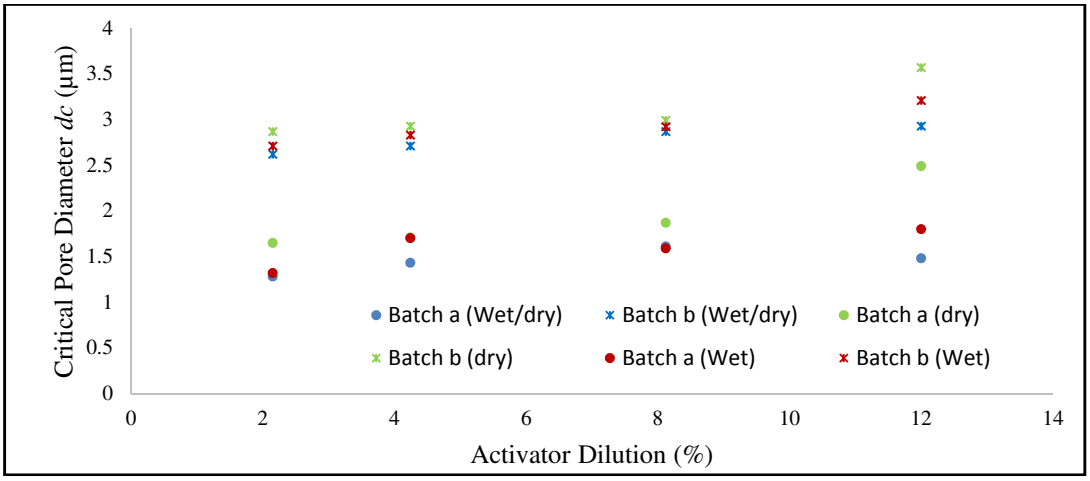

Figure 3. 36: Effect of admixtures (R42 and SRA) on the critical pore diameters of AACM mixes under wet/dry curing.

Batch "a" (with admixtures) possesses lower critical pore diameter d_c than batch "b" (without admixtures). The presence of admixtures (R42 and SRA) in AACM mortar mixes M_2 to M_5 resulted in a lower critical diameter d_c.

The effect of SRA on cement based materials has a positive impact on the capillary porosity depercolation. The diffusivity of fluid and ions is impeded within the mortar matrix when its connecting capillary pores are depercolated, thus improving its durability properties. An increase in the capillary pore depercolation was observed in cement paste by the addition of water reducing admixture (HRWRA, Glenium 3000NS) [158]. Also, 5% by mass of shrinkage-reducing admixture (SRA, Tetraguard AS20) was added to a mix of water/cement ratios 0.3 and 0.5 and OPC content of 360 Kg/m^2, which was cured for 7 days at a temperature of 20^{0}C in lime water. The authors [158] observed a significant reduction of capillary porosity by around 15% – 25% in the OPC paste containing the chemical admixtures compared with cement paste without admixtures. The pore discontinuity (depercolation) within the paste matrix was also observed using low temperature calorimetry (LTC) and electrical impedance spectroscopy techniques. These observations validate the depercolation of intrudable porosity caused by admixtures in concrete, which was proposed by *Bentz and Edward* [113] as discussed in section 3.2.3.1.

On the other hand, *Craeye et al.,* [159] studied the effect of polycarboxylate admixture on the critical pore diameters of self-compacting concrete (SCC) and observed no significant difference between SCC mixes containing the admixture and those without it. The authors concluded that it is not clear if the admixtures have any influence on the concrete microstructure.

3.4.3.2.3 Effect of liquid/binder ratio

The critical pore diameters $\boldsymbol{d_c}$ for AACM mortar mixes M_3 containing three liquid/binder ratios of 0.46, 0.48 and 0.50 were obtained from Appendix 3.5 (a-c). The mixes were subjected to curing regimes wet/dry, wet and dry. The results in Fig. 3.37 show a significant influence of liquid/binder ratio on the critical pore diameter $\boldsymbol{d_c}$ under the three curing regimes.

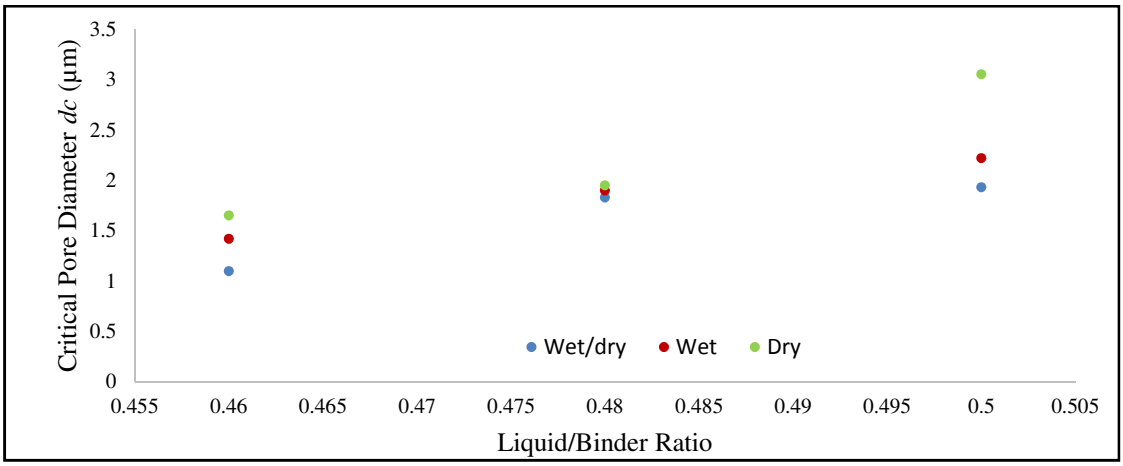

Figure 3. 37: Relationship between liquid/binder ratio and critical pore diameter d_c of AACM mortar mix M_3 (with admixtures)

Depercolation of open pore spaces during geopolymerisation of the gel paste is highest at the lowest liquid binder ratio 0.46. A possible explanation could be that the faster closing of the pore spacing between the binder particles is aided by a lower amount of liquid content present in the mix. These observations are consistent with those of OPC concrete [160]. The gel hydration products of OPC pastes at lower water/cement ratio occupy greater pore spaces that could otherwise have been water-filled spaces. Therefore, water/cement ratio influences the connectivity of cement paste pores. This impacts the overall durability of concrete.

Zeolite formation is the structural framework which has the controlling capacity for the polycondensation and crystal growth in AACMs. In order to maintain a constant molar ratio of H_2O to Na_2O in a fly ash based geopolymer concrete, both the activator concentration and water content was increased but no significant effect was observed on the compressive strength [46]. In other words, the higher molar ratio of Na_2O/SiO_2

(activator concentration) had an insignificant impact on the compressive strength at higher liquid content. The durability properties of AACM material were enhanced by the presence of lower liquid content rather than a higher activator concentration [46]. However, much attention has been given to activator concentration in literature [26][88] while limited data exist on the impact of liquid/binder ratio on porosity parameters of AACM materials.

3.4.3.2.4 Effect of curing regimes (wet/dry, wet and dry)

The critical pore diameters d_c under wet/dry, wet and dry curing were obtained from the differential pore volume graphs presented in Appendix 3.6 (a-c*)* and are shown in Fig. 3.38.

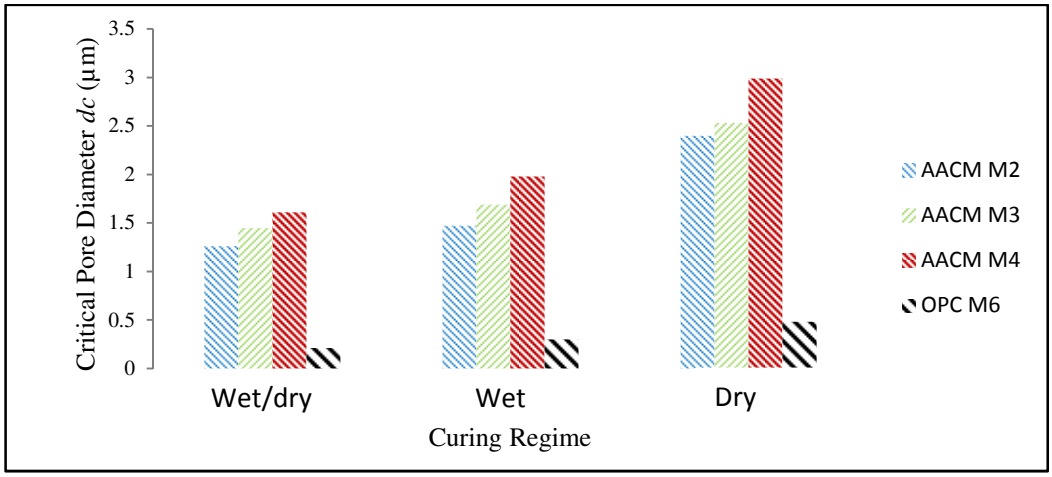

Figure 3. 38: Effect of curing regime (wet/dry, wet & dry) on the critical pore diameters of AACM and OPC mixes (without admixtures)

Fig. 3.38 shows that wet/dry curing regime had the lowest critical pore diameter d_c. This is followed by wet curing which is reasonably close to wet/dry curing while dry curing has the highest critical pore diameter. For example, AACM mortar mix M_2 has critical pore diameter of 1.26 µm under wet/dry curing, 1.47 µm under wet curing and 2.40 µm under dry curing.

On the other hand, OPC mortar mix M_6 under wet/dry curing has the lowest critical pore diameter of 0.21 µm followed by wet curing (0.30 µm) while the highest critical pore diameter d_c is exhibited by dry curing (0.48 µm). The pore blocking effect in OPC concrete was proposed by *Khatib and Mangat* [134] for the wet curing regime. The availability of water during curing allowed for more hydration to take place resulting in the formation of more calcium silicate gel.

OPC mortar mix M_6 has a much lower critical pore diameter d_c than AACM mortar mixes. This may explain the reason for the much higher fire resistance of AACM concrete than OPC concrete. This is because the connected pores in AACM concrete

reduce vapour pressure induced by fire. A notable increase in strength was observed when an alkali-silicate activated concrete was exposed to 1000^0C [161]. This was attributed to the iron oxide content of the fly ash and the better connected microstructure of alkali-silicate activated concrete [161]. *Kong et al.* [162] suggested that the retention of strength in fly ash based AACM concrete was due to the different range of pore sizes present within its matrix and their distribution which is responsible for the escape of pore water during heating, without damaging the structure.

3.4.3.3 Threshold Pore Diameter d_{th}

Threshold pore diameter d_{th} can also be considered as the pore diameter at which an abrupt slope change or point of inflexion occurs on the cumulative porosity curve. This is the point where the intrusion by a small amount of mercury ends, and just before the intrusion by a great portion of mercury begins as shown in Figures 2.4 and 2.5 in section 2.3. The threshold pore diameters d_{th} were investigated to determine the influence of activator dilution, admixtures (R42 & SRA), liquid/binder ratio and curing regimes (wet/dry, wet and dry).

3.4.3.3.1 Effect of activator dilution

The threshold pore diameters d_{th} for AACM mortar mixes M_2 to M_5 were obtained from the combined curves of the cumulative and the differential pore volumes which are presented in Appendix 3.7 (a-c). Fig 3.39 shows the relationship between the threshold pore diameters d_{th} and the activator dilution in AACM mortar mixes M_2 to M_5. A linear relationship between the threshold pore diameters d_{th} and activator dilution is observed by the best-fit regression lines.

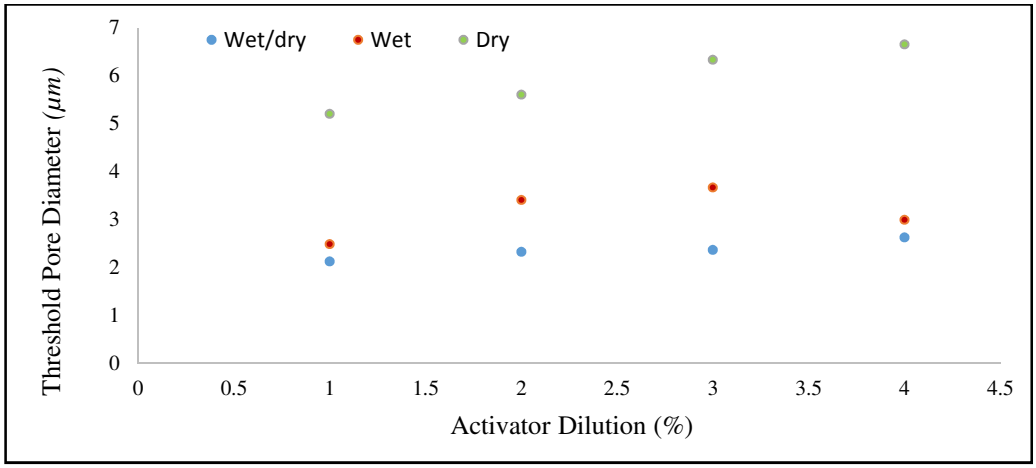

Figure 3. 39: Effect of activator dilution on the threshold pore diameters d_{th} of AACM mortar mixes M_2 to M_5 (without admixtures)

AACM mortar mix M_2 with the least activator dilution of 2.15% possess the lowest threshold pore diameter d_{th} while AACM mortar mix M_5 with the highest activator dilution of 12.0% has the highest threshold pore diameter. For example, the threshold pore diameter d_{th} for mix M_2 is 2.12 µm compared with 2.62 µm for mix M_5 under wet/dry curing.

The high alkali activator concentration especially using sodium silicate on slag based systems facilitates a high degree and rate of reaction, thereby leading to smaller pores [163]. However, the arguments put forward by *Khale et.al,* [24] suggested optimum limits for alkali activator concentration in order to achieve superior AACM concrete qualities. When this limit is exceeded, the unreacted positive ion will interfere with the mortar matrix leading to greater threshold pore diameter d_{th}. A concentration between 8 to 16 molarity was recommended for sodium silicate activator [26] while a concentration of 10 molarity was recommended for potassium hydroxide [24]. The upper limit has not been exceeded in the data presented in Fig. 3.39.

3.4.3.3.2 Effect of admixtures

Fig. 3.40 shows the threshold pore diameters d_{th} of AACM mortar mixes M_2 to M_5 for batch "a" (with admixtures) and batch "b" (without admixture) for wet/dry, wet and dry curing. The combined curves of the cumulative and the differential pore volumes given in Appendix 3.7 (a-c) and 3.8 (a-c) were used to determine the threshold pore diameters d_{th}.

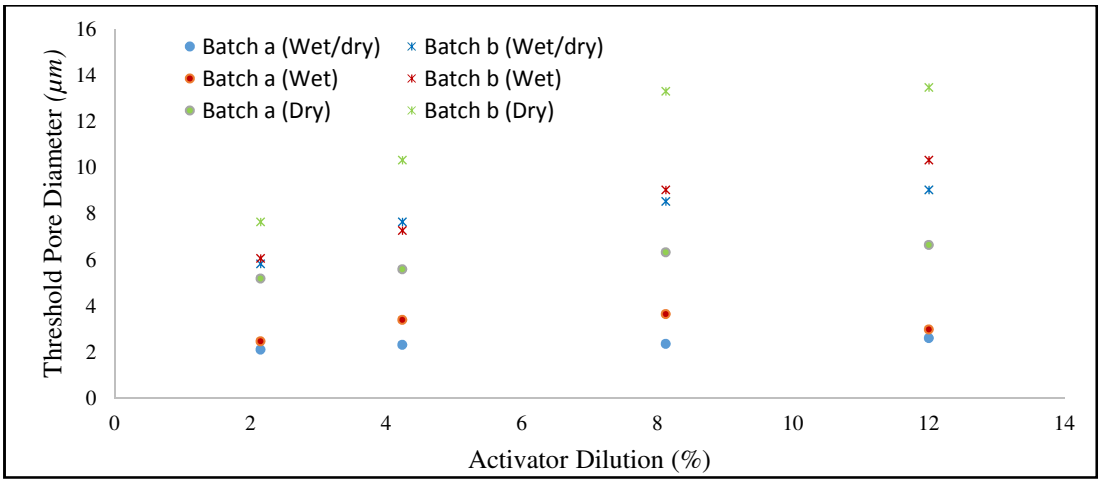

Figure 3. 40: Effect of admixtures (R42 & SRA) on threshold pore diameters d_{th} of AACM mortar mixes

AACM mortar mixes with admixtures have much lower threshold pore diameter than the corresponding mixes without admixtures. The graphs in Fig. 3.40 show a strong linear relationship between activator dilution and threshold pore diameter d_{th}

especially for batch "b" mixes (without admixtures) which show a greater slope of the linear relationship.

Studies show that SRA when added to blended cements reduces the capillary stress and water evaporation in plastic systems thereby increasing the portlandite oversaturation level in solution. This results in higher crystallization stresses which could lead to an expansion [164]. Likewise, the presence of retarders in concrete records an improvement in its performance, particularly its durability [164]. The addition of admixtures (SRA and R42) in AACM mortar also show an improvement similar to that of blended cement mortars. This difference is greater in AACM mortar mixes with high activator dilution (Fig 3.37). For example, AACM mortar mix with 12% activator dilution possesses a threshold pore diameter of 2.62 µm for batch "a" (with admixture) and 9.04µm for batch "b" (without admixture) under wet/dry curing. This is a 71% reduction in the threshold pore diameter due to admixtures. The corresponding difference at 2.15% dilution is 65%.

3.4.3.3.3 Effect of liquid/binder ratio

The relationship between the threshold pore diameters d_{th} and the liquid/binder ratio of AACM mortar mix M_3 is shown in Fig. 3.41. The data are given in Appendix 3.9 (a-c).

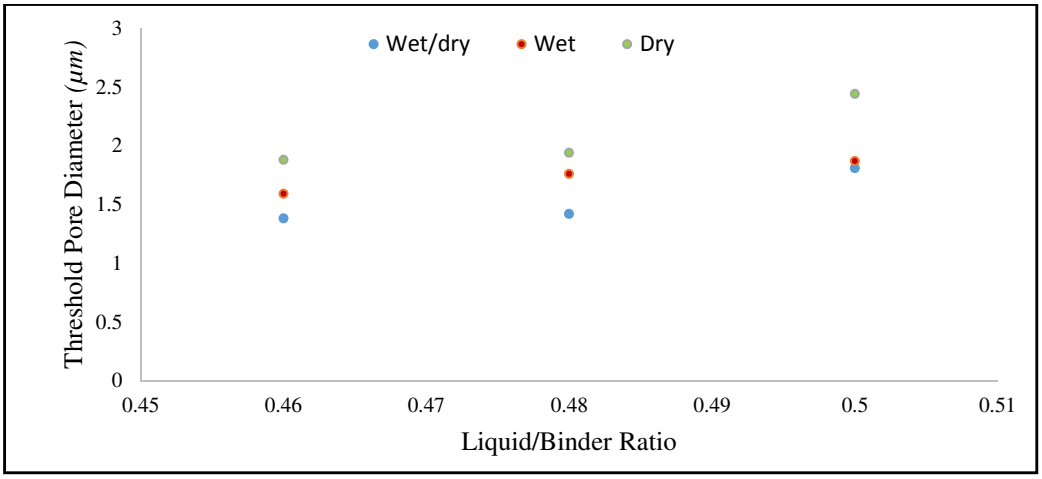

Figure 3. 41: The relationship between threshold pore diameter d_{th} and liquid/binder ratio (with admixtures)

Threshold diameter d_{th} increases linearly with increasing liquid/binder ratio. For example, the mixes with liquid/binder ratios of 0.46, 0.48 and 0.50 had a threshold pore diameter d_{th} of 1.38 µm, 1.42 µm and 1.81 µm respectively under wet/dry curing as shown in Fig 3.38. The wet and dry curing follow the same trend. The results show a significant influence of liquid/binder ratio on the threshold pore diameters d_{th} even at

the small incremental increase of liquid/binder ratio from 0.46 to 0.50, particularly with dry curing. Wet/dry curing displayed lower threshold pore diameters d_{th} than wet or dry curing.

Huajun [165] investigated the porosity and pore structure at higher liquid/binder ratios between 0.6 - 0.8 for a fly-ash based system. The AACM mortar mixes were cured under 20^0C temperature, 95 ± 5% R.H. for 1 day, followed by 14 days wet curing at 20^0C. The activator used was a mixture of sodium hydroxide and sodium silicate in the ratio 2:1. No significant change was observed in the porosity and pore structure of this fly-ash based system compared with OPC mortar. This is possible due to the high temperature of curing (50^0C) which dorminated the influence of other factors on pore structure.

3.4.3.3.4 Effect of curing regime (wet/dry, wet and dry)

The curves of the cumulative and differential pore volumes that were used to determine the effect of curing regimes on the threshold pore diameters d_{th} are presented in Appendix 3.10 (a-c). The threshold pore diameters d_{th} for each AACM and the control OPC mortar mixes are shown in Fig. 3.42 under the three curing regimes.

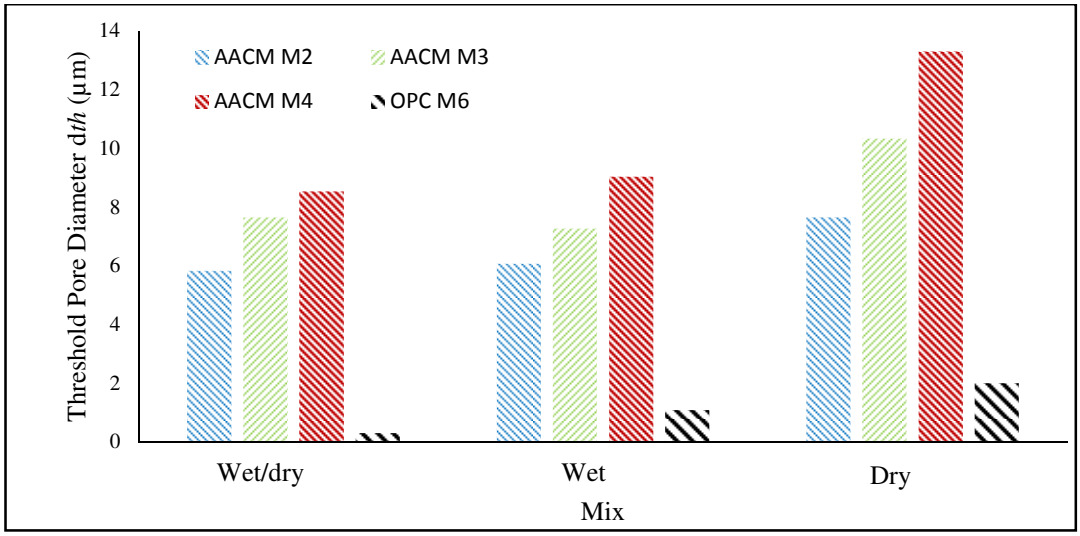

Figure 3. 42: Effect of curing on the threshold pore diameters d_{th} (without admixtures)

Fig. 3.42 shows that d_{th} for the AACM and OPC mortars was optimum under wet/dry curing. AACM mortar mixes displayed higher threshold pore diameters d_{th} than the OPC mortar mix. For example, AACM mortar mix M_2 under wet/dry curing had a threshold pore diameter d_{th} of 5.83 µm compared with 0.31 µm for OPC mortar mix M_6. The huge difference was because d_{th} for OPC mortar occurred just before the unimodal peak (Fig. 3.4) while for AACM mortar, it occurred just before the second bimodal peak (Fig. 3.5). The threshold pore diameters d_{th} of blended cement pastes from *Khatib*

and Mangat [134] also show a similarly big difference between the AACM mortars (M_2 to M_4) and the OPC-pfa paste.

The difference in the threshold pore diameters d_{th} of AACM concrete and OPC mortar could be attributed to the differences in their pore distribution. A large volume of pores for OPC mortar occurs towards the gel pore range while for AACM a greater part of pore volume occurs in the capillary pore range.

3.4.3.4 Effective Porosity

3.4.3.4.1 Effect of activator dilution

The influence of activator dilution under the different curing regimes on porosity of AACM mortar mixes M_2 to M_5 is shown in Fig. 3.43.

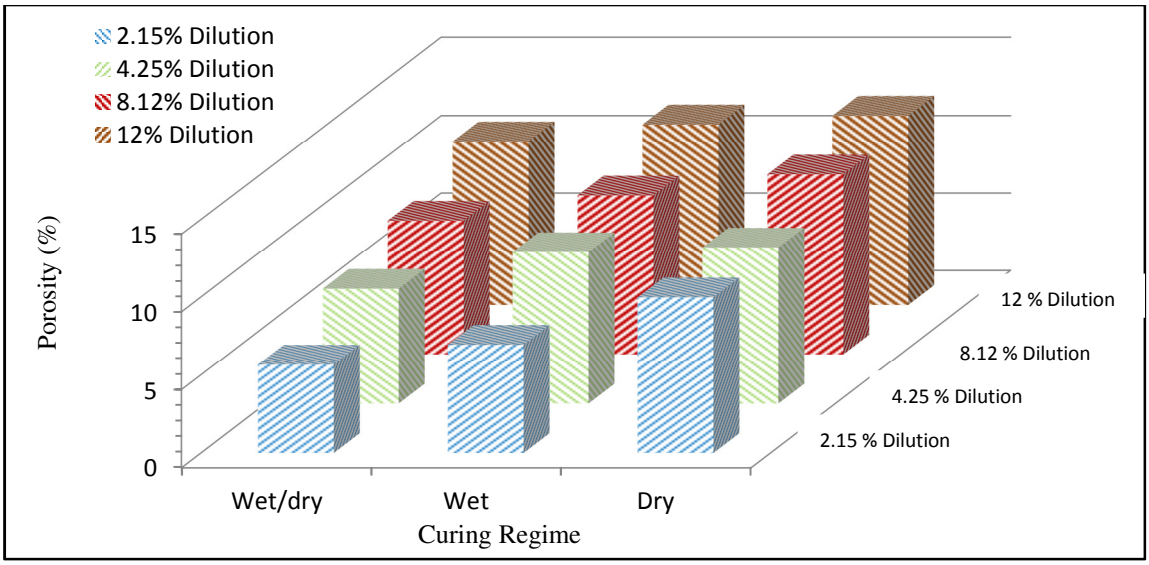

Figure 3. 43: Effect of activator dilution on the porosity of AACM mortar with admixtures under different curing regimes.

The lowest activator dilution in AACM mortar mix (2.15% dilution) had the lowest porosity under each of the three curing regimes. Similarly, the highest activator dilution (12% dilution) had the highest porosity. The lowest porosity at 2.15% dilution suggests a tighter pore structure than the other mixes. For instance, AACM mortar mix with 2.15% activator dilution had 5.67%, 6.94% and 9.98% porosity compared with 10.56%, 11.65% and 12.21% porosity for AACM mortar mix with 12% activator dilution under wet/dry, wet and dry curing respectively. Higher activator concentration in the AACM mortar mixes increases the rate of pozzolanic reaction.

Lloyds et al., [153] and *Zheng et al.,* [154] adopted gas sorption analysis to study the influence of activator concentration in a fly-ash based system. They observed pore

refinement of the fly-ash based alkali activated material with an increase in activator concentration which is similar to results obtained from this study.

3.4.3.4.2 Effect of admixtures (R42 & SRA)

The influence of activator dilution on AACM batch "a" mixes (with admixtures) and batch "b" mixes (without admixtures) under wet/dry, wet and dry curing is shown in Fig. 3.44. The unbroken lines represent batch "a" mixes (with admixtures) while the broken lines represent the batch "b" mixes (without admixtures).

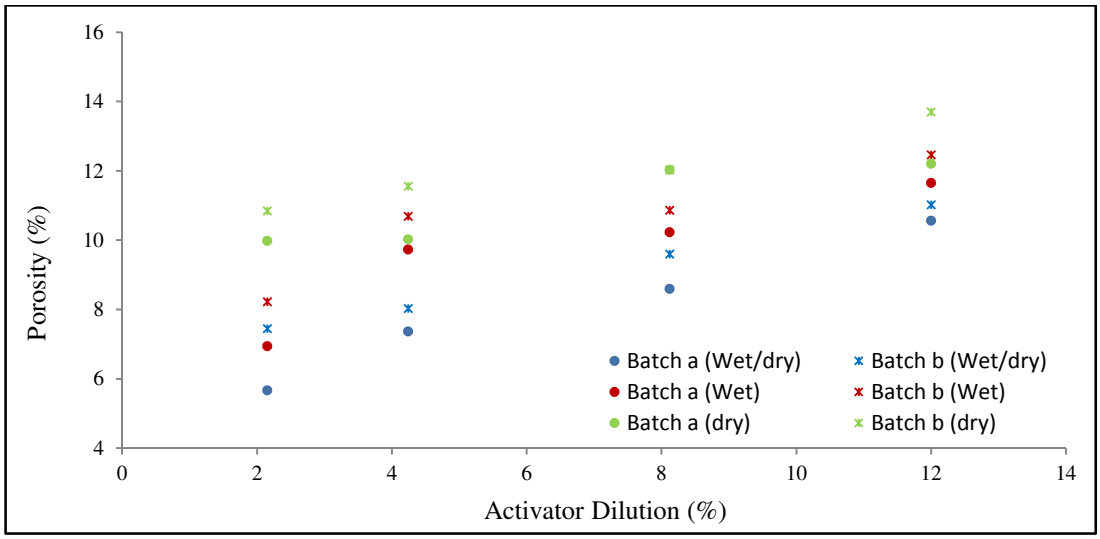

Figure 3. 44: Effect of admixtures on the porosity of AACM mortar under different curing regimes.

AACM mortar mixes containing admixtures (batch "a") have lower porosity compared with those without admixtures (batch "b") under the same curing regime. The presence of admixtures results in the densification of AACM mortar matrix. The shrinkage reducing agent SRA reduces the surface tension of pore water resulting in smaller internal stress during its evaporation (drying shrinkage). It also modifies the pore structure due to the decreased capillary stress of water added during the mixing process [156].

Likewise, the retarder reduces the reaction rate of tricalcium silicate with water, thereby, impeding the early growth of calcium hydroxide in OPC concrete. Realignment of cement particles in the concrete matrix to form denser pore structure evolves [157] during the delayed growth of calcium hydroxide. The admixture R42 has a similar retarding effect on the early age geopolymerisation reaction of the AACMs.

The combined effect of admixtures and low activator dilution in AACM mixes produced lower porosity than mixes without admixtures and with high activator dilution. For example, batch "a" (wet/dry) at 2.15% activator dilution has 5.67% porosity

compared with 11.02% porosity exhibited by batch "b" (wet/dry) at 12% activator dilution. The presence of admixtures as well as the lower activator dilution favoured densification of AACM mortar matrix.

3.4.3.4.3 Effect of liquid/binder ratio

The relationship between porosity and liquid/binder ratio of AACM mortar mix M_3 is shown in Fig. 3.45 for different curing regimes.

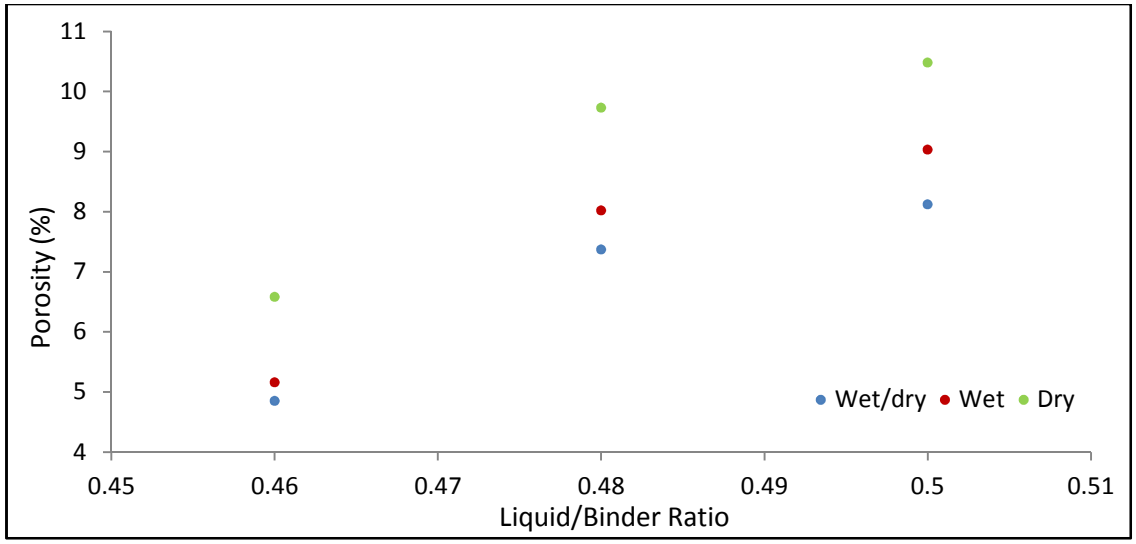

Figure 3. 45: Relationship between porosity and liquid/binder ratio of AACM mortar M_3 under wet/dry, wet and dry curing (with admixture)

The influence of liquid/binder ratio on the porosity of AACM mortar is significant despite the close range of liquid/binder ratio (0.46 – 0.50) as shown in Fig. 3.45. For instance, the porosity of AACM with liquid/binder ratio 0.46 is 4.85%, 5.16% and 6.58% under wet/dry, wet and dry curing respectively compared with 8.12%, 9.03% and 10.48% for liquid/binder ratio 0.50.

These observations are consistent with those of *Bentz and Stutzman* [160] who suggest a strong influence of water/cement ratio on the pore structure of OPC cement paste. The gel hydration products at lower water/cement ratio occupy the spaces which would otherwise be water-filled spaces at higher water/cement ratios, thereby providing lower porosity at low water/cement ratio. This has impact on the overall durability of concrete.

The wet/dry curing produces the lowest porosity at different liquid/binder ratios, followed by wet and lastly dry curing. The 3 days initial curing in water for the wet/dry curing provided the much-needed moisture to improve particle packing around the aggregates in the AACMs. This together with the geopolymer reactions resulted in lower porosity when compared with wet and dry curing.

3.4.3.4.4 Porosity of AACM and OPC mortar

The relationship between porosity and incremental pore diameter range of AACM mortar mix M_2 and OPC mortar mix M_6 under wet/dry, wet and dry curing are shown in Figures 3.46, 3.47 and 3.48 respectively.

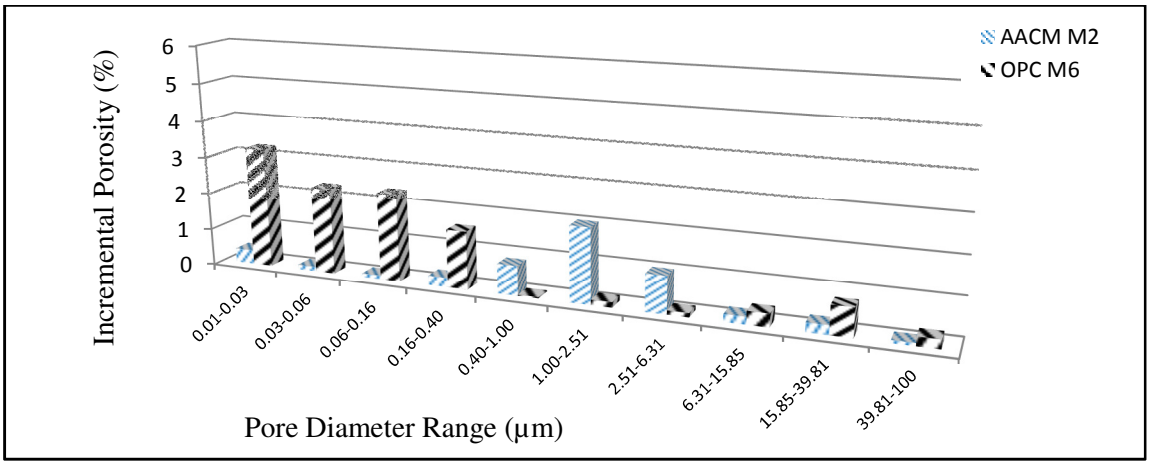

Figure 3. 46: Graph showing the porosity at the incremental diameter (µm) for AACM and OPC mortar mixes M_2 and M_6 under wet/dry curing.

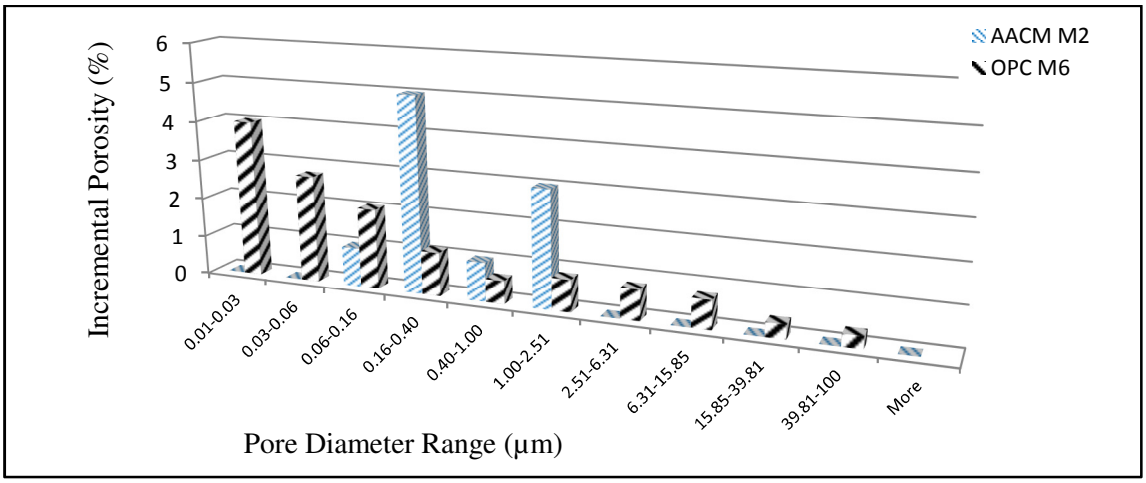

Figure 3. 47*:* Graph showing the porosity at the incremental diameter (µm) for AACM and OPC mortar mixes M_2 and M_6 under wet curing.

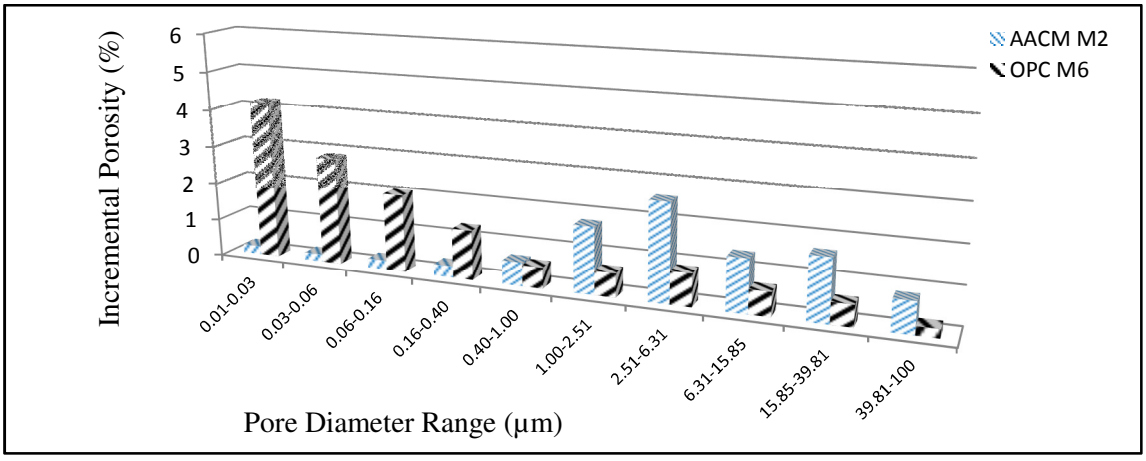

Figure 3. 48: Graph showing the porosity at the incremental diameter (µm) for AACM and OPC mortar mixes M_2 and M_6 under dry curing.

The porosity of AACM Mortar M_2 shows that it was distributed along different pore diameters with more significant porosity at larger diameters. On the other hand, OPC mortar M_6 has its porosity distributed along a range of diameters with more significant porosity at smaller diameters. The distinctive nature of AACM mortars with large volume of pores within the capillary pore zone (0.16 to 6.31 µm) while OPC mortars have large volume of pores within the gel pore zone (0.01 to 0.16 µm) has been discussed fully in section 3.4.2.1.

Fig 3.49 shows the effective porosity of AACM and OPC mortar mixes M_2 and M_6 under wet/dry, wet and dry curing.

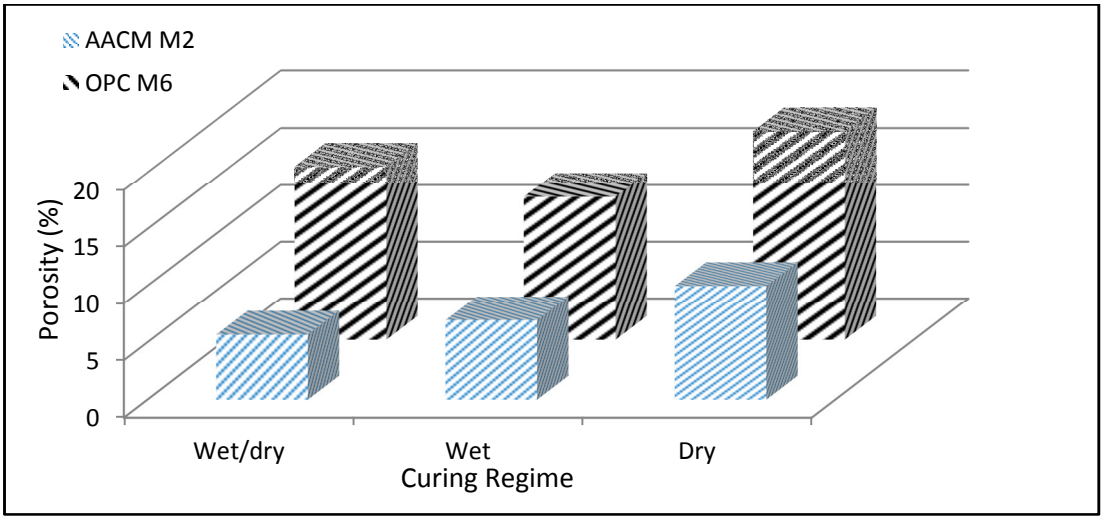

Figure 3. 49: Porosity of AACM and OPC mortar mixes M_2 and M_6 under wet/dry, wet and dry curing.

The porosity of AACM mortar M_2 is much lower than OPC mortar M_6 despite the presence of larger pores in AACM mortar than the OPC mortar. The porosity of AACM mortar M_2 is 5.67%, 6.94% and 9.98% compared with 15.28%, 12.62% and 18.36% for OPC mortar for wet/dry, wet and dry curing respectively. It is clear that wet/dry curing is optimum for AACM mortar while wet curing is best for OPC mortar, the latter being a well-established fact. The densification of AACM is induced by a number of factors which includes the binder particle sizes which are smaller than OPC grains. The smaller particle size enhances the filling of pore spaces [166]. In addition, the geopolymerisation reaction in AACM mortar produces more hydration products compared with OPC mortar [167].

3.4.4 Relationship between Effective Porosity and Strength

The strength of concrete is significantly affected by the porosity of its internal structure like most porous materials. The relationship between porosity and strength of OPC concrete has been well investigated and its literature review is given in Section

3.2.2.4. Total porosity includes both open and closed pores unlike the effective porosity measured by MIP which takes account of open pores only, which provide access for liquid to move within the concrete [112]. The effective porosity which accounts for open pores is presented in this section.

3.4.4.1 Effect of Curing

The relationship between the strength and porosity of AACM mortar mixes under wet/dry, wet and dry curing and the combined plot of wet/dry and dry curing with its regression equation is shown in Fig. 3.47. It is expressed as a linear plot for the different curing regimes, similar to the relationship proposed by Hasselmann [122].

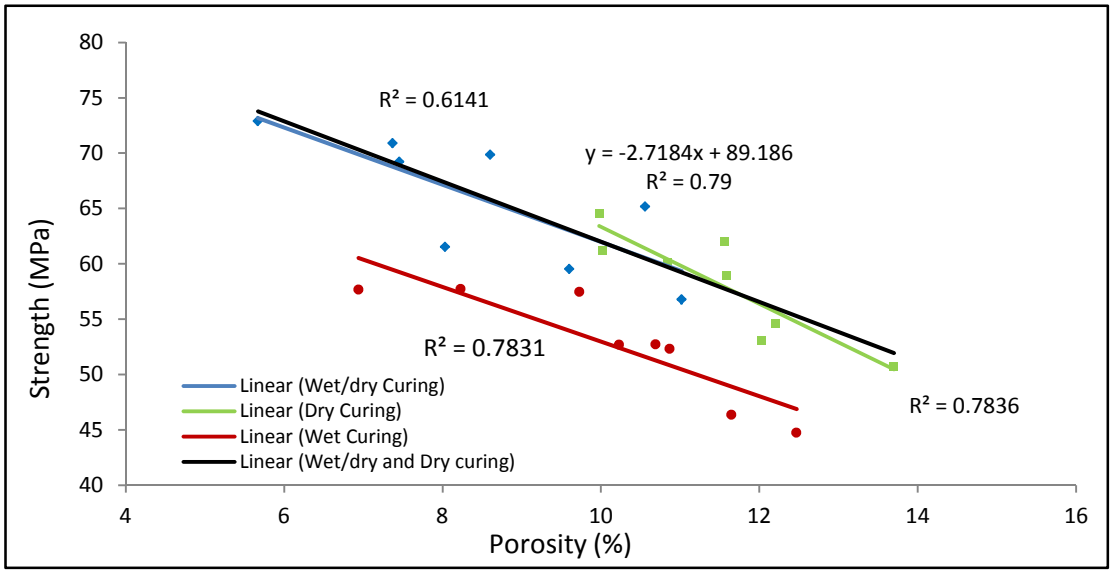

Figure 3. 50: Strength-effective porosity relationship of AACM mortar under different curing.

The Hasselmann [122] linear relationship model (Table 3.2, section 3.2.2) provided the best fit to the AACM experimental data (Fig. 3.50). The results presented by *Roßler and Odler* [168] for OPC mortar showed a similar linear strength-porosity relationship. The wet/dry and dry curing provides a common relationship of the form:

$$y = -2.7184x + 89.186 \qquad 3.2$$

The coefficient of correlation is 0.79. The experimental data for wet/dry curing lies on the upper end of the graph which represents higher strength and lower porosity while the dry curing is represented by the lower end of the common graph representing lower strength and higher porosity. AACM mortar subjected to wet/dry curing has the lowest effective porosity and highest strength (Fig. 3.50). The initial wet curing might have aided the production of more geopolymerisation product while the subsequent dry curing will result in increased compressive strength [26].

On the other hand, AACM mortar subjected to dry curing has a higher effective porosity and higher strength than wet curing as shown in Fig. 3.50. Contrary to the expected increase in strength with decreasing porosity, AACM mortar subjected to dry curing has higher effective porosity than wet curing but the strength is also higher in dry curing than wet curing. For example, effective porosity of 10% possesses compressive strength of 61.2 MPa and 52.7 MPa for dry and wet curing respectively. This suggests that wet curing produces more pore blocking gel than dry curing, thus a more refined AACM pore structure evolves. On the other hand, the alkali reactivity of the pozzolanic material in AACM is higher under dry curing than wet curing, thus promoting rapid strength development which is a well-established fact. In conclusion, the effective porosity is lesser in wet curing than dry curing of AACM but the strength development is faster in dry curing than wet curing.

3.4.4.2 Effect of Liquid/Binder Ratio

The experimental results presented by Lian et al., [118], Bu and Tian [119] for the strength and porosity relationship of OPC concrete together with the author's data on AACM mortar are shown in Fig. 3.48. Lian et al., [118] used OPC cement and fine aggregate with mineral admixtures (quary sand and silica fume) with water/cement ratios within the range of 0.30 to 0.38. The OPC mortar was cured in water for 28 days conforming to AS1012.8.1-2000 [169]. Bu and Tian [119] used a mix proportion of 16% cement, 48% sand and 29% coarse aggregate with water/cement ratios 0.35 to 0.55. The specimens were cured in lime-saturated water at room temperature for 28 days. The author's data is the plot of linear equation obtained from Fig. 3.47 for AACM mortars subjected to wet/dry and dry curing as shown in equation 3.2.

$$y = -2.7184x + 89.186 \qquad 3.2$$

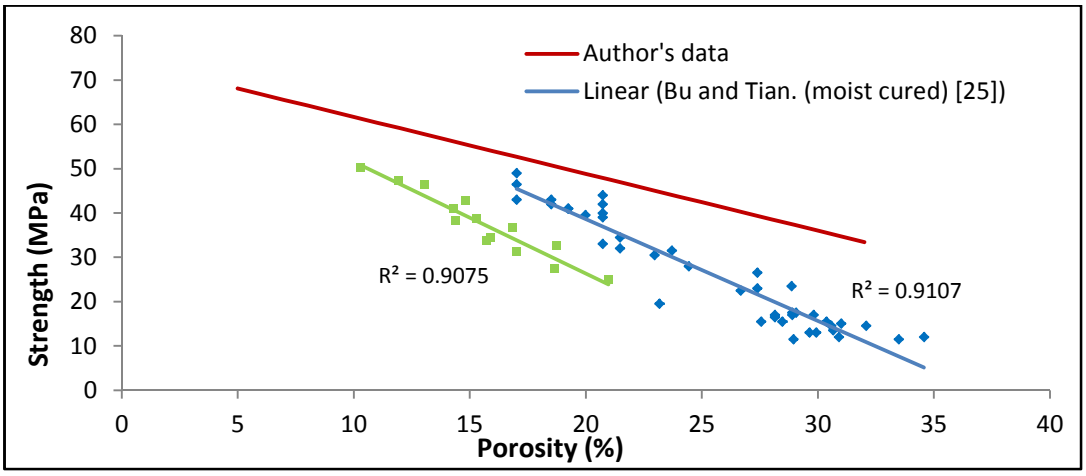

Figure 3. 51: Relationship between porosity and compressive strength.

The experimental results from Lian et al., [118] with water/cement ratios 0.30 to 0.38 and Bu and Tian [119] with water/cement ratios 0.35 to 0.55 show good correlation (R^2 0.91) with the linear model proposed by Hasselmann [122] as shown in Fig. 3.51. The OPC specimens were wet cured for 28 days which provides an optimum condition for hydration process [24, 25] while the AACM mortar results presented by the author were subjected to wet/dry and dry curing, this provides an optimum condition for geopolymerisation.

Fig. 3.51 show different linear porosity-strength relationships for different compositions of OPC concrete and AACM mortars, all conforming to the Hasselmann [122] model. For a given porosity, the strength of AACM mortar is higher. The graph of AACMs extends to much lower porosity than the OPC concretes which results in much higher strength range of AACM mortar.

However, for OPC concrete, the experimental results from Lian et al., [118] with lower water/cement ratio (0.30 to 0.38) displayed higher strength and a lower porosity than Bu and Tian [119] with water/cement ratios 0.35 to 0.55. Admixtures and silica fume were used in Lian et al., [118] concrete mixes.

3.4.4.2.1 Validation of the effect of liquid/binder ratio

Similar influence of liquid/binder ratio on the strength-porosity relationship is shown in Fig. 3.52 for AACM mortar. The liquid/binder ratios are 0.46, 0.48 and 0.50 for AACM mortar mix M_3. The line graph for AACM mortar mix M_3 subjected to wet/dry and dry curing shows similar relationship due to the predominantly dry curing period in both cases.

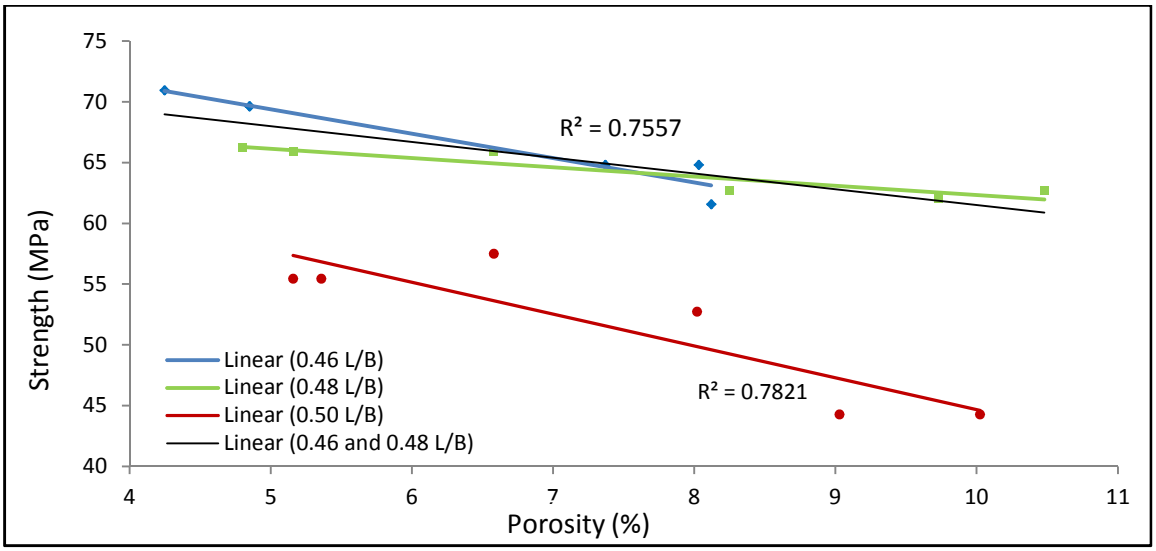

Figure 3. 52: Strength-porosity relationship of AACM mortar mix M_3 (with admixtures) under different liquid/binder ratios

The lowest effective porosity with the highest strength is displayed by liquid/binder ratio 0.46, followed by 0.48 l/b and lastly 0.50 l/b as shown in Fig. 3.52. The effective porosity is influenced by the liquid/binder ratios resulting to the differences in their compressive strength. AACM mortar with liquid/binder ratio 0.46 displayed the least porosity (4.2%) and the highest compressive strength of 70.9 MPa. This is followed by 4.8% and 5.2% porosity by AACM mortars with liquid/binder ratios 0.48 and 0.50 respectively and the corresponding strengths of 66.1 MPa and 57.5 MPa.

The 0.46 l/b and 0.48 l/b shows similar trend in the strength-effective porosity relationship. The correlation is 0.76 for the combined data of 0.46 l/b and 0.48 l/b. On the other hand, 0.50 l/b displayed the lowest strength. This suggests an optimum range of 0.46 to 0.48 liquid/binder ratios to achieve a lower effective porosity and higher strength for AACM mortar.

The effective porosity obtained from mortar mixes with various liquid/binder ratios cannot be used independently to relate to the material strength. Other pore structure parameters such pore size, pore connectivity, pore surface roughness and pore volume fraction (porosity) should be considered when relating to material strength [112].

3.5 CONCLUSIONS

The following conclusions are drawn from the investigation on poorosity and pore structure of AACM and OPC mortars subjected to ambient (wet/dry, wet and dry) curing:

- The 28 days strength of AACM and OPC mortar mixes was significantly influenced by the curing regimes wet/dry curing, wet curing and dry curing. AACM mortar mixes developed maximum strength under wet/dry curing whereas wet curing is optimum for OPC concrete. Dry curing of AACM mortar produced higher strength than wet curing. For example, the 28 days strength of AACM mix M_2 concrete under wet/dry, dry and wet was 73MPa, 65Mpa and 58Mpa respectively.
- An inverse relationship exists between the intrudable porosity and compressive strength of AACM mortar under the different curing regimes and liquid/binder ratios. Similar relationships exist between strength-critical pore and strength and pore diameters (critical and threshold).
- The combined use of a retarder and shrinkage reducing admixture improved the strength of AACM mortar. For example, the 28 days strength mix M_3 containing

both retarder and shrinkage reducing admixture had 71 MPa compared with 62 MPa containing no retarder and shrinkage reducing admixture.

- Strength of AACM mortar increase with decreasing liquid/binder and with increasing activator concentration when the range of activator was maintained between the upper and lower limits of activator molarity.
- AACM shows a bimodal pore structure which is most conspicious under wet/dry and dry curing. Wet curing indicates a small degree of pore continuity possibly due to secondary cementitious hydration reactions overlapping with the geopolymerisation reactions in AACMs.
- AACM mortar cured under the wet/dry regime possessed the lowest intruded pore volume $\boldsymbol{\Phi_{in,}}$ critical pore diameter $\boldsymbol{d_c}$ and threshold pore diameter $\boldsymbol{D_{th.}}$ Similarly, the presence of retarder and shrinkage reducing admixture and a lower degree of activator dilution with water reduced the intruded pore volume $\boldsymbol{\Phi_{in,}}$ critical pore diameter $\boldsymbol{d_c}$ and threshold pore diameter $\boldsymbol{D_{th.}}$
- Lower liquid/binder ratio in AACM mortar M_3 mix displayed a lower intruded pore space $\boldsymbol{\Phi_{in,}}$ critical pore diameter $\boldsymbol{d_c}$ and threshold pore diameter $\boldsymbol{D_{crit}}$.
- AACM mortar has lower porosity than OPC mortar. The gel pore volume (pore size range 0.5nm to 10nm) is lesser in AACM mortar than OPC mortar but the capillary pore volume (pore size range 10nm to 10,000nm) is higher in AACM mortar than OPC mortar.

CHAPTER 4

BOUND CHLORIDES IN ALKALI ACTIVATED CEMENTITIOUS (AACM) CONCRETE

4.1 INTRODUCTION

Chlorides can be present in concrete in three forms namely chemically bound chloride (acid soluble), physically bound chloride (water soluble) and free chloride (pore fluid) [97][25][170]. The ingress of chloride in concrete is mainly influenced by the concrete microstructure as investigated in chapter 3, the curing environment and age amongst others. Chloride ingress in concrete is undesirable because it causes corrosion of reinforcement embedded in the concrete matrix. This corrosion is activated when the passive protective film covering the surface of steel reinforcement is compromised by the presence of chloride ion in the concrete matrix. Chloride-induced corrosion of steel reinforced concrete is a major problem leading to structural failure if not properly addressed.

The presence of chloride ion in concrete is a major durability concern especially when the amount present in concrete has exceeded the corrosion threshold limits. When this threshold limit is exceeded, localised pitting corrosion of the steel reinforcement begins, serving as an active feeding zone to other corrosion sites on the steel surface. The impact is mostly felt on structures exposed to marine environment and de-icing salts e.g bridges, dams and crossings. Huge financial cost is involved in addressing these structural defects. For example, the US spent $552 billion for the total direct and indirect costs of repair, which is 6% of the annual GDP [171].

The mobile chloride ion (free chloride) in the pore solution of OPC concrete is known to initiate corrosion. It is considered to be dependent on the physically bound chloride (chloride bound to the wall of the binder gel) and the chemically bound chloride (chloride forming part of the hydration products in OPC concrete). These relationships, however, are unlikely in AACM concrete [3]. The chloride binding capacity, the bound chlorides (physically and chemically) and pore fluid chloride remain to be fully understood in AACM concrete.

The microstructure of AACM and OPC concrete investigated in chapter 3 reveals differences between the porosity and pore structure of these two concrete materials, possibly leading to differences in the rate of chloride diffusion between the two concretes. The presence of Friedel's salt (calcium chloroaluminate phase) has not been detected in AACM [3]. More research into the chloride diffusion in AACM is

required since the chemistry of the pore fluid and the effect of chlorides on its microstructure are not fully understood [82].

Finally, durability in concrete technology cannot be fully investigated without addressing sustainability which is on the world agenda. For example, the recently held *2nd International Conference on Concrete Sustainability* [172] addressed the issues relating to sustaining the present needs of concrete demand without compromising the needs of future generations to meet their own demands. The use of alkali activated cementitious material as an alternative binder to ordinary Portland cement (OPC) addresses the issues of sustainability.

4.2 LITERATURE REVIEW

4.2.1 Alkali Activated Cementitious Materials (AACMs)

New innovations in low impact construction materials require a reduction in the use of Portland cement with alternative binders, preferably utilising industrial waste materials and aggregates made from recycled waste. The word "Geopolymer" was first introduced by *Davidovits* [19] for alkali activated cementitious materials formed by the chemical reaction between alumino-silicate oxides and alkali polysilicates to yield polymeric Si-O-Al bonds similar in composition to natural zeolites [20][21]. Unlike ordinary Portland cement, the setting mechanism of alkali activated cement is by geopolymerization involving the dissolution of silica and alumina in a pozzolanic compound by a geopolymer activator resulting in the formation of hydrated calcium silicates and aluminates (C-A-S-H) [22][23]. Numerous research advancements have been made on the gel chemistry of alkali-activated binders [24][173][167], heat of hydration [174], fire resistance [175] and acid resistance [176], mechanical strengths [21] with advantageous benefits in comparison to ordinary Portland cement. However, a limited database exists on the durability properties of alkali-activated concretes describing their variation with time which is essential for service life modelling [12][177].

4.2.1.1 Gel Chemistry

The geopolymerisation of an alkali activated cementitious material occurs through an exothemal process. The process entails the dissolution of covalent bonds Si-O-Si and Al-O-Al which is schematised by [19] in Fig. 4.1.

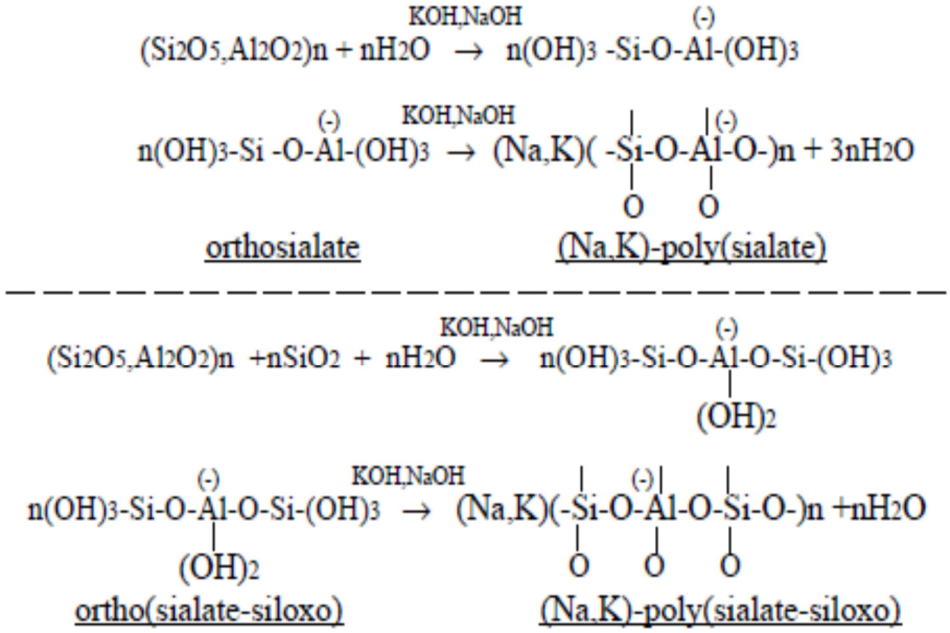

Figure 4. 1: Schematics of exothermic reaction of hydroxide (OH) alkali activators with binder

Recent studies [19][20][24][178] reveal that sodium hydroxide develops high degree of polycondensation compared to silicate, carbonate activators. The high degree of polycondensation results in high crystallinity of the pore structure of the matrix thus improving the stability against aggressive environments. It is also found to buffer the pH of pore fluid thereby directly affecting the geopolymerisation products [26]. On the other hand, sodium silicate when used as activator gives better early and final strength and is found to be less sensitive to impurities like clay residuals, stone dust and fines [3].

4.2.2 Pore Structure of AACM and OPC Concrete

4.2.2.1 AACM Concrete

An investigation on pore structure and permeability of AACM concrete found that the difference in strength was attributed to the difference in pore structure [179]. Porosity and median pore sizes of AACM paste when measured with mercury intrusion porosimetry showed a possible reduction when compared to OPC concrete [173][179][180]. The porosity and pore structure of the AACM concrete investigated in chapter 3 using the mercury intrusion porosimetry techniques equally shows a reduction in the MIP parameters (intrudable porosity, critical and threshold pore diameters) and an increase in the compressive strength compared with OPC concrete.

Findings made by *Provis et al.,* [181] suggested that slag content ≥50% reduces the porosity and increases tortuosity. Research on the relationship between pore structure and water binder ratio of hydrated OPC concrete has also been reported

[25][182][183]. AACM concrete has a porous amorphous matrix that has both solid and liquid phases similar to OPC concrete. There is the potential of pore structure of AACM concrete to affect the penetration of corrosion initiators such as chlorides. The mix composition of the AACM concrete specimens under investigation in this research project was optimised for its liquid binder ratio, alkali content and aggregate proportions to achieve a good pore structure for chloride ingress, carbonation and corrosion tests.

4.2.2.2 OPC Concrete

A relationship between strength and porosity is not only unique to OPC concrete but also applies to other brittle materials. The diffusivity of CO_2 and chloride ions in hardened concrete is a function of the pore structure of the hydrated cement paste [25]. The pore structure determines the diffusion rate of harmful elements like chloride ions and CO_2 (carbonation) through the matrix of OPC concrete until they reach the surface of the embedded steel reinforcement and initiate corrosion [91]. Research on OPC concrete shows that the diffusion through the solid phase of the matrix is negligible when compared to the rate of diffusion through the liquid phase in its pore structure. The rate of diffusion is controlled not only by the diffusion coefficient through the pore solution but by the physical characteristics of the capillary pore structure [111].

4.2.3 Durability Parameters of AACM Concrete

4.2.3.1 Introduction

The structural integrity of any cementitious material is compromised by the ingress of chloride, carbon dioxide and sulphate. Understanding the resistance of AACMs when exposed to aggressive environments is critical to predicting how the material will behave in service. Limited field applications of AACM concrete are due to a lack of knowledge of its structural behaviour when subjected to prolonged exposure to corrosion initiators such as chloride ions and carbonation [3]. The importance of structural stability cannot be overemphasized since the primary aim of design is for a structure to perform optimally during its design lifespan [184]. Structural defects or collapse can be attributed to the rate at which reinforcement steel corrodes under the prolonged influence of chloride diffusion and carbonation.

4.2.3.2 Chloride Ingress and Transportation Mechanism

The penetration of chloride ions in a concrete matrix is a complex interaction of both physical and chemical processes which are predominantly affected by the

environments to which the concrete is exposed [102][170][185]. The presence of chloride ions around the steel bar causes it to corrode as a result of depassivation. Carbonation will neutralise the pH of alkaline concrete thereby causing corrosion of the steel [25]. The threshold level of chloride deposited on the surface of the rebar must be reached to initiate corrosion, thereby activating the surface to form an anode while the inactivated surface will be the cathode [25][170].

The transportation mechanism by which chloride ions can penetrate hardened concrete is governed by the mix composition, degree of saturation within the pore structure, temperature and location. Chloride ingress in a fully saturated hardened matrix is by the diffusion process which occurs when at least one surface of the fully saturated matrix is exposed to a chloride solution [178]. In the process, diffusion occurs as the solution seeks to attain equilibrium by moving the chloride ions from high concentrations to low concentrations within the matrix. A review of chloride diffusion test methods is given by *Stanish et al.* [111].

The bulk chloride diffusion method for determining the basic parameters of the diffusion process was used in this research project. This method uses AACM concrete specimens completely immersed in an aqueous sodium chloride solution at a regulated temperature to attain complete saturation within the pores of the specimen. The chloride ions in the aqueous solution diffuse through the pore matrix of concrete to reach an equilibrium concentration which is further enhanced by the gradient of the free chloride ions in the pore solution [186]. The diffusion of the chloride ions proceeds in one direction from the exposed face while the other faces of the specimen are sealed with a coating [187][98]. The movement of chloride ions within the pores of concrete can be through a combination of mechanisms in marine structures exposed to different conditions outlined in Table 4.1. The test procedure used in this research project for chloride diffusion measurements represents a submerged substructure where diffusion is the sole mechanism of chloride penetration.

Table 4. 1: Chloride transport mechanism for various marine exposure conditions

Exposure	Example of structure	Primary chloride transport mechanism
Submerged	Substructures below low tide.	Diffusion.
	Basement exterior walls or transport tunnel liners below low tide. Liquid containing structures.	Permeation, diffusion and Wick's action.
Tidal	Substructures and superstructures in the tidal zone.	Capillary absorption and diffusion.
Splash and spray	Superstructures above high tide in the open sea.	Capillary absorption and diffusion. (Also carbonation)
Coastal	Land based structures in coastal areas or superstructures above high tide in river estuary or body of water in coastal area.	Capillary absorption. (Also carbonation)

Source: *Cement Concrete and Aggregates Australia* [186].

4.2.3.3 Rate of Chloride Ingress

Factors influencing the rate of chloride migration in AACM concrete can be broadly classified as internal and external factors. The formation of the AACM pore structure is expected to be dependent on various factors such as the alkali activator type and concentration, the pozzolanic material used, liquid binder ratio, binder content in the mix and presence of admixtures. The gel chemistry which is developed as the final AACM pore structure evolves determines its properties [12]. This gel chemistry and the interface with aggregates within the AACM concrete matrix are the primary internal factors that determine the penetration rate of chloride.

On the other hand, the external (environmental) factors that determine the rate of chloride penetration in AACM concrete include the curing condition, duration of exposure, temperature, degree of saturation and the boundary conditions such as the chloride concentration of the surrounding medium. Various studies on chloride ingress in concrete have been reported to determine diffusion parameters under marine spray and tidal cycles [102][188], immersion in NaCl solution [103][189][190].

4.2.3.4 Chloride Diffusion Parameters

Fick's second law of diffusion was suggested as a suitable model for chloride diffusion in concrete by Collepardi et al. [191] as shown in equation 4.1.

$$C_{(x,t)} = C_0 \left(1 - erf\left[\frac{x}{2\sqrt{D_C\, t}}\right]\right) \quad 4.1$$

Where: x = distance from concrete surface (m); t = Time (seconds); D_C = diffusion coefficient (m^2/s); C_0 = equilibrium chloride concentration on concrete surface; $C_{(x,t)}$ = chloride concentration at distance x; time t . This model is used to predict the chloride penetration in concrete with age. However, Fick's second law of diffusion assumes a constant value for the chloride diffusion coefficient for long-term prediction of chloride concentration which has been proven otherwise by recent studies. The diffusivity of concrete with age have been studied by various researchers including Mangat and Gurusamy [96] , Mangat and Molloy [192], Bramforth and Price [193] and Maage et al., [194]. Research findings have shown that the apparent chloride diffusion coefficient D_c varies with time t. It is given by the following power function [192]:

$$D_C = D_i\, t^{-m} \quad 4.2$$

where: D_c is the apparent diffusion coefficient at time t; D_i is diffusion coefficient at reference time t, and m is the age factor.

Equation 4.2 can be written in a linear form as shown in equation 4.3 [192],

$$log\, D_C = log\, D_i - m\, log\, t \quad 4.3$$

Similarly, substituting the time dependency of the diffusion coefficient D_c (equation 4.2) into Fick's second law of diffusion (equation 1), a differential equation is obtained as shown equation 4.4 [192].

$$C_0 = C_{(x,t)} \left(1 - erf\left[\frac{x}{2\frac{\sqrt{D_i\, t^{(1-m)}}}{1-m}}\right]\right) \quad 4.4$$

Where $C_{(x,t)}$ is the chloride concentration at depth $\boldsymbol{x}$ and time *t,* C_0 is the chloride concentration at the concrete surface.

Equation 4.3 can be used to predict the rate of chloride diffusion (Dc) in concrete over a long period of exposure in NaCl laden environment and equation 4.4 can be used to determine the chloride concentration in concrete over a long period [192].

Some authors [195][196] adopted predictive models for chloride ingress by using analytical solutions based on Fick's law to generate equation 4.5

$$C_{(x,t)} = C_i + (C_{sa} - C_i)\, erfc\, \frac{x}{\sqrt{4\,(t - t_{ex})D_a}} \qquad 4.5$$

Where $\boldsymbol{C_{sa}}$ and $\boldsymbol{D_a}$are surface chloride and chloride diffusion coefficients which are assumed to be constants, $\boldsymbol{C_{(x,t)}}$ is the chloride concentration at depth $\boldsymbol{x}$ and time t, $\boldsymbol{C_i}$, is the chloride concentration at the concrete surface and $\boldsymbol{t_{ex}}$ is the reference time which is 28 days.

The relationships between diffusion coefficient, D_C, surface chloride concentration, C_0 and exposure period, t, for marine concrete and repair materials were determined [103] [197][198] which gave diffusion coefficient values ranging between 1 x 10^{-12} m^2/s and 52.3 x 10^{-12} m^2/s (Table 4.2) under short and long-term marine exposure. The maximum value for surface chloride concentration, C_0, at 270days is 0.85% by weight of binder compared with 28 and 90days having 0.32% and 0.56% by weight of binder respectively. Using a semi-empirical relationship between D_C and time, a prediction model for chloride concentrations after long-term (e.g. 10 years) of exposure was established [192]. The build-up of chloride ions in concrete over a passage of time will reach and surpass the threshold value for corrosion initiation at the reinforcing steel surface [170].

Table 4. 2: Published chloride diffusion coefficient Dc values for OPC concrete

D_C ($m^2/s_x 10^{-12}$)	Curing Age	W/C Ratio	Mix Design			Author	Remarks
			Binder (kg/m3)	Water (kg/m3)	Total Aggregate (kg/m3)		
2.5	1.5y	0.43	339	146	-	R.B. Polder, 1997[199]	Fly ash based concrete exposed to salt/dry cycle in the laboratory
3	1.0w	0.40	420	168	-		
2	4.0w	0.40	420	168	-		
1	14.0w	0.40	420	168	-		
4	1.0w	0.54	300	162	-		
3	4.0w	0.54	300	162	-		
2.5	14.0w	0.54	300	162	-		
2.86-3.65	2.0m	0.50	330	165	2066	Zhang & Gjorv 1999 [200]	Theoretical analysis of concrete under RCPT
1.19-1.94	2.0m	0.50	330	165	1894		
2.8-3.1	1.0w	0.35	450	157.5	1695	Luping 1997 [201]	Rapid penetration of chloride in silica fume concrete
4.4-5.4	1.0w	0.40	420	168	1692		
5.6-13.6	1.0w	0.50	390	195	1636		
9.8-39.7	1.0w	0.75	250	187.5	1784		
2.07	28d	0.66	288	190	1900	Bertolini 2013 [202]	-
1.49	28d	0.62	275	170.5	1940		
1.77	28d	0.60	315	189	1835		
1.65	3m	0.50	400	200	1800	Collepardi *et al,*1972 [203]	-
3.24	3m	0.60	384	230.4	1728		
11-14	14d	0.50	423	211.5	1777	Page *et al.,* 1991[204]	Concrete slab exposed to 5% chloride ponding
4.7	90d	0.35	380	133	1924	Hooton, 1997 [197]	Silica fume concrete under bulk diffusion test
5.9	120d	0.35	380	133	1924		
5.0	90d	0.40	374	149	1840		
9.3	120d	0.40	374	149	1840		
7.1	90d	0.45	369	165	1770		
10.8	120d	0.45	369	165	1770		
52.3	28d	0.58	530	307	1309	Mangat & Molloy, 1999 [192]	Steel fibre reinforced concrete exposed to wet/dry cycle in the laboratory
23.8	90d	0.58	530	307	1309		
10.0	270d	0.58	530	307	1309		
6.13	154d	0.40	590	236	1392	Mangat & Gurusamy, 1995 [205]	Steel fibre reinforced concrete under marine exposure (tidal cycles)
3.90	304d	0.40	590	236	1392		
2.81	1250d	0.40	590	236	1392		

4.2.3.5 Chloride Contents and Binding Capacity

The chlorides in concrete can be present in three forms namely chemically bound (acid soluble chloride), physically bound (water soluble chloride) and free chloride (pore fluid chloride) [25][97][170]. The sum of the acid soluble, water soluble and free chloride is termed the total chloride. In practice for OPC concrete, the long term concentration of free chloride in concrete and the chloride concentration of the environment (curing solution) are assumed to be equal [97]. The free chloride is related

to the concentration of the chemically and physically bound chloride. Since acid soluble chlorides are chemically bound (immobile) in the concrete matrix, the physically bound chloride can either release or absorb chloride ions from the free chloride in the concrete pore solution. Only the free chloride which can penetrate into the ferrous oxide protective layer of the steel reinforcement will initiate corrosion in reinforced concrete [95]. Therefore, the critical threshold level for corrosion initiation is evaluated by the amount of free chloride present in the concrete matrix expressed in percentage to the total amount of binder in the mix [206].

The chemically bound chloride is influenced by the volume of unhydrated aluminate (C_3A) and tetracalcium aluminoferrite (C_4AF) phase during ordinary Portland cement hydration. The effective portion of aluminate (C_3A) and tetracalcium aluminoferrite (C_4AF) are those that react during the curing period in the chloride solution to form Friedel's salt ($Ca_6Al_2O_6.CaCl_2.10H_2O$) and calcium chloroferrite ($Ca_6Fe_2O_6.CaCl_2.10H_2O$). The reaction products of aluminate (C_3A) and tetracalcium aluminoferrite (C_4AF) before the curing period in chloride solution do not contribute to chemically bound chloride [207].

The physically bound chloride is influenced by the volume of hydrated and pozzolanic constituents [207]. Physical binding occurs between the interface of the pore solution and hydrated products in the concrete matrix. Physical binding is dependent on the content of the CSH gel [95]. The binding capacity of chloride in concrete removes free chloride present within its pore structure thereby reducing the mobile chloride that can attack passive steel in concrete. Nevertheless, since the diffusion process is based on attaining equilibrium between the free chloride concentration and the external environment (chloride solution), the concentration of free chloride will continue to increase with time [208] and ultimately threshold levels for corrosion initiation in steel may be reached. The pore structure may also be altered due to chloride binding effect by formation of Friedel's salt ($Ca_6Al_2O_6.CaCl_2.10H_2O$). The result is a less porous structure within the concrete matrix to prevent the ingress of chloride [103][209].

4.2.3.6 Chloride Threshold

Chloride induced corrosion in reinforced concrete commences when a critical concentration of chloride is reached at the surface of the embedded steel in the concrete [97]. This is termed the threshold chloride concentration for the initiation of pitting corrosion in steel reinforcement. A number of factors affect critical chloride levels, ranging from concrete mix design, curing method, age, temperature, the presence of

oxygen and moisture [97] and importantly the chemical composition and surface condition of the steel reinforcement. A single value for chloride threshold level is not true for different types of concrete, steels and environment [96]. However, the maximum acceptable chloride concentrations expressed as the percentage of chloride ions by mass of cement have been recommended and are presented in Table 4.3 [74].

The chloride concentration threshold for corrosion initiation in AACM concrete specimens with steel embedded in them will be determined by monitoring electrochemical corrosion in the steel as reported in chapter 7. The specimens have been exposed to a 5% chloride solution since November, 2014.

Table 4. 3: Maximum allowable total chloride content in concrete, BS EN 206 [74]

Concrete use	Chloride content class [a]	Maximum Cl^- content by mass of cement[b] %
Not containing steel reinforcement or other embedded metal with the exception of corrosion-resisting lifting devices	Cl 1,00	1,00
Containing steel reinforcement or other embedded metal	Cl 0,20	0,20
	Cl 0,40[c]	0,40
Containing prestressing steel reinforcement in direct contact with concrete	Cl 0,10	0,10
	Cl 0,20	0,20

a For a specific concrete use, the class to be applied depends upon the provisions valid in the place of use of the concrete.

b Where additions are used and are taken into account for the cement content, the chloride content is expressed as the percentage chloride ion by mass of cement plus total mass of additions that are taken into account.

c Different chloride content classes may be permitted for concrete containing CEM III-cements according to provisions valid in the place of use.

4.2.3.7 Chloride Diffusion Coefficient D_C

Several publications in connection with chloride diffusion coefficients, $\boldsymbol{D_C}$, are presented in Table 4.2. The chloride diffusion coefficients, $\boldsymbol{D_C}$, are conveniently obtained from simulated experiments performed within a short duration [201][200][202]. For long duration predictions, however, semi-empirical expressions based on calculations have been applied to test data obtained over periods extending beyond 6 months. For example, *Polder* [198] obtained the experimental results of chloride diffusion coefficients $\boldsymbol{D_C}$ from 1week to 14 weeks of chloride diffusion tests and the long-term chloride diffusion coefficient $\boldsymbol{D_C}$ value at 1.5 years was determined by using empirical expressions. The chloride diffusion coefficients $\boldsymbol{D_C}$ presented for long durations are best described as predictions due to the complex nature of concrete pore structure and the chloride binding isotherm. Some variation between the predicted values and the actual experimental values of chloride diffusion coefficients $\boldsymbol{D_C}$ are

bound to exist. This research investigation presents the results of chloride diffusion parameters *(D_C and C_0)* of AACM concrete up to 270 days exposure period in 5% NaCl solution.

Chloride diffusion coefficients D_C presented in Table 4.2 are mainly determined for short duration exposure except for *Mangat and Molloy* [192] that presented experimental results for up to 270 days exposure. The values of chloride diffusion coefficients, $\boldsymbol{D_C}$, were mainly influenced by the cement content, water/cement ratio, binder type and exposure period. The relatively high chloride diffusion coefficients, $\boldsymbol{D_C}$, (52.3 x 10^{-12} m^2/s) presented by *Mangat and Molloy* [192] were influenced by the high water/cement ratio of 0.58 in fibre reinforced concrete and wet/dry cyles in the laboratory. These parameters are noted to increase the chloride diffusion rate in concrete. The high water/cement ratio causes a more permeable concrete, a similar observation was reported in chapter 3. *Luping* [201] used a higher water/cement ratio of 0.75 and obtained chloride diffusion coefficients, $\boldsymbol{D_C}$, (39.7 x 10^{-12} m^2/s) but the curing age was not stated.

A longer duration of exposure and higher binder content on the other hand, reduces the chloride diffusion coefficients, $\boldsymbol{D_C}$. For example, *Mangat and Gurusamy* [205] showed a reduction in chloride diffusion coefficients, $\boldsymbol{D_C}$ from 154 to 1250 days exposure. At 154 days, the chloride diffusion coefficient, $\boldsymbol{D_C}$, is 6.13 x 10^{-12} m^2/s but reduces to 2.81 x 10^{-12} m^2/s at 1250 days. The explanation given was the significant decrease in the permeability of concrete with time limiting the diffusion of chloride.

4.3 EXPERIMENTAL PROGRAMME

4.3.1 Mix Composition

This research programme was conducted to determine the durability properties of an alkali activated cementitious concrete (AACM concrete). The AACM concrete comprises of a cementitious binder, fine aggregate, coarse aggregate and the alkali activator. The AACM concrete trial mix S_1 was performed prior to the selection of the mix composition used for the chloride ingress, carbonation and corrosion investigation in this research work. A number of mixes were made with the proprietary AACM binder and activator by incorporating a range of 438 kg/m^3 to 585 kg/m^3 of fine aggregate and 988 kg/m^3 to 1170 kg/m^3 of coarse aggregate. The trial mix S_1 was tested for strength, shrinkage and workability to achieve a practical field mix of AACM concrete with high strength. A compressive strength of 72 MPa was achieved at 28 days age under dry curing, the slump was between 60 - 180 mm and the shrinkage had a

mean value of 683.4 microstrain at 78 days age. The experimental AACM concrete mixes S_2 to S_6 used in this research were produced based on the trial mix S_1. The AACM binder content and fine aggregate content of the mixes S_2 to S_5 was reduced relative to mix S_1 while the liquid/binder and coarse aggregate content was increased to adjust the workability and setting time required for practical mixes. As a result the strength of mixes S_2 to S_5 was lower than the trial mix S_1. The composition of the five series of concrete mixes S_2 to S_6 is given in Table 4.4. S_6 is the control mix produced with 100% OPC binder which gave a 28 days strength of 46 MPa. The reference alkali activator liquid [210] was diluted with tap water by 2.15%, 4.24%, 8.12% and 12% in mixes S_2 to S_5 respectively (Table 4.4).

The total binder content of AACM concrete mix S_2 is 688 Kg/m^3 while AACM concrete S_3 to S_5 have a lower content of 619 Kg/m^3. OPC concrete mix S_6 represents the control specimens used for comparison with the AACM concrete mixes S_2 to S_5. The OPC (binder) content of mix S_6 was 350 Kg/m^3. A varied liquid composition for each mix was used as presented in Table 4.4. The liquid comprised of alkali activator, water, retarder and shrinkage reagents. AACM concrete mix S_2 has the lowest percentage dilution of alkali activator with water (2.15%) while AACM concrete mix S_5 has the highest dilution (12.00%). The ratios of total liquid (alkali activator + water) to binder are 0.41, 0.48, 0.47 and 0.47 for mixes S_2, S_3, S_4 and S_5 respectively. The average 28 day strength of the AACM and control OPC mixes were planned to be fairly similar under wet curing, based on trial mix. Wet curing is standard method for quality testing in concrete [25].

Table 4. 4: Composition of AACM and OPC concrete mixes

Mix	Total Binder (Kg/m^3)	Coarse Aggregate(Kg/m^3)		Fine Aggregate (Kg/m^3)	Alkali activator (Kg/m^3)	Extra water (Kg/m^3)	Total Liquid (Kg/m^3)	Liquid/ Binder Ratio	Activator Dilution (%)	Retarder (Kg/m^3)	SRA (Kg/m^3)
		10mm Gravel	6mm Limestone								
S_2	688	654	334	438	279	6	285	0.414	2.15	8	21
S_3	619	717	374	423	283	12	295	0.477	4.24	7	19
S_4	619	717	374	423	271	22	293	0.473	8.12	7	19
S_5	619	717	374	423	260	31	291	0.470	12.00	7	19
S_6(Control)	350	769	401	585	-	170	170	0.486	-	-	-

4.3.2 Specimen Preparation

All the aggregates were in a saturated surface dry state before mixing. Half of the aggregate content was first poured inside the cretangle concrete mixer of 0.0625 m^3 (150 kg) capacity followed by the binder composition. The remaining half of both the fine and coarse aggregate content was then added to cover the binder. The binder and the aggregates were mixed for one minute. Approximately half of the liquid activator was added to the mixer and mixed for two minutes. To ensure homogeneity, the mix was briefly mixed by hand, particularly concentrating on the material sticking around the edge and corner of the mixer. The retarder was mixed with the second half of the liquid activator and stirred until fully dispersed. The mixture was then added to the mixer and mixed for a further two minutes. A shrinkage admixture (SRA) was then added followed by an additional one minute of mixing.

75 x 75 x 75 mm dimension steel moulds were used for casting cube specimens for compressive strength. Three gang steel moulds of 160 x 40 x 40 mm prisms were used for casting specimens for the shrinkage test. 250 x 250 x 75 mm dimension polystyrene moulds were used for casting chloride diffusion test specimens. The typical 250 x 250 x 75 mm polystyrene mould and the test specimens are shown in Figures 4.2 and 4.3 respectively.

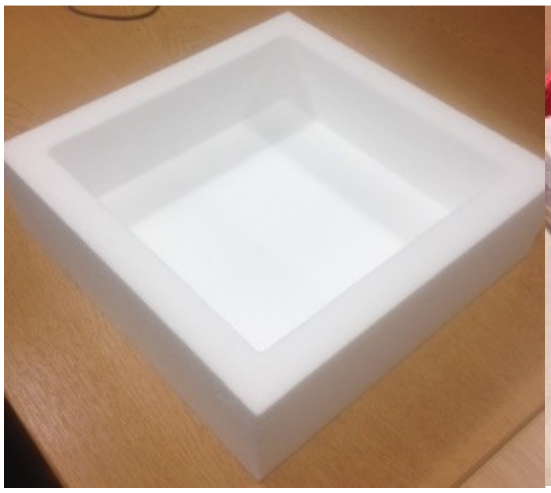

Figure 4. 2: Polystyrene moulds used for casting AACM Concrete

Figure 4. 3: AACM Concrete Specimens after demoulding

Mould oil was applied to internal surfaces of the moulds to prevent the hardened AACM from sticking to the surface. The moulds were filled in three layers. Each layer was compacted on a vibrating table for up to 60 seconds to attain homogeneity and minimise the presence of voids. The AACM concrete surface was gently trowelled to obtain a smooth and level finish. The cast specimens were placed on a flat table surface

in the laboratory environment (20^0C, 65% R.H.) and covered with polythene sheets to prevent moisture loss. The specimens were demoulded after 24 hrs.

4.3.2.1 Chloride Samples

AACM and OPC concrete mixes S_2 to S_6 were cast into slabs of 250 x 250 x 75 mm dimensions as shown in Figures 4.2 and 4.3. After demoulding, the chloride diffusion test samples of the AACM and OPC concrete mixes S_2 to S_6 were cured in water at 20^0C for 27 days (total age 28 days). The specimens were taken out of water and surface dried. Two coats of bituminous paint were applied to five faces of the slabs except the face to be exposed to a chloride solution as shown in Fig. 4.4.

Subsequently after the 27 days of wet curing, the chloride diffusion test samples were fully immersed in a 5% sodium chloride solution. The face cast against the bottom of the polystyrene mould was exposed to the NaCl solution. The chloride diffusion tests were carried out at 55, 90, 120, 180, 270 and 540 days of chloride exposure periods. A total of 75 slabs (15 slabs per each mix S_2 to S_6) were cast for the chloride diffusion test. An average of two slabs for each concrete mix was used at each chloride diffusion test age. For example, chloride diffusion test was performed on two slabs of AACM mix S_2 at 55 days chloride exposure period.

4.3.2.2 Compressive Strength

The compressive strength test was performed in accordance with *BS EN 12390-3* [133]. 75 x 75 x 75 mm cubes of AACM and OPC concrete mixes S_2 to S_6 (Table 4.4) were cast in steel moulds and tested for compressive strength at ages 1, 2, 3, 7, 14, 21 and 28 days. Two sets of cube specimens (S_2 to S_6) which were subjected to wet and dry curing were produced, six cubes for each mix at each test age making forty-two cubes for each mix and one hundred and five cubes for each set of wet and dry curing. A total of two hundred and ten cubes were produced for all the mixes (S_2 to S_6). The first set of the test cube specimens (S_2 to S_6) were cured in air at 20 deg C. and 65% R.H. for 27 days while the second set of the cube specimens were cured in water at 20 deg C. for 27 days. The air cured specimens were covered with polythene sheets to prevent rapid water loss. AACM and OPC concrete cubes were exposed to both dry and wet curing.

4.3.2.3 Shrinkage

The curing of the third batch (shrinkage test samples) was performed in accordance with BS ISO 1920 -8 [211]. Three gang steel moulds of 160 x 40 x 40 mm were used to cast prism specimens for the shrinkage test. The concrete was placed in the prism moulds in three layers and compacted on a vibrating table. The moulds were

covered with polythene sheets to minimise the rate of moisture loss and were stored in the laboratory for 16- 24 hrs at 65% R.H. and 20^{o}C. After de-moulding, stainless steel demec points were fixed along two parallel longitudinal side faces of each prism specimen at a gauge length of 100 mm. The datum reading was taken at 24 hrs age after casting. The specimens were then immersed in water for 7 days and expansion readings were taken at regular intervals with the demec extensometer. The difference between the datum reading at 24 hrs and 7 days was recorded to give the expansion. After 7 days, the specimens were carefully removed from water and surface dried with a damp cloth. A demec extensometer reading was taken before exposing the specimens to laboratory air (65% R.H. and 20^{o}C). The demec extensometer shrinkage readings were taken at regular intervals, initially daily. The difference between the 7 days (datum reading) and subsequent readings was recorded to give the drying shrinkage. The average reading of three specimens (two faces each) per mix was recorded.

4.3.3 Experimental Procedure

4.3.3.1 Chloride Ingress Test

Bulk diffusion tests [187][98] were adopted for measuring the long-term chloride diffusion in the AACM and OPC concrete mixes S_2 to S_6. The two standard test methods have similar procedures apart from the concentration of the chloride exposure solution. *DD CEN/TS 12390-11* [98] specifies 3% NaCl solution (by weight) whereas *NordTest 443* [187] specifies 165 g ± 1g NaCl per dm^3 solution (16.5% NaCl solution by weight). A 5% NaCl solution in tap water was prepared for chloride exposure of the test specimens. The 5% NaCl solution provides an accelerated chloride diffusion test which gives higher chloride concentrations at given depths than under normal marine exposure. Therefore, the permissible chloride concentrations allowed in *DD CEN/TS 12390-11* [98] for different types of chloride exposure cannot be directly related to the data presented in this chapter. The transportation mode of chloride ion was by diffusion only. This was achieved by curing the test specimens in water for 28 days after casting to fully attain saturation of concrete pores thereby eliminating the initial sorption effect upon chloride exposure. All the faces of the chloride diffusion test specimens were coated with 1 mm thick layer of bituminous paint except the 250 x 250 mm face to be exposed to the 5% NaCl solution, as shown in Fig 4.4.

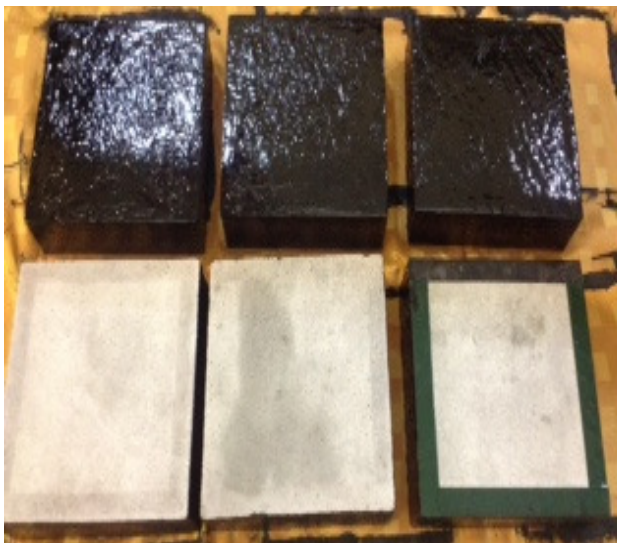

Figure 4. 4: Coated surfaces (top picture), exposed surface (bottom picture)

Figure 4. 5: Specimens immersed in 5% sodium chloride solution.

Figure 4. 6: AACM specimen sawn into half

Figure 4. 7: Some powder sample locations highlighted in red

4.3.3.2 Concrete Powder Sample Collection

At ages of 55, 90, 120, 180 and 270 days, two chloride diffusion test specimens for each series of mixes S_2 to S_6 were removed from the chloride solution. The test specimens were sawn into two equal halves along the plane perpendicular to the uncoated face as shown in Figures 4.6 and 4.7. The direction of the masonry sawing was from the top uncoated surface of the sample to the bottom coated face. The specimens were left to dry in the laboratory for 24 hrs under a temperature of 20^0C and relative humidity of 65% after masonry sawing. Each freshly sawn face perpendicular to the exposed face to the chloride solution was drilled at 8, 15, 20, 25, 35, 50 and 65 mm depths from the top (uncoated) surface. Six holes were drilled per depth making the total of 42 number of holes for each specimen as shown in Fig. 4.7. The diameter of the

holes was 4 mm. They were drilled by means of a SDS drill on the freshly sawn face of the specimens. Each drilling represented a 20 mm deep hole at a constant depth from the chloride-exposed face of the specimen. The initial 5 mm depth of drilled powder was discarded from each hole. A further 15 mm depth hole was drilled to provide a powder sample for the analysis of physically and chemically bound chlorides. The drilling was performed within an area approximately 20 mm from the coated edges of the slab specimens to obviate the risk of edge effects and any disturbances of the bituminous coating which may interfere with the chloride readings. The concrete powder samples were carefully collected to avoid contamination from the bituminous coating. The powder samples collected from the six holes drilled at each depth for each specimen were combined for the analysis. The carefully collected powder samples per depth were stored in a self-sealing polythene bag and labelled accordingly. The concrete powder was sieved through a 150 µm sieve to separate the finer powder as shown in Figures 4.8 and 4.9. The water soluble and acid soluble chloride analysis of the powder samples were carried out in accordance with standards *NordTest 443* [187] and *DD CEN/TS 12390-11* [98].

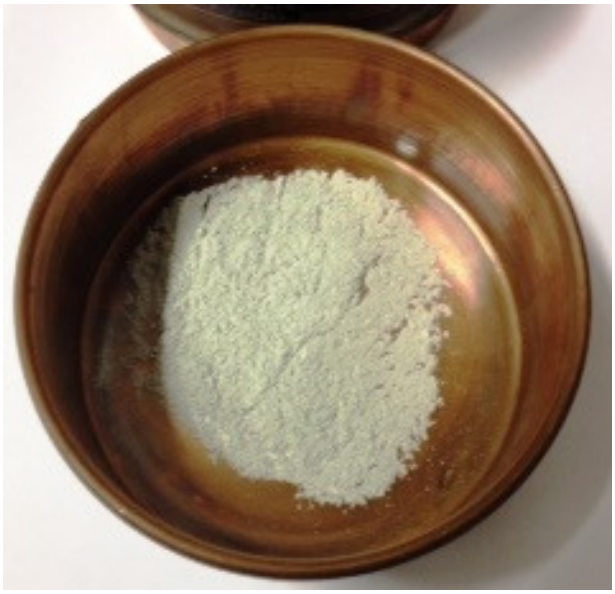

Figure 4. 8: AACM powder passing a 150 µm sieve

Figure 4. 9: AACM powder passing (bottom picture) and retained (top picture) by a 150 µm sieve

4.3.4 Testing Procedure

4.3.4.1 Physically Bound Chloride Analysis

The Chloride Ion Selective Electrode (ISE) used to measure the water-soluble chloride has a solid state poly-crystalline membrane that measures chloride ions (Cl^-) in

aqueous solution. It is suitable for field and laboratory applications. The operation of the device is based on the linear relationship between the electric potential developed between the internal Silver Silver Chloride (Ag/AgCl) reference electrode and the reference electrode immersed in the concrete powder aqueous solution [212]. The Chloride ISE was supplied by Vernier Software and Technology.

Five grams of the concrete powder passing through a 150 µm sieve was dissolved in 50 ml of distilled water. The effective ionic concentration, otherwise known as chloride ion activity within the concrete powder solution, was buffered with $NaNO_3$ to avoid possible interference by other ions like iodine, bromide, cyanide and sulphide [213]. The solution was swirled manually to ensure good, homogeneous contact between it and the ISE membrane. The white reference contact near the tip of the electrode (ISE) was immersed in the solution without entrapping air bubbles below it. The ISE was held in the aqueous solution until the reading stabilized and the displayed reading was then recorded as shown in Fig 4.10. The ISE was rinsed by spraying with a jet of ionised water and dabbed dry with a low-lint laboratory tissue between measurements to prevent hysteresis effects. The ISE was calibrated before and after each measurement to achieve accuracy. The chloride ion reading of powder samples collected at each depth using ISE was repeated thrice to achieve high level of accuracy. The coefficient of variance of repeatability is 10%. The calibration was done by using a pre-prepared 1000 mg/l and 10 mg/l standard NaCl solution.

The pH of the powder solution at each depth was taken as shown in Fig 4.11**.** The pH readings of the powder dissolved in 100 ml distilled water were taken using a digital pH meter. The pH reading was repeated thrice for each powder sample.

Figure 4. 10: ISE reading of concrete powder solution

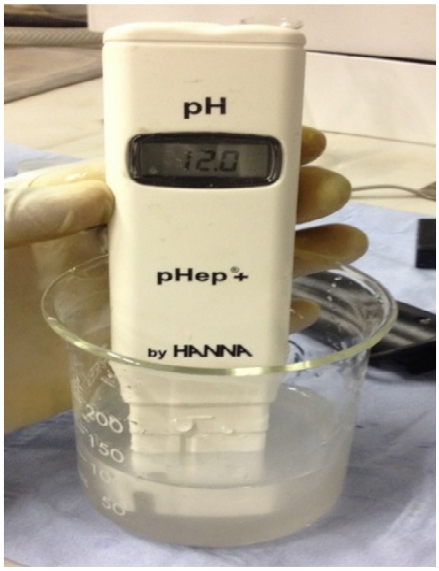

Figure 4. 11: pH reading of concrete powder solution

4.3.4.2 Chemically Bound Chloride Analysis

The determination of chloride content in hardened concrete was performed in accordance with *BS EN 14629* [214].

Volhard's titration method was used to determine the acid soluble chloride concentration on the second part of the concrete powder sample. This involves dissolving 5 grams of powder sample in 50 ml of distilled water and adding 10 ml of 5 mol/l nitric acid followed by 50 ml of hot water. The solution was heated until boiling for 3 mins and stirred continuously. The heated solution was filtered immediately through a medium-textured filter paper. The filter paper was washed with 1% nitric acid to prevent chloride loss. 5 ml of silver nitrate solution was used to precipitate the mixture and ammonium thiocyanate solution was used as titrant while continually agitating the solution until the faint reddish-brown coloration no longer disappears. The volume of ammonium thiocyanate solution used was recorded as V_1.

To obtain V_2, a further 5 ml of silver nitrate solution was added and the titration continued until the end-point was reached a second time. The volume of ammonium thiocyanate solution used was recorded as V_2. The chloride content was calculated as percent of chloride ion by mass of sample using the following formula (equation 4.5):

$$C_C = 3.545 * f * \frac{(V_2 - V_1)}{m} \qquad 4.5$$

V_1 volume of the ammonium thiocyanate solution used in the first titration [ml];

V_2 volume of the ammonium thiocyanate solution used in the second titration [ml];

m mass of the concrete sample [g];

f molarity of silver nitrate solution

4.4 RESULTS AND DISCUSSION

4.4.1 Introduction

The first part of this chapter was to develop an optimal mix of AACM concrete with high compressive strength suitable for structural applications. The mechanical properties and resistance to diffusion of aggressive ions such as chlorides are dependent on the pore structure of cementitious materials. Four AACM concrete mixes were developed and characterised to prepare them for a comprehensive investigation of durability properties. Their mix composition is given in Table 4.4. The compressive

strength and shrinkage of these mixes were determined because they are important controlling factors for the quality and crack resistance of the material. Literature has shown that the strength development and shrinkage of OPC concrete depends on the refinement of its micro-pore structure as does the resistance to diffusion of harmful ions (mainly chloride and carbon dioxide). The basic concepts of micro-pore structure in concrete are expected to apply to AACM concrete generally, but they need to be quantified. The results of micro-pore structure parameters of AACM concrete were presented in chapter 3. The shrinkage results will be discussed in chapter 6 along with carbonation shrinkage.

4.4.2 Compressive Strength

The strength development of concrete is an important property revealing the quality of concrete because it is directly related to the micro structure of the hydrated cement paste [25]. This investigation involves the assessment of AACM concrete mixes in which three liquid/binder ratios, two binder contents and four alkali activator dilution ratios were used, as shown in Table 4.4. The liquid binder ratios were 0.41, 0.47 and 0.48. The binder contents were 688 Kg/m^3 and 619 Kg/m^3. The alkali activator dilution was 2.15%, 4.24%, 8.12% and 12.00%. Control specimens S_6 of concrete made with 100% OPC binder were used to compare the strength of AACM relative to OPC concrete. In addition, a predicted strength-age curve for OPC concrete mix S_7 representing water/cement ratio of 0.4 (to complement w/c of 0.486 for mix S_6), cured at normal temperature [25] is plotted in Fig. 4.12 to compare the strength development of AACM concrete with OPC concrete. The strength development under wet and dry curing is presented in Figures 4.12 and 4.13 respectively.

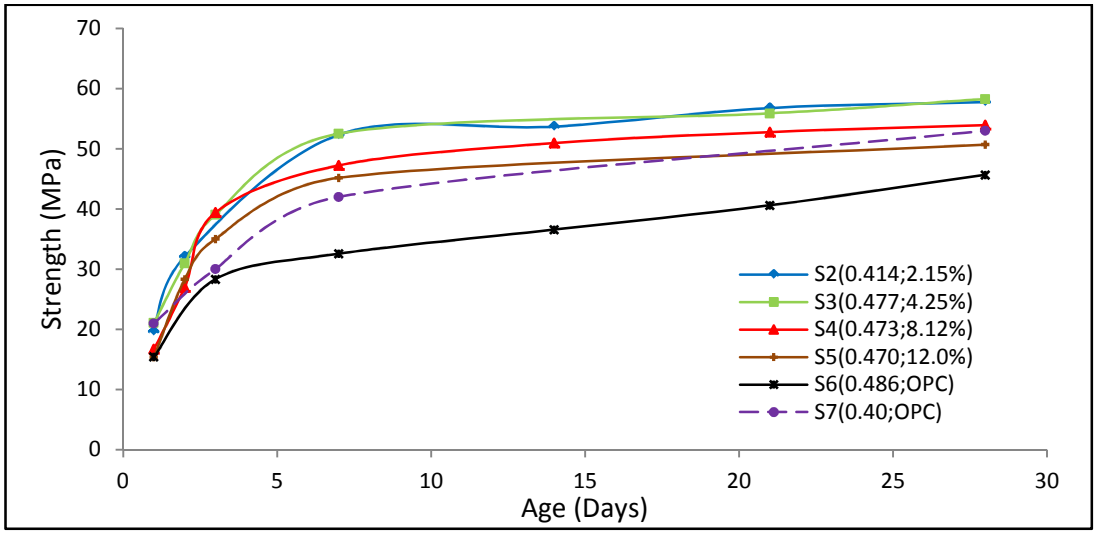

Figure 4. 12: Compressive strength with age of AACM concrete (wet cured, 20^{0}C)

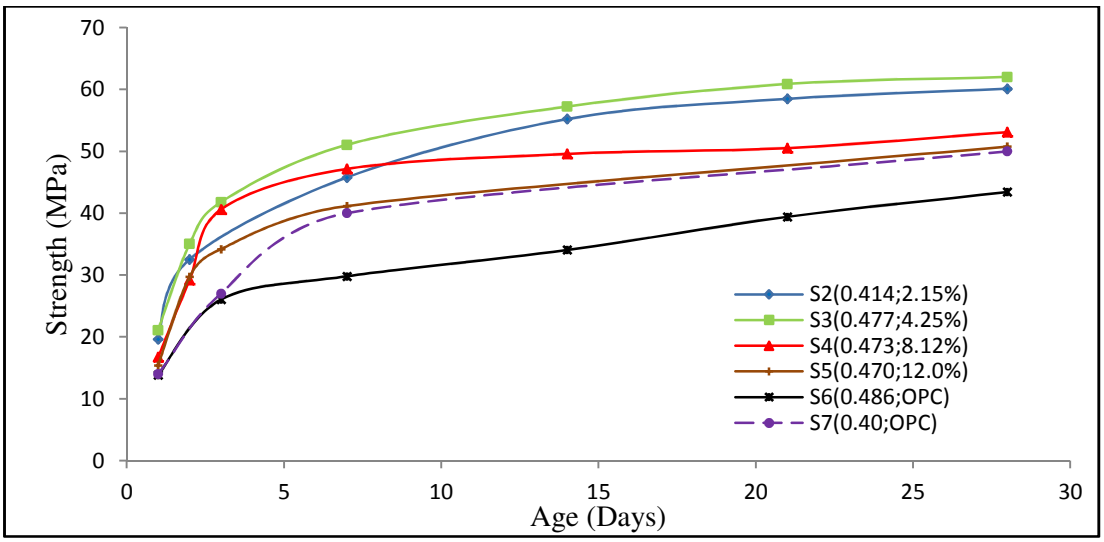

Figure 4. 13: Compressive strength with age of AACM concrete (dry cured, 20^0C, 65% RH)

4.4.2.1 Strength Development of AACM and OPC concrete

Figures 4.12 and 4.13 show the strength development for AACM and OPC concretes under wet and dry curing. AACM concrete mix S_3 with the highest liquid binder ratio of 0.48 reveals a considerably high strength of 62.0 MPa at 28 days under dry curing (Fig. 4.14). This is 30% higher than the strength attained by the dry cured control mix of OPC concrete (mix S_6, 100% OPC) at the same age and similar w/c ratio. Among the AACM concrete mixes, the lowest strength was recorded for AACM mix S_5 of liquid/binder 0.47, which had strength of 51 MPa. Generally, all the AACM concrete mixes had more strength than OPC concrete S_6 and S_7 under both wet and dry curing. The strength difference between AACM concrete and OPC concrete is more pronounced under dry curing.

The predicted strength of OPC mix S_7 with 0.40 w/c ratio, is similar to AACM mix S_5 at later ages while significant difference in strength is observed between AACM mix S_2 and OPC mix S_7. AACM mix S_5 has 0.47 liquid/binder ratio and 12.0% dilution ratio. AACM mix S_2 had similar liquid/binder ratio of 0.41 to OPC mix S_7. The strength gain of AACM concrete is observed to be greater than OPC concrete at the same liquid/binder ratio. The rate of strength gain at early age (up to 3 days) is much greater in AACM concrete compared with OPC concrete.

4.4.2.2 Strength Development at Early Age

A comparison of Figures 4.12 and 4.13 shows that AACM concrete cured in air at room temperature (65% RH, 20^0C) develops higher compressive strength (Fig. 4.13) compared with the wet cured specimens as shown in Fig 4.12. The difference in the 28 day strength between the air and wet cured AACM concrete mixes (S_2 to S_5) are 3.7

MPa, 4.0 MPa, 2.5 MPa and 2.7 MPa respectively. The development of strength in AACM concrete is greater under dry curing than wet curing due to the formation of more crystalline geopolymerisation product [3][26]. Elevated temperatures through steam or dry heat methods, in the range of 50 - 80^0C, have been used to achieve a 15% increase in strength over wet curing methods in AACM concrete [26]. The higher strength achieved by AACM concrete mixes S_2 to S_5 under dry curing is contrary to that of OPC concrete mix S_6 whose strength is higher under wet curing. Similar trend is observed for the 3 day strength.

Rapid early strength development of the AACM concrete mixes S_2 to S_5 was recorded for the first 7 days under dry curing. An average strength development of 92% of 28 days strength was achieved within 7 days by AACM mix S_2 while the lowest value of 81% was obtained for AACM mix S_4. AACM mixes S_3 and S_5 achieved 86% and 85% of the 28 days strength respectively. The control OPC concrete mix S_6 gained 78% of the 28 days strength within 7 days (Fig. 4.13). The differences are even more significant at earlier age (e.g. 3 days) between the rate of strength development of AACM and OPC concrete. For example, the strength under wet curing for AACM mix S_3 and OPC mix S_6 are 39 MPa and 28 MPa respectively while it is 40 MPa for mix S_3 and 26 MPa for mix S_6 under dry curing.

The rate of strength gain increases with a decreasing liquid/binder ratio. AACM mix S_2 with the lowest liquid/binder ratio, gained strength more rapidly than the other AACM concrete mixes. Similarly, OPC mix S_7 with 0.4 w/c gained strength more rapidly than OPC mix S_6 with 0.48 w/c. Lower water/cement ratios in OPC concrete increase early strength development as a result of binder grains coming closer to one another and rapidly forming a continuous system of gel [25]. The rate of strength gain was rapid for AACM and OPC concrete up to 7 days. Beyond 7 days, the strength gain was moderate. This strength gain phenomenon is in agreement with other researchers [21][25][167][178]

4.4.2.3 Influence of binder content

AACM concrete mixes had much higher binder contents (619 and 688 kg/m^3) compared with OPC mix S6 (350 kg/m^3). The strength of the AACM mixes was higher than OPC concrete mix but the increase was not proportional to the much higher binder content. This is due to the entirely different strength development mechanisms of the two materials.

The effect of binder content on the performance of alkali-activated slag concretes relative to OPC concrete has been reported by Susan et al. [22]. AACM achieved compressive strengths of 50, 72 and 75 MPa for slag binder contents of 300, 400 and 500 Kg/m^3 respectively at 28 days, thus classifying it as a high-performance concrete (HPC). The comparative OPC concrete achieved 30, 57 and 62 MPa for cement contents 300, 400 and 500 Kg/m^3 respectively at 28 days. It was also found that regardless of the binder content, alkali-activated slag concretes (AASC) achieved higher compressive strength than comparable concretes.

4.4.2.4 Influence of alkali activator dilution

The alkali activator dilutions are 2.15%, 4.24%, 8.12% and 12.00% for AACM concrete mixes S_2 to S_5 respectively (Table 4.4). The 7 and 28 days compressive strengths for AACM concrete mixes S_2 to S_5 under wet and dry curing (Figures 4.12 and 4.13) are shown in Fig 4.14 against their activator dilution.

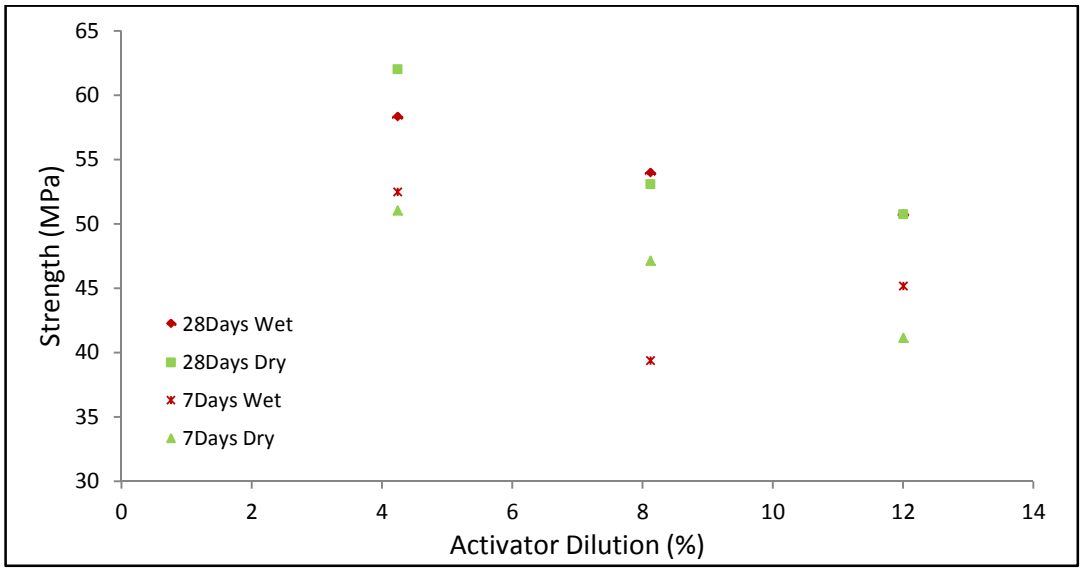

Figure 4. 14: Relationship between Compressive Strength and Activator Dilution

A lower alkali activator dilution resulted in higher strength due to higher reaction rate and the formation of a less porous concrete matrix (reported in sections 3.4.2 and 3.4.3, chapter 3). AACM concrete mix S_3 (4.24% activator dilution) had the highest strength of 62.1 MPa at 28 days under dry curing compared with 50.7 MPa for AACM concrete mix S_5 (12% activator dilution). The poor correlation of 7 day wet is likely due to experimental error. *Morsy et al* [215] studied the effect of sodium silicate activator on the strength of fly ash geopolymer binder. Their results showed that the dissolution of silica and alumina was greater for high activator concentration leading to improvement in compressive strength of the fly ash geopolymer.

4.4.3 Chloride ingress

4.4.3.1 Introduction

Physical and chemical chloride concentration profiles of AACM concrete mixes S_2 to S_5 and OPC concrete mix S_6, whose details are given in Table 4.1, are plotted in Figures 4.15 to 4.25. The experimental data show good correlation with the regression analysis profiles derived from Fick's 2nd law of diffusion which is given by equation 4.1 (section 4.2.3.4) and re-written below**.** The Fick's second law represents one dimensional non-steady condition of diffusion and is used to determine the diffusion coefficient, D_C, and surface chloride concentration, C_0, of AACM and OPC concrete.

$$C_{(x,t)} = C_0 \left(1 - erf\left[\frac{x}{2\sqrt{D_C}\, t}\right]\right) \qquad 4.1$$

Where: x = distance from concrete surface (m); t = Time (seconds); $\boldsymbol{D_C}$ = diffusion coefficient (m^2/s); $\boldsymbol{C_0}$ = equilibrium chloride concentration on concrete surface; $\boldsymbol{C_{(x,t)}}$ = chloride concentration at position x; time t .

Nonlinear regression analysis of the experimental data by a computer package (Microsoft excel) was used to generate the best fitting equation. The analysis determined the chloride concentration on the surface (coefficient $\boldsymbol{C_0}$) of the specimen, at depth zero and the diffusion coefficient, $\boldsymbol{D_C}$.

4.4.3.2 Chloride Diffusion Profiles

The chloride diffusion profiles were derived by the regression analysis of experimental data using the Fick's second law (equation 1). The regression analysis also provides a value for the diffusion coefficient, D_C, surface chloride concentration, C_0 and coefficient of correlation.

Figures (4.15 to 4.18) show the water-soluble chloride profiles for AACM concrete mixes S_2 to S_5 and the OPC concrete mix S_6 immersed in 5% NaCl aqueous solution for 55, 90, 120, 180 and 270 days. Figures (4.20 to 4.24) shows the corresponding acid soluble chloride profiles for the AACM concrete mixes S_2 to S_5 and OPC concrete mix S_6. The chloride concentrations are expressed by percentage weight of the binder. Chloride concentrations that are physically absorbed by the walls of the binder gel are termed as water-soluble chlorides. Acid-soluble chlorides are chemically bound to the concrete matrix which is formed by the hydration/geopolymerisation process. Detailed explanation is given in section 4.2.3.5.

4.4.3.2.1 Water soluble chloride concentration

The water-soluble chloride diffusion profiles for the AACM concrete mixes S_2 to S_5 and OPC concrete mix S_6 at four test ages (55, 90, 120 and 180 days) are presented in Figures. 4.15 to 4.18. The 270 days exposure profiles were not determined for water-soluble chloride because of insufficient test samples. The profiles show the water-soluble chloride content (expressed as % weight of binder) along the depth of the specimens. Non-linear regression analysis was performed on the data using the Fick's second law of diffusion (equation 4.1). The experimental and regression data show high level of correlation ranging between 0.92 and 0.99. This shows very good correlation.

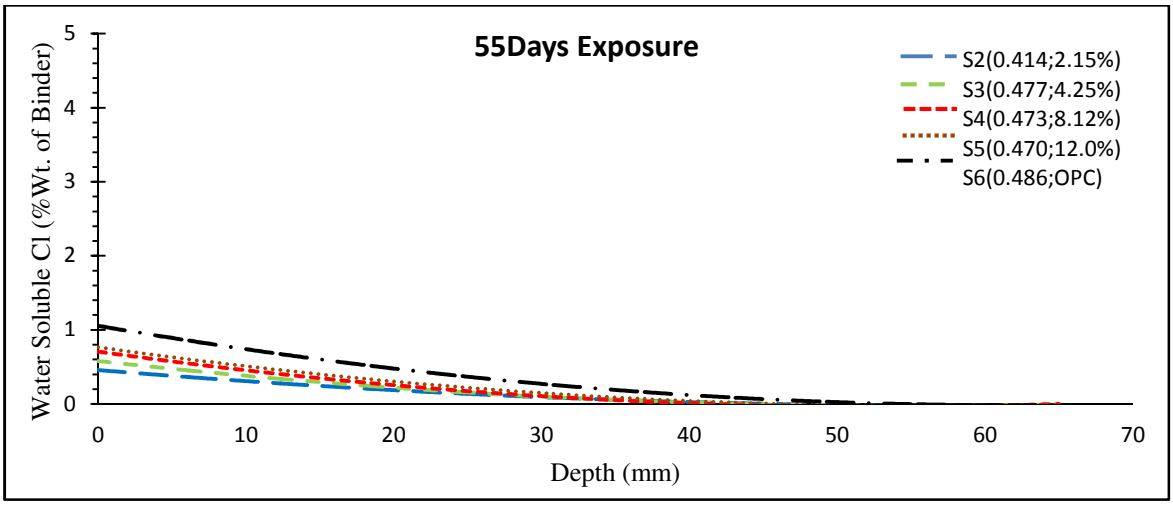

Figure 4. 15: Water-soluble chloride profiles (% weight of binder) at 55days exposure in 5% NaCl solution

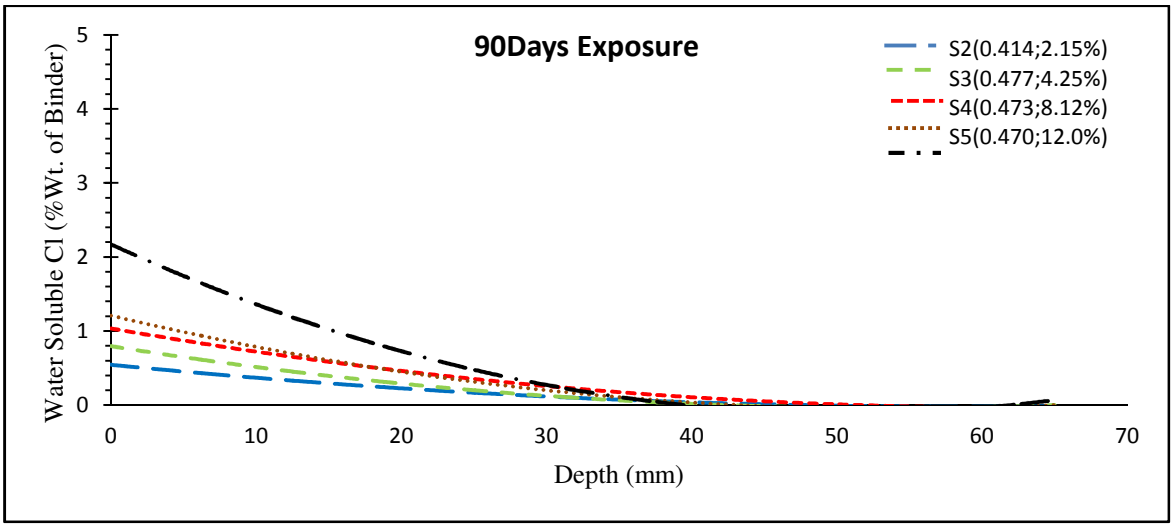

Figure 4. 16: Water-soluble chloride profiles (% weight of binder) at 90days exposure in 5% NaCl solution

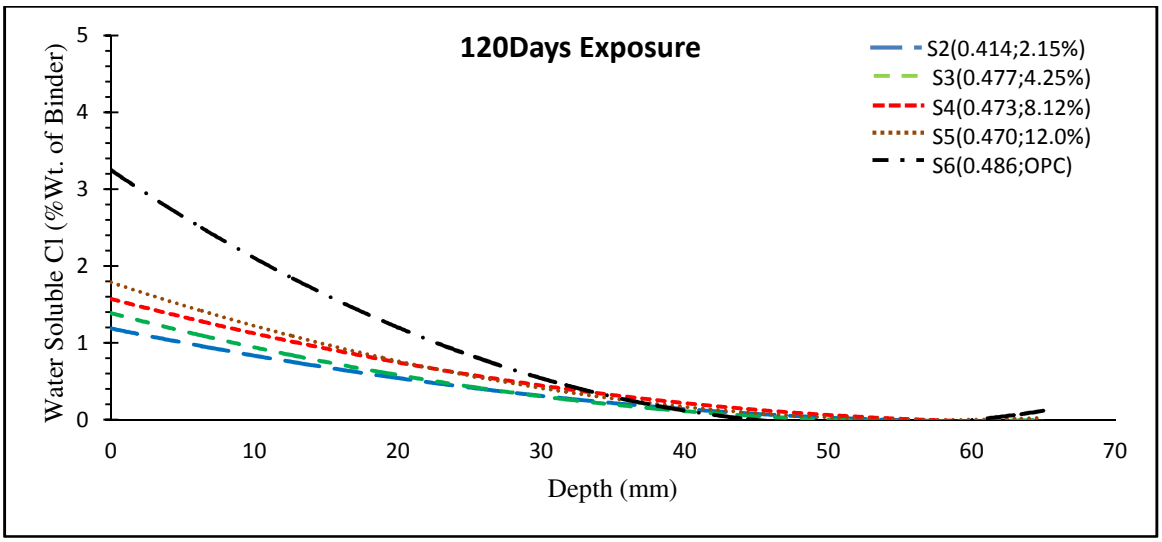

Figure 4. 17: Water-soluble chloride profiles (% weight of binder) at 120days exposure in 5% NaCl solution

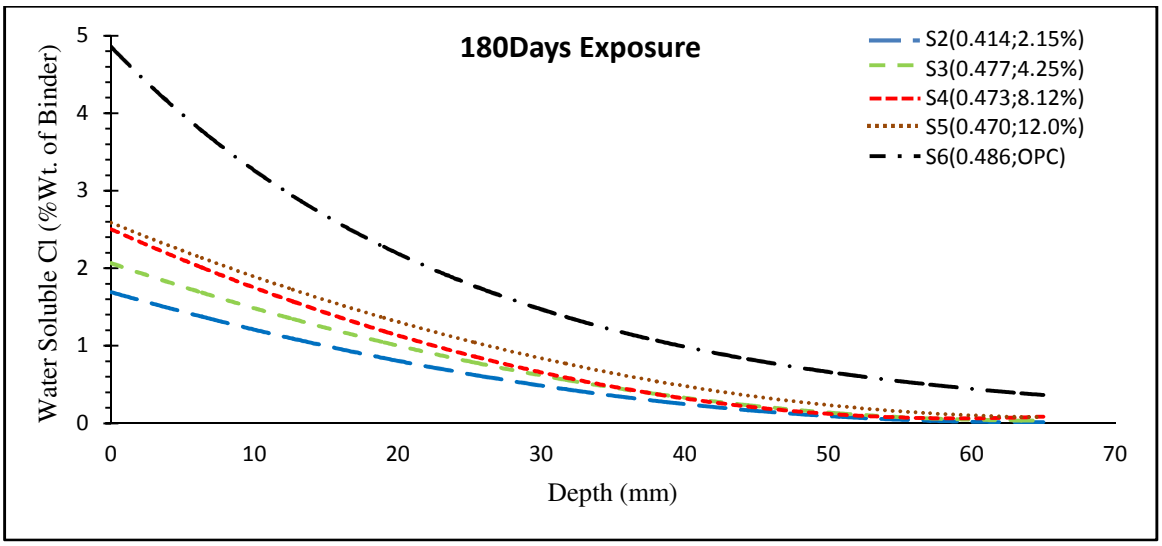

Figure 4. 18: Water-soluble chloride profiles (% weight of binder) at 180days exposure in 5% NaCl solution

The water-soluble chloride concentration for AACM and OPC concrete mixes S_2 to S_6 increases with the period of exposure to the chloride solution as shown in Figures. 4.15 to 4.18. A much lower water-soluble chloride concentration is exhibited by AACM concrete mixes compared with OPC concrete at all ages of exposure (Figures 4.15 - 4.18).

Figure 4.19 shows the relationship between water-soluble chloride content and exposure periods for selected depths of 20, 25 and 35 mm for mixes S_3 and S_6. At depth 20 mm for AACM concrete mix S_3, the chloride concentrations are 0.19%, 0.24%, 0.62% and 1.23% by weight of binder at 55, 90, 120 and 180 days of exposure respectively (Fig. 4.19). The AACM concrete mix S_3, with the same liquid binder ratio (0.48) as the OPC concrete mix S_6, shows a lower chloride content at each depth.

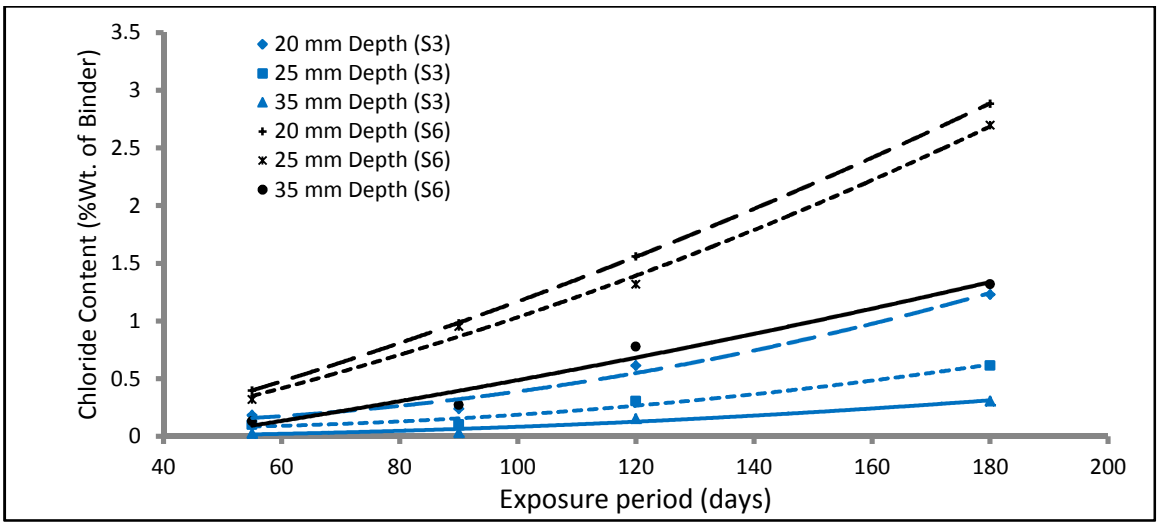

Figure 4. 19: Water-soluble chloride profiles for AACM mix S_3 and OPC mix S_6 at 20, 25 and 35 mm depths

The degree of chloride penetration through these concretes relate to the refinement of the pore structure of AACM concretes, which is reported in chapter 3. The AACM concrete mix S_3 had a porosity of 9.73% at 28 days wet curing (chapter 3, section 3.4.3.4). The OPC concrete mix S_6 had the highest porosity of 12.6% at 28 days under wet curing which resulted in higher water-soluble chloride concentration at all test ages under the same curing conditions. This suggests that refinement of the pore structure of concrete controls the water-soluble chloride penetration. *Tina et al.* [216] observed an apparent difference in water-soluble chloride content between fly ash modified normal concrete and unmodified concrete with passage of time. Fly ash concrete exhibited lower water-soluble chloride concentration than unmodified concrete, which was attributed to lower effective porosity and a high percentage of ink bottle porosity leading to higher resistance to chloride penetration of fly ash concrete. *Costa and Appleton* [217] used an ion selective electrode to measure the rate of water soluble chloride penetration. Their conclusion suggested that shotcrete containing microsilica had better chloride penetration resistance than OPC concrete in all exposure conditions due to the effect of microsilica leading to formation of tighter concrete pores. The relationship between the chloride diffusion parameters and porosity is discussed in detail under section 4.4.4.

4.4.3.2.2 Acid soluble chloride concentration

Figures 4.20 to 4.24 show the acid-soluble chloride diffusion profiles for AACM concrete mixes S_2 to S_5 and the OPC concrete mix S_6 at five test ages under the same exposure conditions used for water-soluble chloride diffusion tests. The results show good correlation with the profiles derived from Fick's 2nd law of diffusion as expressed

in equation 1. The best fit profiles have been derived by a non-linear regression analysis of the experimental data against Fick's 2nd law of diffusion (equation 4.1). The regression analysis also provides a value for the surface chloride concentration, C_0, and the diffusion coefficient, D_c.

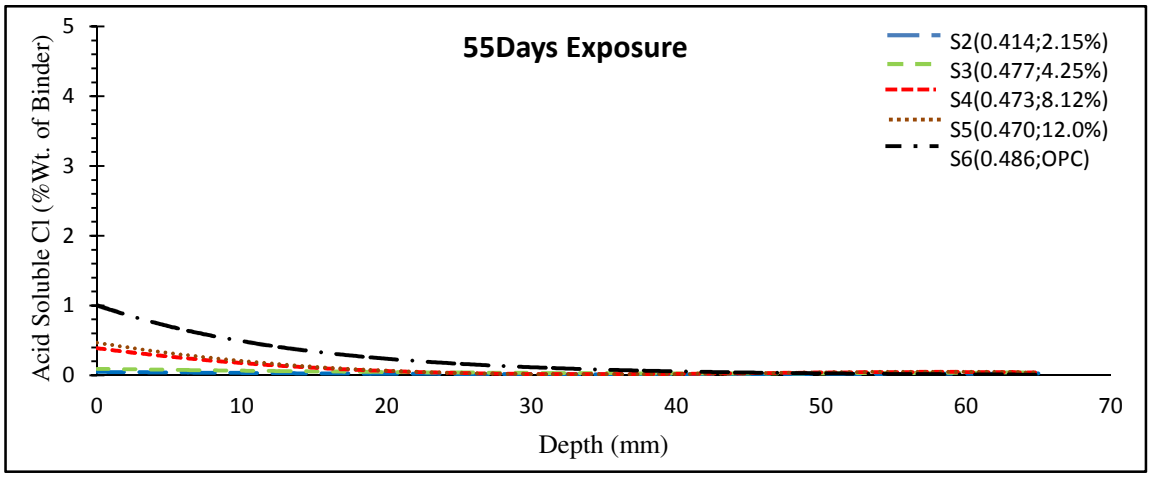

Figure 4. 20: Acid-soluble chloride profiles (% weight of binder) at 55 days exposure in 5% NaCl solution

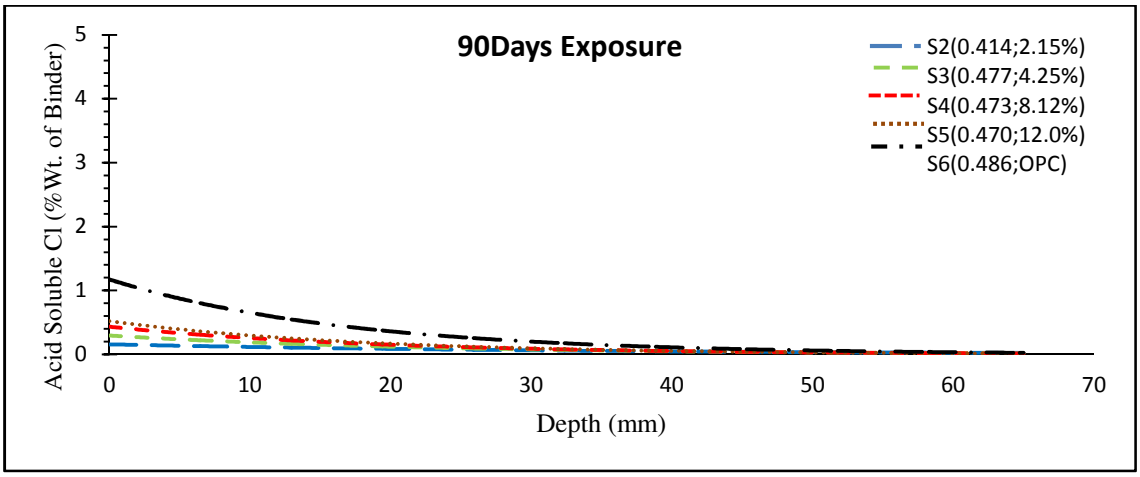

Figure 4. 21: Acid-soluble chloride profiles (% weight of binder) at 90 days exposure in 5% NaCl solution

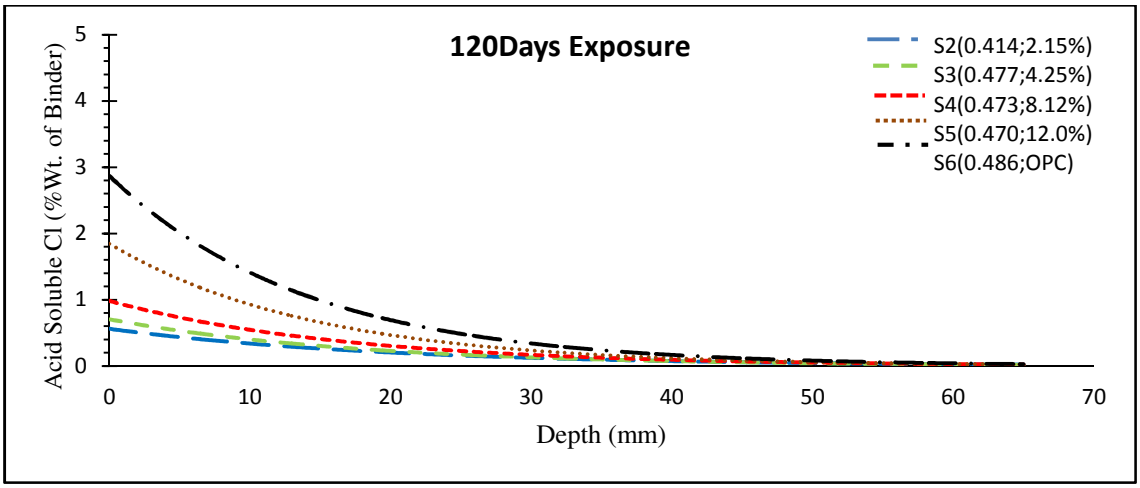

Figure 4. 22: Acid-soluble chloride profiles (% weight of binder) at 120 days exposure in 5% NaCl solution

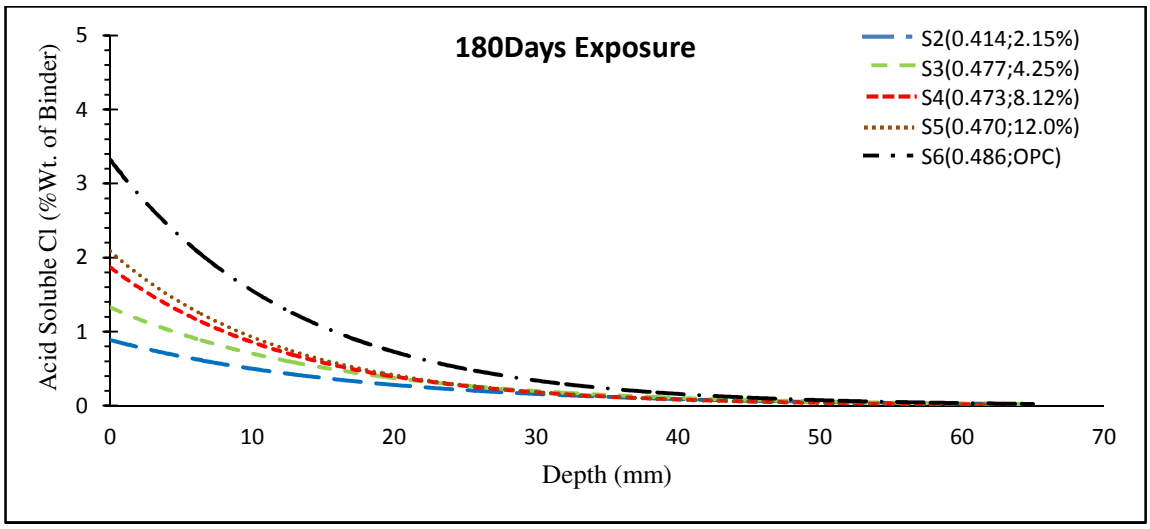

Figure 4. 23: Acid-soluble chloride profiles (% weight of binder) at 180 days exposure in 5% NaCl solution

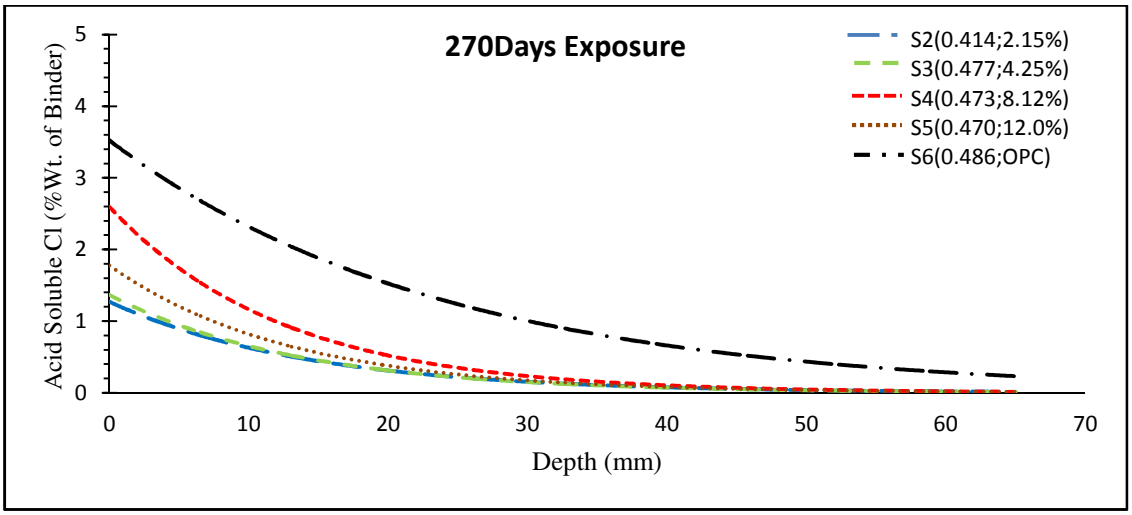

Figure 4. 24: Acid-soluble chloride profiles (% weight of binder) at 270 days exposure in 5% NaCl solution

The acid-soluble chloride concentration profiles for both AACM and OPC concrete mixes S_2 to S_6 show an increase of chloride content with exposure period, both on the concrete surface and at all depths from the exposed concrete surface (figures 4.20 to 4.24).

Figure 4.25 shows the relationship between acid-soluble chloride content and exposure periods for selected depths of 20, 25 and 35 mm for mixes S_3 and S_6. The chloride concentration at a 20 mm depth from the exposed surface of concrete was 0.02% by weight of binder for AACM concrete mixes S_2 to S_5 and 0.1% by weight of binder for the OPC concrete mix S_6 at 55 days of exposure to 5% NaCl solution (Figures 4.20 - 4.25). However, at 270 days of exposure to the same NaCl solution, the chloride concentration at 20, 25 and 35 mm depths were 0.96%, 0.56% and 0.15% by weight of binder for AACM concrete mix S_3 while it was 1.62%, 1.20% and 0.75% by weight of

binder for OPC concrete mixes S_6 respectively. Significant increase in chloride concentration was observed between the 55 and 270 days exposure period. Similar observations were reported by *Mangat and Molloy* [192] on blended cement concretes up to 540 days of exposure in NaCl solution.

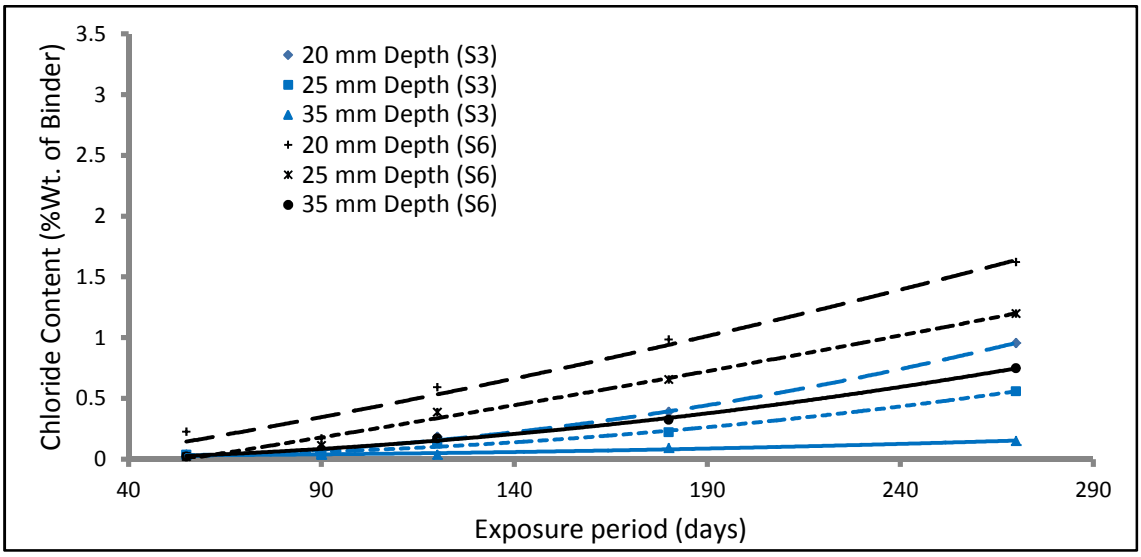

Figure 4. 25: Acid-soluble chloride profiles for AACM Mix S_3 and OPC Mix S_6 at 20, 25 and 35 mm depths

In the case of OPC concrete, the unhydrated portion of aluminate (C_3A) and aluminoferrite (C_4AF) of the binder reacts with chloride ion in the solution during the curing period, transforming it to Friedel's salt and calcium chloroferrite [207]. This is responsible for the increase in acid-soluble chloride concentration in concrete with age. The reaction of hydrated aluminate (C_3A) and aluminoferrite (C_4AF) that takes place before the curing period in NaCl solution does not contribute to chloride chemical binding [207].

The acid-soluble chloride profile for OPC concrete mix S_6 shows a higher chloride concentration than AACM concrete S_3 mix. It was observed that the chloride ingress was influenced by the pore system parameters (intrudable porosity $\boldsymbol{\Phi_{in,}}$ critical pore diameter $\boldsymbol{d_{crit}}$ and threshold pore diameter $\boldsymbol{d_{th}}$). The results of these findings are presented in chapter 3. The refined pore system parameters (intrudable porosity $\boldsymbol{\Phi_{in,}}$ critical pore diameter $\boldsymbol{d_{crit}}$ and threshold pore diameter $\boldsymbol{d_{th}}$) in AACM concrete mixes S_2 to S_5 indicate less interconnected pores within the matrix, thereby resulting in lower diffusivity of harmful ionic species (Cl^-, CO_2 and Sulphate) in AACM concrete compared with OPC concrete mix S_6. *Pierre-Claude and Robert* [218] concluded that the amount of bound chloride strongly depends on the chloride content of exposure, cement type and content, pH of pore solution, porosity and pore size distribution. The

binder type, porosity and pore size distribution of AACMs have already been discussed in chapters 2 and 3 respectively, the pH differences in cement hydration and geopolymerisation in AACMs will be discussed in chapter 5.

4.4.3.3 Surface Chloride Concentration C_0

4.4.3.3.1 Influence of exposure period

The surface chloride concentration, C_0, (% weight of binder) values obtained from the chloride profiles (figures 4.15 to 4.20) at chloride exposures of 55, 90, 120, 180 and 270 days, for acid and water-soluble chlorides are presented in Table 4.5. $(C_0)_{ws}$ and $(C_0)_{as}$ are used to denoted the surface concentrations for water-soluble and acid-soluble chlorides respectively. The 270 days exposure was not determined for water-soluble chloride concentration because of insufficient test samples.

Table 4. 5: Water and acid soluble surface chloride concentrations, C_0, (% weight of binder)

		Chloride Exposure (Days)				
Mix	Type of Cl^-	55	90	120	180	270
S2	Water-Soluble (%)	0.46	0.54	1.19	1.69	-
	Acid-Soluble (%)	0.06	0.15	0.67	0.93	1.42
S3	Water-Soluble (%)	0.58	0.80	1.39	2.07	-
	Acid-Soluble (%)	0.09	0.31	0.81	1.37	1.59
S4	Water-Soluble (%)	0.71	1.04	1.57	2.50	-
	Acid-Soluble (%)	0.35	0.48	1.07	2.04	2.14
S5	Water-Soluble (%)	0.77	1.21	1.79	2.59	-
	Acid-Soluble (%)	0.63	0.62	1.87	2.12	2.86
S6	Water-Soluble (%)	1.06	1.28	2.89	3.27	-
	Acid-Soluble (%)	1.19	2.17	3.25	5.91	4.43

The $(C_0)_{as}$ values listed in Table 4.5 are plotted against their exposure periods in Fig. 4.26. A non linear regression analysis of the test data provide a strong correlation between the water-soluble surface chloride concentration, $(C_0)_{as}$ and chloride exposure period, with the coefficient of correlation ranging from 0.76 to 0.82.

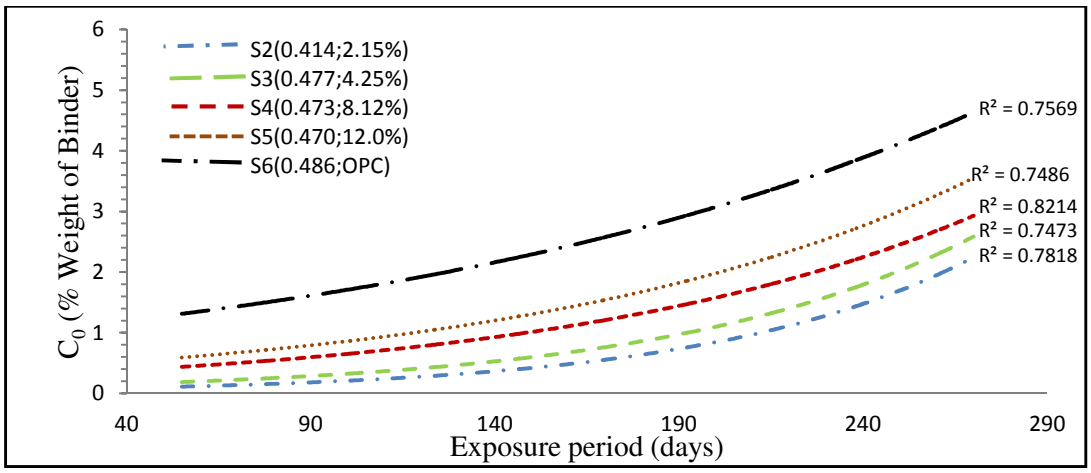

Figure 4. 26: Relationship between the acid-soluble surface chloride concentration, $(C_0)_{as}$ and exposure period

AACM concrete mix S_2 has the lowest surface chloride concentration, $(C_0)_{as}$, of 0.06% and 0.093% by weight of binder at 55 and 180 days exposure periods respectively. The highest $(C_0)_{as}$ for AACM concrete is mix S_5 which has 0.63% and 2.12% by weight of binder at 55 and 180 days exposure periods respectively.

The OPC concrete mix S_6 on the other hand has $(C_0)_{as}$ of 1.19% and 5.91% by weight of binder at 55 and 180 days exposure periods respectively. The $(C_0)_{as}$ of OPC concrete mix S_6 is significantly higher than AACM concrete mixes S_2 to S_5. This shows a higher ingress of acid-soluble chloride in OPC concrete mix S_6 compared with AACM concrete mixes S_2 to S_5 at both early exposure period (55 days) as well as at long period of exposures (180 days).

Increase of chloride concentration at the surface $(C_0)_{as}$ with exposure period (days) is observed for all AACM and OPC concrete mixes as shown in Figures 4.26. The surface chloride concentration $(C_0)_{as}$ for AACM concrete mix S_2 rose from 0.06% at 55 days to 1.42% at 270 days chloride exposure. The chloride concentration values at the surface $(C_0)_{as}$ with exposure period (days) exhibited by OPC concrete mix is within similar range as other research findings [220][221][222][223]. For example, *Chen et al.* [220] presented $(C_0)_{as}$ results of 0.7%, 1.13% and 1.10% by weight of binder at 90, 180 and 360 days exposure periods in seawater for a 45% blast furnace slag cement concrete having a w/c of 0.36. All these results show an increase of C_0 with increased exposure periods in salt laden environment. However, limited data exist in literature for AACM.

AACM concrete mix S_2 has the lowest surface chloride concentration, $(C_0)_{as}$, of 0.06% and 1.42% by weight of binder at 55 and 270 days exposure periods while the highest for AACM concrete is displayed by mix S_5 with 0.63% and 2.86% of binder at 55 and 270 days exposure periods. OPC concrete mix S_6 has the highest surface chloride

concentration, $(C_0)_{as}$, of 1.19% and 4.43% by weight of binder at 55 and 270 days exposure periods.

Costa and Appleton [219] suggested that a concrete submerged in a tank containing sea water (16-21 g/l of NaCl) for more than 1 year has the tendency to reach a constant value of chloride concentration at the concrete surface $(C_0)_{as}$. This, however, is not observed in Figures 4.26 and 4.27 probably due to the leaching of alkali metals from the concrete matrix. This reduces the chloride concentration at the concrete surface, C_0.

Fig. 4.27 shows the corresponding graph for water-soluble surface chloride concentration, $(C_0)_{ws}$, against chloride exposure periods. The coefficient of correlation between the exposure period and acid-soluble surface chloride concentration, $(C_0)_{ws}$ relationship of the test data ranges from 0.91 to 0.99.

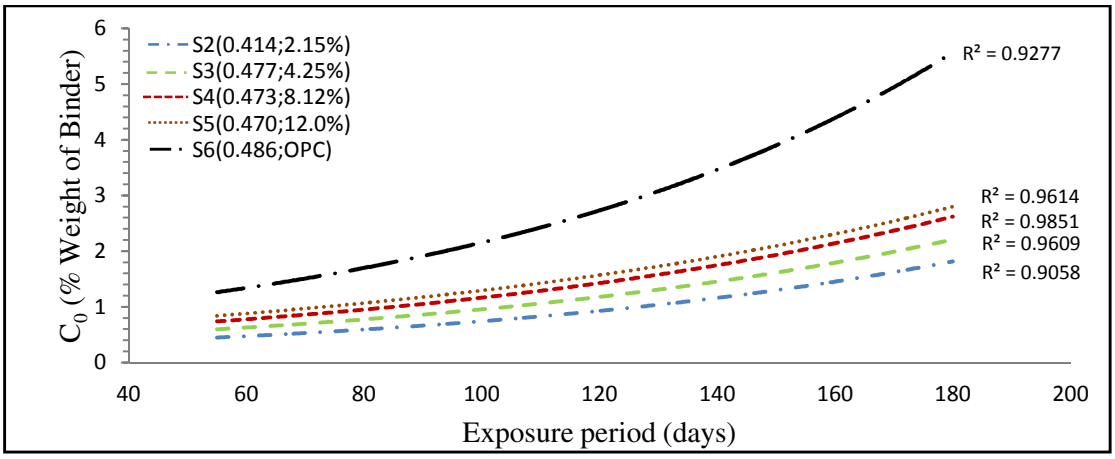

Figure 4. 27: Relationship between the water-soluble surface chloride concentration, $(C_0)_{ws}$ and chloride exposure period

The water-soluble surface chloride concentration $(C_0)_{ws}$ shows similar trend in its relationship with exposure period to that of acid-soluble surface chloride concentration graph. The $(C_0)_{ws}$ value for the water-soluble surface chloride concentration (Fig. 4.27) is higher than the corresponding acid-soluble surface chloride concentration $(C_0)_{as}$ (Fig. 4.28). For example, the $(C_0)_{ws}$ values of water-soluble surface chloride for AACM mortar mix S_2 are 0.46%, 0.54%, 1.19% and 1.69% by weight of binder compared with 0.06%, 0.15%, 0.67% and 0.93% by weight of binder for acid-soluble surface chloride $(C_0)_{as}$ under 55, 90, 120 and 180 days chloride exposure. The water-soluble chloride content within the AACM concrete along its penetration depths was also higher than acid-soluble chloride. The reasons are discussed further in section 4.4.3.3.2.

AACM mix S_2 has the lowest $(C_0)_{as}$ value ranging from 0.06%, 0.15%, 0.67%, 0.93% and 1.42% (by weight of binder) at exposure periods 55, 90, 120, 180 and 270

days respectively. In comparison, the OPC concrete mix S_6 had the highest C_0 values among all mixes of 1.19%, 2.17%, 3.25%, 5.91% and 4.43% at these exposure periods. These values are 63% to 95% higher than the corresponding values of $(C_0)_{as}$ for AACM concrete mix S_2.

4.4.3.3.2 AACM and OPC surface chloride concentrations C_0

The acid-soluble $(C_0)_{as}$ and water-soluble $(C_0)_{ws}$ chloride concentration for AACM and OPC concrete mixes S_2, S_5 and S_6 at 55 and 180 days exposure, are presented in Figures 4.28 and 4.29.

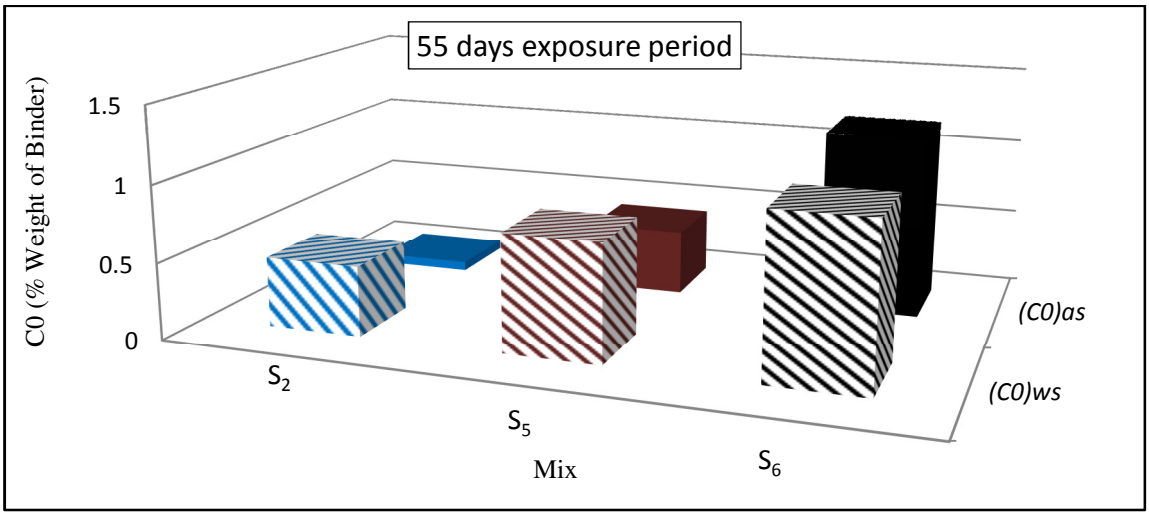

Figure 4. 28: Water-soluble and acid-soluble surface chloride concentrations of mixes S_2, S_5 and S_6 at 55 days exposure.

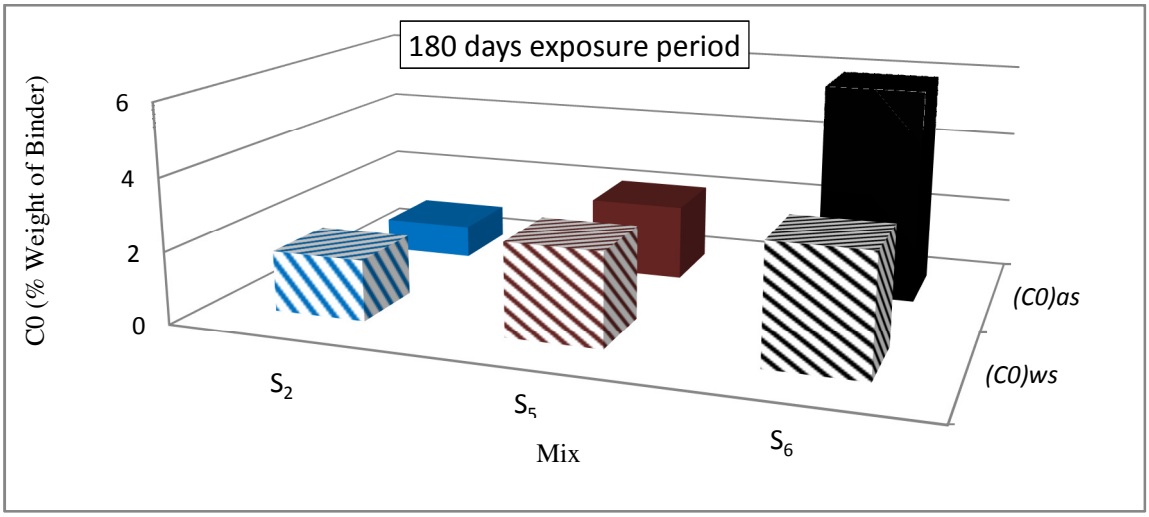

Figure 4. 29: Water-soluble and acid-soluble surface chloride concentrations of mixes S_2, S_5 and S_6 at 180 days exposure.

The acid-soluble surface chloride $(C_0)_{as}$ of AACM mixes S_2 and S_5 are lower than the water-soluble $(C_0)_{ws}$ values. This is opposite to the data of OPC concrete mix S_6 which shows significantly higher acid-soluble surface chloride $(C_0)_{as}$ than water-soluble

surface chlorides $(C_0)_{ws}$. This shows that a higher proportion of chloride is physically bound to the walls of the binder gel in AACMs rather than forming chloride binding compounds during geopolymerisation. It confirms the limited amount of Friedel's salt and any other crystalline chloride compounds in AACM binders which are responsible for the higher chloride binding capacity of OPC concrete as proposed by *RILEM TC 224* [3].

In case of OPC concrete mix S_6, the acid-soluble surface chloride $(C_0)_{as}$ being higher than the water-soluble surface chloride $(C_0)_{ws}$ indicates a much higher acid-soluble chloride binding capacity. Both the acid-soluble and water-soluble surface chlorides of OPC concrete mix S_6 are significantly higher than the AACM mixes S_2 and S_5 indicating both higher chemical and physical chloride binding capacities in OPC concrete. This phenomenon will be discussed further in chapter 5.

The acid-soluble surface chloride concentration, $(C_0)_{as}$ of OPC concrete mix S_6 was higher than that of AACM concrete mixes S_2 and S_5 at both 55 and 180 days exposure. This can be explained by the observation made by *RILEM TC 224* [3] that no Friedel's salt is present in AACM concrete and there is neither any other crystalline chloride compounds unlike those produced in OPC concrete under chloride exposure. In effect, unlike OPC concrete, the chloride exposure period plays an insignificant role in producing acid-soluble chloride in AACM concretes.

4.4.3.3.3 Influence of activator dilution

AACM concrete mixes S_2, S_3, S_4 and S_5 had 2.12%, 4.24%, 8.12% and 12.00% activator dilution respectively as shown in Table 4.4. The relationship between the water-soluble surface chloride concentration, C_0, and the activator dilution is plotted in Fig. 4.30.

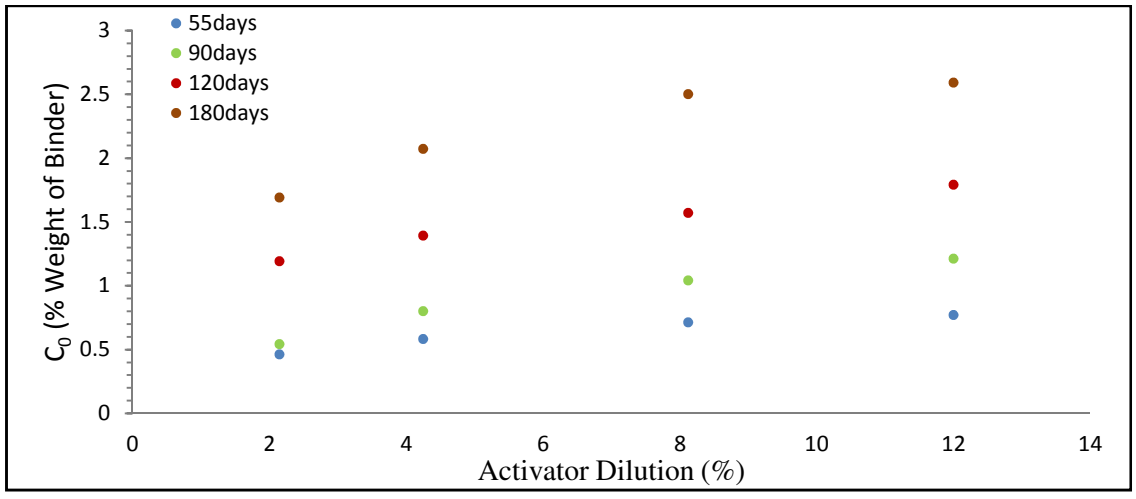

Figure 4. 30: The relationship between water-soluble surface chloride concentration, $(C_0)_{ws}$ and activator dilution.

The surface chloride concentration $(C_0)_{ws}$ decreases with the decrease of alkali activator dilution as shown in Fig. 4.30. Activator dilution of 2.12% had the lowest surface chloride concentration, C_0, while 12% activator dilution had the highest C_0 at all exposure periods as shown in Fig. 4.30. The water-soluble surface chloride concentrations $(C_0)_{ws}$ were 1.70 and 2.70% by weight of binder at 180 days chloride exposure periods for 2.12% and 12% activator dilution respectively. In addition, the water-soluble surface chloride profile increases with the exposure period. The lowest water-soluble surface chloride profile is seen at 55 days exposure period while 180 days exposure period had the highest water-soluble surface chloride profile (Fig. 4.30).

Petermann and Saeed [26] suggested that the activator concentration affects the reaction rate of pozzolans leading to a less porous and stronger cementitious material. The effect of activator concentration on its pore structure is equally observed in AACM concrete mixes S_2 to S_5 which is detailed in section 3.4.3.1.1, chapter 3.

High concentration of soluble silicate was observed to synthesize alumino-silicate gel thereby providing good interparticle bonding and physical strength of geopolymers [227]. *Gao and Brouwers* [228] noted that the presence of high activator modulus (provided by low activator dilution) could have a positive effect on mechanical and durability properties of AACM concrete depending on the slag/fly ash mass ratio. Some researchers, however, recorded a negative impact of high concentration (high modulus) of alkali activator in AACM concrete. For example, *Cheng and Chiu* [229] noted the reduction in compressive strength by inclusion of high concentration of KOH. 10M concentration of KOH produced the highest strength of 60 MPa, while a decrease in strength was witnessed by increasing the KOH concentration from 10M to15M. The reason was attributed to excessive K^+ ions in the framework. The activator dilution (2.12% to 12%) in AACM mixes S_2 to S_5 falls withing the upper and lower limits of optimum molarity range, thus such negative effect of high concentration was not observed.

The acid-soluble surface chloride concentration $(C_0)_{as}$ for AACM concrete mixes with 2.15%, 4.25%, 8.12% and 12% activator dilution at 55, 90, 120, 180 and 270 days exposure period is shown in Fig. 4.31. The surface chloride concentration $(C_0)_{as}$ increases with increasing degree of dilution.

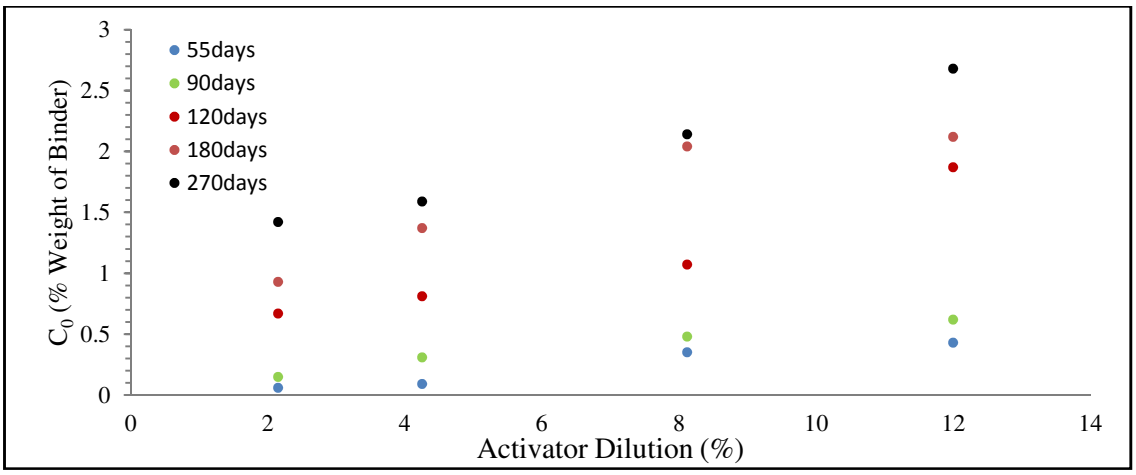

Figure 4. 31: The relationship between acid-soluble surface chloride concentration, $(C_0)_{as}$ and activator dilution.

A lower activator dilution was observed to reduce the volume of larger pores while simultaneously increasing the volume of small pores which generally resulted in lower porosity for fly ash-based systems [230]. Similar findings were observed in chapter 3, whilst investigating the MIP parameters of the hybrid AACM mixes. The maximum reduction in the total porosity of AACM concrete with 2.12% activator dilution could account for its least chloride content in both the acid-soluble $(C_0)_{as}$ and water-soluble $(C_0)_{ws}$ surface chlorides. *Brough and Atkinson* [33] acknowledged the rapid formation of the geopolymerisation products of the binder gel with increased activator concentration. This would also account for the lowest dilution of 2.15% resulting in the least surface chloride content due to densification of binder gel at early age.

4.4.3.4 Chloride Diffusion Coefficient D_c

4.4.3.4.1 Influence of exposure period

Fig. 4.32 shows the relationship between chloride diffusion coefficient, D_C, and chloride exposure period for AACM and OPC concrete mixes S_2 to S_6. A strong coefficient of correlation between 0.87 and 0.99 exists between the D_C and chloride exposure period relationship (non-linear).

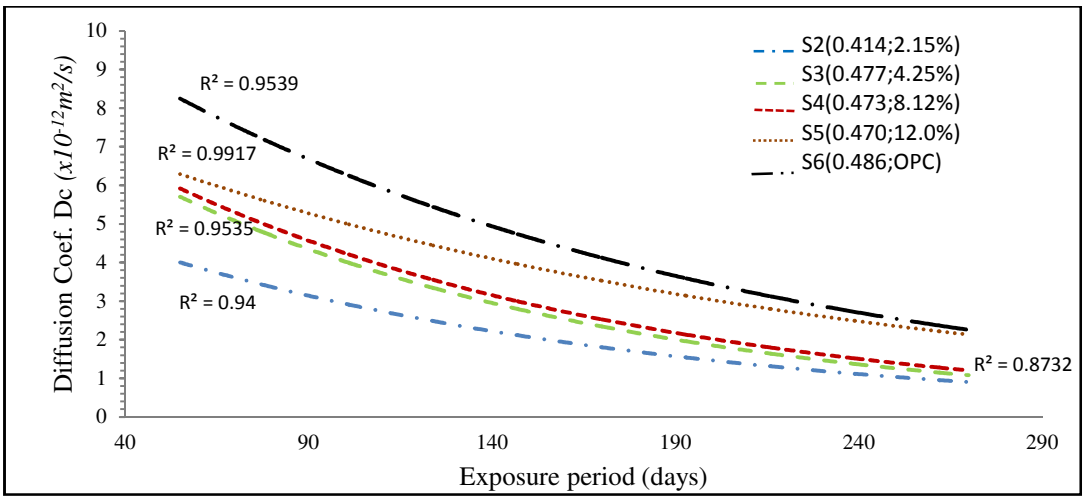

Figure 4. 32: Relationship of acid-soluble chloride diffusion coefficient D_c with exposure period

Fig. 4.32 shows a decrease in the chloride diffusion coefficient, D_C, with exposure period (days) for both AACM and OPC concrete mixes S_2 to S_6. The chloride diffusion coefficient, D_C of 3.5 x 10^{-12} m^2/s at 55 days exposure decreases to 0.89 x 10^{-12} m^2/s at 270 days exposure for AACM mix S_2. The rate of chloride ingress in both AACM and OPC concrete matrix tends to reduce considerably with exposure period.

Higher activator dilution in AACM concrete resulted in a higher chloride diffusion coefficient, D_C. For example, at 55 days chloride exposure period, the chloride diffusion coefficient, D_C is highest in AACM mix S_5 with 12.0% activator dilution (5.5 x 10^{-12} m^2/s) and lowest in AACM mix S_2 with 2.15% activator dilution (3.5 x 10^{-12} m^2/s). This denotes a considerable influence of the alkali activator dilution in resisting the penetration of chloride ion within AACM concrete matrix. This trend was observed for 90, 120, 180 and 270 days exposure periods, where the lowest chloride diffusion coefficient, D_C, was recorded for AACM mix S_2 with the lowest activator dilution.

The chloride diffusion coefficient, D_C is influenced by the concrete pore structure which is discussed in detail in section 4.4.4.1. The refined pore structure of AACM concrete is because of its binder grain size which is lesser than OPC concrete. For example, PFA concrete has pores finer than 0.005 µm whereas OPC concrete pores are within 0.005 µm to 0.02 µm [25]. Similarly, the grain size of silica fume is 100 times finer than the grain size of OPC concrete [25]. These result in a lower total intrudable porosity (i.e. summation of both gel and capillary pores) in PFA mortar than in OPC mortar. Similar results for AACM concrete were presented in chapter 3. The pore blocking effect induced by the secondary reaction of pozzolanic activities has been identified in supplementary cementitious concrete. An example was the faster decrease in the permeability of PFA concrete compared to OPC concrete [192]. The author [192]

suggested that the by-product of hydration, $Ca(OH)_2$, reacts with PFA to produces more calcium silicate hydrate (C-S-H) that reduces the pore sizes of SCM.

The experimental results of chloride diffusion coefficient, $D_{C,}$ for AACM concrete presented in Fig 4.32 are within the limits of 6.5 x 10^{-12} m^2/s and 0.89 x 10^{-12} m^2/s. The corresponding limits for OPC concrete mix S_6 are 8.7 x 10^{-12} m^2/s and 2.5 x 10^{-12} m^2/s. These values lie within the majorirty of published limits presented in Table 4.2 (section 4.2.3.7) obtained from literature for OPC concrete. This table is repeated below.

Table 4. 2: Published chloride diffusion coefficient Dc values for OPC

D_C ($m^2/s_{x}10^{-12}$)	Curing Age	W/C Ratio	Mix Design			Author	Remarks
			Binder (kg/m3)	Water (kg/m3)	Total Aggregate (kg/m3)		
2.5	1.5y	0.43	339	146	-	R.B. Polder, [199]	Fly ash based concrete exposed to salt/dry cycle in the laboratory
3	1.0w	0.40	420	168	-		
2	4.0w	0.40	420	168	-		
1	14.0w	0.40	420	168	-		
4	1.0w	0.54	300	162	-		
3	4.0w	0.54	300	162	-		
2.5	14.0w	0.54	300	162	-		
2.86-3.65	2.0m	0.50	330	165	2066	Zhang & Gjorv [200]	Theoretical analysis of concrete under RCPT
1.19-1.94	2.0m	0.50	330	165	1894		
2.8-3.1	1.0w	0.35	450	157.5	1695	Luping [201]	Rapid penetration of chloride in silica fume concrete
4.4-5.4	1.0w	0.40	420	168	1692		
5.6-13.6	1.0w	0.50	390	195	1636		
9.8-39.7	1.0w	0.75	250	187.5	1784		
2.07	28d	0.66	288	190	1900	Bertolini [202]	
1.49	28d	0.62	275	170.5	1940		
1.77	28d	0.60	315	189	1835		
1.65	3m	0.50	400	200	1800	Collepardi *et al,* [203]	
3.24	3m	0.60	384	230.4	1728		
11-14	14d	0.50	423	211.5	1777	Page *et al.,* [204]	Concrete slab exposed to 5% chloride ponding
4.7	90d	0.35	380	133	1924	Hooton [197]	Silica fume concrete under bulk diffusion test
5.9	120d	0.35	380	133	1924		
5.0	90d	0.40	374	149	1840		
9.3	120d	0.40	374	149	1840		
7.1	90d	0.45	369	165	1770		
10.8	120d	0.45	369	165	1770		
52.3	28d	0.58	530	307	1309	Mangat & Molloy [192]	Steel fibre reinforced concrete exposed to wet/dry cycle in the laboratory
23.8	90d	0.58	530	307	1309		
10.0	270d	0.58	530	307	1309		
6.13	154d	0.40	590	236	1392	Mangat & Gurusamy [205]	Steel fibre reinforced concrete under marine exposure (tidal cycles)
3.90	304d	0.40	590	236	1392		
2.81	1250d	0.40	590	236	1392		

However, a comparison of the chloride diffusion coefficient, D_C, of AACM concrete with OPC concrete in Fig. 4.32 shows significantly higher chloride diffusion coefficients than the AACM concrete mixes at all exposure periods.

4.4.3.4.2 Influence of Activator Dilution

Fig. 4.33 shows the relationship between chloride diffusion coefficients, D_C, and activator dilution at 55, 90, 120, 180 and 270 days of chloride exposure.

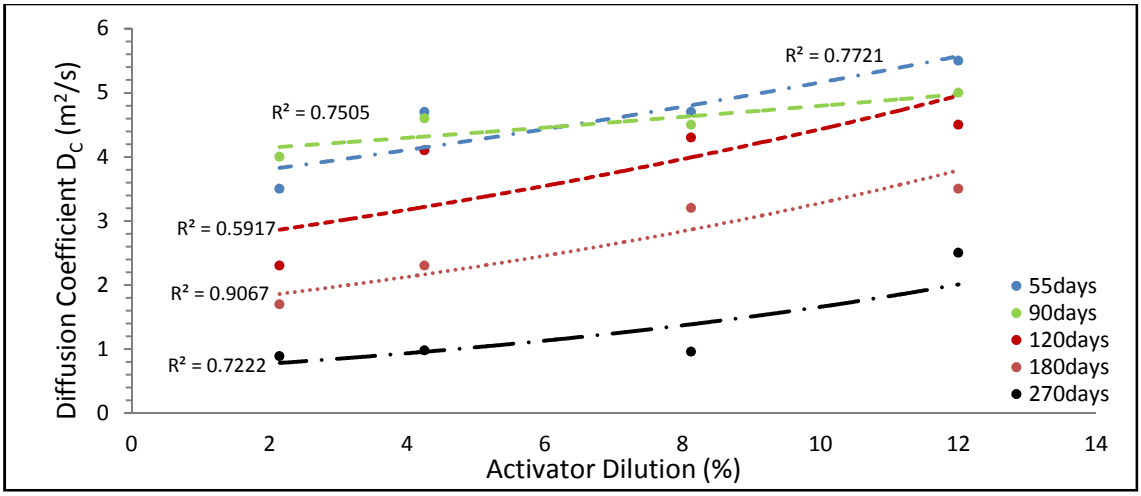

Figure 4. 33: Relationship between acid soluble chloride diffusion coefficient, Dc and activator dilution

The chloride diffusion coefficient, D_C increases as the activator dilution increases. For example, the chloride diffusion coefficient, D_C for 2.12% activator dilution is 0.89 x 10^{-12} m^2/s relative to 2.5 x 10^{-12} m^2/s for 12% activator dilution at 270 days exposure period. The increase in the chloride diffusion coefficients, D_C with increased activator dilution is observed at all exposure periods. The influence of activator dilution on porosity and pore structure of AACM mortar investigated in chapter 3 gives an insight to the rate of chloride ingress through its matrix. The relationship between porosity and chloride diffusion, D_C is detailed in section 4.4.4.1. It was observed that the lower activator dilution in AACM concrete resulted in a more refined intrudable porosity than with high activator dilution. These refined pores limit the ingress of chloride ions.

Unlike the surface chloride concentrations $(C_0)_{ws}$ and $(C_0)_{as}$ which increases with exposure period. The diffusion coefficients D_C versus activator dilution relationships (Fig. 4.33) show the lowest values of chloride diffusion coefficients, D_C, at the oldest exposure period (270 days). This is due to a tighter pore structure evolving after prolonged curing and the likely interference from the bound chlorides which prevent the ingress of chloride. The supersaturation of pores near the concrete surface with chloride ions may also be a possible cause for preventing further chloride ingress.

The phenomenon of higher chloride diffusion coefficients *Dc* during the initial exposure of concrete to salt laden environment followed by a decrease at later exposure periods has been reported since late 70's [188][225][226]. The relative performance of AACM and OPC concrete also depends on the duration of exposure to chloride solution (discussed in section 4.4.3.6). The chloride diffusion coefficients *Dc* in AACM concrete decrease non-linearly with activator dilution, with greater reduction at higher dilution.

4.4.4 Relationship between Porosity and Chloride Diffusion Parameters

4.4.4.1 Chloride Diffusion Coefficient D_C

The relationship between the chloride diffusion coefficient, D_c, at 55, 90, 120, 180 and 270 days exposure and the intrudable porosity obtained from chapter 3 is shown in Fig. 4.34.

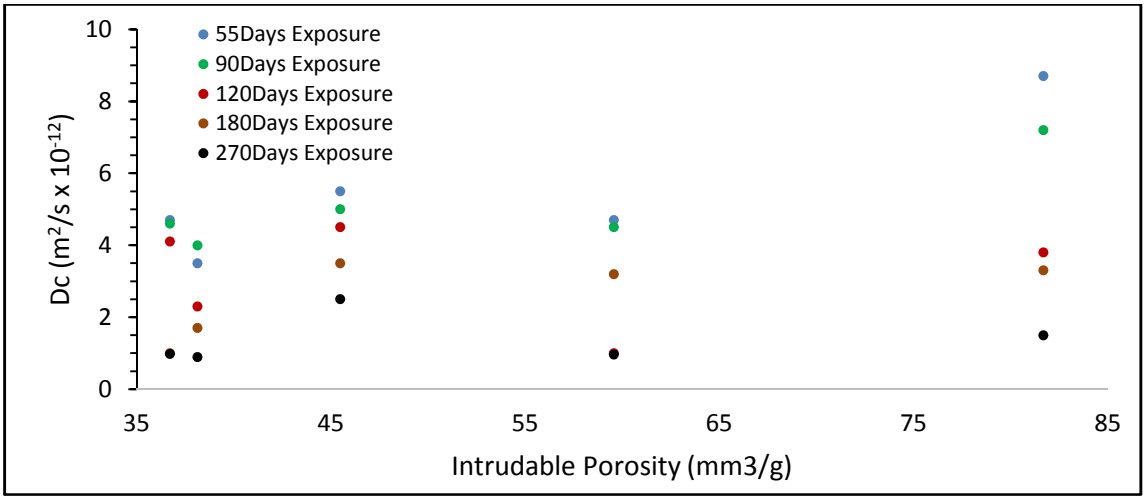

Figure 4. 34: Relationship between the chloride diffusion coefficient and intrudable porosity at different exposure periods.

A fairly-good linear relationship was exhibited at early exposure periods (55 and 90 days) between the chloride diffusion coefficient, D_c, and intrudable porosity. The decline in the linear relationship between chloride diffusion coefficient, D_c, and intrudable porosity at later exposure periods (120, 180 and 270 days) can be explained by the restricted movement of chloride ions within the concrete pore matrix with increasing exposure period. This is because of the continuing hydration and geopolymerization in AACM and OPC concrete with exposure period.

Belch et al. [231] examined the separation of Na^+ and Cl^- when dissolved in water. The sizes of these ionic structures were observed to be in nanomillimeters. The radius of Na+ ion at condensation peak is approximated to be 0.58 nm while the micellar surface of Cl^- ions are not well established for NaCl salt [232]. This suggests

that the penetration of NaCl into concrete matrix is only through intrudable porosity larger than 0.58 nm.

On the other hand, the percentage of large intrudable pores reduces with age. At early age, a high percentage of pore volumes are observed to be above 0.58 nm but as hydration proceeds, the large pore spaces within the concrete matrix reduce, leaving behind smaller pores. Therefore, the linear relationship between the chloride diffusion coefficient D_c and the intrudable porosity were observed at early ages when Cl^- ion could easily penetrate the concrete pore matrix but as the porosity lessens with age, chloride penetration stops, and chloride diffusion coefficient D_c remains constant. The porosity value at 28 days are plotted but they decrease with age and that effect is also reflected in the chloride diffusion coefficient D_c values but not in the porosity values in Fig. 4.34.

4.4.4.2 Surface Chloride Concentration C_0

The relationship between the surface chloride concentration, C_0, at 55, 90, 120, 180 and 270 days exposure and the intrudable porosity at 28 days age is shown in Fig. 4.35. A linear relationship between surface chloride concentration, C_0, and intrudable porosity was obtained from the best-fit curves.

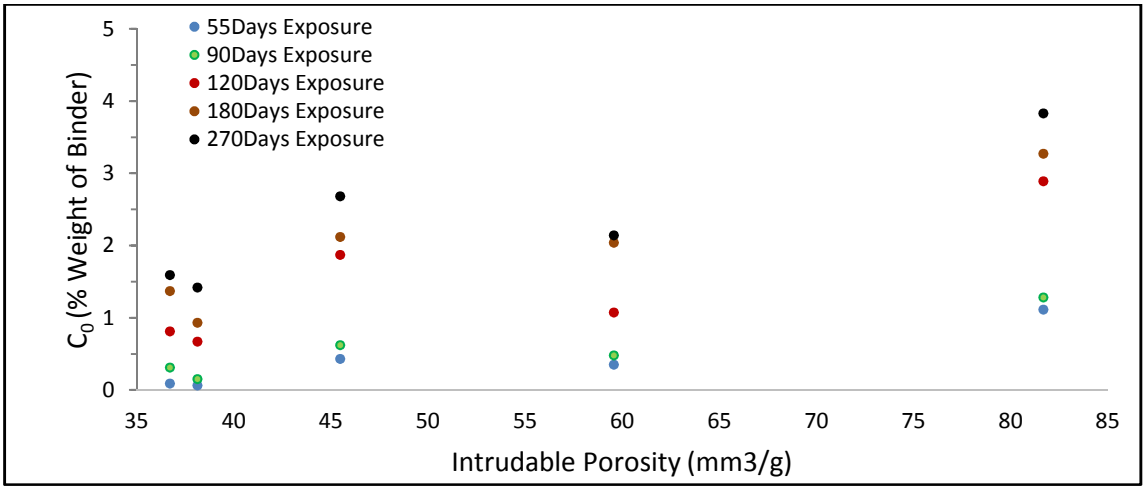

Figure 4. 35: Relationship between the surface chloride concentration and intrudable porosity at different exposure periods to 5% NaCl solution.

The surface chloride concentration, C_0 increases with the period of exposure. The surface chloride concentration, C_0 is as a result of the absorption of Cl^- ion at the surface of the concrete; hence the percentage of pore diameter greater than the diameter of Na+ ion of 0.58 nm within the concrete matrix hardly affects the relationship between these two parameters. The hydration of concrete with age resulting in a reduction of large pores had minimal effect on the surface chloride relationship.

Chisholm and Lee [233] proposed the possibility of precipitation of insoluble salt at the concrete surface over a long period of exposure, this may also account for the high chloride content at the concrete surfaces.

In conclusion, the porosity and chloride diffusion parameters C_0 and D_c of AACM and OPC concrete appear to show a linear relationship especially at earlier exposure periods.

4.5 CONCLUSIONS

The following conclusions are based on the investigation on the strength development of AACM and OPC concrete. The chloride diffusion parameters were also investigated, in particular the water and acid soluble chlorides in AACM concrete, the rate of diffusion and surface chloride profiles.

- The liquid/binder ratio had great impact on the strength of AACM concrete. However, high coarse aggregate content aided an improved compressive strength in AACM concrete. For example, AACM mix S_2 with liquid/binder ratio 0.41 had higher strength than mixes S_4 and S_5 with liquid/binder ratio 0.48. However, mix S_3 had similar strength with mix S_2 because of its higher coarse aggregate and lower activator dilution.
- The activator dilution played a significant role in strength development of AACM concrete similar to AACM mortar in Chapter 3. AACM mixes S_2 (2.15% dilution) and S_3 (4.24% dilurion) with lower activator dilution achieved greater 28 days strength than mixes S_4 (8.12% dilution) and S_5 (12% dilution).
- The strength developed at early age in AACM concrete was faster under dry curing (20^0 C, 65 RH) compared with wet curing (20^0 C) while the reverse is true for OPC concrete. For example, AACM mix S_3 and OPC S_6 under wet curing had 39 MPa and 28 MPa respectively compared with 40 MPa and 26 MPa under dry curing at 7 days age.
- The chloride profiles of water and acid soluble concentration for both AACM and OPC concrete shows good correlation with Fick's second law of diffusion.
- The water and acid soluble surface chloride concentration, $C_{0,}$ increases with exposure periods for AACM and OPC concrete. This increase was more pronounced in water soluble chloride compared with the acid soluble chloride for AACM concrete. On the other hand, OPC concrete revealed more surface chloride concentration, $C_{0,}$ for acid soluble chloride compared with the water soluble chloride. For example, the $C_{0,}$ for AACM mix S_3 and OPC S_6 water

soluble chlorides are 2.07% and 3.27% respectively while it is 1.37% and 5.91% for acid soluble chloride at 180 days exposure.

- A decrease in chloride diffusion coefficient with exposure periods were observed for both AACM and OPC concrete. Generally, AACM concrete possess a lower chloride diffusion coefficient compared with OPC concrete. For example, the chloride diffusion coefficients for AACM mix S_3 and OPC S_6 at 55 days chloride exposure are 5.6 x 10^{-12} m^2/s and 8.7 x 10^{-12} m^2/s respectively while it is 1.8 x 10^{-12} m^2/s and 2.5 x 10^{-12} m^2/s at 180 days chloride exposure.
- The more refined pore structure of AACMs (lower porosity, discontinous pore structure) aided lower chloride diffusion when compared to OPC concrete.

CHAPTER 5

FREE CHLORIDE AND pH OF PORE SOLUTION IN ALKALI ACTIVATED CEMENTITIOUS (AACM) CONCRETE

5.1 INTRODUCTION

The electrochemical reaction between the chloride ions present in the concrete pore solution, also known as free or mobile chloride, and the steel reinforcement or fibres which are embedded within the concrete matrix usually results in chloride induced corrosion in the presence of water and oxygen [25]. This type of corrosion initiates when the pH (alkalinity) of the pore solution reaches a certain limit, normally below 9 for OPC concrete [25], but not yet agreed upon for AACM concrete.

The free or mobile chloride plays a direct role in the corrosion of steel reinforcement in concrete rather than the bound (physically and chemically) chloride because the movement of chloride ions responsible for the corrosion of steel within the concrete matrix is controlled through the pore solution electrolyte when the concrete is saturated [209]. The bound chloride regulates the chloride binding isotherm of the concrete (i.e. the relationship between the free and bound chlorides). It has been suggested that a part of the bound chloride is released into the pore solution when there is a local fall in pH thereby increasing the free chloride content [208]. It is shown that some of the free chlorides are either absorbed by the hydration products of cement or adsorbed by the walls of the binder gel [97] in order to maintain equilibrium between the free and bound chlorides in OPC concrete.

Studies show that the pore solution composition of AACMs is different from that of OPC concrete [3][82][234]. The pore solution composition of AACMs is dependent on the type of activator used, for example, *Puertas et al.* [235] observed a significant change in the ionic composition of pore solution for a slag cement paste within 3 to 24 hrs when activated with either sodium silicate or sodium hydroxide. These changes were different with the two activators and were represented by a decrease in Na and Si contents.

The pH of the pore solution, on the other hand, is a determinant factor for the formation of a passive thin film comprising of iron oxide around the steel surface, which prevents the initiation of corrosion of embedded steel in concrete. The prolonged action of free chloride as well as lower pH due to carbonation in OPC concrete destroys this protective film [25]. However, it is argued that a reduction in pH of the pore solution due to partial replacement of cement by a supplementary cementitious

(pozzolanic) material does not necessarily result in the depletion of the protective thin film around the embedded steel surface [236]. Therefore, the electrochemical reaction between the free chloride and embedded steel in supplementary cementitious concrete is partially affected by the reduction of the concrete pore solution alkalinity.

The corrosion initiating relationship between the free chloride and pH of pore solution in AACMs is not established in literature. This chapter will address this relationship between the two parameters as well as their relationship with bound chlorides from chapter 4.

5.2 LITERATURE REVIEW

5.2.1 Concrete Pore Solution Composition

The hydrated products of OPC concrete produce saturated pore solution containing calcium hydroxide $Ca(OH)_2$ and different ions depending on the type of cement and supplementary cementitious materials (e.g. fly ash, slag and silica fume) [237]. These ionic species are principally alkali oxides of sodium and potassium that exist in the cement. Sulphate ions could also be present in the concrete pore solution due to gypsum added during cement production or from contaminated aggregate or mixing water [25].

The pH of OPC concrete pore solution increases from about 12.5 to 13.5 by the presence of the alkali oxides (Na^+ and K^+) [238][239]. However, the pH decreases when mineral admixtures are added [25]. For example, a 10% replacement of OPC cement with silica fume reduced the pH of the concrete pore solution from 13.5 to 12.6 [236]. This is due to the secondary pozzolanic reactions of the supplementary cementitious material which requires calcium hydroxide $Ca(OH)_2$ from the concrete pore solution to activate these reactions. For a fly-ash based system, the glassy material is only activated when the pH of the concrete pore solution is about 13.2 [25] but for ground granulated blast-furnace slag (GGBS), the glassy material is activated at a lower pH of about 11.5 [240].

Information on the chemistry of AACM pore solution is scanty unlike that of OPC concrete pore solution which is fairly-well documented. *Song and Jennings* [240] performed x-ray diffraction analysis on an alkali-activated ground granulated blast-furnace slag (GGBS) to determine the chemical composition of its pore solution. The ionic species of Si, Ca, Al, and Mg were found to be present in the pore solution and were dependent on the pH of the aqueous phase. The high pH of the pore fluid was associated with high concentrations of Si and Al but lower concentrations of Ca and Mg.

5.2.2 Concrete Chlorides

5.2.2.1 Free Chloride

Free or mobile chlorides are soluble chlorides present in the concrete pore solution. The free chloride content and pH of the pore solution are decisive factors in the initiation and propagation of chloride induced corrosion in reinforced concrete in the presence of oxygen and water [25]. *Wan et al.* [241] suggested that at an early stage of hydration in OPC concrete, the aqueous pore solution contains cations such as sodium, potassium and calcium which leave the pore solution by leaching at later stages of hydration. The displaced cations are replaced by ions such as chloride, sulphate, ammonium and carbon dioxide from the environment. During the ingress of chloride into the concrete matrix, a portion of the chloride ions is adsorbed by the hydration products to form Friedel's salt ($Ca_6Al_2O_6.CaCl_2.10H_2O$), also known as the acid soluble chloride, while some portion is absorbed by the wall of the gel to form Kuzel's salt ($Ca_6Fe_2O_6.CaCl_2.10H_2O$), also known as water soluble chloride [207]. This is discussed in more detail under section 4.2.3.5 in chapter 4. The remaining portion of the total chloride ingress is present in the concrete pore solution, also known as the free chloride. *Xinying et al.* [242] suggested that the free chloride content is about half the quantity of bound chloride content (i.e. summation of acid and water soluble chlorides). The free and total chloride contents for OPC based steel reinforced concrete specimens under laboratory conditions are presented in Table 5.1.

Table 5. 1: Published total and free Cl- content in OPC based concrete (laboratory conditions) [238]

Total Cl^- (% bw)	Free Cl^- (% bw)	Cl^-/OH	Cation	Cl^- Transportation Mechanism	Specimen	W/C	Cement Type	Exposure	Year	Reference
0.5-1.8	0.08-1.07	2.5-6	Na	capillary, diffusion and mix	mortar, concrete	0.3-0.75	OPC, SF	air	1995	*Pettersson* [243]
0.25-0.75	0.06		Na	Introduced in mix	mortar	0.5-0.6	OPC, SF, FA, GGBS	submerged	1998	*Breit* [244]
1.24-3.08	0.39-1.16	1.17-3.98	Na, Ca	Introduced in mix	mortar	0.5	OPC	100% RH	2000	*Alonso et al.* [245]
0.25-1.25	0.03-0.32		Na	Capillary and diffusion	mortar	0.6	OPC		2000	*Zimmermann et al.* [246]
0.62	0.21	1.5	Na	Capillary and diffusion	mortar	0.37	SRPC	95% RH	2002	*Castellote et al.* [247]
0.42	0.19	2.0	Na	migration	mortar	0.37	SRPC	95% RH	2002	
0.04-0.24		0.09-0.62	Na	migration	mortar	0.5	OPC	submerged	2003	*Trejo and Pillai* [248]
0.68-0.97	0.07-0.13	0.16-0.26	Na	Introduced in mix	concrete	0.35-0.55	OPC, FA, GGBS	95% RH	2003	*Oh et al.* [92]
0.45	0.10	0.27	Na	Introduced in mix	concrete	0.35-0.55	SRPC	95% RH	2003	
1.1-2.0	0.4-0.8		Sea water	Capillary and diffusion	Concrete	05	OPC	Air	2006	*Mohammed and Hamada* [249]
2.0	1.2		Na	Capillary and diffusion	Mortar	0.45	OPC, FA	Cycle	1994	
1.8	1.33		NA		Mortar	0.45	OPC	Cycle	1994	*Mangat et al.* [250]

* (% bw) is % by binder weight

The free chloride from Table 5.1 ranges from 0.03 to 1.33% by weight of binder and the lowest total chloride content is 0.04% by weight of binder while the highest is 3.08% by weight of binder. Table 5.1 shows that the cement type and the method of introducing chloride into the concrete had significant influence on the free and total chloride contents. The lowest chloride contents recorded by *Breit* [244] and *Oh et al.* [92] had chloride introduced into the concrete mix during casting and the presence of supplementary cementitious materials. A large portion of the chloride content introduced during concrete mixing would have taken part in the hydration reaction forming Friedel's salt ($Ca_6Al_2O_6.CaCl_2.10H_2O$). The low pH value in concrete containing supplementary cementitious materials and partly inferior binding capacity has resulted in higher free chloride content than normal concrete [251].

The curing method and chloride exposure concentrations equally play vital roles in the amount of total and free chlorides present in the concrete. Information is not provided about the chloride exposure concentrations in Table 5.1 but it is known that high chloride exposure concentrations normally result in high total and free chlorides due to the driving force provided by the concentration gradient. The wet/dry cyclic curing was observed to increase the total and free chlorides significantly. For example, *Mangat et al* [250] gave relatively high free chloride contents of 1.2% and 1.33% by weight of binder for fly ash and OPC concrete respectively which was exposed to marine cycles for 540 days in the laboratory. The salt content of the seawater used in the spray chamber increased with time due to evaporation.

5.2.2.2 Total Chloride

The total chloride is the sum of all the chloride content (i.e. acid-soluble, water soluble and free chloride) present in concrete. There is no fixed or critical amount of total chloride which initiates corrosion of steel or fibres embedded in concrete [25]. Various factors such as binder content and environmental chloride concentration determine the proportion of bound chloride present in the total chloride. The proportion of bound chloride present in the total chloride varies from 80% to about 50% [25]. This in theory means that a larger proportion of the total chloride is either bound to the walls of the binder gel or forms a part of the hydration products than is dissolved in the pore solution. A fraction of the total chloride is present in the free chloride as seen in Table 5.1.

The proportion of free chloride present in the total chloride from Table 5.1 varies from 16% to 65%. This somewhat conforms to the proportion of bound chloride

present in the total chloride varying from 80% to about 50% for OPC concrete. The results of the bound chloride content of AACM concrete presented in chapter 4 reveal that a large proportion (between 65% to 87%) of the total bound chloride is absorbed by the walls of the binder gel (water-soluble chloride) rather than forming a part of the hydration products (acid soluble chloride). This is contrary to OPC concrete, where a large proportion of about 65% of the total bound chloride combines with the hydration products (acid-soluble chloride).

5.2.3 pH of Concrete Pore Solution

The pH of concrete is a measure of the degree of alkalinity of its pore solution. The pH of concrete pore solution is normally high in alkalinity, above 12.6 for OPC concrete. A higher pore solution pH is required to activate the pozzolanic reaction in AACM or supplementary cementitious concrete ranging from, 13.2 for fly-ash based system [25] to 12.8 for ground granulated blast furnace slag concrete and 12.5 for silica fume concrete [238]. The pH of the concrete pore solution is initially dependent on the type of binder but becomes affected by carbonation and leaching of hydration products at a later stage [238].

The pH is defined as the negative logarithm of hydrogen ion [H^+] present in the pore solution. The relationship between pH and hydroxyl ion [OH^-] is shown in equation 5.1.

$$[OH^-] = 10^{-(14-pH)} \quad 5.1$$

The pH of concrete pore solution at considerably low values less than 12 is suggested to aid the participation of bound chloride in corrosion initiation in a reactive solid material [208]. It was argued that the low pH favours the dissolution of chloride ions that are physically or chemically bound to the hydration products thereby increasing the free chloride content in concrete [252]. *Glass and Buenfeld* [208] suggested that an increased binding capacity under certain circumstances may result in a reduced time to initiate corrosion due to bound chlorides participating in the chloride induced corrosion. The explanation given was that an increased binding capacity reduces the free chloride in the pore solution which supports the transport of chloride; this simultaneously increases the chloride concentration differential between the pore solution and the external environment chloride content near the concrete surface exposed to the chloride source. The increased chloride content at the surface over a long period of time will increase the rate of chloride diffusion into the concrete [208].

This hypothesis could only be true when the hydration of the concrete is complete. The pore structure of concrete becomes tighter because of the hydration process over time as detailed in chapter 3. Secondly, the chloride ions physically bound to the wall of the hydration products reduce the mean pore sizes thereby reducing the rate of chloride ingress into the concrete as detailed in chapter 4.

Contrary to the dissolution of bound chloride into the pore solution at low pH when the source chloride is NaCl, *Robert* [253] observed the solubility of Friedel's salt at high pH when the chloride source is from $CaCl_2$, thereby releasing the chemically bound chloride into the concrete pore solution at high pH. The difference in dissolution of bound chloride into the concrete pore solution at various pH for samples containing NaCl and $CaCl_2$ could be attributed to the solubility of their cations at various pH values [254].

The effect of pH on the bound chloride solubility in the concrete pore solution is, therefore, greatly influenced by the source chloride. NaCl is used as the source chloride for this study.

5.2.4 Hydroxyl Ion (OH^-) Concentration

Hydroxyl ion concentration is as important as the chloride content of the pore solution because it affects the corrosion rate of steel in concrete, although no generally valid conclusion exists on its threshold value [25]. There is the possibility of depassivation of steel embedded in concrete with an increase in the chloride/hydroxyl concentration. However, the threshold value of 0.61 for the chloride/hydroxyl ion concentration proposed by *Hausmann* [255] for the initiation of corrosion in cement based materials does not normally apply. For example, *Lambert et al.* [170] presented a chloride/hydroxyl concentration threshold of 3 for steel rods embedded in concrete. The chloride/hydroxyl concentration as high as 320 did not result in corrosion of steel fibres embedded in fly-ash concrete [102]. Similarly high threshold value of chloride/hydroxyl concentration in silica fume concrete was observed by *Page and Havdahl* [256] for corrosion initiation. The reasons attributed to such high values were the lower chloride binding and pH which increases the Cl^-/OH^- ratio in its pore solution. In addition, the reduced chloride ingress and oxygen content due to tight pore structure depresses the steel potential.

Hausmann [255] based the chloride/hydroxyl concentration threshold of 0.61 on an idealized solution to represent the pore solution of hydrated cement. This model electrolyte cannot simulate an oxygen depletion or limited mobility of chloride ion

within the cement matrix unlike the concrete pore solution [252]. The threshold chloride/hydroxyl concentration of 0.61 proposed by *Hausmann* [255] is lower than the threshold values published by other authors as shown in Table 5.1, thus making it unreliable for predicting corrosion behaviour of steel in concrete. The highest Cl^-/OH^- ratios of 2.5 to 6 in Table 5.2 were presented by *Pettersson* [243] for a silica fume mortar and concrete while the lowest values of 0.09 to 0.62 were presented by *Trejo and Pillai* [248] for OPC mortar.

5.2.5 Chloride Binding Isotherms

5.2.5.1 Introduction

Four models commonly adopted to establish the relationship between the bound and free chloride are Freundlich, Langmuir, Linear and BET chloride binding isotherm. These relationships are defined as chloride binding isotherms. These models are suitable for high and low free chloride concentrations [95]. Each model is applicable within a specific range of chloride concentration. Freundlich binding isotherm is adopted for the range of free chloride concentrations in seawater which is usually high concentration while Langmuir binding isotherm is used for low free chloride concentration. The Linear binding isotherm oversimplifies the bound-free chloride relationship and BET isotherm is rarely used [209].

5.2.5.2 Freundlich Isotherm

Regression analysis of the free and bound chloride content relationship were performed on the experimental data of this research project to obtain the best fit curves for the Freundlich, Langmuir and Linear models as shown in Fig 5.1. The Freundlich binding Isotherm showing the relationship between the free and bound chloride concentrations is given in equation 5.2.

$$C_b = \propto C_f^{\beta} \qquad 5.2$$

Where: C_b = Bound Chloride Concentration *(% Wt. by Binder);* C_f = Free Chloride Concentration (mol/L); α *and* β = Binding Constants. The prediction (regression line) of the binding capacity using the Freundlich binding Isotherm (Red dotted line) is shown in Fig 5.1.

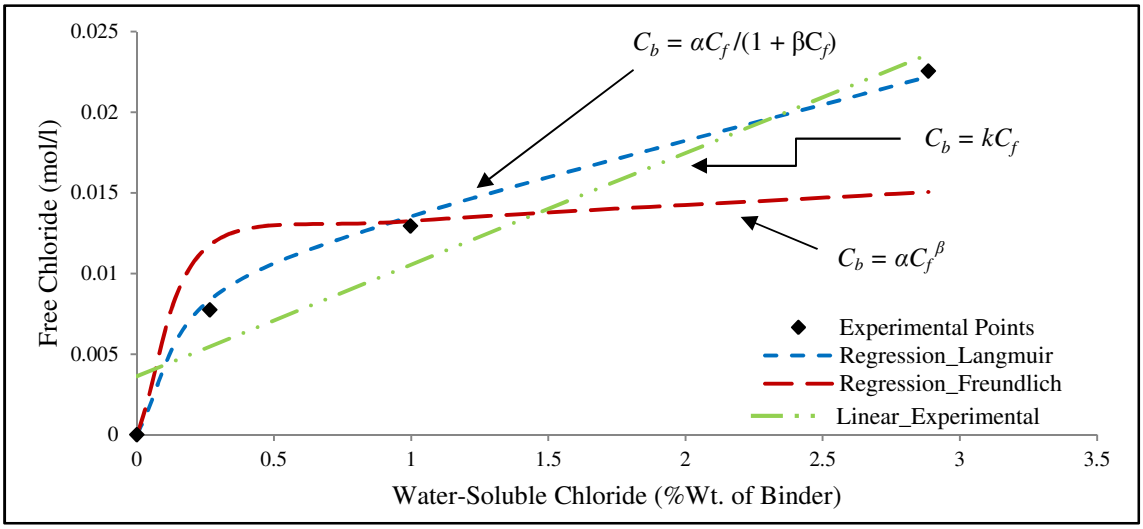

Figure 5. 1: Free and bound chloride relationships using Freundlich, Langmuir and Linear binding isotherms

Freundlich binding isotherms are usually applicable to concrete with high free chloride concentrations. For example, *Thomas et al.* [257] used Freundlich binding isotherm to relate their experimental data to the chloride binding isotherm for supplementary cementitious materials with high concentration of free chlorides. The concrete mixes investigated by *Thomas et al.* [257] showed that 8% cement replacement with silica fume exhibited the lowest chloride binding capacity while 25% cement replacement with fly-ash had the highest binding capacity. The differences in their binding capacities were attributed to the alumina content within the binder gel hydrates. The free chloride concentration in this case was greater than 0.1M (0.1mol/L) of NaCl. In comparison the maximum free chloride concentration in AACM mixes represented in Fig. 5.1 is 0.02 mol/L which is clearly much lower than *Thomas et al.* [257] results.

Similarly, *Yuan et al.* [258] presented the chloride binding capacities for supplementary cementitious materials immersed in 16.5% NaCl for 42 days as well as the chloride migration test with 10% NaCl and 0.3 mol/L of NaOH filled at the cathodic and anodic cells respectively. The results presented suggested a minimal influence of electric voltage on the binding isotherm. The free chloride concentrations present within the concrete matrix are from 0.2 to 1.0 mol/L which fit with Freundlich model.

5.2.5.3 Langmuir Isotherm

The Langmuir binding isotherm shows the relationship between the free and bound chloride concentrations given by equation 5.3. This model is usually used to describe the binding isotherm of free chloride concentration lesser than 0.05 mol/L [95].

$$C_b = (\propto C_f)/(1 + \beta C_f) \qquad 5.3$$

Where: C_b = Bound Chloride Concentration *(% Wt. by Binder);* C_f = Free Chloride Concentration (mol/L); α *and* β = Binding Constants. The free and bound chloride best-fit relationship using non-linear regression analysis of the Langmuir binding Isotherm (Blue dotted line) is shown in Fig 5.1.

Yuan et al. [209] suggested that at high chloride concentration exposures, the Langmuir binding isotherm indicates that all adsorption sites are occupied by chloride ions thereby resulting in lower chloride ion concentration in the pore solution.

Glass and Buenfeld [208] adopted the Langmuir binding isotherm to relate their chloride ingress data for low (2%), medium (8%) and high (14%) C_3A cement which gave good correlation with the model. The concrete mix containing 0-3% by weight of chloride was cured for 130 days without any change in moisture content of the specimen. The values predicted from the best-fit equation by regression analysis of *Glass and Buenfeld* [208] data gave maximum bound chlorides for the low (2%), medium (8%) and high (14%) C_3A cements as 0.97%, 1.32% and 1.67% by weight of cement respectively. The model shows best-fit for (14%) C_3A cement than the low (2%) and medium (8%) C_3A cements.

5.2.5.4 Linear Isotherm

The linear binding isotherm is adopted by many researchers because of its simplicity [92][249][93][259] giving the proposed linear relationship model between the free and bound chloride concentrations in equation 5.4.

$$C_b = k\, C_f \qquad 5.4$$

Where: C_b = Bound Chloride Concentration *(% Wt. by Binder);* C_f = Free Chloride Concentration (mol/L); k = Binding Constant. The relationship between free and bound chloride using the Linear binding isotherm (Green dotted line) is shown in Fig 5.1.

Several controversial views on the validity of adopting the linear binding isotherm to predict the relationship between free and bound chloride concentration has been put forward. *Ramachandran et al.* [260] and *Yuan et al.* [209] suggested that the results from linear binding isotherm are not valid because the linear binding isotherm over-estimates the chloride binding capacity at high concentration of exposures and under-estimates the chloride binding capacity at low concentration of exposures.

On the other hand, the linear binding isotherm was validated to predict the relationship between free and bound chloride for field-exposed concrete under a marine environment for long exposure periods of 10 to 30years [249]. *Sandberg* [261] noted the differences between the linear relationship of free and total chloride of the field-exposed

and laboratory cured concretes. The differences in their linear binding isotherms were ascribed to the leaching of hydroxyl ions.

5.2.5.5 Chloride Binding Capacity

The chloride binding capacity of sulphate-resisting Portland cement SRPC and supplementary cement replacement concrete was reported to be lower than OPC concrete [25]. This was due to the differences in the binding effect which was influenced by the Tricalcium aluminate C_3A content in each cement (OPC ~ 15% and SRPC~ 2%) [170]. An increase in the Tricalcium aluminate C_3A decreases the free chloride concentration in the pore solution. Similarly, an increase in the alkali content and OH^- concentration decreases the free chloride concentration in pore solution thus improving the chloride binding capacity [92].

Fig. 5.2 shows the binding isotherm of the published total and free chloride content in cement based materials (Table 5.1). Lower limits of the total and free chloride contents from the data of *Pettersson* [243], *Alonso et al.* [245], *Trejo and Pillai* [248], *Oh et al.* [92] and *Mohammed and Hamada* [249] were used from Table 5.1. The linear binding isotherm was adopted because of the single value of total and free chloride available for the analysis.

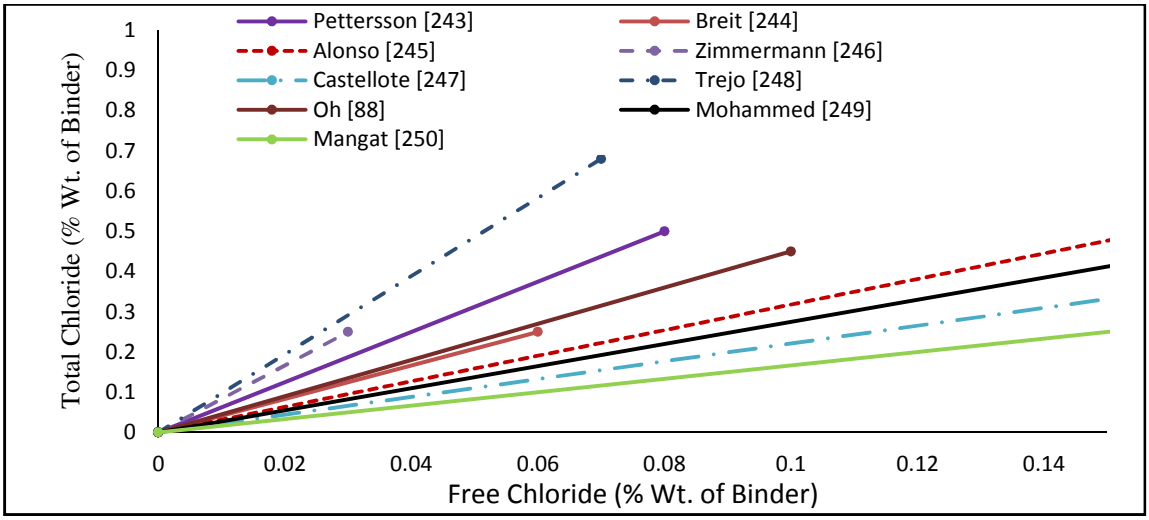

Figure 5. 2: Linear binding isotherm of published chloride concentrations from Table 5.1

Trejo [248] had the highest binding capacity followed by *Pettersson* [243]. Supplementary materials were incorporated in the mix compositions of these concrete and mortar mixes. The binding capacity increases for a fly-ash slag concrete because of its high Al-bearing phase although the increase in the binding capacity is dependent on the property of the ash [209]. *Florea and Brouwers* [262] presented the binding capacities of slag blended cement pastes containing 0%, 25% and 50% slag content. The slag blended cement paste containing 50% slag had the highest binding capacity which

was attributed to the aluminate phases in the slag blended cement. AACM materials are likely to have high binding capacity because of the high alkali content of mix as a result of the alkali activator concentration and due to the use of supplementary binders.

On the other hand, the lowest binding capacity was observed in the results presented by *Mangat et al.* [250] which contain microsilica and the concrete was exposed to the longest curing period under marine spray cycles in the laboratory for 520 days.

5.3 EXPERIMENTAL PROGRAMME

5.3.1 Mix Composition

The specimens used for free chloride and pH analysis were obtained from the same AACM concrete mixes that were used to determine the bound chloride concentrations, which are detailed in chapter 4. The AACM concrete comprises of a cementitious binder, fine aggregate, coarse aggregate and the alkali activator as shown in Table 5.2. Trial mix S_1 was performed prior to the selection of the mix composition used for the free chloride and pH investigation. The mixes for the investigation were made with the proprietary AACM binder and activator by incorporating a range of 438 kg/m^3 to 585 kg/m^3 of fine aggregate and 988 kg/m^3 to 1170 kg/m^3 of coarse aggregate (Table 5.2). The trial mix S_1 was tested for strength, shrinkage and workability to achieve a practical field mix of AACM concrete with high strength. A compressive strength of 72.25 MPa was achieved at 28 days age, the slump was between 60 - 180 mm and the shrinkage had a mean value of 683.4 microstrain at 78 days age. The experimental AACM concrete mixes S_2 to S_6 used in this research were produced based on the trial mix S_1 (Table 5.2). The AACM binder content and fine aggregate content of the mixes S_2 to S_5 was reduced relative to mix S_1 while the liquid/binder and coarse aggregate content was increased to adjust the workability and setting time required for practical mixes. The mix composition of the five series of concrete mixes S_2 to S_6 is given in Table 5.2. S_6 is the control mix produced with 100% OPC binder of C40 grade concrete. The reference *alkali activator liquid* [210] was diluted with tap water by 2.15%, 4.24%, 8.12% and 12% in mixes S_2 to S_5 respectively (Table 5.2). The liquid composition of each mix comprised of alkali activator, water, retarder and shrinkage admixture. AACM Mix S_2 had the lowest percentage dilution of alkali activator with water, which was 2.15%, while AACM Mix S_5 had the highest with 12.00%. The ratios of total liquid (alkali activator + water) to binder are 0.41, 0.48, 0.47 and 0.47 for mixes

S_2, S_3, S_4 and S_5 respectively. The water cement ratio of the control OPC concrete mix S_6 is 0.48.

Table 5. 2: Composition of AACM and OPC concrete mixes

Mix	Total Binder (Kg/m^3)	Coarse Aggregate(Kg/m^3)		Fine Aggregate (Kg/m^3)	Alkali activator (Kg/m^3)	Extra water (Kg/m^3)	Total Liquid (Kg/m^3)	Liquid/ Binder Ratio	Activator Dilution (%)	Retarder (Kg/m^3)	SRA (Kg/m^3)
		10mm Gravel	6mm Limestone								
S_2	688	654	334	438	279	6	285	0.41	2.15	8	21
S_3	619	717	374	423	283	12	295	0.48	4.24	7	19
S_4	619	717	374	423	271	22	293	0.47	8.12	7	19
S_5	619	717	374	423	260	31	291	0.47	12.00	7	19
S_6(Control)	350	769	401	585	-	170	170	0.48	-	-	-

5.3.2 Experimental Procedure

5.3.2.1 Concrete Coring

Four cores of 50 mm diameter x 60 mm height were drilled using a diamond core drill bit from the AACM and OPC concrete specimens of dimensions 250 x 250 x 75 mm (Fig. 5.3) which were used for the chloride diffusion investigation (section 4.3.4.1, chapter 4). The coring was performed at 180, 270 and 540 days exposure period in 5% NaCl solution. At exposure periods of 180 and 270 days, the concrete cores were obtained from the sawn halves of concrete specimens (250 x 125 x 75 mm) that were used to collect powder samples for the acid and water-soluble chloride analysis in chapter 4. The concrete coring performed at exposure period of 540 days was carried out on a complete specimen (250 x 250 x 75 mm) as shown in Fig. 5.3.

(a) (b)

Figure 5. 3: Coring of AACM and OPC specimens exposed to 5% NaCl solution. (a) Sawn halves, dimensions 250x125x75mm (180 and 270 days exposure) (b) Full specimen, dimensions 250x250x75 mm (540 days exposure).

Each core specimen of 50 mm diameter x 60 mm depth was sawn into three discs of 50 mm diameter x 20 mm depth representing depths of 0 - 20 mm, 20 - 40 mm and 40 - 60 mm from the surface of the concrete (Figures 5.4 and 5.5).

Figure 5. 4: Cutting the concrete cores into discs of 50 mm diameter x 20 mm depth.

The discs were labelled 1, 2 and 3 for depths of 0 - 20 mm, 20 - 40 mm and 40 - 60 mm respectively. Four discs for each depth from the concrete surface were produced i.e 4 Nos of 0 - 20 mm, 20 - 40 mm and 40 - 60 mm as shown in Fig. 5.5.

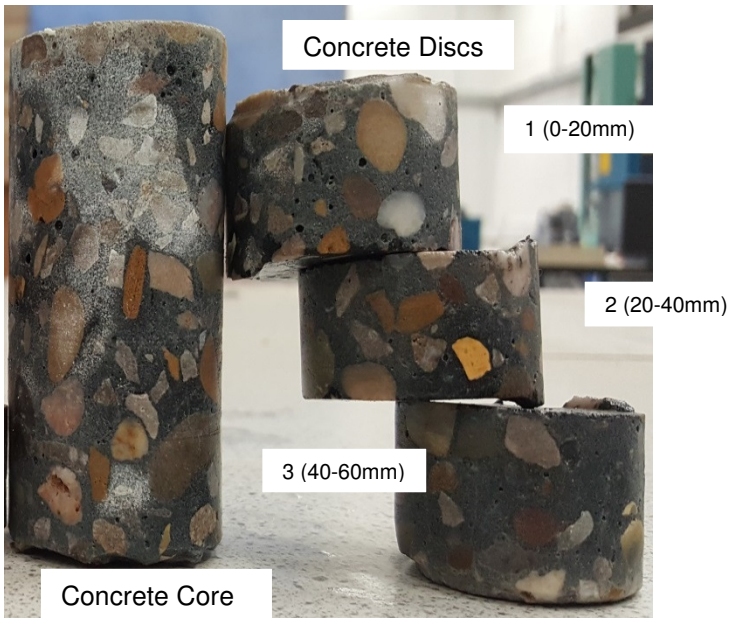

Figure 5. 5: Obtaining discs of 50mm diameter, 20mm depth from the concrete core.

The bituminous coating which was applied to the five faces of the chloride diffusion specimens to prevent the ingress of chloride was carefully removed from the cores. The coating was removed to prevent possible interference with the measured free chloride content. The concrete discs were immediately stored separately for each concrete specimen in self-sealing bags to avoid the effects of carbonation of the test samples (Fig. 5.6). The test samples were stored in the environmental simulation

chamber at 100% R.H. to retain the concrete pore solution within the sample and prevent carbonation. Expression of the pore fluid was performed on all the samples within 10 days.

Figure 5. 6: Concrete discs stored in self-sealing bags

5.3.2.2 Pore Solution Expression

The extraction process of pore solution from concrete required compressing the concrete discs at high pressure up to 190 tonnes using the OpiCAD pore fluid extraction device (Fig. 5.7). The OpiCAD device consists of the crushing cone, piston and punching head, all made from high resistance metal. The core samples were subjected to high triaxial pressures of up to1000 MPa in the pore fluid extraction device by the compression testing machine.

Three concrete discs each of 50 mm diameter x 20 mm depth, which were numbered 1 (representing 0-20 mm depth) from the three cores of each AACM concrete mix S_2 to S_5 were combined and placed inside the pore fluid extractor. The pore fluid extractor comprised the following parts: the crushing cone, Teflon disc, piston and the punching head as shown in Fig. 5.8. The punching head was centrally positioned on the teflon disc and the whole assembly was then placed on top of the core discs inside the pore fluid extraction device with the punching head pressing on the core discs (Fig. 5.8). The teflon discs provide an airtight joint and prevent air intrusion into the pore fluid extractor from the outside environment during the application of high pressure through the punching head to squeeze the pore solution from concrete (Fig. 5.9). In addition to preventing air intrusion, the function of the teflon disc is to centrally position the

punching head which might otherwise damage the piston or the crushing cone if not placed centrally.

Figure 5. 7: Pore fluid extraction device

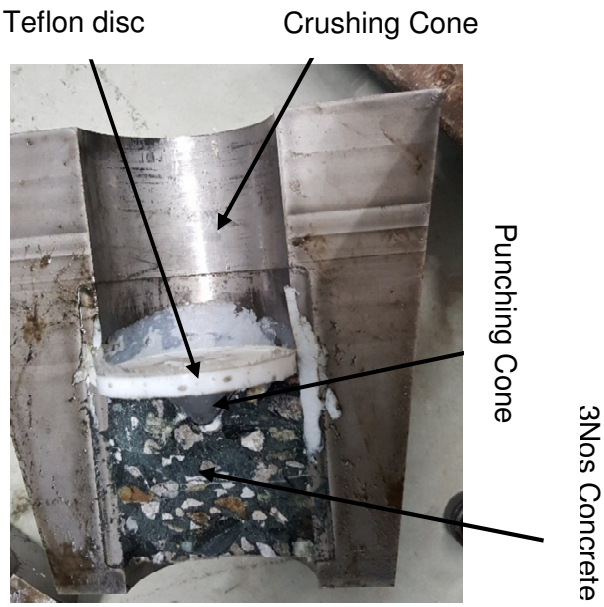

Figure 5. 8: Cross section of pore fluid extraction device and concrete discs

The piston (Fig. 5.7) was placed on the teflon disc. Pressure on the core discs was applied by the compression testing machine. The pore fluid extraction device with the concrete discs in it was placed under the loading platen (Fig 5.9) in the compression testing machine. Compressive load was applied at a steady rate and the pore solution was extracted through a suction action without allowing contact with air and was immediately stored in plastic vials, labelled and sealed with parafilm (Fig 5.10). The same procedure was repeated on concrete core discs labelled 2 (representing 20-40 mm depth) and 3 (representing 40-60 mm depth).

Figure 5. 9: Pore fluid extractor placed under the compression testing machine platen

Figure 5. 10: Air tight plastic vials containing concrete pore solution.

5.3.2.3 Concrete Pore Solution

The data of the pore fluid extraction performed on both AACM and OPC concrete mixes S_2 to S_6 are presented in Table 5.4. The pore fluid extraction was performed on AACM and OPC concrete at 180, 270 and 540 days of chloride exposure periods. A total of 24 pore fluid extractions were performed on the concrete core discs.

Table 5. 3: Details of AACM and OPC concrete pore fluid extraction

540 days chloride exposure			
Mix	Depth (mm)	Extraction Pressure (MPa)	Weight of Pore Fluid Sample (g)
S_2	0-20	954.75	2.05
	20-40	969.53	2.83
	40-60	949.69	2.4
270 days chloride exposure			
Mix	Depth (mm)	Extraction Pressure (MPa)	Weight of Pore Fluid Sample (g)
S_2	0-20	992.6	1.00
	20-40	895.7	0.83
	40-60	896.1	1.15
S_4	0-20	902.4	2.49
	20-40	901.5	0.94
	40-60	900.7	1.40
S_5	0-20	980.4	1.35
	20-40	894.7	1.93
	40-60	892.8	1.72
S_6	0-20	967.03	1.49
	20-40	981.23	1.82
	40-60	975.93	1.40
180 days chloride exposure			
Mix	Depth (mm)	Extraction Pressure (MPa)	Weight of Pore Fluid Sample (g)
S_2	0-20	987.5	1.37
	20-40	891.4	1.79
	40-60	893.0	3.08
S_3	0-20	923.1	2.42
	20-40	908.3	2.04
	40-60	889.8	2.60
S_4	0-20	784.6	2.28
	20-40	713.9	3.12
	40-60	747.1	2.90

An average pressure of 900 MPa was applied by the compression testing machine on the piston head to squeeze the three combined concrete core discs to obtain a quantity of pore solution within the range of 0.94 to 3.12 g. Once the pore solution was extracted, it was immediately transferred to an air tight plastic vial (Fig. 5.10). The plastic vial containing the concrete pore solution was placed in an air tight container and stored in a

humidity chamber at 100% R.H. to prevent evaporation of the pore solution. The determination of free chloride content and pH was done within 7 days.

5.3.3 Analytical Procedures

5.3.3.1 Determination of Free Chloride Concentration

The Chloride Ion Selective Electrode (ISE) that was used to obtain the water-soluble chloride concentration in chapter 4 was used to measure the free chloride content. It has a solid-state poly-crystalline membrane that measures chloride ions (Cl^-) in aqueous solution, which is suitable for field and laboratory applications. The operation of the device is based on the linear relationship between the electric potential developed between the internal Silver/Silver Chloride (Ag/AgCl) reference electrode and the reference electrode immersed in the concrete pore solution [212]. The Chloride ISE was supplied by Vernier Software and Technology.

The small quantity of concrete pore solution obtained during the extraction process necessitated the use of an analytical procedure. 0.2 ml of concrete pore solution was dissolved in 10 ml of distilled water, which is a ratio of 1:50. The solution was swirled manually to ensure good, homogeneous contact between the solution and the ISE membrane. The white reference contact near the tip of the electrode (ISE) was immersed in the solution without entrapping air bubbles below it. The ISE was held in the aqueous solution until the reading stabilized and the displayed reading was then recorded. The ISE was rinsed by spraying with a jet of ionised water and dabbed dry with a low-lint laboratory tissue between measurements to prevent hysteresis effects. The ISE was calibrated before and after each measurement to achieve accuracy. The free chloride concentration readings for the pore solution of concrete core discs labelled 1 (representing 0 - 20 mm depth), 2 (representing 20 - 40 mm depth) and 3 (representing 40 - 60 mm depth) were determined with the ISE thrice to achieve high level of accuracy. The coefficient of variance of repeatability was less than 10%. The calibration was done by using a pre-prepared 1000 mg/l and 10 mg/l of standard NaCl solution.

5.3.3.2 Determination of pH

A number of methods have been proposed to measure pH of concrete and the free alkali content in the pore solution of mortars amongst which are the pore water expression (PWE) and ex-situ leaching methods (ESL) [263]. The ex-situ leaching methods use hot or cold water to extract hydroxyl ions by dissolving the concrete powder samples in solution and then leaving the solution for leaching process to take

place before measuring the pH with an electrode [263]. The pore water expression on the other hand does not require adding hot or cold water as described in section 5.3.2.2.

Limitations in the accuracy of pH values for ex-situ leaching methods were observed when compared with pore water expression due to the addition of water to the ground material. The added water to the ground material could lead to secondary hydration of the previously unhydrated part, this will lead to the further release of OH^- ions into the solution and subsequently higher pH [264]. In addition, the partial dissolution of the hydration prone phase is observed such as the Portlandite, but no impact on the pore solution composition was recorded as long as the phase is not modified when water is added [265].

The pH in this study was determined using the pore water extraction method explained in section 5.3.2.2 and then dipping a double junction electrode in the pore solution. The pH readings from the pore solution were displayed on a benchtop meter 3-in-1 (Fig. 5.11). This device measures pH ranging from 0.00 to 14.00.

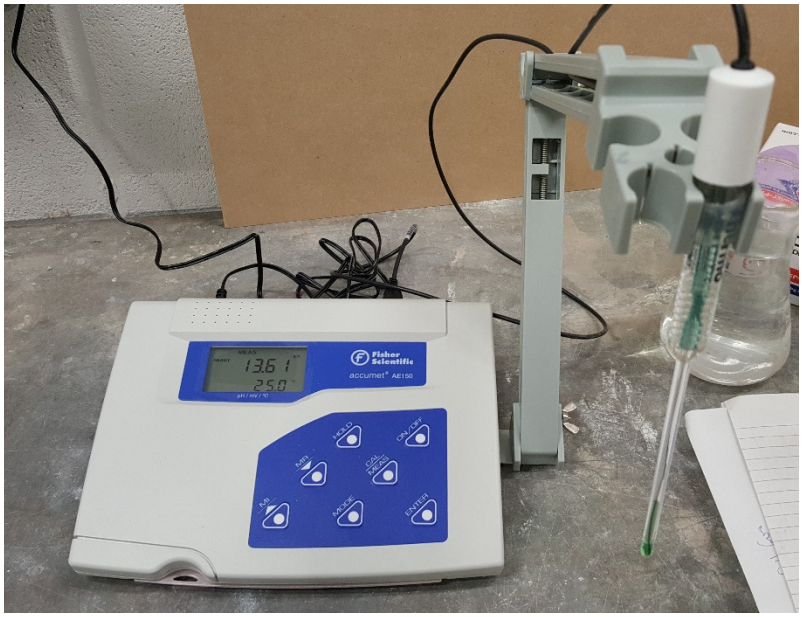

Figure 5. 11: Double junction electrode and benchtop meter 3-in-1 used to measure pH

The pH device can measure samples as small as 0.2 mL with an accuracy of ± 0.01. The body of the double junction electrode is made of glass which makes it suitable in very acidic or alkaline solutions. The internal reference comprises of Ag/AgCl double junction electrode resulting in exceptionally stable and minimal long-term drift.

5.4 RESULTS AND DISCUSSION

5.4.1 Free Chloride Concentration

The free chloride concentration obtained from the pore solution of AACM and OPC concrete discs is presented in Table 5.5. The three variable parameters that will be

used to analyse the free chloride contents are the exposure periods to chloride solution, activator dilution ratio and the mean depth of the samples from the exposed surface to the chloride environment.

Table 5. 4: Free chloride concentration (mg/L) for AACM and OPC concrete

Mix S_2				
Depth (mm)	Mean Depth (mm)	S2(180days)	S2(270days)	S2(540days)
0 - 20	10	521.81	951.89	1266.56
20 - 40	30	278.22	641.48	822.50
40 - 60	50	194.99	478.68	550.97
Mix S_3				
0 - 20	10	383.92	x	x
20 - 40	30	215.65	x	x
40 - 60	50	162.19	x	x
Mix S_4				
0 - 20	10	662.74	999.88	x
20 - 40	30	331.67	673.67	x
40 - 60	50	278.22	515.13	x
Mix S_5				
0 - 20	10	x	1086.75	x
20 - 40	30	x	734.42	x
40 - 60	50	x	544.89	x
Mix S_6				
0 - 20	10	x	800.63	x
20 - 40	30	x	459.24	x
40 - 60	50	x	274.57	x

The AACM and OPC concrete specimens were cured in a 5% NaCl (by weight) aqueous solution up to 540 days. The exposure periods used for this analysis are 180, 270 and 540 days. The activator dilution ratios of the AACM concrete mixes are 2.15%, 4.25%, 8.12% and 12% (Table 5.4) which are common with the bound chloride investigation. The free chloride profiles with depth of both the AACM and OPC concretes at 270 days exposure period were also investigated.

5.4.1.1 Free Chloride Diffusion Profiles

The effects of chloride exposure on the free chloride concentration of AACM concrete mixes S_2 and S_4 are presented in Fig. 5.12. The free chloride concentration of AACM concrete mix S_2 was determined at 180, 270 and 540 days of chloride exposure periods while for mix S_4 it was determined at 270 and 540 days of chloride exposure.

The measuring unit of free chloride concentration (mg/L) from Table 5.5 was converted to mol/L using equations 5.5.

$$mol/L = \frac{mg/L}{1000 * unit\ wt.of\ Cl\ (\frac{g}{mol})} \qquad 5.5$$

The unit weight of Cl is 35.5 g/mol and mg/L is divided by 1000 to convert it to g/L.

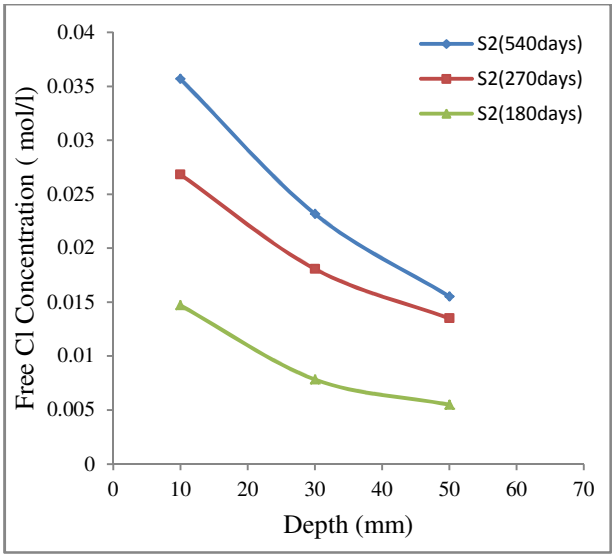

(a) Free chloride profiles for AACM mix S_2

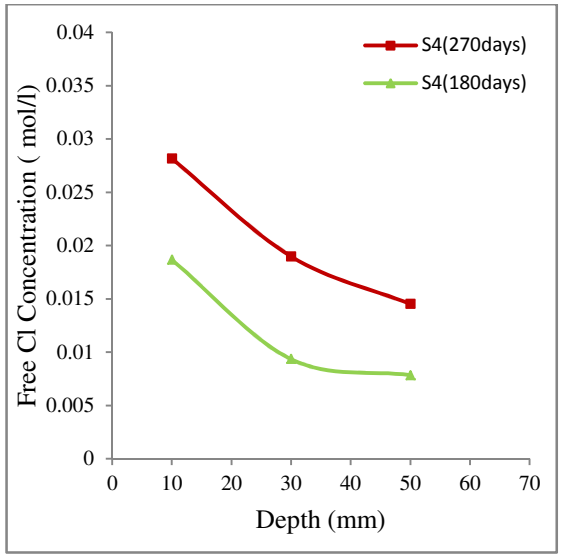

(b) Free chloride profiles for AACM mix S_4

Figure 5. 12: Free chloride concentration profiles of AACM concrete exposed to 5% chloride solution.

An increase in the free chloride concentration within AACM concrete mixes S_2 and S_4 is observed with increase in the chloride exposure periods in Fig 5.12. The free chloride concentration is 0.036 mol/L at a mean depth of 10 mm for AACM concrete mix S_2 at 540 days (Fig 5.12a) while it is 0.028 mol/L at a depth of 10 mm for mix S_4 at 270 days of chloride exposure (Fig 5.12b). The free chloride concentration increases with the exposure period as the chloride from the external source tends to attain concentration equilibrium with the concrete pore solution with passage of time. Similar increase in the free chloride concentration has been reported by many researchers [93][266][267].

Mangat and Gurusamy [266] presented free chloride concentration for a 26% pulverised fly-ash replacement fibre reinforced concrete with water/cement ratio of 0.4. The free chloride concentration under 1200 and 2000 tidal cycles (corresponding to 640 and 1250days of exposure) was 0.1mol/L and 0.3mol/L respectively. The reason for the high free chloride concentration presented by *Mangat and Gurusamy* [266] relative to this investigation could be attributed the wet/dry cycles regime provided by the tidal exposure and longer exposure period (cycles).

The free chloride concentration of OPC concrete over a long period (10 years) of chloride exposure was presented by *Cheewaket et al.* [267]. The specimens were exposed to tidal zone in the gulf of Thailand which has chloride concentration between 16,000 to 18,000 mg/L. Concrete cores were obtained from the specimen after 10 years of chloride exposure which was then dry cut into 10-mm thick slices. The 10-mm thick slices were ground to obtain powder which was mixed with water similar to water-soluble chloride extraction method. The free chloride concentrations at 20 mm depth from concrete surface was 0.42%, 0.7%, 2.0%, 2.7%, 3.3%, 3.8% by weight of binder at 2, 3, 4, 5, 7 and 10 years respectively. However, the chloride extraction method adopted by the authors is used to determine water-soluble chloride concentration. The free chloride values given by the authors [267] are in fact the water-soluble chloride values. The free chloride gets bound (physically or chemically) to gel paste as it penetrates through the AACM and OPC concrete matrix. This phenomenon is known as the chloride binding capacity or binding isotherm which is discussed fully in Section 5.4.3.

5.4.1.2 Activator Dilution

The influence of activator dilution on the free chloride concentrations for AACM concrete at 180 and 270 days of chloride exposure is shown in Fig 5.13a and b. The activator dilutions with water represented at 180 days of chloride exposure period are 2.15%, 4.25% and 8.12% (Fig 5.13a). The dilutions at 270 days exposure (Fig. 5.13b) are 2.15%, 8.12% and 12%.

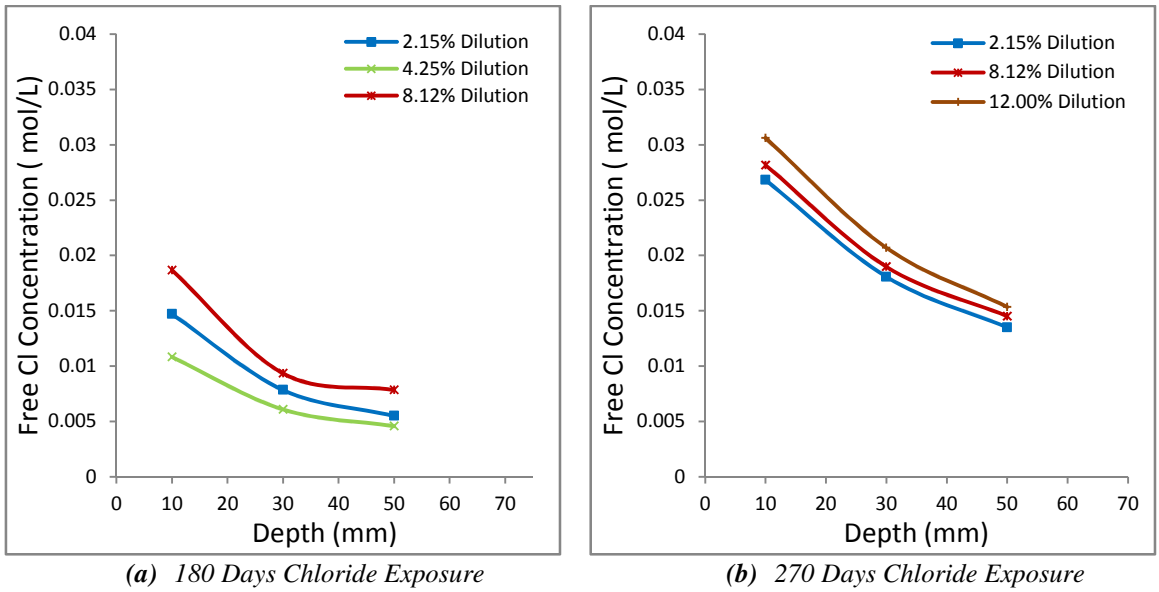

(a) *180 Days Chloride Exposure* ***(b)*** *270 Days Chloride Exposure*

Figure 5. 13: Effect of activator dilution on the free chloride concentrations of AACM concrete at 180 and 270 days of chloride exposure.

Fig. 5.13a shows that the free chloride profiles and its concentration (0.011 mol/L) at 10 mm mean depth is lowest at 4.25% activator dilution compared with

8.12% (0.019 mol/L) dilution. This low free chloride concentration at 4.25% activator dilution (AACM mix S_3) follows the results of the better mechanical performance of AACM concrete mix S_3 detailed in chapter 4. This suggests that the free chloride concentration in AACM concrete is related to its total porosity. The intrudable porosity of the AACM mortar representing the concrete mixes of the pore fluid investigation was presented in chapter 3. It gave the lowest intrudable porosity for the matrix of AACM concrete mix S_3 and highest compressive strength 62 MPa which explains its lowest free chloride values. Ideally, however, the total porosity (not intrudable porosity) is related to chloride diffusion.

Fig. 5.13b shows a close range of free chloride concentration between the three dilution ratios at 270 days of chloride exposure. For example, the free chloride concentrations at 10 mm mean depth are 0.031mol/L and 0.028mol/L for 12% and 8.12% activator dilution respectively. The difference, however, is more significant at 180 days of chloride exposure (Fig. 5.13a). For example, the free chloride concentration at 10 mm mean depth is 0.019mol/L and 0.011mol/L for 8.12% and 4.25% activator dilution respectively (Fig. 5.13a). This represents a difference of 0.008mol/L in free chloride concentration between 8.12% and 4.25% activator dilution for 180 days chloride exposure, which is quite significant. The free chloride concentration is likely to attain greater stability (equilibrium) with the chloride concentration of its exposure environment at the later chloride exposure period (270 days) and also the matrix evolves a finer pore structure than at 180 days age, thereby, slowing the rate of chloride penetration within the concrete pore solution.

In addition to the activator dilution, the liquid/binder ratio clearly influences the free chloride concentration in AACM concrete. Mix S_2 with the lowest liquid/binder ratio 0.41 (Table 5.2) has higher free chloride content than mix S_3 with liquid/binder ratio 0.48 (Fig. 5.13a) at 180 days chloride exposure. A negligible difference of 0.001 mol/L free chloride concentration was observed between 8.12% (mix S_4) and 2.15% (mix S_2) activator dilution (Fig. 5.13b) at 270 days chloride exposure. Further investigation on the effect of liquid/binder ratio on the free concentration in AACM concrete will be required to enable a clear conclusion.

5.4.1.3 Free Chloride Content of AACM and OPC Concrete

The comparative results of free chloride concentrations for AACM and OPC concrete are presented in Fig. 5.14. The free chloride concentrations were determined for AACM concrete mixes S_2, S_4, S_5 and OPC concrete mix S_6 at 270 days chloride

exposure. OPC concrete mix S_6 has the lowest free chloride concentration profile compared with AACM concrete mixes in Fig. 5.14. The free chloride concentration for OPC concrete mix S_6 is 0.023mol/L at 10 mm mean depth while AACM concrete mixes S_2, S_4 and S_5 have 0.027mol/L, 0.028mol/L and 0.031mol/L respectively. AACM concrete mix S_2, S_4 and S_5 has 15%, 18% and 26% more free chloride concentration than OPC concrete mix S_6.

It is noteworthy to mention that the increase in strength of the control OPC mix required to match AACM strength may require the use of mineral admixtures (silica fume, GGBS and fly ash). This will likely reduce its C_3A content which is partly responsible for the low free chloride content in OPC concrete.

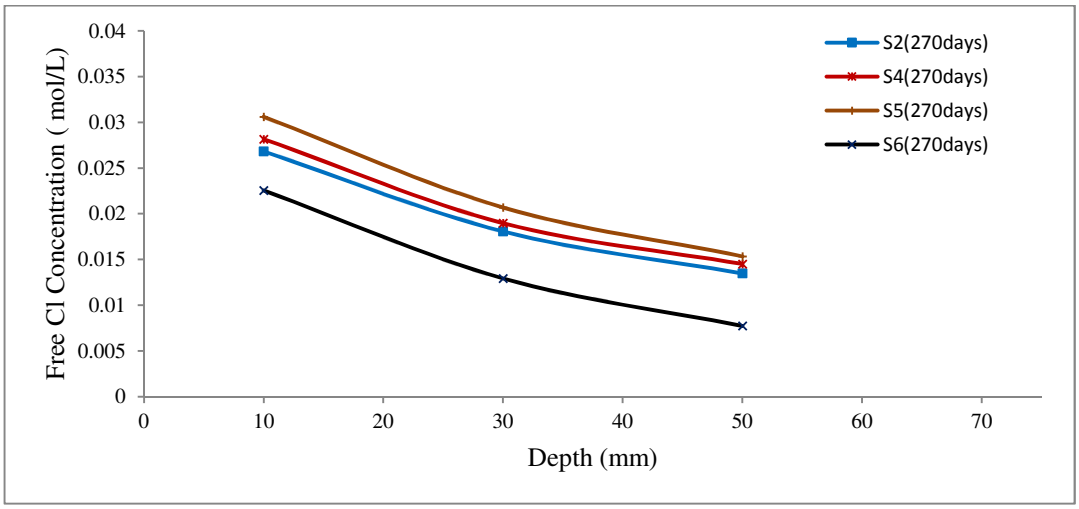

Figure 5. 14: Free chloride concentration profile of AACM and OPC concrete

The high free chloride concentration present in the pore solution of AACM concrete compared with OPC concrete could be attributed to the low chemically bound (acid-soluble) chloride observed in AACM concrete, which was reported in chapter 4. *RILEM TC 224* [3] observed that no Friedel's salt is present in AACM concrete neither is there any other crystalline chloride compounds unlike in the OPC concrete. In effect, the acid soluble chlorides in AACM concrete play an inconsequential role in chloride ingress compared with OPC concrete.

Therefore, the physically bound (water-soluble) chloride and free chloride will add up to make the bulk of total chloride present in AACM concrete. However, the total chloride present in OPC concrete is the summation of chemically bound (acid-soluble) chloride, physically bound (water-soluble) chloride and the free chloride [25][97][170].

5.4.2 Free Chloride Diffusion Parameters

5.4.2.1 Chloride Profiles

The experimental and Fick's law based regression profiles of free chloride concentrations of AACM and OPC concrete at 180, 270 and 540 days exposure periods are shown in Figures 5.15, 5.16 and 5.17 respectively.

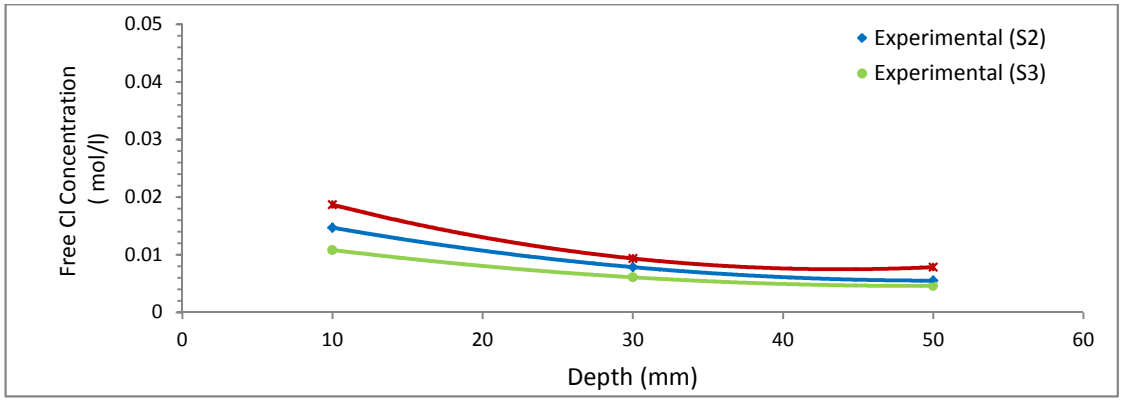

Figure 5. 15: Experimental data and regression analysis profiles of free chloride concentration of AACM concrete at 180 days chloride exposure.

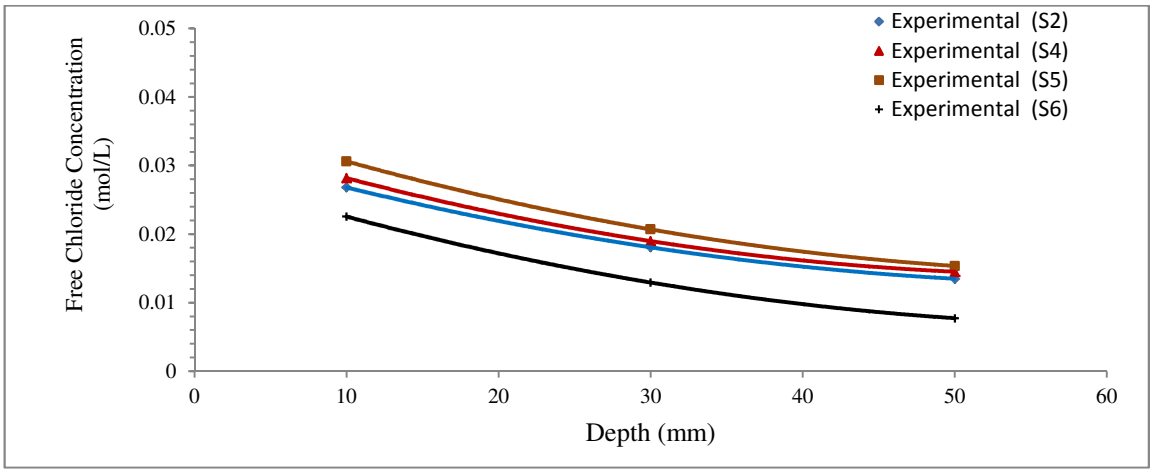

Figure 5. 16: Experimental data and regression analysis profiles of free chloride concentration of AACM and OPC concrete at 270 days chloride exposure.

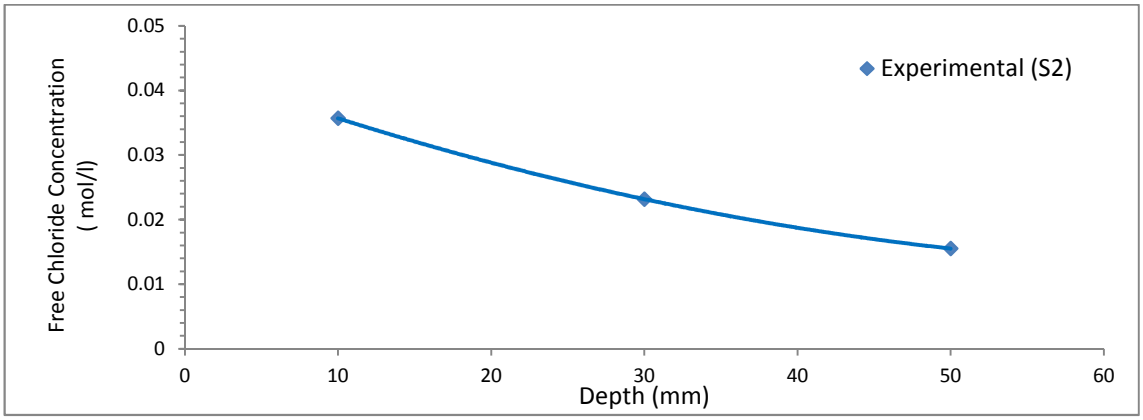

Figure 5. 17: Experimental data and regression analysis profiles of free chloride concentration of AACM concrete at 540 days chloride exposure.

The experimental data show strong correlation with the regression analysis profiles derived from Fick's 2nd law of diffusion which is given by equation 5.6. The Fick's second law represents one dimensional non-steady condition of diffusion and is used to determine the diffusion coefficient, $D_{C(f),}$ and surface chloride concentration, $C_{0(f),}$ of AACM and OPC concrete.

$$C = C_{\circ}\left(1 - erf\left[\frac{x}{2\sqrt{D_C\, t}}\right]\right) \qquad 5.6$$

Where: x = distance from concrete surface (m); t = Time (seconds); $D_{C(f)}$= diffusion coefficient (m^2/s); $C_{0(f)}$ = equilibrium chloride concentration on concrete surface (mol/L); $C_{(x,t)}$ = chloride concentration at distance x, time t (mol/L).

Nonlinear regression analysis of the experimental data by a computer package (Microsoft excel) was used to generate the best fitting equation. The analysis determined the chloride concentration on the surface of the specimen, at depth zero, $C_{0(f)}$, and the diffusion coefficient, $D_{C(f)}$. The free chloride diffusion parameters $C_{0(f)}$, $D_{C(f)}$ and level of correlation R^2 of the regression analysis, obtained from the data in Figures 5.15, 5.16 and 5.17 are presented in Table 5.6.

Table 5. 5: Free Chloride diffusion parameters $C_{0(f)}$, $D_{c(f)}$ and the coefficient of correlation R^2

	S_2 Exposure (Days)			S_3Exposure (Days)	S_4 Exposure (Days)		S_5 Exposure (Days)	S_6 Exposure (Days)
	540	270	180	180	270	180	270	270
C_0 (mol/L)	0.053	0.032	0.025	0.018	0.035	0.029	0.039	0.032
D_c x 10^{-12} (m^2/s)	0.65	5.1	3.6	4.2	5.4	4.5	5.6	2.7
R^2	0.85	0.97	0.93	0.92	0.96	0.99	0.97	0.97

5.4.2.2 Surface Chloride Concentration $C_{0(f)}$

The free surface chloride concentrations, $C_{0(f)}$, for AACM concrete mixes S_2, S_3, S_4, S_5 and OPC concrete mix S_6 at 180, 270 and 540 days of chloride exposure are presented in Fig. 5.18.

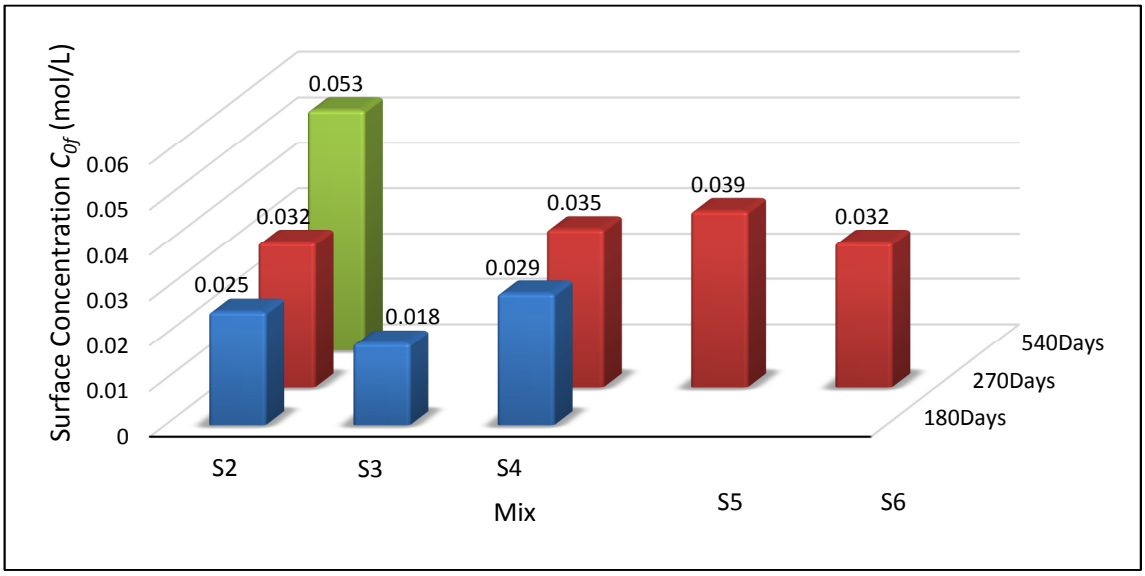

Figure 5. 18: Free surface chloride concentration, $C_{0(f)}$, of AACM and OPC concrete at 180, 270 and 540 days of chloride exposure.

The free surface chloride concentration, $C_{0(f)}$, increases with chloride exposure periods as seen in Fig. 5.18. For example, $C_{0(f)}$ values for AACM concrete mix S_2 are 0.025 mol/L, 0.032 mol/L and 0.053 mol/L for 180, 270 and 540 days of chloride exposure respectively. Similarly, for mix S_4, the $C_{0(f)}$ increases from 0.029 mol/L to 0.035 mol/L at 180 and 270 days of chloride exposure respectively. *Glass and Buenfeld* [268] stated that the increase of free chloride concentration at the surface $C_{0(f)}$, in OPC concrete could be attributed to a high moisture content of the concrete mix and prolonged exposure to chloride laden environment. The chloride concentration in the pore solution will be diluted by its high moisture content which will induce further chloride ingress through the concrete boundary. The difference in concentration gradient between the pore solution and external environment is due to the high moisture content within the concrete matrix which will induce further accumulation of free surface chloride concentration, $C_{0(f)}$ over time [268].

An experimental investigation carried out by *Jun et al.* [269] on concrete specimens immersed in 5% NaCl solution (5.6 mol/L) shows that an increase in water/cement ratio increases the free chloride concentration at the surface, $C_{0(f)}$. However, with prolonged chloride exposure, the difference in surface chloride concentration induced by w/c becomes smaller. The liquid/binder ratios in AACM mixes S_2, S_3, S_4 and S_5 in this research investigation are within the same range of 0.41 to 0.48, therefore, the impact of liquid/binder on the free surface chloride concentration $C_{0(f)}$, could not be ascertained due to the close range of liquid/binder.

The free surface chloride concentration, $C_{0(f)}$, of AACM concrete is slightly higher than OPC concrete at 270 days chloride exposure. $C_{0(f)}$ values of AACM concrete mixes S_2, S_4 and S_5 are 0.032 mol/L, 0.035 mol/L and 0.039 mol/L respectively while it is 0.032 mol/L for OPC concrete mix S_6. *Angst et al.* [238] suggested that the secondary pozzolanic reaction by mineral admixtures with hydration products of cement may have induced high chloride concentration at the concrete surface, $C_{0(f)}$, than the hydration product of OPC concrete. The additional hydration product in supplementary cementitious materials creates more chloride sorption sites compared to OPC concrete. There is a tendency for chloride at the concrete surface, $C_{0(f)}$, to increase due to additional chloride sorption sites within its matrix. In the case of AACM, the geopolymerisation products are greater than the hydration products of OPC concrete [3]. The affinity of chloride at the geopolymerisation sites may have induced more chloride build up at the surface, $C_{0(f)}$, than in OPC concrete.

5.4.2.3 Diffusion Coefficient $D_{c(f)}$

The diffusion coefficients, $D_{c(f)}$, for AACM concrete mixes S_2, S_3, S_4, S_5 and OPC concrete mix S_6 at 180, 270 and 540 days of chloride exposure are presented in Fig. 5.19.

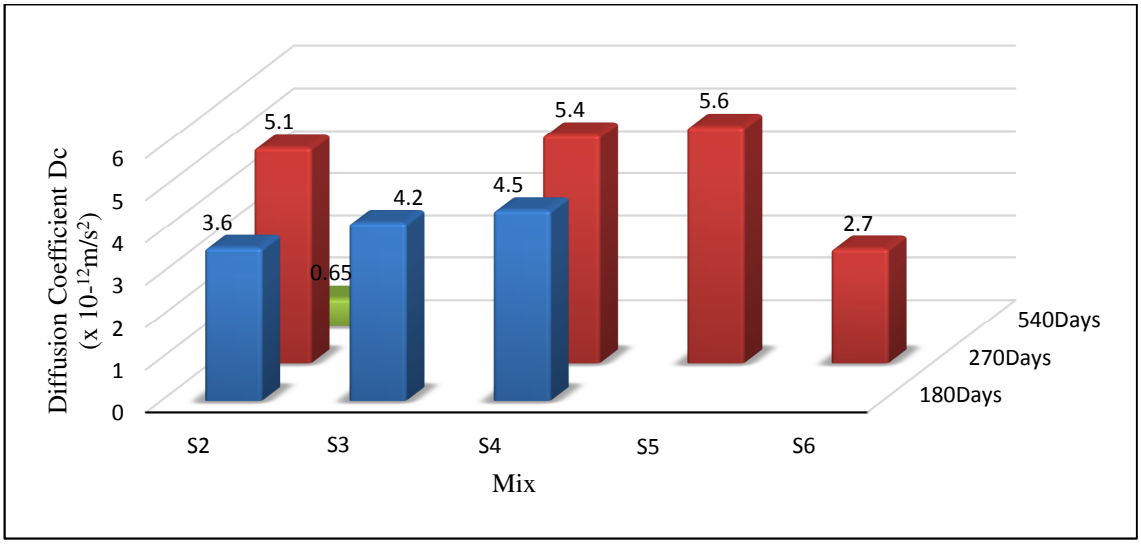

Figure 5. 19: Diffusion coefficient, $D_{c(f)}$, of AACM and OPC concrete at 180, 270 and 540 days of chloride exposure.

The highest chloride diffusion coefficient, $D_{C(f)}$, was attained at 270 days chloride exposure as seen in Fig. 5.19. For example, $D_{C(f)}$ for AACM concrete mix S_2 is 3.6 x 10^{-12} m^2/s, 5.1 x 10^{-12} m^2/s and 0.65 x 10^{-12} m^2/s for 180, 270 and 540 days respectively. The saturation of the wall of the gel hydrates with chloride ions (i.e. water-bound chloride) may be responsible for preventing further chloride ingress beyond 270

days of chloride exposure. These water-soluble chlorides narrow the concrete pore diameter thereby interfering with the progressive chloride ingress with exposure period.

Between 0 to 270 days of chloride exposure, the concentration gradient of the concrete pore solution and the external environment lead to an increased free chloride diffusion. The concentration gradient outweighs the possibility of resistance to chloride ingress by narrow pores due to geopolymerization of AACM at early age. However, the impact of concentration gradient over prolonged chloride exposure periods (beyond 270 days) is insignificant because of equilibrium in chloride concentration within the concrete matrix and its curing environment.

On the other hand, the impact of tightened pores in AACM concrete due to geopolymerization is observed when comparing different AACM mixes at the same age. AACM mix S_2 has the lowest chloride diffusion coefficient $D_{C(f)}$, of 3.6 x 10^{-12} m^2/s at 180 days exposure compared with 4.2 x 10^{-12} m^2/s and 4.5 x 10^{-12} m^2/s for mixes S_3 and S_4. A similar trend is evident at 270 days exposure with $D_{C(f)}$ values of 5.1 x 10^{-12} m^2/s, 5.4 x 10^{-12} m^2/s and 5.6 x 10^{-12} m^2/s for mixes S_2, S_4 and S_5 respectively. The lowest rate of chloride diffusion coefficient, $D_{C(f)}$, for AACM mix S_2 is as a result of its lowest intrudable porosity (Chapter 3, Section 3.4.2.1) compared to the other AACM mixes. The low intrudable porosity is facilitated by the fast rate of geopolymerisation due to the lowest activator dilution (2.12%) in AACM mix S_2.

OPC concrete mix S_6 has the lowest free chloride diffusion coefficient, $D_{C(f)}$, compared with AACM concrete mixes at 270 days of chloride exposure. It has $D_{C(f)}$ of 2.7 x 10^{-12} m^2/s compared with 5.1 x 10^{-12} m^2/s, 5.4 x 10^{-12} m^2/s and 5.6 x 10^{-12} m^2/s for AACM concrete mixes S_2, S_4 and S_5 respectively at 270 days of chloride exposure. The bound chloride isotherm which is presented in later sections (section 5.4.3 and 5.4.4) is solely responsible for the reduced chloride diffusion coefficient, $D_{C(f)}$, in OPC compared with AACM concrete. Significantly higher amount of free chloride is physically and chemically bound (acid-soluble and water-soluble chloride) to OPC concrete which slows the chloride diffusion rate, whereas, free chloride is mainly physically bound (water-soluble chloride) to AACM concrete.

Contrary to the free lower chloride diffusion rate observed in OPC compared to AACM concrete in Fig. 5.19, results from *Qianmin et al.* [234] suggested a lower chloride diffusion rate in alkali activated slag concrete compared to OPC concrete. The chloride diffusion coefficient, $D_{C(f)}$, of pore fluid in OPC concrete was compared with alkali activated slag (AAS) concrete by measuring the resistivity of their pore solutions [234]. The $D_{c(f)}$ of the pore fluid in AAS concrete is suggested to be lower than the OPC

concrete due to its low ionic nature. The lower the ionic activity and conductivity of AAS concrete, the lesser the ionic flow within its pore solution [234]. However, the limitation of using this method to determine $D_{c(f)}$ of AAS concrete is the limited ionic flow within its pore solution attributed to their dense tortuous pore structure. It is noteworthy to mention that cyclic ponding and drying regime of chloride solution was adopted during the investigation of *Qianmin et al.* [234]. The capillary absorption of concrete will significantly influence the chloride ingress due to this curing regime unlike the diffusion mechanism of the chloride bulk diffusion test used in this investigation.

5.4.3 Chloride Binding Isotherms

5.4.3.1 Free and Water-Soluble Chloride Relationship

Regression analysis using the three chloride binding isotherms (Freundlich, Langmuir and Linear) were used to determine the relationship between free and physically bound chloride concentrations for AACM concrete mixes S_2, S_3 and S_4 at 180 days of chloride exposure and 270 days chloride exposure for OPC concrete mix S_6. The chloride binding isotherms for AACM and OPC concrete mixes S_2, S_3, S_4 and S_6 are presented in Figures 5.20, 5.21, 5.22 and 5.23 respectively. The experimental data points, Freundlich model (red dotted lines), Langmuir model (blue dotted lines) and the Linear model (black straight lines) are shown in Figures 5.20, 5.21, 5.22 and 5.23. The unit of measurement for free chloride concentrations is mol/L because it was obtained by expression of concrete pore fluid. Other authors expressed it as a percentage weight by binder because concrete powder was dissolved in water (water-soluble bound chloride) to measure the free chloride concentration [92][93]. These values do not strictly represent free chloride concentration and are more representative of water soluble chloride.

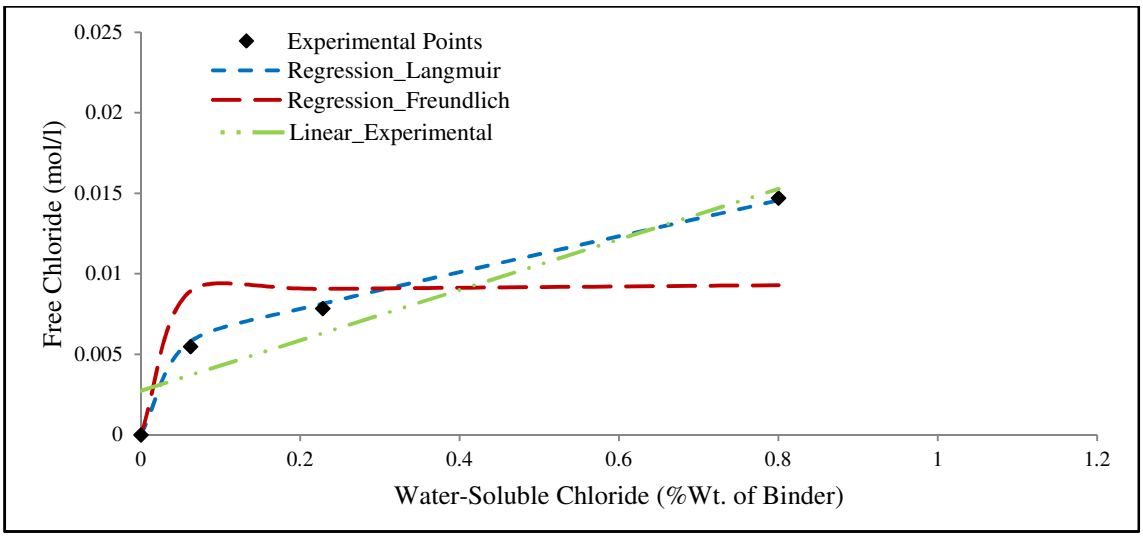

Figure 5. 20: Langmuir, Freundlich and Linear binding isotherms for AACM concrete mix S_2 at 180 days chloride exposure.

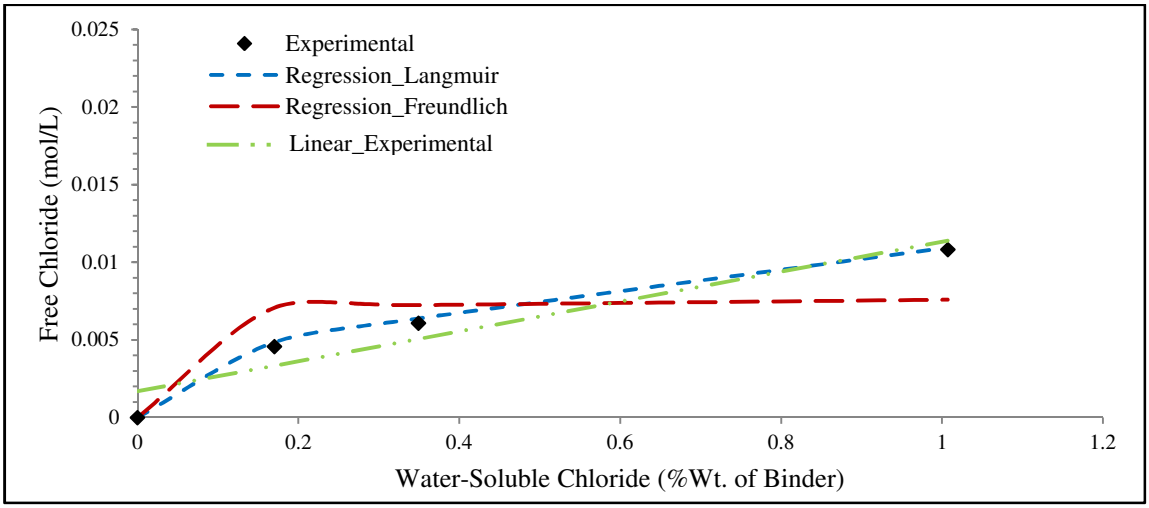

Figure 5. 21: Langmuir, Freundlich and Linear binding isotherms for AACM concrete mix S_3 at 180 days chloride exposure.

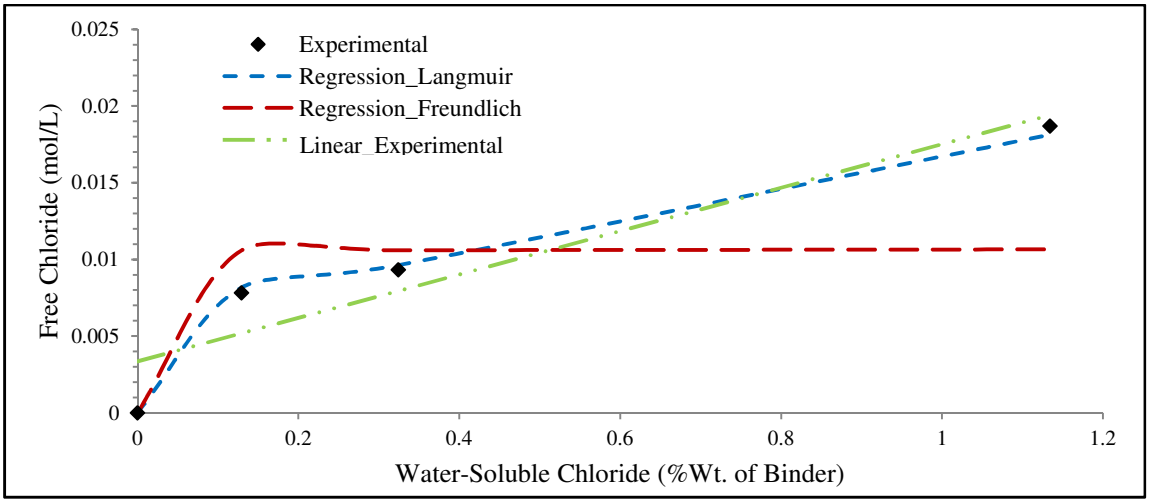

Figure 5. 22: Langmuir, Freundlich and Linear binding isotherms for AACM concrete mix S_4 at 180 days chloride exposure.

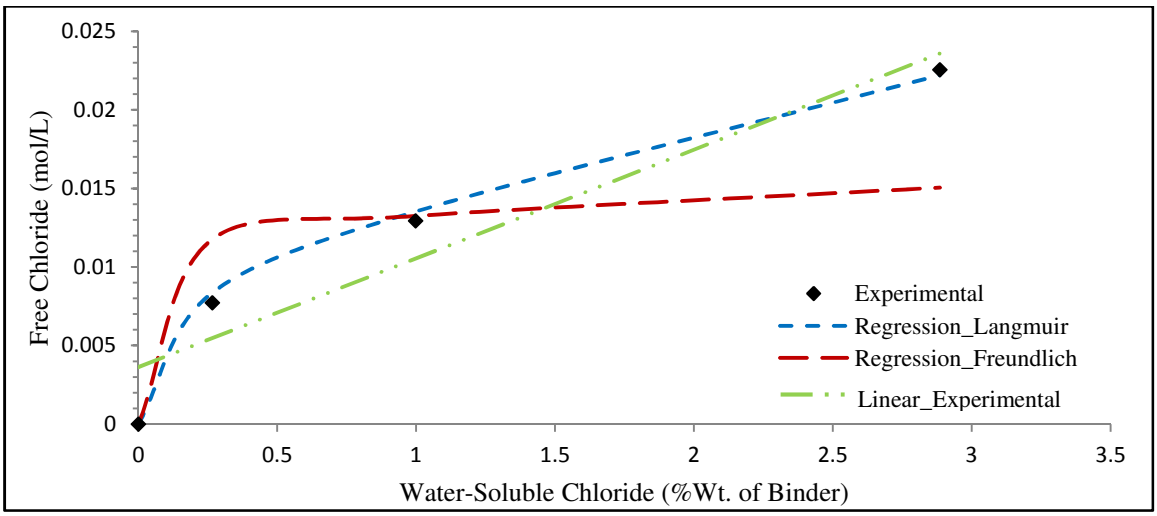

Figure 5. 23: Langmuir, Freundlich and Linear binding isotherms for OPC concrete mix S_6 at 270 days chloride exposure.

The Langmuir binding isotherm best fits the experimental data as shown in Figures 5.20, 5.21, 5.22 and 5.23**.** This is followed by the Linear binding isotherm which shows good correlation at high chloride values while the Freundlich binding isotherm shows a poor correlation. The level of correlation R^2 and binding constants *α, β and k* of equations 5.2, 5.3 and 5.4 are presented in Table 5.7. These parameters were derived from the non-linear regression analysis of the experimental data.

Table 5. 6: Binding coefficients for Langmuir, Freundlich and Linear isotherms

	Langmuir			Freundlich			Linear	
Mix	α	β	R^2	α	β	R^2	K	R^2
S_2	1.1	7.5	0.99	0.011	0.040	0.62	0.0157	0.88
S_3	1.1	8.0	0.99	0.011	0.082	0.70	0.0096	0.90
S_4	1.1	7.2	0.99	0.011	0.008	0.58	0.0141	0.88
S_6	1.2	7.0	0.99	0.036	0.23	0.73	0.0069	0.91

The maximum free chloride concentrations are 0.0147mol/L (Fig. 5.20), 0.0108mol/L (Fig. 5.21) and 0.0187mol/L (Fig. 5.22) for AACM concrete mixes S_2, S_3 and S_4 respectively and 0.0222mol/L (Fig. 5.23) for OPC concrete mix S_6 at 10 mm mean depth. These concentrations are less than 0.05 mol/L limit at any concrete depth suggested by *Tang and Nilsson* [95] at which the Langmuir isotherm is valid.

Langmuir binding isotherm has the highest correlation of 0.99 with the experimental data, followed by Linear binding isotherm of 0.88 to 0.91 while the least correlation of 0.58 to 0.70 is exhibited by Freundlich binding isotherm as shown in Table 5.7. The binding coefficient α is constant for each isotherm while β and K vary

for AACM concrete mixes S_2, S_3 and S_4. The binding coefficient α is 1.1 for Langmuir while it is 0.011 for Freundlich binding isotherm. The binding coefficients β for Langmuir binding isotherm are 7.5, 8.0 and 7.2 while they are 0.040, 0.082 and 0.008 for Freundlich binding isotherm for AACM concrete mixes S_2, S_3 and S_4 respectively. The binding coefficient k for linear binding isotherm is 0.0157, 0.0096 and 0.0141 for AACM concrete mixes S_2, S_3 and S_4 respectively. The binding coefficients α, β and K for OPC concrete vary for Langmuir, Freundlich and linear binding isotherms

The Langmuir binding isotherm shall be adopted for analysing the relationship between the physically bound and free chloride concentrations because of its good correlation with the experimental data.

5.4.3.1.1 Influence of Activator Dilution

The relationship between the free and water-soluble bound chloride using the Langmuir binding isotherm for AACM concrete with different degrees of activator dilution is shown in Fig. 5.24.

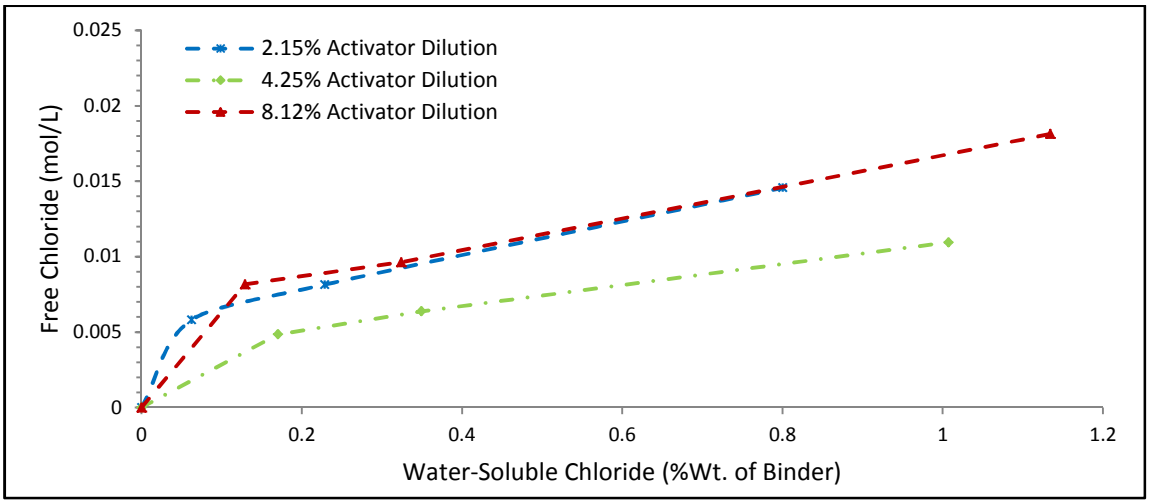

Figure 5. 24: Effect of activator dilution on Langmuir binding isotherms of AACM concrete at 180 days chloride exposure.

AACM mix S_4 which represents activator dilution of 8.12% has the highest free chloride concentration isotherm followed by the mixes with 2.15% (AACM mix S_2) and 4.25% (AACM mix S_3) dilution respectively. This also indicates the order of physical chloride binding capacity with 8.12% providing the lowest chloride binding capacity followed by 2.15% and 4.15%.

The higher chloride binding capacity of the mix with 4.25% dilution compared with 2.15% dilution is unexpected when considering the case of ordinary Portland cement concrete where it is established that higher cement content and lower w/c ratio provide higher binding capacity due to formation of C_3S and C_2S content in binder

[209]. The likelihood of the result of AACM mix S_3 with 4.25% dilution to have higher binding capacity is due to mix design parameters rather than activator dilution alone.

The silicate phases C_3S and C_2S and alumina phase C_3A of cement binder in OPC concrete are primarily responsible for the physical absorption of chloride ion present in the pore solution by the wall of hydration products, thereby reducing the free chloride content. The higher the C_3S and C_2S content in binder, the higher the binding capacity [209]. In the case of AACM binder, silica and alumina monomer phases are formed during the dissolution of aluminosilicate source. The chloride binding mechanisms of these monomers are yet to be fully understood.

Glass and Buenfeld [208] investigated the chloride binding capacities for low (2%), medium (8%) and high (14%) C_3A cements. The results presented show the chloride binding capacity is highest at high (14%) C_3A cement content and lowest at low (2%) C_3A cement content. Similarly, *Oh et al.* [92] suggested that the difference in the binding capacity between type I ordinary Portland cement and type V sulphate-resisting cement is their C_3A content, OH^- concentration and alkali content of their pore solutions.

5.4.3.2 Free and Acid-Soluble Chloride Relationship

5.4.3.2.1 Influence of Activator Dilution

The relationships between free and acid-soluble chloride of AACM concrete mixes with different levels of activator dilution at 180 and 270 days chloride exposure periods are shown in Figures 5.25 and 5.26 respectively.

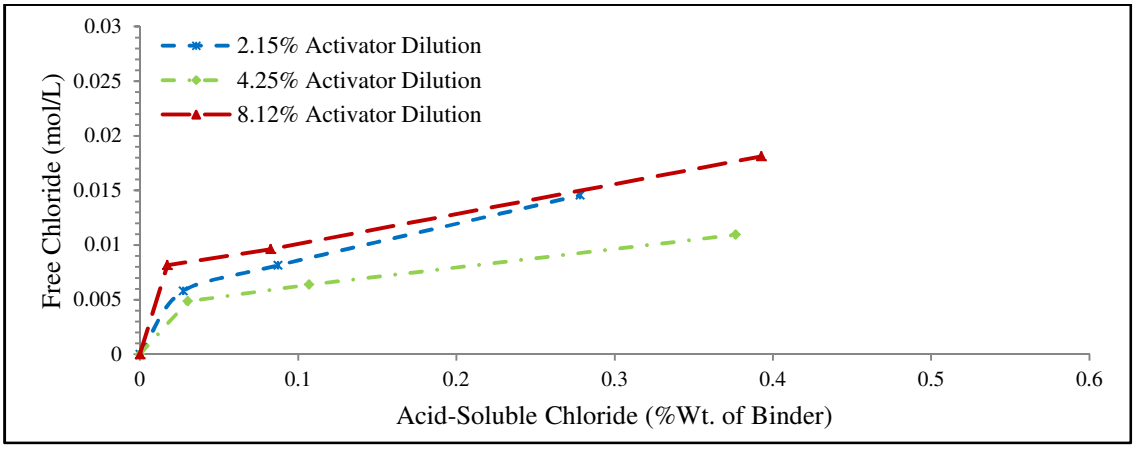

Figure 5. 25: Effect of activator dilution on Langmuir binding isotherms of AACM concrete at 180 days chloride exposure

The free and acid soluble chloride binding relationship at 180 days chloride exposure (Fig. 5.25) is similar to the free and water-soluble chloride binding

relationship shown in Fig. 5.24. AACM concrete S_3 with 4.25% activator dilution possesses the highest binding capacity followed by 2.15% activator dilution (S_2) while 8.12% (S_4) has the lowest binding capacity.

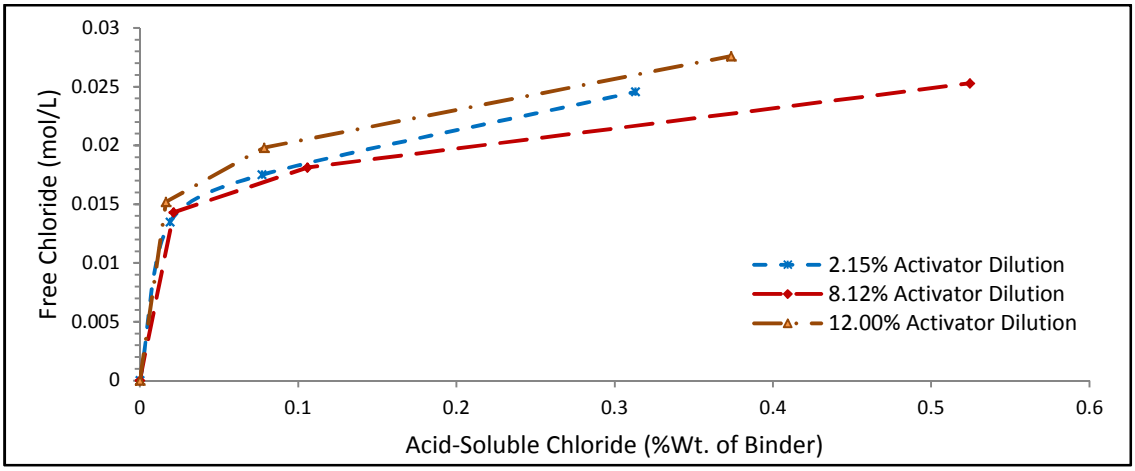

Figure 5. 26: Effect of activator dilution on Langmuir binding isotherms of AACM concrete at 270 days chloride exposure.

Fig. 5.26 shows that at 270 days chloride exposure period, AACM concrete mix S_4 with activator dilution ratio of 8.12% possesses the highest binding capacity followed by 2.15% and lastly AACM concrete mix S_5 with 12.00% activator dilution which had the lowest binding capacity. The better performance of AACM concrete mix S_4 with 8.12% activator dilution at 270 days chloride exposure period may be attributed to the rise in pH at 0 - 20 mm depth (from 13.45 to 13.48) between 180 and 270 days chloride exposure. AACM concrete mix S_2 with 2.15% activator dilution on the other hand witnessed a drop in the pH at 0 - 20 mm depth (from 13.64 to 13.58) near the concrete surface. A comprehensive analysis of the pH of AACM concrete pore solution is presented in section 5.4.5.

Nilsson et al. [97] stated that the increase in the amount of chloride binding in OPC concrete was due to the effect of drop in pH close to the concrete surface. Deterioration of C-S-H gel by the leaching of hydroxides was suggested as the reason for the drop in the pH. Similarly, *Tritthart* [254] cured cement pastes in chloride solution and found that chloride binding increases with decrease in pH value. The conclusion drawn was that chloride and hydroxyl ions compete for absorption sites on the cement gel surfaces.

On the contrary, *Reddy et al.* [270] observed calcium aluminate cement, CAC, releasing most of the bound chlorides into the pore solution before the pH drops to 11. The drop in the pH was attributed to the dissolution of the chloride-containing phase. In the case of AACM concrete, the presence of Friedel's salt (calcium chloroaluminate

phase) which is responsible for chemical binding is not evident as shown in chapter 4. Thus, the possibility of chloride that should have been chemically bound to the hydration products being released into the pore solution as the pH value drops is unlikely in AACM concrete.

As previously stated, AACM concrete has a different pore solution chemistry compared with OPC concrete. Therefore, the influence of leaching on pH value and how it adversely affects chloride binding is different from that of OPC.

5.4.3.2.2 Influence of Chloride Exposure Period

The relationship between free and acid-soluble chloride under 180 and 270 days of chloride exposure periods are presented in Fig. 5.27. Only AACM concrete mix S_2 with 2.15% activator dilution is investigated under this category.

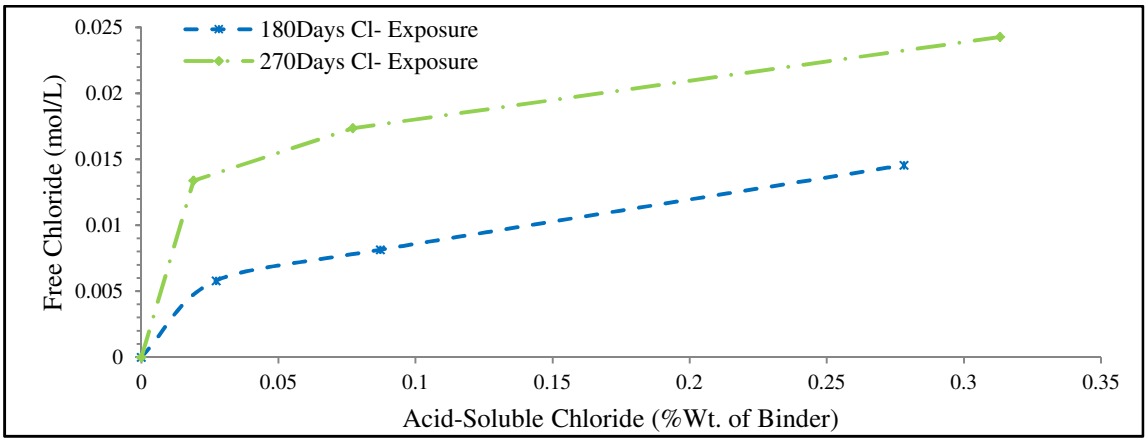

Figure 5. 27: Effect of chloride exposure period on Langmuir binding isotherms of AACM concrete.

A decrease in the chloride binding capacity is observed with an increase in the chloride exposure period. The chloride binding capacity is higher at 180 days than 270 days of chloride exposure period. The free chloride concentration is up to 0.015mol/L at 180 days exposure period while it is up to 0.024mol/L at 270 days of chloride exposure period. The possible explanation for the differences in binding capacities is the oversaturation of the concrete pore solution as chloride diffusion occurs over time from the environment without being adsorbed during gel formation and also less gel formation in the long term.

The binding isotherm curves of free and acid-soluble chloride show higher binding capacity at greater depth from the concrete surface while the depth near the concrete surface has lower chloride binding. This denotes that the concrete surface zone can no longer adsorb chloride ions as the chloride diffuses into the concrete matrix from its environment.

On the other hand, the binding isotherm curves of free and water-soluble chloride (Figures 5.20, 5.21 and 5.22) show the chloride absorption near and at greater depths from the concrete surface to be similar. The chloride is physically bound by the wall of the binder gel as chloride ingress occurs into the concrete pore solution from its environment.

5.4.3.3 AACM and OPC Chloride Binding Capacity

The relationships between free-acid soluble chloride and free-water soluble chloride of AACM and OPC concrete mixes are shown in Figures 5.28 and 5.29 respectively. The chloride binding capacity of AACM concrete mixes S_2, S_4, S_5 and OPC concrete mix S_6 are presented in these Figures.

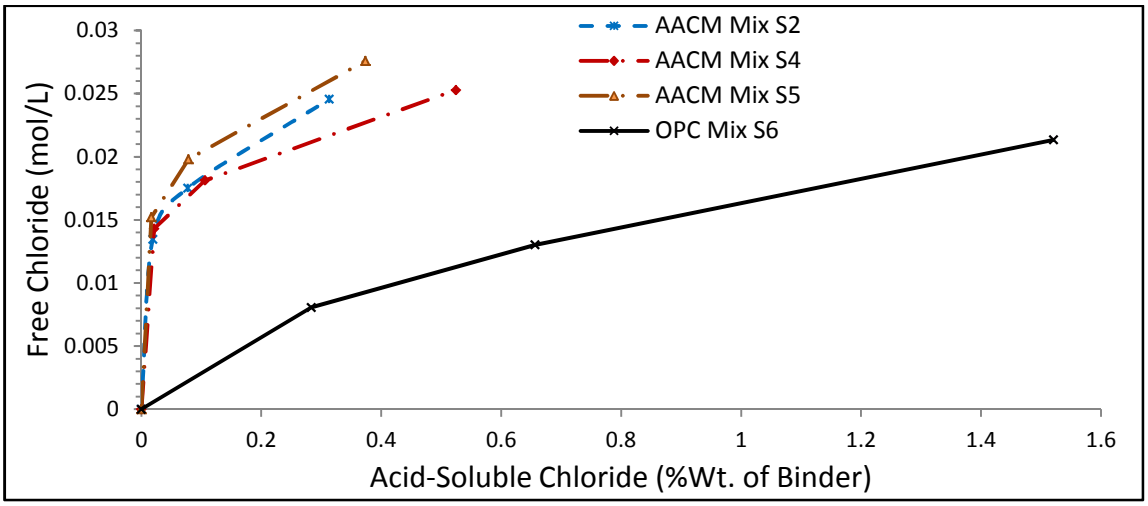

Figure 5. 28: Acid-soluble chloride binding capacity of AACM and OPC concrete at 270 days chloride exposure period

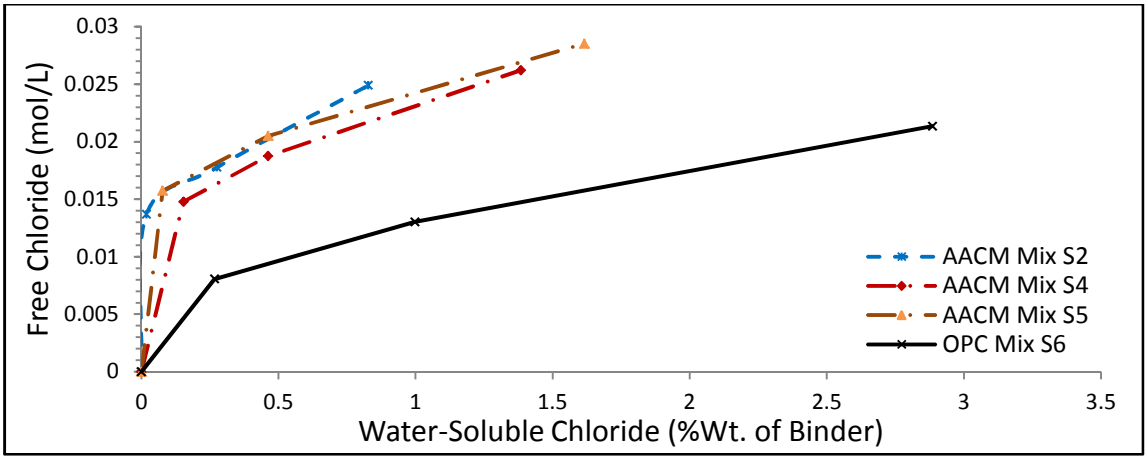

Figure 5. 29: Acid-soluble chloride binding capacity of AACM and OPC concrete at 180 days chloride exposure period

Clearly, the binding capacity of OPC concrete is higher than that of AACM concrete. The maximum free chloride concentration of OPC concrete is 0.0213 mol/L while it is 0.0253 mol/L, 0.0246 mol/L and 0.0276 mol/L for AACM concrete mixes S_2,

S_4 and S_5 respectively (Figures 5.28 and 5.29). This represents an increase of 13.4% to 22.8% in the free chloride concentration of AACM concrete relative to OPC concrete. The chemical binding capacity of OPC concrete is superior to AACM concrete. This is because of the presence of Friedel's salt ($Ca_6Al_2O_6.CaCl_2.10H_2O$) in OPC concrete which is responsible for the chemical binding but AACM concrete lacks it. On the other hand, Kuzel's salt ($Ca_6Fe_2O_6.CaCl_2.10H_2O$) is found in both OPC and AACM concrete [3]. The water soluble chloride concentration range is much higher than the acid soluble chloride concentration range in Figures 5.28 and 5.29 respectively.

The binding capacity of OPC concrete is influenced by other factors beside the C_3A content of cement. These factors include the water/cement ratio, mineral and chemical admixtures and temperature *Glass and Buenfeld* [208]. These factors contribute substantially to the binding capacity of OPC concrete. An increase in water/cement ratio was observed to increase the chloride binding capacity of OPC concrete. The increased water content was suggested to have a dilution effect on the chloride concentration within the pore solution and lowers the OH^- concentration thereby increasing the binding capacity [271]. On the other hand, increasing the water/cement ratio increases the concrete porosity and the chloride diffusion rate is increased proportionately. This reduces the binding capacity.

Supplementary cementitious materials like silica fume, fly-ash, ground granulated blast furnace slag and gypsum influence the binding capacity. Silica fume decreases the binding capacity by reducing the pH of the concrete pore solution [209]. In addition, it decreases the binding capacity by reducing the C_3A content of cement required for chloride binding [271]. On the other hand, fly-ash and ground granulated blast furnace slag increase the binding capacity due to the high alumina content which promotes the formation of Friedel's salt ($Ca_6Al_2O_6.CaCl_2.10H_2O$) in OPC concrete [272].

The addition of chemical admixtures such as superplasticisers SP was observed to reduce the chloride binding in OPC concrete and it was suggested that the SP impacts negative charges on the cement particles resulting in the release of bound chloride ions into the concrete pore solution [273].

High temperature decreases the binding capacity of OPC concrete. Elevated temperature causes thermal vibration of gel particles resulting in the release of physically bound chloride ions while the chemically bound chloride ions present in the hydration products (Friedel's salt) become highly soluble in the concrete pore solution.

The influence of these factors on AACM concrete can be investigated in future. Overall, it can be deduced that the chloride binding capacity of OPC concrete is better than AACM concrete because OPC concrete is effective in binding both water and acid soluble chlorides whereas the AACM concrete is effective in binding water-soluble chlorides while the acid-soluble chloride binding is limited. The free chloride concentration of the AACM concrete pore fluid is 13.4% to 22.8% greater than control OPC concrete.

5.4.4 pH and OH^- of AACM Concrete

5.4.4.1 Introduction

The pH and hydroxyl ion [OH^-] concentration for AACM and OPC concrete pore solution at 180, 270 and 540 days are presented in Table 5.8. The hydroxyl ions [OH^-] content was determined from equation 5.7.

$$[OH^-] = 10^{-(14-pH)} \qquad 5.7$$

The dominant factors influencing the pH and hydroxyl ion concentrations in this study are the concrete depths at which the pore solution is extracted (0-20 mm, 20-40 mm and 40-60 mm), activator dilution and the chloride exposure periods. There is limited information available in literature on the free chloride/hydroxyl ion [Cl/OH^-] ratios of OPC mortars while information on the free chloride/ hydroxyl ion [Cl/OH^-] ratio on OPC concrete is lacking [238]. Information on the free chloride/ hydroxyl ion [Cl^-/OH^-] ratios for AACM materials is not available in literature. The data in Table 5.7 have been used to determine the [Cl^-/OH^-] ratios of AACM concrete, which will be discussed in section 5.4.6.

Table 5. 7: pH and OH^- concentration of AACM and OPC concrete pore solution

Mix	Mean Depth (mm)	pH	$[OH^-]$ *(mol/L)*
		540 Days	
S_2	10	13.27	0.186
	30	13.68	0.479
	50	13.77	0.589
		270 Days	
	Mean Depth (mm)	pH	$[OH^-]$ *(mol/L)*
S_2	10	13.58	0.380
	30	13.75	0.562
	50	13.85	0.708
S_4	10	13.48	0.302
	30	13.53	0.339
	50	13.63	0.427
S_5	10	13.33	0.214
	30	13.5	0.316
	50	13.58	0.380
S_6	10	12.82	0.066
	30	13.27	0.186
	50	13.69	0.490
		180 Days	
	Mean Depth (mm)	pH	$[OH^-]$ *(mol/L)*
S_2	10	13.64	0.437
	30	13.73	0.537
	50	13.74	0.550
S_3	10	13.58	0.380
	30	13.73	0.537
	50	13.85	0.708
S_4	10	13.45	0.281
	30	13.56	0.363
	50	13.57	0.372

5.4.4.2 Effect of Activator Dilution and Penetration Depths

The pH and hydroxyl ion concentration of AACM and OPC concrete mixes at a mean depth of 10, 30 and 50 mm from the concrete surfaces for 180 and 270 days of chloride exposure periods is shown in Figures 5.30 and 5.31 respectively. Similarly, the relationship between hydroxyl ion concentration and depths (10, 30 and 50 mm) for AACM and OPC mixes for 180 and 270 days of chloride exposure are shown in Figures 5.32 and 5.33 respectively.

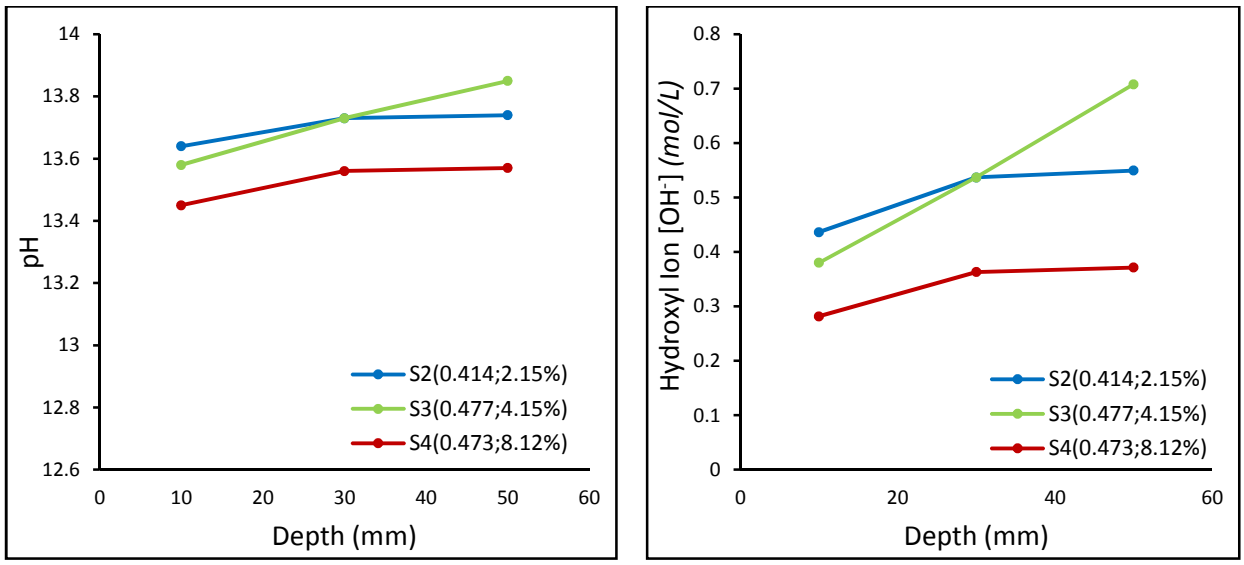

Figure 5. 30: pH and OH^- profiles of AACM concrete at 180 days of chloride exposure

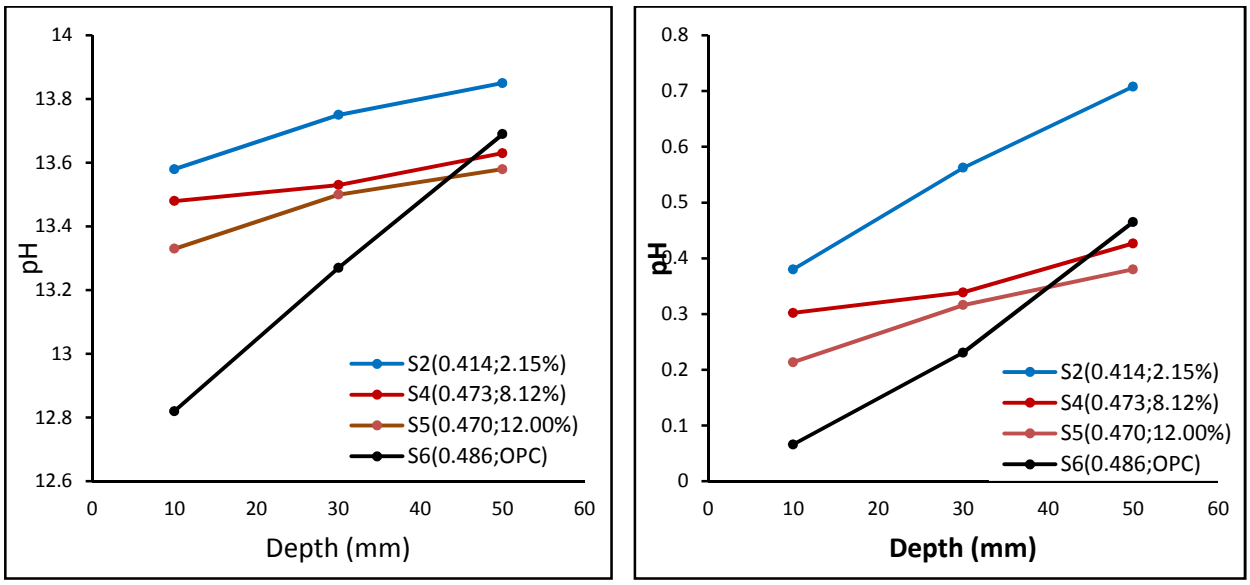

Figure 5. 31: pH and OH^- profiles of AACM and OPC concrete at 270 days of chloride exposure

There is a gradual depletion of hydroxyl ions towards the concrete surface for all profiles shown in Figures 5.30 to 5.33. The depletion is more in OPC concrete mix S_6 at 270 days chloride exposure (Figures 5.31 and 5.33). OPC concrete mix S_6 has hydroxyl ion content of 0.066mol/L, 0.186mol/L and 0.490mol/L at 10, 30 and 50 mm mean depths respectively from the concrete surface. The gradual depletion of hydroxyl ions towards the concrete surface could be caused by leaching or accumulation of alkali content on the concrete surface [274]. All precautions were taken to prevent carbonation which, therefore, is unlikely to be a cause of PH reduction in the surface zone. Results of the carbonation investigation are given in Chapter 6.

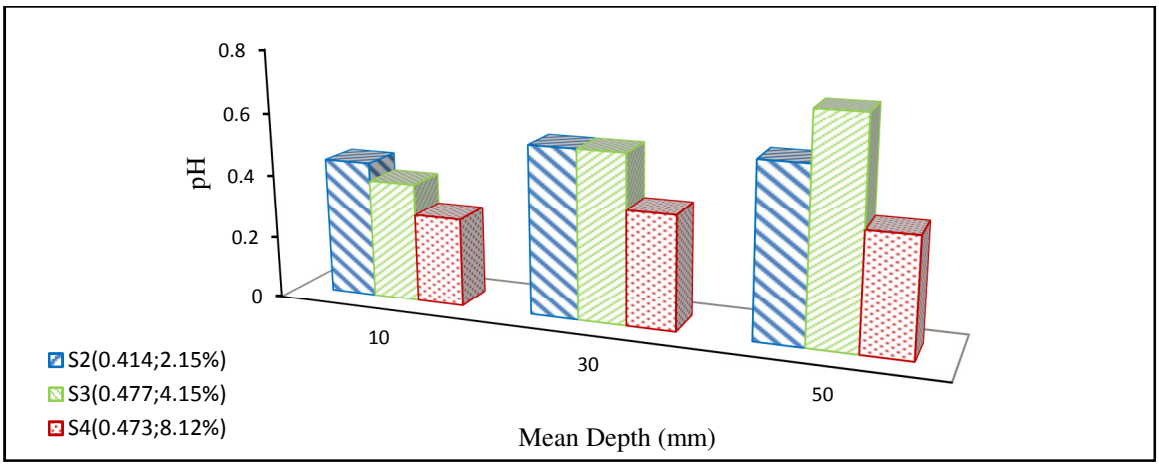

Figure 5. 32: The relationship between [OH^-] and mean depths (10, 30 and 50 mm) for AACM mixes S_2, S_3 and S_4 at 180 days of chloride exposure.

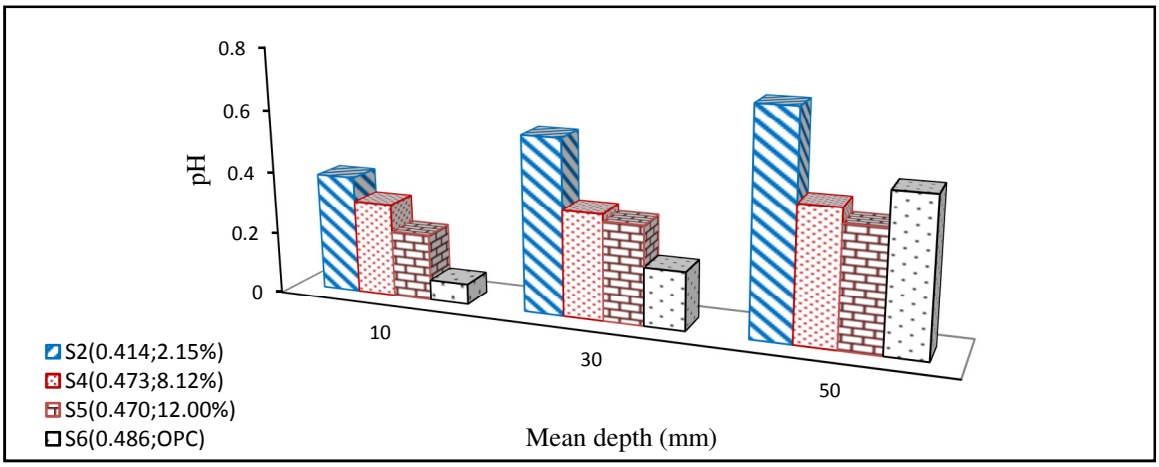

Figure 5. 33: The relationship between [OH^-] and mean depths (10, 30 and 50 mm) for AACM and OPC mixes S_2, S_4 , S_5 and S_6 at 270 days of chloride exposure.

Tuuti [90] suggested the possibility of undissolved alkali content which is enclosed in the unhydrated slag cement to be responsible for boosting the pH of concrete pore solution especially at greater depth from the concrete surface. In the case of AACM concrete, the possibility of alkali activator concentration that was not utilised during geopolymerisation could account for the high pH when compared with OPC concrete as seen in Figures 5.31 and 5.33. AACM concrete mix S_2 exhibited high pH of 13.58 *(OH^- = 0.380 mol/L)* and 13.85 *(OH^- = 0.708 mol/L)* at 10 and 50 mm mean depths compared with OPC concrete mix S_6 with pH of 12.82 *(OH^- = 0.066 mol/L)* and 13.69 *(OH^- = 0.490 mol/L)* at 10 and 50 mm mean depths respectively as shown in Figures 5.31 and 5.33.

Another possible explanation for the gradual depletion of hydroxyl ion towards the concrete surface was proposed by *Mangat and Gurusamy* [266]. Depressed pH was observed at the surface zone for concrete submerged in water free of chloride. The tendency towards the neutralisation of concrete surface was attributed to outward

diffusion of hydroxyl ion. On the contrary, *Tritthart* [271] proposed that under chloride exposure a competition exists between OH^- and Cl^- at the adsorption sites of the hydration products. It was observed that as more chloride ions were chemically adsorbed, fewer adsorption sites were left for other ions such as OH^- which could be adsorbed simultaneously. This hypothesis was suggested as the reason for higher binding capacity for concrete with a low pH, the low pH results in more adsorption sites for free chloride compared with concrete which has high pH. This may not be entirely true for AACM concrete because its poor binding capacity was largely due to the absence of Friedel's salt (acid-soluble chloride) or any form of crystallised salt, leaving only the kuzel's salt (water-soluble chloride) to be actively involved in the chloride binding reported in chapter 4. Also, less binding in AACM leaves more sites for OH^-.

5.4.4.3 Effect of Chloride Exposure Period

The pH and hydroxyl ion concentration profiles of AACM concrete mix S_2 at 180, 270 and 540 days of chloride exposure periods are shown in Fig. 5.34 while the corresponding pH and hydroxyl profiles of AACM concrete mix S_4 at 180 and 270 days of chloride exposure periods are shown in Fig. 5.35.

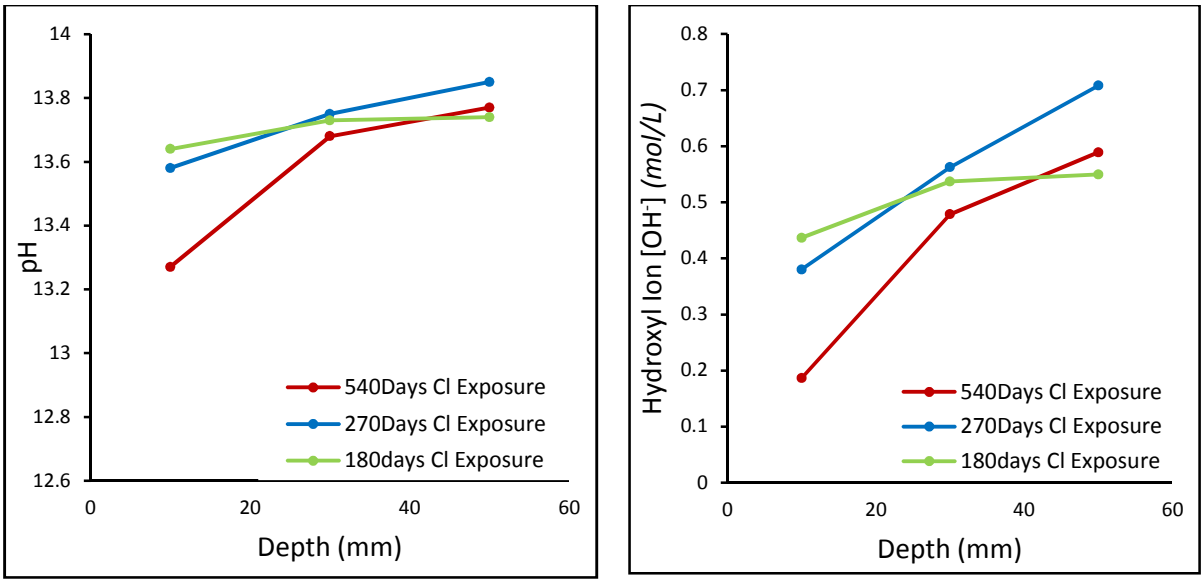

Figure 5. 34: pH and OH^- profiles of AACM concrete mix S_2 at 180, 270 and 540 days of chloride exposure

A significant reduction of pH and hydroxyl ions is observed at the 10 mm mean depth from the concrete surface in Fig. 5.34 at 540 days of chloride exposure period. This process involves the release of alkali metals from AACM into a leaching solution thereby reducing its pH. A possible reason for such release is the higher concentration gradient induced when chloride solution is in contact with the AACM binder, which can lead to leaching by the low ionic strength of the solution [3].

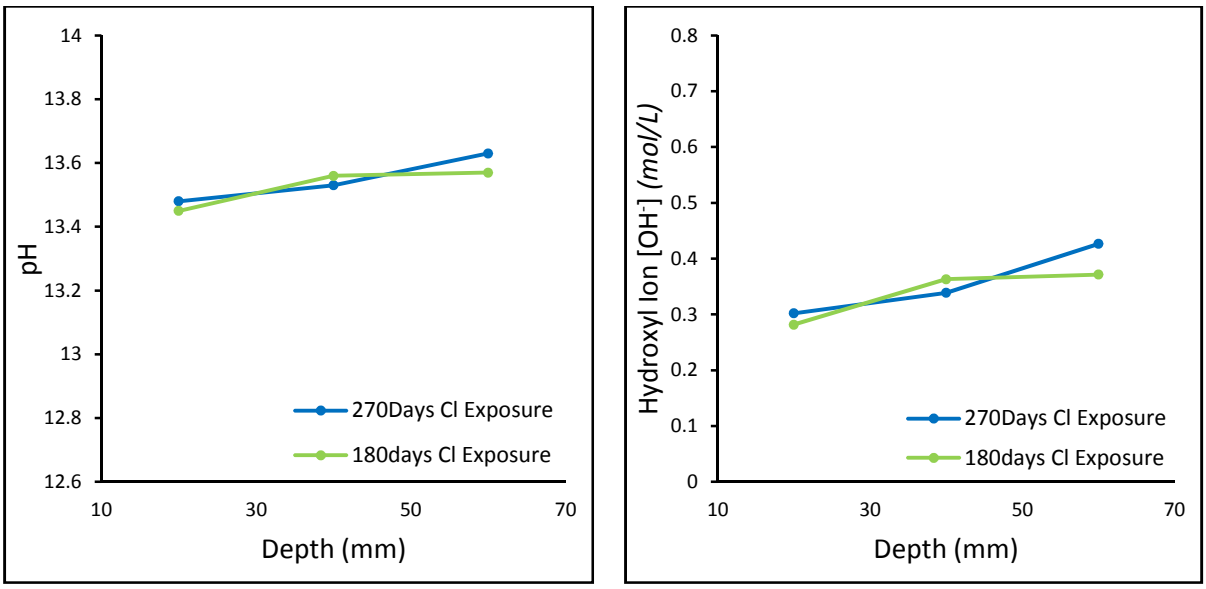

Figure 5. 35: pH and OH^- profiles of AACM concrete mix S_4 at 180 and 270 days of chloride exposure

The difference in pH and hydroxyl ions profiles between 180 and 270 days (Figures 5.34 and 5.35) is not significant compared to 540 days of chloride exposure period.

5.4.5 Free Chloride/ Hydroxyl ion Ratio [Cl^-/OH^-]

5.4.5.1 Effect of Activator Dilution

Two parameters used to express the critical chloride thresholds for corrosion initiation in steel reinforced concrete are the total chloride content relative to the weight of binder and the ratio of free chloride to hydroxyl ion concentration present in the pore solution which is usually expressed as [Cl^-/OH^-]. The former is presented in Chapter 4 and the latter [Cl^-/OH^-] ratio is discussed in this section.

The relationships between chloride/hydroxyl ion [Cl^-/OH^-] ratio and penetration depth at 180 and 270 days of chloride exposure periods are shown in Figures 5.36 and 5.37 respectively. Similarly, the relationship between [Cl^-]/[OH^-] and depths (10, 30 and 50 mm) for AACM and OPC mixes for 180 and 270 days of chloride exposure are shown in Figures 5.38 and 5.39 respectively.

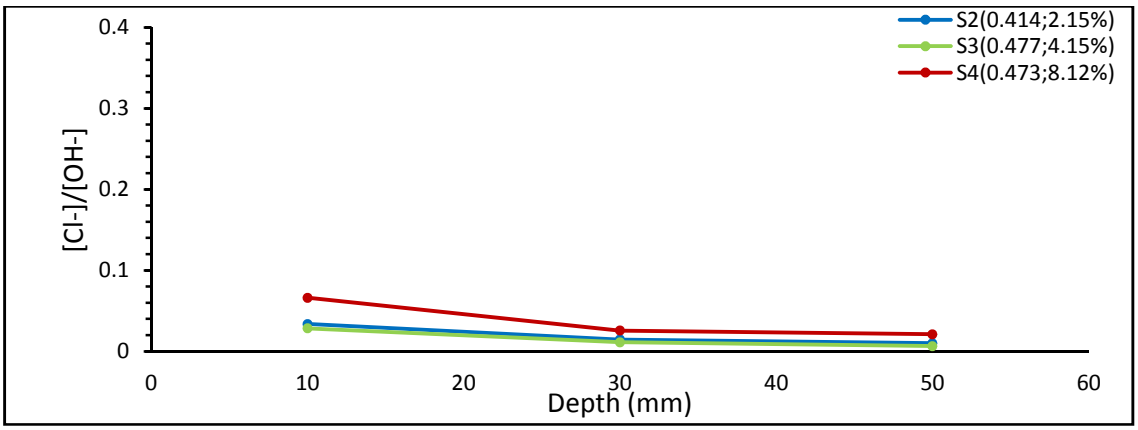

Figure 5. 36: Chloride/Hydroxyl ion [Cl^-]/[OH^-] of AACM concrete at 180 days of chloride exposure

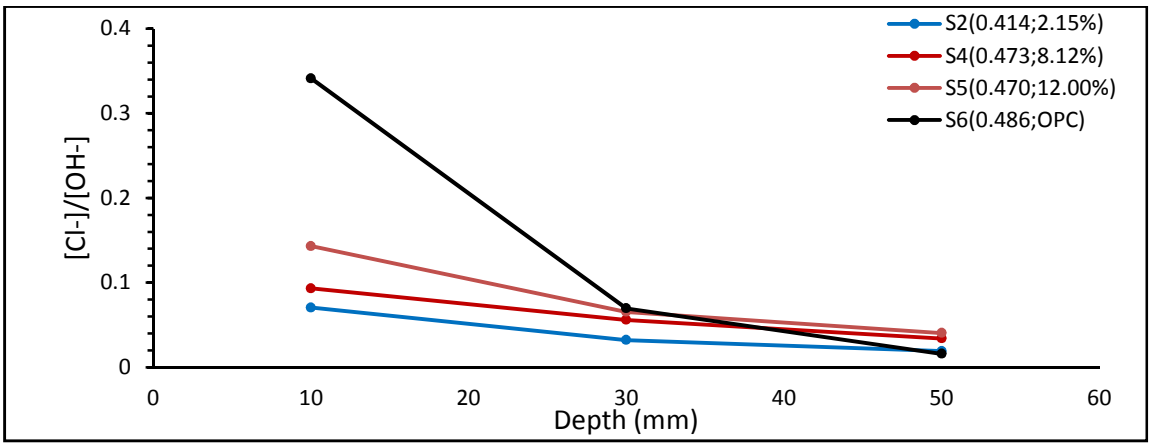

Figure 5. 37: Chloride/Hydroxyl ion [Cl^-]/[OH^-] of AACM concrete at 270 days of chloride exposure

The influence of activator dilution on the free Cl^-/OH^- ratio is more pronounced at 270 days (Figure 5.37 and 5.39) than 180 days (Figures 5.36 and 5.38) of chloride exposure. The activator dilution has a negative influence on the free Cl^-/OH^- ratio. The highest free Cl^-/OH^- ratio at 180 days of chloride exposure (Figures 5.36 and 5.38) was observed in AACM concrete mix S_4 (8.12% dilution), likewise mix S_5 (12% dilution) had the highest free Cl^-/OH^- ratio at 270 days of chloride exposure (Figure 5.37 and 5.39). AACM concrete mix S_2 (2.15% dilution) has the lowest free Cl^-/OH^- ratio at both 180 and 270 days of chloride exposure. For example, the free Cl^-/OH^- ratios are 0.07 and 0.14 for AACM mixes S_2 and S_5 respectively at 10 mm mean depth (Figure 5.37 and 5.39). Figures 5.36 and 5.38 similarly show AACM concrete mix S_4 having the highest free Cl^-/OH^- ratio 0.07 while its 0.03 for mix S_2.

The hydroxyl ion content in the pore solution is boosted by the presence of high concentration of activator in the pore solution. *RILEM TC 224* [3] stated that the silicate sites present in the alkali activator will lose protons once or twice to become more basic when used in AACMs. Silicate activators are buffered by the silicate deprotonation

equilibria (i.e. removal of protons) to provide a remarkable high level of available alkalinity [3].

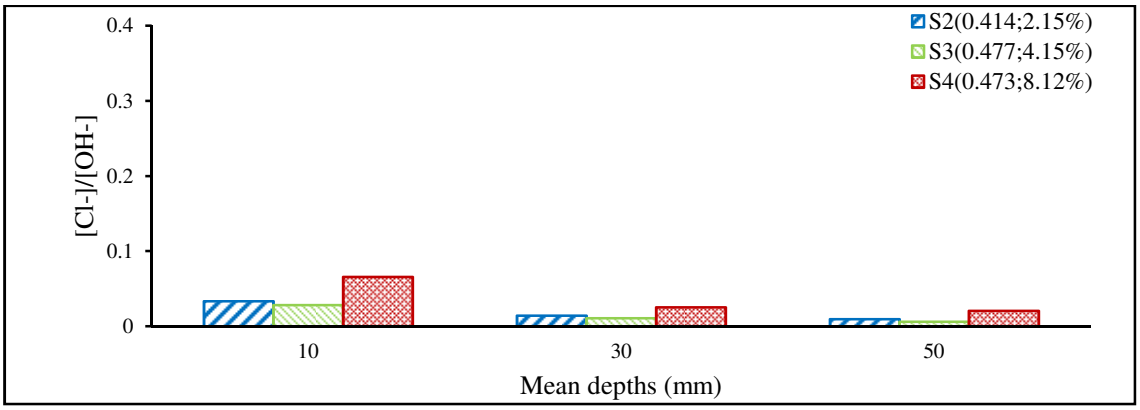

Figure 5. 38: The relationship between $[Cl^-]/[OH^-]$ and mean depths (10, 30 and 50 mm) for AACM mixes S_2, S_3 and S_4 at 180 days of chloride exposure.

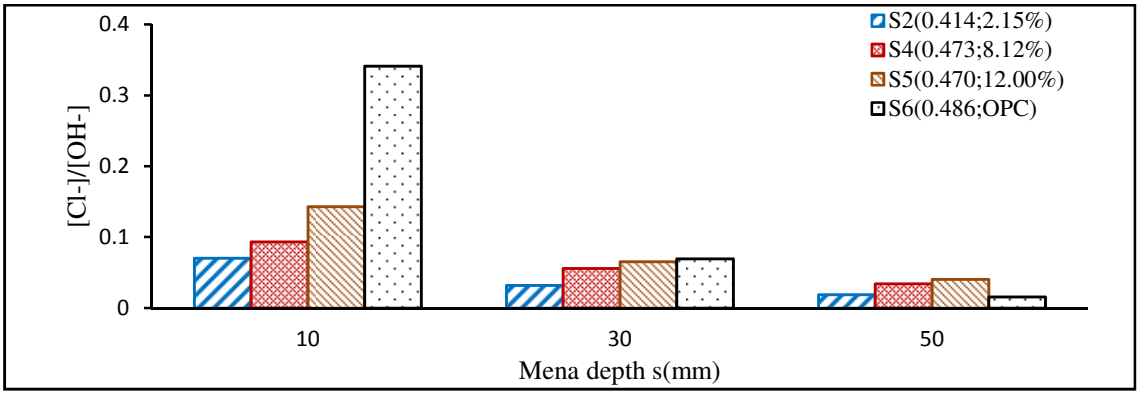

Figure 5. 39: The relationship between $[Cl^-]/[OH^-]$ and mean depths (10, 30 and 50 mm) for AACM and OPC mixes S_2, S_4 , S_5 and S_6 at 270 days of chloride exposure**.**

The positive influence of high hydroxyl ion content in AACM concrete which resulted in low free Cl^-/OH^- ratios is evident when compared with OPC concrete as shown in Figure 5.37 and 5.39. OPC concrete mix S_6 possesses the highest free Cl^-/OH^- of 0.34 at 10 mm mean depth compared to AACM concrete. Despite OPC concrete having the lowest free chloride content due to its better chloride binding capacity as shown in Fig. 5.28, the presence of lower hydroxyl ion content of 0.066 mol/L in its pore solution at 10 mm mean depth resulted in the highest free Cl^-/OH^- ratio compared with AACM concrete. In conclusion, therefore, even with the lowest free chloride content, a higher free Cl^-/OH^- ratio is observed in OPC concrete pore solution. AACM concrete on the other hand has higher chloride content but a lower free Cl^-/OH^- ratio in its pore solution. The Cl^-/OH^- parameter is often considered important for corrosion initiation of steel in concrete. The effect of this on the corrosion resistance of steel reinforcement in AACMs is investigated in chapter 7.

5.4.5.2 Effect of Chloride Exposure Period

The influence of chloride exposure periods on free Cl^-/OH^- ratio for AACM concrete mixes S_2 and S_4 are presented in Figures 5.40 and 5.41 respectively. Fig. 5.40 shows the relationship between free Cl^-/OH^- and concrete depth at 180, 270 and 540 days of chloride exposure periods while Fig. 5.41 has free Cl^-/OH^- profiles at 180 and 270 days of chloride exposure periods.

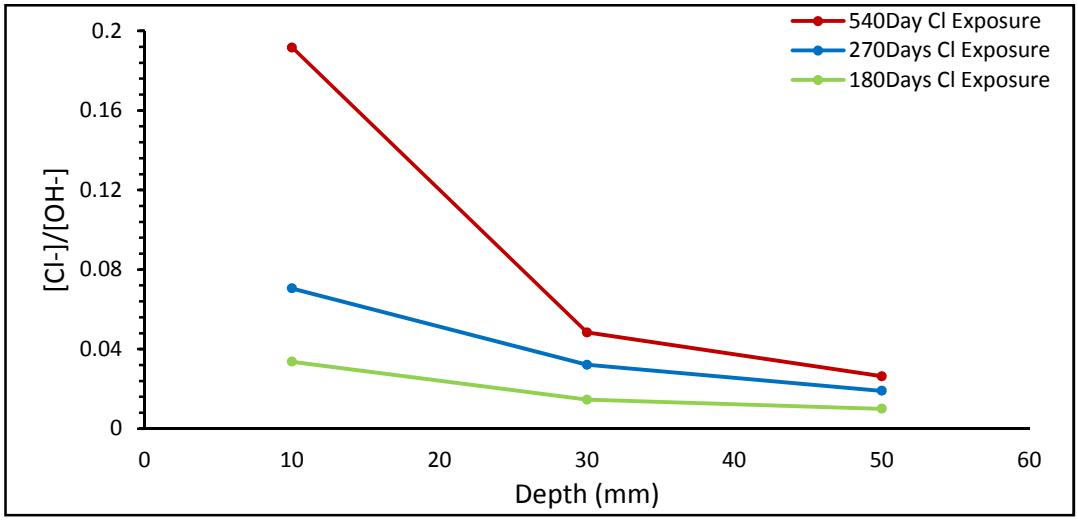

Figure 5. 40: $[Cl^-]/[OH^-]$ of AACM concrete mix S_2 at 180, 270 and 540 days of chloride exposure

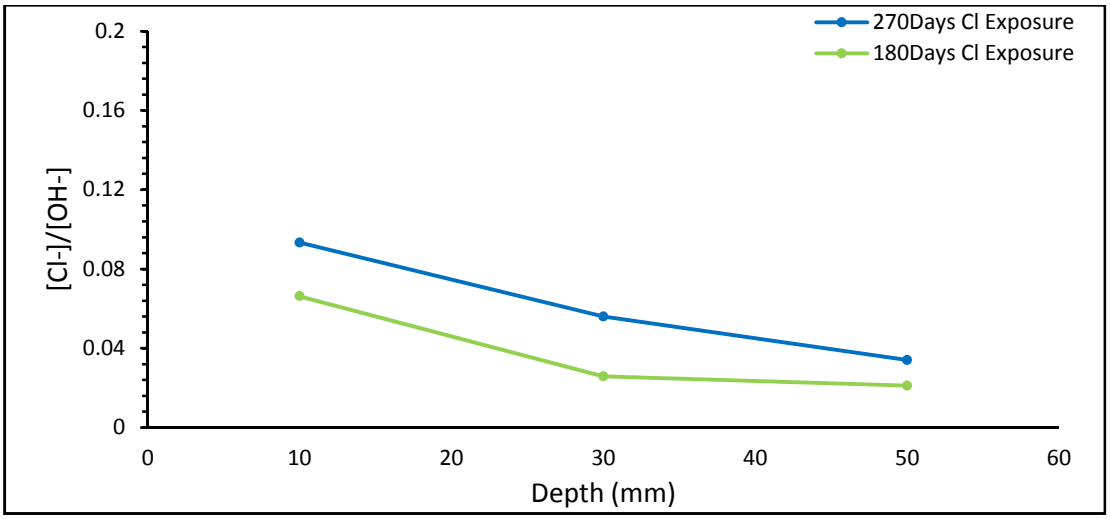

Figure 5. 41: $[Cl^-]/[OH^-]$ of AACM concrete mix S_4 at 180 and 270 days of chloride exposure

Higher values of free Cl^-/OH^- ratios were observed at latter chloride exposure periods. The highest free Cl^-/OH^- ratio 0.19 was recorded at 540 days of chloride exposure period while 180 days of chloride exposure has the lowest free Cl^-/OH^- ratio 0.03 at 10 mm mean depth for mix S_2 (Fig. 5.40). Similarly, for mix S_4, the highest free Cl^-/OH^- ratio of 0.09 was recorded at 270 days of chloride exposure period while 180 days of chloride exposure has the lowest free Cl^-/OH^- ratio of 0.07 at 10 mm mean

depth (Fig. 5.41). The free Cl^-/OH^- ratio of AACM concrete is greatly influenced by the depletion of hydroxyl ion within its pore solution with age.

A gradual reduction in hydroxyl ion content towards the concrete surface is observed with age due to leaching (Figures 5.32 and 5.33). *RILEM TC 224* [3] gives three major causes of leaching in AACMs as porous microstructure, high alkali concentration and weak Na^+ binding. The solutions offered to reduce leaching were to replace Na^+ with K^+, which improves binding with the aluminosilicate gel and provides a more stable alkali binding capacity. The second solution is to produce AACM with low permeability properties.

Since AACM mix S_2 contains the same mix composition that was subjected to 180, 270, 540 days of chloride exposure periods, this eliminates the possibility of discrepancies in their microstructure and alkali concentrations thus suggesting a weak alkali binding capacity of Na^+ with the aluminosilicate gel as the reason for rapid leaching in AACM mix S_2 at 540 days of chloride exposure period (Fig. 5.40).

In addition to the depletion of hydroxyl ion content towards the surface, the high concentration of free chloride near the concrete surface over time equally contributed to the high values of free Cl^-/OH^- ratios observed at 540 days of chloride exposure (Fig. 5.40). For example, the free chloride concentration at 10 mm mean depth (0.036mol/L) is high at 540 days exposure compared to 0.015mol/L at 180 days exposure (Fig. 5.12). A similar trend was observed for AACM mix S_4 having high free chloride concentration of 0.028mol/L at 270 days exposure compared to 0.019mol/L at 180 days exposure both at 10 mm mean depths (Fig. 5.12).

5.5 CONCLUSIONS

The following conclusions can be drawn based on the study carried out on the pore fluid chloride and pH and the relationship between chloride/hydroxyl raio of AACM concrete.

- OPC concrete exhibited the lowest amount of free chloride compared with AACM concrete because of its better binding capacity.
- The experimental data of free chloride concentration show strong correlation with the regression analysis profiles derived from Fick's second law of diffusion.
- The chloride diffusion parameters *[$C_{0(f)}$ and $D_{c(f)}$]* increase with an increase in chloride exposure periods except for $D_{c(f)}$ at 540 days. For example, $C_{0(f)}$ *and* $D_{c(f)}$ for AACM S_2 at 180 days exposure are 0.025mol/L and 3.6 x 10^{-12}m/s^2 respectively while it is 0.032mol/L and 5.1 x 10^{-12}m/s^2 at 270 days exposure.

The values are 0.053mol/L and 0.36 x 10^{-12}m/s^2 for $C_{0(f)}$ *and* $D_{c(f)}$ respectively at 540 days exposure.

- Langmuir binding isotherm best-fits the free and bound chloride relationship of AACM and OPC concrete because of its lower free chloride concentration (≤0.02 mol/L).
- The binding capacity decreases as the chloride exposure periods increases. OPC concrete had better chloride binding capacity compared with AACM concrete. This due to the presence of higher concentrations of water and acid soluble bound chlorides OPC concrete compared to AACM concrete (Chapter 4).
- The free chlorides and pH are much higher in AACMs than OPC. For example, the free chloride concentrations at 10mm mean depth of AACM mix S_2 and OPC S_6 are 0.027mol/L and 0.023mol/L respectively at 270 days exposure. The corresponding pH for AACM mix S_2 and OPC S_6 are 0.38mol/L and 0.066mol/L respectively. The higher free chloride in AACMs is due to its lower water and acid soluble binding capacity while the higher pH was influenced its activator concentration.
- The Cl^-/OH^- ratio of pore solution increases with increasing activator dilution. The highest activator dilution (12%) produced the highest free Cl^-/OH^- ratio while the lowest activator dilution (2.15%) produced the lowest free Cl^-/OH^- ratio within AACM pore solution. For example, the Cl^-/OH^- ratio at 10mm mean depth is 0.071 and 0.143 for 2.15% and 12% activator dilutions respectively at 270 days exposure.
- The AACM concrete had the lowest free Cl^-/OH^- ratio despite the high free chloride concentration compared with OPC concrete. The impact of high pH and hydroxyl ion present within pore solution of AACM concrete aided the low free Cl^-/OH^- ratio. For example, the free Cl^-/OH^- ratio at 10mm mean depth for AACM mix S_2 is 0.071 while it is 0.34 for OPC S_6 at 270 days exposure.

CHAPTER 6

CARBONATION OF ALKALI ACTIVATED CEMENTITIOUS (AACM) CONCRETE

6.1 INTRODUCTION

The primary effect of carbonation in OPC concrete is to reduce the pH of its pore solution to below 9 [275][276]. The pH is reduced when atmospheric carbon dioxide, CO_2, dissolves in the pore solution to form carbonic acid HCO_3 and then reacts with the main hydration products of concrete, $Ca(OH)_2$ and C-S-H, to form calcium carbonates $CaCO_3$ [277][278]. The hydroxyl ion [OH^-] within the pore solution is displaced by this reaction thereby causing the depletion of the protective passive film around the reinforcing steel in concrete. The progression of these reactions will result in carbonation induced corrosion when oxygen and water are present.

The geopolymerisation products of AACM do not contain calcium hydroxide $Ca(OH)_2$ which reacts with carbonic acid, HCO_3, to produce calcium carbonates, $CaCO_3$, unlike the OPC and supplementary replacement concrete that has calcium hydroxide $Ca(OH)_2$ as hydration products. Therefore, the use of phenolphthalein indicator method to determine the carbonation front may not give a true carbonation performance in AACM concrete [3]. The question of the suitability of phenolphthalein indicator method in AACM concrete will be addressed in this chapter.

In addition to the lowered pH of the concrete pore solution, the porosity and pore structure is altered by increasing the concrete pore sizes to more than 100 nm [279] because the relatively large calcium hydroxide molecules are replaced by the smaller calcium carbonate molecules. The increased pore size facilitates further carbonation. The increase in the porosity of concrete reduces the relative gel volume but the absolute concrete volume may remain the same. The concrete permeability is increased in the process affecting both the durability and mechanical properties of concrete negatively [280]. Carbonation in concrete is, therefore, considered as one of the leading causes of degradation in cement based structure [3].

The rate of carbonation in concrete is a slow process which sometimes takes years to manifest. Concrete structures in large cities are prone to carbonation due to human activities involving high emissions of CO_2, up to 1% by volume of air. Concrete linings in road tunnels where a high concentration of CO_2 is emitted [25] and reinforced concrete car parks are examples where carbonation is important. The CO_2 concentration in the carbonation chamber which was used to simulate the effect of carbonation on

AACM and OPC concrete was maintained at 5% to provide accelerated carbonation conditions. A relative humidity between 50 to 70 per cent should be maintained to achieve the highest rate of carbonation in OPC concrete [281][282]. If the pores of concrete are fully saturated, the CO_2 diffuses in it at 4 orders of magnitude slower than oxygen while its diffusion remains inactive if the concrete pores are insufficiently saturated [25]. Therefore, the moisture level within the concrete pores has considerable influence on the rate of carbonation. The relative humidity of the carbonation chamber used for this study was maintained at 65% R.H. and a temperature of 20^0C.

6.2 LITERATURE REVIEW

6.2.1 Carbonation in Concrete

The chemistry and the geopolymerisation products of AACM concrete are different from the hydration products of OPC concrete and consequently, the carbonation process of these two types of concrete is also different. The reaction of atmospheric CO_2 with the by-products of geopolymerisation/hydration of AACM and OPC concrete is dependent on the amount and type of the by-product formed. The by-products containing alkali metals or alkali-earth metal cations were suggested to be most susceptible to carbonation [283]. These alkali metals which are classed as group 1 elements in the periodic table react vigorously with water to produce metallic hydroxide and hydrogen. An investigation was carried out on the carbonation of different types of cement by adding heavy metal wastes originating from electroplating, galvanising and metal finishing operations [284]. An increase in the carbonation front was observed in the following order for the different types of cement: ordinary Portland cement (OPC) > sulphate-resistant Portland cement (SRPC) > white Portland Cement (WOPC). The presence of high amount of these metal wastes up to 60% increased the carbonation in these cement types. Two major reasons were suggested for the increase of carbonation in the OPC concrete [284]. The first reason was the presence of high ferrite content in OPC leading to the formation of ettringite which reacts with CO_2 to form gypsum, calcium carbonate and alumina gel [284]. The second reason was that the presence of metal waste which promotes the gas-permeability of a cement product [284]. These factors result in a high degree of decalcification of the anhydrous calcium silicate phase as well as accelerated hydration leading to rapid formation of $CaCO_3$.

In the case of concrete with supplementary cement replacement materials, the secondary reactions of the pozzolanic material with the hydration products will lead to lower $Ca(OH)_2$ content. This results in a faster rate of carbonation since small amount of

CO_2 will be needed to cause decalcification of the anhydrous calcium silicate phase. An investigation on the carbonation of OPC mortar, 30% fly ash replacement mortar and 50% blast furnace slag replacement mortar was performed by exposing to a 2% CO_2 concentration at a temperature of 20^0C and 65% R.H [285]. The highest depth of carbonation was recorded for the 30% fly ash replacement mortar (8.8 mm) followed by the 50% blast furnace slag replacement mortar (6.9 mm) and the lowest carbonation depth was observed in OPC mortar (0.4mm) at 154 days of CO_2 exposure. The polarization and fluorescence microscopy (PFM) was used to observe the capillary porosity at the carbonated zones of these mortars. It was discovered that the capillary porosity of OPC mortar was lower than the 30% fly ash replacement mortar and 50% blast furnace slag replacement mortar. The carbonation effect resulted in a lower capillary porosity at the carbonated zone for OPC mortar compared with 30% fly ash replacement mortar and 50% blast furnace slag replacement mortar. However, a higher capillary porosity was observed at the noncarbonated zone for OPC mortar compared with the 30% fly ash replacement mortar and 50% blast furnace slag replacement mortar.

The diffusivity of CO_2 within the supplementary replacement concrete is reduced by the dense structure evolving from the secondary reaction between the pozzolanic material and hydration product. This is particularly observed in silica fume replacement concrete which has 100 times smaller particle sizes than an average particle size of ordinary Portland cement. A study was carried out on the effect of supplementary cementing materials (silica fume, low-calcium and high-calcium fly ashes) to determine concrete resistance against carbonation [286].

Published results on the carbonation of AACM concrete are incoherent in comparison to OPC concrete. For example, high depths of carbonation were recorded for silicate-activated blast furnace slag concrete compared with OPC concrete under accelerated carbonation conditions [287][288]. Other studies show that the depth of carbonation of alkali activated blast furnace slag concrete and mortar is comparable to those of OPC concrete or mortar [289]. The author concluded that the refinement of the pore structure of alkali activated blast furnace slag concrete is responsible for its carbonation resistance [289]. However, a high relative humidity of 90% was adopted during the accelerated carbonation of these test samples [289]. The high relative humidity used during the carbonation will slow the diffusion of CO_2 within the concrete matrix which may have invalidated the author's results. A relative humidity between 50% to 70% was recommended for optimum degree of carbonation in concrete [281][282].

6.2.2 Chemistry of Carbonation in Concrete

The chemistry of carbonation in OPC concrete is fairly well documented while limited knowledge is available for AACM concrete [3]. Like other durability properties, the carbonation of AACM is significantly influenced by its pore solution chemistry which is significantly different from that of OPC concrete. The mechanism of carbonation in OPC concrete is represented in equation 6.1 - 6.3:

$$H_2O + CO_2 = HCO_3^- (Bicarbonate\ ion) + H^+ \quad 6.1$$

$$HCO_3^- = CO_3^{2-} (Carbonate\ ion) + H^+ \quad 6.2$$

$$Ca(OH)_2 + 2H^+ + CO_3^{2-} = CaCO_3 + 2H_2O \quad 6.3$$

Bicarbonate ions are formed when CO_2 reacts with water at the carbonated zone (equation 6.1). These bicarbonate ions dissociate near the uncarbonated zone within the OPC concrete to form carbonate ions due to the high pH of the pore solution (equation 6.2). The carbonate ions precipitate as calcium carbonate ($CaCO_3$) crystals when they react with the hydration product of OPC concrete ($Ca[OH]_2$) (equation 6.3). These crystals are present in OPC concrete in two forms: vaterite and calcite, the metastable vaterite turns to calcite over time [290]. This process will continue until all the hydration product of OPC concrete $Ca(OH)_2$ is consumed by the carbonate ions. The pH of OPC concrete drops because of the low calcium ions present in the pore solution due to this process.

Other hydration products of OPC concrete, calcium silicate hydrates C-S-H and ettringite/monosulphate [AFt/AFm], dissolve as pH of the pore solution drops. First, the calcium silicate hydrate C-S-H dissolves followed by monosulphate (AFm) at a pH of around 11.6 and then ettringite (AFt) at around 10.6. The phenolphthalein indicator method in OPC concrete does not change colour when the pH remains below 9 indicating that the calcium containing phases have been dissolved [290].

In cement replacement concrete, the hydration products (calcium silicate hydrate, C-S-H and ettringite/monosulphate, AFt/AFm) will dissolves faster leading to a faster rate of carbonation. This is due to the secondary pozzolanic reaction that consumes part of the free lime, $Ca(OH)_2$, responsible for the high pH of its pore solution.

The geopolymerization product of AACM concrete does not contain free lime, $Ca(OH)_2$, responsible for the high pH in concrete. The high pH in AACM is influenced by the concentration of alkali activator. The chemistry of how carbonate ions will react with different activators and subsequently dissolve other geopolymerization products of

AACM concrete is a grey area of research. Also, the suitability of phenolphthalein indicator method in AACM concrete is in doubt [3] since its functionality depends on the non-availability of the stable calcium phase within the concrete matrix.

6.2.3 Factors Affecting Carbonation in Concrete

Several factors have been identified to affect the carbonation in OPC concrete. These factors range from humidity, temperature, curing regime, binder content, CO_2 exposure concentration, concrete quality, cracks and fissures. Prominent amongst these factors are the humidity, binder content and CO_2 exposure concentration.

6.2.3.1 Humidity

The environmental humidity around the concrete boundary plays a vital role in the carbonation of concrete. The diffusion rate of carbonate ions in concrete depends on the saturation level within its pores. The optimum speed of carbonation in OPC concrete was achieved at a relative humidity between 50 to 70 per cent [281][282]. A dry concrete with relative humidity below 50% will permit faster diffusion rate of carbon dioxide but it will remain chemically inactive within the concrete pores by not forming carbonate ions. This is because only the carbonate ions react with the stable calcium phase within concrete matrix which leads to carbonation. However, in a water saturated concrete with relative humidity above 70%, the carbonate ions can move freely within the concrete matrix but the carbonation is slow. This is because the diffusion of CO_2 in the saturated concrete will be 4 orders of magnitude slower than for partially saturated concrete (50 to 70% R.H.) [25]. Studies were carried out to determine the influence of humidity on the carbonation of concrete by adopting three relative humidities of 50%, 70% and 90% [291]. The highest coefficient of carbonation occurred at 70% relative humidity.

The porosity of the carbonated zone in concrete was suggested to control the optimum humidity necessary for carbonation in concrete [290]. It was further explained that the possibility of water blocking the pore connectivity in concrete could prevent the CO_2 gas diffusion which results in slow carbonation for dense concrete.

6.2.3.2 Binder Content

Carbonation occurs only in the binder gel and not the aggregates. The depth of carbonation decreases with an increased amount of binder content in the concrete mix. The effect of carbonation results in the drop of pore solution pH as the free lime $Ca(OH)_2$ depletes. Other hydration products of OPC concrete (calcium silicate hydrates

C-S-H and ettringite/monosulphate [AFt/AFm]) dissolve as the pH of the pore solution drops. First, the calcium silicate hydrate C-S-H dissolves followed by monosulphate (AFm) at a pH of around 11.6 and then ettringite (AFt) at around 10.6 [290].

The rates of carbonation in supplementary replacement concrete have been observed to be faster than OPC concrete [275][292][293]. This was largely due to the secondary pozzolanic reaction in supplementary replacement concrete producing more calcium silicate hydrate C-S-H but less free lime $Ca(OH)_2$. The reduction of free lime $Ca(OH)_2$ induced by the secondary pozzolanic reaction promotes the faster rate of carbonation compared with OPC concrete. The depletion of free lime $Ca(OH)_2$ by the secondary reaction in supplementary replacement concrete is influenced by the pozzolanic activity. The lower the pozzolanic activity of a supplementary binder the more the demand for $Ca(OH)_2$ for it to be activated, thus the speed of carbonation is faster than when the pozzolanic activity of the binder is lower. The carbonation of binary and ternary blended cementitious systems based on ordinary Portland cement (OPC), pulverised fuel ash (PFA) and silica fume (SF) was investigated [292]. The depth of carbonation of pulverised fuel ash (PFA) based system increased significantly compared with OPC and SF based systems. This was due to the lower pozzolanic activity of PFA compared with SF. Similarly, the author suggested that the blast furnace slag (BFS) based system is more susceptible to carbonation than OPC and SF based systems [293].

However, AACM concrete does not contain free lime $Ca(OH)_2$ but has hydrates of calcium silicates. The high pH of AACM concrete pore solution is determined by the solution modulus of the type of alkali activator used. The dissolution of the hydrates of calcium silicates and other hydrates containing calcium in AACM concrete will occur when the pH is reduced to a certain level. AACM concrete becomes carbonated when this calcium containing phase is dissolved at lower pH. The chemistry of pH reduction of AACM pore solution by the action of carbonation requires further investigation. However, the accelerated carbonation testing of AACM concrete was suggested to be a far more aggressive test method when compared to OPC concrete [294]. This is because the carbonation effect on AACM concrete by using the accelerated testing method may have overestimated its actual degradation in service life.

6.2.3.3 CO_2 Exposure Concentration

The volume of CO_2 concentration in the atmosphere will affect the rate of carbonation in concrete. High rate of carbonation in concrete is found in large cities due

to various human activities resulting in the emission of high volume of CO_2, for example in road tunnels and car parks. Some environments in which concrete structures are located may reduce the rate of carbonation such as coastal areas; these structures are least susceptible to carbonation because water absorbs CO_2 by a physio-chemical process.

Accelerated concrete carbonation test method is often used to simulate the carbonation of concrete in service life. Concrete specimens are subjected to a high-volume concentration of CO_2 under this method. The rate of carbonation of concrete in service can be estimated by the ratio of the accelerated CO_2 concentration divided by the natural CO_2 concentration [285]. For example, a 5% accelerated CO_2 concentration will increase the degradation of concrete in service by 125-fold (carbonation coefficient) when the natural CO_2 concentration is 0.04%. Whilst this may be applicable to OPC concrete, the carbonation effect on AACM concrete by using the accelerated testing method may have overestimated its actual degradation in service life [294]. The change in pore solution equilibria was suggested to have caused the formation of sodium bicarbonates under accelerated carbonation instead of hydrous sodium carbonate under natural carbonation. This favours faster reaction rate and consequently the carbonation of AACM concrete under accelerated conditions of high CO_2 concentration gives higher apparent carbonation rate [294].

6.2.4 Rate of Carbonation

The rate of carbonation in concrete is principally governed by the accessibility of carbonate ions (CO_2 dissolved in pore solution) and the reactivity of the diffused carbonate ions with the binder gel. These principal factors relate to the concrete permeability and the free lime content of the binder gel, the pore solution should also be taken into consideration. Other factors such as humidity, porosity, CO_2 concentration and binder type and content influence these two governing factors.

Carbonation of concrete in service is a complex process that could not be easily described by Fick's law of diffusion, unlike the chloride ingress in concrete. This is because the rate of carbonation in a structure varies at different sections when subjected to the same CO_2 concentration [3]. It was suggested that the factors which affect carbonation, such as humidity, wet/dry condition, sunlight exposure differ at different sections in a structure.

Many authors have used the following equation to approximate the rate of carbonation in concrete [90][275].

$$d_k = d_0 + kt^n \qquad 6.4$$

Where d_k is depth of carbonation; d_0 is the initial depth of carbonation which is insignificantly small; k is carbonation coefficient (mm/year$^{(n)}$); n is the power series constant.

The carbonation coefficient ***k,*** is a variable that depends on the microclimate especially the humidity inside the concrete [290]. On the other hand, the power series constant ***n***, depends on the exposure condition. ***n*** is assumed to be 0.5 for OPC concrete but could be lesser [90].

The carbonation coefficient ***k,*** as shown in Table 6.1 for CEM I type concrete exposed to various environmental conditions for 35years was presented in literature [290]. The carbonation coefficient ***k,*** for compressive strength class ranging from less than 15 MPa to strength greater than 35 MPa is given in Table 6.1.

Table 6. 1: Depth of carbonation of concrete produced with CEM I Type Cement exposed to typical Nordic climate for 35 years.

Strength	< 15 MPa	15-20 MPa	25-35 MPa	> 35 MPa
Wet/submerged	2mm/√year	1.0mm/√year	0.75mm/√year	0.5mm/√year
Underground	3mm/√year	1.5mm/√year	1.0mm/√year	0.75mm/√year
Outdoor	5mm/√year	2.5mm/√year	1.5mm/√year	1.0mm/√year
Indoors	15mm/√year	9.0mm/√year	6mm/√year	3.5mm/√year

Table 6.1 gives estimated values of carbonation coefficient ***k,*** under various environmental conditions when the concrete surfaces are without finishes like paint, tiles or any wall coverings. The rate of carbonation could be reduced between 30% to 50% by these wall coverings depending on their thickness [290].

The value of carbonation coefficient ***k*** decreases as the strength increases for all exposure conditions as shown in Table 6.1. The lowest value of carbonation coefficient ***k*** was observed at strength > 35 MPa while strength < 15 MPa has the highest carbonation coefficient ***k,*** for all exposure conditions. It is generally accepted that the compressive strength of concrete is directly related to its porosity. Hence, the carbonation coefficient, ***k,*** increases as the concrete porosity increases at lower strength while it decreases as the porosity decreases at higher strength. Another study on the carbonation depth for different strength class of OPC concrete (25 to 41 MPa) exposed to accelerated CO_2 concentration (4 + 0.5%) in a chamber (23^0C and 50% R.H.) up to 1

year was reported [275]. The concrete with the highest strength (41 MPa) had the lowest carbonation depth of 1 mm while the highest carbonation depth of 6.9 mm was observed for concrete with the lowest strength (25 MPa). The influence of porosity on the rate of carbonation equally applies to supplementary replacement and AACM concretes when investigated independently. However, when these three different concrete types (OPC, supplementary replacement and AACM concrete) are compared together, other influencing factors like the free lime content $Ca(OH)_2$ played vital roles in the rate of carbonation [275].

The exposure conditions shown in Table 6.1 reflect the importance of degrees of humidity surrounding the concrete. Wet/submerged exposure condition had the lowest carbonation coefficient, ***k,*** for all strength grades while indoors exposure conditions have the highest carbonation coefficient ***k.*** The lowest carbonation coefficient, ***k,*** possessed by wet/submerged exposure condition was because of the diffusion of CO_2 is about 4 orders of magnitude slower than for partially saturated concrete (50 to 70% R.H.) [25]. On the other hand, the indoor exposure has environmental conditions that favour faster rate of carbonation. For example, the bathroom often has water vapour ideal for faster carbonation. The underground exposure condition has less access to atmospheric CO_2. However, the biological decay produces CO_2 that could contribute to carbonation of buried structures [290]. For the outdoor exposure conditions, the rate of carbonation is subject to the environment.

6.2.5 Carbonation Shrinkage

Carbonation shrinkage in concrete occurs due to stresses induced in the cement paste as the calcium carbonate $CaCO_3$ is formed [3]. This happens at the carbonated zone of the OPC concrete where free lime, $Ca(OH)_2$, is dissolved to form calcium carbonate $CaCO_3$. The reorganisation of the pores at the carbonated zone reduces the total porosity depending on the crystals formed, which is 3% for aragonite, 12% for calcite and 19% for vaterite [295]. The reduced porosity at the carbonated zone causes a differential shrinkage between the carbonated and the uncarbonated zones of the concrete which produces surface crazing.

The underlying mechanism of carbonation shrinkage is not fully understood for supplementary replacement and AACM concrete, unlike drying shrinkage. Recent studies were carried out on the carbonation shrinkage of AACM paste activated by mixing NaOH and KOH pellets in water [296]. The conclusion was that the carbonation shrinkage resulted in mass gain unlike the situation in drying shrinkage which results in

mass loss. The carbonation shrinkage induced mass gain together with moisture change was due to the drying and pore modification in the carbonated concrete. This produces a misleading phenomenon of equilibrium because the drying of concrete should result in mass loss rather than mass gain but the $CaCO_3$ formed during carbonation precipitates into the pore spaces unlike the pore spaces of concrete undergoing drying shrinkage that is partially filled with air. Decalcification of cement paste due to carbonation resulted in significant and irreversible shrinkage when the Ca/Si ratio of the C–S–H gel was reduced below 1.2 [297]. The carbonation shrinkage is constrained to the surface of the concrete unlike drying shrinkage which penetrates the entire concrete. However, drying and carbonation shrinkage in AACMs are dependent on relative humidity, curing condition, temperature and specimen size [298].

6.3 EXPERIMENTAL PROGRAMME

6.3.1 Mix Composition

The composition of AACM concrete used for the carbonation investigation was the same as used to investigate the chloride diffusion which is detailed in chapter 4 and 5. Four compositions of AACM concrete, mixes S_2 to S_5, were produced which are given in Table 6.2. S_6 is the control mix produced with 100% OPC binder of C40 grade concrete. The AACM concrete comprises of a cementitious binder, fine aggregate, coarse aggregate and the alkali activator. The AACM concrete trial mix S_1 was performed prior to the selection of the mix compositions used for the chloride ingress, carbonation and corrosion investigation in this research work. The AACM cementitious binder used is a proprietary hybrid alkali activated precursor comprising of low and high calcium constituents, which has been developed at Sheffield Hallam University [131]. A version of the AACM cementitious binder used for this research work is currently manufactured under licence. Several mixes were made with the AACM binder and activator by incorporating a range of fine aggregate (438 to 585 kg/m^3) and coarse aggregate content (988 to 1170 kg/m^3). The reference alkali activator liquid [131] was diluted with tap water by 2.15%, 4.24%, 8.12% and 12% in mixes S_2 to S_5 respectively, similar to the AACM concrete specimens produced for chloride ingress investigation reported in chapters 4 and 5 and published [132]. S_6 is an OPC concrete control mix with water/cement ratio of 0.486.

Two groups of AACM and OPC concrete specimens were produced for the carbonation investigation. The first group were prisms of dimensions 300 x 75 x75 mm that were used to determine the carbonation shrinkage and the rate of carbonation. The

second group were cylinders of 50 mm diameter x 60 mm depth that were used to investigate the pH of the carbonated and uncarbonated AACM and OPC concrete.

Table 6. 2: Composition of AACM and OPC concrete mixes

Mix	Total Binder (Kg/m^3)	Coarse Aggregate(Kg/m^3)		Fine Aggregate (Kg/m^3)	Alkali activator (Kg/m^3)	Extra water (Kg/m^3)	Total Liquid (Kg/m^3)	Liquid/ Binder Ratio	Activator Dilution (%)	Retarder (Kg/m^3)	SRA (Kg/m^3)
		10mm Gravel	6mm Limestone								
S_2	688	654	334	438	279	6	285	0.414	2.15	8	21
S_3	619	717	374	423	283	12	295	0.477	4.24	7	19
S_4	619	717	374	423	271	22	293	0.473	8.12	7	19
S_5	619	717	374	423	260	31	291	0.470	12.00	7	19
S_6(Control)	350	769	401	585	-	170	170	0.486	-	-	-

6.3.2 Specimen Preparation

Two different dimensions of AACM and OPC concrete specimens were produced to determine the rate of carbonation, carbonation shrinkage and the concrete pH. Prism specimens of dimensions 300 x 75 x 75 mm were used to determine the rate of carbonation and carbonation shrinkage (section 6.3.2.1). Cylindrical specimens of 50 mm diameter x 60 mm depth were used to determine the pH of the concrete (section 6.3.2.2).

6.3.2.1 Prism Specimens (300 x 75 x 75 mm)

The prisms were cast into lightly oiled metal moulds. No air entraining admixture was added to the mix. The specimens were then demoulded 24 hrs after casting and cured in water for 27 days at a temperature of 20 ± 2^0C. After curing in water for 27 days, the specimens were grouped into two batches. The first batch of AACM and OPC concrete prism specimens was used to determine the rate of carbonation while the second batch was used to determine the carbonation shrinkage. Four specimens were cast per mix (i.e. S_2 to S_6) and a total of twenty specimens were produced for both carbonation rate and shrinkage.

6.3.2.1.1 Rate of carbonation specimens

The first batch of AACM and OPC concrete prism specimens were used to determine the rate of carbonation. The specimens were removed from water after 27 days curing (28 days age) and allowed to dry in the laboratory air (20 ± 2^0C, 65% R.H.) before applying two coats of bitumen paint to the two end faces and two longitudinal faces (total of 4 faces) of the 300 x 75 x75 mm prisms. The remaining two longitudinal (300 x 75 mm) faces which were left uncoated for exposure to CO_2 are shown in Fig 6.1. The two uncoated faces were the side faces while the top (trowelled) and bottom faces of the prisms were coated. After the 28 days preconditioning in water, the specimens were placed inside an accelerated carbonation chamber (Fig 6.2). The AACM and OPC concrete specimens in the carbonation chamber were exposed to 5% CO_2 concentration in the air. The relative humidity and temperature inside the carbonation chamber were within 50% to 70% and 20 ± 2^0C respectively. The specimens were exposed to 5% CO_2 concentration in the carbonation chamber for 327 days. The depths of concrete carbonation were determined by using the phenolphthalein indicator method at 28, 55, 90, 145 and 327 days of CO_2 exposure. A total number of ten concrete specimens (2 per

mix) were used to investigate the rate of carbonation. The test procedure of the rate of carbonation is detailed in section 6.3.3.1.

Figure 6. 1: Four sides coated with bitumen paint; the remaining two longitudinal (300 x 75mm) faces uncoated.

Figure 6. 2: Specimens exposed to 5% CO_2 concentration inside the accelerated carbonation chamber.

6.3.2.1.2 Carbonation shrinkage specimens

Two stainless steel demec points were fixed, 24 hrs after casting, along the two-parallel longitudinal (300 x 75 mm) side faces at a gauge length of 200 mm (Fig 6.3). The specimens were cured in water at (20 ± 2^0C) for 7 days. The specimens were removed from water after 7 days and allowed to dry in the laboratory air (20 ± 2^0C, 65% R.H.) for 42 days (Fig 6.3). This was to ensure even moisture condition within the concrete matrix before accelerated CO_2 exposure. No bitumen paint was applied to the face(s) of the concrete. The AACM and OPC concrete specimens in the carbonation chamber were exposed to 5% CO_2 concentration within 50% to 70% relative humidity while the temperature was 20 ± 2^0C. The period of exposure in the carbonation chamber was 327 days. The readings of carbonation shrinkage were taken and recorded at regular intervals. Two specimens were used per mix (i.e. S_2 to S_6) with a total of ten specimens for the carbonation shrinkage investigation. The test procedure for the carbonation shrinkage is detailed in section 6.3.3.2.

Figure 6. 3: Stainless steel demec points fixed along the two-parallel longitudinal (300 x 75 mm) faces

6.3.2.2 Cylindrical Specimens (50mm diameter X 60mm Depth)

AACM and OPC concrete specimens were cast in plastic cylinders of 50 mm diameter X 60mm depth as shown in Fig. 6.4. Self-adhesive bitumen tape was fixed at the bottom of the plastic cylinder moulds before casting to prevent the concrete from pouring out (Fig. 6.5). The top cast surface was carefully trowelled to achieve a plain surface. No air entraining admixture was used in the mix. A total of 50 specimens were produced to determine the pH of carbonated and uncarbonated concrete specimens. The specimens, inside the moulds, were air cured in the laboratory air (20 ± 2^0C, 65% R.H.) for 24 hrs after casting while covered with polythene sheets to prevent rapid moisture loss. After 24 hrs, the specimens were not demoulded to prevent the ingress of CO_2 through the bottom face and the circumference of the specimens when subsequently placed inside the carbonation chamber. The specimens within the plastic moulds were cured in water for 27 days at a temperature of 20 ± 2^0C. The specimens were then cured at 65% R.H. and a temperature of 50 ^{0}C until the change in their unit weight was less than 0.2% in a 24-hour period. After the preconditioning to 65% R.H., the specimens were placed inside the accelerated carbonation chamber as shown in Fig. 6.2. The specimens were exposed to 5% CO_2 concentration in the carbonation chamber for 327 days at a relative humidity of 50 to 70% and temperature 20 ± 2^0C.

Figure 6. 4: Concrete specimens in 50mm diameter X 60mm depth cylindrical plastic moulds


Figure 6. 5: Self-adhesive tape fixed at the bottom of cylindrical moulds

6.3.3 Experimental Procedure

6.3.3.1 Rate of Carbonation Test

The rate of carbonation was determined by the standard phenolphthalein test for concrete [299]. The 300 x 75 x 75 mm dimension specimens were marked at 50 mm intervals along the longitudinal face. An incremental 50 mm long piece was cut at each test age (28, 55, 90, 145 and 327 days of CO_2 exposures) from the previously cut prism cross-section by tensile splitting across the prism cross-section at the first 50 mm interval marking from the end face of the specimen. Splitting was performed by placing 8 mm diameter cylindrical rods along the first 50 mm interval marking at the top and bottom face of the prism and performing a tensile split test by applying a compressive load through the cylinders. A fairly neat cut was achieved by this method across the prism face at a 50 mm incremental length from the end face at each test age. The cut face (cross section) of the remaining whole prism e.g. 250 mm length after the first cut at 28 days together with the freshly cut face of the 50 mm long end piece were exposed to the phenolphthalein test to determine depth of carbonation (Fig. 6.6). Subsequently, the cut face of the remaining whole prism was sealed by coating with bitumen paint (Fig. 6.7) and the specimen returned to the carbonation chamber until the next test age.

At each test age (28, 55, 90, 145 and 327 days) of CO_2 exposure, therefore, two freshly cut faces of the prism cross-section were exposed to the phenolphthalein test. The depth of carbonation was measured from the two uncoated longitudinal faces of the prism, which were directly exposed to carbonation (Fig. 6.8). The carbonation depth was measured at four points from each of the uncoated longitudinal faces, thereby

providing 8 readings per freshly cut face. A total of 16 depth of carbonation readings, therefore, were obtained from the two faces exposed by the freshly cut cross section at each test age.

Figure 6. 6: Phenolphthalein indicator applied to the two freshly cut faces.

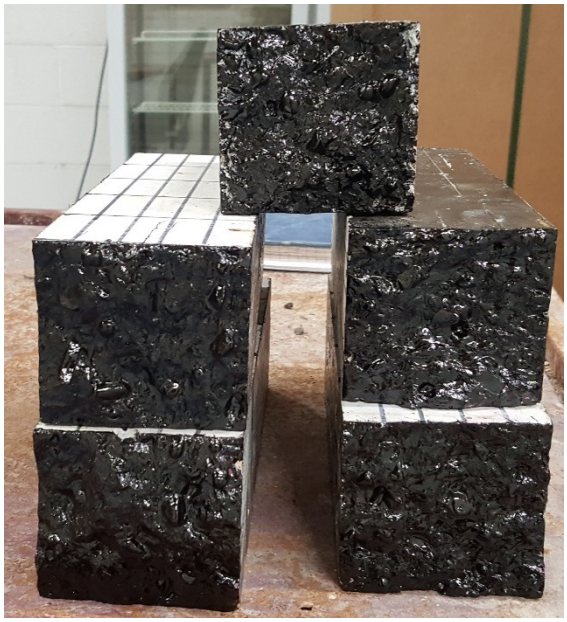

Figure 6. 7: Bitumen paint applied to the freshly cut face of the prism.

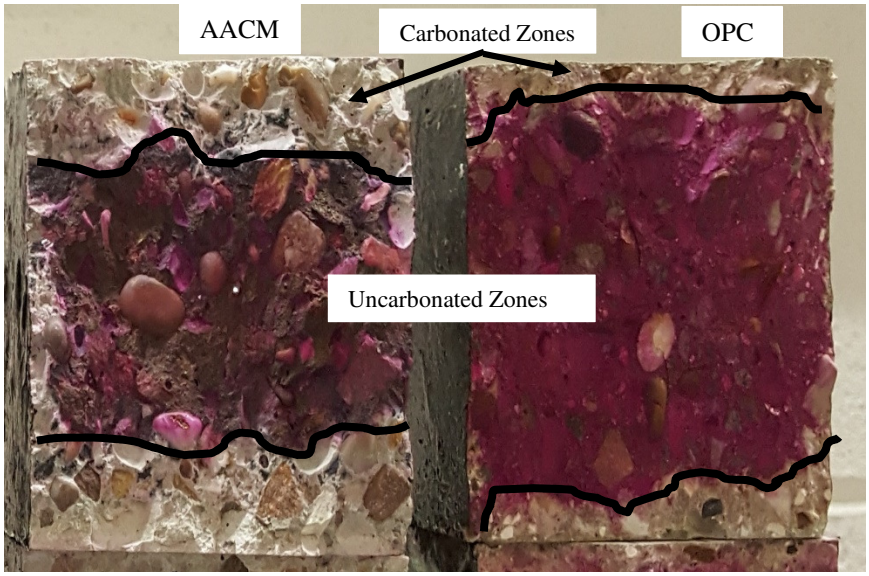

Figure 6. 8: Depth of carbonation d_k measured from the two uncoated longitudinal faces of a prism

6.3.3.1.1 Depth of carbonation d_k

A solution of 1g phenolphthalein dissolved in 70ml ethyl alcohol and 100 ml distilled water [300] was sprayed on the freshly broken face as shown in Figures 6.6 and 6.8. The phenolphthalein indicator was just sufficient to wet the concrete surface without running down the surface. An instantaneous colour change to red-purple was observed at the inner core of the sprayed surface, this is referred to as the uncarbonated

zone (Fig. 6.8). The colour at the edge of the sprayed surface did not change; this is referred to as the carbonated zone (Fig. 6.8). The spraying of phenolphthalein was performed on the two freshly cut faces of the prism cross-section for each concrete mix S_2 to S_6. The depth of carbonation d_k for each mix is the average of these 16 readings.

6.3.3.2 Carbonation Shrinkage Test

The shrinkage test was performed in accordance with the standard method [211] on 75 X 75 X 300 mm prism specimens which were cured in water for 7 days (20 ± 2^0C) and then cured in laboratory air (20 ± 2^0C, 65% R.H.) for 42 days before exposing to accelerated carbonation. The datum shrinkage reading of AACM and OPC concrete mixes S_2 to S_6 specimens was taken before exposing the specimens to CO_2 in the accelerated carbonation chamber. The specimens were exposed to 5% CO_2 at a relative humidity of 50 to 70% and 20 ± 2^0C temperature. The carbonation shrinkage readings were taken at regular intervals with the demec extensometer over a gauge length of 200 mm. The difference between the datum reading obtained before exposing it to CO_2 concentration inside the carbonation chamber and the periodical readings gave the carbonation shrinkage values. The carbonation shrinkage readings were taken on the two longitudinal side faces (i.e. 300 x 75 mm) of the prism specimens. The average reading of two specimens (two faces each) per mix was recorded.

6.3.3.3 Powder Collection

pH analysis was performed on the 50 mm diameter X 60 mm depth cylindrical specimens which were detailed in section 6.3.2.2. The cylindrical specimens were removed from the accelerated carbonation chamber after 327 days exposure. These specimens were demoulded from their plastic moulds (sleeves) and split into halves longitudinally along their depths as shown by section A-A in Fig. 6.9. The splitting tensile strength test procedure was adopted to break the cylinders into two longitudinal halves. The surface of the split cylinder halves revealed the depth of carbonation resulting from the top unsealed face of the cylinder, which was exposed to CO_2 in the carbonation chamber. All the remaining surfaces of the cylinder were sealed as described in Section 6.3.2.2.

The depth of carbonation was determined by spraying phenolphthalein on the exposed (split) surface of the first broken half of each cylinder according to standard procedure [300]. The depth of carbonation profile from the exposed face of the cylinder, which was revealed by no colour change of the phenolphthalein test, was clearly marked. However, phenolphthalein was not applied to the surface of the second half of each split

cylinder. The depth of carbonation profile obtained from the first half cylinder was marked on the second half of the cylinder that was not sprayed with phenolphthalein. The marked depth of carbonation zone on the second half of the specimen was carefully chiselled to obtain concrete chunks of the carbonated and uncarbonated zones. This procedure was performed on five specimens for each AACM and OPC concrete mixes S_2 to S_6 to obtain sufficient concrete chunks for the pH test. The chunks were ground to powder and passed through a 150 µm sieve to obtain concrete powder for the carbonated and uncarbonated zones.

A second set of powder test samples was similarly obtained but by removing the coarse aggregate particles from the concrete chunks. The concrete pieces were crushed to separate the coarse aggregate particles from the matrix and they were removed by sieving. The remaining mortar material was ground to obtain mortar powder for the carbonated and uncarbonated zones. The concrete and mortar powder for the carbonated and uncarbonated zones for mixes S_2 to S_6 was stored separately in air proof plastic vials and labelled accordingly as shown in Fig. 6.10. pH analysis was performed on these carbonated and uncarbonated powder samples.

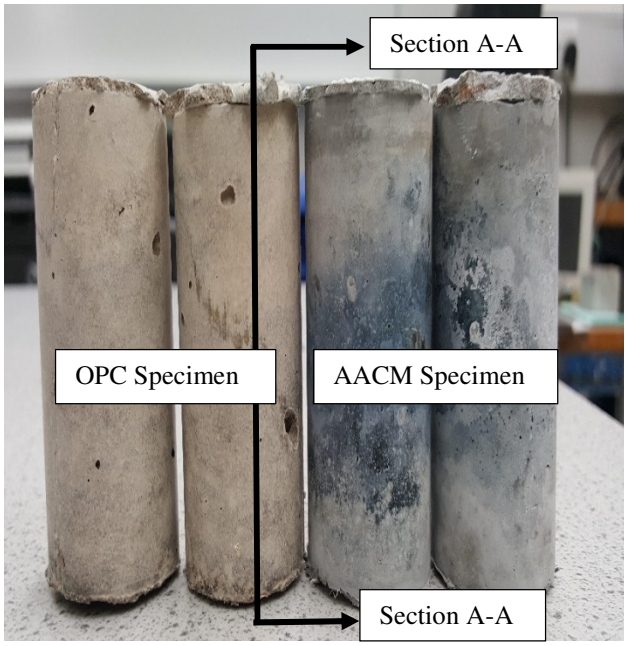

Figure 6. 9: Demoulded cylinders showing the section A-A of splitting

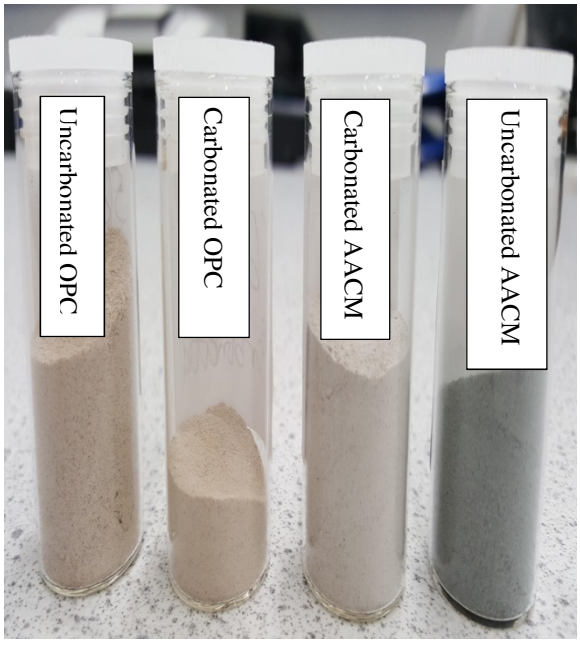

Figure 6. 10: AACM and OPC concrete/mortar powder stored in air-proof plastic vials

6.3.3.3.1 pH analysis

The ex-situ leaching method of concrete [263] was adopted to obtain the solution used for pH analysis of the concrete and mortar samples. This was carried out by dissolving 5 grams of the concrete powder in distilled water at a liquid/solid ratio of 1:1 in the air-tight plastic vials. The solution was shaken thoroughly for 10 seconds to

ensure a homogenous mix of the concrete powder. The concrete powder solution in the air-tight plastic vial was left undisturbed for 5 mins to allow for leaching. The concrete powder solution was then filtered as shown in Fig. 6.11 to obtain a solution that does not contain concrete powder particles.

A double junction electrode connected to a benchtop meter 3-in-1 (Fig. 6.12) was dipped inside the filtered solution to measure its pH. This device measures pH ranging from 0.00 to 14.00 and can measure sample volumes as small as 0.2mL with an accuracy of ± 0.01. The body of the double junction electrode is made of glass which makes it suitable in very acidic or alkaline solutions. The internal reference comprises of Ag/AgCl double junction electrode resulting in exceptionally stable and minimal long-term drift.

Figure 6. 11: Filtering of AACM and OPC concrete/mortar powder

Figure 6. 12: Double junction electrode and benchtop meter 3-in-1 used to measure pH

6.4 RESULTS AND DISCUSSION

6.4.1 Depth of Carbonation (Prism Tests)

The depth of carbonation readings obtained from tests on 300 x 75 x 75 mm prism specimens described in section 3.3.1.1 are presented in Table 6.3. The readings were taken at 28, 55, 90, 145 and 327 days of exposure to 5% CO_2 concentration in the carbonation chamber.

Table 6. 3: Depth of Carbonation d_k (mm) for AACM and OPC concrete mixes S_2 to S_6 at different exposure periods to accelerated carbonation

		1st cut face		2nd cut face		Carbonation depth
Age	Mix	side 1 Av.	side 2 Av.	side 1 Av.	side 2 Av.	d_k *(mm)*
28 days exposure	S_2	4.75	4.25	4	3.75	4.19
	S_3	6.75	6	5.75	5.75	6.06
	S_4	7	8	6.5	8	7.38
	S_5	8.75	8.75	8.25	8.75	8.63
	S_6	1.5	1	1	1	1.13
55 days exposure	S_2	8.75	7.75	7.25	6	7.44
	S_3	13	13.25	12.5	12.5	12.81
	S_4	11	10	9.5	11.5	10.5
	S_5	12.25	12.25	11.5	11.5	11.88
	S_6	3	3.75	4.5	4.5	3.94
90 days exposure	S_2	10	10.75	8.75	10	9.88
	S_3	17	17.75	16.75	15.75	16.81
	S_4	15.25	16.75	15	17.25	16.06
	S_5	17.5	16.75	16	15.75	16.5
	S_6	2.5	6.5	8.5	6.25	5.94
145 days exposure	S_2	10	11.5	10.75	10	10.56
	S_3	22.25	19.5	22.5	22.5	21.69
	S_4	23	21.5	21.25	24.5	22.56
	S_5	26.5	26	25.5	25.75	25.94
	S_6	9.25	9.5	10.75	11.5	10.25
327 days exposure	S_2	14	13.5	12.25	13.5	13.31
	S_3	26	23.5	25	26.25	25.19
	S_4	25.75	26.25	27.25	27.75	26.75
	S_5	29.5	29.5	29.25	28.75	29.25
	S_6	15.75	14.75	12.75	13.25	14.13

6.4.1.1 AACM and OPC Concrete

The relationship between the depth of carbonation and exposure period in 5% $C0_2$ concentration for AACM and OPC concrete mixes S_2 to S_6 is shown in Fig. 6.13. The 5% $C0_2$ concentration is 125 times higher than the atmospheric $C0_2$ concentration of 0.04%.

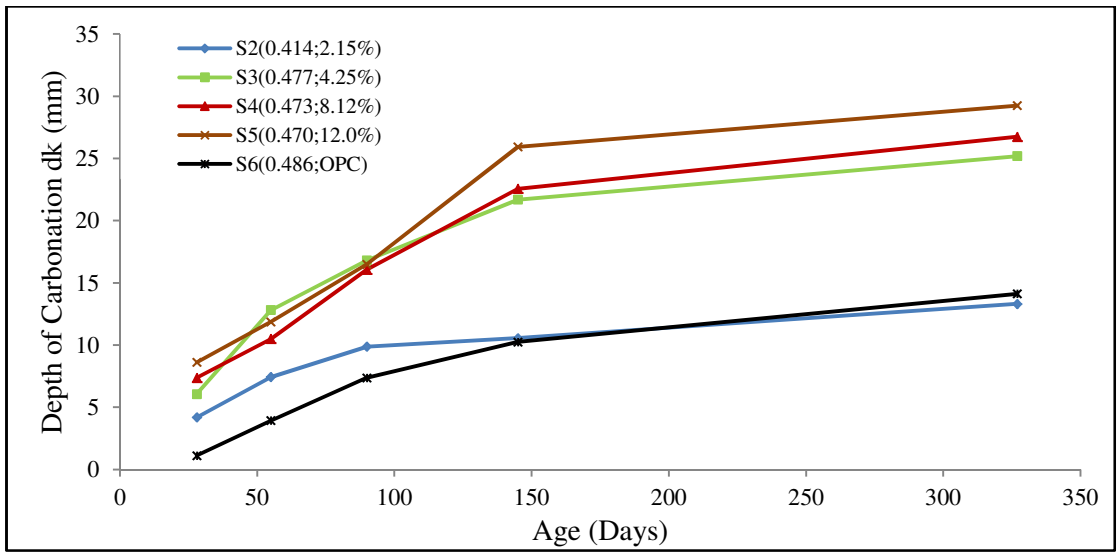

Figure 6. 13: Relationship between depth of carbonation d_k and exposure period of AACM and OPC concrete (300 X 75 X 75 mm prism tests).

A lower depth of carbonation was observed in OPC concrete compared with AACM concrete except for AACM concrete mix S_2 (Fig. 6.13). AACM concrete mix S_2 shows a similar depth of carbonation to OPC concrete mix S_6 after 150 days of exposure. The depth of carbonation is 10.3 mm for AACM and OPC concrete mixes S_2 and S_6 at 150 days exposure while it is in the range of 21.69 to 25.94 mm for AACM concrete mixes S_3, S_4 and S_5 at 150 days of exposure. Mix S_2 is an exception for the reasons discussed in Section 6.4.1.2. This trend is in agreement with other authors, which shows deeper carbonation fronts in AACM concrete than OPC concrete [287][288].

A significant depth of carbonation was recorded for AACM concrete mixes S_3, S_4 and S_5 as shown in (Fig. 6.13). It was suggested that the pH buffer effect of $Ca(OH)_2$ in OPC concrete is responsible for its lower depth of carbonation compared with AACM concrete [301]. However, AACM concrete does not produce $Ca(OH)_2$, its main geopolymerization product is C-A-S-H. The $Ca(OH)_2$ maintains the pH of OPC concrete between 12.5 to 13.5 while this is not the case in AACM concrete. The CO_2 reacts directly with the C-A-S-H product in AACM concrete to generate decalcification of the binder gel [289].The decalcification of the binder gel in AACM results in the loss of cohesion and ultimately larger pore structure [302]. This accounts for the loss in compressive strength of carbonated AACM concrete observed by many authors [288][303]. For OPC concrete, the calcium carbonate produced during carbonation precipitates around the surface area of the concrete to form a barrier which reduces further ingress of CO_2 [302]. In addition to the ongoing hydration in OPC concrete, the precipitated calcium carbonate contributes to the dense structure which leads to higher compressive strength observed by some authors [289][301][302].

The presence of high volume of micro cracks in AACM concrete was suggested to influence its greater depth of carbonation despite low porosity compared with OPC concrete [289][301]. Surface crazing is observed in AACM concrete when it is not properly cured. However, the specimens of this study were free from visible crazing and cracking.

6.4.1.2 Effect of liquid/binder ratio

Lower carbonation front depths were observed for AACM mix S_2 as shown in Fig. 6.13. The increase in the carbonation depth was significant between Mix S_2 and Mix S_3 especially at longer exposure periods. For instance, the carbonation depth of Mix S_2 is 13.31 mm while it is 25.19 mm for Mix S_3 at 327 days exposure. This represents 90% increase in the carbonation depths between Mix S_2 and Mix S_3. Mix S_2 has the lowest activator dilution (2.15%) and also the lowest liquid/binder ratio of 0.41 (Table 6.2).

On the other hand, Mixes S_3, S_4 and S_5 have the same liquid/binder ratio of 0.48 while the degrees of activator dilution increases from 4.25% to 12.0% respectively. This shows an increase in the depth of carbonation profile with the increasing activator dilution (Fig. 6.14) which is discussed in detail in the next section. The increase in the depth of carbonation between Mix S_3 to Mix S_5 was much less significant (Fig. 6.13). For instance, the carbonation depth is 25.19mm for Mix S_3 while it is 29.25mm for Mix S_5 at 327 days exposure.

In addition to the low activator dilution and liquid/binder in AACM concrete mix S_2, its tight pore structure (Chapter 3, Section 3.4.3.4) reduces the ingress of CO_2 and its lower capillary absorption (Chapter 7, Section 7.4.1) reduces moisture movement, both of which reduce carbonation. The porosity of Mix S_2 is 5.67%, 6.94% and 9.98% under wet/dry, wet and dry curing as shown in Fig. 3.40 (Chapter 3, Section 3.4.3.4) while its capillary absorption gave a sorptivity value of 0.041 mm/sec$^{0.5}$ (Chapter 7, Section 7.4.1). The prescence of more binder gel in Mix S_2 provided a tighter pore structure. This will lead to a decrease in diffusion of CO_2 and carbonation [304]. The presence of lower liquid/binder ratio in AACM concrete mix S_2 resulted in lower porosity and lower carbonation than any other AACM mixes.

6.4.1.3 Effect of Activator Dilution

The relationship between depth of carbonation and activator dilution is shown in Fig. 6.14. The depths of carbonation were measured at 28, 55, 90, 145 and 327 days of

exposure to 5% CO_2 concentration in an accelerated carbonation chamber. The chamber was maintained at a temperature of 20 ± 2^0C and 65% R.H.

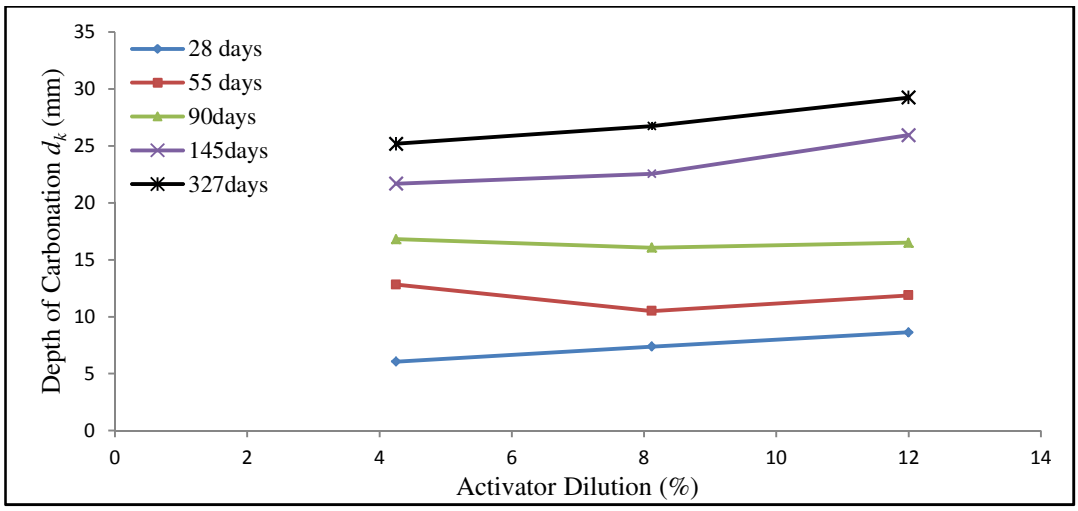

Figure 6. 14: Influence of activator dilution on the depth of carbonation d_k in AACM concrete

Increase in the depth of carbonation is modest with increasing activator dilution at 28, 55, 90, 145 and 327 days exposure. A similar trend of lower carbonation front was observed for a metakaolin-containing system that has high alkalinity [303]. This is because the formation of more C-A-S-H takes longer for the carbonate ions to consume the C-A-S-H product produced by the high alkalinity of AACM concrete. An increased rate of carbonation in an alkali activated slag concrete with lower activator modulus (0.75) was observed compared with that of higher activator modulus (1.25) [301]. It was suggested that the increase in the carbonation front for the lower activator modulus was because of the high penetration rate of CO_2 and water absorption [301].

6.4.1.4 Effect of Exposure Period

The carbonation front of AACM and OPC concrete mixes S_2 to S_6 at 28 and 145 days of CO_2 exposure is shown in Figures 6.15 and 6.16 respectively.

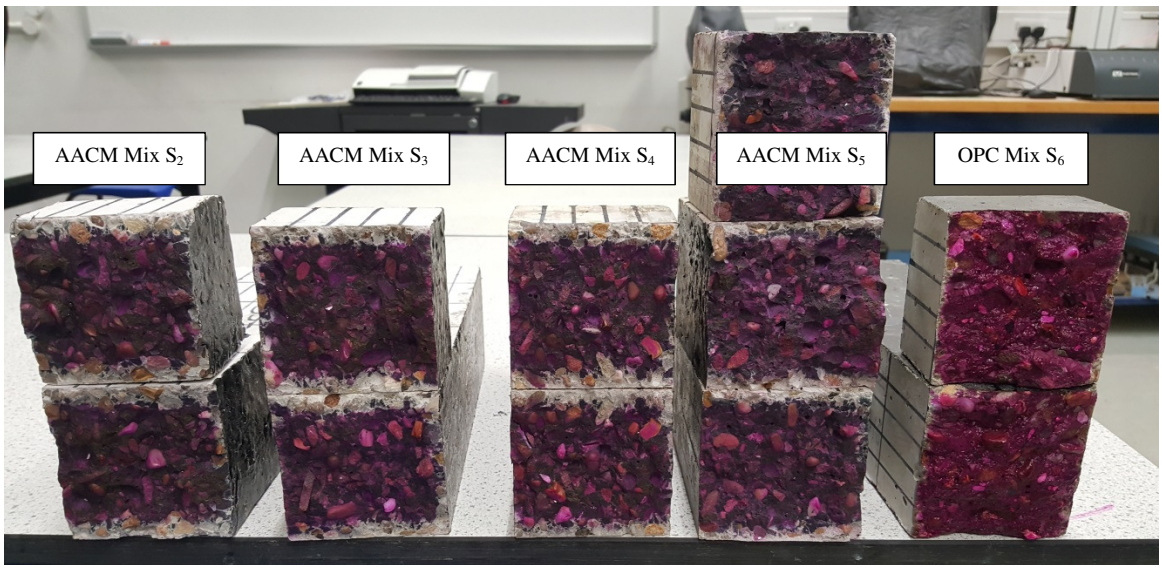

Figure 6. 15: Carbonation front at 28 days exposure to 5% CO_2 concentration.

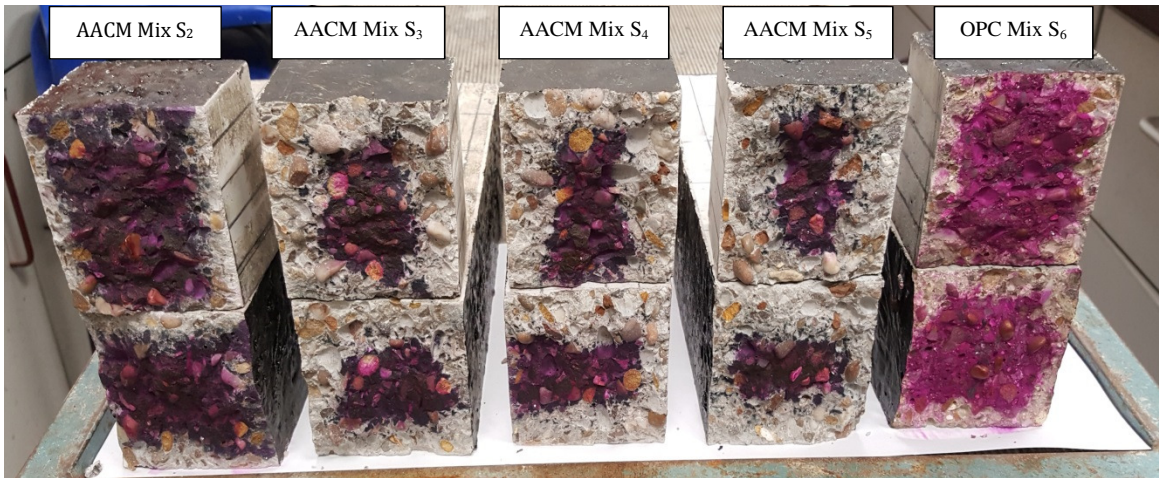

Figure 6. 16: Carbonation front at 145 days exposure to 5% CO_2 concentration.

Significant increase in the depth of carbonation is observed between 28 and 145 days of CO_2 exposures for both AACM and OPC concrete as shown in Figures 6.14, 6.15 and 6.16. The highest increase in the carbonation depth is observed in AACM concrete mix S_5 while mix S_2 displayed the least increase in carbonation depth with age. For example, the depth of carbonation for AACM mix S_2 and S_5 at 28 days are 4.19 mm and 8.63 mm respectively while it is 10.25 mm and 25.94 mm at 145 days exposure. An increase of 144% and 200% was observed in the carbonation depths between 28 and 145 days exposure for AACM concrete mixes S_2 and S_5 respectively. After 145 days exposure, the increase in the depth of carbonation was moderate for all mixes, Fig. 6.14.

Similar increase in the depth of carbonation was observed for water-glass activated slag mortar [302]. The author observed a much deeper and intense carbonation between 28 and 120 days while moderate increase in the carbonation depth was observed between 120 and 240 days. The specimens were cured in a closed chamber

containing K_2CO_3 solution, kept at a relative humidity of 43.2%. The chamber was saturated with CO_2 gas twice daily but the concentration of the CO_2 was not stated.

Figure 6.16 show that the depths of carbonation front occurred at all the four edges of the concrete cross-section at 145 days of exposure even though only two of the longitudinal prism faces were free from the bitumen paint sealant. This is because the CO_2 gas which diffused into the concrete circulated throughout its matrix since the moisture content was uniform within the concrete matrix. The presence of optimum moisture content and high CO_2 gas concentration within the concrete matrix resulted in the decalcification of the Ca-rich gel binder at the four edge zones of the concrete cross-section. The carbonation depth recorded in Fig. 6.15, in contrast, extends only from the CO_2 exposed (uncoated) surfaces of the prisms since 28 days of CO_2 exposure is an insufficient period for carbonation to circulate throughout the matrix.

6.4.2 Rate of Carbonation

Equation 6.4 is used by many authors to predict the rate of carbonation in concrete [275][90].

$$d_k = d_0 + kt^n \qquad 6.4$$

Where $\boldsymbol{d_k}$ is the depth of carbonation; $\boldsymbol{d_o}$ is the initial depth of carbonation which is insignificantly small; $\boldsymbol{k}$ is carbonation coefficient (mm/time$^{(n)}$); $\boldsymbol{n}$ is the power series constant which is assumed to be 0.5 [90]; $\boldsymbol{t}$ is time in years.

The depth of carbonation with accelerated carbonation exposure period is plotted against √years in Fig. 6.17 for the data of mixes S_2 to S_6. A linear relationship is clearly evident in Fig. 6.17 and the carbonation coefficient $\boldsymbol{k}$ has been calculated by regression analysis.

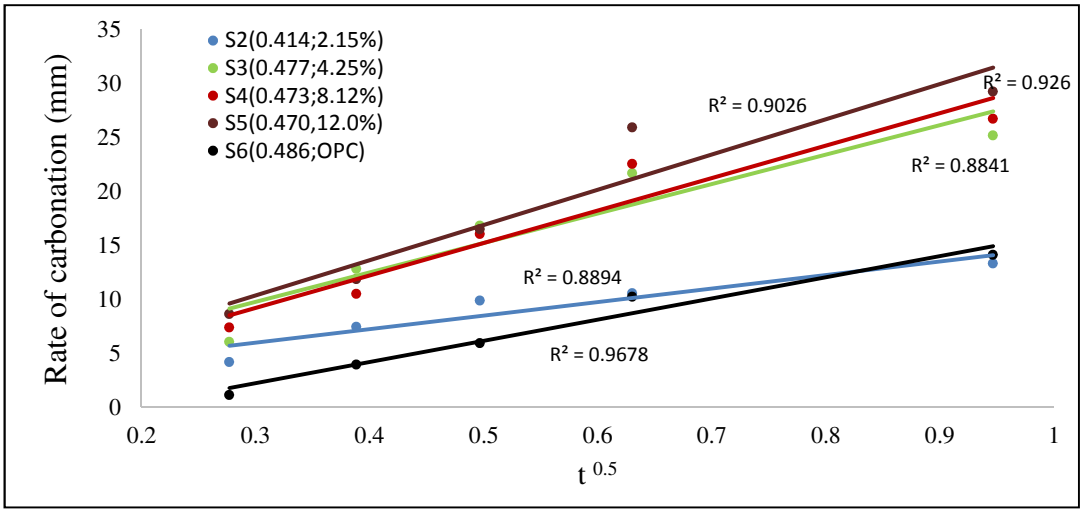

Figure 6. 17: Rate of carbonation graph for AACM and OPC concrete S_2 to S_6

Fig. 6.17 shows the rate of carbonation (represented by coefficient ***k***) of AACM and OPC concrete mixes exposed to 5% CO_2. Each point on the graph represents an average of 16 depths of carbonation readings from two cut faces of prism test samples, which are presented in Table 6.3. The best-fit curve is linear with strong correlation of 0.88 to 0.97. The carbonation coefficient ***k*** (mm/time$^{(0.5)}$) is determined from Fig. 6.17 by applying equation 6.4. The carbonation coefficient ***k*** (mm/time$^{(0.5)}$) is shown Fig. 6.18.

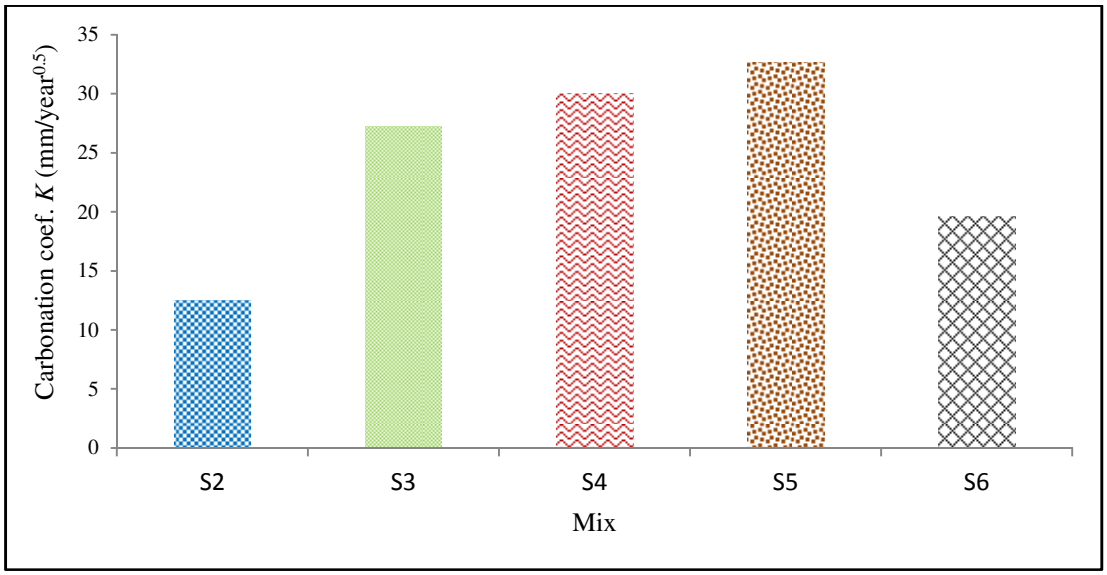

Figure 6. 18: The carbonation coefficient k (mm/yr$^{0.5}$) for AACM and OPC concrete mixes

AACM concrete mix S_2 has the lowest carbonation coefficient *k* of 12.55 mm/yr$^{0.5}$ followed by OPC concrete mix S_6 19.62 mm/yr$^{0.5}$ while the coefficient for AACM concrete mixes S_3, S_4 and S_5 is 27.29 mm/yr$^{0.5}$, 30.08 mm/yr$^{0.5}$ and 32.68 mm/yr$^{0.5}$ respectively. The lowest carbonation coefficient *k* in AACM concrete mix S_2 is an indication of lower rate of carbonation, which is aided by the refinement of its pore structure while that of OPC concrete is aided by the buffer effect provided by $Ca(OH)_2$ in OPC concrete. The relationship between carbonation coefficient *k (mm/yr$^{0.5}$)* and the activator dilution is shown in Fig. 6.19. The influence of lower activator dilution on the carbonation of AACM concrete is due, firstly, to the production of more geopolymerisation products within its matrix which take longer to carbonate, secondly the evolution of a tighter pore structure which will reduce the penetration of CO_2 and moisture and thirdly a higher pH compared with AACM concrete with higher activator dilution.

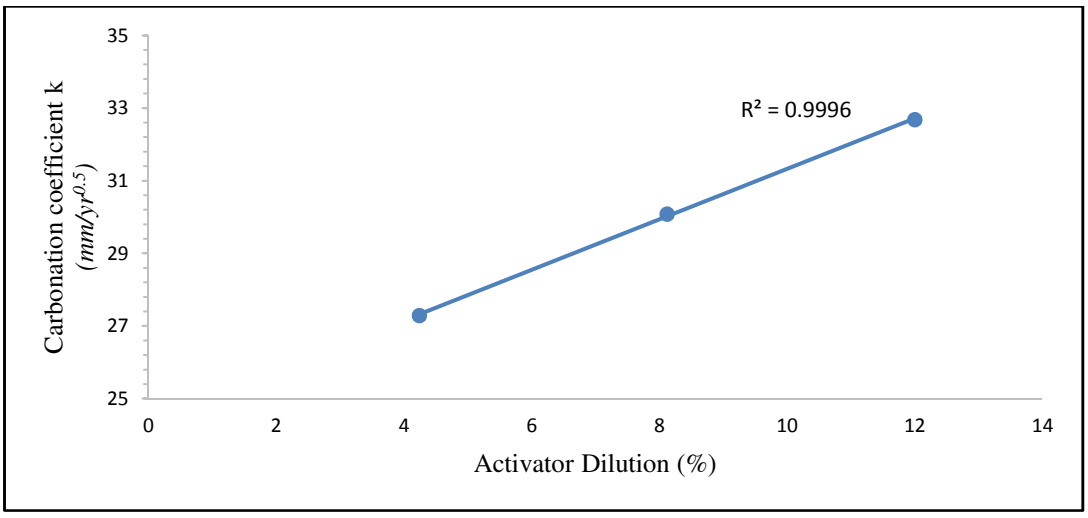

Figure 6. 19: Relationship between carbonation coefficient k ($mm/yr^{0.5}$) and activator dilution

Geopolymerization reaction of AACMs do not produce $Ca(OH)_2$, its main product is C-A-S-H. It has been reported that the rate of carbonation of OPC concrete of 5 to 10% replacement with silica fume increases by 5% compared with 100% OPC concrete that has the same strength class [290]. Similarly, an increase of 2 to 3 times in the carbonation coefficient ***k*** was observed for concrete containing 50% fly ash compared with OPC concrete [305]. The increase in carbonation is due to the consumption of $Ca(OH)_2$ produced by cement hydration for the pozzolanic reactions. This reaction results to a lesser concentration of $Ca(OH)_2$ which increases carbonation.

6.4.3 Shrinkage of AACM and OPC concrete

6.4.3.1 Carbonation Shrinkage

The carbonation shrinkage of the AACM and OPC concrete cured in the accelerated carbonation chamber is shown in Fig. 6.20. The shrinkage samples (300 x 75 x 75 mm prisms) were exposed to 5% CO_2 concentration for 360 days at a temperature of 20 ± 2^0 C and 50 to 70% R.H.

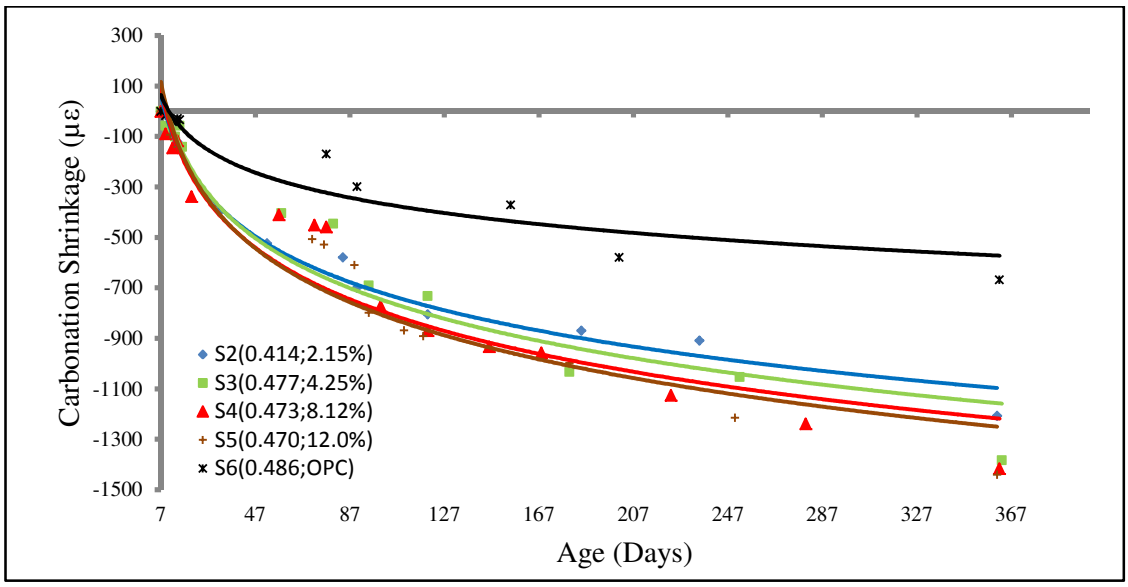

Figure 6. 20: Carbonation shrinkage of AACM and OPC concrete

High carbonation shrinkage strain is observed in AACM concrete compared with OPC concrete. The carbonation shrinkage strains in AACM concrete mixes are within the range of 1100 με to 1250 με while it is 670 με for OPC concrete exposed to 5% $C0_2$ concentration for 360 days. The high carbonation shrinkage strain in AACM concrete mixes could be attributed to the high volume of capillary pores > 1 μm. AACM concrete has a lower effective porosity but higher volume of capillary pores compared with OPC concrete when measured with mercury intrusion porosimetry (Chapter 3, section 3.4.3.4). The high volume of the capillary pores will facilitate the diffusion of moisture from AACM concrete.

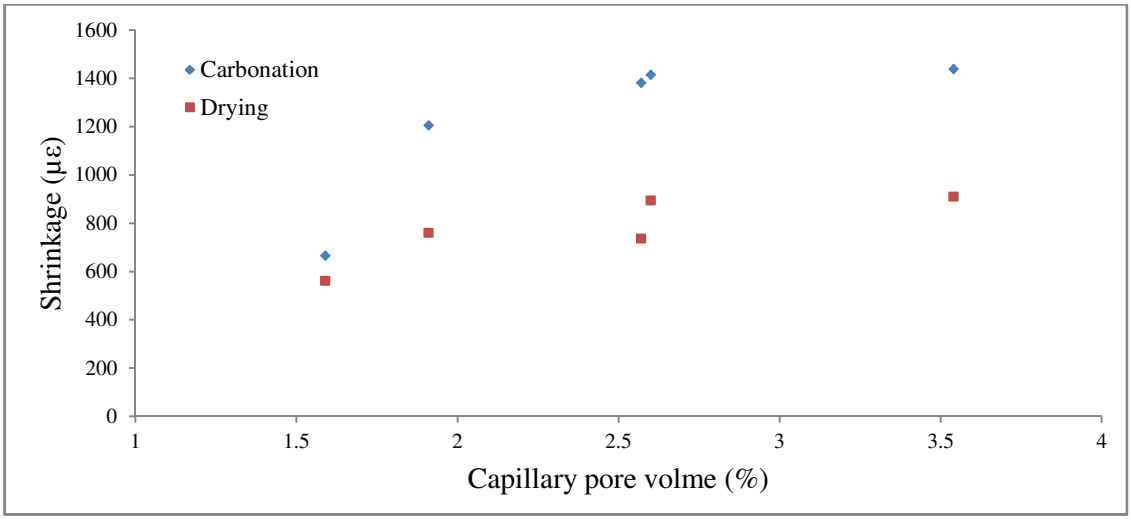

Figure 6. 21: Effect of capillary pores on carbonation and drying shrinkage

Fig. 6.21 shows the effect of capillary pore volumes on the carbonation and drying shrinkage of AACM and OPC concrete. An increase in both carbonation and drying shrinkage is observed at higher percentages of capillary pore volumes.

The correlation between the rate of accelerated and natural carbonation of AACM concrete is very dissimilar to OPC concrete [294]. The carbonation and shrinkage caused by the accelerated carbonation in AACM concrete is much higher. The authors [294] observed the formation of sodium bicarbonates during accelerated carbonation of AACM concrete compared with hydrous sodium carbonate formed during natural carbonation. The shift in the pore solution equilibria was suggested to cause high degree of carbonation in AACM concrete compared with OPC concrete [294].

Carbonation shrinkage strain increases with an increase in activator dilution. AACM concrete with 12% activator dilution (mix S_5) has the highest carbonation shrinkage strain of 1250 με while it is 1100 με for the lowest activator dilution 2.15% (mix S_2). The lowest carbonation shrinkage strain observed in mix S_2 (Fig. 6.20) is because of its finer pore structure rather than the restraining effect of coarse aggregate observed in drying shrinkage.

6.4.3.2 Drying Shrinkage

The drying shrinkage of AACM and OPC concrete is shown in Fig. 6.22. The AACM and OPC concrete samples were air cured at a temperature of 20 ± 2^0 C and 65% R.H for 80 days subsequent to 7 days of wet curing after demoulding the shrinkage specimens.

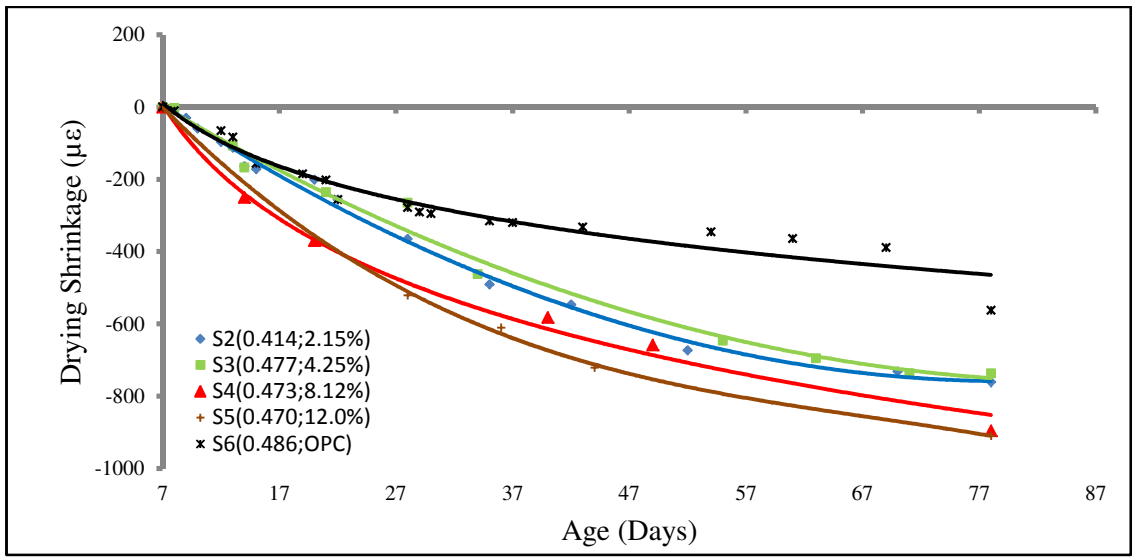

Figure 6. 22: Drying shrinkage of AACM and OPC concrete

The drying shrinkage of AACM concrete is higher than OPC concrete. The drying shrinkage strains for AACM concrete mixes S_2 to S_5 are within the range of 736 με to 910 με while it is 562 με for OPC concrete at 80 days. The high shrinkage strain

for AACM concrete correlates with the high volume of large capillary pores (> 1 μm) within its matrix compared with OPC concrete.

Drying shrinkage strains of 800 με to 1400 με were observed by other researchers in AACM concrete while the shrinkage of comparative OPC concrete was 700 με [308]. The specimens were cured at a temperature of 20 ± 2^0 C and 50 ± 5% R.H for 380 days. The author attributed the higher shrinkage observed in AACM concrete to its pore structure.

AACM concrete mix S_3 has slightly lower drying shrinkage strain of 736 με compared with 761 με observed in mix S_2. The reverse would have been expected since Mix S_2 has a lower liquid/binder ratio (0.41) and lower activator dilution (2.15%) than mix S_3which has a liquid/binder ratio of 0.48 and activator dilution of 4.25%. The lower shrinkage recorded by mix S_3 is attributed to two reasons; the total coarse aggregate content of mix S_3 is 1091 Kg/m^3 compared with 988 Kg/m^3 for mix S_2 as shown in Table 6.2. The presence of more coarse aggregate in mix S_3 provided greater restraint to the shrinkage of the matrix. The shrinkage restraining effect of coarse aggregates in concrete, due to their higher elastic modulus than the surrounding matrix, is well recognised [25]. A direct relationship was observed between the shrinkage of hydrated cement paste and water/cement ratio of 0.2 - 0.6 [309]. This relationship is affected by the coarse aggregate content of concrete, which restrains its shrinkage [25].Interestingly, the performance of mix S_2 and S_3 was reversed for carbonation shrinkage (Figures 6.20 and 6.22) due to the dominant role of pore structure instead of coarse aggregate content on carbonation shrinkage.

6.4.3.3 Carbonation and Drying Shrinkage

The carbonation and drying shrinkage graphs up to about 80 days for AACM concrete mixes S_2 and S_5 and OPC mix S_6 are shown in Fig. 6.23. The solid lines represent the carbonation shrinkage while the dashed lines are the drying shrinkage.

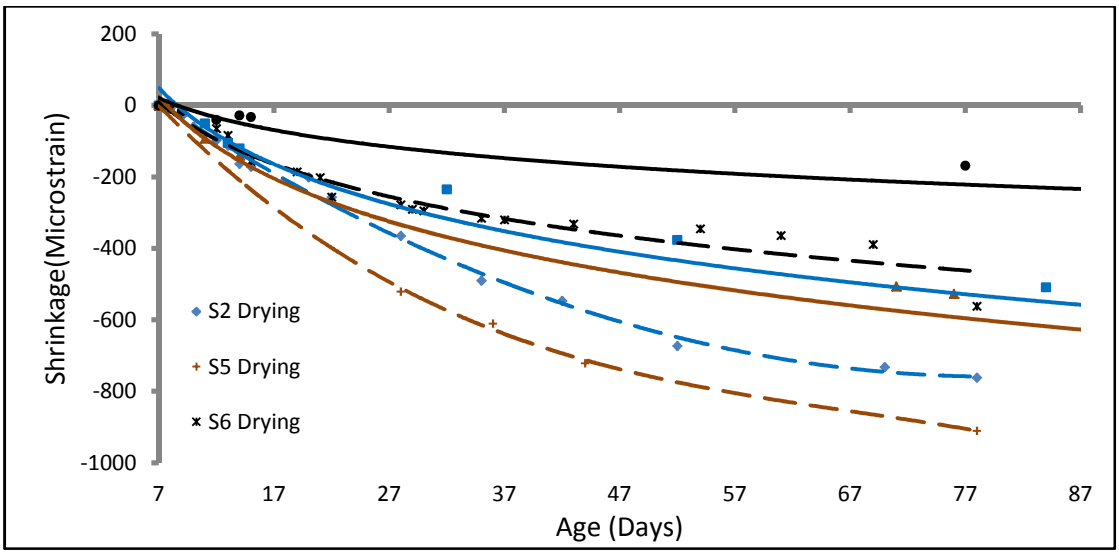

Figure 6. 23: Relationship between carbonation and drying shrinkage of AACM and OPC concrete

The carbonation shrinkage strain is lower than the drying shrinkage strain in both AACM and OPC concrete. The carbonation shrinkage strain at 80 days is 700 με, 798 με and 300 με for mixes S_2, S_5 and S_6 respectively. The corresponding drying shrinkage strain is 761 με, 910 με and 562 με for mixes S_2, S_5 and S_6 respectively. The drying shrinkage is higher due to greater water loss when compared with carbonation shrinkage. The lower volume change in the carbonated OPC concrete could be due to the water released when carbonate ion CO_3^{2-} reacts with $Ca(OH)_2$. This reaction releases two molecules of water during carbonation in OPC concrete as shown in equation 6.3: [310]

$$Ca(OH)_2 + 2H^+ + CO_3^{2-} = CaCO_3 + 2H_2O \qquad 6.3$$

In addition to the release of water during the carbonation in OPC concrete, precipitation of $CaCO_3$ is observed within the matrix of OPC concrete [302]. The precipitated $CaCO_3$ fills the capillary pores thereby reducing the stress induced by the loss of water during carbonation. The precipitation of $CaCO_3$ results in the densification and increased strength of carbonated OPC concrete [302][311].

On the other hand, the carbonated AACM concrete does not contain $Ca(OH)_2$. Instead the CO_3^{2-} reacts directly with C-A-S-H to produce decalcification within the AACM concrete matrix. The decalcification produces white spongy particles which have a low Ca content [302] which is shown in Fig. 6.24. Larger pores evolve during the carbonation of AACM concrete as a result of the decalcification of the C-S-H. The decalcification during the carbonation of AACM concrete reduces its strength

[302][311] unlike the precipitation of $CaCO_3$ in OPC concrete which increases its strength.

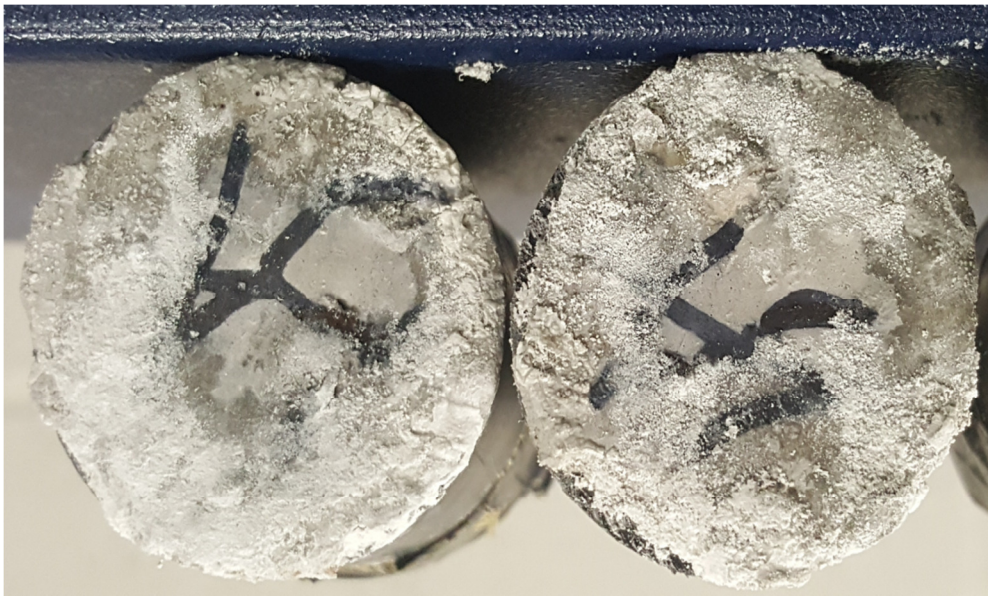

Figure 6. 24: Decalcification of C-A-S-H in AACM concrete

6.4.4 pH of Carbonated Zone

6.4.4.1 AACM and OPC Concrete and Mortar

The pH of the solutions extracted from AACM and OPC concrete and mortar powder at the carbonated zones is shown in Fig. 6.25. The pH of solutions at the carbonated zones for both AACM and OPC mortar are lower than the corresponding concrete. The difference in their solution pH is due to the release of alkaline content by the coarse aggregate present in the concrete. OPC concrete S_6 which had the highest coarse aggregate content of 1170 kg/m^3 (Table 6.2) shows the highest pH difference between the pore fluid extracted from concrete powder and mortar powder. The pH of the mortar pore fluid is considered a more realistic value of the actual pore fluid in the

mixes.

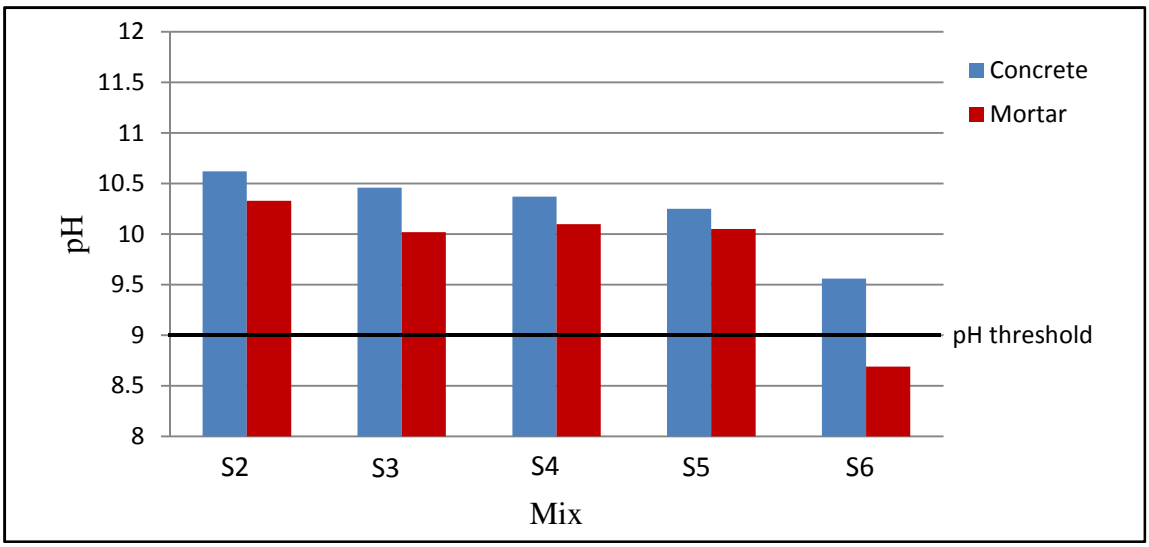

Figure 6. 25: pH of pore solutions extracted from AACM and OPC concrete and mortar powder at the carbonated zones after 360 days exposure to 5% CO_2.

The pH of pore solutions extracted from the powder at the carbonated zones of AACM concrete mixes S_2 to S_5 is above the pH threshold of 9 as shown in Fig. 6.25. The pH of the solution at the concrete carbonated zones is 10.62, 10.46, 10.37, 10.25 and 9.56 for mixes S_2, S_3, S_4, S_5 and S_6 respectively. The corresponding pH of the solutions of AACM and OPC mortar mixes M_2, M_3, M_4, M_5 and M_6 at the carbonated zones are 10.33, 10.02, 10.1, 10.05 and 8.69 respectively. The pH of the mortar pore fluid is also greater than the carbonation threshold value of 9 for all AACM mixes whereas the OPC mix S_6 has a pH value significantly lower than the carbonation threshold of 9 for the mortar fluid. The pH of the carbonated AACM mortar fluid, which is significantly above the pH threshold of 9, indicates that the phenolphthalein indicator method provides an inadequate assessment of carbonation in AACM concrete compared with OPC concrete.

The phenolphthalein test method detects carbonation in the OPC concrete when the mortar pH is below the threshold value of 9 (Fig. 6.25). However, for AACM mixes S_2 to S_5 it detects carbonation at mortar pH value exceeding 10 (Fig. 6.25) which is in the high alkalinity range. An alternative method to the phenolphthalein indicator test is required for assessing the carbonation in AACM concrete. This has also been suggested by some authors [3][294][312].

6.4.4.2 Effect of Activator Dilution

The influence of activator dilution on the pH of solutions extracted from AACM concrete and mortar powder at the carbonated zones is shown in Fig 6.26.

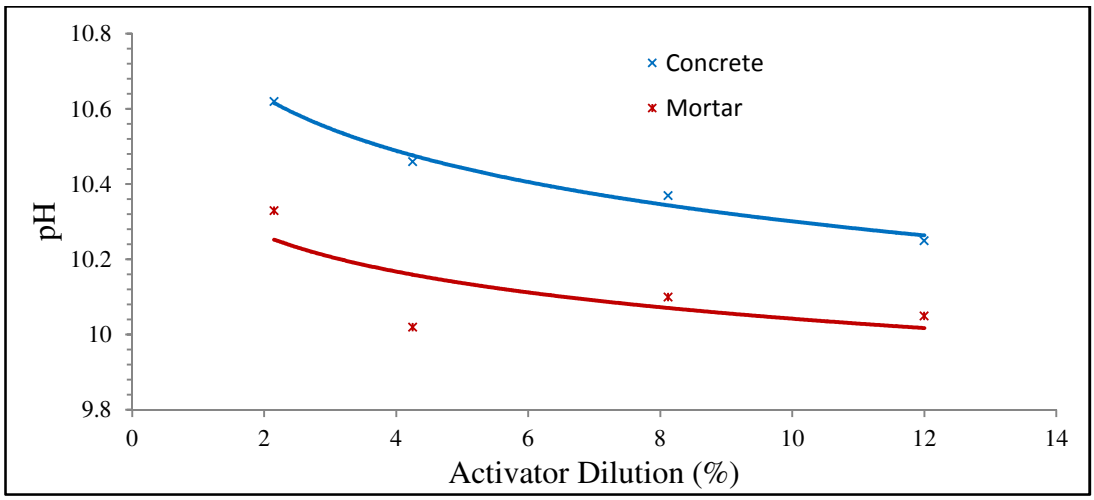

Figure 6. 26: Alkali activator dilution versus pH of pore solution extracted from carbonated AACM concrete and mortar powder.

The difference in the pH of pore solutions extracted from AACM concrete and mortar powder at the carbonated zones is fairly constant at different activator dilutions (Fig. 6.26). This is because the coarse aggregate content in AACM concrete mixes S_2 to S_5 are within the same range of 988 kg/m^3 to 1091 kg/m^3 (Table 6.2). The release of alkaline content by the coarse aggregate present in the AACM concrete mixes S_2 to S_5 accounts for the difference in the pH of solutions extracted from concrete and mortar. On the other hand, carbonation reacts chemically with AACM mortar while the concrete will influence the diffusion rate of CO_2 and moisture because of the interfacial transition zones around the coarse aggregate [290].

The pH of pore solutions extracted from AACM concrete and mortar powders is highest at the lowest activator dilution (Fig. 6.26). The difference in the pH of pore solution extracted from AACM concrete is attributed to the rate of carbonation which is discussed in section 6.4.1.3 and the leaching of alkali content from the coarse aggregate into its pore solution.

6.4.5 Relationship between Carbonation Depth and Porosity

The relationship between the carbonation depth at 327 days exposure to 5% CO_2 and effective porosity of AACM mixes S_2 to S_5 at 28 days is presented in Fig 6.27. The effective porosity of the AACM mixes S_2 to S_5 is obtained from chapter 3, section 3.4.3.4. A linear relationship is established between the effective porosity and the depth of carbonation with a correlation of 0.98

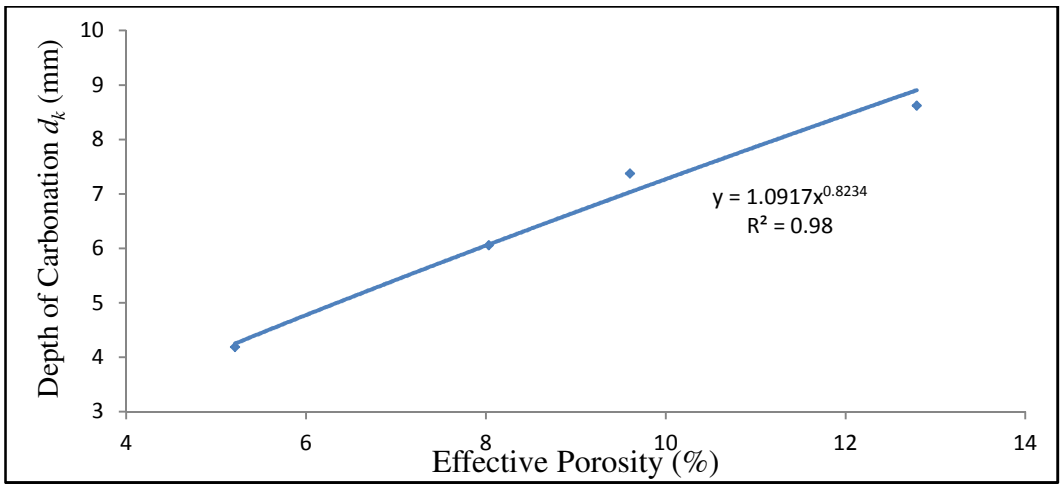

Figure 6. 27: The relationship between depth of carbonation d_k and effective porosity of AACM concrete

The lower the effective porosity of AACM concrete the lower the depth of carbonation within its matrix. The effective porosity of 5.21% produced a carbonation depth of 4.19mm while effective porosity of 12.79% resulted in 8.63 mm carbonation depth. Concrete diffusivity which is a function of porosity is a major controlling factor for carbonation [25]. The speed of carbonation at lower effective porosity is inhibited by limiting the ingress of CO_2 and moisture from the environment into the concrete.

The carbonation process is complicated because it involves the transport of liquid and gas which can not be represented with Fick's law [290]. *Lagerblad* [290] stated that it is difficult to apply Fick's law because of the simultaneous inward and outward diffusions involving these ions. The pore structure is altered during the inward and outward diffusions involving carbonate ions and calcium ions. For OPC concrete, a dense pore structure evolves as the outward diffusion of $CaCO_3$ forms precipitates that block the concrete pores. In the case of AACM, the calcium ions from the geopolymerization products disintegrate by a process of decalcification and diffuse outward into the environment. Whilst the chemical compound ($CaCO_3$) formed during the carbonation in OPC concrete blocks the pores, the disintegration of calcium ion during carbonation in AACM concrete enlarges the pores.

6.5 CONCLUSIONS

The following conclusions can be drawn based on the study carried out on the carbonation of AACM concrete.

- A lower depth of carbonation was observed in OPC concrete compared to AACM concrete. For example, the carbonation depth for AACM mix S_3 is 25.19 mm while it is 14.13 mm for OPC S_6 at 327 days CO_2 exposure. This is due to

the main hydration product of $Ca(OH)_2$ in OPC while AACMs does not have it as its geopolymerisation product.

- The rate of carbonation is higher in AACMs than OPC. For example, the rate of carbonation in AACM mixes S_3, S_4 and S_5 are 27.29mm/yr$^{0.5}$, 30.08mm/yr$^{0.5}$ and 32.68mm/yr$^{0.5}$ respectively while it is 19.62mm/yr$^{0.5}$ for OPC S_6. However, the rate of carbonation for AACM mix S_2 is lowest because of it lowest liquid/bindar ratio 0.41 compared to the liquid/binder 0.48 of other mixes.
- The carbonation and drying shrinkage is considerably higher in AACMs than OPC concrete. For example, the carbonation and drying shrinkage of AACM mix S_2 at 80 days are 700 με and 761 με while it is 300 με and 562 με for OPC S_6. This is due to the precipitation of $CaCO_3$ which fills the pore spaces in OPC concrete thereby reducing the stress induced by water loss during shrinkage.
- The drying shrinkage values are higher than carbonation shrinkage for both AACM and OPC concrete. This is because of high water loss during drying shrinkage, on the other hand, the carbonation shrinkage shows precipitation of $CaCO_3$ within the pores of OPC concrete which restrict further shrinkage.
- The pH of the carbonated zones of AACM mortar is above the carbonation threshold value of 9 while OPC mortar is below it. For example, the pH at the carbonated zone of AACM mix M_3 is 10.02 while it is 8.69 for OPC S_6. This suggests that the phenolpthalein test method might not be appropriate to determine the carbonation of AACMs.
- The pH of AACM and OPC concrete is higher than mortar which suggests the release of alkaline content by the aggregates. For example, the pH of concrete mixes S_3 and S_6 are 10.46 and 9.56 compared with 10.02 and 8.69 of its corresponding mortar mixes M_3 and M_6 respectively.
- A non-linear relationship of the form $y = 1.0917x^{0.8234}$ and a coefficient of 0.99 is established between depth of carbonation and the porority of AACM concrete.

CHAPTER 7

CHLORIDE-INITIATED REINFORCEMENT CORROSION IN AACM CONCRETE

7.1 INTRODUCTION

The integrity of reinforced concrete structures may be undermined by the corrosion of steel reinforcement embedded in them. Factors affecting the durability and sustainability of reinforced concrete structures are attributed to the rate at which steel reinforcement corrodes under the prolonged influence of corrosion initiators like chloride and carbon dioxide. Addressing these durability concerns require specialist skills and incur huge maintenance cost and time. For example, an estimated £550m per year have been accrued in repairs and structural failures of OPC concrete structures in the UK alone due to this corrosion mechanism [15].

Chloride ingress and carbonation of concrete are the leading factors that induce corrosion of steel bars or fibres embedded in concrete [314][315]. The presence of moisture and oxygen within the concrete matrix will sustain the corrosion mechanism induced by these corrosion initiators [252][316]. The chloride and CO_2 interact with the concrete matrix in ionic solutions while oxygen is consumed during the corrosion process. There is the possibility of a cost reduction in the repairs and structural failures due to chloride induced corrosion in AACM concrete structures compared with OPC concrete structures. This is because the rate of chloride ingress in an AACM concrete matrix is lower than for OPC concrete (Chapter 4, Section 4.4.3). This suggests a longer time for chloride-induced corrosion to initiate in reinforced AACM concrete compared with reinforced OPC concrete structures. This will be validated in this chapter while also conseidering other key factors which initiate corrosion.

On the other hand, the rate of carbonation in AACM concrete seems to be higher than OPC concrete when using the phenolphthalein test method (Chapter 6, Section 6.4.1). The suitability of the phenolphthalein test method for the carbonation of AACM concrete has raised some concerns. This is because of the high pH of the pore solution at the carbonated zone (indicated by phenolpthlein test) of AACM concrete which is above the threshold level of 9 (Chapter 6, Section 6.4.2). The phenolpthlein test, however, applies to the control OPC concrete and the pH of the carbonated zone remains below the threshold of 9. This suggests that an alternative test method should be adopted for AACM concrete instead of the phenolphthalein indicator method. *RILEM TC 224-AAM* [3] states that the use of phenolphthalein indicator method for

carbonation of AACM concrete may be over simplified. The phenolphthalein indicator method detects the depletion of $Ca(OH)_2$ in OPC concrete, which is responsible for its alkalinity, whereas AACM geopolymerization products do not contain $Ca(OH)_2$. Carbonation-initiated corrosion in OPC concrete is activated when its pore solution pH is less than 9 [25]. Therefore, AACM concrete is likely to have good resistance to chloride and carbonation induced corrosion. Only the chloride induced corrosion will be investigated in this chapter.

The diffusion of chloride and CO_2 in concrete is in solution with water, which is largely dependent on the pore structure of the concrete. The pore structure of AACM concrete reveals lower intrudable porosity than OPC concrete (Chapter 3, Section 3.4.3). The refined pore structure of AACM will contribute to resisting the ingress of these deleterious substances.

The reaction of the diffused corrosion initiators with the steel reinforcement is well documented in literature for OPC concrete but only partially understood in AACM concrete. The steel reinforcement in OPC concrete is largely protected from corroding by the hydration product $Ca(OH)_2$ which is not present in AACM concrete [3]. Chloride ions and carbonic acid, when present in the OPC concrete matrix, will deplete the thin protective layer around the steel reinforcement [314][316]. This thin protective film of (Fe_2O_3 or Fe_3O_4) produced during the hydration process in OPC concrete is destroyed when the pH of the concrete pore solution is low to about 9. Once the protective thin film is disrupted, chloride ions and carbonic acid (formed when carbon dioxide dissolves into the pore water) react with the steel reinforcement surface to form ferrous chloride $FeCl_2$ and ferrous carbonate $FeCO_3$ respectively [25]. The ferrous chloride or carbonate reacts with moisture to form ferrous hydroxide $Fe(OH)_2$ which is commonly referred to as rust [317]. For AACM concrete, the corrosion resistance is maintained by the high pH provided by the alkali activator concentration [318] unlike the thin protective oxide layer, $Ca(OH)_2$, present in reinforced OPC concrete. The influence of activator concentration of AACM concrete in resisting the chloride-initiated corrosion will be investigated in this chapter.

7.2 LITERATURE REVIEW

7.2.1 Introduction

Steel reinforcement corrodes in a neutral or acidic medium but remains passive in an alkali medium. The high alkali pH of OPC concrete pore solution prevents the embedded steel reinforcement from corroding. A thin protective film develops around

the steel reinforcement in OPC concrete which acts as an effective barrier to aggressive elements such as carbonic acid and chloride ions. This protective film is composed of an inner anhydrous oxide layer (Fe_2O_3 or Fe_3O_4) which is approximately 2.5nm thick and an outer hydrous layer approximately 1nm thick [319]. Khan [320] monitored the development of passivity of steel reinforcement embedded in concrete for 648 days from the day of casting. The curing period included 53 days immersion in potable water followed by 595 days exposure to laboratory air. The author observed that it took more than a year for the embedded steel reinforcement to attain a passive state.

The geopolymerisation of AACM concrete does not produce $Ca(OH)_2$ [3] nor does it generate a protective thin film in the manner of OPC concrete. The corrosion behaviour of steel in AACM concrete is strongly dependent on the type and concentration of activator used [318]. It is suggested that a high resistance to steel reinforcement corrosion is provided by NaOH and KOH when monitored by galvanic corrosion and half-cell potential. The high alkalinity of the pore solution provides the protective barrier against the corrosion initiators.

The passivity of the embedded steel reinforcement is destroyed once a low pH reaches the vicinity of the steel surface [25]. This is because the protective thin film adhering to the surface of steel reinforcement in OPC concrete is no longer maintained and corrosion begins in the presence of oxygen and moisture. This process is termed depassivation of steel. The depassivation of steel reinforcement in AACM concrete is not fully understood. However, it has been suggested that the corrosion resistance of steel reinforcement in AACM concrete is aided by the nature and dosage of the binder, type of activator and the prevailing internal condition of the concrete [321][322]. The nature and dosage of the binder will play a vital role in the concrete microstructure while the reaction products will not generate a protective oxide layer formed over the steel surface in the manner of OPC concrete. The activator type is suggested to induce a protective barrier against the corrosion of steel reinforcement [318]. The effect of prevailing internal conditions on the corrosion of steel reinforcement in AACM concrete would then be similar to OPC concrete.

Many authors investigated the corrosion behaviour of steel reinforcement in concrete by using accelerated corrosion techniques such as applying an anodic current to the rebar. Limited information is available on natural corrosion techniques. The chloride-induced corrosion was investigated by using the natural technique of bulk immersion of specimens in 5% NaCl solution and drying in laboratory air which is modelled after a reinforced marine structure [91]. It is unlikely that the accelerated

corrosion techniques will provide true representation of steel corrosion behaviour in AACM concrete while in service [3]. Hanson [239] stated that any technique designed to accelerate the corrosion process should be considered with sceptism.

7.2.2 Corrosion process

The corrosion process of steel reinforcement is the same in both AACM and OPC concrete structures. Corrosion of steel is an electrochemical process involving two reactions; oxidation (anode) and reduction (cathodic). Fig. 7.1 shows a schematic representation of the corrosion cell of the anodic and cathodic sites on the steel surface. The anodic and cathodic reactions on the steel surface are mutually dependent on each other and must be in balance.

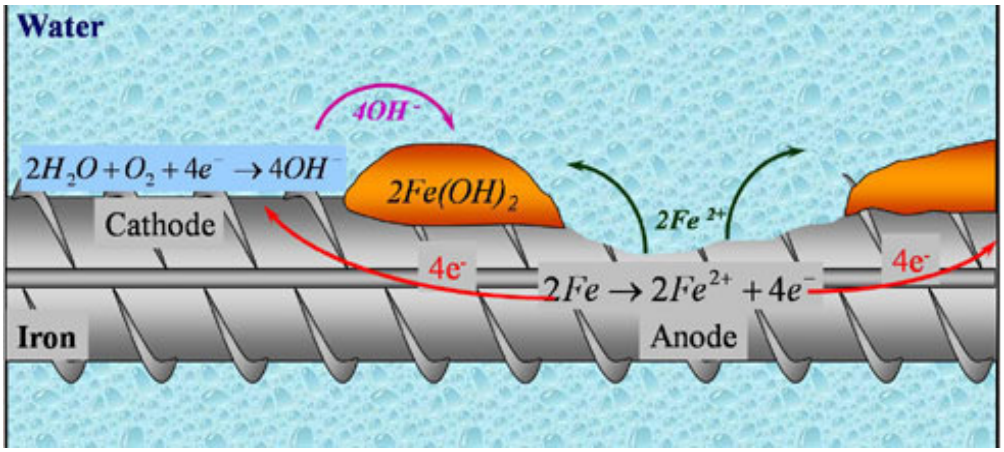

Figure 7. 1: Schematic illustration of steel reinforcement corrosion showing the anodic and cathodic sites on the steel surface [323]

The potential difference between adjacent areas on the steel reinforcement causes the release of electrons in order to preserve electrical neutrality [324]. The electrons are released from the most negative sites which are the anodic sites. This release of electrons from the most negative site creates a positive site which is the cathodic site. Therefore, the surface of the corroding steel functions as a mixed electrode that is a composite of both anodes and cathodes electrically connected through the body of the steel. The pore solution of the concrete serves as the electrolyte to complete the corrosion cell as shown in Fig 7.1.

7.2.2.1 The Anodic Reaction

The corrosion of steel reinforcement dissolves iron into the concrete pore solution as ferrous ions at the anodic site as shown in Fig 7.1. The oxidation of iron atoms in the pore solution releases two electrons which are negatively charged. In order to maintain electrical neutrality on the steel surface, the build-up of negatively charged electrons at the anodic site will be consumed elsewhere on the steel surface at the

cathodic sites [325]. This is because there cannot be large amounts of electrical charge building up at one place on the steel surface [324]. Equation 7.1 shows the the anodic reaction.

$$Fe \rightarrow Fe^{2+} + 2e^{-} \qquad 7.1$$

7.2.2.2 The Cathodic Reaction

The negatively charged electrons at the cathodic site react with oxygen and water from the concrete pore solution as shown in Fig 7.1. Hydroxyl ions are generated by this reaction which increases the local alkalinity thus strengthening the passitivity of steel reinforcement at the cathodic site [324]. The passivation of the steel surface decreases at the anodic site but increases at the cathodic site. The reverse reaction of corrosion by applying current can be used to address the decrease in the steel surface passivation at the anodic site which is reffered to as cathodic and galvanic protection. Equation 7.2 shows the the cathodic reaction.

$$2e^{-} + H_2O + \frac{1}{2}O_2 \rightarrow 2OH^{-} \qquad 7.2$$

The redox (oxidation – reduction) reactions are shown in equations 7.3 - 7.5

$Fe^{2+} + 2OH^{-} \rightarrow Fe(OH)_2$ Ferrous hydroxide *7.3*

$4Fe(OH)_2 + O_2 + 2H_2O \rightarrow 4Fe(OH)_3$ Ferric hydroxide *7.4*

$2Fe(OH)_3 \rightarrow Fe_2O_3.H_2O + 2H_2O$ Hydrated ferric oxide (rust) *7.5*

7.2.2.3 The Pourbaix Diagrams

The potential of steel reinforcement embedded in a concrete depends on a set of factors such as the standard potentials of the anodic and cathodic reactions, temperature, and composition of the concrete pore solution with its ionic concentration [326]. The influence of concrete pore solution and its ionic concentration on the steel potential is expressed by Pourbaix [327] using pH–potential diagrams (Fig. 7.2). These diagrams represent the conditions of potential and pH where a particular corrosion reaction is thermodynamically favourable. It should be noted that the diagrams are based on the thermodynamics of the reactions and are not empirical. The diagram is divided into three main zones: corrosion, immunity and passivation.

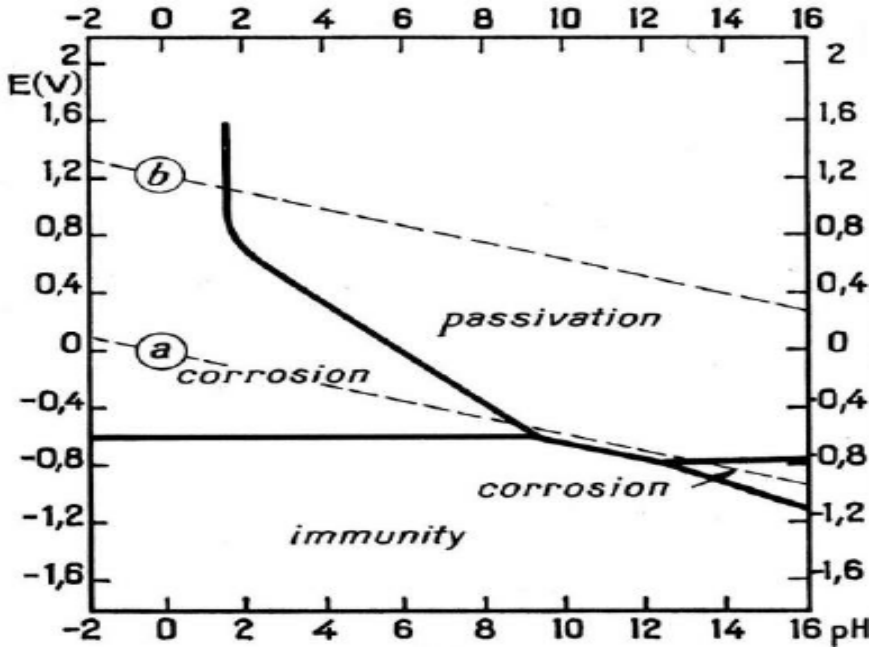

Figure 7. 2: Pourbaix diagram showing the potential pH of iron in aqueous solutions [327]

7.2.3 Types of Corrosion

Corrosion may proceed by uniform dissolution of steel surface which is referred to as generalised corrosion or localised corrosion which attacks metal grains locally to form pits [328][329][330].

7.2.3.1 General or Uniform Corrosion

The rate of corrosion under this category proceeds uniformly over the entire steel surface. The corrosion rate is slower under the general corrosion than the localised corrosion [330] although, a greater overall quantity of rust may be generated in the general corrosion type because of the large surface area affected. General corrosion is characterized by a uniform distribution of anodes and cathodes over the metal surface [331] unlike localised corrosion which has essentially fixed positions of the anode and cathode. General corrosion will lead to a gradual thinning of the metal until the section fails [331].

7.2.3.2 Localised Corrosion

In the case of localised corrosion, the corrosion is focussed on certain parts of the metal surface before spreading out as the corrosion develops [331]. There are three common form of localised corrosion: pitting, crevice and bimetallic corrosion.

7.2.3.2.1 Pitting corrosion

Pitting corrosion is initiated in reinforced concrete due to a localized breakdown of the protective oxide film on the steel surface by aggressive elements such as chloride

[331][332]. The rate of corrosion is rapid, preferentially attacking small phases on the metal [332]. Pitting corrosion produces cavities or mouths which can be open or occluded (covered) with semi permeable corrosion products [333]. The cavities become visible over a period of time which is dependent on the material and its environment [332]. These cavities can induce fatigue or stress corrosion at the base which, under certain conditions, could lead to catastrophic failure [333]. Such catastrophic failure induced by pitting corrosion occurred in Mexico, where a single pit in a gasoline line running over a sewer line was blamed for the death of 215 people in Guadalajara [333].

7.2.3.2.2 Crevice corrosion

Crevice corrosion is another localized form of corrosion involving the attack of stagnant solution in crevices such as washers, lap joints and clamps, under gaskets, insulation material, surface deposits, fastener heads, disbonded coating and threads [333]. Poor welding can also form crevices, which can then lead to corrosion [332]. Crevice corrosion is initiated when there is a depletion of oxygen within the crevice, the shift in acid condition and build-up of aggressive ions at the crevice can also initiate this form of corrosion [333].

7.2.3.2.3 Bimetallic corrosion

Bimetallic corrosion, also known as galvanic corrosion, is encountered when two metals with significant potential difference are in contact within a common electrolyte. A number of factors contribute to bimetallic corrosion such as an environment able to induce thermodynamic instability in the anode, the presence of an electrolyte bridging the two metals, electrical connection between the two metals and a sustained cathodic reaction on the more noble metal [332].

7.2.4 Corrosion Mechanisms in Concrete

Chloride and carbonation have been identified as the two major corrosion initiators for steel reinforcement in concrete and do not require degradation of the concrete before the steel is attacked [334]. The increased volume of the corrosion product induces the degradation of the concrete though cracking, delamination and spalling, which in turn further promotes the problem [334]. These corrosion initiators have been investigated independently in Chapters 4, 5 and 6.

7.2.4.1 Chloride induced corrosion

Corrosion induced by chloride attack on reinforced concrete is a common cause of deterioration in structures [3]. Chloride ions which are responsible for this type of

corrosion are described as "a specific and unique destroyer" [335]. The chloride contamination can be from cast-in calcium chloride used as a set accelerator, cast-in salt from contaminated mix constituents, chloride ingress from marine environments or de-icing salt ingress from roads [336]. Chloride can be present in OPC concrete in three forms which are free chloride dissolved in pore solution, physically bound chlorides to the wall of the binder and chemically bound chlorides to the hydrates of calcium aluminates [90]. However, the presence of chemically bound chlorides in AACM concrete is minimal compared to OPC concrete as shown in Chapter 4, Section 4.4.3.7. *RILEM TC 224,* [3] describes how, unlike OPC concrete, there is no Friedel's salt present in AACM concrete nor any other crystalline chloride compounds which can chemically bind chlorides..

The presence of chlorides at the vicinity of the steel surface can locally destroy the passive film, thus initiating localised corrosion. Chloride induced corrosion occurs as pitting. The breakdown of the passive film described by *Jovancicevic et al.* [337] involves the adsorption-displacement, chemico-mechanical and migration-penetration of the steel passive layer. *Legault et al.* [338] reported that the destruction of the protective film on the steel surface is due to the adsorption of Cl^- with simultaneous displacement of O^{2-} at its surface. A model developed by Chao [339] suggests that the Fe^{2+} complexes are formed when Cl^- reaches the steel occupying O^{2-}. This results in a decrease in oxygen vacancies while the Cl^- increases at the film/solution interface. The formation of voids leading to pit growth evolves from this reaction.

The reaction of Cl^- and the displacement of oxygen at the film/solution interface for steel reinforced OPC concrete may not necessary apply to AACM concrete. The mechanism of steel protection by the passive thin film where oxygen is displaced during pit growth is not present in the case of steel reinforcement embedded in AACM.

The depassivation of steel reinforcement in concrete is influenced by the concrete mix, type of binder, C_3A content of binder, curing method, water content in the concrete and presence of mineral admixtures because they influence chloride diffusion in concrete. AACM concrete has a more refined pore structure than OPC concrete and thus higher resistance to chloride penetration as shown in Chapter 4, Section 4.3. Significant reduction of chloride ingress is observed in concrete containing mineral admixtures compared with OPC concrete. For example, It was observed that higher resistance to chloride ingress occurs in concrete containing fly ash, microsilica and slag compared with OPC concrete [50][188]. The use of mineral admixtures improves the concrete pore refinement thus providing resistance to chloride ingress. However, the

tricalcium aluminate (C_3A) content which plays a vital role in chloride binding is higher in OPC concrete than AACM concrete. Increases in the water/cement ratio results in higher chloride diffusion [340], although it has been suggested that the water-cement ratio does not affect chloride penetration at depths greater than 20 mm [188].

The chloride content at the steel depth that is required for the breakdown of the local passive film and thereby initiate corrosion is referred to as the chloride threshold level [341]. This can be presented as the ratio of chloride to hydroxyl ions [Cl^-/OH^-] in the pore solution. Much research has been been carried out on the threshold levels of chloride in concrete but a universal value has not been established.

The threshold value of 0.61 for the [Cl^-/OH^-] concentration proposed by *Hausmann* [255] for the initiation of corrosion in cement based materials does not always apply. For example, *Lambert et al.* [170] presented a [Cl^-/OH^-] concentration threshold of 3 for steel rods embedded in OPC concrete. A [Cl^-/OH^-] concentration as high as 320 did not result in corrosion of steel fibres embedded in fly-ash concrete [102]. The reasons attributed to such high values were the lower chloride binding capacity and pH of Hausmann composition [255], which increases the [Cl^-/OH^-] ratio in its pore solution. In addition, the reduced chloride ingress and oxygen content due to tight pore structure depresses the steel potential.

7.2.4.2 Carbonation induced corrosion

The primary effect of carbonation on concrete is to reduce the pH of the pore solution to below 9 [275][276]. The pH of concrete pore solution is reduced when atmospheric carbon dioxide CO_2 dissolves in concrete pore water to form carbonic acid (HCO_3) which can then react with the main hydration products of OPC concrete, $Ca(OH)_2$ and C-S-H, to form calcium carbonates ($CaCO_3$) [277][278]. The hydroxyl ion $(OH)_2$ within the pore solution of OPC concrete is displaced by this reaction thereby causing the depletion of the protective passive film around the steel in concrete. The progression of these reactions can result in carbonation induced corrosion when oxygen and water are present.

The rate of carbonation depends on both the quality of the OPC concrete (mainly its alkalinity and permeability) and a number of environmental factors (humidity, temperature and CO_2 concentration). It has been reported that concrete with low permeability typically has good resistance to CO_2 penetration [90][342]. Increased OPC cement content of concrete is reported to retard the rate of CO_2 penetration [343]. The hydration products of OPC concrete (calcium silicate hydrates [C-S-H] and

ettringite/monosulphate [AFt/AFm]) dissolve as the alkalinity of the pore solution drops due to carbonation. First, the C-S-H dissolves at around pH11.6 and then ettringite at around pH10.6. In concrete with partial cement replacement, the hydration products will dissolve faster, leading to a faster rate of carbonation. This is due to the secondary pozzolanic reaction that consumes part of the free lime ($Ca(OH)_2$) responsible for the high pH of its pore solution. The geopolymerization products of AACM concrete do not contain the free lime responsible for the high pH in OPC concrete. The high pH in AACM is influenced by the concentration of alkali activator. The chemistry of how carbonate ions will react with different activators and subsequently dissolve other geopolymerization products of AACM concrete is not yet fully researched.

7.2.5 Service Life of Reinforced Concrete Structures

The service life of reinforced concrete structures is reduced by the action of corrosion on the embedded steel reinforcement. The synergetic effect of mechanical and environmental loads on reinforced concrete structures will give a realistic design load for service life predictions [344]. Mechanical loads such as the design live and dead loads combined with the time dependent induced damage from the environment such as carbonation, chloride ingress and frost damage, act simultaneously to reduce the service life of the structure.

7.2.5.1 Service life models

A number of models have been developed to characterize the corrosion of reinforcement in concrete and predict its service life. A widely used service life model was proposed by *Tuttii* [90] as shown in Fig. 7.3. This model is subdivided into the initiation and propagation stages of corrosion in reinforced concrete. The initiation stage is the period when deleterious substances such as chloride and CO_2 penetrate the concrete cover to induce steel depassivation. Corrosion commences at the end of the initiation period [90]. There is a threshold interface between the initiation and propagation stages of corrosion. This threshold gives the amount of deleterious substances around the steel reinforcement that might initiate the corrosion process. The propagation stage is when reduction in the metal thickness commences which leads to concrete deterioration such cracking, delamination and spalling.

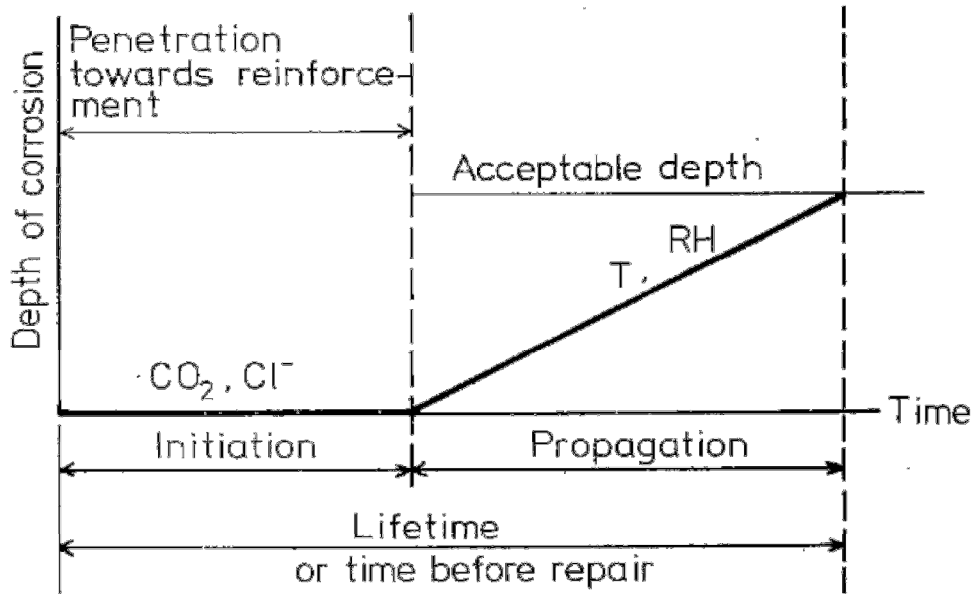

Figure 7. 3: Schematic model of corrosion process in steel reinforced concrete [90]

Beaton and Stratfull [345] developed a model to evaluate the environmental influence on the corrosion of 239 bridges constructed over the past 50 years across the state of California. The model predicts the estimated time of cracking in a reinforced concrete submerged in sea water. The modified version of the model of *Beaton and Stratfull* [345] was presented by *Virmani et al.,* [346]. The corrosion data used for the model was based on the application of 3% solution of sodium chloride to a reinforced concrete slab. Other models presented in literature [347][348][349] assume chloride induced corrosion based on the diffusion theory whilst neglecting the interaction of chloride ions with the gel phase. However, the reliability of these models were disputed by *Papadakis* [350] who argued that the ingress of chloride in concrete is a more complex and complicated transport process than was described by Fick's law of diffusion. These models capture only the corrosion initiation stage (Fig. 7.3).

Predictive models that capture the corrosion propagation in reinforced concrete often assume a uniform loss of steel thickness [351]. Examples of such models were presented by *Thoft-Christensen* [352] and *Vu* [353]. However, this assumption does not accurately depict the chloride induced corrosion of reinforced concrete which usually experiences pitting corrosion. An alternative model for the corrosion of RC slab bridges was developed by *Val and Melchers* [354]. This model takes into account the pit formations due to chloride induced corrosion as shown in Fig. 7.4. *Gonzalez et al.*, [355] used the same model on small dimensions (50 x 50 x 10 cm and 20 x 15 x 10 cm) of reinforced concrete. The author suggested that the maximum depth of pit due to chloride induced corrosion is about four to eight times the average general corrosion.

The size of the embedded steel is 0.8 cm and the first batches (50 x 50 x 10 cm) were exposed to repeated wet/dry cycles. The wet curing of the specimens was in an aqueous solution of 3% $CaCl_2$ by water weight and the dry curing in the laboratory air at a relative humidity of 50% to 60%. However, the second batch (20 x 15 x 10 cm) were submerged in natural sea water at insituto de cinencias del mar (CSIC) of Barcelona. The salinity of the seawater was 28 g/l, the temperature varies between 14^0 C to 24^0 C in summer and oxygen content of 5 ppm. The two batches were cured for 6 years [355].

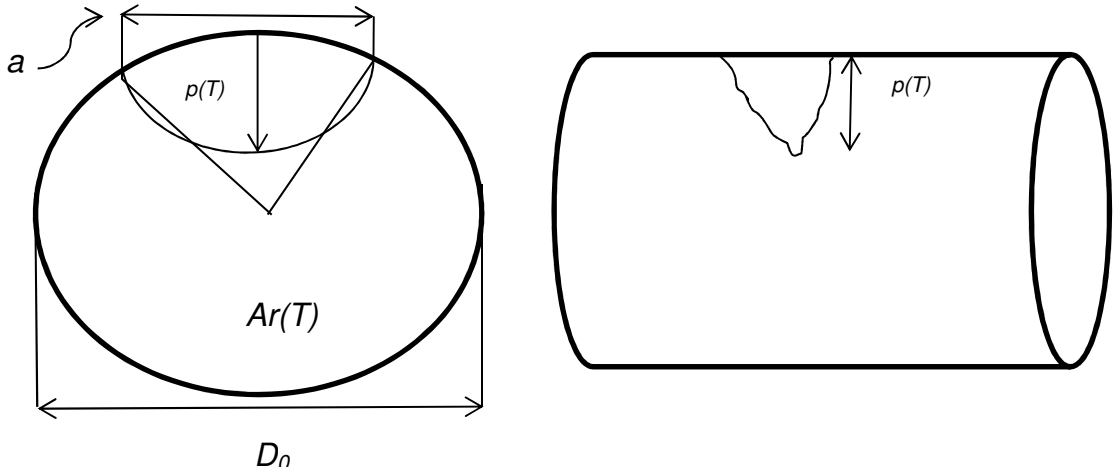

Figure 7. 4: Schematic model of pit formation during chloride induced corrosion [354]

The symbols in Figure 7.4 are as follows: ***p(T)*** is the time of pit formation; ***D_0*** is the initial diameter of rebar (mm); ***a*** is the net section of the corroded rebar and ***Ar(T)*** is the section of the un-corroded bar. Pits may be of various shapes, but the author assumed a hemispherical shape of pits for simplicity sake.

Darmawan and Sterwart [356] adopted the model on a larger prestressed concrete speciamen (150 cm x 100 cm x 25 cm) embedded with wires/strands. The authors suggested that the distribution of maximum pits for prestressing wires is best represented by the Gumbe (EV-type 1). The concrete mix design has 0.5 w/c ratio, $f_c^{'}$ of 40 MPa and a 3% $CaCl_2$ by concrete weight was added during concrete mixing. The specimens were cured for 28 days before performing an accelerated corrosion test.

The service life assessment of steel reinforced structures does not account for the synergy of combined loads from the environment (chloride and CO_2) and mechanical (live and dead) loads. These combined loads acting simultaneously are crucial for structural safety and should therefore be incorporated in the service life design [357]. Somodikova et al., [357] suggested that the mechanical loading may cause cracking and pore structure changes in concrete that can result in reduced service life for the structure. *Val and Melchers* [354] used a probabilistic approach to investigate the effect of material fatigue and overloading on the corrosion behaviour of a reinforced concrete

bridge. The two corrosion types (general and localised) were used in the reliability model. The authors suggested that the main risk associated with the general corrosion type is the loss of bond between the concrete and the corroding steel while the localised corrosion is dominated by ductile failure which affects the bridge reliability significantly.

7.2.5.2 Corrosion damage in steel reinforced concrete

The corrosion of steel reinforcement is the leading cause of deterioration in concrete structures. This deterioration process does not attack the concrete directly unlike, for example, the actions of sulphate and acid which can disintegrate the concrete before the embedded steel reinforcement is affected. Severe cases of corrosion damage are observed in marine structures that are constantly exposed to wet and dry cycles of salt spray. For example, about 40% of the 581,862 bridges in the USA were observed to be either structurally or functionally deficient due to the extensive loss of serviceability and reduced safety [358]. In the United Kingdom, the estimated annual cost of corrosion damage is £616.5 million (approximately one billion US dollars per year) which is largely caused by salt-induced corrosion on motorway and trunk road bridges in England and Wales [359]. The conclusion was based on the survey carried out on 10% of the total bridges constructed in the UK [359].

The rust produced during corrosion leads to volume increase at the steel/concrete interface. The volume increase at the interface has been observed to be six to ten times more than the space occupied by uncorroded steel [324] consequently developing tensile stresses within the concrete matrix. The reinforced concrete cannot accommodate the tensile stresses induced by the rust product at the steel/concrete interface thus resulting in cracking and spalling of the concrete cover [25]. The loss of concrete cover will expose the rebar to further corrosion process at an accelerated rate. Moreover, corrosion reduces the cross-section of the steel thereby reducing the load bearing capacity. The cross-section of the rebars are reduced faster by pitting (i.e. localised) corrosion than the generalised corrosion [331]. The reduction in the cross-section will reach a point where it can no longer withstand the applied load, potentially leading to catastrophic failure of the structures [360].

McLeish [361] pointed out several factors which may impair the ultimate load capacity of structural elements, such as; loss of reinforcement area and ductility, delamination of cover to tension reinforcement, bulking of compressive reinforcement, loss of cover in the compression zone, reduction of bond strength and possible

secondary actions. Similarly, *Almusallam et al.* [362] suggested that the load carrying capacity of corroded reinforced concrete slab decreases due to the reduction in the cross-sectional area of the rebars particularly where corrosion was concentrated. In addition to the strength reduction of the slab, brittle failure was also observed. The load carrying capacity of corroded beams was not only reduced by the strength reduction of the rebar, but also by the cracks formed during the corrosion process *Uomoto* [363]. The author observed a reduction in load carrying capacity by 4% to 17% which results from a weight loss of 1% to 2.4% in the main reinforcing steel [363]. In another experiment performed by *Cabrera* [364], the author reported a 20% reduction in the ultimate bending moment due to the reduction of the cross section of the bottom bar by 9%.

The bond behaviour of steel reinforced concrete is significantly affected by the corrosion process. A study on the influence of reinforcing bar corrosion and cracking on the bond strength of reinforced concrete was carried out by *Al-Sulaimani* [365]. The author used a beam dimension of 150 x 150 x 1000 mm reinforced with one 12 mm Ø bottom bar, two 10 mm Ø top bars and 6 mm Ø closed stirrups at 50 mm spacing. Accelerated corrosion of the 12 mm Ø bottom bar was achieved by applying a constant current density of 2 mA/cm^2. The test load has a shear span of 300 mm; the beam shows a reduction in the load carrying capacity which was attributed to the reduction of cross section of the bar. Also, the ultimate bond capacity increases when corrosion was up to 0.5% and then decreased beyond 5% corrosion. A similar trend was observation by *Mangat and Elgarf* [366] on the bond characteristics of reinforced concrete beams which were subjected to corrosion. The bond strength at the steel and concrete interface increased when the degree of corrosion was up to 0.4% and the decreased beyond 0.4% corrosion [366]. A maximum increase of 25% bond strength was observed at 0.4% degree of corrosion. On the other hand, *Val et al*., [367] observed that a complete loss of bond has insignificant effect on bridge reliability in flexure. The author used a non-linear finite element model and probabilistic model for bond characteristics, corrosion propagation, material properties and reinforcement placement to analyse the effect of reinforcement corrosion on the reliability of highway bridges [367].

7.3 EXPERIMENTAL PROGRAMME

7.3.1 Sample Preparation

7.3.1.1 Preparation of steel bars and electrical connection

The corrosion test specimens were prepared by embedding 8 mm Ø high strength plain steel reinforcement bars in AACM and control OPC concrete. The length

of the steel reinforcement bar is 400 mm. The steel reinforcement bars were grit blasted to remove all mill scale, rust and foreign matter as shown in Fig 7.5 The steel bars were prepared to the visual standard Grade Sa $2^1/_2$ during the grit blast cleaning [368]. Grade Sa $2^1/_2$ involves thorough blast cleaning to remove almost all mill scale, rust and foreign matter, followed by dry vacuum cleaning with compressed air or a clean brush [368]. The steel surface colour after the grit blast cleaning was greyish as shown in Fig 7.5.

Each steel bar was weighed to the nearest milligram after grit blasting. A 4 mm thread was tapped at one end of the reinforcing steel bar to accommodate a copper wire connection. This was followed by casting a thin cylindrical layer of cement slurry having a w/c ratio 0.5 between 100 mm and 20 mm from the bar end (Fig 7.6). The thickness of the slurry was nominally 3 mm around the steel bar. An epoxy resin was applied over the hardened cement slurry and beyond to end of the bar, which covered the copper wire connection at the end. All this was carried out to avoid crevice corrosion at the electrical junction. The epoxy was cured in air to completely seal the end connections of the steel bars from chloride ion penetration (Fig. 7.7). Care was taken to prevent the epoxy from coming in direct contact with the steel surface to be embedded in the AACM and OPC concrete matrix. This is to prevent isolation of the electrical connection and the possible formation of a crevice. Each corrosion specimen had three steel bars embedded in the AACM and OPC concrete as shown in Fig. 7.8.

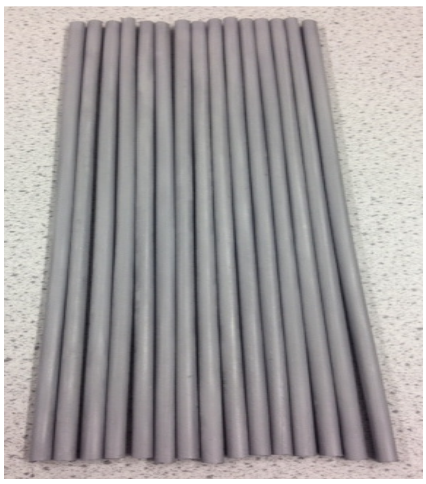

Figure 7. 5: Grit blasted steel bars

Figure 7. 6: Cement slurry cast at the bar end.

Figure 7. 7: Wire connection at one end

Figure 7. 8: Bars positioned in moulds

7.3.1.2 Casting

Expanded polystyrene moulds were used to cast 250 x 250 x 75 mm reinforced slabs for AACM and the control OPC concrete**.** The expanded polystyrene moulds were drilled at the opposite side faces to allow for proper placing of the three steel bars in each specimen as shown in Fig. 7.8. The concrete cover to the steel bars was 30 mm. This was measured from the bottom of the expanded polystyrene mould to the surface of the steel bars. The expanded polystyrene mould opening around the steel bar was completely sealed off to prevent outward pouring of concrete through any gap in the opening. The inside of the expanded polystyrene mould was lightly covered with mould oil to prevent the concrete from sticking. This was followed by cleaning of the steel surface with acetone to degrease the surface and remove any other dirt. The expanded polystyrene moulds with the properly positioned steel bars inside were placed on the vibrating table for casting.

The mix compositions used for the corrosion specimens were the same as those for the chloride ingress investigation which is detailed in Section 4.3.1, Chapter 4. They are given in Table 7.1. All the aggregates were in a saturated surface dry state before mixing. Half of the aggregate content was first poured into a forced action concrete mixer of 150 kg capacity followed by the binder. The remaining half of both the fine and coarse aggregate content was then added to cover the binder. The binder and the aggregates were mixed for one minute. Approximately half of the liquid activator was added to the mixer and mixed for two minutes. To ensure homogeneity, the mix was briefly mixed by hand, particularly concentrating on the material adhering to the edge and corner of the mixer. The retarder reagent was mixed with the second half of the liquid activator and stirred until fully dispersed. The mixture was then added to the

mixer and mixed for a further two minutes. A shrinkage reducing admixture was then added followed by an additional one minute of mixing.

The expanded polystyrene moulds with the correctly positioned steel bars inside were filled with concrete in three layers. Each layer was compacted on the vibrating table for up to 60 seconds to attain homogeneity and minimise the presence of voids. The AACM and control OPC concrete surface was gently trowelled to obtain a smooth and level finish. The cast specimens were placed on a flat table surface and covered with polythene sheets to prevent moisture loss. Two specimens were cast for each AACM and the control OPC concrete mixes (S_2 to $S_{6,}$ Table 7.1). A total of ten concrete specimens which consist of batches "a" and "b" (five specimens in each batch) were cast for the corrosion test. Each batch ("a" and "b") were subjected to different corrosion inducing curing regimes as detailed in Section 7.3.1.3 and as shown in Table 7.2.

Table 7. 1: Composition of AACM and control OPC concrete mixes

Mix	Total Binder (Kg/m^3)	Coarse Aggregate(Kg/m^3)		Fine Aggregate (Kg/m^3)	Alkali activator (Kg/m^3)	Extra water (Kg/m^3)	Total Liquid (Kg/m^3)	Liquid/ Binder Ratio	Activator Dilution (%)	Retarder (Kg/m^3)	SRA (Kg/m^3)
		10mm Gravel	6mm Limestone								
S_2	688	654	334	438	279	6	285	0.414	2.15	8	21
S_3	619	717	374	423	283	12	295	0.477	4.24	7	19
S_4	619	717	374	423	271	22	293	0.473	8.12	7	19
S_5	619	717	374	423	260	31	291	0.470	12.00	7	19
S_6(Control)	350	769	401	585	-	170	170	0.486	-	-	-

Table 7. 2: Exposure duration of corrosion specimens (batches "a" and "b") under different environments

	Exposure Period (days)								
	0 - 90 days	90 - 190	190 - 220	220 - 260	260 - 340	340 - 440	440 - 510	510 - 690	690 - 860
Batch "a"	Chloride diffusion (20 ± 2^0C) 5% NaCl Soln	Laboratory air (20 ± 2^0C, 65% R.H.)	Chloride diffusion (20 ± 2^0C) 5% NaCl Soln	Chloride diffusion (20 ± 2^0C) 5% NaCl Soln	Climate chamber (50^oC, 75% RH)	Chloride diffusion (20 ± 2^0C) 5% NaCl Soln	Laboratory air (20 ± 2^0C, 65% R.H.)	Chloride diffusion (20 ± 2^0C) 5% NaCl Soln	1 day wet/6 days dry cycles
Batch "b"	Chloride diffusion (20 ± 2^0C) 5% NaCl Soln	Laboratory air (20 ± 2^0C, 65% R.H.)	Chloride diffusion (20 ± 2^0C) 5% NaCl Soln	Climate chamber (50^oC, 75% RH)	Chloride diffusion (20 ± 2^0C) 5% NaCl Soln	Laboratory air (20 ± 2^0C, 65% R.H.)	Chloride diffusion (20 ± 2^0C) 5% NaCl Soln	Laboratory air (20 ± 2^0C, 65% R.H.)	1 day wet/6 days dry cycles

7.3.1.3 Curing and exposure to corrosion environment

The two batches (a and b) of corrosion specimens were kept under ambient conditions in the laboratory (approximately 20 deg C, 65% RH) immediately after casting and demoulded after 24 hrs. After demoulding, the specimens were cured in water at 20 ^{0}C up to 28 days age. After 28 days, the specimens were taken out of the water and surface dried. Two coats of bituminous paint were applied to five faces of the slabs except the exposed face (300 x 300 mm) which provided the concrete cover of 30 mm to the embedded steel bars (Fig. 7.9). The un-coated face allowed the unidirectional ingress of chloride ions into the concrete cover zone when the specimens were exposed to chloride solution. The smooth face cast against the bottom of the polystyrene mould was used as the concrete cover face exposed to the chloride solution. The corrosion specimens were cured in water for 28 days to saturate the concrete pore spaces. This was followed by subjecting the corrosion specimens to NaCl solution, laboratory air, an aggressive alternative climate chamber exposure and wet/dry cycles to accelerate corrosion initiation in the steel.

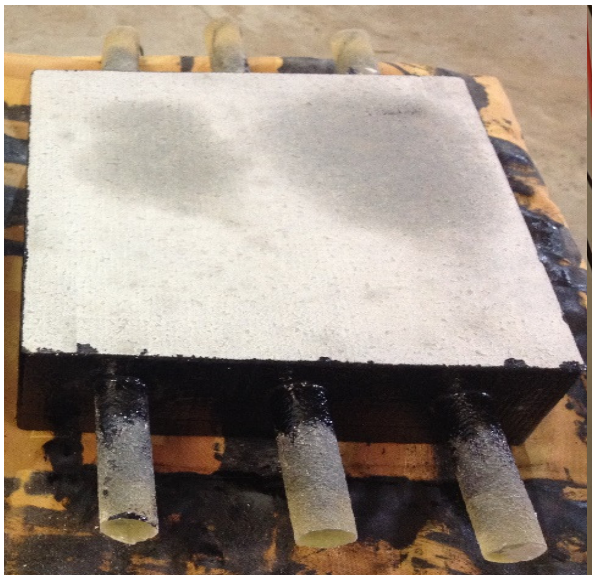

Figure 7. 9: Two coats of bituminous paint applied to five faces of the specimen

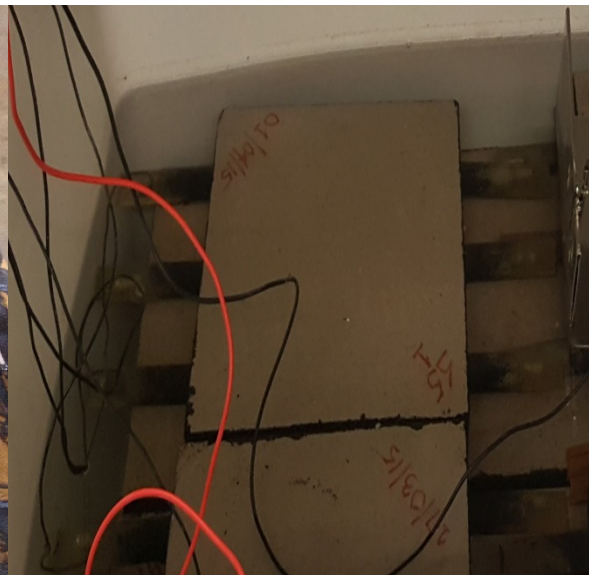

Figure 7. 10: Specimens immersed in 5% NaCl solution

7.3.1.3.1 Chloride diffusion

Bulk diffusion test, *NordTest* [99] and *DD CEN/TS 12390-11* [369] method was adopted for the exposure of the corrosion specimens of AACM and control OPC concrete mixes S_2 to S_6. The two standard test methods have similar procedures apart from the concentration of the chloride exposure solution. *DD CEN/TS 12390-11* [369] specifies 3% NaCl solution (by weight) whereas *NordTest* [99] specifies 165g ± 1g NaCl per dm^3 solution (16.5% NaCl solution by weight). A 5% NaCl solution in tap

water was prepared for chloride exposure of the corrosion specimens. The 5% NaCl solution allows for accelerated chloride diffusion which gives higher chloride concentrations at the steel reinforcement's depth (30 mm). The transportation mode of chloride ion was by diffusion only. This was achieved by curing the batches "a" and "b" of the corrosion specimens in water for 28 days after casting to attain full saturation of concrete pores thereby eliminating the initial sorption effect upon chloride exposure. All the faces of the corrosion specimens were coated with 1 mm thick layer of bituminous paint except the concrete cover face to the steel bars (250 mm x 250 mm face) which was exposed to the 5% NaCl solution, as shown in Fig 7.10. The NaCl solution was replaced every month to maintain a constant concentration of 5% by weight.

7.3.1.3.2 Accelerated corrosion inducing environment

The two batches (a and b) of corrosion investigation specimens were subjected to wet/dry exposure cycles (Table 7.2) to accelerate the corrosion of steel bars in the concrete. The wet exposure involved the bulk diffusion of the specimens in 5% NaCl solution as detailed in Section 7.3.1.3.1. The NaCl solution provided moisture which maintains saturated pore spaces of the concrete while also diffusing chloride ions which induce corrosion. However, the corrosion process is retarded when the concrete specimens are immersed in NaCl solution since a limited amount of oxygen (less than 1%) was available to sustain the corrosion process [370]. The dry exposure cycle was achieved by placing the concrete specimens in the laboratory air (20 + 2^0C and 65% R.H.) as shown in Fig 7.11. The laboratory air contains about 21% oxygen which recovers any oxygen depletion in submerged specimens and aids the corrosion process [252][316]. The corrosion specimens were exposed to long wet and dry cycles up to 690 days age, after which they were subjected to weekly cycles of 1 day wet (submerged in water) and 6 days dry (laboratory air) up to 860 days age (Table 7.2).

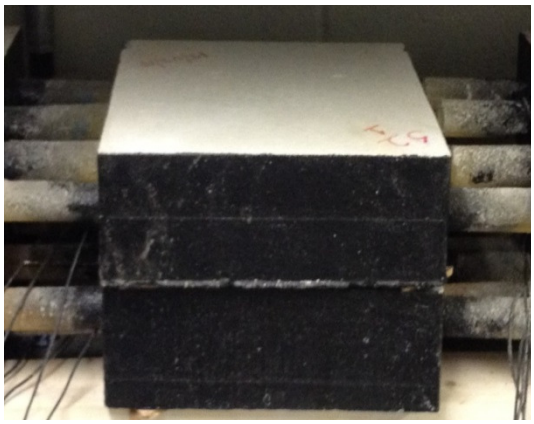

Figure 7. 11: Specimens cured in laboratory air

Figure 7. 12: Specimens cured in alternative climate chamber

7.3.1.3.3 Climate chamber

The climate chamber was supplied by Binder GmgH. The chamber has a temperature range of -50 ^{o}C to 200 ^{o}C and the humidity ranges from 0% to 100%. The chamber was set to a temperature of 50 ^{o}C and 75% relative humidity (Fig. 7.12). The elevated temperature (50 ^{o}C) was selected to aid the corrosion process of the AACM and control OPC concrete samples. Batch "a" of the corrosion specimens were placed inside the climate chamber from 260 days to 340 days age (80 days exposure period). Batch "b" was placed in the chamber for 40 days starting from 220 days to 260 days age as shown in Table 7.2. The use of the climate chamber was discontinued after the first exposure period due to the precipitation of chloride ion within the chamber under high humidity.

7.3.2 Test Procedure

7.3.2.1 Corrosion potential E_{corr}

The half - cell potential investigation of the corrosion specimens was performed using a digital voltmeter (DVM) in accordance with TR 60 [371] and ASTM C876 - 15 [372]. A silver-silver chloride (SSC) reference electrode was connected to the digital voltmeter for taking the potential reading in order to avoid chloride contamination when immersed in NaCl solution unlike a copper-copper sulphate electrode that is prone to such contamination [372]. The positive terminal of the voltmeter was connected to the connecting wire from the embedded steel bars while the reference electrode was placed on the exposed surface of the concrete cover to the steel as shown in Fig. 7.13. The reading was taken when the corrosion specimen was in NaCl solution, but care was taken to ensure that no electrically conductive part other than the porous tip of the reference electrode was in the solution. Corrosion potentials of specimens exposed in the climate chamber and laboratory air were measured after wetting the exposed concrete cover with a water saturated sponge. The sponge was placed on the concrete surface while the reference electrode was placed on top of it for the duration of the potential readings. The pre-wetting of the concrete surface was required to reduce the high electrical resistance of the dry concrete [372].

The potential of the embedded steel is passive when the measurement is > -200 mV while a potential reading between -200 mV to -350 mV can indicate the possibility of corrosion happening on the steel surface [324][372]. The steel bar is actively corroding at a higher negative potential than -350 mV [324][372]. However, in the case of submerged concrete structures, a higher negative potential than -350 mV is observed

due to the absence of oxygen, even when the steel is passive. This could produce misleading interpretation during analysis, which is often considered as a limitation of the potential measurement of reinforced concrete [324].

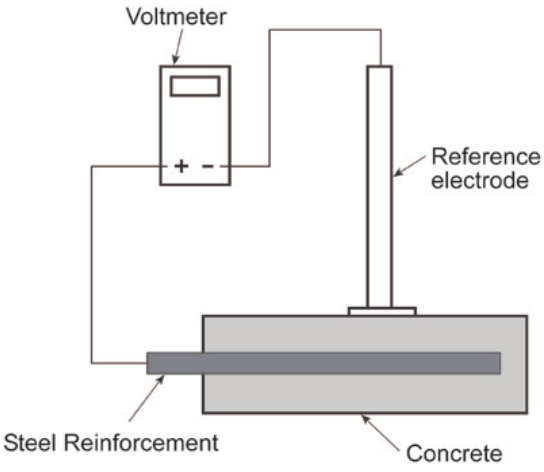

Figure 7. 13: Schematic diagram showing the Half-cell potential test [373]

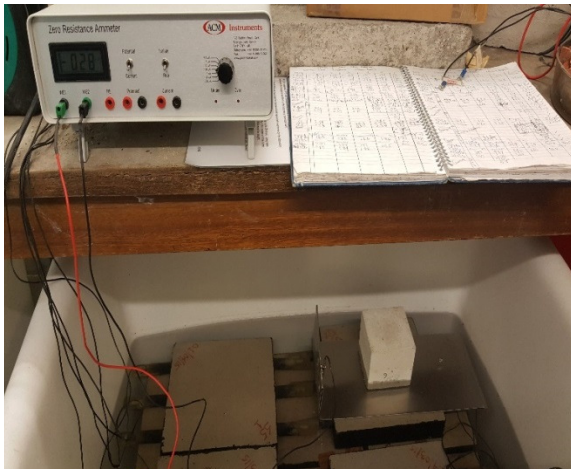

Figure 7. 14: Galvanic current reading using the Zero Resistance Ammeter.

7.3.2.2 Corrosion current density I_{corr}

A zero-resistance ammeter (ZRA) was used to measure the corrosion current of AACM and the control OPC concrete. The 1st working electrode from the ammeter was connected to the wire connection from the steel bar while the 2nd working electrode was connected to a stainless steel plate placed over the surface of the concrete cover as shown in Fig. 7.14. A concrete cube was placed on the stainless-steel plate to ensure full contact between the concrete surface and the plate. The instrument was switched to isolate and a range of 100 µA was selected. The 100 µA range did not illuminate the under/over range LED which indicates that it was suitable to measure the galvanic current between the 1st and 2nd working electrodes. After the selection of the correct range, the instrument was switched to run to measure the galvanic current between the two working electrodes. The readings of the galvanic current between the two working electrodes were viewed on the digital meter, which became stable after 3 minutes. The procedure was repeated for AACM and the control OPC concrete specimens of mixes S_2 to S_6. The corrosion current density was calculated by dividing the galvanic current by the area of the 8-mm diameter steel rod electrode embedded in the concrete specimens using the following equation.

$$i_{corr} = \frac{I}{A} \qquad 7.6$$

where i_{corr} is the corrosion current density ($\mu A/cm^2$), and A is the surface area of the exposed reinforcing steel in concrete matrix. In this study, the exposed steel has the nominal surface area of Π x d x l = 3.142 x 0.8 x 40 = 100 cm^2.

The results of the corrosion densities of the AACM and control OPC concrete specimens of mixes S_2 to S_6 are presented in Section 7.4.2.

7.3.2.3 Sorptivity

The sorptivity test was used to determine the capillary absorption tendencies in AACM and the control OPC concrete. 75 x 75 x 75 mm cubes were produced to investigate the capillary sorptivity of AACM and the control OPC concrete S_2 to S_6. Three cubes were produced for each concrete mix, giving fifteen cubes in total. The specimens were cast in a similar procedure to that detailed in Chapter 4, Section 4.3.3. The preconditioning procedure used for the sorptivity test were, however, different from the chloride diffusion test. The specimens were oven dried for 7 days at 50^0C to a constant moisture condition. After the 7 days oven drying, the specimens were placed in a sealed container for 3 days for cooling and redistribution of the moisture to a uniform level within the specimen matrix. Afterwards, five faces of the specimens were sealed with self-adhesive PVC tape, leaving one side face exposed (Fig 7.15). The partially sealed specimens were weighed to the nearest 0.01g. The specimens were placed on a support device at the bottom of a container as shown in Fig 7.16. The container was filled with tap water at 20 ± 2^0C to a level that was within 1 to 3 mm above the top of the supporting device during the tests. At selected times of 5, 10, 15, 20, 25 and 30 minutes, the specimens were removed from the water and excess water on the exposed surface blotted off with a paper towel. The specimens were weighed to the nearest 0.01g. The gain in mass per unit area divided by the density of water was plotted against the square root of the elapsed time. The slope of the best-fit line of these points (ignoring the origin) was reported as the sorptivity value [374][375].

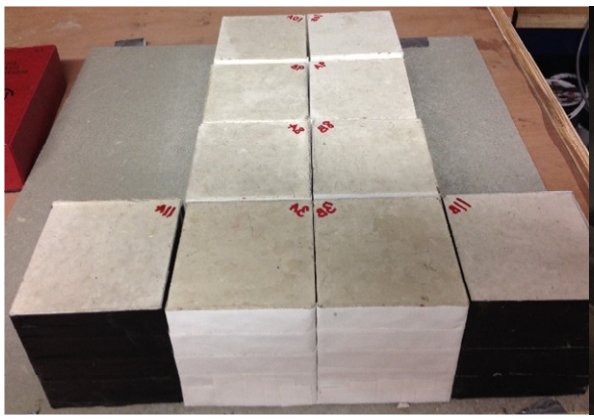

Figure 7. 15: PVC tape wrapped on five concrete faces

Figure 7. 16: Specimen supported on a strip of porous membrane.

7.3.2.4 Determination of [Cl/OH$^-$] ratio

7.3.2.4.1 Concrete coring

Concrete coring was performed on the corrosion specimens at 860 days age to produce core samples similar to the specimens used to investigate chloride ingress (Section 5.3.2.1, Chapter 5). The cores were obtained from locations between the embedded steel bars. This was achieved by carefully marking out 50 mm diameter circles with a permanent marker on the surface of the concrete cover. The 50 mm diameter circles were drawn between the three number of embedded steel bars in each concrete specimen as shown in Fig. 7.17. Adequate allowance was provided to prevent any damage to the embedded steel bars when performing the coring operation. Four number of concrete cores with the dimension of 50 mm diameter X 60 mm depth were obtained from each corrosion specimen as shown in Fig. 7.18. A total of forty concrete cores were obtained from the ten AACM and control OPC corrosion specimens.

The concrete cores were immediately stored in an enclosed container. The moisture content within the core matrix was preserved by placing it on a suspended support inside a container that is partially filled with water as shown in Fig. 7.19. The water level inside the enclosed container was below the level of the support. Each concrete core was sawn into three discs from 0 - 20, 20 - 40 and 40 - 60 mm depths (Fig. 7.20) similar to Section 5.3.2.1, Chapter 5 which were then returned back to the enclosed container until the pore fluid expression was carried out from the disc. The pore solution expression was performed within 7 days after the coring operation was carried out.

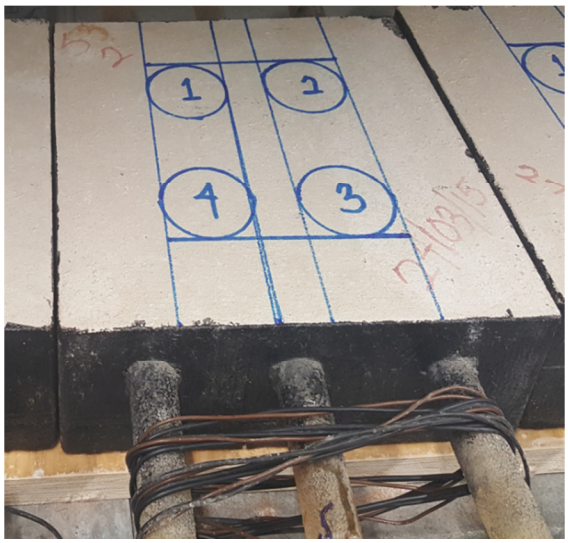

Figure 7. 17: Marked 50 mm diameter circle for coring

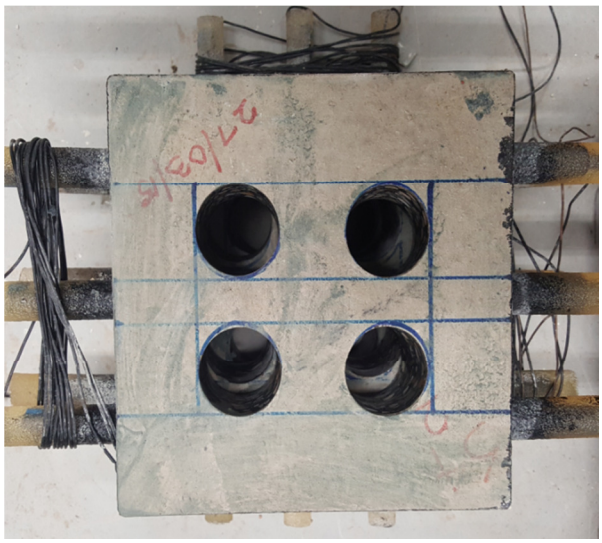

Figure 7. 18: Four cores (50 mm dia X 60 mm depth) drilled from corrosion specimens

Figure 7. 19: Concrete cores placed above water-filled enclosed container

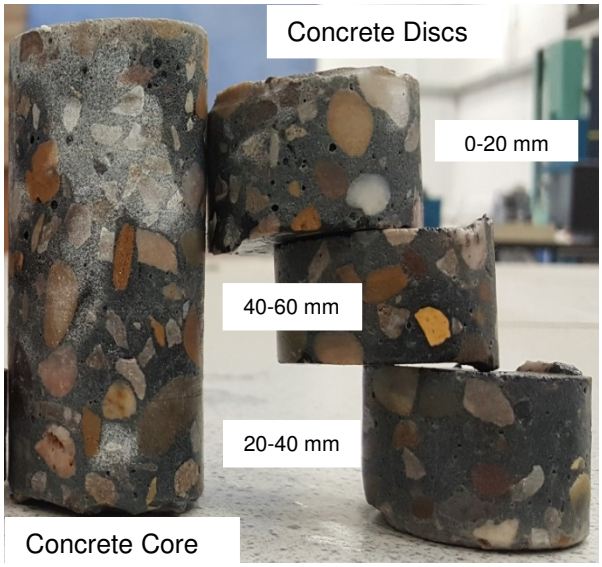

Figure 7. 20: Concrete discs obtained from cores

The cored holes in the AACM and control OPC corrosion specimens (Fig. 7.18) were repaired with AACM and OPC concrete respectively as shown in Fig. 7.21 and the specimen surfaces re-coated on the bottom and the four side faces with bitumen paint, leaving the top cover face uncoated (Fig. 7.22). The samples were then further subjected to a continuous wet/dry curing regime while monitoring the corrosion activity of the steel bars.

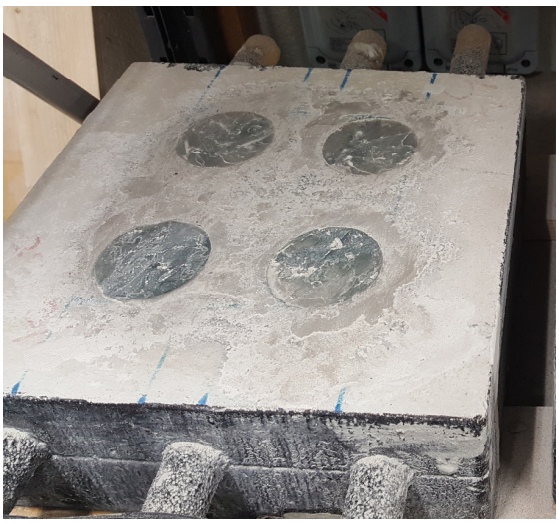

Figure 7. 21: Repaired core holes

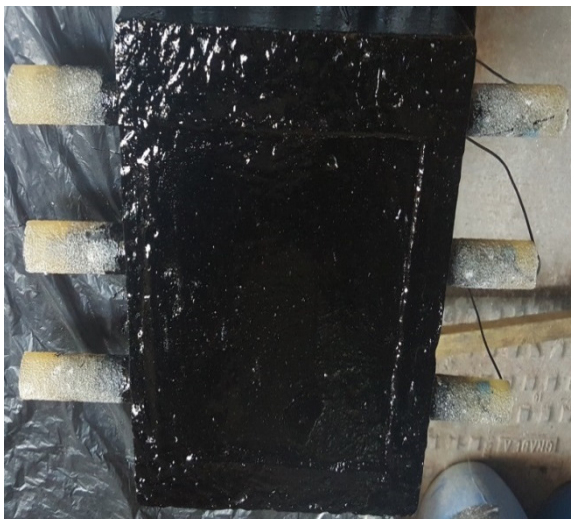

Figure 7. 22: Re-coating of bottom and the four side faces with bitumen paint

7.3.2.4.2 Concrete pore solution expression

The pore fluid expression was performed on the concrete discs obtained from the cores of corrosion specimens. Similar pore solution expression technique used for specimens under chloride ingress (Chapter 5, Section 5.3.2.2) was adopted for the corrosion specimens. The technique entails placing 3 core discs of the same depth e.g. 0 - 20 mm depth only, at a time, from each corrosion specimen core into a pore fluid extraction device. The pore solution extraction device with the core discs in it was placed in the compression testing machine under the loading platen (Fig 7.23). Compressive load was applied at a steady rate and the pore solution was extracted through a suction action without allowing contact with air and was immediately stored in plastic vials, labelled and sealed with parafilm (Fig 7.24). The same procedure was repeated on concrete core discs labelled 2 (representing 20-40 mm depth) and 3 (representing 40-60 mm depth) (Fig 7.20).

Figure 7. 23: Pore fluid extraction device

Figure 7. 24: Air tight plastic vials containing concrete pore solution.

7.3.2.4.3 Determination of free chloride and pH of pore solution

The free chloride and pH of AACM and OPC corrosion specimens were determined by dipping a chloride ion selective electrode (ISE) and a double junction pH electrode into its pore solution.

For the free chloride measurement, the white reference contact near the tip of the electrode (ISE) was immersed in the solution without entrapping air bubbles below it (Fig 7.25). The ISE was held in the aqueous solution until the reading stabilized and the displayed reading was then recorded. The ISE was rinsed by spraying with a jet of deionised water and dabbed dry with a low-lint laboratory tissue between measurements to prevent hysteresis effects. The ISE was calibrated before and after each measurement to achieve accuracy. Triplicate free chloride concentration readings for the pore solution of concrete core discs labelled 1 (representing 0 - 20 mm depth), 2 (representing 20 - 40 mm depth) and 3 (representing 40 - 60 mm depth) were taken with the ISE to achieve a high level of accuracy.

The pH readings from the pore solution of AACM and the control OPC corrosion specimens were displayed on a benchtop meter 3-in-1 (Fig. 7.26). This device measures pH ranging from 0.00 to 14.00.

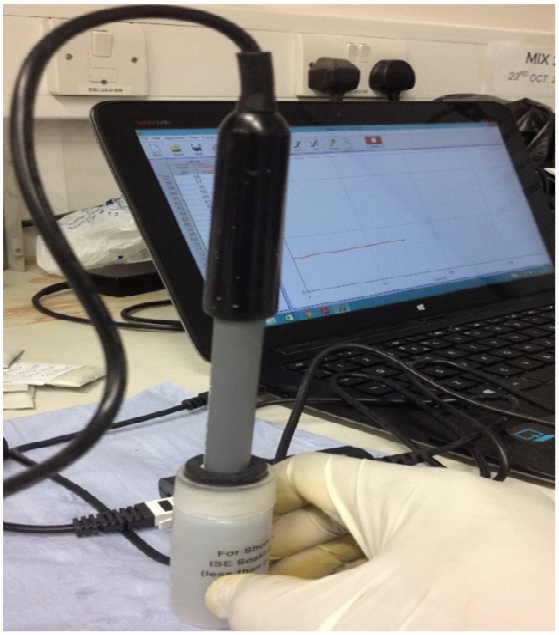

Figure 7. 25: Free chloride measurement from concrete pore solution

Figure 7. 26: Double Junction Electrode and Benchtop Meter 3-in-1 used to measure pH

7.4 RESULTS AND DISCUSSION

7.4.1 Sorptivity

The sorptivity results of AACM and the control OPC concrete mixes S_2 to S_6 are presented in Fig. 7.27 which shows the capillary absorption tendencies of the AACM and control OPC concrete mixes. The sorptivity index of each material is given by the slope of the graph.

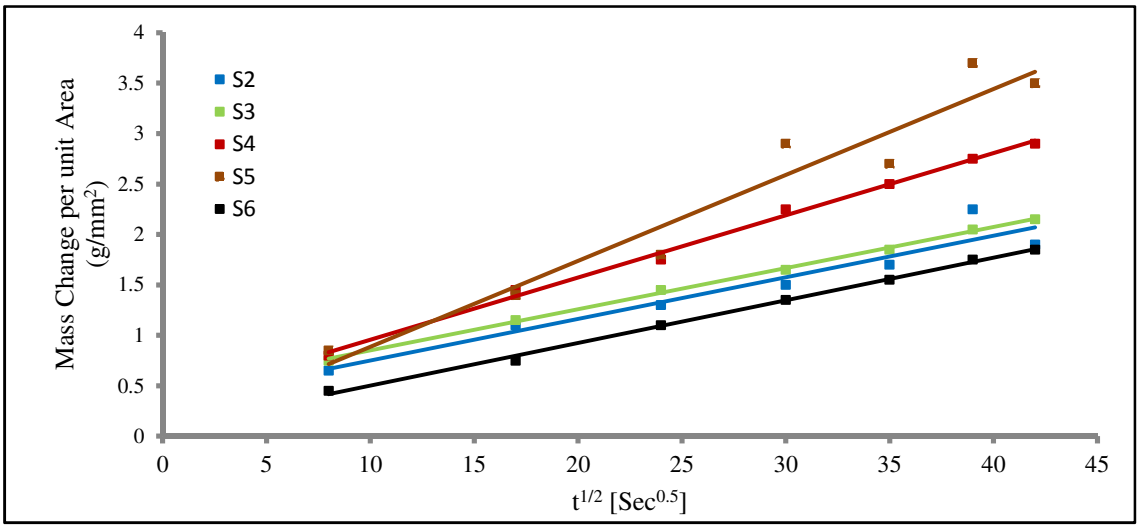

Figure 7. 27: Relationship between increase in mass of water per unit area and square root of time

The sorptivity graphs of AACM concrete mixes S_2 to S_5 show higher absorption values than the control OPC concrete mix S_6, notably AACM mix S_5 which shows sorptivity of 0.085 mm/sec$^{0.5}$ while it is 0.0413 mm/sec$^{0.5}$, 0.0422 mm/sec$^{0.5}$ and 0.0617 mm/sec$^{0.5}$ for AACM mixes S_2, S_3 and S_4 respectively. The control OPC concrete has sorptivity of 0.0408 mm/sec$^{0.5}$. This is in agreement with the research findings by *Law et al*. [301] on alkali activated slag AAS concrete showing a higher sorptivity value than OPC concrete. The authors [301] related the higher sorptivity values observed in AAS concrete to the capillary absorption tendencies of the concrete. The results of the microstructure of AACM concrete presented in Section 3.4.3.4, Chapter 3 of this research project support this observation. The results show that the capillary pore volume (pores sizes within 0.01 to 10 µm) of AACM concrete is more than that of the control OPC concrete mix S_6. The volume of the capillary pores is greatest in the AACM mix S_5 thus having the highest sorptivity value of 0.085 mm/sec$^{0.5}$.

The diffusion of deleterious substances such as chlorides is controlled by the total pore volume of concrete which is the summation of the capillary and gel pore volumes. AACM concrete mixes S_2 to S_5 have lower total pore volumes than the control

OPC concrete mix S_6 while their capillary pore volume is greater (Section 3.4.3.4, Chapter 3). In addition to the lower total volume of pores possessed by AACM concrete mixes S_2 to S_5, a high volume of their pores is discontinuous (Section 3.4.3.4, Chapter 3). This factor also contributes to the lower diffusion of deleterious substances in AACM concrete compared with the control OPC concrete.

7.4.2 Corrosion Potential E_{corr}

The half-cell potential readings for batches "a" and "b" of the corrosion specimens are presented in Figures 7.28 and 7.29. Each figure gives the corrosion potential readings for AACM and the control OPC concrete mixes S_2 to S_6. The corrosion potential readings for AACM concrete mixes S_2 to S_5 were recorded for 860 days under different exposure conditions which are detailed in Table 7.2, Section 7.3.1.2. However, the corrosion potential readings for the control OPC concrete mix S_6 are for 690 days due to 170 days of delay in starting the test. The two batches "a" and "b" of the corrosion specimens were subjected to chloride diffusion, laboratory air and environmental chamber exposure for accelerated corrosion.

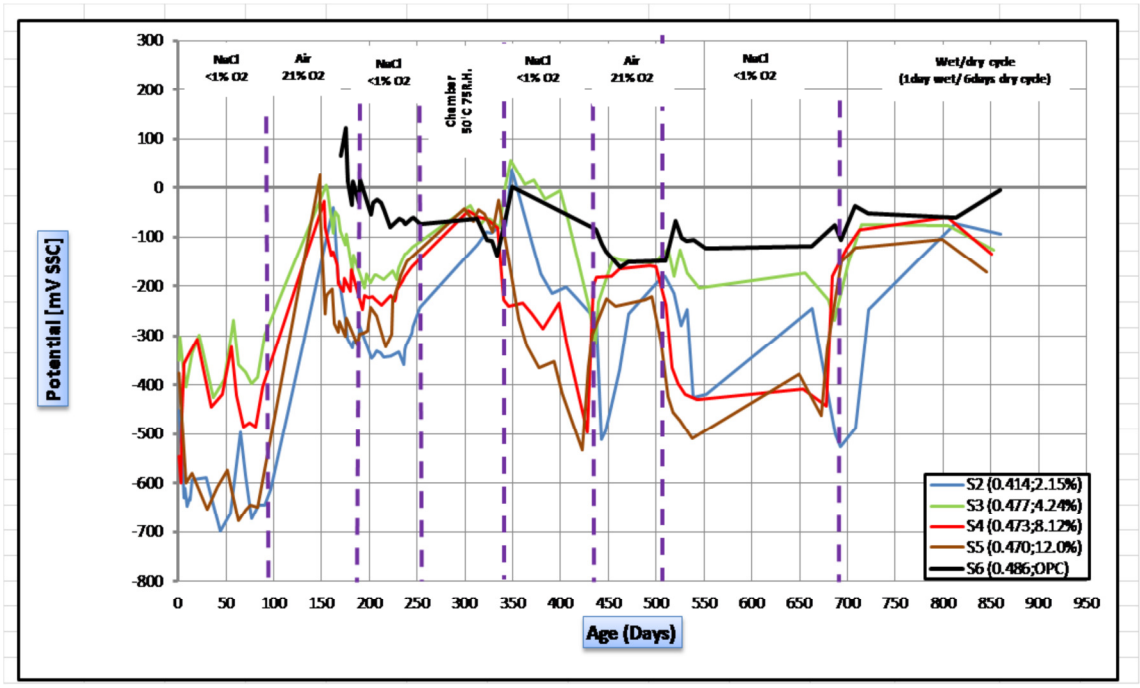

Figure 7. 28: Graph of corrosion potential E_{corr} with exposure period for batch "a" corrosion specimens

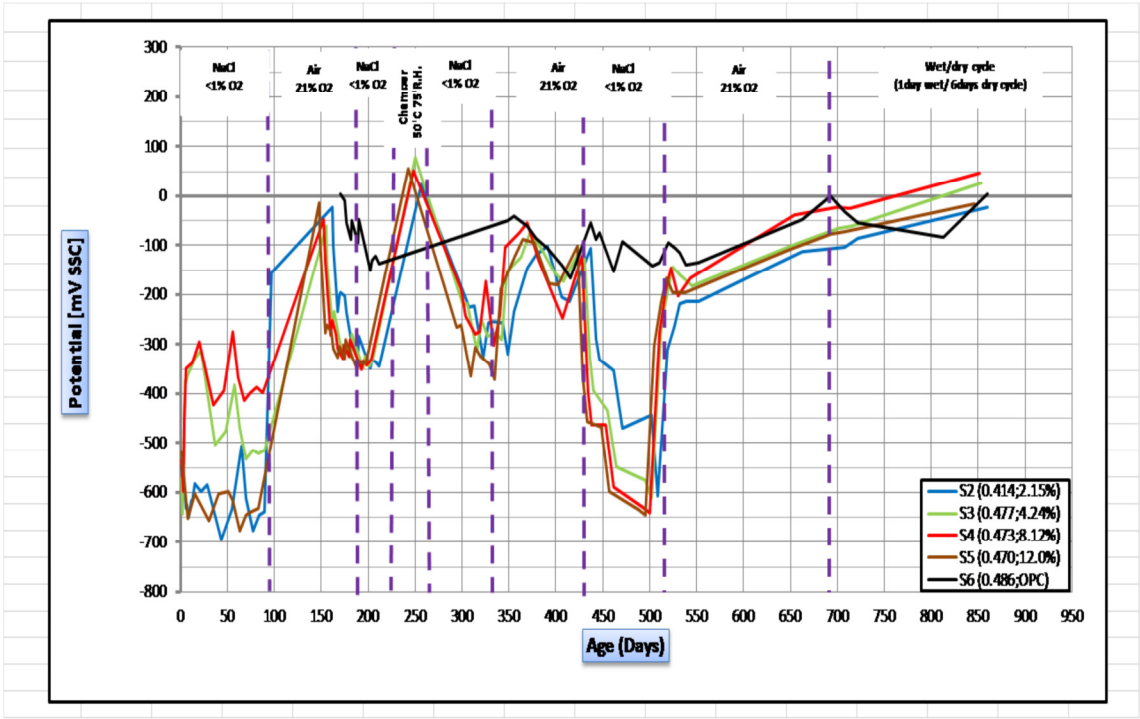

Figure 7. 29: Graph of corrosion potential E_{corr} with exposure period for batch "b" corrosion specimens

7.4.2.1 Chloride diffusion period

AACM concrete mixes S_2 to S_5 were subjected to four exposure periods of chloride diffusion. Batch "a" corrosion specimens were exposed to 5% NaCl solution at ages 0 - 90, 190 – 260, 340 – 440 and 510 – 690 days (Fig. 7.28). The corresponding exposure periods for batch "b" were 0 -90, 190 – 220, 260 – 340 and 440 – 510 days (Fig. 7.29). However, the control OPC concrete mix S_6 was exposed to three exposure cycles of chloride diffusion for each batch, omitting the 1st exposure cycle (0 – 90 days).

The corrosion potentials E_{corr} under these exposure periods in the chloride solution show a more negative potential, as much as -700 mV, for AACM concretes of both batches "a" and "b". The corrosion potential E_{corr} is more negative during the 1st cycle (0 -90 days) of exposure of the AACM concrete to 5% chloride solution. The control OPC concrete in both Figures 7.28 and 7.29 showed insignificant drop in the corrosion potential E_{corr} during chloride solution exposure, unlike the AACM concrete. An embedded steel bar is expected to be actively corroding at a more negative potential than -350 mV [324][372] but in this case it does not represent intense corrosion activity in AACM concrete during these periods. On the contrary, it signifies a deficiency of oxygen concentration at the steel rebar/concrete interface. The presence of both moisture and oxygen within the concrete matrix is required to initiate and sustain corrosion of the steel [252][316] but insufficient oxygen shifts the corrosion potential

E_{corr} to an even more negative value than -350 mV (Figures 7.28 and 7.29). Similar trends have been observed by other researchers [373].

The dense (lower total porosity) concrete cover in AACM concrete appears to limit the diffusion of oxygen which is necessary to drive the corrosion process at the surface of the steel bars. The microstructure of AACM and the control OPC concrete was investigated in Chapter 3 which shows a significant reduction of pore volume in AACM concrete compared with the control OPC concrete. This suggests there may be a siginifcantly restricted corrosion process due to oxygen depletion when AACM concrete is submerged in NaCl solution unlike the control OPC concrete that did not show such a negative shift in corrosion potential. In addition to the dense concrete cover that prevents oxygen from diffusing into the concrete matrix, the oxygen concentration in NaCl solution is very low. *Page and Lambert* [370] reported the solubility of oxygen in saturated solution of water as 1.50 x 10^6, 1.23 x 10^6 and 1.03 x 10^6 mol/cm^3 at 15^0C, 25^0C and 35^0C respectively. The available oxygen concentration in NaCl solution is insufficient to sustain the corrosion process in AACM concrete. OPC concrete shows signs of no significant corrosion activity during these exposure periods.

7.4.2.2 Laboratory air exposure periods

AACM concretes in batch "a" corrosion specimens were subjected to two exposure periods in the laboratory air (20 ± 2^0C, 65% R.H.) which are (90 – 190) days and (440 – 510) days as shown in Fig. 7.28 while in batch "b", they were subjected to three exposure periods which are 90 – 190, 340 – 440 and 510 – 690 days as shown in Fig. 7.29. The control OPC concrete specimens in batches "a" and "b" were subjected to one and two exposure periods in the laboratory air respectively.

AACM concrete shows a sharp positive rise in the corrosion potentials E_{corr} from -700 mV to +50 mV at 90 - 190 days exposure period (Fig.7.28 and 7.29). The oxygen concentration in air is about 20 times more than in water. There is sufficient oxygen available at the concrete/steel interface which reflects on the corrosion potential significantly. The rise in corrosion potential of AACM concrete is observed in both the laboratory air and the environmental chamber exposure periods.

Bastidas et al. [322] studied the passive state stability of steel embedded in alkali activated fly ash mortars. The fly ash reinforced mortar was cured for 94 days at 95% R.H. followed by 150 days in laboratory air and then 220 days at 95% R.H. The corrosion potential E_{corr} decreases by 400 mV when moved from a dry to a wet environment. The authors attributed the low resistivity of the fly ash mortar to the wetness of the concrete pores. E_{corr} was influenced by the degree of wetness of the fly

ash mortar, shifting to more negative values (more active) from a dry to a wet atmosphere [322]. Contrary to the conclusion of *Bastidas et al.* [322] about more active corrosion happening when the pores of fly ash mortar are saturated with water, the negative shift in E_{corr} in the present study is attributed to the insufficient oxygen available at the concrete/steel interface [239][376]. Care must, therefore, be taken when interpreting the results of E_{corr} of AACM under different exposure conditions. The control OPC concrete in Figures 7.28 and 7.29 does not show much variation of E_{corr} under the different exposures and there is no sign of oxygen depletion under saturated conditions. The likely reason is the higher total pore volume of OPC concrete relative to the AACMs.

7.4.2.3 Climate chamber exposure

Batches "a" and "b" corrosion specimens were exposed in the climate chamber for a single period due to the chloride precipitate from the concrete surface causing the inner chamber to corrode. The exposure periods of the corrosion specimens in the climate chamber were 260 - 340 days and 220 - 260 days for batches "a" and "b" respectively. The climate chamber was set to 50^0C and 75% R.H. Exposure to the elevated temperature of 50^0C accelerates the diffusion and corrosion processes while the 75% R.H. induces partial saturation of the concrete pore spaces which supports corrosion.

A rise in the corrosion potentials E_{corr} is observed when the AACM concrete is cured at a temperature of 50^0C and 75% R.H (Fig.7.28 and 7.29). The combined effect of temperature and humidity that causes partial saturation of the pores of AACM concrete resulted in a rise of E_{corr} to around +70 mV. The corrosion behaviour of AACM and the control OPC concrete under these exposure parameters is considered to be passive.

Véronique et al. [377] concluded that the temperature and humidity interaction increases the corrosion rate from 0.1 $\mu A/cm^2$ when cured at 20^0C and 60% R.H to 10 $\mu A/cm^2$ at 45^0C and 80% R.H. The corrosion rate is influenced by the diffusivity of O_2 in concrete similar to the diffusivity of CO_2 during accelerated carbonation in concrete provided by an optimum temperature and humidity. This is because the diffusion of O_2 and CO_2 in the saturated concrete will be approximately 4 orders of magnitude slower than for partially saturated concrete (50 to 70% R.H.) [25]. The climate chamber has the potential of accelerating the corrosion process if continued.

7.4.3 Corrosion Current Density I_{corr}

The corrosion current density I_{corr} for AACM and the control OPC corrosion specimens was measured by using a zero-resistance ammeter. The output results of corrosion current density (I_{corr}) against time are shown in Fig. 7.30. The I_{corr} measurements were taken between 290 and 860 days. The differences in the I_{corr} profiles are associated with the variation of binder type, mix proportions and exposure conditions. The I_{corr} values provide a basis for the measurement of corrosion severity in the concrete specimens.

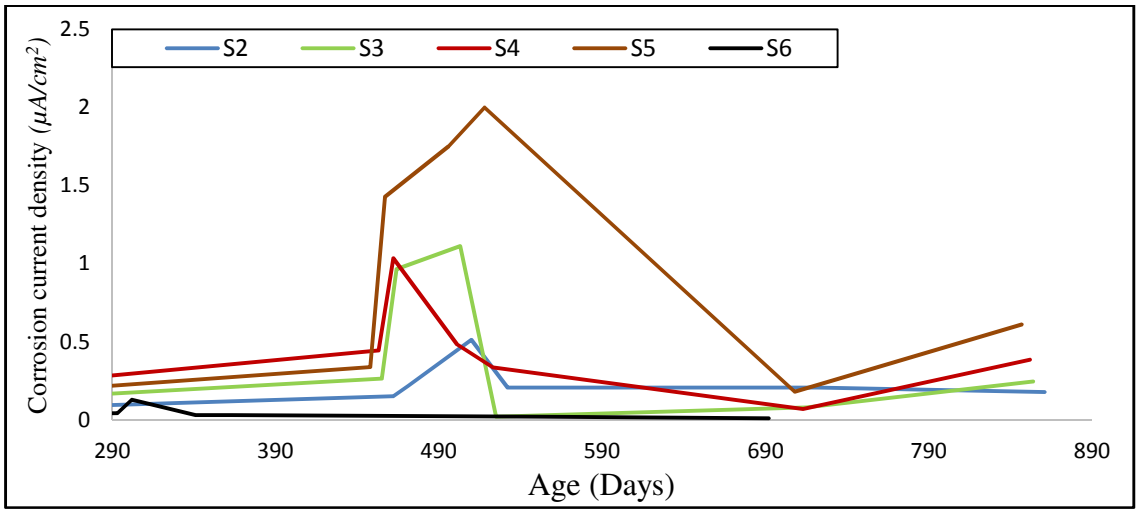

Figure 7. 30: Graph of corrosion current density I_{corr} of AACM and control OPC concrete

The corrosion current density I_{corr} for AACM is higher than the control OPC corrosion specimens as shown in Fig. 30. The I_{corr} in AACM corrosion specimen is relatively low from 290 days up until 450 days before showing high peak values. AACM mix S_5 has the highest I_{corr} value of 2 µA/cm^2 at 520 days age, followed by AACM mix S_3, S_4 and S_2 with I_{corr} values of 1.11 µA/cm^2, 1.03 µA/cm^2 and 0.51 µA/cm^2 respectively. On the other hand, the control OPC concrete S_6 has the lowest I_{corr} value of 0.13 µA/cm^2 at 300 days age followed by a lower I_{corr} (0.03 µA/cm^2). Nevertheless, the values of I_{corr} for AACM and the control OPC corrosion samples are considered to remain in the passive range.

The process of corrosion induced by chloride is anodically controlled [170]. The dissolution of iron into the electrolyte (pore solution) at the anodic site on the steel surface is impeded by the limited cathodic reaction for AACM corrosion samples. The cathodic reaction involves the reaction of oxygen with negatively charged electrons. These negatively charged electrons are released by the iron atom in the pore solution. In the case of the AACM corrosion samples, the oxygen demand at the cathodic sites for the continuous corrosion process is impeded by the dense microstructure and limited

dissolved oxygen in water (< 1%). Thus, the reaction at the anodic sites on the steel embedded in AACM concrete is hindered.

Bastidas et al., [322] observed an increase of two orders of magnitude in I_{corr} for steel reinforcements embedded in a fly ash mortar when subjected to wet curing compared with dry curing. *Holloway and Sykes* [378] observed a decrease in the I_{corr} as the passive film develops around the steel surface embedded in slag cement mortar (Fig 7.31a). This is followed by the steady increase of I_{corr} exceeding 1 µA/cm^2 at 107 days. The shift in the I_{corr} is associated with the depletion of the cathodic reactant. The second conclusion drawn by the authors was the sulphur deposition at the cathodic site. The sulphur deposits are the products formed from the oxidation of hydrogen sulphide in the slag [378]. The inhibition of the cathodic reaction produces a low I_{corr} and a negative E_{corr} (Fig 7.31b) whereas the inhibition of anodic reactions will result in lower I_{corr} and a more negative E_{corr} [378].

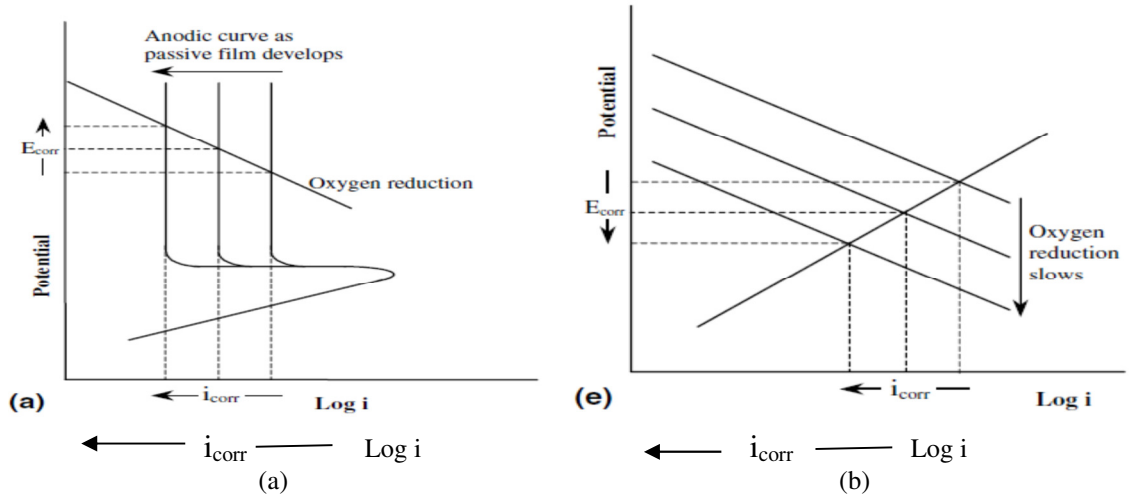

Figure 7. 31: Schematic diagram illustrating (a) change of corrosion potential and current density as passive film grows (b) fall in corrosion potential and decrease in corrosion density as cathode is inhibited [378]

7.4.4 Pore Solution

7.4.4.1 Free Cl concentration (mol/L)

Figure 7.32 shows the graph of free chloride concentrations against depth of AACM and the control OPC concrete mixes S_2, S_3 and S_6 at 850 days exposure to the different corrosion inducing environments presented in Table 7.2. Lower free chloride concentrations are observed in batch "b" corrosion specimens compared with batch "a" for mixes S_2, S_3 and S_6. The differences in the exposure environments of batches "a" and "b" (Table 7.2) are responsible for the variation of free chloride concentrations within the two batches.

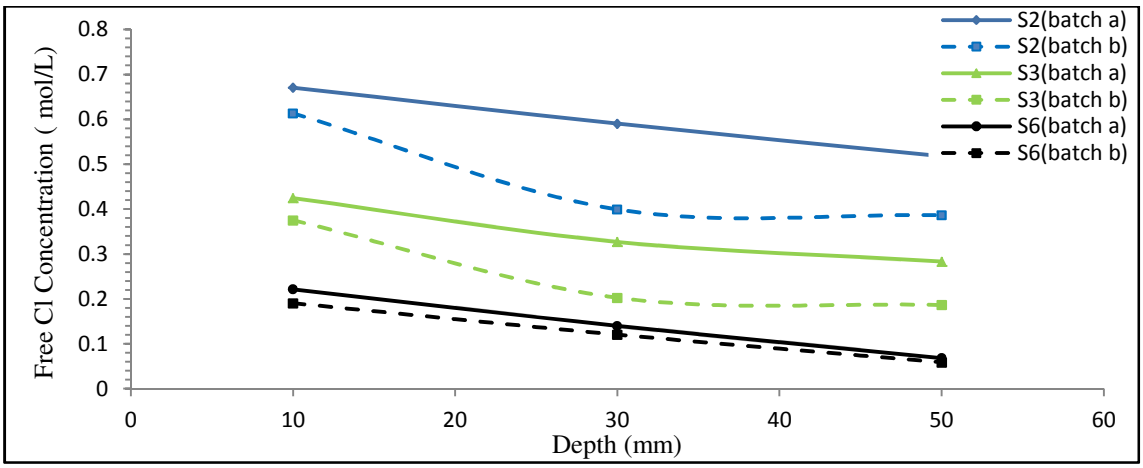

Figure 7. 32: Free chloride concentration (mol/L) of AACM and OPC concrete mixes S_2, S_3 and S_6 at 850 days exposure period

The exposure of corrosion specimens (batches "a" and "b") presented in Table 7.2 is different from the exposure method described in Section 4.3.4.1 Chapter 4 although the mix compositions for these samples are the same. Whilst the AACM and the control OPC concrete samples used to investigate the chloride ingress in Chapter 4 and 5 were completely immersed in NaCl solution (chloride bulk diffusion) throughout the exposure period, the corrosion specimens of this chapter were subjected to cycles of chloride bulk diffusion, laboratory air and climate chamber exposure as described in Section 7.3.1.3. The mechanism of chloride penetration in the specimens immersed in NaCl solution (Chapter 4) was diffusion whereas the corrosion specimens reported in this chapter were subjected to diffusion and absorption of chloride ions. The free chloride concentration data from Chapter 4 at 270 days exposure are plotted in Figure 7.33 together with the free chloride concentrations at 850 days obtained from the corrosion specimens of this chapter. The graphs in Fig. 7.33 show an exponential increase of free chloride concentration at the exposure period of 850 days age due to the alternative wetting and drying exposure cycles of the corrosion specimens during the 850 days of exposure (Table 7.2). Concrete exposed to cyclic wetting and drying has been observed by many researchers to aid rapid chloride ingress [91][25] due to combined diffusion and absorption of chloride ions. Fick's 2nd law of diffusion does not apply to the chloride absorption transportation mechanism.

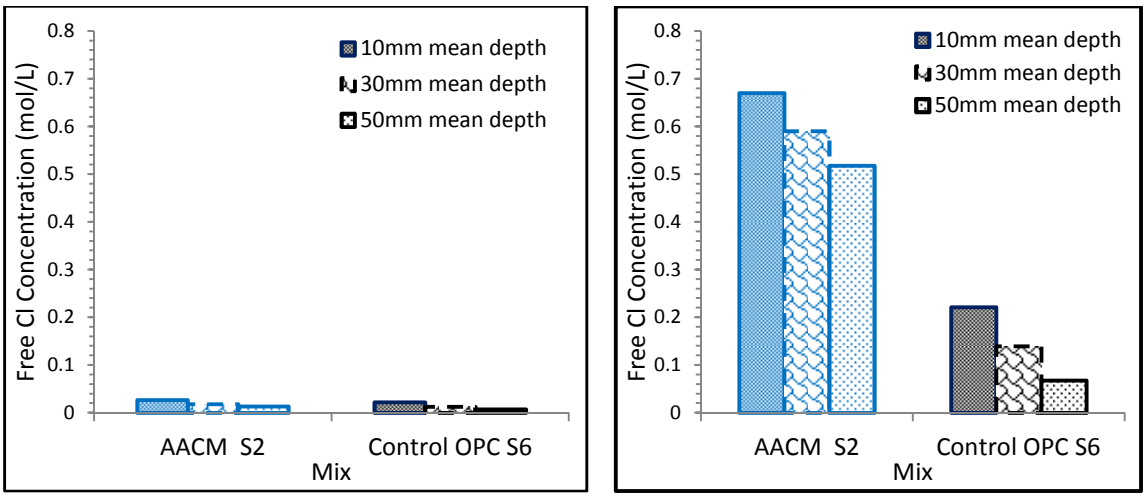

Figure 7. 33: Free chloride concentration (mol/L) of AACM S_2 and control OPC concrete S_6 specimens under (a) diffusion (b) water absorption and diffusion.

7.4.4.2 Hydroxyl ion concentration (mol/L)

The graph of hydroxyl ion concentration with depth for corrosion specimens of batches "a" and "b" is shown in Fig. 7.34. AACM concrete mixes S_2 and S_3 have considerably higher OH^- concentration compared with the control OPC concrete mix S_6. This trend is similar to the results of hydroxyl ion content presented for chloride ingress specimens in Section 5.4.5, Chapter 5. The hydroxyl ion concentration of AACM concrete mixes S_2 and S_3 is within the range 0.13 to 0.2 mol/L at 10 mm mean depth and 0.3 to 0.36 mol/L at 50 mm mean depth from the concrete surface. The control OPC concrete mix S_6 has 0.02 mol/L at 10 mm mean depth and 0.08 mol/L at 50 mm mean depth from the concrete surface. This clearly shows that the pore solution of AACM concrete has significantly higher alkalinity than the control OPC concrete when subjected to diffusion and absorption transportation mechanisms over long exposure periods of 850 days.

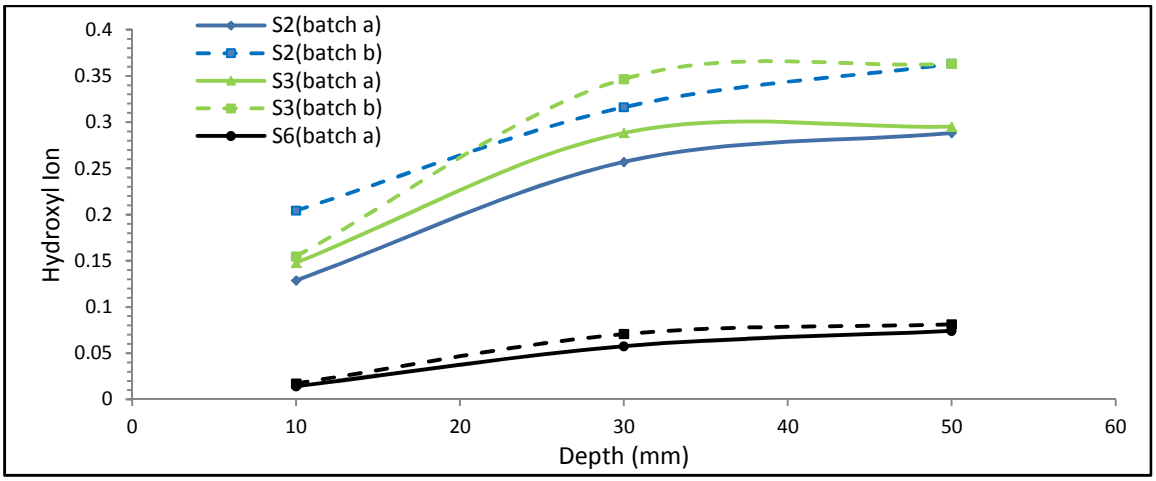

Figure 7. 34: Hydroxyl Ion concentration of AACM and OPC concrete mixes S_2, S_3 and S_6 at 850 days exposure period

The influence of diffusion and absorption exposure conditions presented in Table 7.2 is minimal on the hydroxyl ion concentrations (Fig. 7.35) unlike the free chloride concentration (Fig. 7.33). A decrease in the hydroxyl ion concentration is observed with exposure period as shown in Fig. 7.35. Significant decrease in the hydroxyl ion concentration is particularly observed in the control OPC concrete mix S_6 between 270 (0.49 mol/L) to 850 (0.07 mol/L) days exposure at 50 mm mean depths. This suggests that the combined effect of diffusion and absorption mechanisms has significant effect on the ingress of ions into the concrete and less prevelant in the leaching of ions from the concrete matrix.

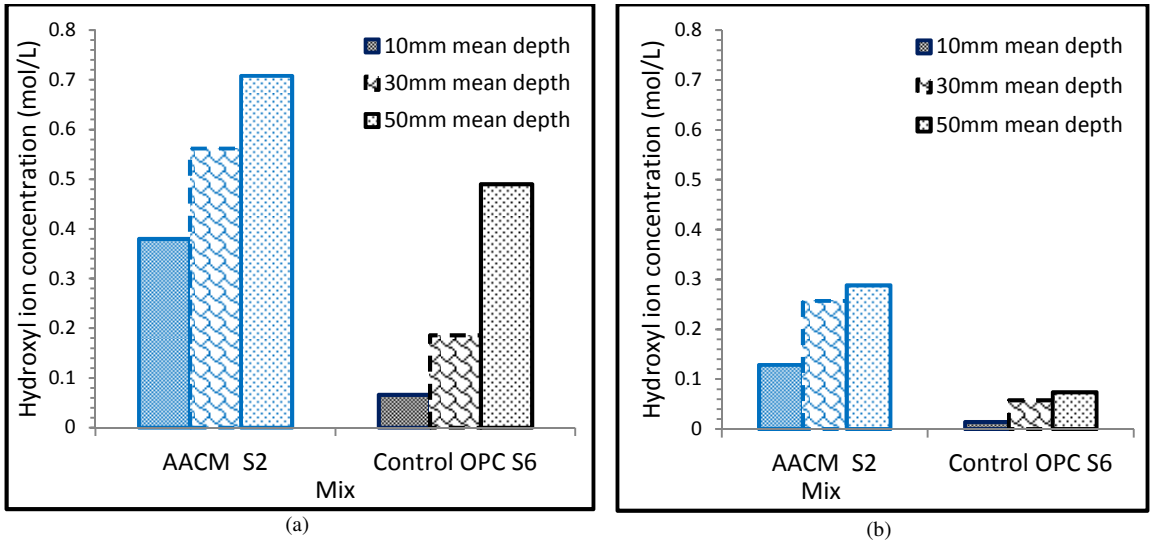

Figure 7. 35: Hydroxyl Ion concentration (mol/L) of AACM S_2 and control OPC concrete S_6 specimens under (a) diffusion (b) water absorption and diffusion**.**

7.4.4.3 Chloride/Hydroxyl ion concentration [Cl⁻]/[OH⁻]

The free chloride/hydroxy ion concentration graph is presented in Fig. 7.36. The free [Cl^-]/[OH^-] profiles of AACM and the control OPC concrete specimens of batches "a" and "b" of mixes S_2, S_3 and S_6 is shown are Fig. 7.36.

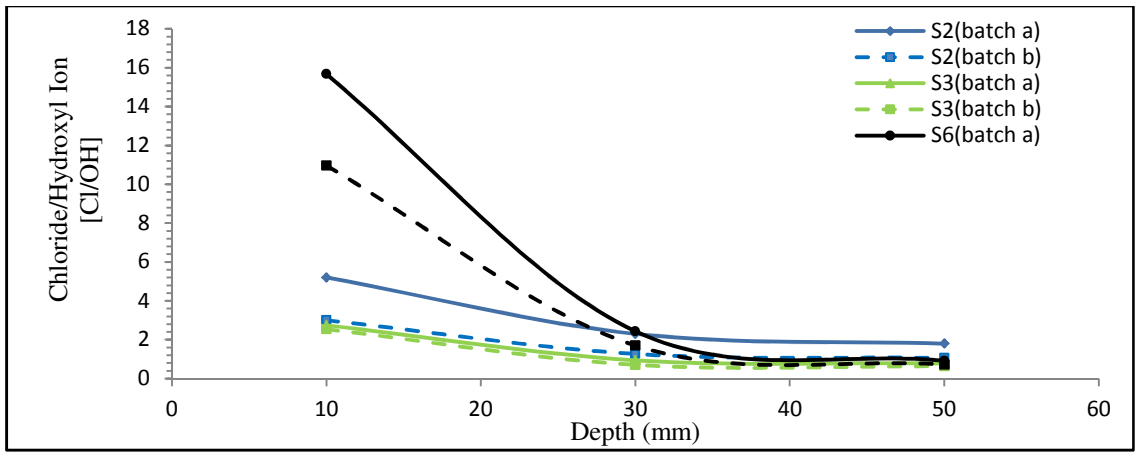

Figure 7. 36: [Cl^-]/[OH^-] of AACM and OPC concrete mixes S_2, S_3 and S_6 at 850 days exposure period

The free $[Cl^-]/[OH^-]$ ratio of the control OPC concrete mix S_6 for batch "a" corrosion specimen shows a value of 15.66 at 10 mm mean depth, which decreases sharply at 30 and 50 mm mean depths with ratios of 2.43 and 0.63 respectively. This trend is also observed for the control OPC concrete mix S_6 in the chloride ingress study (Section 5.4.6, Chapter 5), at an exposure period of 270 days, as shown in Fig. 7.37. The results of chloride diffusion (Chapter 4) also show similarly sharp reduction of chloride concentration in the surface zone due to leaching. This shows that the depletion of both hydroxyl and the chloride ion is high near the surface of the control OPC concrete, ultimately resulting in a high free $[Cl^-]/[OH^-]$ ratio.

AACM concrete mix S_3 has the lowest free $[Cl^-]/[OH^-]$ ratio of 2.54 at 10 mm mean depth while mix S_2 has free $[Cl^-]/[OH^-]$ ratio of 5.21 at 10 mm mean depth for batch "a" corrosion specimen. The exposure conditions of batch "a" corrosion specimen (Table 7.2) resulted in a higher free $[Cl^-]/[OH^-]$ ratio and chloride concentration than for batch "b" specimen while the OH^- concentration was lower. The longer exposure period of batch "a" corrosion specimen in the climate chamber *[50^0C, 75% R.H.]* (80 days) and bulk chloride diffusion solution (440 days) accounts for the high chloride concentration and a lower hydroxyl ion concentration. The batch "b" corrosion specimens were exposed to the climate chamber *[50^0C, 75% R.H.]* for 40 days and bulk chloride diffusion solution for 270 days (Table 7.2). The exposure period to laboratory air is less for batch "b" (100 days) than batch "a" (170 days). The exposure periods of 1 day wet/6 days dry cycles (170 days) is the same for batch "a" and "b" corrosion specimens.

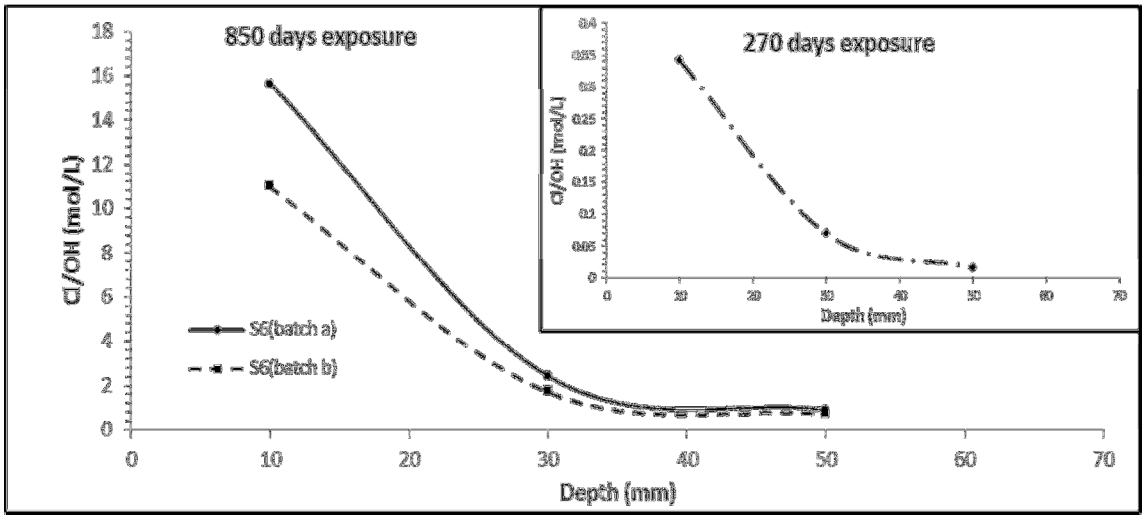

Figure 7. 37: Chloride/Hydroxyl Ion $[Cl^-]/[OH^-]$ of OPC concrete mix S_6 at 270 and 850 days exposure period

In conclusion, the corossion activity in AACM and the control OPC concrete remains passive at higher free $[Cl^-]/[OH^-]$ ratio than the threshold value of 0.61

suggested by Hausmann [255]. The free $[Cl^-]/[OH^-]$ ratios of AACM and the control OPC concrete mixes S_2, S_3 and S_6 for batch "a" specimens are 2.29, 0.94 and 2.43 (Fig. 7.36) and their corresponding potential readings are -100 mV, -125 mV and -16 mV (Fig. 7.28) respectively. The corresponding free $[Cl^-]/[OH^-]$ ratios for batch "b" specimens are 1.26, 0.70 and 1.70 (Fig. 7.36) and corresponding potential readings of -25 mV, +27 mV and -5 mV (Fig. 7.29) for mixes S_2, S_3 and S_6 respectively.

The threshold value of 0.61 for the $[Cl^-/OH^-]$ concentration proposed by *Hausmann* [255] for the initiation of corrosion in OPC based materials does not always apply. For example, *Lambert et al.* [170] presented a $[Cl^-/OH^-]$ concentration threshold of 3 for steel rods embedded in OPC concrete. The $[Cl^-/OH^-]$ concentration as high as 320 did not result in corrosion of steel fibres embedded in fly-ash concrete [102]. The reasons attributed to such high values of $[Cl^-/OH^-]$ are the lower chloride binding capacity in the AACM concrete and a lowered pH for the control OPC concrete. These factors increase the $[Cl^-/OH^-]$ ratio in its pore solution.

7.5 CONCLUSIONS

The following conclusions can be drawn based on the study carried out on the chloride initiated corrosion in AACM concrete. The half-cell potential and zero resistance ammeter were used to monitor the corrosion activies of the reinforcing steel. Investagtion on the sorptivity tendency and chloride/hydroxyl ratio of AACM concrete provided an insight to the corrosion activities of the embedded reinforcing steel.

- The absorption tendency of AACMs is higher than the control OPC concrete. For example, the soptivity of AACM mix S_3 is 0.0422 $mm/sec^{0.5}$ while it is 0.0408 $mm/sec^{0.5}$ for the control OPC S_6 concrete. These results compliment the higher volume of capillary pores in AACM concrete (chapter 3).
- The corrosion potential E_{corr} for AACM concrete shows high negative potentials as high as -700 mV at early age and during the bulk chloride diffusion exposures. The control OPC concrete shows E_{corr} values within the passive range of > -200 mV. The high negative potentials in AACM concrete is due to the deficiency of oxygen concentration at the steel rebar/concrete interface.
- The E_{corr} for AACM concrete exposed to air and corrosion inducing environment shows a sharp rise from -700 mV to passive range of > -200 mV. There is sufficient oxygen concentration available at the steel rebar/concrete interface at these exposure environments which reflected significantly on the E_{corr} of AACM concrete. The E_{corr} values for the control OPC concrete shows no significant

variation when exposed to air and corrosion inducing environment compared with the bulk chloride diffusion exposures.

- The corrosion potential E_{corr} shows less corrosion activities in AACMs than the control OPC concrete at 860 days exposure. For example, E_{corr} for AACM mix S_2 and the control OPC S_6 concrete are +27 mV and -5 mV respectively. The steel reinforcing bars in both AACM and OPC concrete remains passive at 860 days exposure.
- The corrosion current densities I_{corr} is higher in AACMs than control OPC concrete. The cathodic reaction at the steel surface for AACM corrosion samples is impeded due to the limited oxygen concentration at the reaction site. The high I_{corr} value of AACM concrete may not be the the true indication of its corrosion severity. Visual inspection is required to ascertain the corrosion severity of the steel embedded in AACM concrete.
- The free chloride concentration is higher in AACMs than the control OPC concrete at 850 days exposure period. For example, the free chloride concentrations for batch "b" AACM mix S_3 and the control OPC S_6 corrosion specimens at 30 mm depth are 0.20 mol/L and 0.12 mol/L respectively.
- The corresponding hydroxyl ion concentration is similarly higher in AACMs than the control OPC concrete at 850 days exposure period. For example, the hydroxyl ion concentrations for batch "b" AACM mix S_3 and the control OPC S_6 corrosion specimens at 30 mm depth are 0.35 mol/L and 0.07 mol/L respectively.
- The free chloride/hydroxyl ion ratio of AACMs is considerably lower than the control OPC concrete. For example, the free chloride/hydroxyl ion ratios for batch "b" AACM mix S_3 and the control OPC S_6 corrosion specimens at 30 mm depth are 0.7 and 1.7 respectively. This is due to the high pH of the pore solution in AACMs compared with the control OPC concrete.
- The corrosion activity in AACM and OPC concrete remains passive at higher free chloride/hydroxyl ion ratio than the historic Hausmann threshold value of 0.61. This is because the model developed by Hausmann for corrosion threshold did not consider the effect of chloride binding.

CHAPTER 8

CONCLUSIONS AND RECOMMENDATIONS FOR FUTURE WORK

8.1 INTRODUCTION

This research project investigated the durability properties of alkali activated concrete and a parallel control OPC concrete under the long term influence of chloride and CO_2 attack. The mechanical and microstructure properties was also investigated. A summary of the conclusions and area of further research are given in this chapter.

8.2 CONCLUSIONS

8.2.1 Porosity and pore structure of AACM and OPC mortars

- The 28 days strength of AACM and OPC mortar mixes was significantly influenced by the curing regimes wet/dry curing, wet curing and dry curing. AACM mortar mixes developed maximum strength under wet/dry curing whereas wet curing is optimum for OPC concrete. Dry curing of AACM mortar produced higher strength than wet curing. For example, the 28 days strength of AACM mix M_2 concrete under wet/dry, dry and wet was 72.9MPa, 64.6Mpa and 57.7Mpa respectively.
- An inverse relationship exists between the intrudable porosity and compressive strength of AACM mortar under the different curing regimes and liquid/binder ratios. Similar relationships exist between strength-critical pore and strength and pore diameters (critical and threshold).
- The combined use of a retarder and shrinkage reducing admixture improved the strength of AACM mortar. For example, the 28 days strength mix M_3 containing both retarder and shrinkage reducing admixture had 70.9MPa compared with 61.6MPa containing no retarder and shrinkage reducing admixture.
- Strength of AACM mortar increase with decreasing liquid/binder and with increasing activator concentration when the range of activator was maintained between the upper and lower limits of activator molarity.
- AACM shows a bimodal pore structure which is most conspicious under wet/dry and dry curing. Wet curing indicates a small degree of pore continuity possibly due to secondary cementitious hydration reactions overlapping with the geopolymerisation reactions in AACMs.
- AACM mortar cured under the wet/dry regime possessed the lowest intruded pore volume $\boldsymbol{\Phi_{in,}}$ critical pore diameter $\boldsymbol{d_c}$ and threshold pore diameter $\boldsymbol{D_{th.}}$

Similarly, the presence of retarder and shrinkage reducing admixture and a lower degree of activator dilution with water reduced the intruded pore volume $\Phi_{in,}$ critical pore diameter d_c and threshold pore diameter $D_{th.}$

- Lower liquid/binder ratio in AACM mortar M_3 mix displayed a lower intruded pore space $\Phi_{in,}$ critical pore diameter d_c and threshold pore diameter D_{crit}.
- AACM mortar has lower porosity than OPC mortar. The gel pore volume (pore size range 0.5nm to 10nm) is lesser in AACM mortar than OPC mortar but the capillary pore volume (pore size range 10nm to 10,000nm) is higher in AACM mortar than OPC mortar.

8.2.2 Strength, shrinkage and bound chlorides of AACM and OPC concrete

- The liquid/binder ratio had great impact on the strength of AACM concrete. However, high coarse aggregate content aided an improved compressive strength in AACM concrete. For example, AACM mix S_2 with liquid/binder ratio 0.41 had higher strength than mixes S_4 and S_5 with liquid/binder ratio 0.48. However, mix S_3 had similar strength with mix S_2 because of its higher coarse aggregate and lower activator dilution.
- The activator dilution played a significant role in strength development of AACM concrete similar to AACM mortar in Chapter 3. AACM mixes S_2 (2.15% dilution) and S_3 (4.24% dilurion) with lower activator dilution achieved greater 28 days strength than mixes S_4 (8.12% dilution) and S_5 (12% dilution).
- The strength developed at early age in AACM concrete was faster under dry curing (20^0 C, 65 RH) compared with wet curing (20^0 C) while the reverse is true for OPC concrete. For example, AACM mix S_3 and OPC S_6 under wet curing had 39.1MPa and 28MPa respectively compared with 40.1MPa and 26MPa under dry curing.
- The chloride profiles of water and acid soluble concentration for both AACM and OPC concrete shows good correlation with Fick's second law of diffusion.
- The surface chloride concentration, $C_{0,}$ increases with exposure periods for AACM and OPC concrete water and acid soluble chlorides. This increase was more pronounced in water soluble compared with the acid soluble chloride for AACM concrete. On the other hand, OPC concrete revealed more surface chloride concentration, $C_{0,}$ for acid soluble compared with water soluble. For example, the $C_{0,}$ for AACM mix S_3 and OPC S_6 water soluble chlorides are

2.07% and 3.27% respectively while it is 1.37% and 5.91% for acid soluble chloride at 180 days exposure.

- A decrease in chloride diffusion coefficient with exposure periods were observed for both AACM and OPC concrete. Generally, AACM concrete possess a lower chloride diffusion coefficient compared with OPC concrete. For example, the chloride diffusion coefficients for AACM mix S_3 and OPC S_6 at 55 days chloride exposure are 5.6 x 10^{-12} m^2/s and 8.7 x 10^{-12} m^2/s respectively while it is 1.8 x 10^{-12} m^2/s and 2.5 x 10^{-12} m^2/s at 180 days chloride exposure.
- The more refined pore structure of AACMs (lower porosity, discontinous pore structure) aided lower chloride diffusion when compared to OPC concrete.

8.2.3 Free chloride and pH of AACM and OPC concrete pore solution

- OPC concrete exhibited the lowest amount of free chloride compared with AACM concrete because of its better binding capacity.
- The experimental data of free chloride concentration show strong correlation with the regression analysis profiles derived from Fick's second law of diffusion.
- The chloride diffusion parameters *[$C_{0(f)}$ and $D_{c(f)}$]* increase with an increase in chloride exposure periods except for $D_{c(f)}$ at 540 days. For example, $C_{0(f)}$ *and* $D_{c(f)}$ for AACM S_2 at 180 days exposure are 0.025mol/L and 3.6 x $10^{-12}m/s^2$ respectively while it is 0.032mol/L and 5.1 x $10^{-12}m/s^2$ at 270 days exposure. The values are 0.053mol/L and 0.36 x $10^{-12}m/s^2$ for $C_{0(f)}$ *and* $D_{c(f)}$ respectively at 540 days exposure.
- Langmuir binding isotherm best-fits the free and bound chloride relationship of AACM and OPC concrete because of its lower free chloride concentration ($\leq$0.02 mol/L).
- The binding capacity decreases as the chloride exposure periods increases. OPC concrete had better chloride binding capacity compared with AACM concrete. This due to the presence of higher concentrations of water and acid soluble bound chlorides OPC concrete compared to AACM concrete (Chapter 4).
- The free chlorides and pH are much higher in AACMs than OPC. For example, the free chloride concentrations at 10mm mean depth of AACM mix S_2 and OPC S_6 are 0.027mol/L and 0.023mol/L respectively at 270 days exposure. The corresponding pH for AACM mix S_2 and OPC S_6 are 0.38mol/L and 0.066mol/L respectively. The higher free chloride in AACMs is due to its lower water and

acid soluble binding capacity while the higher pH was influenced its activator concentration.

- The Cl^-/OH^- ratio of pore solution increases with increasing activator dilution. The highest activator dilution (12%) produced the highest free Cl^-/OH^- ratio while the lowest activator dilution (2.15%) produced the lowest free Cl^-/OH^- ratio within AACM pore solution. For example, the Cl^-/OH^- ratio at 10mm mean depth is 0.071 and 0.143 for 2.15% and 12% activator dilutions respectively at 270 days exposure.
- The AACM concrete had the lowest free Cl^-/OH^- ratio despite the high free chloride concentration compared with OPC concrete. The impact of high pH and hydroxyl ion present within pore solution of AACM concrete aided the low free Cl^-/OH^- ratio. For example, the free Cl^-/OH^- ratio at 10mm mean depth for AACM mix S_2 is 0.071 while it is 0.34 for OPC S_6 at 270 days exposure.

8.2.4 Carbonation of AACM and OPC concrete

- A lower depth of carbonation was observed in OPC concrete compared to AACM concrete. For example, the carbonation depth for AACM mix S_3 is 25.19 mm while it is 14.13 mm for OPC S_6 at 327 days CO_2 exposure. This is due to the main hydration product of $Ca(OH)_2$ in OPC while AACMs does not have it as its geopolymerisation product.
- The rate of carbonation is higher in AACMs than OPC. For example, the rate of carbonation in AACM mixes S_3, S_4 and S_5 are 27.29mm/yr$^{0.5}$, 30.08mm/yr$^{0.5}$ and 32.68mm/yr$^{0.5}$ respectively while it is 19.62mm/yr$^{0.5}$ for OPC S_6. However, the rate of carbonation for AACM mix S_2 is lowest because of it lowest liquid/bindar ratio 0.41 compared to the liquid/binder 0.48 of other mixes.
- The carbonation and drying shrinkage is considerably higher in AACMs than OPC concrete. For example, the carbonation and drying shrinkage of AACM mix S_2 at 80 days are 700 με and 761 με while it is 300 με and 562 με for OPC S_6. This is due to the precipitation of $CaCO_3$ which fills the pore spaces in OPC concrete thereby reducing the stress induced by water loss during shrinkage.
- The drying shrinkage values are higher than carbonation shrinkage for both AACM and OPC concrete. This is because of high water loss during drying shrinkage, on the other hand, the carbonation shrinkage shows precipitation of $CaCO_3$ within the pores of OPC concrete which restrict further shrinkage.

- The pH of the carbonated zones of AACM mortar is above the carbonation threshold value of 9 while OPC mortar is below it. For example, the pH at the carbonated zone of AACM mix M_3 is 10.02 while it is 8.69 for OPC S_6. This suggests that the phenolpthalein test method might not be appropriate to determine the carbonation of AACMs.
- The pH of AACM and OPC concrete is higher than mortar which suggests the release of alkaline content by the aggregates. For example, the pH of concrete mixes S_3 and S_6 are 10.46 and 9.56 compared with 10.02 and 8.69 of its corresponding mortar mixes M_3 and M_6 respectively.
- A non-linear relationship of the form $y = 1.0917x^{0.8234}$ and a coefficient of 0.99 is established between depth of carbonation and the porority of AACM concrete.

8.2.5 Chloride initiated corrosion in AACM and OPC concrete

- The absorption tendency of AACMs is higher than the control OPC concrete. For example, the soptivity of AACM mix S_3 is 0.0422 mm/sec$^{0.5}$ while it is 0.0408 mm/sec$^{0.5}$ for the control OPC S_6 concrete. These results compliment the higher volume of capillary pores in AACM concrete (chapter 3).
- The corrosion potential E_{corr} for AACM concrete shows high negative potentials as high as -700 mV at early age and during the bulk chloride diffusion exposures. The control OPC concrete shows E_{corr} values within the passive range of > -200 mV. The high negative potentials in AACM concrete is due to the deficiency of oxygen concentration at the steel rebar/concrete interface.
- The E_{corr} for AACM concrete exposed to air and corrosion inducing environment shows a sharp rise from -700 mV to passive range of > -200 mV. There is sufficient oxygen concentration available at the steel rebar/concrete interface at these exposure environments which reflected significantly on the E_{corr} of AACM concrete. The E_{corr} values for the control OPC concrete shows no significant variation when exposed to air and corrosion inducing environment compared with the bulk chloride diffusion exposures.
- The corrosion potential E_{corr} shows less corrosion activities in AACMs than the control OPC concrete at 860 days exposure. For example, E_{corr} for AACM mix S_2 and the control OPC S_6 concrete are +27 mV and -5 mV respectively. The steel reinforcing bars in both AACM and OPC concrete remains passive at 860 days exposure.

- The corrosion current densities I_{corr} is higher in AACMs than control OPC concrete. The cathodic reaction at the steel surface for AACM corrosion samples is impeded due to the limited oxygen concentration at the reaction site. The high I_{corr} value of AACM concrete may not be the the true indication of its corrosion severity. Visual inspection is required to ascertain the corrosion severity of the steel embedded in AACM concrete.
- The free chloride concentration is higher in AACMs than the control OPC concrete at 850 days exposure period. For example, the free chloride concentrations for batch "b" AACM mix S_3 and the control OPC S_6 corrosion specimens at 30 mm depth are 0.20 mol/L and 0.12 mol/L respectively.
- The corresponding hydroxyl ion concentration is similarly higher in AACMs than the control OPC concrete at 850 days exposure period. For example, the hydroxyl ion concentrations for batch "b" AACM mix S_3 and the control OPC S_6 corrosion specimens at 30 mm depth are 0.35 mol/L and 0.07 mol/L respectively.
- The free chloride/hydroxyl ion ratio of AACMs is considerably lower than the control OPC concrete. For example, the free chloride/hydroxyl ion ratios for batch "b" AACM mix S_3 and the control OPC S_6 corrosion specimens at 30 mm depth are 0.7 and 1.7 respectively. This is due to the high pH of the pore solution in AACMs compared with the control OPC concrete.
- The corrosion activity in AACM and OPC concrete remains passive at higher free chloride/hydroxyl ion ratio than the historic Hausmann threshold value of 0.61. This is because the model developed by Hausmann for corrosion threshold did not consider the effect of chloride binding.

8.2 RECOMMENDATIONS FOR FUTURE RESEARCH

A few areas have been identified where further research could be carried out based on the observations and conclusions from this study.

- Some limitation has been identified with MIP test, which was used to investigate the porosity and pore structure of AACM and OPC concrete. These limitations include;
    - ✓ MIP measures only the effective porosity of concrete and not the total porosity. The effective porosity relates to the permeability and diffusion properties in concrete but less to its strength properties unlike the total

porosity. The nitrogen gas absorption test can be used to investigate the pore structure of concrete in order to address this limitation.

- ✓ The minimum accessible pores volume by the mercury intrusion is 0.0073 µm. The cummulative and differential pore volume graphs suggests the possibility of lesser pores than 0.0073 µm could be present in the AACM and OPC concrete. This requires futher research.

- The phenolpthalein indicator method used for investigating the carbonation of AACM concrete may not be suitable. This is because of the high pH above the threshold value of 9 observed at the carbonated zones in AACM concrete. An improved testing method to investigate carbonation in AACM concrete is required.
- The corrosion behaviour of steel embedded in AACM concrete shows false higher values of corrosion potential and current densities than OPC concrete. This requires further study through breaking up the specimens for visual inspection when corrosion activity begins. The steel reinforcing bars is passive in both AACM and OPC concrete as at the time of writing this report.

APPENDIX I

List of Publications

- **Ojedokun O.Y.** and P.S. Mangat, Chloride Diffusion in Alkali Activated Concrete**,** Second International Conference on Concrete Sustainability ICCS2016 held in Madrid, Spain, June 13th – 15th, 2016.
- **Ojedokun O.Y.** and P.S. Mangat, Pore size distribution of an Alkali Activated Cementitious (AACM) Mortar, 3rd World congress on materials science and engineering, held in Barcelona, Spain, August 24th – 26th, 2017.
- **Ojedokun O.Y.** and P.S. Mangat, Chloride Profiling in Alkali Activated Concrete, Proceedings of the 2015 annual Material Engineering Research and Institute (MERI) Symposium, Sheffield Hallam University.
- **Ojedokun O.Y.** and P.S. Mangat, Chloride Diffusion in Alkali Activated Concrete, Proceedings of the 2016 annual Material Engineering Research and Institute (MERI) Symposium, Sheffield Hallam University.

APPENDIX II

Pore size distribution of AACM and OPC concrete

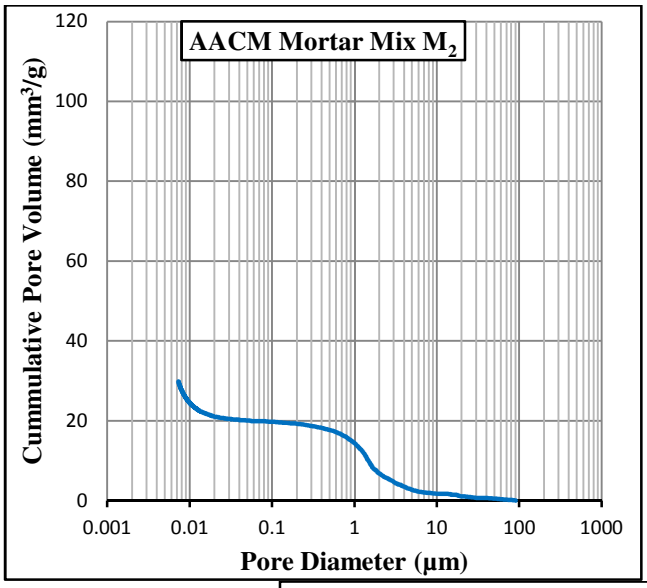

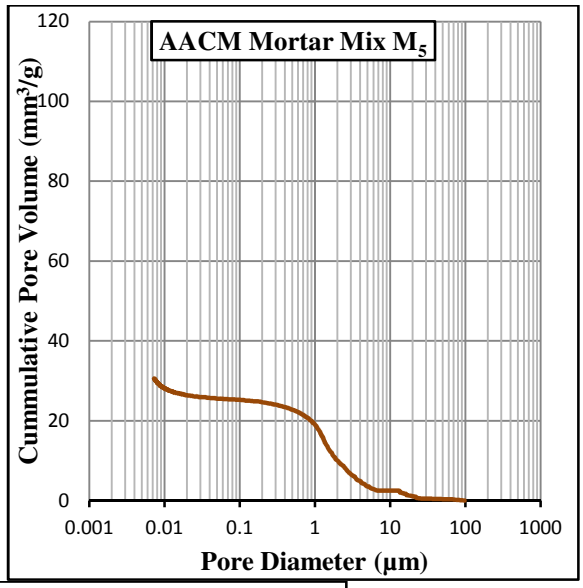

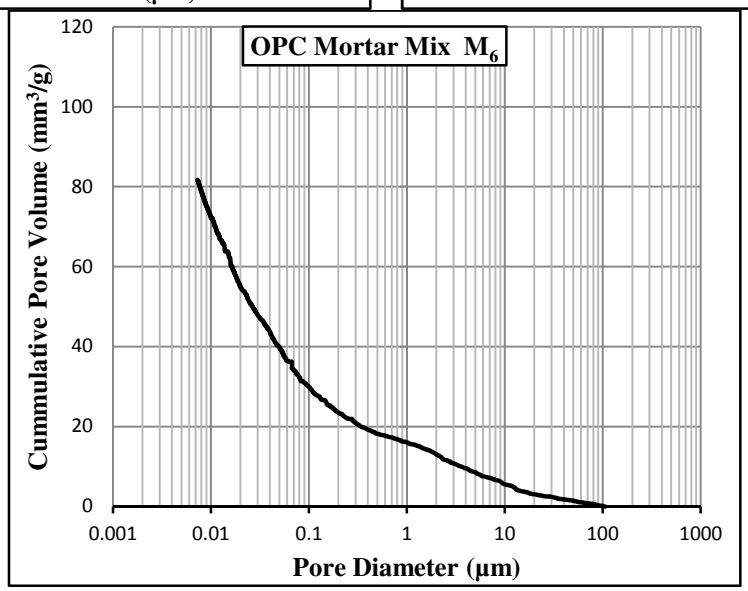

***Appendix 3.1a**: Intrudable Porosity for AACM and OPC Mixes under Wet/dry Curing*

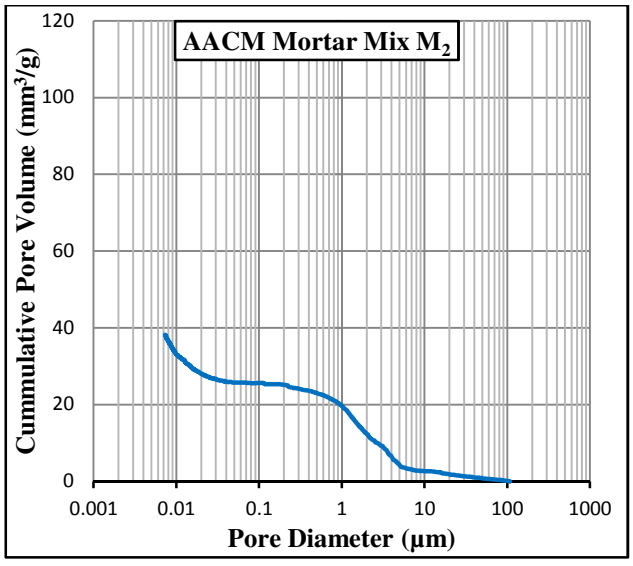

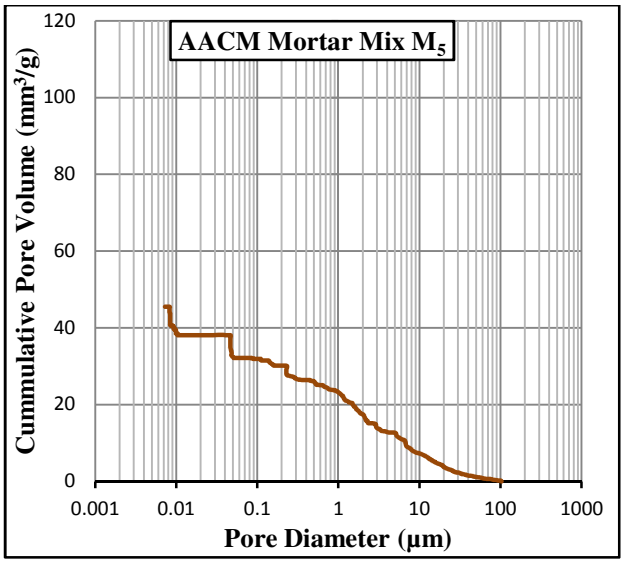

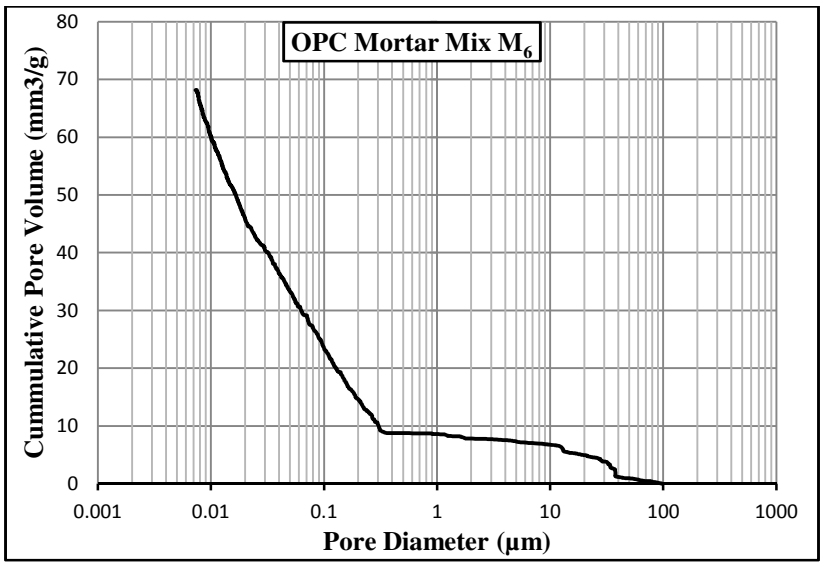

***Appendix 3.1b**: Intrudable Porosity for AACM and OPC Mixes under Wet Curing*

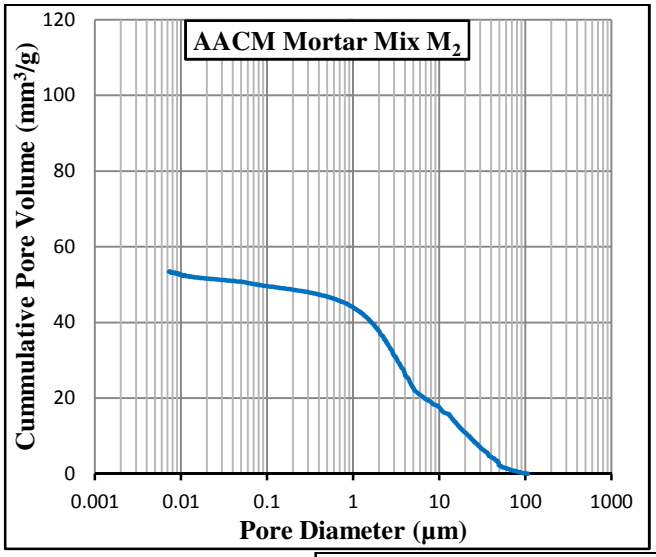

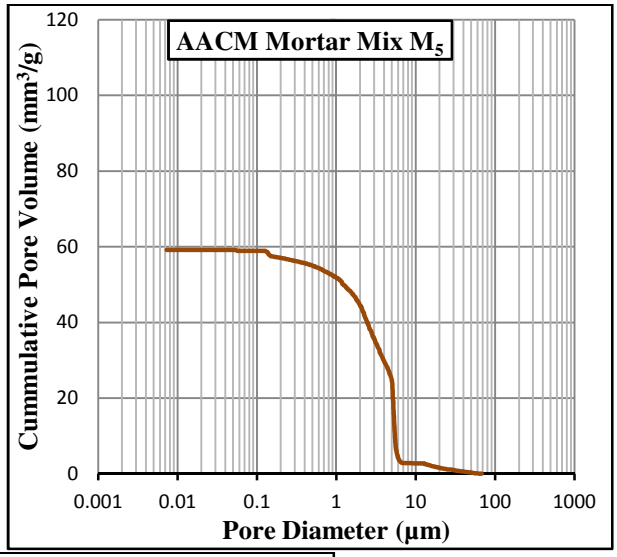

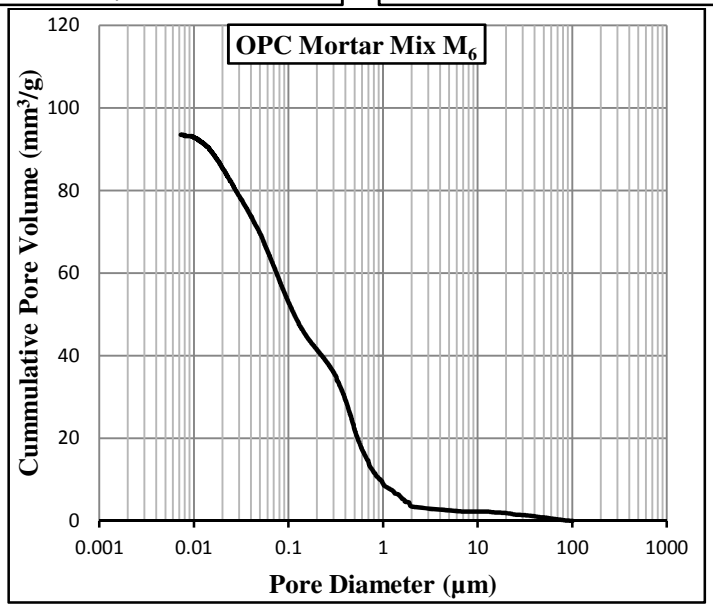

***Appendix. 3.1c**: Intrudable Porosity for AACM and OPC Mixes under Dry Curing*

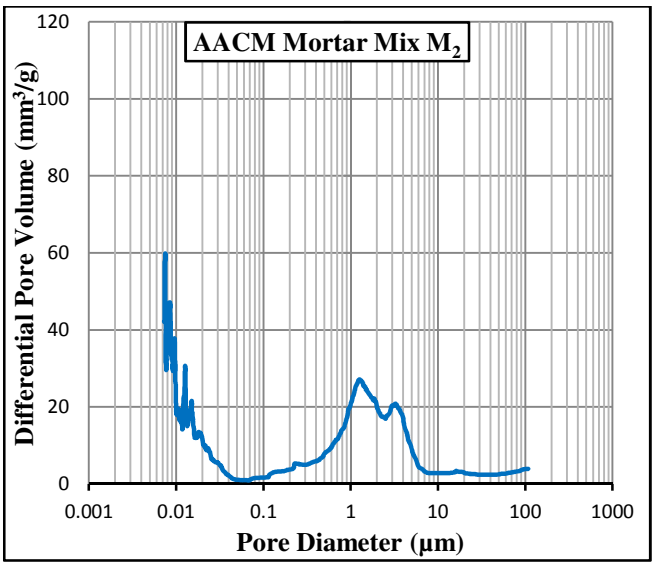

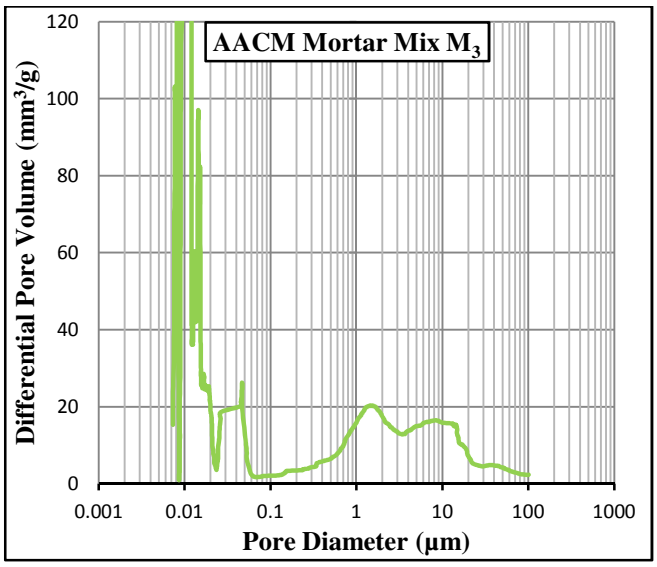

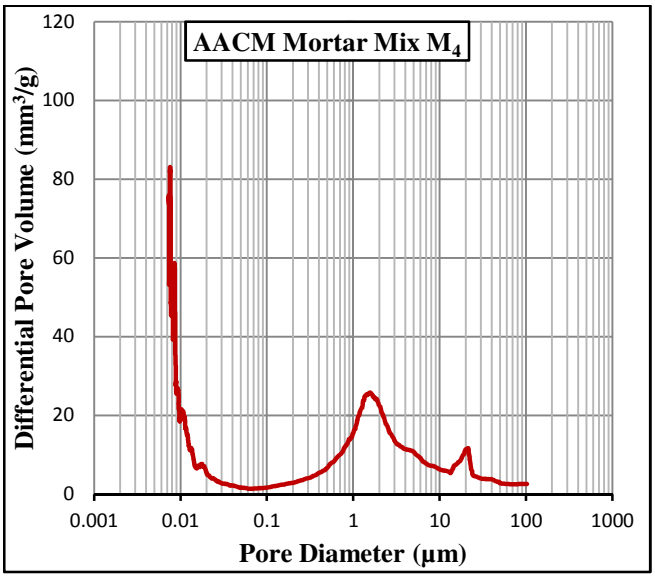

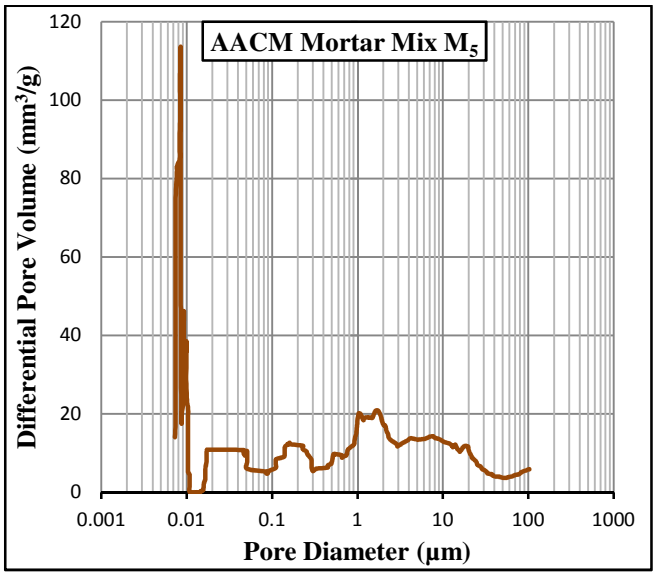

Appendix. 3.2a: *Pore Size Distribution of AACM mixes (with Admixtures) under Wet Curing*

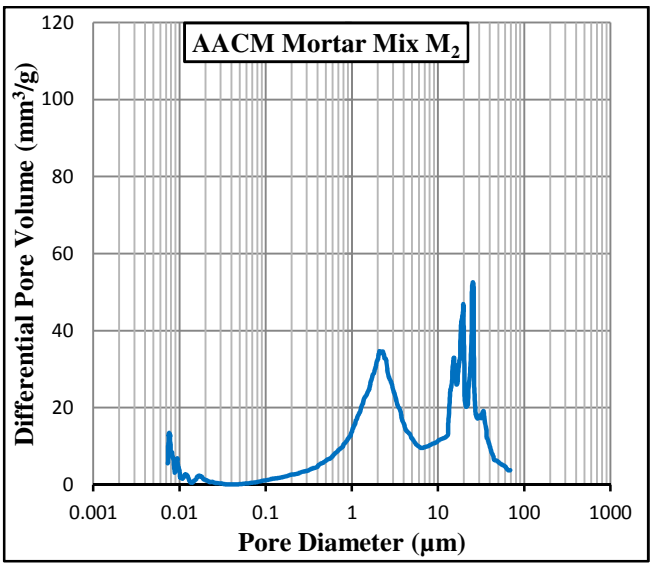

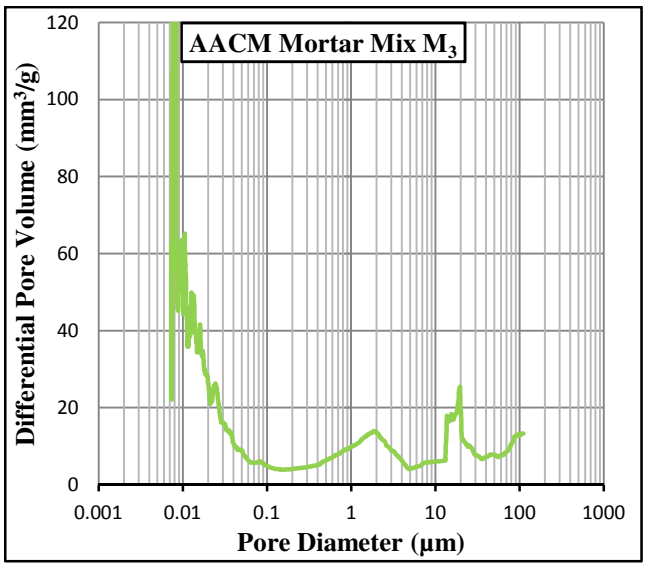

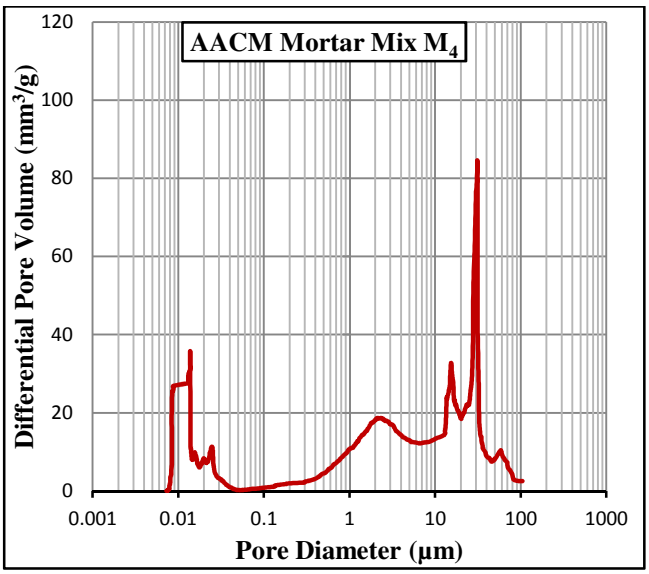

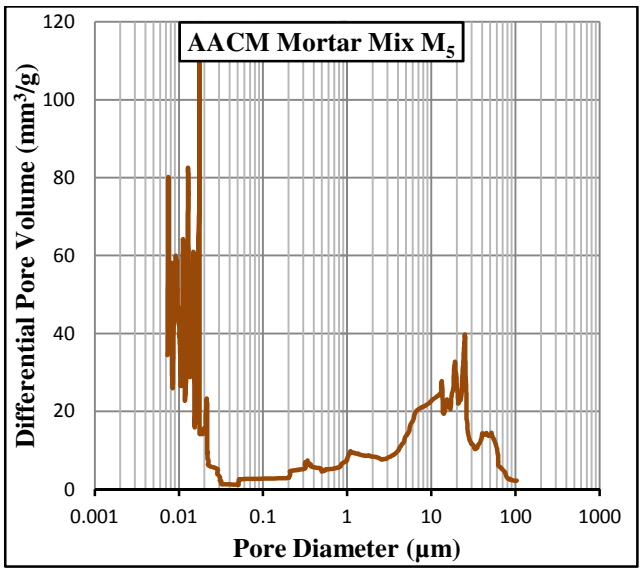

Appendix. 3.2b: *Pore Size Distribution of AACM mixes (Without Admixtures) under Wet Curing*

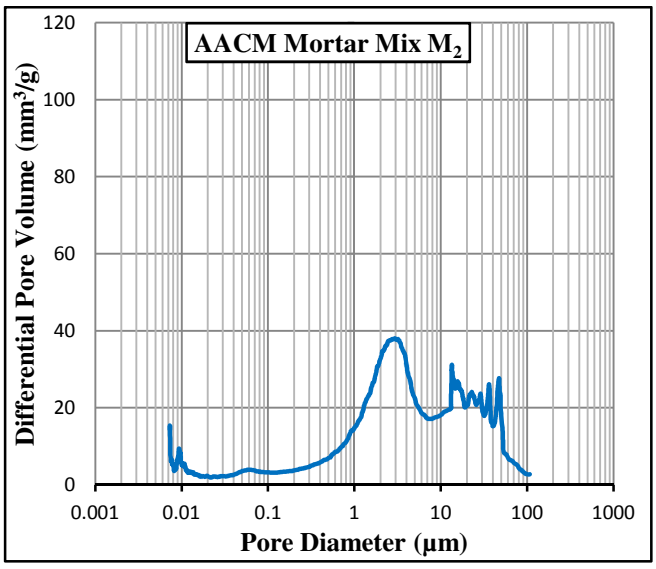

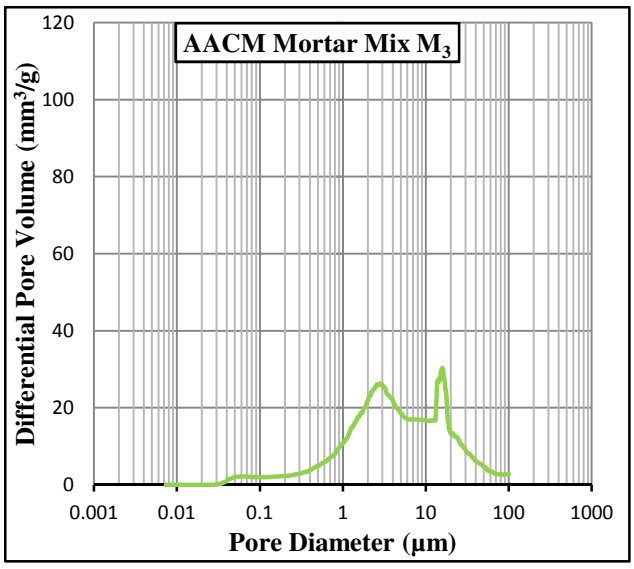

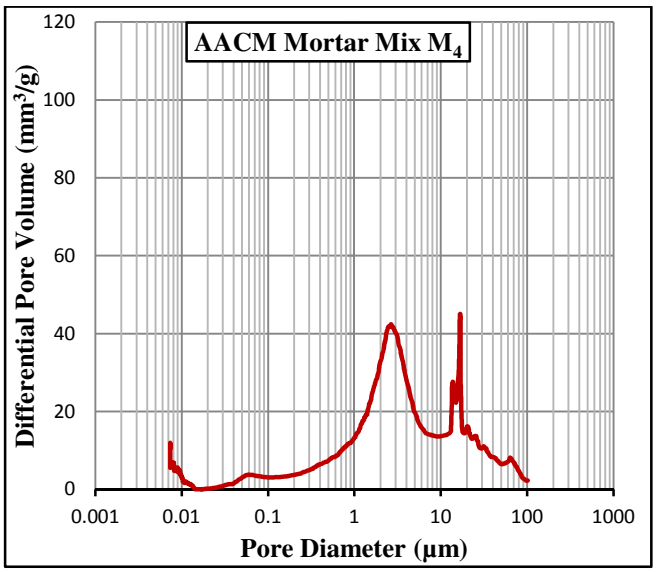

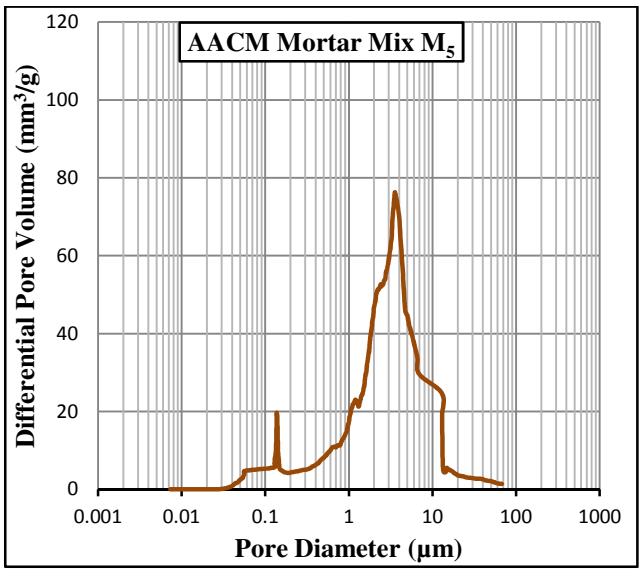

Appendix. 3.2c: *Pore Size Distribution of AACM mixes (with Admixtures) under Dry Curing*

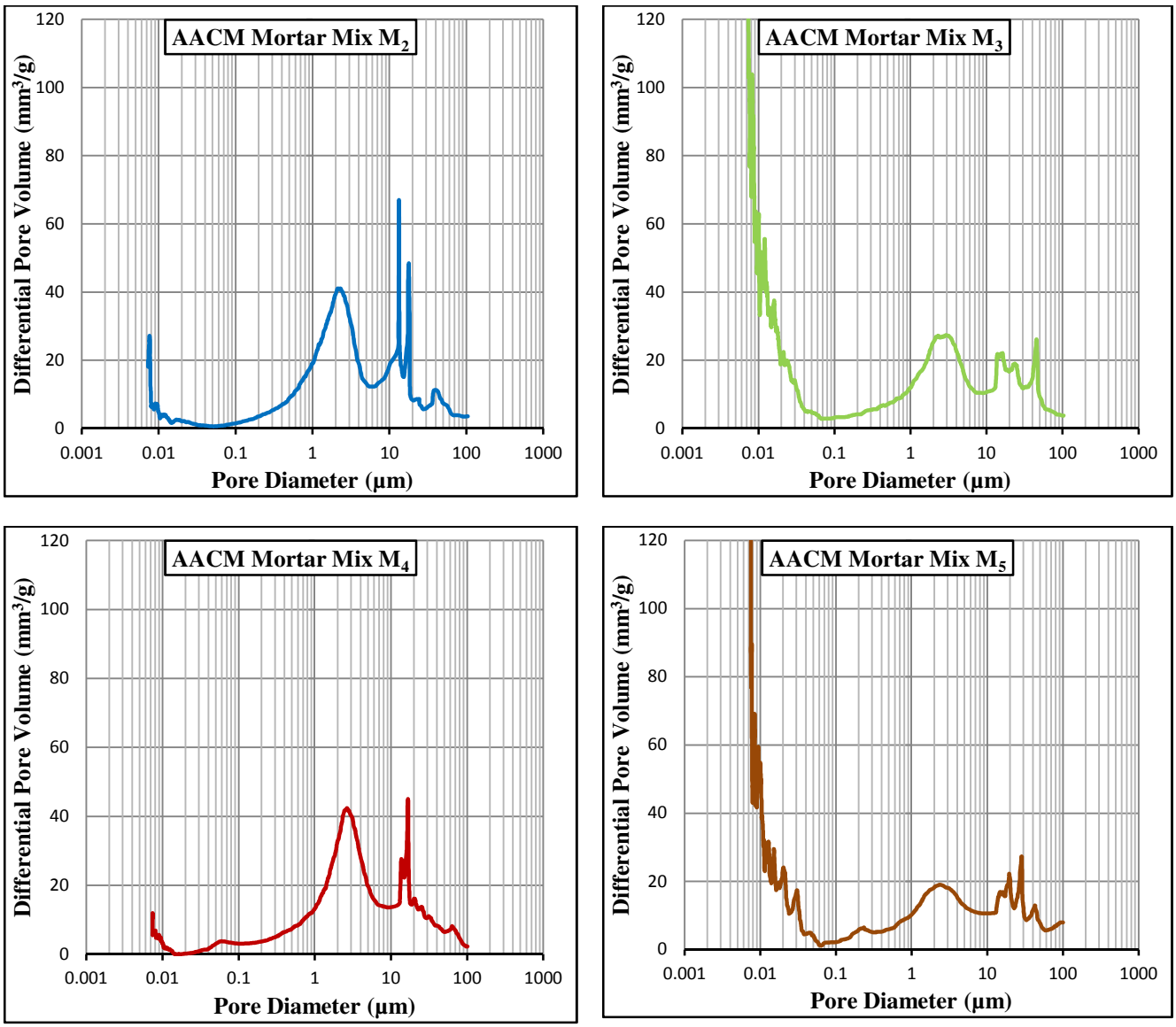

Appendix. 3.2d: *Pore Size Distribution of AACM mixes (without Admixtures) under Dry Curing*

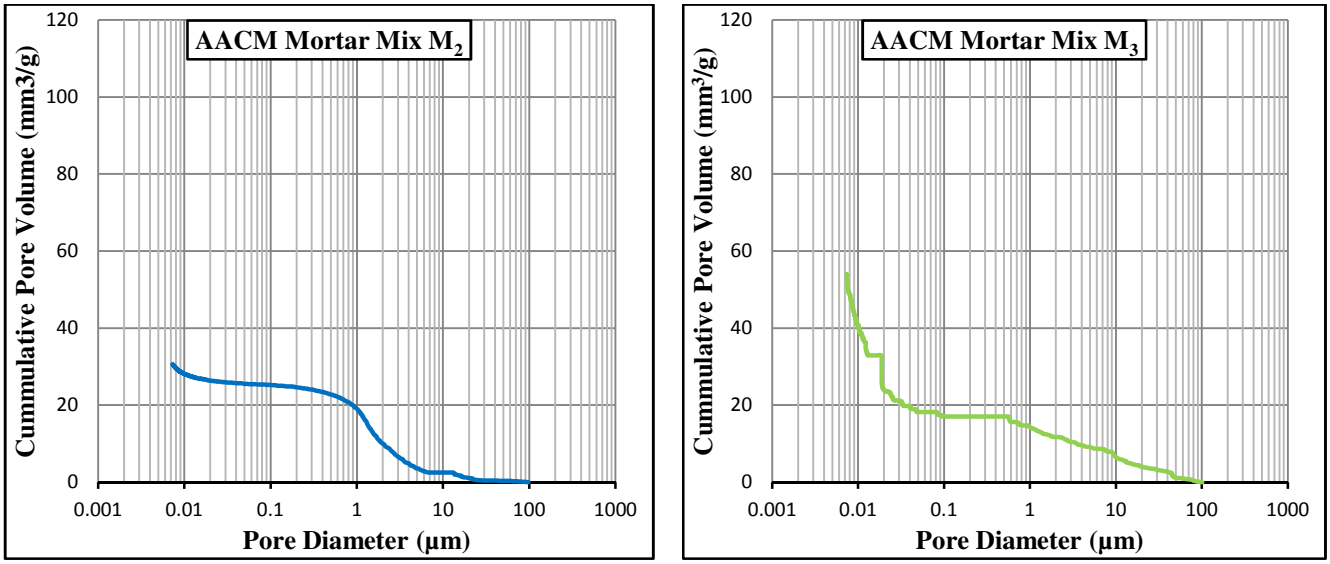

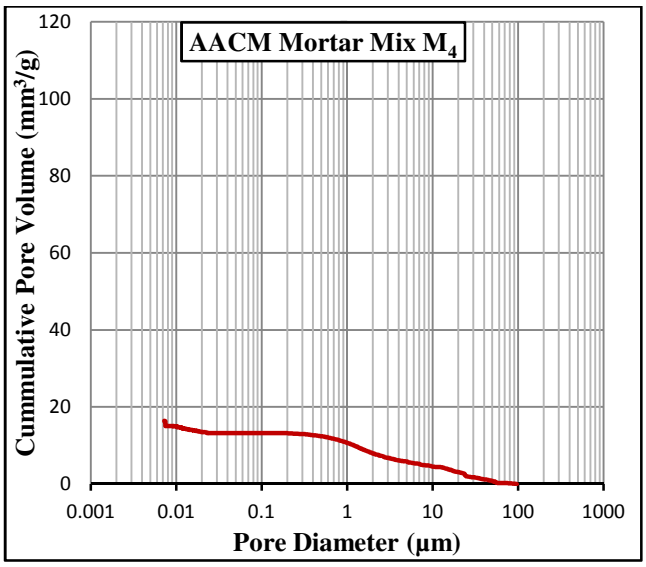

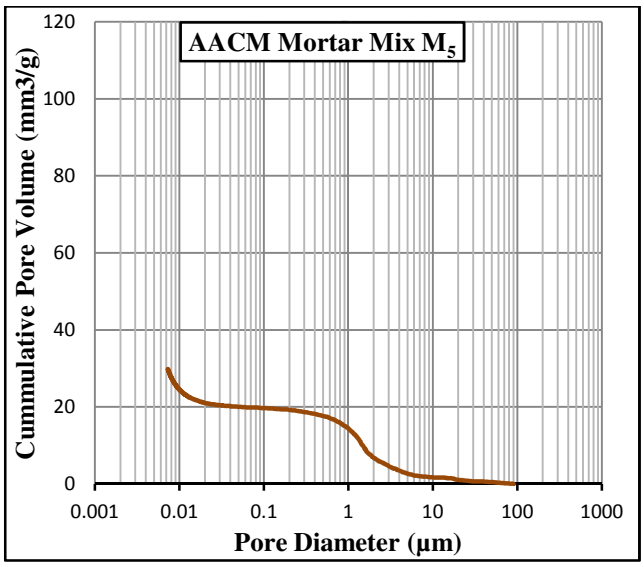

Appendix 3.3a: *Cumulative Pore Volume of AACM mixes (with Admixtures) under Wet/dry Curing*

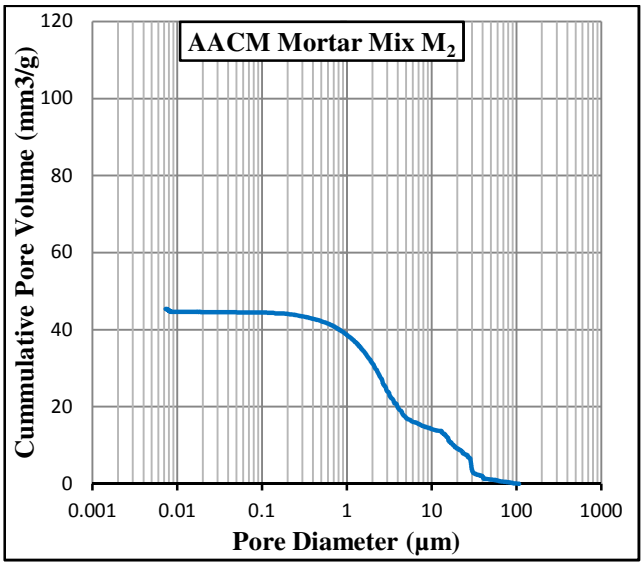

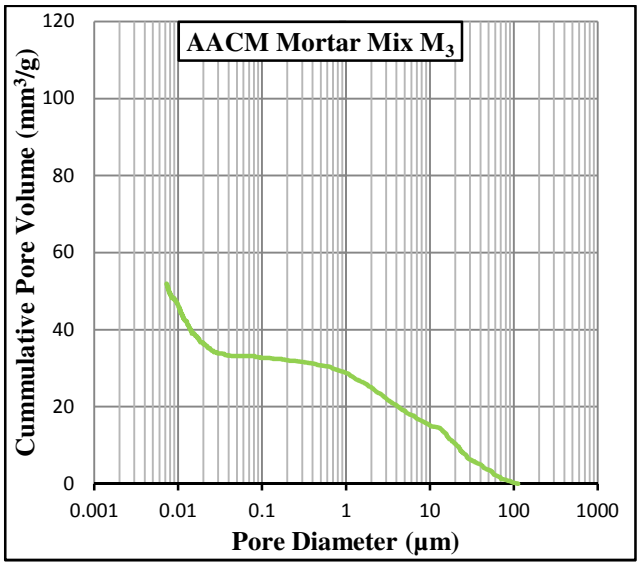

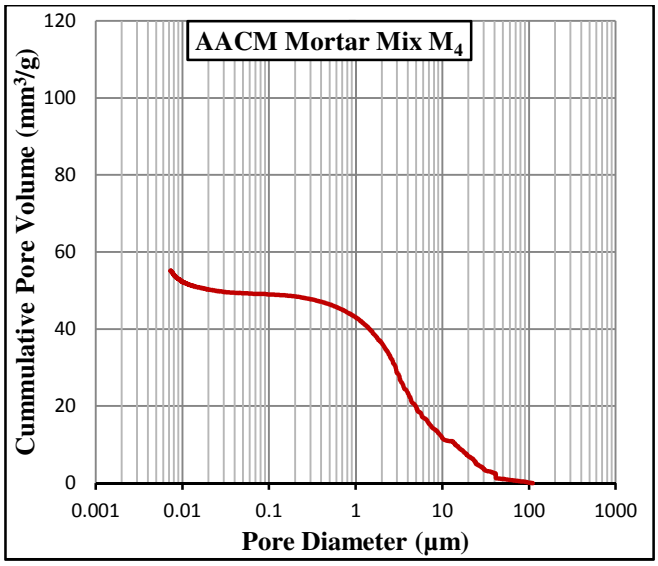

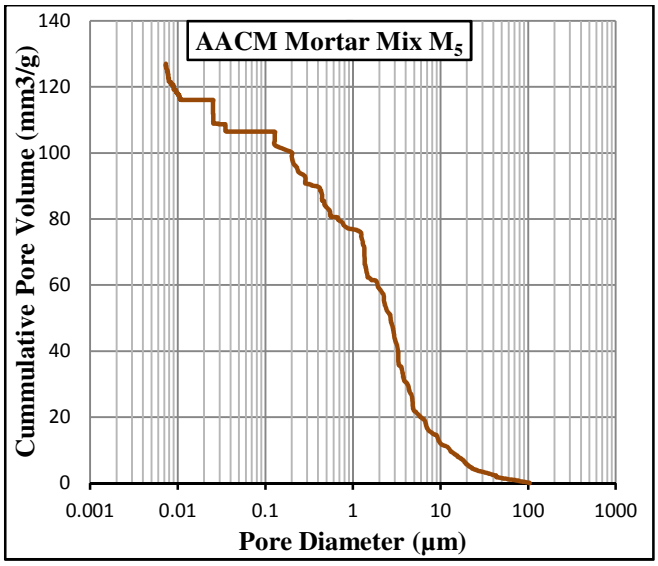

Appendix 3.3b: *Cumulative Pore Volume of AACM mixes (without Admixtures) under Wet/dry Curing*

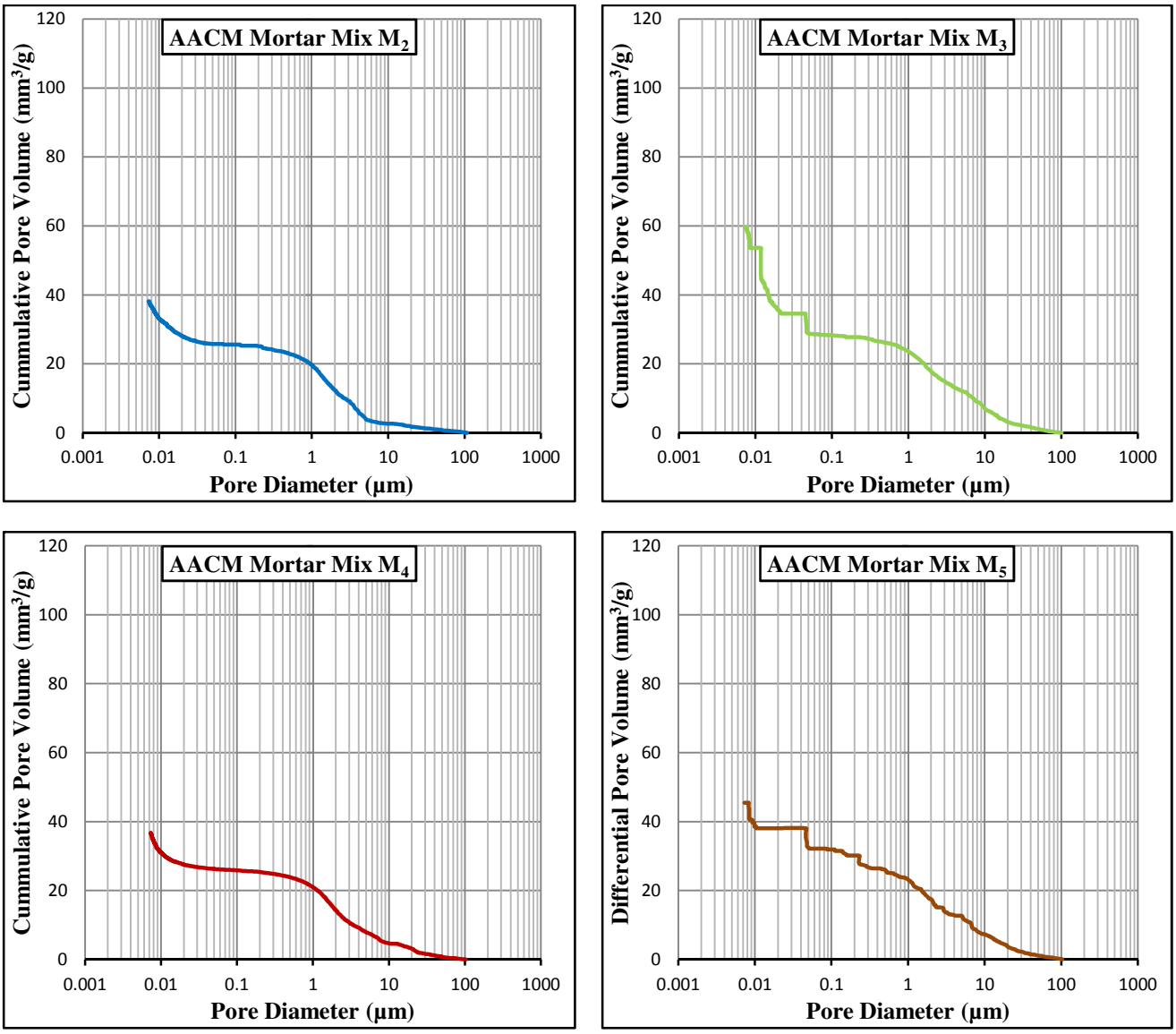

Appendix 3.3c: *Cumulative Pore Volume of AACM mixes (with Admixtures) under Wet Curing*

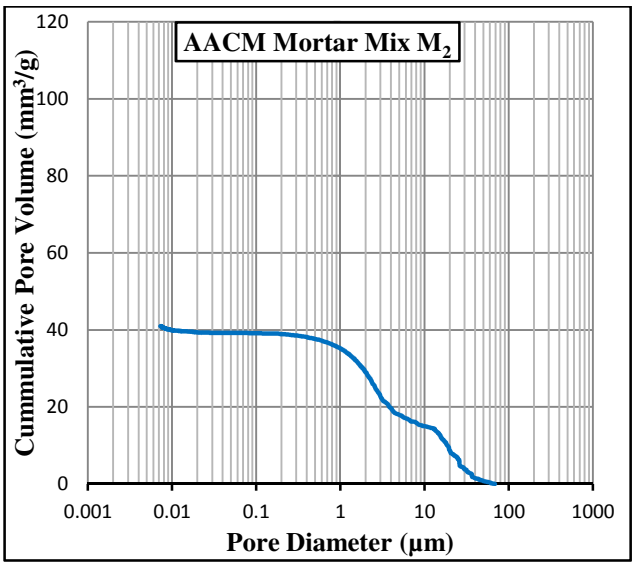

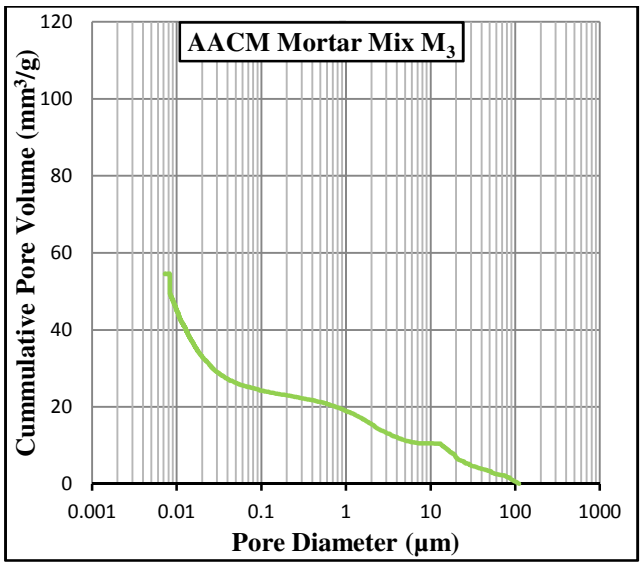

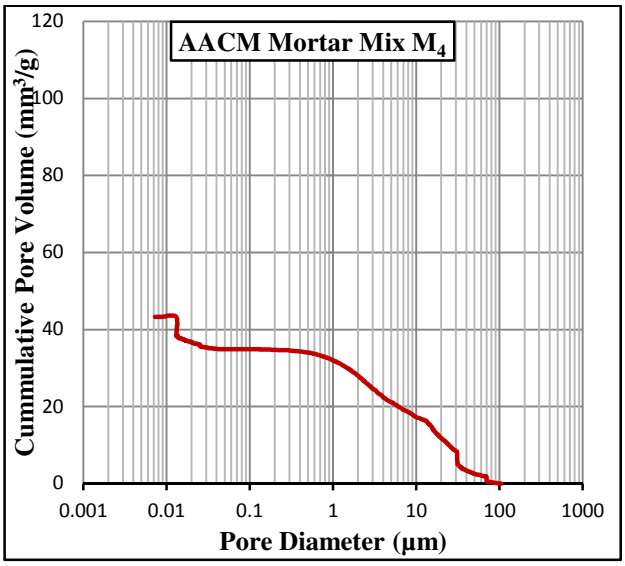

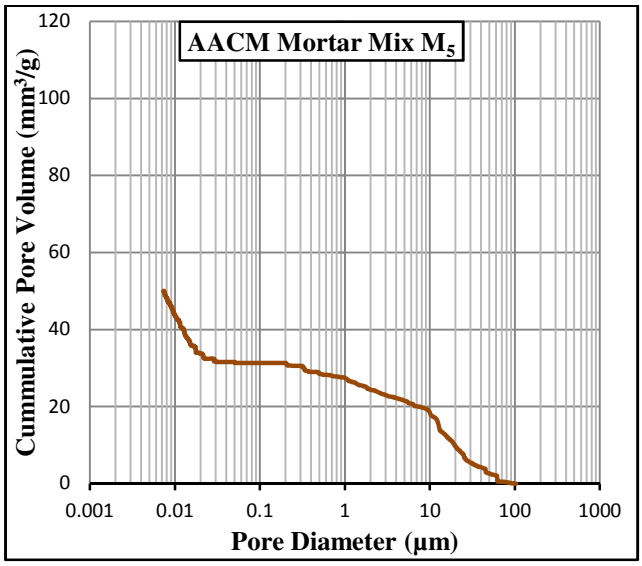

Appendix 3.3d: *Cumulative Pore Volume of AACM mixes (without Admixtures) under Wet Curing*

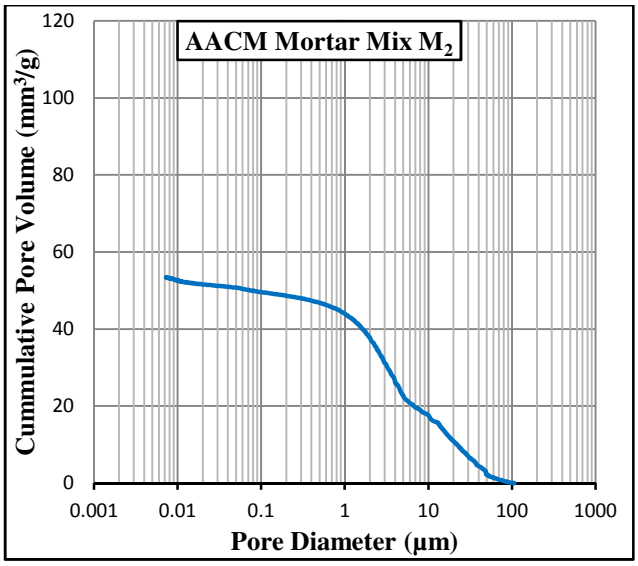

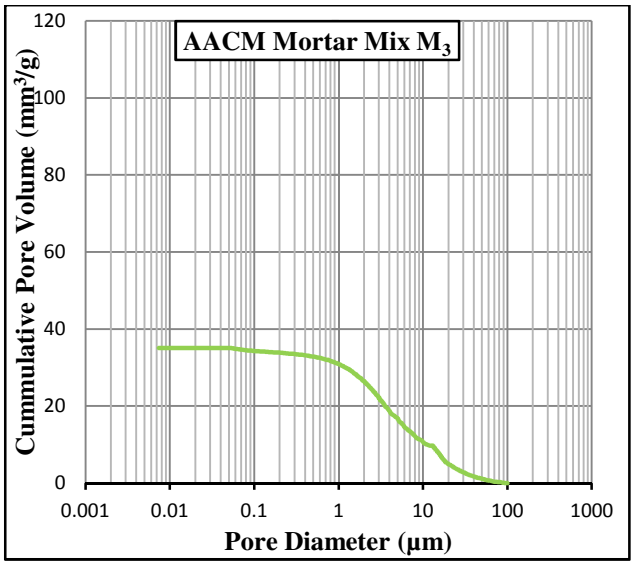

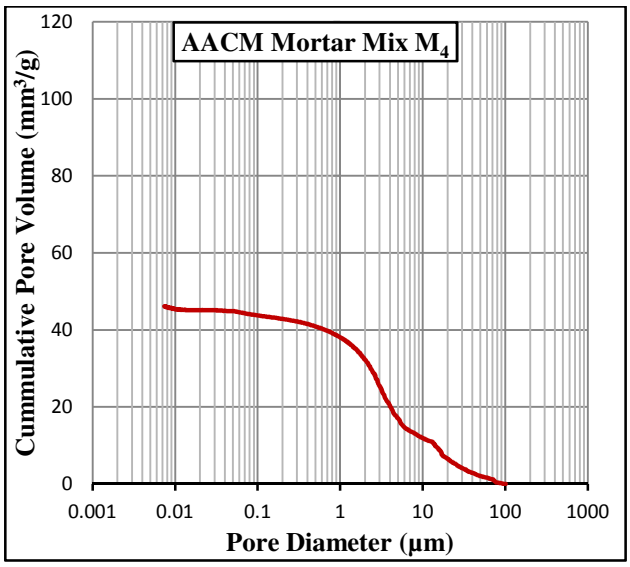

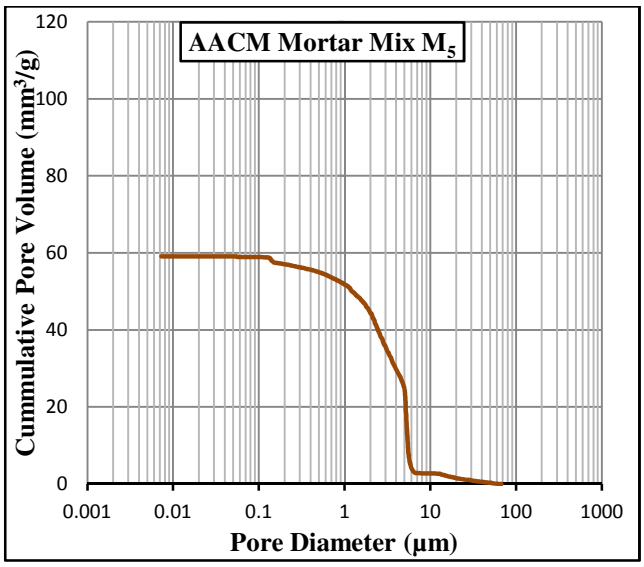

Appendix 3.3e: *Cumulative Pore Volume of AACM mixes (with Admixtures) under Dry Curing*

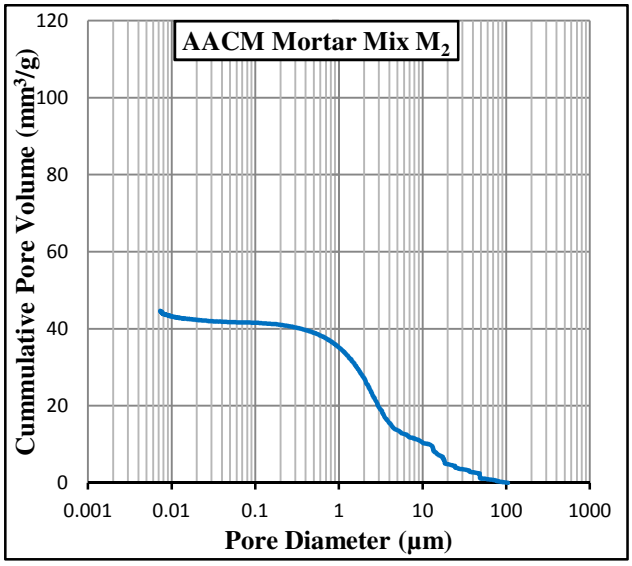

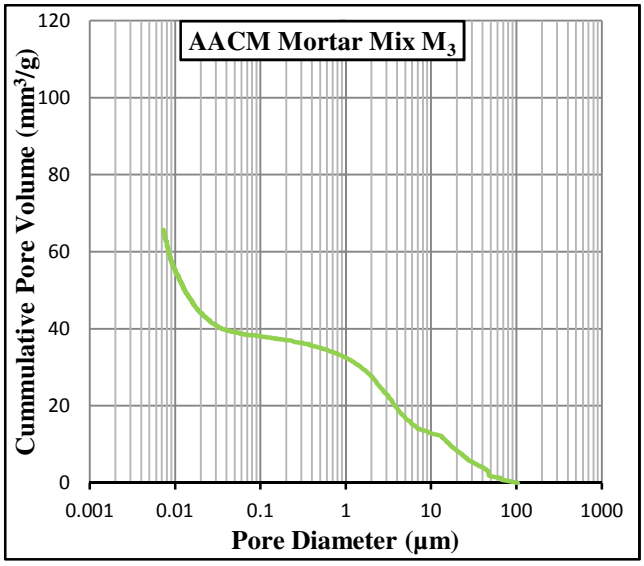

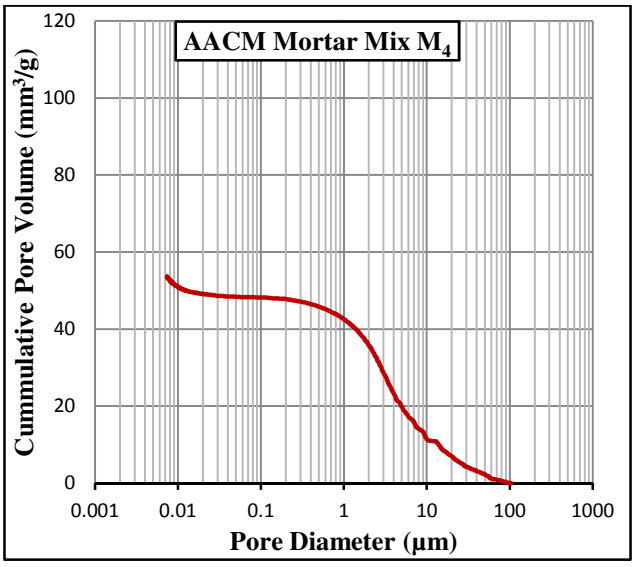

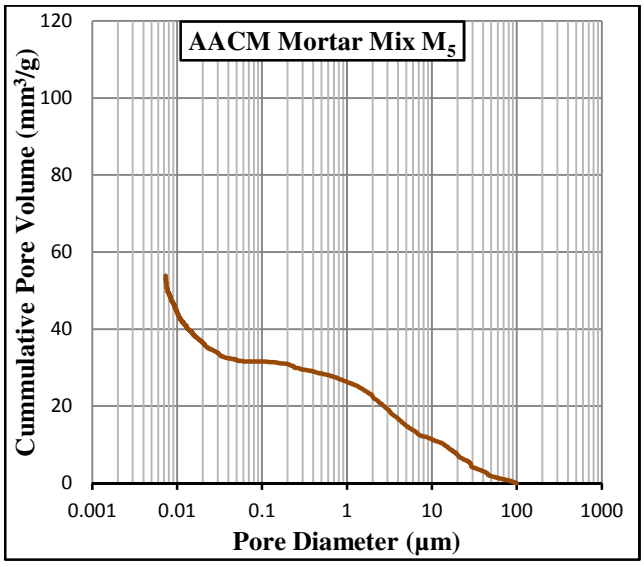

Appendix 3.3f: *Cumulative Pore Volume of AACM mixes (without Admixtures) under Dry Curing*

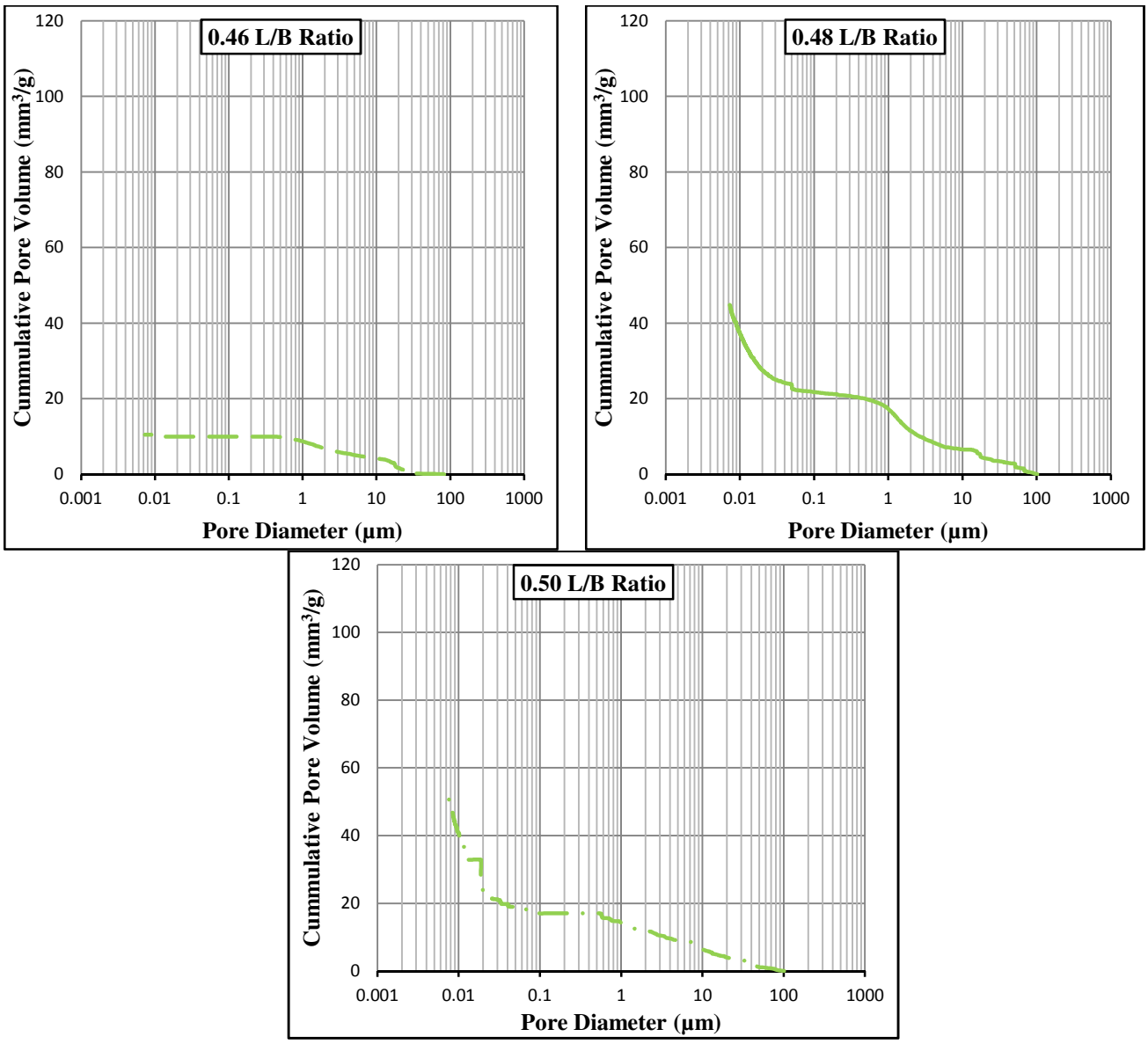

Appendix 3.4a: *Cumulative Pore Volume of AACM Mortar Mix M_3 (different Liquid/Binder Ratio) under Wet/dry curing*

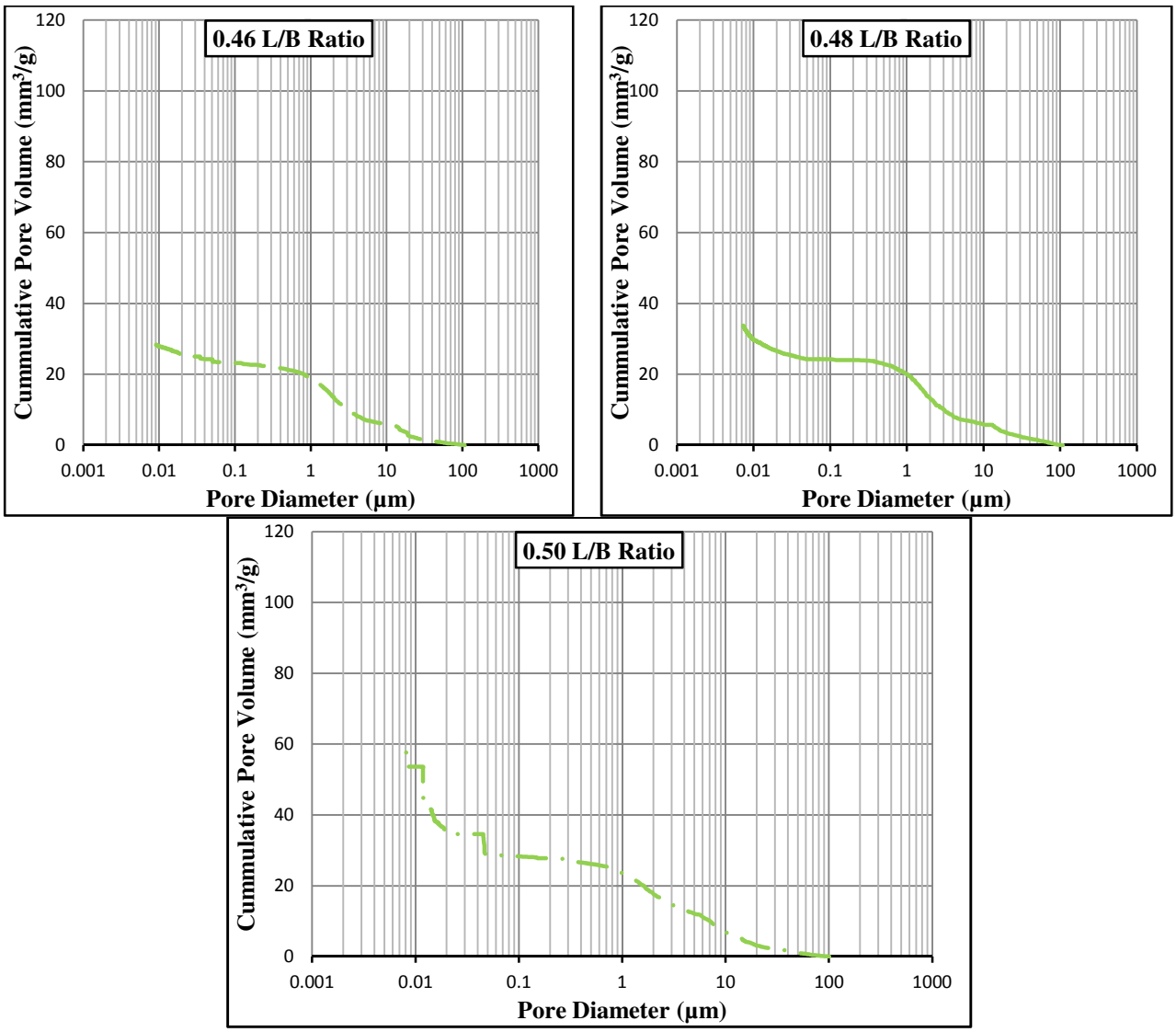

Appendix 3.4b: *Cumulative Pore Volume of AACM Mortar Mix M_3 (different Liquid/Binder Ratio) under Wet curing*

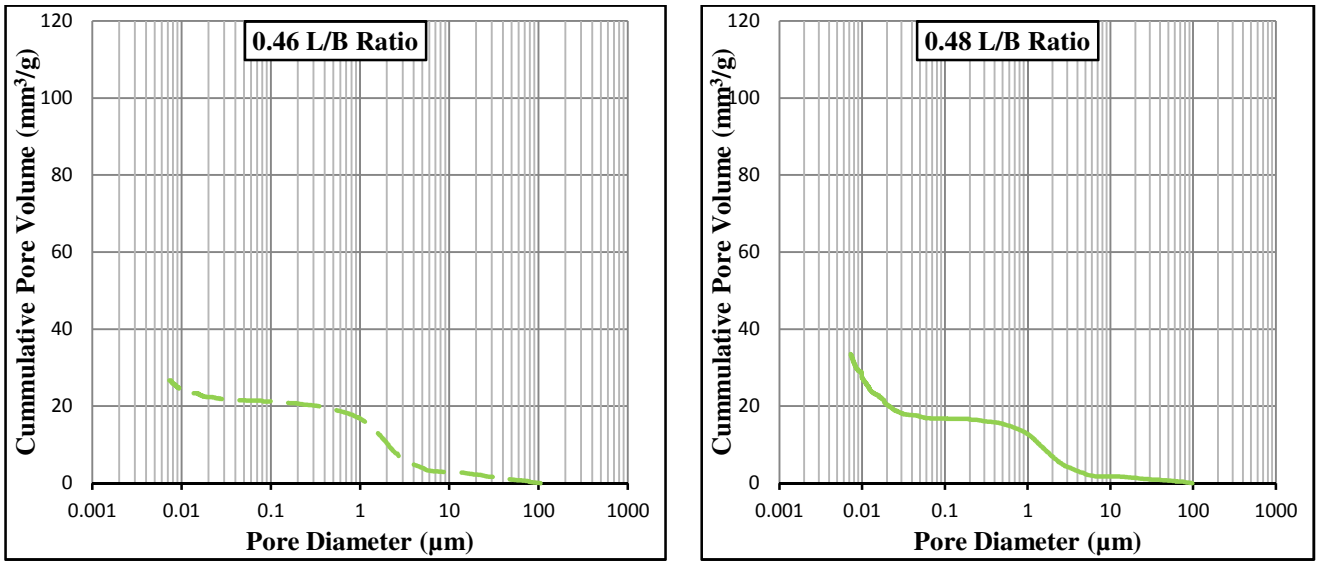

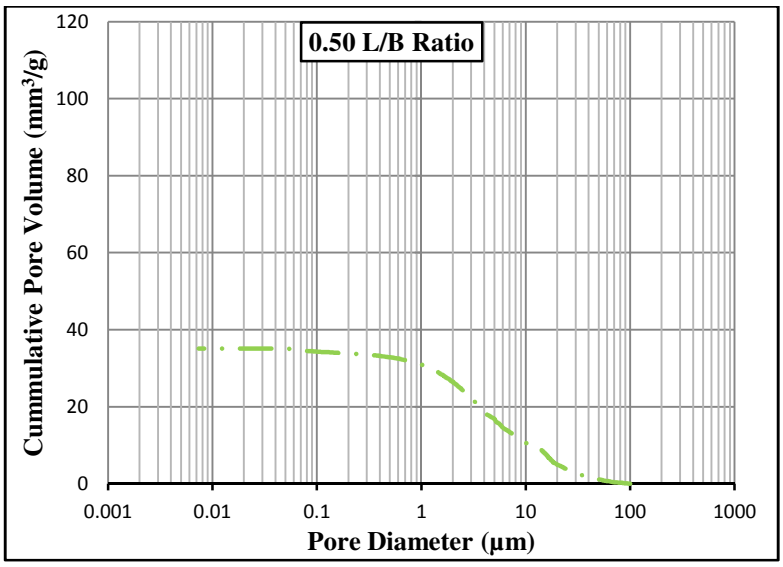

Appendix 3.4c: *Cumulative Pore Volume of AACM Mortar Mix M_3 (different Liquid/Binder Ratio) under Dry curing*

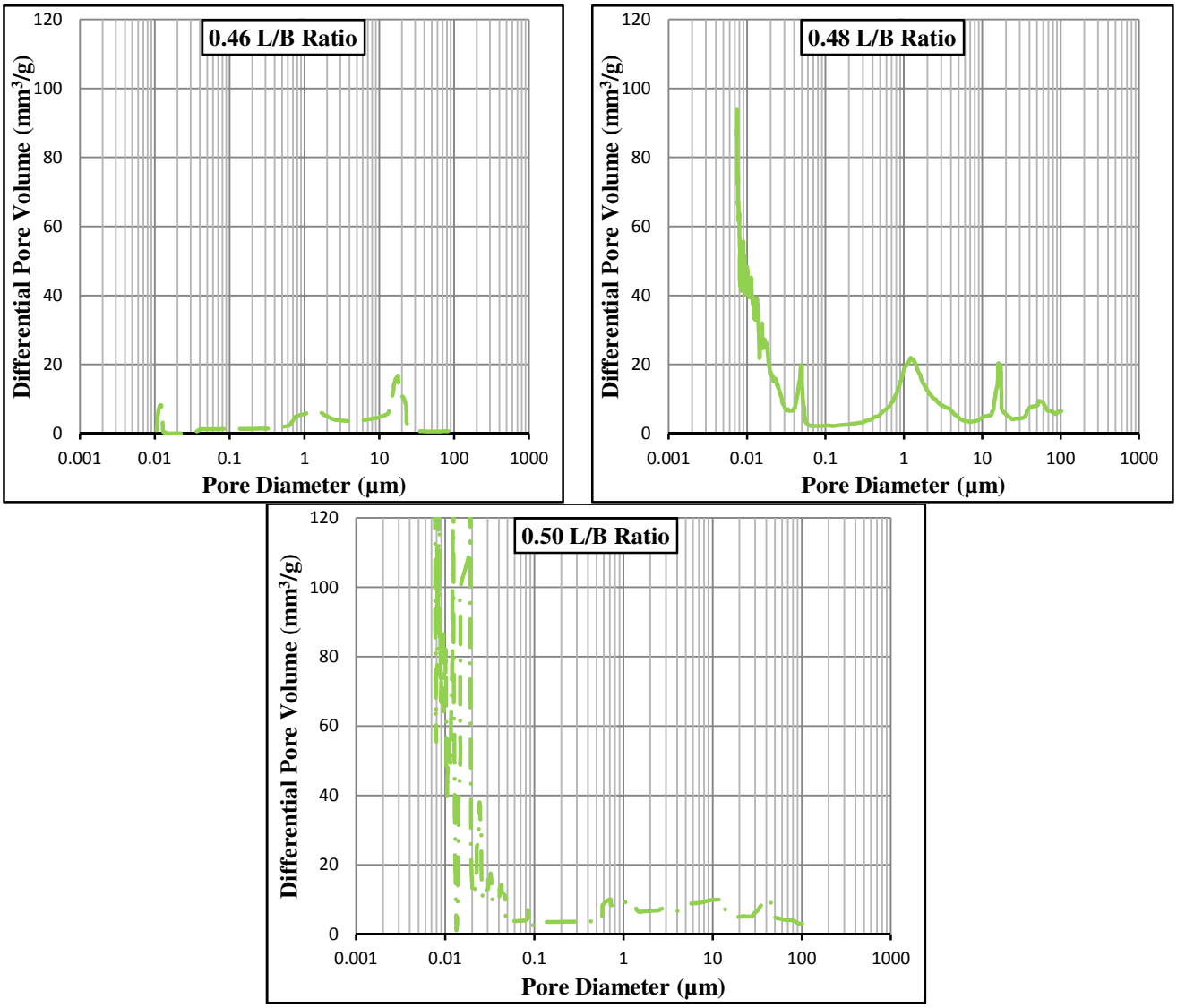

Appendix 3.5a: *Differential Pore Volume of AACM Mortar Mix M_3 (different Liquid/Binder Ratio) under Wet/dry curing*

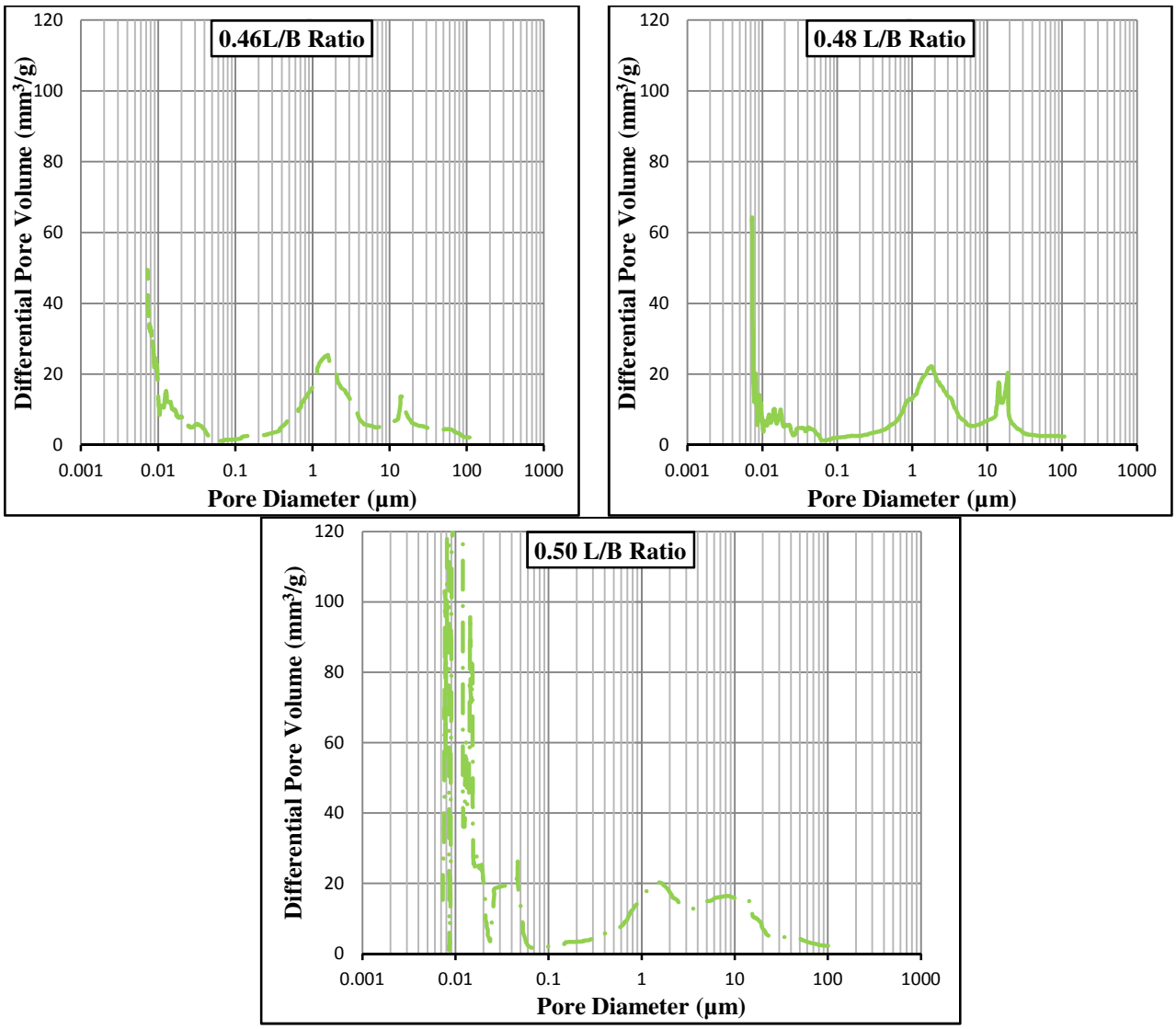

Appendix 3.5b: *Differential Pore Volume of AACM Mortar Mix M_3 (different Liquid/Binder Ratio) under Wet curing*

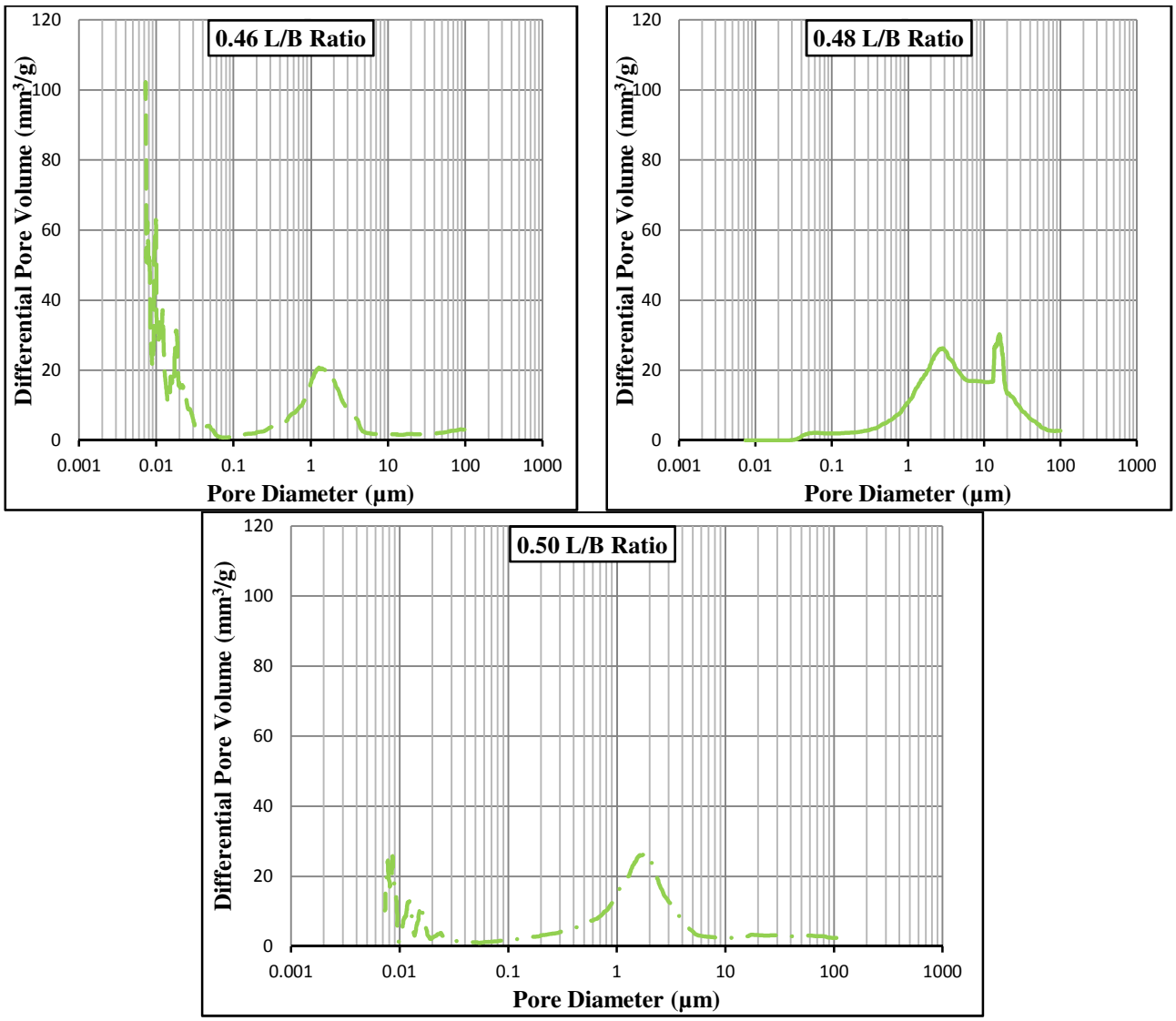

Appendix 3.5c: *Differential Pore Volume of AACM Mortar Mix M_3 (different Liquid/Binder Ratio) under Dry curing*

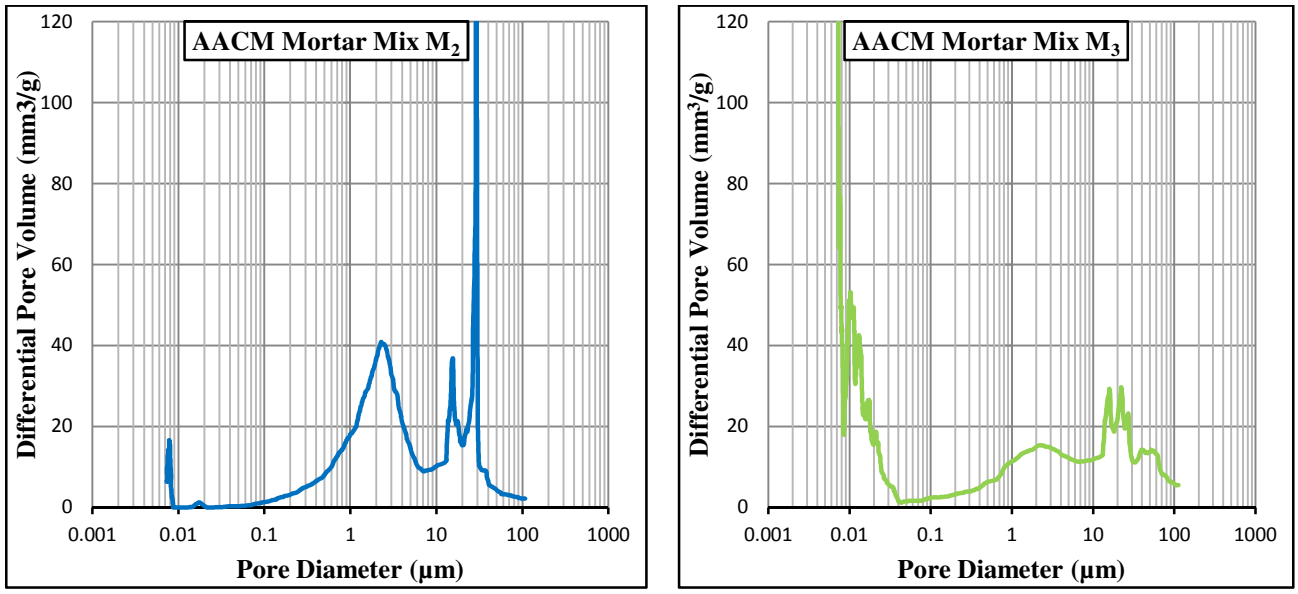

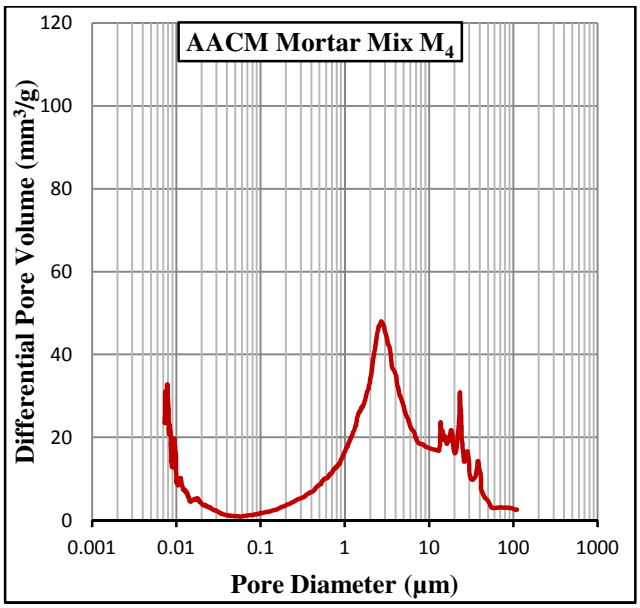

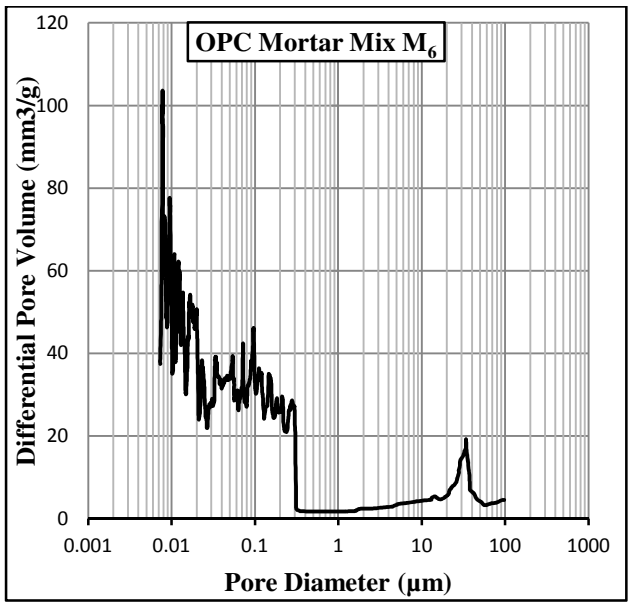

Appendix 3.6a: *Pore Size Distribution of AACM and OPC mixes (without Admixtures) under Wet/dry Curing*

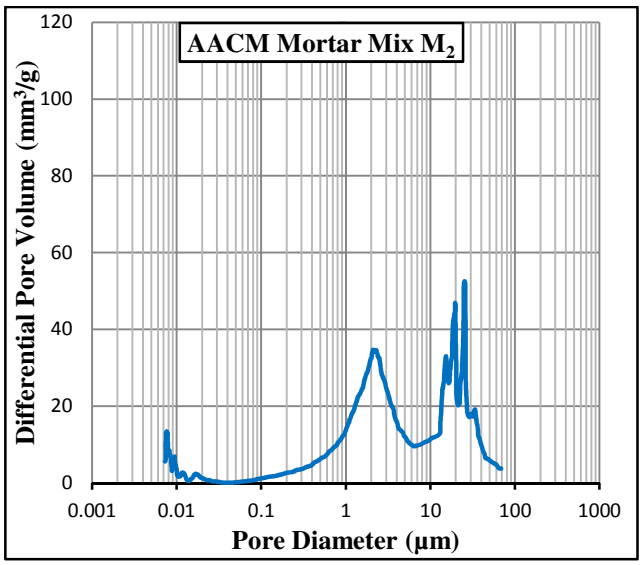

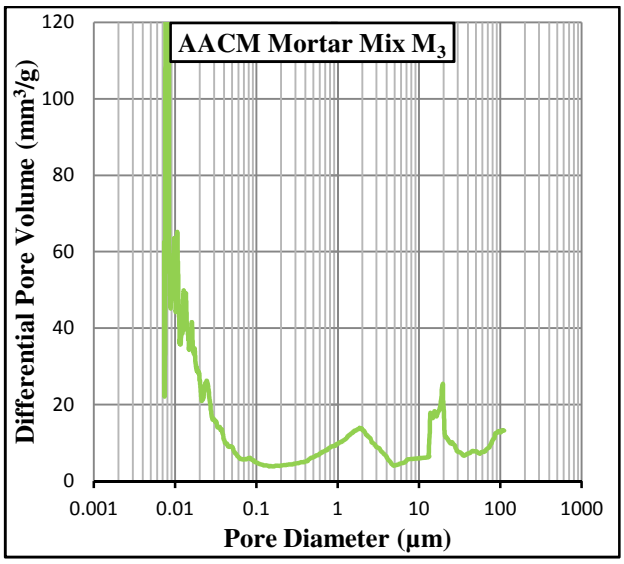

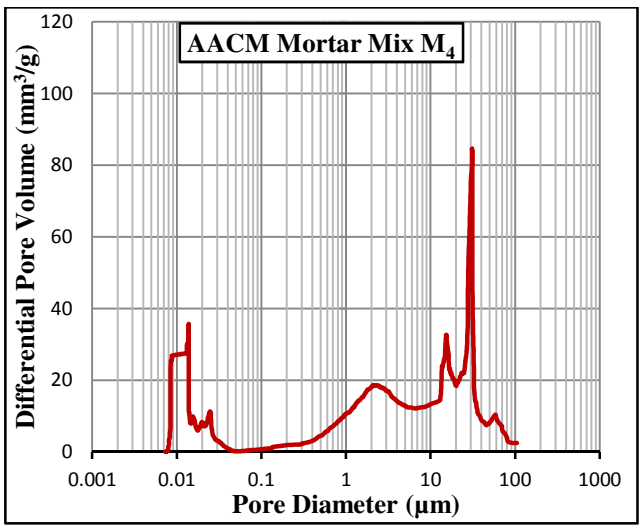

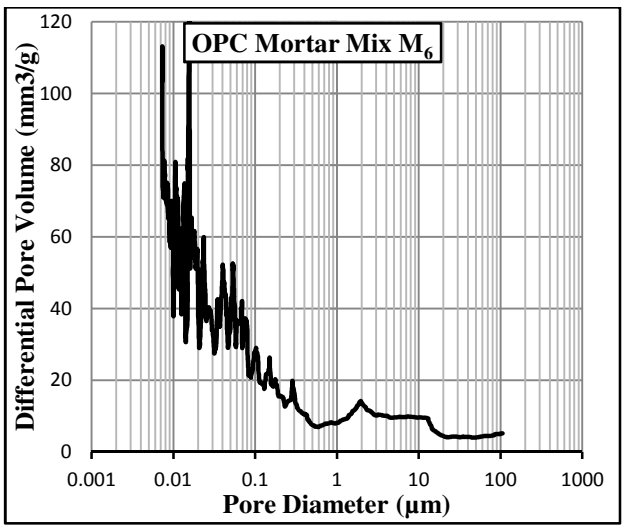

Appendix 3.6b: *Pore Size Distribution of AACM and OPC mixes (Without Admixtures) under Wet Curing*

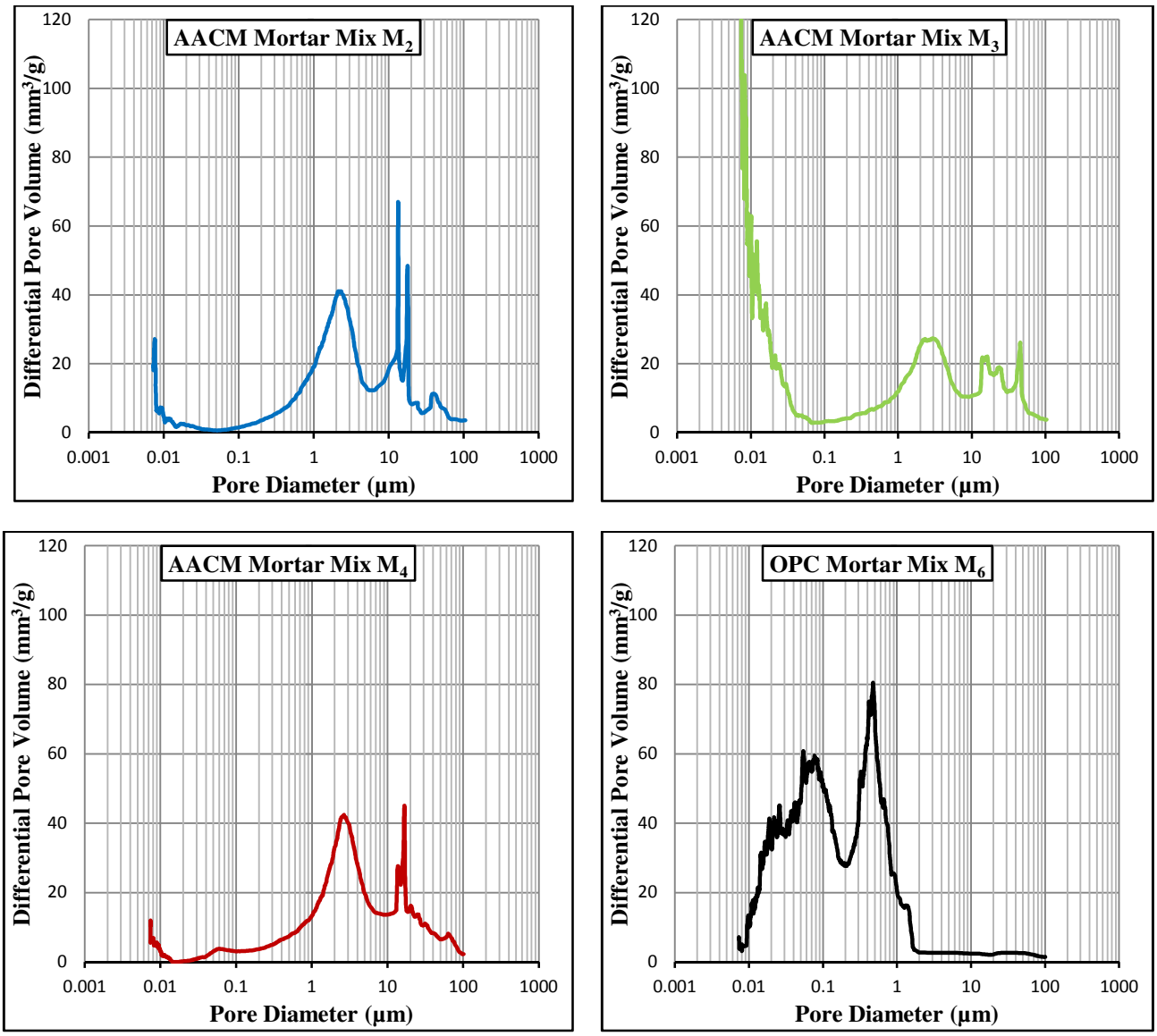

Appendix 3.6c: *Pore Size Distribution of AACM and OPC mixes (without Admixtures) under Dry Curing*

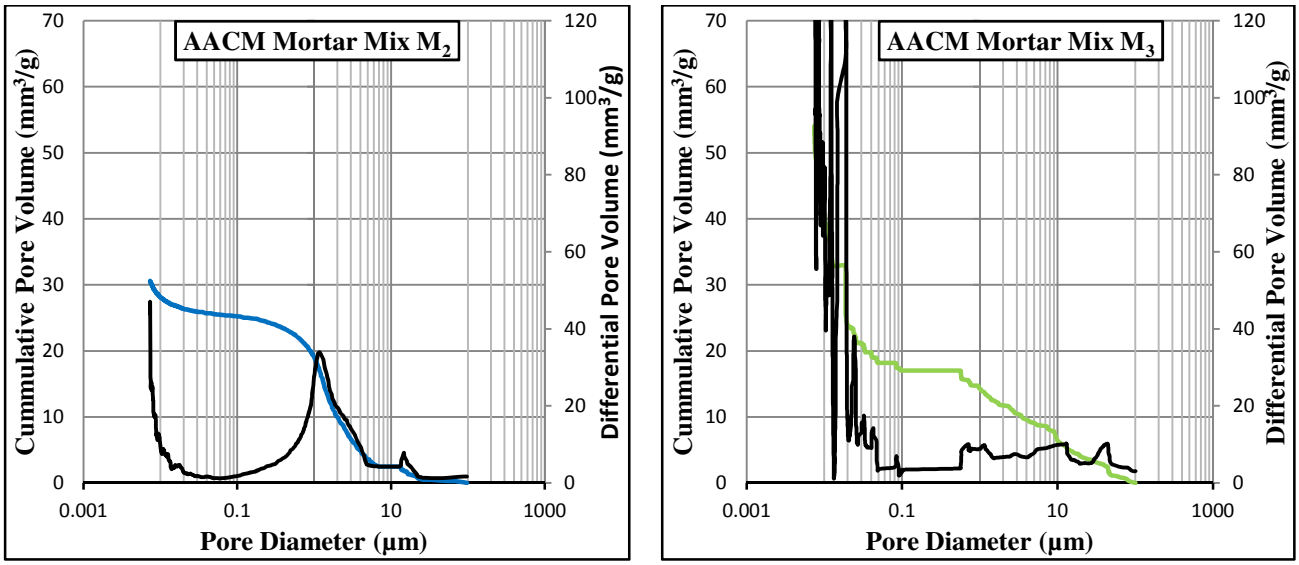

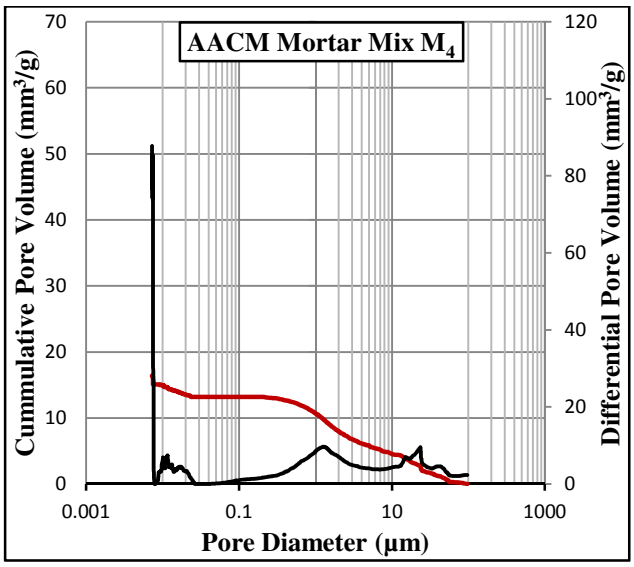

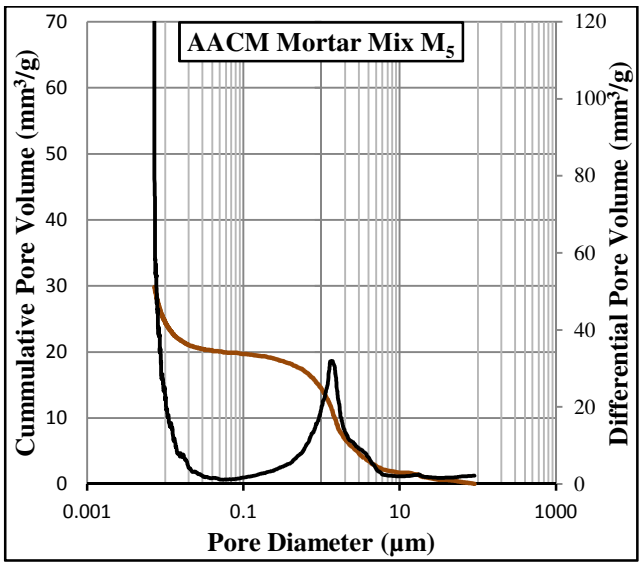

Appendix 3.7a: *Cumulative and Differential Pore Volumes of AACM Mortar Mixes M_2 to M_5 under Wet/dry Curing (batch a).*

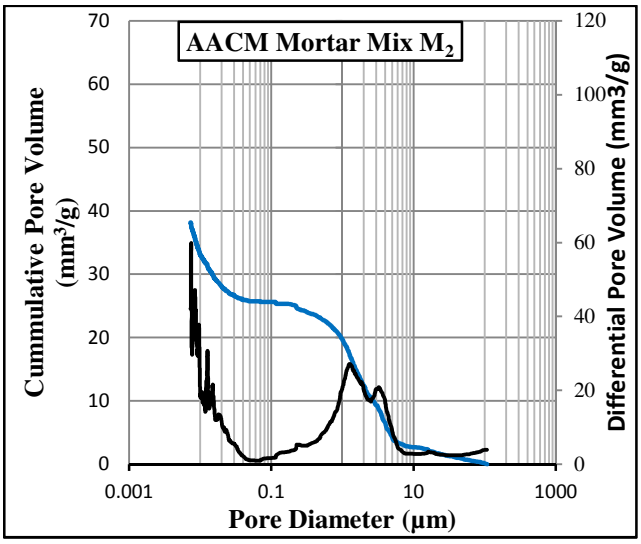

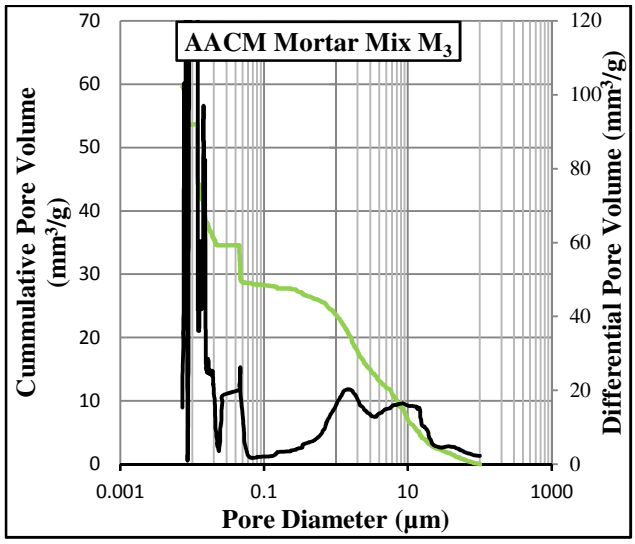

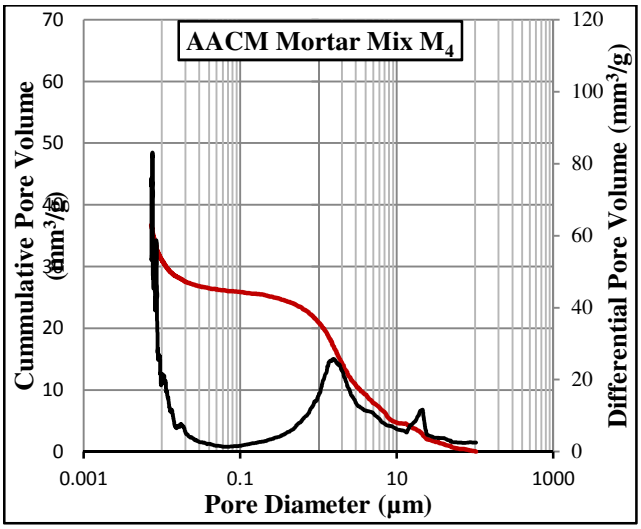

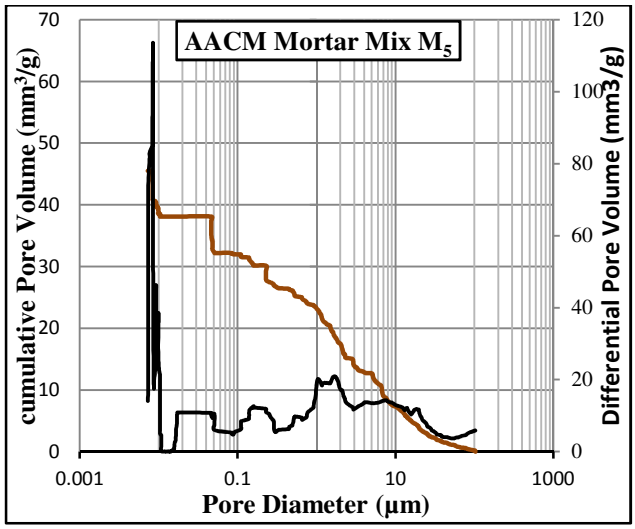

Appendix 3.7b: *Cumulative and Differential Pore Volumes of AACM Mortar Mixes M_2 to M_5 under Wet Curing (batch a).*

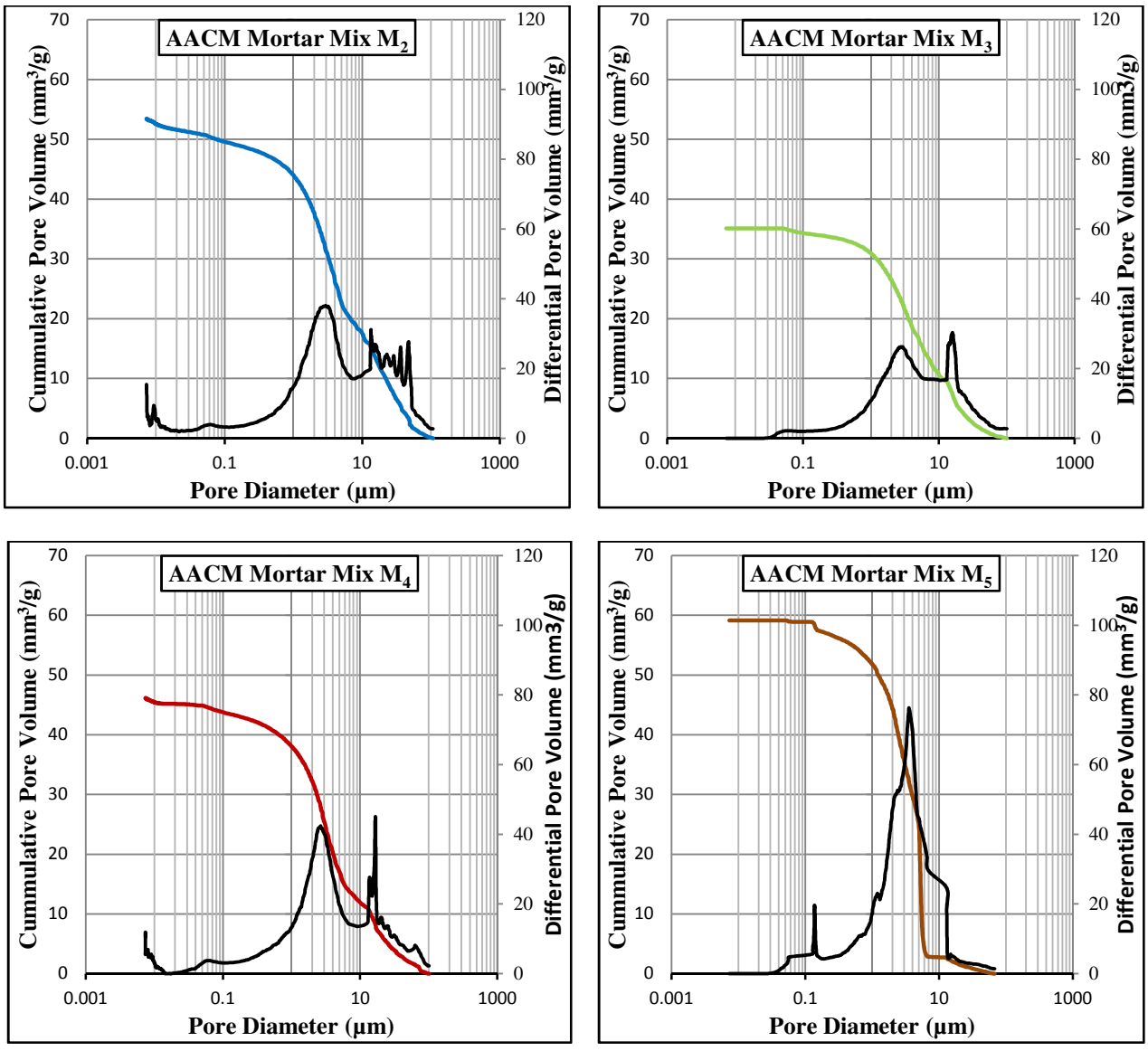

Appendix 3.7c: *Cumulative and Differential Pore Volumes of AACM Mortar Mixes M_2 to M_5 under Dry Curing (batch a).*

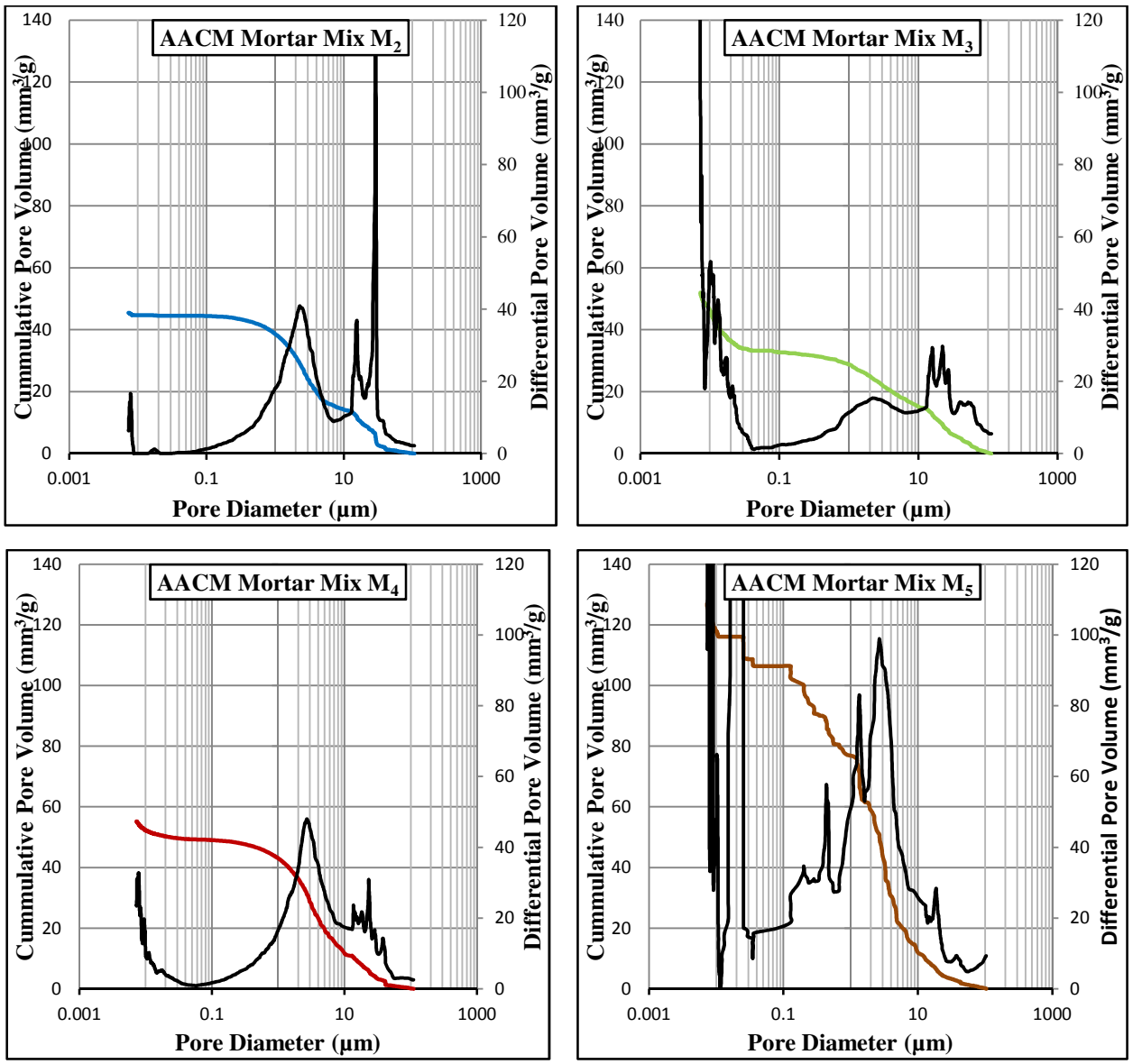

Appendix 3.8a: *Cumulative and Differential Pore Volumes of AACM Mortar Mixes M_2 to M_5 under Wet/dry curing*

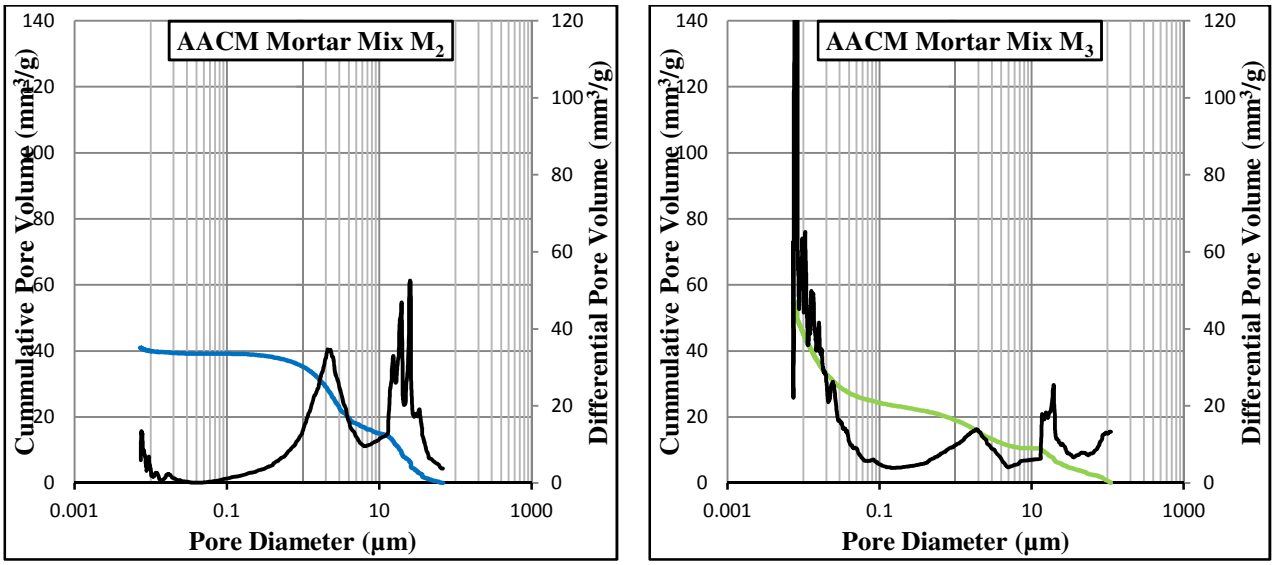

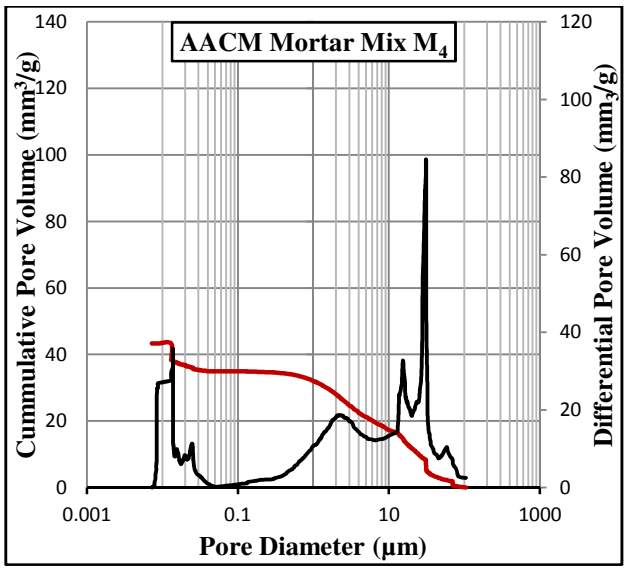

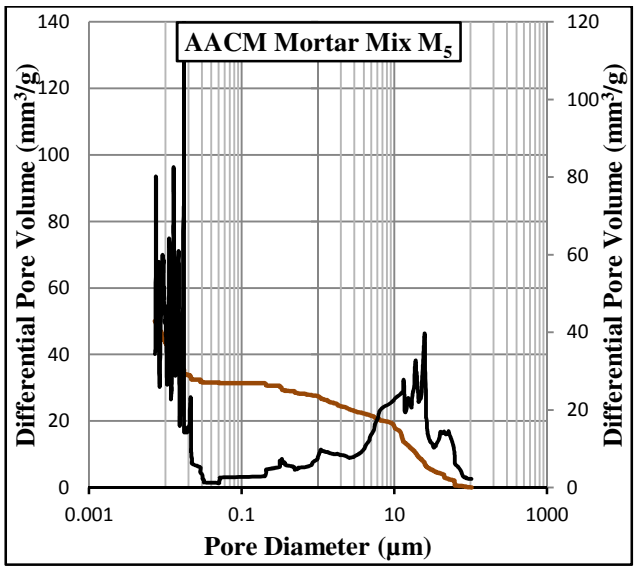

Appendix 3.8b: *Cumulative and Differential Pore Volumes of AACM Mortar Mixes M_2 to M_5 under Wet Curing (batch b).*

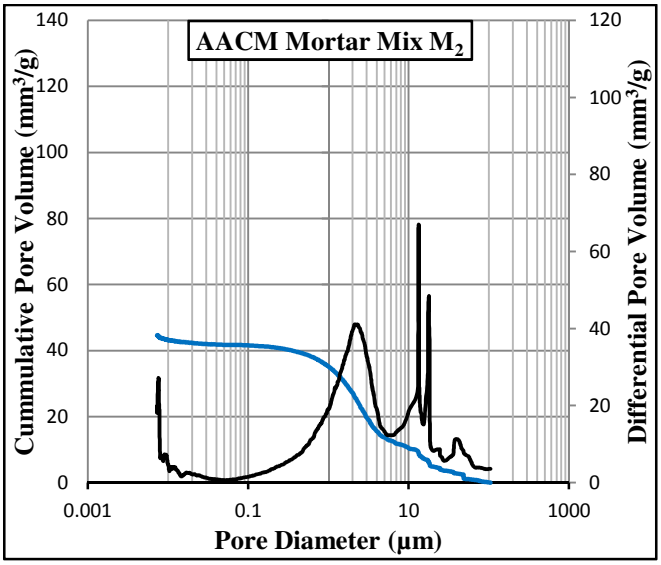

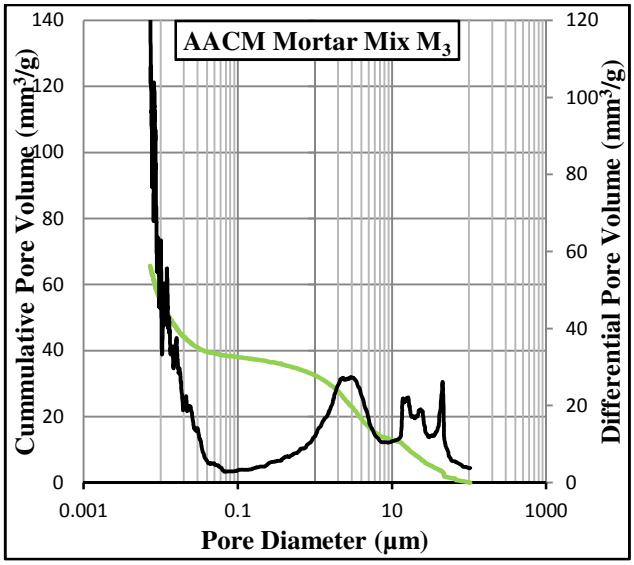

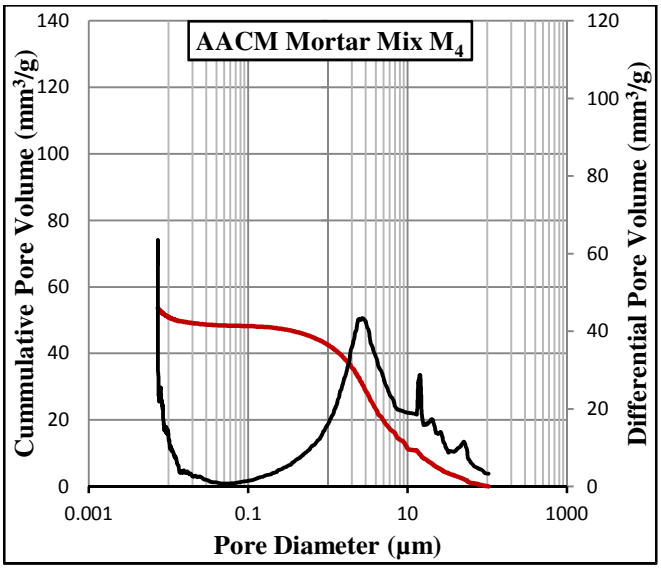

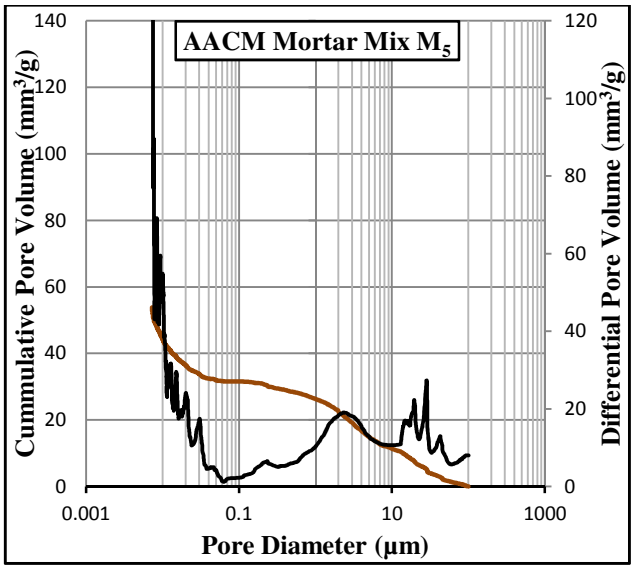

Appendix 3.8c: *Cumulative and Differential Pore Volumes of AACM Mortar Mixes M_2 to M_5 under Dry Curing (batch b).*

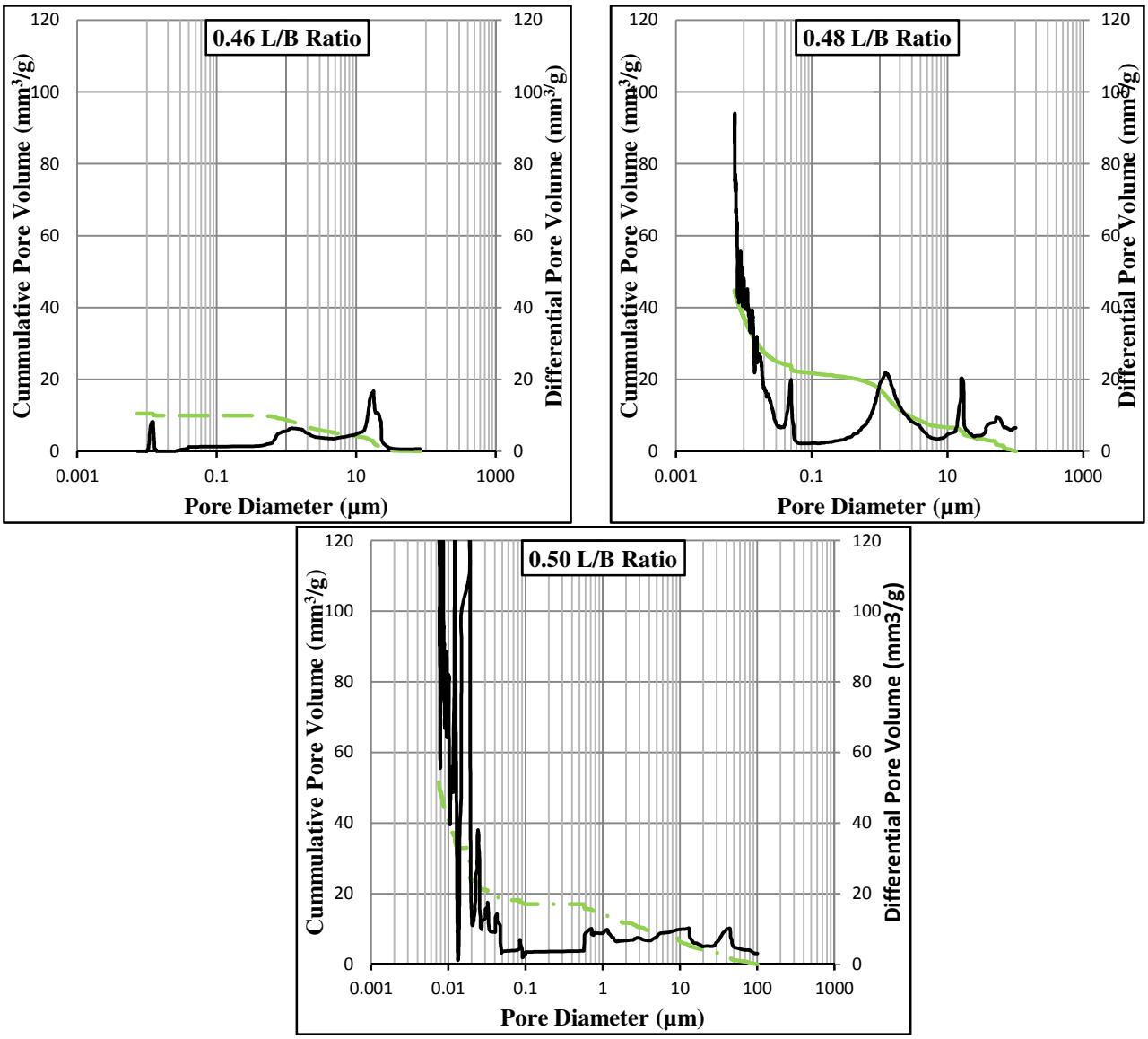

Appendix 3.9a: *Cumulative and Differential Pore Volumes of AACM Mortar Mixes M_2 to M_5 under Wet/dry Curing (batch a).*

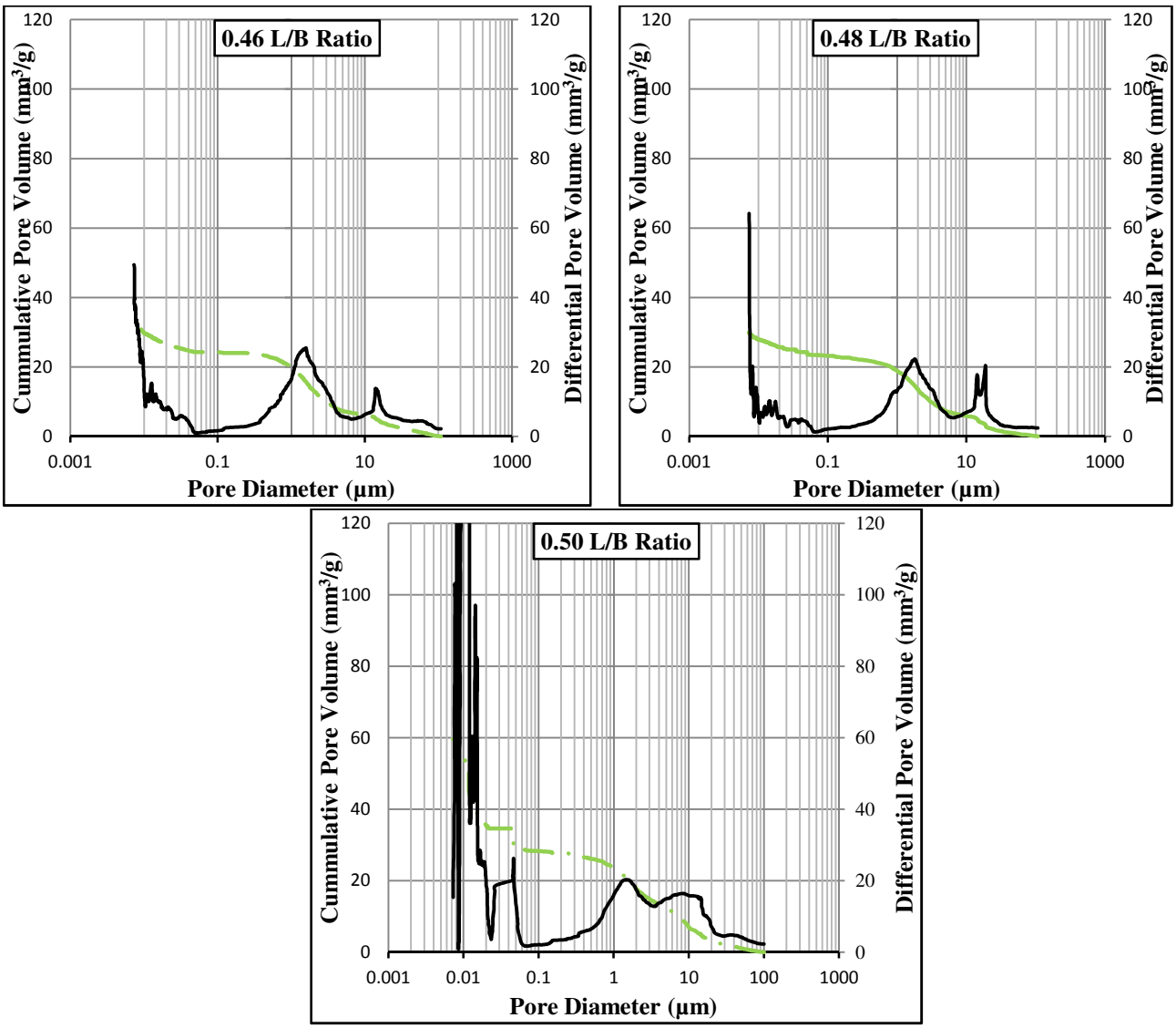

Appendix 3.9b: *Cumulative and Differential Pore Volumes of AACM Mortar Mixes M_2 to M_5 under Wet Curing (batch a).*

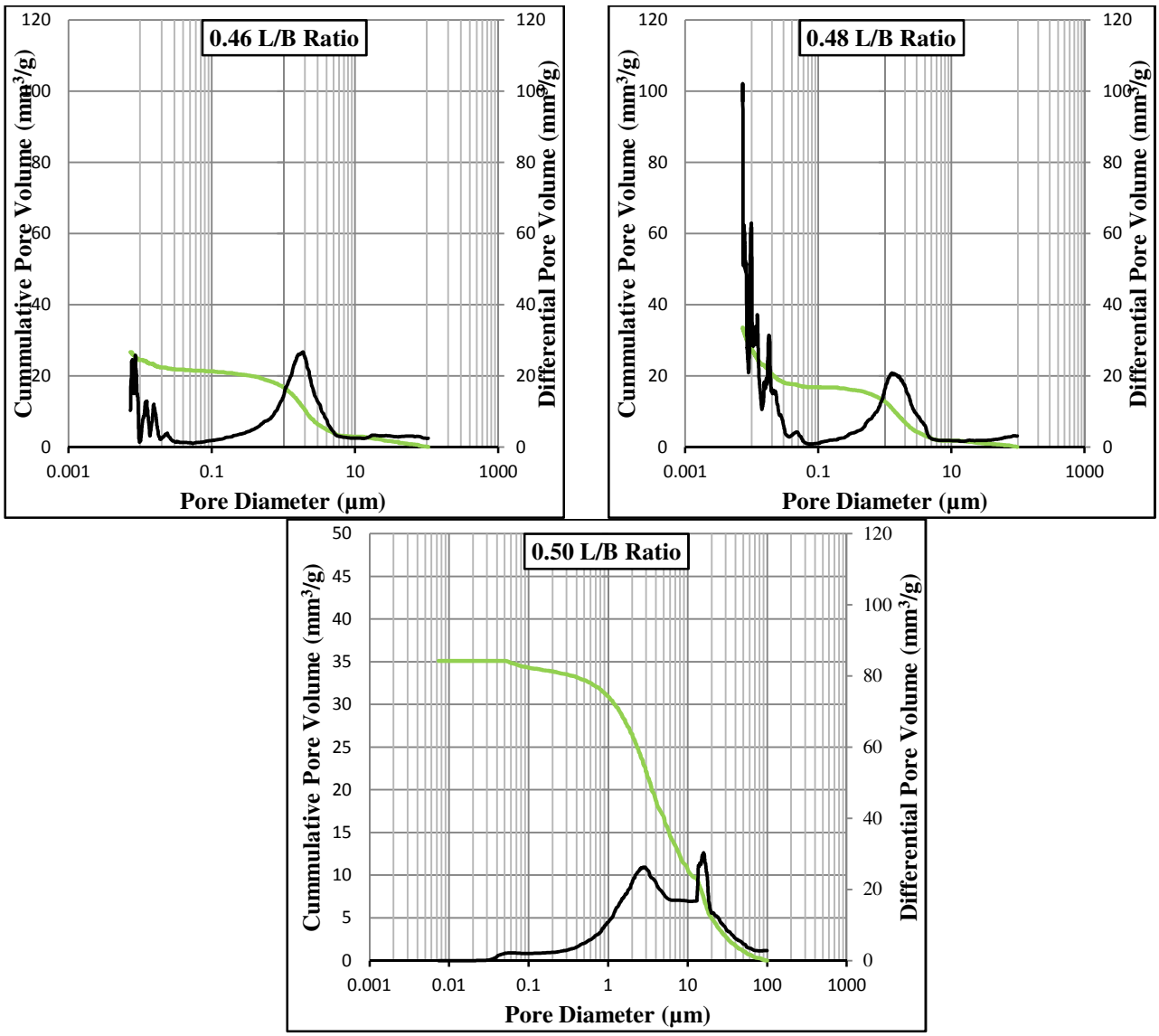

Appendix 3.9c: *Cumulative and Differential Pore Volumes of AACM Mortar Mixes M_2 to M_5 under Dry Curing (batch a).*

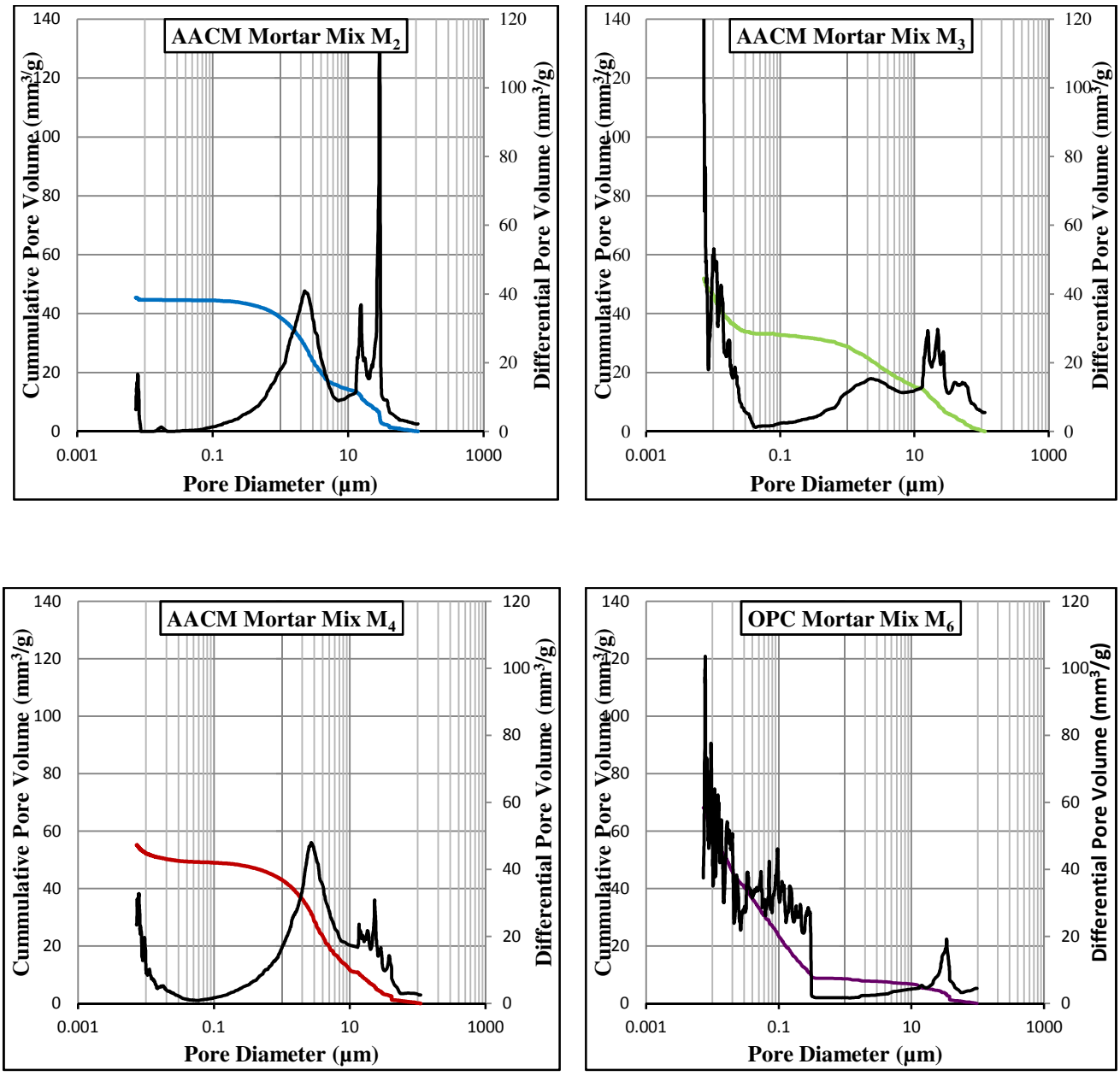

Appendix 3.10a: *Cumulative and Differential Pore Volumes of AACM and OPC Mortar Mixes under Wet/dry Curing (batch b).*

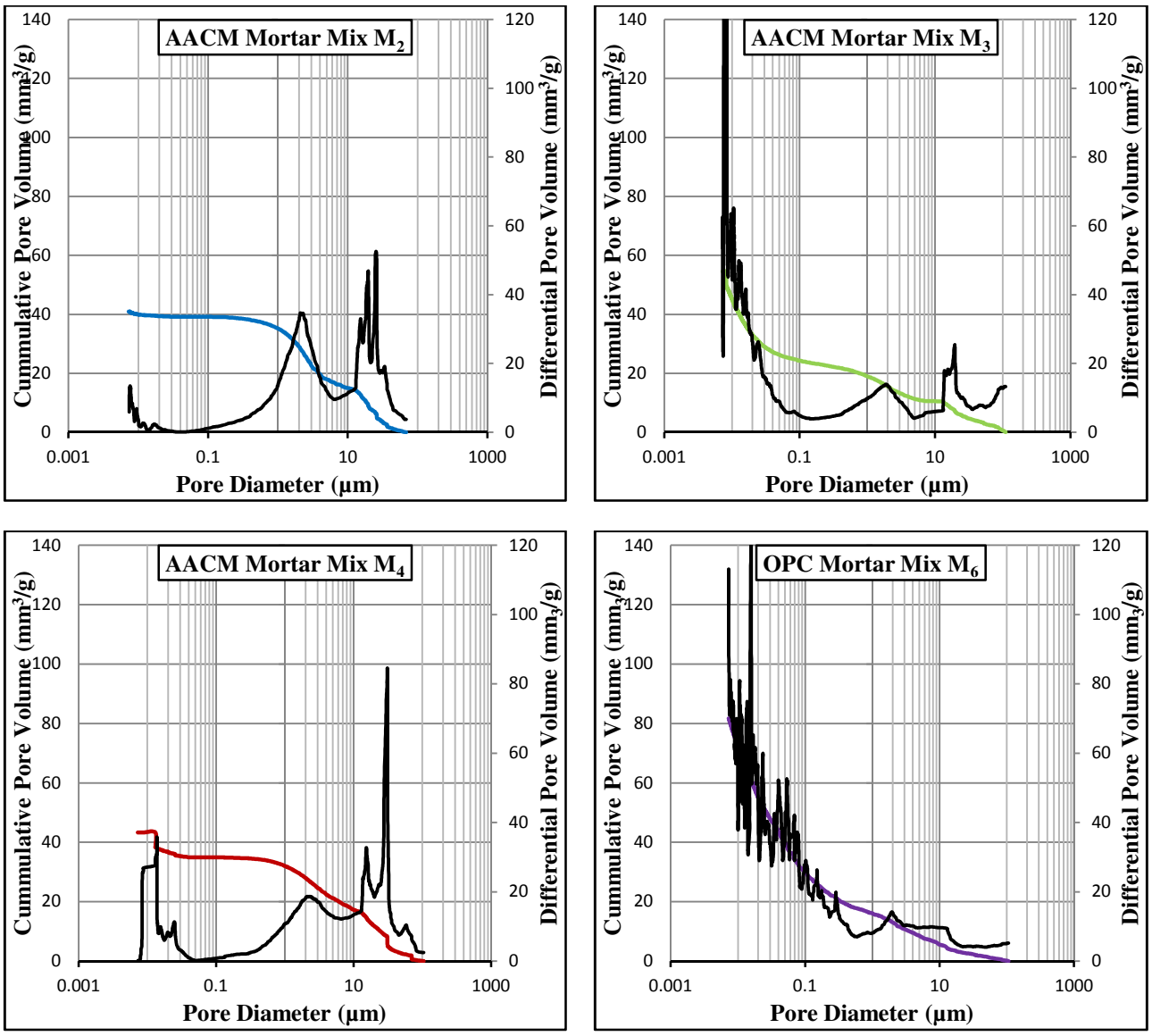

Appendix 3.10b: *Cumulative and Differential Pore Volumes of AACM and OPC Mortar Mixes under Wet Curing (batch b).*

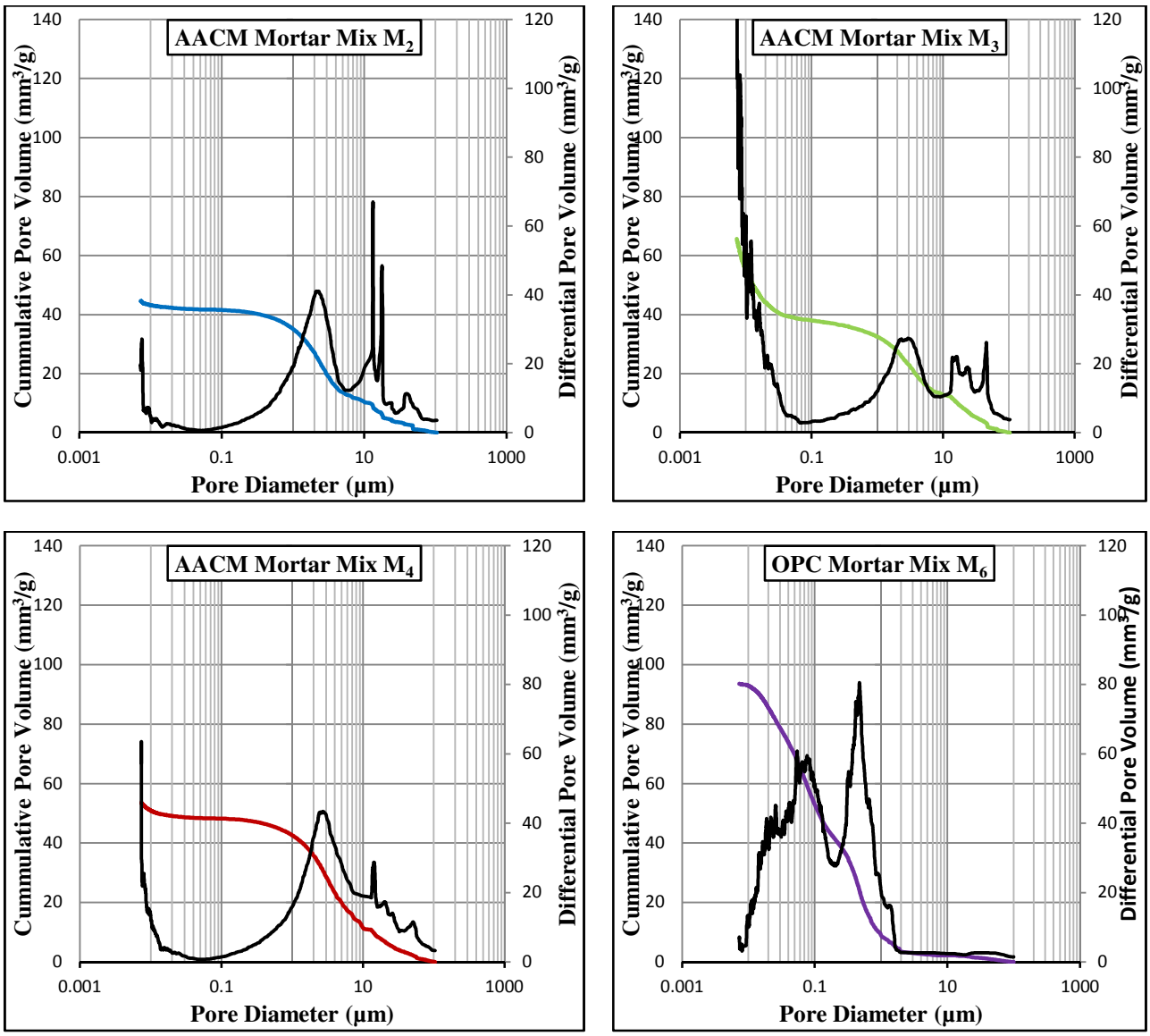

Appendix 3.10c: *Cumulative and Differential Pore Volumes of AACM and OPC Mortar Mixes under Dry Curing (batch b).*

REFERENCES

[1] P. C. Aïtcin, "Cements of yesterday and today - concrete of tomorrow," *Cem. Concr. Res.*, vol. 30, no. 9, pp. 1349–1359, 2000.

[2] Portland Cement Association, "Green in Practice 102 - Concrete, Cement, and CO2." [Online]. Available: http://www.concretethinker.com/technicalbrief/Concrete-Cement-CO2.aspx. [Accessed: 06-Oct-2017].

[3] John L. Provis and J. S. J. van Deventer, "Alkali-Activated Materials State-of-the-Art Report, RILEM TC 224-AAM," 2014.

[4] N. A. Madlool, R. Saidur, M. S. Hossain, and N. A. Rahim, "A critical review on energy use and savings in the cement industries," *Renewable and Sustainable Energy Reviews*, vol. 15, no. 4. pp. 2042–2060, 2011.

[5] S.-D. Wang and K. L. Scrivener, "Hydration products of alkali activated slag cement," *Cem. end Concr. Res.*, vol. 25, no. 3, pp. 561–571, 1995.

[6] P. G. Malone and C. A. Randall, "Potential Applications of Alkali-Activated Alumino-Silicate Binders in Military Operations Library Branch," 1985.

[7] British Standards Institution, *Construction materials : Alkali-activated cementitious material and concrete : specification.* 2016.

[8] US Geological survey, "USGS - Minerals Information: Cement," 2017.

[9] K. L. Scrivener and R. J. Kirkpatrick, "Innovation in use and research on cementitious material," *Cem. Concr. Res.*, vol. 38, no. 2, pp. 128–136, 2008.

[10] European commission, "Roadmap for moving to a low-carbon economy in 2050," *DG Clim. Action portal*, pp. 1–2, 2011.

[11] M. C. G. Juenger, F. Winnefeld, J. L. Provis, and J. H. Ideker, "Advances in alternative cementitious binders," *Cem. Concr. Res.*, vol. 41, no. 12, pp. 1232–1243, 2011.

[12] S. A. Bernal and J. L. Provis, "Durability of alkali-activated materials: Progress and perspectives," *J. Am. Ceram. Soc.*, vol. 97, no. 4, pp. 997–1008, 2014.

[13] British Standards Institution, "Structural Use of Concrete - Part 2: Code of practice for special circumstances (BS 8110-2: 1985)," *Incorporating Amendments Nos 1- 3*. p. 68, 2005.

[14] M. Webster and L. Clark, "The structural effect of corrosion–an overview of the mechanism," *Proc. Concr.*, pp. 409–421, 2000.

[15] F. O'Flaherty, P. Mangat, P. Lambert, and E. H. Brown, "Influence of shear reinforcement corrosion on the performance of under-reinforced concrete beams," *Biophysical journal*. 2010.

[16] Hans Kuehl, "Slag cement and process of making the same.," US900939 A, 1907.

[17] A. O. Purdon, "The action of alkalis on blast-furnace slag," *J Soc Chem Ind*, vol. 59, no. 9, pp. 191–202.

[18] Arthur Oscar Purdon, “Improvements in processes of manufacturing cement, mortars and concretes,” GB19340012244 19340423, 1935.

[19] J. Davidovits, “Geopolymers - Inorganic polymeric new materials,” *J. Therm. Anal.*, vol. 37, pp. 1633–1656, 1991.

[20] A. Palomo, P. Krivenko, I. Garcia-Lodeiro, E. Kavalerova, O. Maltseva, and A. Fernández-Jiménez, “A review on alkaline activation: new analytical perspectives ; Activación alcalina: Revisión y nuevas perspectivas de análisis,” *Mater. Construcciónn*, vol. 64, no. 315, 2014.

[21] A. Palomo, M. W. Grutzeck, and M. T. Blanco, “Alkali-activated fly ashes: A cement for the future,” *Cem. Concr. Res.*, vol. 29, pp. 1323–1329, 1999.

[22] S. A. Bernal, R. Mejia De Gutierrez, A. L. Pedraza, J. L. Provis, E. D. Rodriguez, and S. Delvasto, “Effect of binder content on the performance of alkali-activated slag concretes,” *Cem. Concr. Res.*, vol. 41, pp. 1–8, 2011.

[23] M. Ben Haha, B. Lothenbach, G. Le Saout, and F. Winnefeld, “Influence of slag chemistry on the hydration of alkali-activated blast-furnace slag - Part II: Effect of Al2O3,” *Cem. Concr. Res.*, vol. 42, pp. 74–83, 2012.

[24] D. Khale and R. Chaudhary, “Mechanism of geopolymerization and factors influencing its development: A review,” *J. Mater. Sci.*, vol. 42, pp. 729–746, 2007.

[25] A. M. Neville, *Properties of Concrete*, vol. Fifth. Pearson Education Limited, 2011.

[26] J. C. Petermann, A. Saeed, and M. I. Hammons, “Alkali-activated geopolymers: a literature review air force research laboratory materials and manufacturing directorate,” 2010.

[27] A. Fernández-Jiménez, F. Puertas, I. Sobrados, and J. Sanz, “Structure of Calcium Silicate Hydrates Formed in Alkaline-Activated Slag: Influence of the Type of Alkaline Activator,” *J. Am. Ceram. Soc.*, vol. 86, no. 8, pp. 1389–1394, 2003.

[28] J. I. Escalante-García, A. F. Fuentes, A. Gorokhovsky, P. E. Fraire-Luna, and G. Mendoza-Suarez, “Hydration Products and Reactivity of Blast-Furnace Slag Activated by Various Alkalis,” *J. Am. Ceram. Soc.*, vol. 86, no. 12, pp. 2148–2153, 2003.

[29] P. L. Pratt, S.-D. Wang, X.-C. Pu, and K. L. Scrivener, “Alkali-activated slag cement and concrete: a review of properties and problems,” *Adv. Cem. Res.*, vol. 7, no. 27, pp. 93–102, 1995.

[30] Z. Huanhai, W. Xuequan, X. Zhongzi, and T. Mingshu, “Kinetic study on hydration of alkali-activated slag,” *Cem. Concr. Res.*, vol. 23, no. 6, pp. 1253–1258, 1993.

[31] J. Schneider, M. A. Cincotto, and H. Panepucci, “Si-29 and Al-27 high-resolution NMR characterization of calcium silicate hydrate phases in activated blast-furnace slag pastes,” *Cem. Concr. Res.*, vol. 31, no. 7, pp. 993–1001, 2001.

[32] B. Lothenbach and a. Gruskovnjak, “Hydration of alkali-activated slag:

thermodynamic modelling," *Adv. Cem. Res.*, vol. 19, no. 2, pp. 81–92, 2007.

[33] A. R. Brough and A. Atkinson, "Sodium silicate-based, alkali-activated slag mortars - Part I. Strength, hydration and microstructure," *Cem. Concr. Res.*, vol. 32, no. 6, pp. 865–879, 2002.

[34] S. A. Bernal, J. L. Provis, V. Rose, and R. Mej??a De Gutierrez, "Evolution of binder structure in sodium silicate-activated slag-metakaolin blends," *Cem. Concr. Compos.*, vol. 33, no. 1, pp. 46–54, 2011.

[35] C. Shi, P. V Krivenko, and D. M. Roy, *Alkali-Activated Cements and Concretes*. 2006.

[36] C. Shi and R. L. Day, "Selectivity of Alkaline Activators for the Activation of Slags," *Cem. Concr. Aggregates*, vol. 18, no. 1, pp. 8–14, 1996.

[37] M. Ben Haha, G. Le Saout, F. Winnefeld, and B. Lothenbach, "Influence of activator type on hydration kinetics, hydrate assemblage and microstructural development of alkali activated blast-furnace slags," *Cem. Concr. Res.*, vol. 41, no. 3, pp. 301–310, 2011.

[38] S. D. Wang, K. L. Scrivener, and P. L. Pratt, "Factors affecting the strength of alkali-activated slag," *Cem. Concr. Res.*, vol. 24, no. 6, pp. 1033–1043, 1994.

[39] B.F.M. Bakker, "Diffusion within and into concrete," in *13th Annual convention of the institute of concrete technology, University of Technology, Loughborough*, 1985.

[40] R. D. Hooton and J. J. Emery, "Sulfate resistance of a Canadian slag cement," *ACI Mater. J.*, vol. 87, no. 6, pp. 547–555, 1990.

[41] C. Costa, "Hydraulic Binders," in *Materials for Construction and Civil Engineering*, Cham: Springer International Publishing, 2015, pp. 1–52.

[42] S. Song, D. Sohn, H. M. Jennings, and T. O. Mason, "Hydration of alkali-activated ground granulated blast furnace slag," *J. Mater. Sci.*, vol. 35, no. 1, pp. 249–257, 2000.

[43] A. Fernández-Jiménez and A. Palomo, "Characterisation of fly ashes. Potential reactivity as alkaline cements," *Fuel*, vol. 82, no. 18, pp. 2259–2265, 2003.

[44] Edwin R. Dunstan Jr., "Fly ash and fly ash concrete," 1984.

[45] a. L. a. Fraay, J. M. Bijen, and Y. M. de Haan, "The reaction of fly ash in concrete a critical examination," *Cem. Concr. Res.*, vol. 19, no. 2, pp. 235–246, 1989.

[46] B. V. Rangan, "Fly Ash-Based Geopolymer Concrete," in *Proceedings of the International Workshop on Geopolymer Cement and Concrete, December*, 2010, vol. 2010, pp. 68–106.

[47] U.S. Department of Transportation, "Silica Fume manual," FWHA-IF-05-016, 2005.

[48] D. M. Roy, "Fly Ash and Silica Fume Chemistry and Hydration," *Spec. Publ.*, vol. 114, pp. 117–138, May 1989.

[49] J. A. Larbi, “Microstructure of the interfacial zone around aggregate particles in concrete,” *Heron*, vol. 39, no. 1, pp. 1–69, 1993.

[50] P. S. Mangat and B. T. Molloy, “Influence of PFA, slag and microsilica on chloride induced corrosion of reinforcement in concrete,” *Cem. Concr. Res.*, vol. 21, no. 5, pp. 819–834, 1991.

[51] Min-Hong Zhang and V. Mohan Malhotra, “High-Performance Concrete Incorporating Rice Husk Ash as a Supplementary Cementing Material,” Title nos. 93-M72, 1996.

[52] S. Kumar, P. Sangwan, D. R. M. V, and S. Bidra, “Utilization of Rice Husk and Their Ash : A Review,” *J. Chem. Environ. Sci.*, vol. 1, no. 5, pp. 126–129, 2013.

[53] P. K. Mehtra and K. J. Folliard, “Rice Husk Ash--a Unique Supplementary Cementing Material: Durability Aspects,” *Spec. Publ.*, vol. 154, pp. 531–542, May 1995.

[54] K. J. D. MacKENZIE, I. W. M. BROWN, R. H. MEINHOLD, and M. E. BOWDEN, “Outstanding Problems in the Kaolinite-Mullite Reaction Sequence Investigated by 29Si and 27Al Solid-state Nuclear Magnetic Resonance: I, Metakaolinite,” *J. Am. Ceram. Soc.*, vol. 68, no. 6, pp. 293–297, 1985.

[55] D. R. Collins, A. N. Fitch, and C. R. A. Catlow, “Time-Resolved Powder Neutron-Diffraction Study of Thermal-Reactions in Clay-Minerals,” *J. Mater. Chem.*, vol. 1, no. 6, pp. 965–970, 1991.

[56] M. R. Wang, D. C. Jia, P. G. He, and Y. Zhou, “Influence of calcination temperature of kaolin on the structure and properties of final geopolymer,” *Mater. Lett.*, vol. 64, no. 22, pp. 2551–2554, 2010.

[57] R. Cioffi, L. Maffucci, and L. Santoro, “Optimization of geopolymer synthesis by calcination and polycondensation of a kaolinitic residue,” *Resour. Conserv. Recycl.*, vol. 40, no. 1, pp. 27–38, 2003.

[58] F. Puertas, S. Martínez-Ramírez, S. Alonso, and T. Vázquez, “Alkali-activated fly ash/slag cements. Strength behaviour and hydration products,” *Cem. Concr. Res.*, 2000.

[59] J. G. S. Van Jaarsveld, J. S. J. Van Deventer, and G. C. Lukey, “A Comparative Study of Kaolinite Versus Metakaolinite in Fly Ash Based Geopolymers Containing Immobilized Metals,” *Chem. Eng. Commun.*, vol. 191, no. 4, pp. 531–549, 2004.

[60] J. G. . van Jaarsveld, J. S. . van Deventer, and G. . Lukey, “The effect of composition and temperature on the properties of fly ash- and kaolinite-based geopolymers,” *Chem. Eng. J.*, vol. 89, no. 1–3, pp. 63–73, 2002.

[61] Y. Zhang, Z. Li, W. Sun, and W. Li, “Setting and hardening of geopolymeric cement pastes incorporated with fly ash,” *ACI Mater. J.*, vol. 106, no. 5, pp. 405–412, 2009.

[62] A. Palomo and A. Fernández-Jiménez, “Alkaline activation, procedure for transforming fly ash into new materials. Part I: Applications.”

[63] Pavel V. Krivenko, “Alkaline cements and concretes,” in *Proceedings of the first*

International Conference held at the Scientific-Research Institute on Binders and Materials named after V.D. Glukhovsky, 1994, pp. 11–14.

[64] Mike McDonald and Judy LaRosa Thompson, "Sodium Silicate a Binder for the 21st Century," Philladelphia, U.S.A.

[65] A. Fernández-Jiménez, A. Palomo, and M. Criado, "Microstructure development of alkali-activated fly ash cement: A descriptive model," *Cem. Concr. Res.*, vol. 35, no. 6, pp. 1204–1209, 2005.

[66] D. Feng, H. Tan, and J. S. J. Van Deventer, "Ultrasound enhanced geopolymerisation," *J. Mater. Sci.*, vol. 39, no. 2, pp. 571–580, 2004.

[67] F. Pacheco-Torgal, J. Castro-Gomes, and S. Jalali, "Alkali-activated binders: A review. Part 2. About materials and binders manufacture," *Construction and Building Materials*, vol. 22, no. 7. pp. 1315–1322, 2008.

[68] A. Fernández-Jiménez and A. Palomo, "Composition and microstructure of alkali activated fly ash binder: Effect of the activator," *Cem. Concr. Res.*, vol. 35, no. 10, pp. 1984–1992, 2005.

[69] A. Fernández-Jiménez, J. G. Palomo, and F. Puertas, "Alkali-activated slag mortars," *Cem. Concr. Res.*, vol. 29, no. 8, pp. 1313–1321, 1999.

[70] J. L. Provis, "Green concrete or red herring? – future of alkali-activated materials," *Adv. Appl. Ceram.*, vol. 113, no. 8, pp. 472–477, 2014.

[71] S. A. Bernal, J. L. Provis, R. J. Myers, R. San Nicolas, and J. S. J. van Deventer, "Role of carbonates in the chemical evolution of sodium carbonate-activated slag binders," *Mater. Struct.*, vol. 48, no. 3, pp. 517–529, 2015.

[72] X. Ke, S. A. Bernal, and J. L. Provis, "Controlling the reaction kinetics of sodium carbonate-activated slag cements using calcined layered double hydroxides," *Cem. Concr. Res.*, vol. 81, pp. 24–37, 2016.

[73] S. A. Bernal, R. S. Nicolas, J. S. J. van Deventer, and J. L. Provis, "Alkali-activated slag cements produced with a blended sodium carbonate/sodium silicate activator," *Adv. Cem. Res.*, vol. 28, no. 4, pp. 262–273, Apr. 2016.

[74] BS EN 206, *Concrete — Specification, performance, production and conformity*. British Standards Institution, 2014.

[75] BSI 12, *Specification for Portland cement*. British Standards Institution, 1996.

[76] BS EN 1008, *Mixing water for concrete — Specification for sampling, testing and assessing the suitability of water, including water recovered from processes in the concrete industry, as mixing water for concrete*. British Standards Institution, 2002.

[77] BS 882:1992, *Specification for aggregates from natural sources for concrete*. British Standards Institution, 1992.

[78] BS EN 12620:2002+A1, *Aggregates for concrete –*. British Standards Institution, 2008.

[79] BS 812 - 103.2, *Testing aggregates.* British Standards Institution, 1975.

[80] N. Smaoui, M. A. Bérubé, B. Fournier, B. Bissonnette, and B. Durand, “Effects of alkali addition on the mechanical properties and durability of concrete,” *Cem. Concr. Res.*, vol. 35, no. 2, pp. 203–212, 2005.

[81] S. Adu-Amankwah, J. M. Khatib, D. E. Searle, and L. Black, “Effect of synthesis parameters on the performance of alkali-activated non-conformant en 450 pulverised fuel ash,” *Constr. Build. Mater.*, vol. 121, pp. 453–459, 2016.

[82] P. Mangat and P. Lambert, “Sustainability of alkali-activated cementitious materials and geopolymers,” in *Sustainability of Construction Materials*, Elsevier Ltd, 2016, pp. 459–476.

[83] T. Williamson and M. C. G. Juenger, “The role of activating solution concentration on alkali-silica reaction in alkali-activated fly ash concrete,” *Cem. Concr. Res.*, vol. 83, pp. 124–130, 2016.

[84] M. Rowles and B. O’Connor, “Chemical optimisation of the compressive strength of aluminosilicate geopolymers synthesised by sodium silicate activation of metakaolinite,” *J. Mater. Chem.*, vol. 13, no. 5, pp. 1161–1165, 2003.

[85] DD ENV 197:part 1, *Cement. Composition, specifications and conformity criteria. Common cements*. Bsi, 1995.

[86] Duff Andrew Abrams, *Design of Concrete Mixtures - Duff Andrew Abrams - Google Books*. Structural Materials Research Laboratory, Lewis Institute, 1919.

[87] J. G. S. van Jaarsveld and J. S. J. van Deventer, “Effect of the Alkali Metal Activator on the Properties of Fly Ash-Based Geopolymers,” *Ind. Eng. Chem. Res.*, vol. 38, no. 10, pp. 3932–3941, 1999.

[88] A. Fernández-Jiménez, J. G. Palomo, and F. Puertas, “Alkali-activated slag mortars: Mechanical strength behaviour,” *Cem. Concr. Res.*, vol. 29, no. 8, pp. 1313–1321, 1999.

[89] D. Krizan and B. Zivanovic, “Effects of dosage and modulus of water glass on early hydration of alkali-slag cements,” *Cem. Concr. Res.*, vol. 32, no. 8, pp. 1181–1188, 2002.

[90] K. Tuutti, “Corrosion of steel in concrete,” *Swedish Cem. Concr. Res. Inst.*, vol. 26, p. 469, 1982.

[91] Page C.L. and Lambert, “Analytical and Electrochemical Investigations of Reinforcement Corrosion, Contractor Report 30, Department of Transportation, Transport and Road Research Laboratory,” 1986.

[92] B. H. Oh, S. Y. Jang, and Y. S. Shin, “Experimental investigation of the threshold chloride concentration for corrosion initiation in reinforced concrete structures,” in *Magazine of Concrete Research*, 2003, pp. 1–9.

[93] J. Backus, D. McPolin, M. Basheer, A. Long, and N. Holmes, “Exposure of mortars to cyclic chloride ingress and carbonation,” *Adv. Cem. Res.*, vol. 25, no. 1, pp. 3–11, 2013.

[94] P. Lambert, C. L. Page, and N. R. Short, “Pore solution chemistry of the hydrated system tricalcium silicate/sodium chloride/water,” *Cem. Concr. Res.*, vol. 15, no. 4, pp. 675–680, 1985.

[95] T. Luping and L. O. Nilsson, “Chloride binding capacity and binding isotherms of OPC pastes and mortars,” *Cem. Concr. Res.*, vol. 23, pp. 247–253, 1993.

[96] P. S. Mangat and K. Gurusamy, “Long-term properties of steel fibre reinforced marine concrete,” *Mater. Struct.*, vol. 20, no. 4, pp. 273–282, 1987.

[97] S. H. E. O. K. Nilsson L. O., Poulsen E., Sandberg P., “Chloride Penetration into Concrete, State-of-the-Art, Transport Processes, Transport Processes, Corrosion Initiation, Test Methods and Prediction Models,” 1996.

[98] British Standards, “DD CEN/TS 12390-11: Testing hardened concrete, Part 11: Determination of the chloride resistance of concrete, unidirectional diffusion,” 2010.

[99] Nordtest 443, “Hardened concrete: Accelerated chloride penetration,” FIN-02150 ESPOO, Finland, 1995.

[100] R. Kumar and B. Bhattacharjee, “Assessment of permeation quality of concrete through mercury intrusion porosimetry,” *Cem. Concr. Res.*, vol. 34, no. 2, pp. 321–328, 2004.

[101] E. J. Garboczi, “Permeability, Diffusivity, and Microstructural Parameters: A Critical Review,” *Cem. Concr. Res.*, vol. 20, pp. 591–601, 1990.

[102] P. S. Mangat and K. Gurusamy, “Corrosion resistance of steel fibres in concrete under marine exposure,” *Cem. Concr. Res.*, vol. 18, no. 1, pp. 44–54, 1988.

[103] P. S. Mangat and M. C. Limbachiya, “Effect of initial curing on chloride diffusion in concrete repair materials,” *Cem. Concr. Res.*, vol. 29, no. 9, pp. 1475–1485, 1999.

[104] *BS ISO 15901-1:2016 - Evaluation of pore size distribution and porosity of solid materials by mercury porosimetry and gas adsorption. Mercury porosimetry*. 2016.

[105] D. Mindess, Sidney; Young, J. Francis; Darwin, *Concrete*. Prentice Hall, Pearson Education, Inc. Upper Saddle River, NJ 07458, U.S.A., 2003.

[106] Y. Ma, J. Hu, and G. Ye, “The effect of activating solution on the mechanical strength, reaction rate, mineralogy, and microstructure of alkali-activated fly ash,” *J. Mater. Sci.*, vol. 47, no. 11, pp. 4568–4578, 2012.

[107] Glukhovsky V.D., *Soil Silicates*. Gosstroyizdat, Kiev, 1959.

[108] P. Duxson, A. Fernández-Jiménez, J. L. Provis, G. C. Lukey, A. Palomo, and J. S. J. Van Deventer, “Geopolymer technology: The current state of the art,” *J. Mater. Sci.*, vol. 42, no. 9, pp. 2917–2933, 2007.

[109] J. C. H. Llewellyn Everard Copeland, “The Determination of Non-evaporable Water in Hardened Portland Cement Paste,” *Volume 47 of Bulletin (Portland Cement Association. Research and Development Laboratories. Research Department)*, p. 9, 1953.

[110] Y. Li and J. Li, “Capillary tension theory for prediction of early autogenous shrinkage of self-consolidating concrete,” *Constr. Build. Mater.*, vol. 53, pp. 511–516, 2014.

[111] K. D. Stanish, R. D. Hooton, and M. D. A. Thomas, “Testing the Chloride Penetration Resistance of Concrete: A Literature Review,” 1997.

[112] K. K. ALIGIZAKI, *Pore structure of cement-based materials: testing, interpretation and requirements*. Abingdon [England]: Taylor & Francis, 2006.

[113] D. P. Bentz and E. J. Garboczi, “Percolation of phases in a three-dimensional cement paste microstructural model,” *Cem. Concr. Res.*, vol. 21, pp. 325–34, 1991.

[114] P. K. Mehta and D. Manmohan, “Pore size distribution and permeability of hardened cement pastes,” in *7th International Congress on the Chemistry of Cement. Vol. 3*, 1980, p. VII-1-5.

[115] A. T. C. Guimarães, G. De Vera, F. T. Rodrigues, C. Antõn, and M. A. Climent, “Comparison between Dcrit Considering the Abrupt Variation and Inflexion in the Concrete Mercury Intrusion Porosimetry Curve,” *Exp. Tech.*, 2015.

[116] H. Ma, “Mercury intrusion porosimetry in concrete technology: Tips in measurement, pore structure parameter acquisition and application,” *J. Porous Mater.*, vol. 21, pp. 207–215, 2014.

[117] H. Zhao, Q. Xiao, D. Huang, and S. Zhang, “Influence of Pore Structure on Compressive Strength of Cement Mortar,” *Sci. World J.*, p. 12, 2014.

[118] C. Lian, Y. Zhuge, and S. Beecham, “The relationship between porosity and strength for porous concrete,” *Constr. Build. Mater.*, vol. 25, no. 11, pp. 4294–4298, 2011.

[119] J. Bu and Z. Tian, “Relationship between pore structure and compressive strength of concrete: Experiments and statistical modeling,” *Sadhana - Acad. Proc. Eng. Sci.*, vol. 41, no. 3, pp. 337–344, 2016.

[120] Balshin M.Y., “Relation of Mechanical Properties of Powder Metals and their Porosity and the Ultimate Properties of Porous-Metal Ceramic Materials,” *Dokl Askd SSSR*, vol. 67, no. 5, pp. 831–834, 1949.

[121] Ryshkevitch R, “Compression Strength of Porous Sintered Alumina and Zirconia,” *J Am Ceram Soc*, vol. 36, no. 2, pp. 65–68, 1953.

[122] Hasselman DPH, “Griffith Flaws and the Effect of Porosity on Tensile Strength of Brittle Ceramics,” *J Am Ceram Soc*, vol. 52, p. 457, 1969.

[123] Schiller K.K., “Strength of Porous Materials,” *Cem Concr Res*, vol. 1, pp. 419–422, 1971.

[124] M. A. I. Laskar, R. Kumar, and B. Bhattacharjee, “Some aspects of evaluation of concrete through mercury intrusion porosimetry,” *Cem. Concr. Res.*, vol. 27, no. 1, pp. 93–105, 1997.

[125] S. Diamond and D. Bonen, “Microstructure of Hardened Cement Paste???A New Interpretation,” *J. Am. Ceram. Soc.*, vol. 76, no. 12, pp. 2993–2999, 1993.

[126] R. A. Cook and K. C. Hover, “Mercury porosimetry of hardened cement pastes,” *Cem. Concr. Res.*, vol. 29, pp. 933–943, 1999.

[127] Raymond Avery Cook, *Fundamentals of mercury intrusion porosimetry and its*

application to concrete materials science. Cornell University, 1991.

[128] R. Kumar and B. Bhattacharjee, "Study on some factors affecting the results in the use of MIP method in concrete research," *Cem. Concr. Res.*, vol. 33, no. 3, pp. 417–424, 2003.

[129] R. J. Myers, S. A. Bernal, R. San Nicolas, and J. L. Provis, "Generalized structural description of calcium-sodium aluminosilicate hydrate gels: The cross-linked substituted tobermorite model," *Langmuir*, 2013.

[130] R. F. Feldman and P. J. Sereda, "A New Model for Hydrated Portland Cement and its Practical Implications," *Repr. from Eng. J.*, vol. 53, no. 819, pp. 53–59, 1970.

[131] P. S. Mangat, "Liquid Granite: Building Material Of The Future Unveiled," *Science Daily*, Sheffield Hallam University, U.K., pp. 2016–2017, 04-Nov-2009.

[132] Olalekan O. Ojedokun and Pal Mangat, "Chloride diffusion in alkali activated concrete," in *II International Conference on Concrete Sustainability ICCS16, Madrid, Spain*, 2016, vol. 3, pp. 521–530.

[133] BS EN 12390-3:2009, "BS EN 12390-3:2009 Testing Hardened Concrete Part 3: Compressive Strength of Test Specimens," 2009.

[134] J. M. Khatib and P. S. Mangat, "Porosity of cement paste cured at 45C as a function of location relative to casting position," *Cem. Concr. Compos.*, vol. 25, no. 1, pp. 97–108, 2003.

[135] M. M. Reda Taha, A. S. El-Dieb, and N. G. Shrive, "Sorptivity: a reliable measurement for surface absorption of masonry brick units," *Mater. Struct. Constr.*, vol. 34, pp. 438–445.

[136] British Standard, "BS 1902-316: 1990 Refractory materials — Part 3: General and textural properties — Section 3.16 Determination of pore size distribution (method1902-316)," 2011.

[137] N. Hearn and R. D. Hooton, "Sample mass and dimension effects on mercury intrusion porosimetry results," *Cem. Concr. Res.*, vol. 22, no. 5, pp. 970–980, 1992.

[138] Thermo Scientific, "Mercury Porosity PASCAL 240 Series Instruction Manual," 2014.

[139] P. S. Deb, P. Nath, and P. K. Sarker, "Drying shrinkage of slag blended fly ash geopolymer concrete cured at room temperature," in *Procedia Engineering*, 2015, vol. 125, pp. 594–600.

[140] M. Palacios and F. Puertas, "Effect of superplasticizer and shrinkage-reducing admixtures on alkali-activated slag pastes and mortars," *Cem. Concr. Res.*, vol. 35, no. 7, pp. 1358–1367, 2005.

[141] K. H. Yang, J. K. Song, K. S. Lee, and A. F. Ashour, "Flow and compressive strength of alkali-activated mortars," *ACI Mater. J.*, vol. 106, no. 1, pp. 50–58, 2009.

[142] M. Chi, "Effects of modulus ratio and dosage of alkali-activated solution on the

properties and micro-structural characteristics of alkali-activated fly ash mortars," *Constr. Build. Mater.*, vol. 99, pp. 128–136, 2015.

[143] A. Fernández Jiménez and A. Palomo, "Factors affecting early compressive strength of alkali activated fly ash (OPC-free) concrete," *Mater. Construcciónn*, vol. 57, no. 287, pp. 7–22, 2007.

[144] A. Wardhono, D. W. Law, and A. Strano, "The strength of alkali-activated slag/fly ash mortar blends at ambient temperature," *Procedia Eng.*, vol. 125, pp. 650–656, 2015.

[145] M. A. Salih, N. Farzadnia, A. A. Abang Ali, and R. Demirboga, "Effect of different curing temperatures on alkali activated palm oil fuel ash paste," *Constr. Build. Mater.*, vol. 94, pp. 116–125, Sep. 2015.

[146] E. Altan and S. T. Erdoğan, "Alkali activation of a slag at ambient and elevated temperatures," *Cem. Concr. Compos.*, vol. 34, no. 2, pp. 131–139, 2012.

[147] K. Tan and O. E. Gjorv, "Performance of concrete under different curing conditions," *Cem. Concr. Res.*, vol. 26, no. 3, pp. 355–361, 1996.

[148] B. Ozer and M. H. Ozkul, "The influence of initial water curing on the strength development of ordinary portland and pozzolanic cement concretes," *Cem. Concr. Res.*, vol. 34, no. 1, pp. 13–18, 2004.

[149] F. P. Glasser, "Progress in the immobilization of radioactive wastes in cement," *Cem. Concr. Res.*, vol. 22, no. 2–3, pp. 201–216, Mar. 1992.

[150] T. C. Powers, "A discussion of cement hydration in relation to the curing of concrete," *Highw. Res. Board Proc.*, vol. 27, 1948.

[151] R. G. Patel, D. C. Killoh, L. J. Parrott, and W. A. Gutteridge, "Influence of curing at different relative humidities upon compound reactions and porosity in Portland cement paste," *Mater. Struct.*, vol. 21, no. 3, pp. 192–197, 1988.

[152] F. Puertas, H. Santos, M. Palacios, and S. Martinez-Ramirez, "Polycarboxylate superplasticiser admixtures: effect on hydration, microstructure and rheological behaviour in cement pastes," *Adv. Cem. Res.*, vol. 17, no. 2, pp. 77–89, 2005.

[153] R. R. Lloyd, J. L. Provis, K. J. Smeaton, and J. S. J. van Deventer, "Spatial distribution of pores in fly ash-based inorganic polymer gels visualised by Wood's metal intrusion," *Microporous Mesoporous Mater.*, vol. 126, no. 1–2, pp. 32–39, 2009.

[154] L. Zheng, W. Wang, and Y. Shi, "The effects of alkaline dosage and Si/Al ratio on the immobilization of heavy metals in municipal solid waste incineration fly ash-based geopolymer," *Chemosphere*, vol. 79, no. 6, pp. 665–671, Apr. 2010.

[155] J. M. Khatib and P. S. Mangat, "Influence of superplasticizer and curing on porosity and pore structure of cement paste," *Cem. Concr. Compos.*, vol. 21, no. 5–6, pp. 431–437, 1999.

[156] M. Palacios and F. Puertas, "Effect of shrinkage-reducing admixtures on the properties of alkali-activated slag mortars and pastes," *Cem. Concr. Res.*, vol. 37, no. 5, pp. 691–702, 2007.

[157] V. H. Dodson, *Concrete Admixtures*. Springer US, 1990.

[158] G. Sant, D. Bentz, and J. Weiss, "Capillary porosity depercolation in cement-based materials: Measurement techniques and factors which influence their interpretation," *Cem. Concr. Res.*, vol. 41, pp. 854–864, 2011.

[159] B. Craeye *et al.*, "Effect of mineral filler type on autogenous shrinkage of self-compacting concrete," *Cem. Concr. Res.*, vol. 40, pp. 908–913, 2010.

[160] D. P. Bentz and P. E. Stutzman, "Curing, hydration, and microstructure of cement paste," *ACI Mater. J.*, vol. 103, no. 5, pp. 348–356, 2006.

[161] W. D. A. Rickard, R. Williams, J. Temuujin, and A. van Riessen, "Assessing the suitability of three Australian fly ashes as an aluminosilicate source for geopolymers in high temperature applications," *Mater. Sci. Eng. A*, vol. 528, no. 9, pp. 3390–3397, 2011.

[162] D. L. Y. Kong and J. G. Sanjayan, "Damage behavior of geopolymer composites exposed to elevated temperatures," *Cem. Concr. Compos.*, vol. 30, no. 10, pp. 986–991, 2008.

[163] F. Sajedi and H. A. Razak, "The effect of chemical activators on early strength of ordinary Portland cement-slag mortars," *Constr. Build. Mater.*, vol. 24, no. 10, pp. 1944–1951, 2010.

[164] J. Plank, E. Sakai, C. W. Miao, C. Yu, and J. X. Hong, "Chemical admixtures - Chemistry, applications and their impact on concrete microstructure and durability," *Cem. Concr. Res.*, vol. 78, pp. 81–99, 2015.

[165] H. Zhu, Z. Zhang, Y. Zhu, and L. Tian, "Durability of alkali-activated fly ash concrete: Chloride penetration in pastes and mortars," *Constr. Build. Mater.*, vol. 65, pp. 51–59, 2014.

[166] M. Thomas, "The effect of supplementary cementing materials on alkali-silica reaction: A review," *Cement and Concrete Research*, vol. 41, no. 12. pp. 1224–1231, 2011.

[167] F. Pacheco-Torgal, J. Castro-Gomes, and S. Jalali, "Alkali-activated binders: A review Part 1. Historical background, terminology, reaction mechanisms and hydration products," *Constr. Build. Mater.*, vol. 22, no. 7, pp. 1305–1314, 2008.

[168] M. Robler and I. Odler, "Investigations on the relationship between porosity, structure and strength of hydrated portland cement paste I. effect of porosity," *Cem. Concr. Res.*, vol. 15, pp. 320–330, 1985.

[169] Australian Standard AS1012.8-1999:, "Method of testing concrete – Method of making and curing concrete compression, indirect tensile and flexural test specimens, in the laboratory or in the field," 1999.

[170] P. Lambert, C. L. Page, and P. R. W. Vassie, "Investigations of reinforcement corrosion. 2. Electrochemical monitoring of steel in chloride-contaminated concrete," *Mater. Struct.*, vol. 24, no. 5, pp. 351–358, 1991.

[171] NACE International, "Corrosion Costs and Preventive Strategies in the United States [summary of the US FHWA publication No. FHWA-RD-01-156]," *Mater. Perform.*, vol. 41, no. 7 (cost of corrosion supplement), p. 12, 2002.

[172] J. C. Galvez, A. A. de Cea, D. F. Ordonez, K. Sakai, and et al., “2nd International conference on concrete sustainability,” in *Concrete Sustainability ICCS 2016*, 2016, pp. 1–1100.

[173] D. M. Roy, W. Jiang, and M. R. Silsbee, “Chloride diffusion in ordinary, blended, and alkali-activated cement pastes and its relation to other properties,” *Cem. Concr. Res.*, vol. 30, pp. 1879–1884, 2000.

[174] S. Vaidya, E. I. Diaz, and E. N. Allouche, “Experimental Evaluation of Self-Cure Geopolymer Concrete for Mass Pour Applications,” in *World of coal ash (WACO)*, 2011.

[175] Pal Mangat, “Revolutionary building material developed at Materials & Engineering Research Institute, Sheffield Hallam University,” 2014. [Online]. Available: https://vitruvianas.wordpress.com/tag/granite/. [Accessed: 07-Aug-2017].

[176] T. Bakharev, J. G. Sanjayan, and Y. B. Cheng, “Resistance of alkali-activated slag concrete to acid attack,” *Cem. Concr. Res.*, vol. 33, pp. 1607–1611, 2003.

[177] M. Leivo *et al.*, “Effect of interacted deterioration parameters on service life of concrete structures in cold environments.”

[178] F. Puertas and A. Fernández-Jiménez, “Mineralogical and microstructural characterisation of alkali-activated fly ash/slag pastes,” *Cem. Concr. Compos.*, vol. 25, pp. 287–292, 2003.

[179] C. Shi, “Strength, pore structure and permeability of alkali-activated slag mortars,” *Cem. Concr. Res.*, vol. 26, no. 12, pp. 1789–1799, 1996.

[180] P. Rovnaník, “Influence of C12A7 admixture on setting properties of fly ash geopolymer,” *Ceram. - Silikaty*, vol. 54, no. 4, pp. 362–367, 2010.

[181] J. L. Provis, R. J. Myers, C. E. White, V. Rose, and J. S. J. Van Deventer, “X-ray microtomography shows pore structure and tortuosity in alkali-activated binders,” *Cem. Concr. Res.*, vol. 42, no. 6, pp. 855–864, 2012.

[182] A. Ahmad and A. Kumar, “Chloride ion migration/diffusion through concrete and test methods,” *Int. J. Adv. Sci. Tech. Res.*, vol. 6, no. 3, pp. 151–180, 2013.

[183] G. Ye, “Percolation of capillary pores in hardening cement pastes,” *Cem. Concr. Res.*, vol. 35, pp. 167–176, 2005.

[184] British Standards Institution., “BS 8110-1:1997 Structural use of concrete — Part 1: Code of practice for design and construction,” 1997.

[185] M. A. Climent, G. De Vera, J. F. López, E. Viqueira, and C. Andrade, “A test method for measuring chloride diffusion coefficients through nonsaturated concrete Part I. The instantaneous plane source diffusion case,” *Cem. Concr. Res.*, vol. 32, pp. 1113–1123, 2002.

[186] Cement Concrete & Aggregates Australia Chloride, “Chloride Resistance of Concrete,” 2009.

[187] NT BUILD 443, “Concrete, Hardened: Accelerated Chloride Penetration,” 1995.

[188] O. E. Gjørv and Vennesland, “Diffusion of chloride ions from seawater into

concrete," *Cem. Concr. Res.*, vol. 9, no. 2, pp. 229–238, 1979.

[189] Z. Song, L. Jiang, H. Chu, C. Xiong, R. Liu, and L. You, "Modeling of chloride diffusion in concrete immersed in CaCl2 and NaCl solutions with account of multi-phase reactions and ionic interactions," *Constr. Build. Mater.*, vol. 66, pp. 1–9, 2014.

[190] M. Olivia and H. Nikraz, "Properties of Fly Ash Geopolymer Concrete in Seawater Environment," in *Hokkaido university collection*, 2013, pp. 1–9.

[191] Collepardi et al., "The Kinetics of Chloride ions Penetration in Concrete," *II Cem.*, vol. 67, pp. 157–164, 1970.

[192] P. S. Mangat and B. T. Molloy, "Prediction of long term chloride concentration in concrete," *Mater. Struct.*, vol. 27, no. 6, pp. 338–346, 1994.

[193] P. B. Bamforth, W. F. Price, and M. Emerson, "An international review of chloride ingress into structural concrete," *Contract. report.*, no. 301, p. 162, 1997.

[194] M. Maage, S. Helland, E. Poulsen, Ø. Vennesland, and J. E. Carlsen, "Service life prediction of existing concrete structures exposed to marine environment," *ACI Mater. J.*, vol. 93, no. 6, pp. 602–608, 1996.

[195] E. Maahn, "PENETRATION RATE OF CHLORIDE IN MARINE CONCRETE STRUCTURES," *Nord. Concr. Res.*, no. 1, Dec. 1982.

[196] R. D. Browne, "Mechanisms of Corrosion of Steel in Concrete in Relation to Design, Inspection, and Repair of Offshore and Coastal Structures," *Spec. Publ.*, vol. 65, pp. 169–204, Aug. 1980.

[197] R. D. Hooton, P. Pun, T. Kojundic, and P. Fidjestol, "INFLUENCE OF SILICA FUME ON CHLORIDE RESISTANCE OF CONCRETE," in *PCI/FHWA International Symposium on High Performance Concrete*, 1997, pp. 245–256.

[198] R. B. Polder, "Critical chloride content for reinforced concrete and its relationship to concrete resistivity," in *Materials and Corrosion*, 2009, vol. 60, no. 8, pp. 623–630.

[199] Polder R.B., "Chloride diffusion and resistivity testing of five concrete mixes for marine environment," in *RILEM International Workshop on Chloride Penetration into Concrete*, 1997, pp. 225–233.

[200] T. Zhang and O. E. Gjørv, "An electrochemical method for accelerated testing of chloride diffusivity in concrete," *Cem. Concr. Res.*, vol. 24, no. 8, pp. 1534–1548, 1994.

[201] T. Luping, "On chloride diffusion coefficients obtained by using the electrically accelerated methods," in *RILEM International Workshop on Chloride Penetration into Concrete*, 1997, pp. 126–134.

[202] L. Bertolini, B. Elsener, P. Pedeferri, E. Redaelli, and R. Polder, *Corrosion of Steel in Concrete : Prevention, Diagnosis, Repair.* Wiley, 2013.

[203] M. COLLEPARDI, A. MARCIALIS, and R. TURRIZIANI, "Penetration of Chloride Ions into Cement Pastes and Concretes," *J. Am. Ceram. Soc.*, vol. 55, no. 10, pp. 534–535, Oct. 1972.

[204] C. L. Page, P. Lambert, and P. R. W. Vassie, “Investigations of reinforcement corrosion. 1. The pore electrolyte phase in chloride-contaminated concrete,” *Mater. Struct.*, vol. 24, no. 4, pp. 243–252, 1991.

[205] “Chloride diffusion in steel fibre reinforced concrete containing PFA,” *Cem. Concr. Res.*, vol. 17, no. 4, pp. 640–650, Jul. 1987.

[206] C. Arya, N. R. Buenfeld, and J. B. Newman, “Assessment of simple methods of determining the free chloride ion content of cement paste,” *Cem. Concr. Res.*, 1987.

[207] T. Sumranwanich and S. Tangtermsirikul, “A model for predicting time-dependent chloride binding capacity of cement-fly ash cementitious system,” *Mater. Struct.*, vol. 37, no. 6, pp. 387–396, Jul. 2004.

[208] G. K. Glass and N. R. Buenfeld, “The influence of chloride binding on the chloride induced corrosion risk in reinforced concrete,” *Corros. Sci.*, 2000.

[209] Q. Yuan, C. Shi, G. De Schutter, K. Audenaert, and D. Deng, “Chloride binding of cement-based materials subjected to external chloride environment - A review,” *Constr. Build. Mater.*, vol. 23, pp. 1–13, 2009.

[210] Sheffield Hallam University, “Liquid Granite: Building Material Of The Future Unveiled -- ScienceDaily,” 2009. [Online]. Available: https://www.sciencedaily.com/releases/2009/10/091029161253.htm. [Accessed: 07-Aug-2017].

[211] CIA, “Testing of concrete,” 1966.

[212] Vernier Software and Technology, “Chloride Ion-Selective Electrode (Order Code CL-BTA),” 2014.

[213] ELIT 8261, “Method for determining the concentration of Chloride (Cl-) in Aqueous Solutions,” 2015. [Online]. Available: http://www.nico2000.net/analytical/chloride.htm. [Accessed: 07-Aug-2017].

[214] BS EN 14629:2007, “Products and systems for the protection and repair of concrete structures — Test methods — Determination of chloride content in hardened concrete,” 2007.

[215] M. S. Morsy, S. H. Alsayed, Y. Al-Salloum, and T. Almusallam, “Effect of Sodium Silicate to Sodium Hydroxide Ratios on Strength and Microstructure of Fly Ash Geopolymer Binder,” *Arab. J. Sci. Eng.*, vol. 39, no. 6, pp. 4333–4339, Jun. 2014.

[216] T. Simcic, S. Pejovnik, G. De Schutter, and V. B. Bosiljkov, “Chloride ion penetration into fly ash modified concrete during wetting-drying cycles,” *Constr. Build. Mater.*, vol. 93, pp. 1216–1223, 2015.

[217] A. Costa and J. Appleton, “Chloride penetration into concrete in marine environment - Part II : Prediction of long term chloride penetration,” *Mater. Struct.*, vol. 32, no. June, pp. 354–359, 1999.

[218] P. C. Aitcin and R. J. Flatt, *Science and technology of concrete admixtures*. 2015.

[219] a Costa and A. Appleton, “Chloride penetration into concrete in marine

environment -Part I: Main parameters affecting chloride penetration," *Mater. Struct. Constr.*, vol. 32, no. May, pp. 252–259, 1999.

[220] H.-J. Chen, S.-S. Huang, C.-W. Tang, M. A. Malek, and L.-W. Ean, "Effect of curing environments on strength, porosity and chloride ingress resistance of blast furnace slag cement concretes: A construction site study," *Constr. Build. Mater.*, vol. 35, pp. 1063–1070, Oct. 2012.

[221] M. G. Stewart and D. V. Rosowsky, "Structural Safety and Serviceability of Concrete Bridges Subject to Corrosion," *J. Infrastruct. Syst.*, vol. 4, no. 4, pp. 146–155, Dec. 1998.

[222] M. K. Kassir and M. Ghosn, "Chloride-induced corrosion of reinforced concrete bridge decks," *Cem. Concr. Res.*, vol. 32, no. 1, pp. 139–143, 2002.

[223] R. N. Swamy, *Corrosion and corrosion protection of steel in concrete*. Sheffield Academic Press, 1994.

[224] R. Malheiro, G. Meira, M. Lima, and N. Perazzo, "Influence of mortar rendering on chloride penetration into concrete structures," *Cem. Concr. Compos.*, 2011.

[225] Baker J.M., Davies H., Majumdar A.J., and Nixon p.j., "Durability of Building Materials and Components: Proceedings of the Fifth ... - Google Books," in *Proceedings of the Fifth International Conference*, 1990, p. 766.

[226] P. S. S. Mangat and B. T. T. Molloy, "Predicting of long term chloride concentration in concrete," *Mater. Struct.*, vol. 27, no. 6, pp. 338–346, 1994.

[227] W. K. W. Lee and J. S. J. van Deventer, "Effects of anions on the formation of aluminosilicate gel in geopolymers," *Ind. Eng. Chem. Res.*, vol. 41, pp. 4550–4558, 2002.

[228] X. Gao, Q. L. Yu, and H. J. H. Brouwers, "Reaction kinetics, gel character and strength of ambient temperature cured alkali activated slag-fly ash blends," *Constr. Build. Mater.*, vol. 80, pp. 105–115, 2015.

[229] T. W. Cheng and J. P. Chiu, "Fire-resistant geopolymer produced by granulated blast furnace slag," *Miner. Eng.*, vol. 16, no. 3, pp. 205–210, 2003.

[230] T. Chareerat and P. Lee-Anansaksiri, A. and Chindaprasirt, "Synthesis of High Calcium Fly Ash and Calcined Kaoline Geopolymer Mortar," in *International Conference on Pozzolan, Concrete and Geopolymer, Khhon Kaen*, 2006, p. 456.

[231] A. C. Belch, M. Berkowitz, and J. A. McCammon, "Solvation structure of a sodium chloride ion pair in water," *J. Am. Chem. Soc.*, vol. 108, no. 8, pp. 1755–1761, Apr. 1986.

[232] M. Sammalkorpi, M. Karttunen, and M. Haataja, "Ionic Surfactant Aggregates in Saline Solutions: Sodium Dodecyl Sulfate (SDS) in the Presence of Excess Sodium Chloride (NaCl) or Calcium Chloride ($CaCl_2$)," *J. Phys. Chem. B*, vol. 113, no. 17, pp. 5863–5870, Apr. 2009.

[233] D.H. Chisholm and N.P. Lee, "Actual and Effective Diffusion Coefficient of Concrete Under Marine Exposure Conditions," in *20th Biennial Conference of the Concrete Institute of Australia*, 2001, pp. 11–14.

[234] Q. Ma, S. V. Nanukuttan, P. A. M. Basheer, Y. Bai, and C. Yang, “Chloride transport and the resulting corrosion of steel bars in alkali activated slag concretes,” *Mater. Struct.*, vol. 49, no. 9, pp. 3663–3677, Sep. 2016.

[235] F. Puertas, A. Fernández-Jiménez, and M. T. Blanco-Varela, “Pore solution in alkali-activated slag cement pastes. Relation to the composition and structure of calcium silicate hydrate,” *Cem. Concr. Res.*, vol. 34, pp. 139–148, 2004.

[236] V. K. Ortolan, M. Mancio, and B. F. Tutikian, “Evaluation of the influence of the pH of concrete pore solution on the corrosion resistance of steel reinforcement,” *J. Build. Pathol. Rehabil.*, vol. 1, no. 10, pp. 1–7, 2016.

[237] P. Ghods, O. B. Isgor, G. McRae, and T. Miller, “The effect of concrete pore solution composition on the quality of passive oxide films on black steel reinforcement,” *Cem. Concr. Compos.*, vol. 31, no. 1, pp. 2–11, 2009.

[238] U. Angst, B. Elsener, C. K. Larsen, and O. Vennesland, “Critical chloride content in reinforced concrete - A review,” *Cem. Concr. Res.*, vol. 39, pp. 1122–1138, 2009.

[239] A. Poursaee and C. M. Hansson, “Potential pitfalls in assessing chloride-induced corrosion of steel in concrete,” *Cem. Concr. Res.*, vol. 39, no. 5, pp. 391–400, 2009.

[240] S. Song and H. M. Jennings, “Pore solution chemistry of alkali-activated ground granulated blast-furnace slag,” *Cem. Concr. Res.*, vol. 29, no. 2, pp. 159–170, 1999.

[241] X. Wan, F. H. Wittmann, T. Zhao, and H. Fan, “Chloride content and pH value in the pore solution of concrete under carbonation,” *J. Zhejiang Univ. Sci. A*, vol. 14, no. 1, pp. 71–78, 2013.

[242] M. Te Liang, R. Huang, and H. Y. Jheng, “Relationship between the free and total chloride diffusivity in concrete,” *J. Mar. Sci. Technol.*, vol. 32, pp. 323–326, 2002.

[243] Pettersson K., “Chloride Threshold Value and the Corrosion Rate in Reinforced Concrete,” in *Proc. of the Nordic Seminar*, 1995, pp. 257–266.

[244] W. Breit, “Kritischer korrosionsausl??sender Chloridgehalt - Untersuchungen an M??rtelelektroden in chloridhaltigen alkalischen L??sungen,” *Mater. Corros.*, vol. 54, no. 6, pp. 430–439, 2003.

[245] C. Alonso, C. Andrade, M. Castellote, and P. Castro, “Chloride threshold values to depassivate reinforcing bars embedded in a standardized OPC mortar,” *Cem. Concr. Res.*, vol. 30, no. 7, pp. 1047–1055, 2000.

[246] L. Zimmermann, “Korrosionsinitiierender Chloridgehalt von Stahl in Beton,” ETH Zürich, Jan. 2000.

[247] M. Castellote, C. Andrade, and C. Alonso, “Accelerated simultaneous determination of the chloride depassivation threshold and of the non-stationary diffusion coefficient values,” *Corros. Sci.*, vol. 44, no. 11, pp. 2409–2424, 2002.

[248] D. Trejo and R. G. Pillai, “Accelerated chloride threshold testing - Part II: Corrosion-resistant reinforcement,” *ACI Mater. J.*, vol. 101, no. 1, pp. 57–64,

2004.

[249] T. U. Mohammed and H. Hamada, “Corrosion of steel bars in concrete with various steel surface conditions,” *ACI Mater. J.*, vol. 103, no. 4, pp. 233–242, 2006.

[250] P. S. Mangat, J. M. Khatib, and B. T. Molloy, “Microstructure, chloride diffusion and reinforcement corrosion in blended cement paste and concrete,” *Cem. Concr. Compos.*, 1994.

[251] C. Arya and Y. Xu, “Effect of cement type on chloride binding and corrosion of steel in concrete,” *Cem. Concr. Res.*, vol. 25, no. 4, pp. 893–902, 1995.

[252] C. L. Page and Vennesland, “Pore solution composition and chloride binding capacity of silica-fume cement pastes,” *Matériaux Constr.*, vol. 16, no. 1, pp. 19–25, 1983.

[253] M. H. Roberts, “Effect of calcium chloride on the durability of pre-tensioned wire in prestressed concrete,” *Mag. Concr. Res.*, vol. 14, no. 42, pp. 143–154, 1962.

[254] J. Tritthart, “Chloride binding in cement II. The influence of the hydroxide concentration in the pore solution of hardened cement paste on chloride binding,” *Cem. Concr. Res.*, vol. 19, no. 5, pp. 683–691, 1989.

[255] D. A. Hausmann, “Steel corrosion in concrete -- how does it work?,” *Mater. Prot.*, vol. 6, no. 11, pp. 19–23, Nov. 1967.

[256] C. L. Page and J. Havdahl, “Electrochemical monitoring of corrosion of steel in microsilica cement pastes,” *Mater. Struct.*, vol. 18, no. 1, pp. 41–47, Jan. 1985.

[257] M. D. A. Thomas, R. D. Hooton, A. Scott, and H. Zibara, “The effect of supplementary cementitious materials on chloride binding in hardened cement paste,” *Cem. Concr. Res.*, vol. 42, pp. 1–7, 2012.

[258] Q. Yuan, D. Deng, C. Shi, and G. De Schutter, “Chloride binding isotherm from migration and diffusion tests,” *J. Wuhan Univ. Technol. Mater. Sci. Ed.*, vol. 28, no. 3, pp. 548–556, 2013.

[259] K. Tuutti, “Analysis of pore solution squeezed out of cement paste and mortar,” *Nord. Concr. Res.*, no. 1, pp. 1–16, Dec. 1982.

[260] V. S. Ramachandran, R. C. Seeley, and G. M. Polomark, “Free and combined chloride in hydrating cement and cement components,” *Mat??riaux Constr.*, vol. 17, no. 4, pp. 285–289, 1984.

[261] P. Sandberg, “Studies of chloride binding in concrete exposed in a marine environment,” *Cem. Concr. Res.*, vol. 29, no. 4, pp. 473–477, 1999.

[262] M. V. A. Florea and H. J. H. Brouwers, “Modelling of chloride binding related to hydration products in slag-blended cements,” *Constr. Build. Mater.*, vol. 64, pp. 421–430, 2014.

[263] G. Plusquellec, M. R. Geiker, J. Lindgard, J. Duchesne, B. Fournier, and K. De Weerdt, “Determination of the pH and the free alkali metal content in the pore solution of concrete: Review and experimental comparison,” *Cem. Concr. Res.*,

vol. 96, pp. 13–26, 2017.

[264] V. Rasanen and V. Penttala, “The pH measurement of concrete and smoothing mortar using a concrete powder suspension,” *Cem. Concr. Res.*, vol. 34, no. 5, pp. 813–820, 2004.

[265] K. Haga, M. Shibata, M. Hironaga, S. Tanaka, and S. Nagasaki, “Change in pore structure and composition of hardened cement paste during the process of dissolution,” *Cem. Concr. Res.*, 2005.

[266] P. S. Mangat and K. Gurusamy, “Pore fluid composition under marine exposure of steel fibre reinforced concrete,” *Cem. Concr. Res.*, vol. 17, pp. 734–742, 1987.

[267] T. Cheewaket, C. Jaturapitakkul, and W. Chalee, “Initial corrosion presented by chloride threshold penetration of concrete up to 10 year-results under marine site,” *Constr. Build. Mater.*, vol. 37, pp. 693–698, 2012.

[268] G. K. Glass and N. R. Buenfeld, “The presentation of the chloride threshold level for corrosion of steel in concrete,” *Corros. Sci.*, vol. 39, no. 5, pp. 1001–1013, 1997.

[269] J. Liu, K. Tang, D. Pan, Z. Lei, W. Wang, and F. Xing, “Surface chloride concentration of concrete under shallow immersion conditions,” *Materials (Basel).*, vol. 7, pp. 6620–6631, 2014.

[270] B. Reddy, G. K. Glass, P. J. Lim, and N. R. Buenfeld, “On the corrosion risk presented by chloride bound in concrete,” *Cem. Concr. Compos.*, vol. 24, pp. 1–5, 2002.

[271] J. Tritthart, “Pore solution of concrete: The equilibrium of bound and free chloride,” *Mater. Corros.*, vol. 60, no. 8, pp. 579–585, Aug. 2009.

[272] R. K. Dhir, M. A. K. El-Mohr, T. D. Dyer, and C. D. Pomeroy, “Developing chloride resisting concrete using PFA,” *Cem. Concr. Res.*, vol. 27, no. 11, pp. 1633–1639, 1997.

[273] M. N. Haque and O. A. Kayyali, “Free and water soluble chloride in concrete,” *Cem. Concr. Res.*, vol. 25, no. 3, pp. 531–542, 1995.

[274] R. R. Lloyd, J. L. Provis, and J. S. J. Van Deventer, “Pore solution composition and alkali diffusion in inorganic polymer cement,” *Cem. Concr. Res.*, vol. 40, p. 2010, 2010.

[275] D. W. S. Ho and R. K. Lewis, “Carbonation of concrete and its prediction,” *Cem. Concr. Res.*, 1987.

[276] V. G. Papadakis, M. N. Fardis, and C. G. Vayenas, “Effect of composition, environmental factors and cement-lime mortar coating on concrete carbonation,” *Mater. Struct.*, vol. 25, no. 5, pp. 293–304, 1992.

[277] D. W. Hobbs, “Concrete deterioration: causes, diagnosis, and minimising risk,” *Int. Mater. Rev.*, vol. 46, no. 3, pp. 117–144, 2001.

[278] B. Johannesson and P. Utgenannt, “Microstructural changes caused by carbonation of cement mortar,” *Cem. Concr. Res.*, vol. 31, pp. 925–931, 2001.

[279] T. A. Bier, “Influence of type of cement and curing on carbonation progress and

pore structure of hydrated cement paste," in *Materials Research Society Proceedings*, 1986, vol. 85, pp. 123–134.

[280] F. P. Glasser, J. Marchand, and E. Samson, "Durability of concrete - Degradation phenomena involving detrimental chemical reactions," *Cem. Concr. Res.*, vol. 38, no. 2, pp. 226–246, 2008.

[281] V. G. Papadakis, C. G. Vayenas, and M. N. Fardis, "Experimental Investigation and Mathematical-Modeling of the Concrete Carbonation Problem," *Chem. Eng. Sci.*, vol. 46, no. 5–6, pp. 1333–1338, 1991.

[282] Y. F. Houst, "The role of moisture in the carbonation of cementitious materials TT - Bauinstandsetzen und Baudenkmalpflege: eine internationale Zeitschrift," *Restor. Build. Monum. an Int. J. = Bauinstandsetz. und Baudenkmalpfl. eine Int. Zeitschrift*, vol. 2, no. 1, pp. 67–82, 1996.

[283] Rasheeduzzafar, "Influence of cement composition on concrete durability," *ACI Mater. J.*, vol. 89, no. 6, pp. 574–586, 1992.

[284] L. C. Lange, C. D. Hills, and A. B. Poole, "The influence of mix parameters and binder choice on the carbonation of cement solidified wastes," *Waste Manag.*, 1996.

[285] J. H. M. Visser, "Accelerated carbonation testing of mortar with supplementary cementing materials - Limitation of the acceleration due to drying," *Heron*, 2012.

[286] V. G. Papadakis, "Effect of supplementary cementing materials on concrete resistance against carbonation and chloride ingress," *Cem. Concr. Res.*, vol. 30, no. 2, pp. 291–299, 2000.

[287] K. Byfors, G. Klingstedt, V. Lehtonen, H. Pyy, and L. Romben, "Durability of Concrete Made With Alkali-Activated Slag," in *Third International Conference Proceedings. Fly Ash, Silica Fume, Slag, and Natural Pozzolans in Concrete*, 1989, pp. 1429–1466.

[288] T. Bakharev, J. G. Sanjayan, and Y.-B. Cheng, "Resistance of alkali-activated slag concrete to carbonation," *Cem. Concr. Res.*, vol. 31, pp. 1277–1283, 2001.

[289] J. Deja, "Carbonation aspects of alkali activated slag mortars and concretes," *Silic. Ind.*, no. 3–4, pp. 37–42, 2002.

[290] B. Lagerblad, *Carbon dioxide uptake during concrete life cycle – State of the art*, vol. CBI 2005:2, no. February. 2005.

[291] C.-T. Chen and C.-W. Ho, "Influence of Cyclic Humidity on Carbonation of Concrete.," *J. Mater. Civ. Eng.*, vol. 25, no. 12, pp. 1929–1935, 2013.

[292] M. I. Khan and C. J. Lynsdale, "Strength, permeability, and carbonation of high-performance concrete," *Cem. Concr. Res.*, 2002.

[293] E. Gruyaert, P. Van Den Heede, and N. De Belie, "Carbonation of slag concrete: Effect of the cement replacement level and curing on the carbonation coefficient - Effect of carbonation on the pore structure," *Cem. Concr. Compos.*, 2013.

[294] S. A. Bernal, J. L. Provis, D. G. Brice, A. Kilcullen, P. Duxson, and J. S. J. Van Deventer, "Accelerated carbonation testing of alkali-activated binders

significantly underestimates service life: The role of pore solution chemistry," *Cem. Concr. Res.*, vol. 42, no. 10, pp. 1317–1326, 2012.

[295] B. F. Houst, "Carbonation shrinkage of hydrated cement paste," in *Fourth CANMET/ACI International Conference on Durability of Concrete, Sydney,* 1997, pp. 481–491.

[296] H. Ye, A. Radlińska, and J. Neves, "Drying and carbonation shrinkage of cement paste containing alkalis," *Mater. Struct.*, 2017.

[297] J. J. Chen, J. J. Thomas, and H. M. Jennings, "Decalcification shrinkage of cement paste," *Cem. Concr. Res.*, 2006.

[298] G. J. Verbeck, "Carbonation of Hydrated Portland Cement," *ASTM Spec. Tech. Publ.*, vol. 205, no. 205, pp. 17–36, 1958.

[299] British Standards Institution., "Testing hardened concrete Part 210: Determination of the potential carbonation resistance of concrete – Accelerated carbonation method," 2013.

[300] "Products and systems for the protection and repair of concrete structures — Test methods — Determination of carbonation depth in hardened concrete by the phenolphthalein method," 2006.

[301] D. W. Law, A. A. Adam, T. K. Molyneaux, and I. Patnaikuni, "Durability assessment of alkali activated slag (AAS) concrete," *Mater. Struct.*, 2012.

[302] F. Puertas, M. Palacios, and T. Vázquez, "Carbonation process of alkali-activated slag mortars," *J. Mater. Sci.*, 2006.

[303] S. A. Bernal, R. M. de Gutierrez, J. L. Provis, and V. Rose, "Effect of silicate modulus and metakaolin incorporation on the carbonation of alkali silicate-activated slags," *Cem. Concr. Res.*, 2010.

[304] S. Kandasami, T. A. Harrison, M. R. Jones, and G. Khanna, "Benchmarking UK concretes using an accelerated carbonation test," *Mag. Concr. Res.*, vol. 64, no. 8, pp. 697–706, 2012.

[305] J. Khunthongkeaw, S. Tangtermsirikul, and T. Leelawat, "A study on carbonation depth prediction for fly ash concrete," *Constr. Build. Mater.*, 2006.

[306] F. Collins and J. G. Sanjayan, "Microcracking and strength development of alkali activated slag concrete," *Cem. Concr. Compos.*, vol. 23, no. 4–5, pp. 345–352, 2001.

[307] F. Collins and J. G. Sanjayan, "Cracking tendency of alkali-activated slag concrete subjected to restrained shrinkage," *Cem. Concr. Res.*, vol. 30, no. 5, pp. 791–798, 2000.

[308] R. J. Thomas, D. Lezama, and S. Peethamparan, "On drying shrinkage in alkali-activated concrete: Improving dimensional stability by aging or heat-curing," *Cem. Concr. Res.*, 2017.

[309] J. J. Brooks, "Influence of mix proportions, plasticizers and superplasticizers on creep and drying shrinkage of concrete," *Mag. Concr. Res.*, vol. 41, no. 148, pp. 145–153, 1989.

[310] N. B. (Nicholas B. . Winter, *Understanding cement : an introduction to cement production, cement hydration and deleterious processes in concrete*. WHD Microanalysis Consultants, 2012.

[311] E. Douglas, A. Bilodeau, and V. M. Malhotra, "Properties and durability of alkali-activated slag concrete," *ACI Mater. J.*, vol. 89, no. 5, pp. 509–516, 1992.

[312] R. M. de G. and J. S. J. van D. Bernal A. Susan, John L. Provis, "Accelerated carbonation testing of alkali-activated slag/metakaolin blended concretes: effect of exposure conditions," *Mater. Struct.*, vol. 48, pp. 653–669, 2015.

[313] Y. Qin and H. Yang, "Carbonation dominates the acid intake of recycled concrete aggregate subjected to intermittent leaching," *Constr. Build. Mater.*, vol. 89, pp. 110–114, 2015.

[314] Page C.L. and Lambert P., "Analytical and Electrochemical Investigations of Reinforcement Corrosion," Crowthorne, Berkshire, UK, 1986.

[315] V. K. Gouda, "Corrosion and Corrosion Inhibition of Reinforcing Steel: I. Immersed in Alkaline Solutions," *Br. Corros. J.*, vol. 5, no. 5, pp. 198–203, Sep. 1970.

[316] C. L. Page and K. W. J. Treadaway, "Aspects of the electrochemistry of steel in concrete," *Nature*, vol. 297, no. 5862, pp. 109–115, May 1982.

[317] K. Kupwade-Patil, E. N. Allouche, S. Vaidya, and E. I. Diaz-Loya, "Corrosion analysis of reinforced geopolymer concretes," *Concr. Solut.*, 2012.

[318] J. W. Park, K. Y. Ann, and C.-G. Cho, "Resistance of Alkali-Activated Slag Concrete to Chloride-Induced Corrosion," *Adv. Mater. Sci. Eng.*, vol. 2015, pp. 1–7, Oct. 2015.

[319] Nishimura R. and Sato N., "potential-pH diagram of composition/structure of passive film on iron," in *International congress on metallic corrosion*, 1984, pp. 96–101.

[320] Mohammad Shamid Khan, "Corrosion State of Reinforcing Steel in Concrete at Early Ages," vol. 88, no. 1, pp. 37–40, 1991.

[321] J. M. Miranda, A. Fernández-Jiménez, J. A. González, and A. Palomo, "Corrosion resistance in activated fly ash mortars," *Cem. Concr. Res.*, vol. 35, no. 6, pp. 1210–1217, 2005.

[322] D. M. Bastidas, A. Fernández-Jiménez, A. Palomo, and J. A. González, "A study on the passive state stability of steel embedded in activated fly ash mortars," *Corros. Sci.*, vol. 50, no. 4, pp. 1058–1065, 2008.

[323] America's cement manufacturers, "Corrosion of Embedded Materials," *PCA*, 2017. [Online]. Available: http://www.cement.org/learn/concrete-technology/durability/corrosion-of-embedded-materials. [Accessed: 06-Jul-2017].

[324] J. P. Broomfield, *Corrosion of steel in concrete : understanding, investigation and repair*. Taylor & Francis, 2007.

[325] A. Poursaee, *Corrosion of steel in concrete structures*, 1st ed. Woodhead Publishing, 2016.

[326] C. Andrade, “Corrosion of steel reinforcement,” in *Environmental Deterioration of Materials*, 1st ed., A. Moncmanova, Ed. Southampton, England: WIT Transactions on State-of-the-art in Science and Engineering , 2007, pp. 185–216.

[327] M. Pourbaix, *Atlas of electrochemical equilibria in aqueous solutions.* Houston, TX: Nat’L Assoc. Of Corrosion, 1974.

[328] R. W. (Robert W. Revie and H. H. Uhlig, *Corrosion and corrosion control : an introduction to corrosion science and engineering*, 4th ed. New Jersey: John Wiley & Sons, 2008.

[329] W. S. Tait, *An introduction to electrochemical corrosion testing for practicing engineers and scientists*. PairODocs Publications, 1994.

[330] R. W. Revie, Ed., *Uhlig’s Corrosion Handbook*. Hoboken, NJ, USA: John Wiley & Sons, Inc., 2011.

[331] E. McCafferty, *Introduction to corrosion science*. Springer, 2010.

[332] P. Lambert, “Corrosion Mechanisms – an Introduction to Aqueous Corrosion,” pp. 1–5, 2002.

[333] NACE International, “Pitting Corrosion,” 2017. [Online]. Available: https://www.nace.org/Pitting-Corrosion/. [Accessed: 16-Jul-2017].

[334] J. P. Broomfield, “Repair Guidance Note 1: Corrosion of steel in concrete,” *Concrete*, vol. 41, no. 4, pp. 13–15, 2007.

[335] G. J. Verbeck, “Mechanisms of Corrosion of Steel in Concrete,” *Spec. Publ.*, vol. 49, pp. 21–38, Jan. 1975.

[336] Portland Cement Association, “Types and Causes of Concrete Deterioration,” *PCA R&D Spec. N. 2617*, pp. 1–16, 2002.

[337] V. Jovancicevic, J. O. Bockris, J. L. Carbajal, P. Zelenay, and T. Mizuno, “Adsorption and Absorption of Chloride Ions on Passive Iron Systems,” *J. Electrochem. Soc.*, vol. 133, no. 11, p. 2219, Nov. 1986.

[338] R. A. Legault, S. Mori, and H. P. Leckie, “An Electrochemical-Statistical Study of the Effect of Chemical Environment on the Corrosion Behavior of Mild Steel,” *CORROSION*, vol. 26, no. 6, pp. 221–228, Jun. 1970.

[339] C. Y. Chao, L. F. Lin, and D. D. Macdonald, “A Point Defect Model for Anodic Passive Films,” *J. Electrochem. Soc.*, vol. 128, no. 6, p. 1187, Jun. 1981.

[340] J. Tritthart, “Chloride binding in cement I. Investigations to determine the composition of porewater in hardened cement,” *Cem. Concr. Res.*, vol. 19, no. 4, pp. 586–594, 1989.

[341] M. Schiessl, P. and Raupach, “Influence of concrete composition and microclimate on the critical chloride content in concrete,” in *Corrosion of reinforcement in concrete*, K. W. J. T. and P. B. B. C.J. Page, Ed. Published for the Society of Chemical Industry by Elsevier Applied Science, 1990, pp. 49–58.

[342] P. Schiessl, *Corrosion of steel in concrete : report of the Technical Committee 60 CSC, RILEM (the International Union of Testing and Research Laboratories for Materials and Structures)*. London ; Chapman and Hall, 1988.

[343] R. A. M. Watkins, A. P. Pitt Jones, and A. P. P. Jones, “Carbonation: A durability model related to site data,” *Proc. Inst. Civ. Eng. - Struct. Build.*, vol. 99, no. 2, pp. 155–166, May 1993.

[344] Z. P. and J. F. Wittman F.H., Zhao T., “Service life of reinforced concrete structures under combined mechanical and environmental loads,” in *2nd International Symposium on Service Life Design for Infrastructure*.

[345] J. L. Beaton and R. F. Stratfull, “Environmental Influence on Corrosion of Reinforcing in Concrete Bridge Substructures,” *Highw. Res. Board*, vol. Record No., pp. 60–78, 1963.

[346] Y. P. Virmani, K. C. CLEAR, and T. J. Pasko Jr, “Time-to-corrosion of reinforcing steel in concrete slabs,” *Mater. Technol. Chem. Div. 1200 New Jersey Ave. SE*, vol. 5, p. 76, Sep. 1983.

[347] K. Hong and R. D. Hooton, “Effects of cyclic chloride exposure on penetration of concrete cover,” *Cem. Concr. Res.*, vol. 29, no. 9, pp. 1379–1386, Sep. 1999.

[348] C. Q. Li, “Initiation of Chloride-Induced Reinforcement Corrosion in Concrete Structural Members—Prediction,” *ACI Struct. J.*, vol. 99, no. 2, pp. 133–141, Mar. 2002.

[349] P. B. Bamforth, “The derivation of input data for modelling chloride ingress from eight-year UK coastal exposure trials,” *Mag. Concr. Res.*, vol. 51, no. 2, pp. 87–96, Apr. 1999.

[350] Vagelis G Papadakis, “Service life prediction of a reinforced concrete bridge exposed to chloride induced deterioration,” *Adv. Concr. Constr.*, vol. 1, no. 3, pp. 201–213, 2013.

[351] M. S. Darmawan, “Pitting corrosion model for reinforced concrete structures in a chloride environment,” *Mag. Concr. Res.*, vol. 62, no. 2, pp. 91–101, 2010.

[352] Palle Thoft-Christensen, “Modelling of the deterioration of reinforced concrete structures,” *Struct. Reliab. Theory*, vol. R0020, no. 199, p. 12, 2000.

[353] K. Vu and M. Stewart, “Structural reliability of concrete bridges including improved chloride-induced corrosion models,” *Struct. Saf.*, vol. 22, no. 4, pp. 313–333, 2000.

[354] D. V. Val and R. E. Melchers, “Reliability of Deteriorating RC Slab Bridges,” *J. Struct. Eng.*, vol. 123, no. 12, pp. 1638–1644, Dec. 1997.

[355] J. A. González, C. Andrade, C. Alonso, and S. Feliu, “Comparison of rates of general corrosion and maximum pitting penetration on concrete embedded steel reinforcement,” *Cem. Concr. Res.*, vol. 25, no. 2, pp. 257–264, Feb. 1995.

[356] M.S. Darmawan and M.G. Stewart, “Effect of Spatially Variable Pitting Corrosion on Structural Reliability of Prestressed Concrete Bridge Girders,” *Aust. J. Struct. Eng.*, vol. 6, no. 2, pp. 148–158, 2006.

[357] D. V. & D. L. M. Šomodíková, B. Teplý, “Modelling of the service life of concrete structures under combined mechanical and environmental actions,” in *Safety and Reliability of Complex Engineered Systems* , Podofillini et al. (Eds), Ed. London: Taylor & Francis Group, 2015, pp. 4219–4224.

[358] Y. Paul Virmani and Gerardo G. Clemena, “Corrosion protection - Concrete bridges,” McLean, Virginia 22102 -2296, 1998.

[359] E. J. Wallbank, Great Britain. Department of Transport., and G. Maunsell & Partners., *The Performance of Concrete in Bridges : A Survey of 200 Highway Bridges*. UK: H.M.S.O, 1989.

[360] S. Ahmad, “Reinforcement corrosion in concrete structures, its monitoring and service life prediction—a review,” *Cem. Concr. Compos.*, vol. 25, no. 4–5, pp. 459–471, May 2003.

[361] McLeish A., *Manual for life cycle aspects of concrete in buildings and structures*. Taywood Engineering, 1987.

[362] A. A. Almusallam, A. S. Al-Gahtani, A. R. Aziz, F. H. Dakhil, and Rasheeduzzafar, “Effect of Reinforcement Corrosion on Flexural Behavior of Concrete Slabs,” *J. Mater. Civ. Eng.*, vol. 8, no. 3, pp. 123–128, 1996.

[363] T. Uomoto and S. Misra, “Behavior of Concrete Beams and Columns in Marine Environment When Corrosion of Reinforcing Bars Takes Place,” *Spec. Publ.*, vol. 109, pp. 127–146, Aug. 1988.

[364] J. G. Cabrera, “Deterioration of concrete due to reinforcement steel corrosion,” *Cem. Concr. Compos.*, vol. 18, no. 1, pp. 47–59, Jan. 1996.

[365] G. J. Al-Sulaimani, M. Kaleemullah, I. A. Basunbul, and Rasheeduzzafar, “Influence of Corrosion and Cracking on Bond Behavior and Strength of Reinforced Concrete Members,” *ACI Struct. J.*, vol. 87, no. 2, pp. 220–231, Mar. 1990.

[366] P. S. Mangat and M. S. Elgarf, “Bond characteristics of corrding reinforcement in concrete beams,” *Mater. Struct.*, vol. 32, no. 2, pp. 89–97, Mar. 1999.

[367] D. V. Val, M. G. Stewart, and R. E. Melchers, “Effect of reinforcement corrosion on reliability of highway bridges,” *Eng. Struct.*, vol. 20, no. 11, pp. 1010–1019, Nov. 1998.

[368] British Standards Institution., “Preparation of steel substrates before application of paints and related products. Group E. Metallic blast-cleaning abrasives. Part E4. Specification for low-carbon cast-steel shot,” British Standards Institution, 1994.

[369] British Standard, “Testing hardened concrete. Determination of the chloride resistance of concrete, unidirectional diffusion,” UK, BS EN 12390-11:2015, 2015.

[370] C. L. Page and P. Lambert, “Kinetics of oxygen diffusion in hardened cement pastes,” *J. Mater. Sci.*, vol. 22, no. 3, pp. 942–946, 1987.

[371] The Concrete Society, “TR60 Electrochemical tests for reinforcement corrosion,” Surrey, 2004.

[372] G01.14 Corrosion of Metals, “ASTM C876 - 15: Standard Test Method for Corrosion Potentials of Uncoated Reinforcing Steel in Concrete,” 2009.

[373] P. Gu and J. J. Beaudoin, “Obtaining Effective Half-Cell Potential Measurements

in Reinforced Concrete Structures," *Inst. Res. Constr.*, vol. 18, 1998.

[374] ASTM C1585, "Standard Test Method for Measurement of Rate of Absorption of Water by Hydraulic-Cement Concretes."

[375] C. Hall and T. K.-M. Tse, "Water movement in porous building materials—VII. The sorptivity of mortars," *Build. Environ.*, vol. 21, no. 2, pp. 113–118, Jan. 1986.

[376] M. Babaee and A. Castel, "Chloride-induced corrosion of reinforcement in low-calcium fly ash-based geopolymer concrete," *Cem. Concr. Res.*, vol. 88, pp. 96–107, 2016.

[377] V. Bouteiller, J.-F. Cherrier, V. L'Hostis, N. Rebolledo, C. Andrade, and E. Marie-Victoire, "Influence of humidity and temperature on the corrosion of reinforced concrete prisms," *Eur. J. Environ. Civ. Eng.*, vol. 16, no. 3–4, pp. 471–480, Apr. 2012.

[378] M. Holloway and J. M. Sykes, "Studies of the corrosion of mild steel in alkali-activated slag cement mortars with sodium chloride admixtures by a galvanostatic pulse method," *Corros. Sci.*, vol. 47, no. 12, pp. 3097–3110, Dec. 2005.